بسم الله الرحمن الرحیم

Collection of Full Papers

8th Iranian Fuel Cell Seminar

Islamic Azad University
Najafabad branch
(Feb. 25-26, 2015)

With Collaboration of:
Iranian Electrochimical Society

Dear Participant,

Welcome to 8th Iranian Fuel Cell Seminar

The Iranian Fuel Cell Seminar with collaboration of Iranian Electrochemical Society was established in 8 years ago for the purpose of exploring new finding, latest researches and exchange information in different fields of fuel cells systems.

Fuel cell is the best way for clean energy production in Hydrogen economy. It can help for producing electricity with low noise and good efficiency. As fuel cells generate electricity through a chemical reaction, rather than combustion, they do not produce harmful emissions. Currently, technologists are developing and adapting fuel cell technology for practical use in exhaust-free automobiles and in electricity-generating plants.

Participants at this seminar celebrate 70 paper presentations, posters sessions. Professor Hossien Gharibi as especial invited speaker, Professor Jahan Bakhsh Raoof as Director of Electrochemical Society of Iran and Dr. Rasol Abdullah Mirzaie as invited speaker provided insightful ideas and questions for many seminar participants by tackling issues in renewable energy, fuel cell systems.

This seminar would not be possible without your participation and support. We would like to thank you for your participation and also all those involved in the organization of this conference. We hope that you have had a fruitful and memorable seminar and a delightful stay in Islamic Azad University of Najafabad.

Ahmad Nozad Golikand
Head of Scientific Committee

8th Iranian fuel cell seminar

Organizing Committee

Prof. Hossein Gharibi	Seminar Honorary Chairman
Dr Seyed Mohammad Amiri	Seminar Chairman
Prof. Ahmad Nozad Golikand	Head of Scientific Committee
Dr. Reza Ebrahimi	Head of Coordination
Dr Farid Naeimi	Head of Executive Committee
Dr Iman Ebrahimzadeh	Manager of Executive
Mr. Reza Ghasemi	I.A.U. Najafabad branch
Mr. Mostafa Salehi	I.A.U. Najafabad branch
Mr. Noor Mohamadi	I.A.U. Najafabad branch
Mr. Rastegar	I.A.U. Najafabad branch
Mr. Nahvi	I.A.U. Najafabad branch

8th Iranian fuel cell seminar

Scientific Committee

Prof. Hossein Gharibi	Tarbiat Modares University
Prof. Jahan Bakhsh Raoof	University of Mazandaran
Prof. Ahmad Nozad Golikand	Material Research School, NSTRI
Prof. Majid Jafarian	K. N. Toosi University
Dr. Rasol Abdullah Mirzaie	Shahid Rajaee Teacher Training University
Prof. Reza Ojani	University of Mazandaran
Prof. Ghasem Hosseini	Tabriz University
Prof. Mohsen Shakeri	Babol Noshirvani University of Technology
Dr Majid Amidpour	K.N.Toosi University of Technology
Dr Mohsen Asadi	Material Research School, NSTRI
Dr Habib Ashassi	Tabriz University
Dr Mojtaba Bagherzadeh	Material Research School, NSTRI
Dr Niloufar Bahrami Panah	Payame Noor University
Dr Javad Beheshtian	Shahid Rajaee university
Dr Mostafa Dehghani Mobarake	Research Institute of Petroleum Industry
Dr Reza Ebrahimi-Kahrizsangi	Islamic Azad University of Najafabad
Dr Iman Ebrahimzadeh	Islamic Azad University of Najafabad
Dr Ali Ehsani	University of Qom
Dr Mohammad Hasan Eikani	Iranian Research Organization for Science and Technology (IROST)
Dr Ali Eliassi	Iranian Research Organization for Science and Technology (IROST)
Dr Soheila Javadian Farzaneh	Tarbiat Modares University
Dr Hamid Ghayour	slamic Azad University of Najafabad
Dr Seyed Mehdi Golabi	Tabriz University
Dr Biuck Habibi	Azarbaijan Shahid Madani University
Dr Seyed Majid Hashemianzadeh	Iran University of Science of Technology
Dr Majid Jafari	Islamic Azad University of Najafabad
Dr Mehran Javanbakht	Amirkabir University of Technology
Dr Hasan Karimi Maleh	Graduate University of Advanced Technology
Dr Pejman Kazempoor	Tarbiat Modares University
Dr Mohammad Jafar Kermani	Amirkabir University of Technology
Dr Mehdi Kheirmand	Yasouj University
Dr Amir Maghsoudipour	Materials and Energy Research Centre
Dr Reza Majidi	Tabriz University
Dr Farid Naeimi	Islamic Azad University of Najafabad
Dr Mojtaba Nasr-Esfahanni	Islamic Azad University of Najafabad
Dr Saeed Olyaee	Shahid Rajaee Teacher Training University
Dr Soosan Rowshanzamir	Iran University of Science of Technology
Dr Ehsan Saebnoori	Islamic Azad University of Najafabad
Dr Mohammad Safi Rahmanifar	Shahed University
Dr Mohammad Zhiani	Isfahan University of Technology
Dr Mahmoud Ziarati	Malek Ashtar University of Technology

8_{th} Iranian fuel cell seminar
Student Executive Committee:

Seyed Sina Khalifeh Soltani	I.A.U. Najafabad branch
Rasoul Sanjari	I.A.U. Najafabad branch
Rasoul Naderi	I.A.U. Najafabad branch
Mohammad Reza Rostami	I.A.U. Najafabad branch
Keyvan Ahmadi	I.A.U. Najafabad branch
Zahra Ashouri	I.A.U. Najafabad branch
Zahra Nouri	I.A.U. Najafabad branch
Forough Hemat gir	I.A.U. Najafabad branch
Elham Fathiyan	I.A.U. Najafabad branch
Mahdis Salehi	I.A.U. Najafabad branch
Sepideh Nasiri	I.A.U. Najafabad branch
Nakisa Amini	I.A.U. Najafabad branch
Shakiba Saghir Zadeh	I.A.U. Najafabad branch

Table of Content

Fuel Cell Stack Components

Investigation of Nanostructured Bimetallic Pt-Pd Alloy on Functionalized Carbon Supports as a New Cathode for Oxygen Reduction Reaction in Proton Exchange Membrane Fuel Cells …….….15
Fatemeh Yasi, Hussein Gharibi, Ahmad Heydari

Preparation of Cu/Pt Bimetallic Nanocomposite on the MOF-199 Derived Nanoporous Carbon and its Application for Hydrogen Evolution Reaction ……..25
Sakineh Mandegarzad, Jahan-Bakhsh Raoof, Sayed Reza Hosseini, Reza Ojani

A Complete Research about Synthesizing of PtO in the Form of Octahedral; Some Findings about the Anodic Material of Solid State Oxide Fuel Cells ……..….33
Kourosh Motevalli1, Zahra Yaghoubi

Electrodeposition of Platinum on Glassy Carbon Electrode for Electrooxidation of Glucose in Alkaline Medium ……..37
Mehdi khairmand, Abolfath Eshghi

Study of Oxygen Reduction on Pt/ Glassy Carbon Electrode for PEM Fuel Cell Application …….…41
Mehdi kheirmand, Abolfath Eshghi

Metal Oxide/Pt Based Nanocomposites as Electrocatalysts for Oxygen Reduction Reaction ……...45
Tahere Mohammadghasabi, Nasrin Talebian

Performance Comparison of the Two Commercial PEMFC Electrode Substrates: Toray and Ballard Carbon Paper ……..51
Mohammad Zhiani, Mohammad Mohammadi taghiabadi, Ismaeil Mohammadi, Mohsen Keivannejad

Synthesis and Characterization of $PrNiO_3$ Perovskite with Various Ratios of Gelatin as Cathode of Solid Oxide Fuel Cell ……..……57
Bita Roomi, Ahmad Yazdani

Facile Synthesis of Pd/MWCNT Nanocomposite for Ethanol Fuel Cell …….….63
Biuck Habibi, Soheila Mohammadyari

Investigation of Ethylene Glycol Electrooxidation on Fe_3O_4@Pt Core-Shell Nanoparticles Decorated Carbon-Ceramic Substrate ……..……..…71
Biuck Habibi, Serveh Ghaderi

Synthesis, Characterization and Electrocatalytic Activity of Fe_3O_4@Pt Core-Shell Nanoparticles for Formic Acid Electrooxidation ……..….79
Biuck Habibi, Serveh Ghaderi

Production of Chromium oxide using as Modified Thin Film for Lithium Ion Batteries …….85
Bagher-Aziz kalantari, Mohamad Reza-Talei Bavil Olya

Exploring of the Oxygen Reduction Reaction on the Gas Diffusion Electrode for Zinc Air Fuel Cell ……....91
Parisa Akbarian, Mehdi Kheirmand

Core-Shell Co@Pt Nanoparticles as Highly Active Electrocatalyst for Ethanol Oxidation in Fuel Cells …...95
Biuck Habibi, Serveh Ghaderi

Electro-Oxidation Ethanol Using Modified Carbon Paste Electrode with MWCNTs and VSB-5 Nanozeolite for Fuel Cell ……...……99
Mojtaba Gholami-Esfidvajani, Seyed Karim Hassaninejad-Darzi

Evaluation of a Porous Nano Structure Electrode Base on Pt-Free Nano Catalyst for Direct 2-Propanol Fuel Cell ……...…107
S. Samadinejada,M. Zhiania

Electrocatalytic Activity of Green Synthesized CuO Nanoparticles/Conductive Polymer Composite Film in DMFC …….……111
A. Ehsani, M. Ahmadi, A. Rostami-Vartooni

Electrooxidation of Acetaldehyde Using $PtSnO_2$/C and $PtSnO_2$/CNT Catalysts Prepared by Modified Alcohol-Reduction Process …….115
S. Sadeghi, H. Gharibi, F. Golmohammadi, F. Dehghan

Preparation and Evaluation of New Anode Electrode Microstructures Based on Iron-Nickel-Cobalt Nano Catalyst for Direct Fuel Cell 1-Propanol …….…….119
M. Zhiani, K. Esteghlal

Investigation the Performance of Pt-Sn Nanoparticles Supported by Carbon-Polyaniline Composite in a Passive DMFC …….……129
Mitra Amani, Hussein Gharibi, Mohammad Kazemeini, Fereshteh Dehghan

Investigation of Three Metallic Electrocatalyst Activity for ORR in PEMFC ……...……..135
Masoumeh Javaheri

Surfce Enhanced Graphene Supported Pt Nanoparticles for Oxygen Reduction Reaction in PEM Fuel Cells .143
Monireh Faraji, Anil Virkar, Hussein Gharibi

Study of Process Parameters in Preparing Platinum Nano Electrocatalyst by Cyclic Electrodeposition Method Effect on Glucose Oxidation Reaction in Glucose Alkaline Fuel Cell …….……167
Rasol Abdullah Mirzaie, Behnam Moeini, Tahereh Gholian Avval

Nanosilver/TiO_2 Composite as Photoanode of Water Splitting System under Visible Light Illumination …173
Maryam Azimzadehirani, Hussein Gharibi

Study of Increasing Reaction Layer Surface Area Effect on Performance of Gas Diffusion Electrode Prepared by Electrocatalyst Electrodeposition Method for Oxygen Reduction Reaction …….……177
Rasol Abdullah Mirzaie, Mohammad safi Rahmanifar, Narges mohammadkhani

بررسی تاثیر فلز منگنز بر اندرکنش اتانول/الکترود در پیل های سوختی غشا پلیمری ۱۸۱
محسن رضایتمند، احسان صائب نوری

بررسی پوشش کبالت تولید شده به روش لایه نشانی الکتریکی به عنوان کاتد پیل سوختی غشا پلیمری ۱۸۹
امیرحسین آرامی پارچه باف، محمود فاضل نجف آبادی

طراحی سیستم کنترلی تست استیشن پیل سوختی بر اساس برنامه نویسی Labview ۱۹۹
بهزاد ارحامی،عباسعلی ملک برمی، سیامک توکلی

ارزیابی رفتار الکتریکی فولاد ضدزنگ Crofer 22 APU مورد استفاده در پیل‌های سوختی اکسید جامد در حضور اسپینل‌های کبالت .۲۰۹
هادی ابراهیمی فر، مرتضی زند رحیمی

تهیه وشناسایی نانوساختارهای Fe-Ni- Pd و مطالعه خواص الکتروکاتالیستی آنها در جهت اکسیداسیون سوختهای متداول در پیلهای سوختی ..۲۱۷
سید سعید میررضی

استفاده از مواد مختلف پایه کربنی به عنوان الکترود کاتد در پیل سوختی میکروبی ۲۲۹
مهرداد مشکور، مصطفی رحیم نژاد، مهدی مشکور، مریم اصغری

بررسی تاثیر زمان پوشش‌دهی کبالت و منگنز به روش لایه نشانی الکتریکی در پیل‌های سوختی غشا پلیمری ۲۳۷
امیرحسین آرامی پارچه باف، محسن رضایت مند

تهیهٔ الکتروکاتالیست Ni-Pt/C و بررسی تاثیر شرایط عملیاتی بر عملکرد پیل‌های سوختی با سوخت مستقیم بورهیدرید ۲۵۱
میرقاسم حسینی، مهدیه صادقی، رعنا محمودی

ایجاد پوشش محافظ برای اتصال‌دهنده فلزی پیل سوختی اکسید جامد ۲۵۹
زهرا رنجبرنوری، منصور سلطانیه، سعید رستگاری

بررسی استحکام کششی و ضربه ای صفحات دوقطبی تولید شده از پلی استر/دوده ۲٦۷
سید احمد مرتضوی، احمد نوزاد گلی کند، اکرم حیدری

مطالعه تأثیر ثابت دی الکتریک محلول مورد استفاده در تهیه الکتروکاتالسیت پلاتین به روش الکتروشیمیایی در واکنش کاهش اکسیژن در پیل سوختی پلیمری ۲۷۳
رسول عبداله میرزائی، مریم مهدی پور، مهتاب گودرز، صدف دلپذیریان، بهنام معینی

Fuel Cell and Energy

A Nanostructure Magnetic Based Graphene Oxide Electrocatalyst for Methanol Oxidation ……281
R. Sadeghi, H. Karimi-Maleh, Necip Atar

GrapheneNanosheets/CarbonNanotube/Pt/Polyaniline Nanocompositeas Electrode Material for Supercapacitor ……..……..285
Mojtaba Bagherzadeh, Zeinab Shirazi, Ahmad Nozad, Vahid Esfahdani

Effect of Noncovalan Attachment of Magnetic Nanoparticles on Supercapacitive Performance of Reduced Graphene Oxide Nanosheets …….…….289
Mojtaba Bagherzadeh, Vahid Esfahdani, Mahdi Jabouri-Abassi

Effect of Titanium Foil Surface in Anodized Titanium Oxide Nanotubes as Electrode for Lithium-Ion Batteries ……..…….295
Hamideh Kashani, Hussein Gharibi

Evaluation of the Activity of Binary PtM/C Alloy Catalysts Towards the (HOR) for PEMFCS ……..……299
S. Ordoukhani, A. Nozad Golikand

Palladium-Based Catalysts for Oxygen Reduction Reaction in Fuel Cells …….……..309
Fereshteh Dehghani sanij, Hussein Gharibi, Farhad Golmohammadi

Biomass, Resources and Technology for Use in PEMFC ……313
Akram Heidari, Ahmad Nozad Golikand, Seyed Ahmad Mortazavi, Maryam Heidari

Synthesis of Fe:Pt Nanoalloy and Application of it in Preparation of Modified Carbon Paste Electrode in Methanol Oxidation ……....323
Hassan Karimi-Maleh, Sahebe Khosravi

پیل‌های سوختی با سوخت مستقیم بورهیدرید و تاثیر شرایط عملیاتی بر عملکرد پیل‌های سوختی ۳۲۷
میرقاسم حسینی، رعنا محمودی

Simulation and Computational Methods

High Performance Nanocomposite Proton-Exchange Membranes for Fuel Cell Applications 339
Ghasem Bahlakeh

Investigation of Characteristics of Hybrid PEMs from Atomistic Molecular Dynamics Simulations …….345
Ghasem Bahlakeh

شبیه‌سازی سیستم الکترونیکی برای اندازه‌گیری اختلاف فاز متناظر با ضریب شکست مایع پیل سوختی ۳۵۱
زهرا دشتبان، سعید علیائی

Applications

A Total Research about Quick Synthesis of Ultrafine NiPd Bimetallic Nanoparticles and Their High Performance in relation with Methanol Electrooxidation …….…365
Kourosh Motevalli, Zahra Yaghoubi

Study and Fabrication of Monocell and Stack Fuel Cell

Synthesis, Studing and Performance Comparing of Membrane Electrode Assembly Fabricated by Pt/N-rGO with Pt/Vulcane ……..371
Ahmad Heydari, Hussein Gharibi, Fatemah Yasi

Electrochemical Analysis of Anodic Catalysts in Direct Borohydride Fuel Cell ……..377
M. Zhiani, I. Mohammadi, M.M. Taghiabadi

Effect of Potential Cyclic and External Humidity Injection on Proton Exchange Membrane Fuel Cell Performance ……..……..383
M. Zhiani, I. Mohammadi, M.M. Taghiabadi

Performance of Membrane-Electrode Assembly in the PEMFC under the Constant Voltage Procedure …389
Somayeh Majidi, Hussein Gharibi

Investigation of Electrochemical Impedance Spectroscopy Response of Membrane-Electrode Assembly with Time in the PEMFCs ……..393
Somayeh Majidi, Mohammad Zhiani

Analysis of Membrane-Electrode Assembly Performance with Time in the PEMFC …….397
Somayeh Majidi, Mohammad Zhiani

Exploring of the Oxygen Reduction Reaction on the Gas Diffusion Electrode for Zinc Air Fuel Cell …..…401
Parisa Akbarian, Mehdi Kheirmand

بهینه‌سازی جریان سیال درکانال‌های پیل سوختی اکسید جامد صفحه‌ای ٤٠٥
رضا خندابی، رفعت محمّدی

طیف‌سنجی الکتروشیمیایی و بررسی توان و ولتاژ پیل سوختی با غشاء خود مرطوب شونده و آند انتها بسته در زمان پرج هیدروژن .٤١٥
محمدرضا نریمانی، سعیداصغری

Fuel Cell Stack Components

8th Iranian Fuel Cell Seminar
FEBRUARY 25,26
2015

Investigation of Nanostructured Bimetallic Pt-Pd Alloy on Functionalized Carbon Supports as a New Cathode for Oxygen Reduction Reaction in Proton Exchange Membrane Fuel Cells

Fatemeh Yasi*, Hussein Gharibi, Ahmad Heydari
Department of Chemistry, Faculty of Science, Tarbiat Modares University, Tehran, Iran
** fatemeh.yasi@gmail.com*

Abstract
Carbon supported Pt-Pd alloy electrocatalysts of different Pt Pd_x atomic ratios (x = 0.25, 0.5, 1 and 2) were prepared by the impregnation synthesis method using $NaBH_4$ as a reductive agent. To improve the utilization and activity of cathodic catalysts for ORR reaction, the alloy nanoparticles were loaded on the mixture of Vulcan XC-72 and MWCNT (1:3), which were functionalized in the mixture of 96% sulfuric acid and 4-aminobenzenesulfonic acid using sodium nitrite to produce intermediate diazonium salts. For the synthesized Pt Pd_x/C electrocatalysts, the highest catalytic activity for the ORR was found for a Pt:Pd atomic ratio of 2:1 in acidic media. A membrane-electrode assembly (MEA) has been prepared by employing of the modified carbon supported catalyst as a cathode for single cell test and characterized by polarization curves and impedance diagrams. The PEMFC test results indicate that the MEA prepared from modified Pt_2Pd/C cathode exhibits better performance compared to the MEA prepared from Pt/C (Electrochem), in terms of maximum power density and minimum charge transfer resistance.

Keywords: Pt-Pd alloy electrocatalysts, Modified carbon support, Polymer electrolyte fuel cell, Membrane–electrode assembly.

Introduction

Polymer electrolyte membrane fuel cells (PEMFCs) are attractive power sources due to their safe emission, high conversion efficiency, and high energy density [1-2]. To enhance both activity and durability of PEM fuel cell catalysts, there are several approaches in literature: (1) Optimizing the size and shape of the Pt particles: reducing the particles' size alone can increase the total surface area of catalyst available to participate in reactions per volume of Pt used. (2) Alloying Pt with various transition metals to form binary or ternary catalysts. In particular, the Pt–transition metal alloys have attracted much interest due to their enhanced catalytic activities toward ORR in PEM fuel cell developments. Metallic palladium presents considerable catalytic activity for the ORR in acid electrolyte, which preferentially proceeds through a four-electron pathway. The use of Pd is of interest as it is at least 50 times more abundant than Pt on the earth and they belong to similar group in the periodic table. The enhancement of the activity for Pt in the presence of Pd originates from the (3) Developing more durable catalyst supports to overcome the issue of carbon support corrosion. Several studies have also been focused on enhancing the catalyst utilization in the PEFC electrodes by extending the so called triple-phase boundaries. Among them, sulfonation of carbon materials [3-24] and its use as a support for catalysts as mixed electronic and protonic conductors has been demonstrated to be an efficient

way to improve the structure of the triple-phase boundaries. In addition, the proton-conducting polymer stabilized surface of carbon may not only enhance the interactions between Pt nanoparticles and carbon support, but also slow down the Pt nanoparticles migration and inhibit the coalescence of Pt nanoparticles in comparison with the Pt catalysts supported on the carbon support without treatment [12].

Experimental

Surface modification of MWCNTs (p-MWCNTs)

The surfaces of commercial MWCNTs were functionalized with carboxyl functional groups. For this purpose, commercial MWCNTs and concentrated nitric acid were refluxed at 120 °C for 12 h. They were then washed well with deionized water and dried to produce a modified catalyst [22].

Anchoring phenyl-sulfonic groups to Vulcan XC-72R

In a typical experiment of synthesis of S-Vulcan XC-72R, carbon support was mixed with hot aqueous solution of p-amino phenyl sulfonic acid (Merck, Germany) to form slurry. The required amount of concentrated hydrochloric acid was added drop wise to the carbon slurry with constant stirring at 80ºC. The resulting suspension was cooled below 20ºC. Subsequently, the aqueous solution of sodium nitrite was added with stirring forming 4-sulfobenzenediazonim salts in situ that reacted with carbon support. The mixture was stirred for 30 min, filtered, washed copiously with hot distilled water to remove the unbounded residues, and then dried in an air oven at 120ºC for 2 h [9].

Functionalization of MWCNTs (f-MWCNTs)

The preparation procedure of benzenesulfonic functionalized MWCNTs consisted of dispersing p-MWNT in 96% H_2SO_4 and $(NH_4)_2S_2O_8$ with magnetic stirring (6 h). When the mixture was dispersed, the substituted 4-aminobenzenesulfonic acid was added and homogenized for 2 h in order to effectively disperse the aniline throughout the mixture. This was followed by addition of solid $NaNO_2$ and slow addition of di-tert-butylperoxide (AIBN and di-tert-butylperoxide produced similar results). The mixture was stirred at 80°C and homogenized for 6 h. The resulting product was filtered and washed with deionized water, acetone, and fresh N,N-dimethylformamide (DMF) in order to remove any impurity and then dried at 30°C for 24 h in a vacuum oven [22].

Preparation of the Pt-Pd/C electrocatalyst

Carbon-supported Pd–Pt alloys (Pd–Pt/C) with different Pd/Pt mass ratios were synthesized using sodium borohydride as a reductive agent. The preparation process is described in detail as follows: s-Vulcan XC-72 (5 w/o) + s-MWCNT (1:3) was used as the support. $Pd[NO_3]_2{\cdot}2H_2O$ and $H_2PtCl_6.6H_2O$ dissolved in deionized water were used as the precursors of Pd and Pt, respectively. The Pd/Pt mass ratios were ranged from 1:1 to 1:2, 2:1, 1:4 and the total metal loading was kept as 10 wt.%. The designed amount of support was ultrasonically dispersed in deionized water and 2-propanol. Then metal precursors ($H_2PtCl_6.6H_2O$ + $Pd[NO_3]_2{\cdot}2H_2O$) were added to the result ink in different atomic ratios of Pd to Pt under constant stirring . The mixture was heated up to 80 °C. Afterward, excessive $NaBH_4$ solution was added dropwisely to reduce these precursors. The catalysts were obtained after centrifuging, washing and drying the mixture. For comparison, 10 wt% Pt/(s-Vulcan XC-72 (5 w/o)+s-MWCNT (1:3))was prepared with the same method, too.

Results and discussion

Physical characterization

The composition of the alloy surfaces were investigated using energy dispersive X-ray (EDX) Spectroscopy. The transmission electron microscope (TEM) operated at 200 kV (Philips Model CM200) was applied for analysis of the morphology of electrocatalysts. XRD study was carried out for the catalysts by using an XPERT MPD Philips diffractometer with a Co X-ray source operating at 40 kV and 40 mA. The XRD patterns were obtained at a scanning rate of 1° min^{-1} with a step size in the 2θ scan of in the range 10–90°. The average particle size of the nanoparticles (d) was estimated from the (220) diffraction plane using Scherrer equation [25]. The lattice parameter and Pt–Pt interatomic distance were calculated from the (111) diffraction plane using Bragg equation [8]. The amount of Pt-Pd electrocatalysts coated on the support was determined by using the inductive coupled plasma (ICP) technique (ICPOES, Varian Vista-PRO, Australia). Ones dissolved 5 mg of each sample (synthesized Pt-Pd on the support) in a mixture of hydrochloric acid and nitric acid (3/1). The solutions were refluxed at 150°C and finally the percentage of Pt and Pd were determined by ICP according to the standard solution of Pt and Pd.

Electrochemical characterization

Activity of the Pt/C and Pt:Pd (1:1, 2:1, 4:1, 1:2)/C electrocatalysts were determined by cyclic voltammetry using EG&G Princeton Applied Research Model 2273 instrument. All experiments were performed at room temperature in a conventional three-electrode cell assembled with glassy carbon (GC) disk as the working electrode, Ag/AgCl, as a reference and Pt foil as the counter electrodes, respectively [26]. The amount of loading of catalyst is 0.5 mg metal cm^{-2}. The reduction of oxygen was investigated with the porous GDE (geometric exposed area of 1.3 cm^2) in 0.5 M H_2SO_4 solution. The electrochemical cell was connected to a potentiostat–galvanostat (EG&G Model 2273) for I–V polarization measurements (LSV), chronoamperometry (CA), and electrochemical impedance spectroscopy (EIS).

Catalytic activity of Pt/C and the different ratio of Pt-Pd/C bimetallic electrocatalysts

Cyclic voltammetry (CV) study

Figure 1 showed the cyclic voltammograms (CV) of Pt-Pd bimetallic nanoparticles with different ratios in the nitrogen atmosphere with scan rate of 50 mV s^{-1} between −0.25 and 1.1 V relative to an Ag/AgCl reference electrode in 0.5 M sulfuric acid. It can be seen that the Pt-Pd/C electrocatalyst produces higher currents in the hydrogen region, compared with that of Pt/C electrocatalyst. The calculations showed that the Pt-Pd/C electrocatalyst has higher EAS in relative to Pt/C electrocatalyst. So, with increasing of available active surface area, catalytic activity of electrocatalyst towards ORR has been raised. In spite of larger particle size of Pt-Pd/C electrocatalyst, these samples have higher EAS whereas generally, it occurs conversely. This matter can be related to synergetic effect, which is playing a critical role in hydrogen adsorption/desorption reaction and is not only dependent to particle size parameter. The synergetic effect of the simultaneous presence of Pd and Pt in the electocatalyst can be explained by the spill-over effect of hydrogen and oxygen from Pt surface to Pd and resultant freedom for Pt active sites. Other electrochemical results confirm the better electrocatalytic performance of Pt-Pd/C electrocatalyst, too. The influence of the surface composition on hydrogen adsorption capacity of the alloys is shown in Table 1.

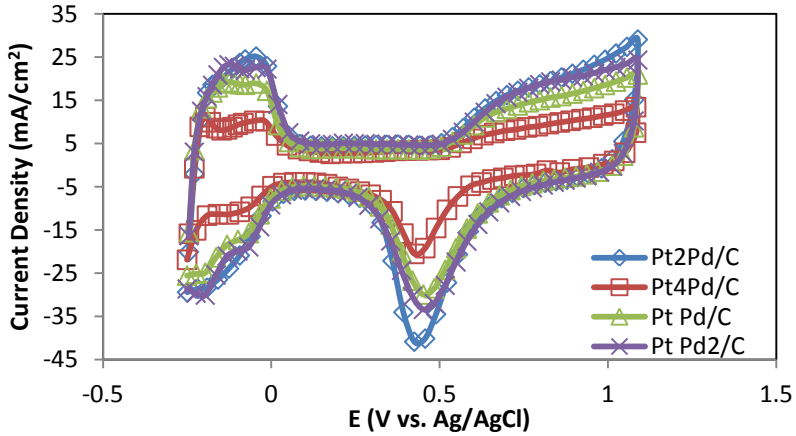

Figure 1. Cyclic voltammograms of electrodes in 0.5 M H_2SO_4 under an argon atmosphere at 298 K and at a scan rate of 50 mV/s in the potential range from -0.25 to 1.1 V vs. Ag/AgCl.

Table 1. Structural and electrochemical characteristics of the carbon supported Pd and the PdxCo bimetallic electrocatalysts with different atomic ratios.

Catalyst	EDX analysis of Pt-Pd	2θ (220)(◦)	Lattice parameter (nm)	Particle size (nm)	Electrochemical area (m^2g^{-1}metal)	ECSA (m^2/g Pt)
Pt Pd/C	1:1.099	80.19	0.39232	6.39	26.43	152.72
Pt_1 Pd_2/C	1:2.185	80.64	0.39128	6.03	16.93	127.44
Pt_2Pd_1/C	1:0.46	80.43	0.39245	5.64	48.70	188.27
Pt_4Pd/C	1:0.225	80.33	0.39217	11.99	29.77	127.58
Pt/C Electrochem	-	79.48	0.39602	5.24	53.5	35.84

Linear sweep voltammetry

Figure 2 depicts the polarization curves for electrocatalysts, in a conventional three electrode cell. Polarization curves were produced at a scan rate of 5 mVs^{-1} between 1 and −0.3V relative to the Ag/AgCl in oxygen saturated in 0.5 M H_2SO_4 solution. In order to obtain information about the kinetic parameters of oxygen reduction reaction in the fabricated GDEs, a Tafel plot was drawn and its data were fitted by the following equations:

$$\eta = \frac{2.303RT}{\alpha nF \log\left({}^{i}/_{i_0}\right)}$$

where η = (E−E_0) is the over potential, R is gas constant, T is the absolute temperature, α is the transfer coefficient, i_0 is exchange current density, i is current density, n is the number of electrons, and F is Faraday's constant. The results showed that the ORR current density in Pt-Pd/C GDEs is higher than in Pt/C GDE, which indicated that the GDEs containing Pt-Pd/C has a much better performance which has been caused by weakening of the O-O bond on Pd-modified Pt nanoparticles, synergic effect between Pt and Pd nanoparticles, and uniform dispersion of Pd and Pt on the carbon support. The kinetic parameters have been obtained in Table 2. The lower Tafel slope and higher exchange current density in Pt-Pd/C GDE can be attributed to an enhanced electrocatalytic activity of Pt-Pd/C electrocatalyst in relative to Pt/C electrocatalyst. Comparison of the GDEs with different compositions of Pt and Pd in the catalyst layer, showed that GDE with 2:1 ratio of Pt–Pd presented smaller Tafel slope and higher exchange current density. Based on this result, the Pt_2Pd/C catalyst favors the reduction of OH at the surface compared with other catalysts, allowing a weaker interaction of OH with the surface compared with other catalysts. This result is in good agreement with other results.

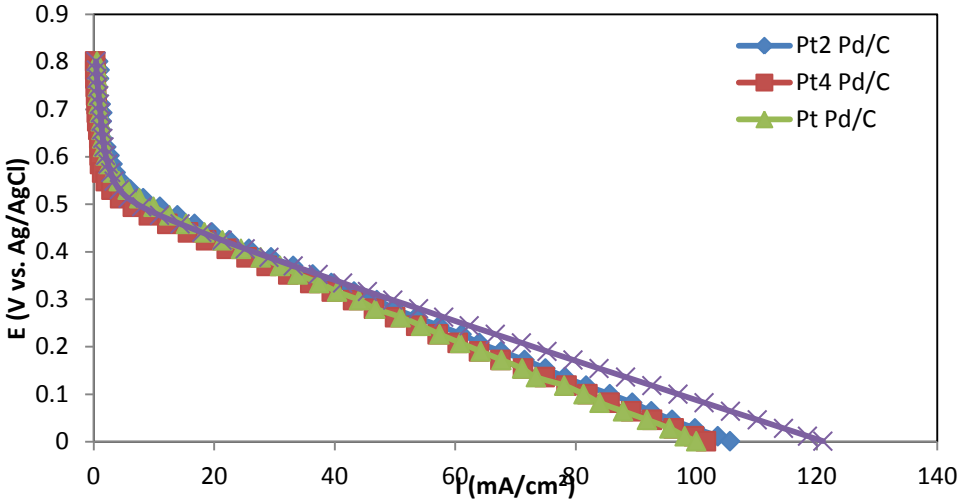

Figure 2. I–V curves at 25°C for the electrodes with Pt loading of 0.5 mg/cm^2 in 0.5 mol L^{-1} H_2SO_4 solution at a scan rate of 1 mVs^{-1}.

Table 2. Parameters obtained from EIS diagrams with the equivalent circuit shown in Figure 4 using nonlinear least-squares fitting (Zview, ver. 2.0), Kinetic parameters, and permeability values for ORRs in 0.5 M H_2SO_4 at 298 K, under an oxygen atmosphere.

Catalyst	R at 0.3V	R at 0.5V	i_0	Tafel slope (mV dec^{-1})	$D_b^{0.5}C_b$
Pt Pd/C	0.97	3.14	1.35*10^{-4}	86.75	1.10*10^{-4}
Pt_1 Pd_2/C	0.79	3.97	5.53*10^{-5}	98.03	1.08*10^{-4}
Pt_2Pd/C	0.91	3.00	1.68*10^{-4}	69.72	1.16*10^{-4}
Pt_4Pd/C	1.10	3.71	1.33*10^{-5}	106.34	1.07*10^{-4}
Pt/C Electrochem	3.38	4.00	1.55*10^{-5}	110.55	4.47*10^{-6}

Chronoamperometry

The oxygen diffusion coefficients from electrodes were determined by chronoamperometry. Chronoamperograms were obtained by holding the potential of the electrode at 1.2 V for 60 s and then holding it at 0.2 V relative to the Ag/AgCl electrode for 10 s with oxygen flowing along the back of the electrode. Figure 3 shows the chronoamperograms of GDEs at 0.2 V in relative to the Ag/AgCl in oxygen saturated in 0.5 M H_2SO_4 solution. The results confirmed that the permeability of oxygen in the Pt-Pd/C alloy electrocatalysts is slightly higher than that of the Pt/C electrocatalyst, suggesting that the permeability of O_2 on the alloy surface is more favored than that on pure Pt surface, and this is in agreement with the results of ECSA. The highest Cottrell slope and D is found with a Pt:Pd atomic ratio of 2:1. Cottrell parameters are listed in Table 2.

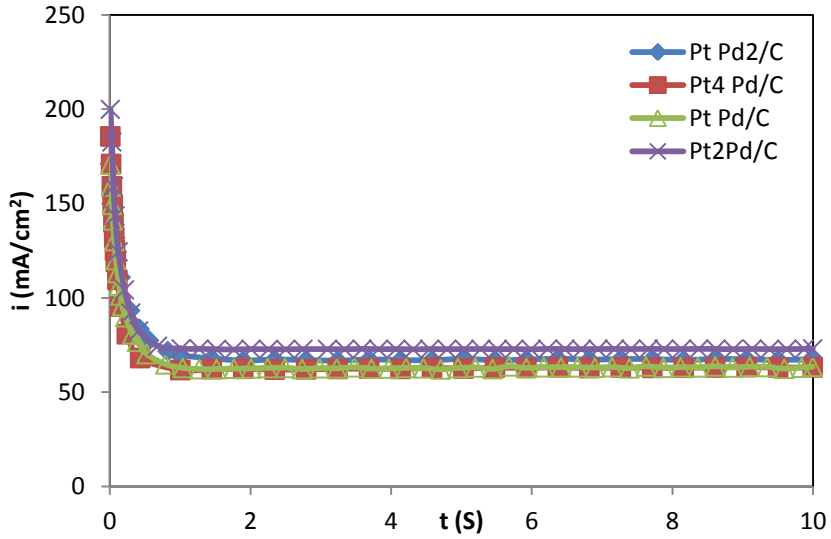

Figure 3. Chronoamperograms of various electrodes with Pt loading of 0.5 mg/cm^2 in the presence of O_2, at 0.2 V potential vs. Ag/AgCl, at 25°C.

Impedance spectroscopy

The Nyquist plots of the different electrodes were obtained as be shown in Figure 4. Impedance spectra were collected for frequencies between 100 kHz and 50 mHz, in oxygen saturated 0.5 M H_2SO_4 solution at 25°C and 0.3 V relative to the Ag/AgCl. An AC potential of 5 mV was superimposed on the DC potential. The low frequency impedance is corresponded to the kinetic impedance of the ORR and it becomes smaller as the cathode over potential decreases, whereas the high-frequency is independent of the over potential, which indicates the impedance dependency to an Ohmic process. As can be seen, Pt_2Pd/C GDE has minimum electronic resistance and slightly better performance towards ORR in relative to other GDEs. Impedance spectroscopy was used to characterize the ionic resistance. The corresponding data are shown in Table 2. These data show that the ionic resistance in GDE containing Pt-Pd/C is smaller than in the GDE with Pt/C Electrochem, confirming the previous outcomes about the dual role of support as both electronic and protonic conductors.

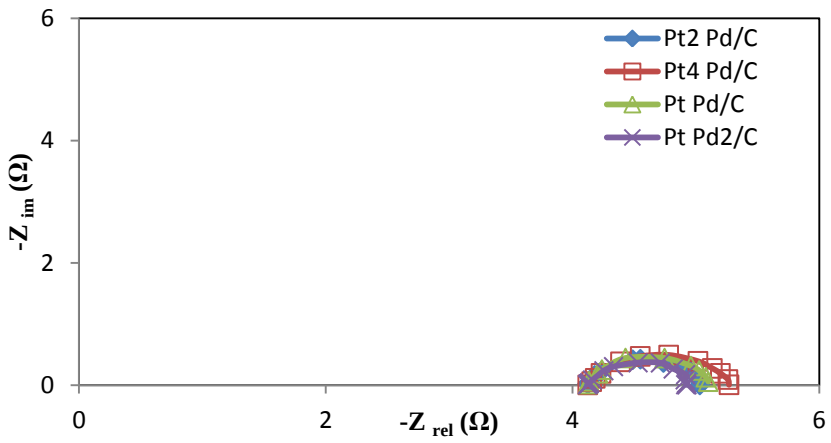

(b)

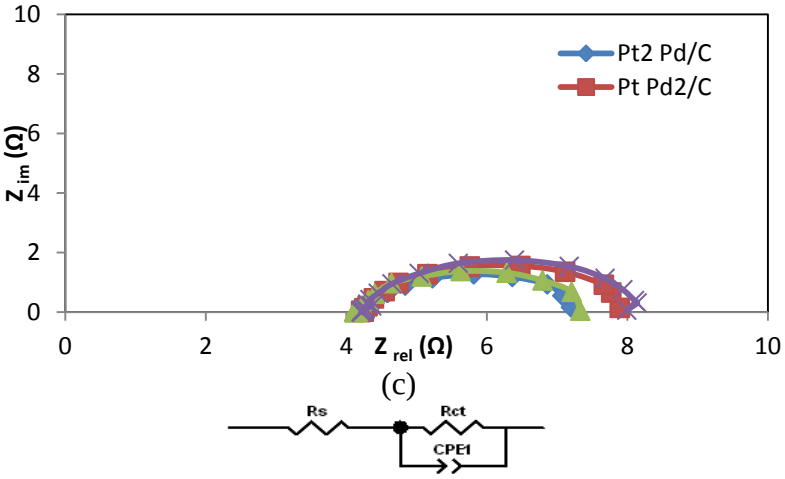

Figure 4. Nyquist plots of the impedance response from 100 KHz to 50 mHz for gas diffusion electrodes, a) 0.3 V and (b) 0.5 V vs. Ag/AgCl

under an oxygen-saturated atmosphere. Schematic representation of the equivalent circuit for the different electrodes, where R_s : electrolyte resistance (subtracted from results), R_{ct} : charge transfer resistance, and CPE: constant-phase element.

Physical characterization of Pt-Pd/C bimetallic electrocatalysts

Powder X-ray diffraction (XRD) analysis was conducted to confirm the crystalline structures of the Pt–Pd/C catalysts and commercial Pt/C with the X-ray diffractometer (X´PERT MPD Philips diffractometer) using Co target (λ=1.7902 A°) excited at 40kV and 40 mA. The XRD patterns were recorded over a 2θ range of 10–90°. Figure 5 represents a typical powder X-ray diffraction (XRD) pattern obtained for the commercial catalyst and those prepared in the laboratory. The peak located at around 24° in all patterns arises from the (002) hexagonal phase of carbon support. The other four peaks are the characteristic peaks of the face centered cubic (FCC) crystalline structure of platinum. The peaks correspond to the planes (111), (200) and (220) at 2θ of around 46°, 54° and 80° respectively. These XRD patterns reveal that our catalysts are single-phase solid solutions. Compared with the plane (111) of commercial Pt/C, the diffraction peaks of catalysts are shifted to higher angles, which indicate that the addition of Pd to Pt leads to a decrease in the lattice parameters of Pt.Pd alloy nanoparticles due to contraction of the unit cells. The average crystallite size and the lattice parameters were evaluated by Scherrer formula and Bragg's equation [21,22], respectively. For this purpose, the (220) reflection of the Pt face centered cubic (fcc) structure around 2θ ≈ 80° was used. The average particle sizes are provided in Table 1. It is noteworthy that the crystallite size, calculated from XRD data, is related to the area of coherent diffraction and, in general, can be smaller than the true particle size. Surface area of the catalysts was calculated using the equation, $S = 6000/\rho d$ where ρ (ρ_{Pd} = 12.0 g cm^{-3}, ρ_{Pt} = 21.4 g cm^{-3}, $\rho_{alloy} = W_{Pd}\% \times \rho_{Pd} + W_{Co}\% \times \rho_{Pt}$, where W% means weight percent) is the metal density, d is the particle size (in nm) with S given in m^2 g^{-1}. The obtained results are given in Table 1. The morphology of electrocatalyst was observed using transmission electron microscopy (TEM. Philips model EM280). Specimens for TEM observation were prepared by placing a drop of the particle-dispersed solution onto a copper grid. TEM images of the synthesized catalyst are shown in Figure 6. As the figure shows, the metal clusters are well dispersed on the carbon support.

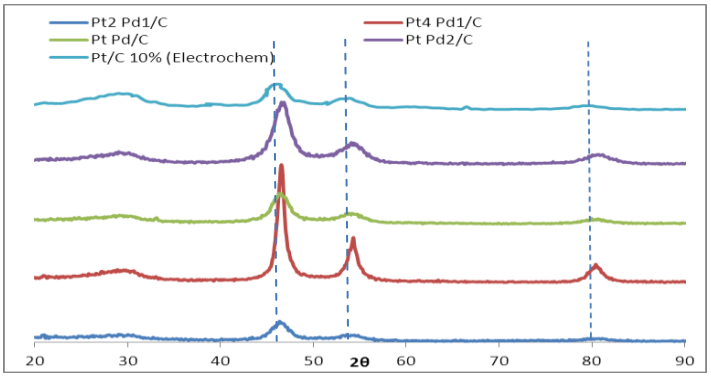

Figure 5. XRD patterns of the Pt/C and the Pt-Pd (x = 0.25, 0.5, 1 and 2)/C bimetallic electrocatalysts with different atomic ratios.

(a)

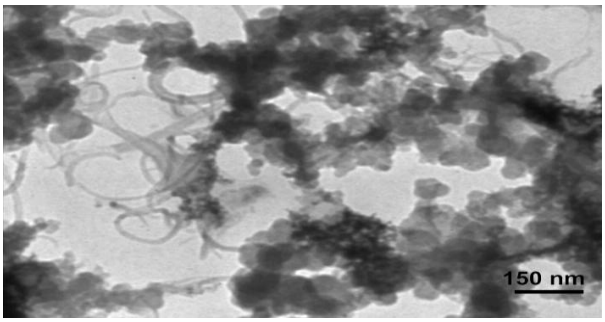

(b)

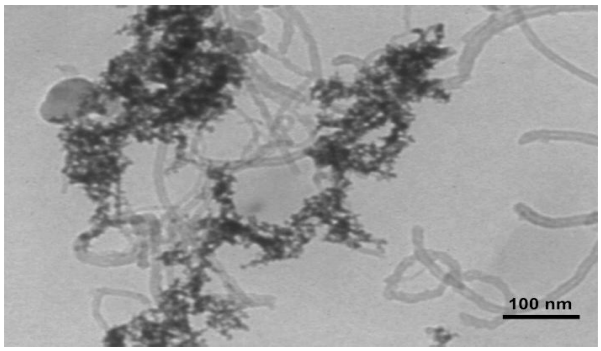

(c)

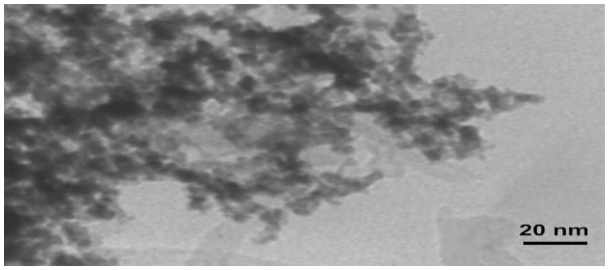

Figure 6. (a)-(c).TEM images of Pt_2Pd/C electrocatalyst.

Conclusion

It was proposed that, anchoring the phenyl-sulfonic group on the carbon support of the platinum catalyst enhanced the performance of the PEFC. The combination of modified supports (i.e.; 75% f-MWCNT + 25% f-Vulcan XC-72 (5%) was determined to be the optimum mixture. The electrochemical properties of Pt-based binary alloy catalysts supported on modified support, have been investigated in acidic media in the present research. Comparison of GDEs with different Pd/Pt mass ratios showed that Pt_2 Pd/C electrocatalyst presented the smallest Tafel slope value in acidic electrolytes. This comparison indicates that the amount of transition metals in the catalyst may be one of the factors effective in determining the performance of the GDEs. Chronoamperometry showed that Pt_2 Pd/C electrocatalyst presented the highest permittivity value. These results suggest a change in crystallographic structure of the alloy electrocatalysts with respect to Pt.

References

1. Chortip Termpornvithit, N.C.a.M.H., Stability of Pt–Co/C and Pt–Pd/C based oxygen reduction reaction electrocatalysts prepared at a low temperature by a combined impregnation and seeding process in PEM fuel cells. journal of applied electrochemistry, 2012. **42**: p. 169-178.
2. Chang, S.-H., et al., Structural and Electronic Effects of Carbon-Supported PtxPd1−x Nanoparticles on the Electrocatalytic Activity of the Oxygen-Reduction Reaction and on Methanol Tolerance. Chemistry – A European Journal, 2010. **16**(36): p. 11064-11071.
3. Mazumder, V., Y. Lee, and S. Sun, Recent Development of Active Nanoparticle Catalysts for Fuel Cell Reactions. Advanced Functional Materials, 2010. **20**(8): p. 1224-1231.
4. Madhu Sudan Saha, V.N., Dave Ghosh and Jiujun Zhang, Nanomaterials-supported Pt catalysts for proton exchange membrane fuel cells. WIREs Energy Environ 2013. **2**: p. 31-51.
5. Zignani, S.C., E. Antolini, and E.R. Gonzalez, Evaluation of the stability and durability of Pt and Pt–Co/C catalysts for polymer electrolyte membrane fuel cells. Journal of Power Sources, 2008. **182**(1): p. 83-90.
6. Takako Toda, H.I., Hiroyuki Uchida, and Masahiro Watanabe, Enhancement of the Electroreduction of Oxygen on Pt Alloys with Fe, Ni, and Co. Journal of The Electrochemical Society, 1999. **146**(10): p. 3750-3756.
7. Maghsodi, A., et al., Exploration of bimetallic Pt-Pd/C nanoparticles as an electrocatalyst for oxygen reduction reaction. Applied Surface Science, 2011. **257**(15): p. 6353-6357.
8. Carmo, M., et al., Enhanced activity observed for sulfuric acid and chlorosulfuric acid functionalized carbon black as PtRu and PtSn electrocatalyst support for DMFC and DEFC applications. International Journal of Hydrogen Energy, 2011. **36**(22): p. 14659-14667.
9. Kim, H., W. Lee, and D. Yoo, Functionalized carbon support with sulfonated polymer for direct methanol fuel cells. Electrochimica Acta, 2007. **52**(7): p. 2620-2624.
10. choi, Y., et al., A composite electrolyte membrane containing high-content sulfonated carbon spheres for proton exchange membrane fuel cells. Carbon, 2011. **49**(4): p. 1367-1373.
11. Carmo, M., et al., A novel electrocatalyst support with proton conductive properties for polymer electrolyte membrane fuel cell applications. Journal of Power Sources, 2009. **191**(2): p. 330-337.

12. Cheng, N., et al., Enhanced life of proton exchange membrane fuel cell catalysts using perfluorosulfonic acid stabilized carbon support. Electrochimica Acta, 2011. **56**(5): p. 2154-2159.
13. Du, C.Y., T.S. Zhao, and Z.X. Liang, Sulfonation of carbon-nanotube supported platinum catalysts for polymer electrolyte fuel cells. Journal of Power Sources, 2008. **176**(1): p. 9-15.
14. Hung, T.F., et al., Effect of sulfonated carbon nanofiber-supported Pt on performance of Nafion®-based self-humidifying composite membrane for proton exchange membrane fuel cell. Journal of Power Sources, 2011. **196**(1): p. 126-132.
15. Hung, T.-F., et al., Sulfonation of graphene nanosheet-supported platinum via a simple thermal-treatment toward its oxygen reduction activity in acid medium. International Journal of Hydrogen Energy, 2012. **37**(19): p. 14205-14210.
16. Pak, C., et al., Direct sulfonation of ordered mesoporous carbon for catalyst support of direct methanol fuel cell, in Studies in Surface Science and Catalysis, S.Q.Y.T. Dongyuan Zhao and Y. Chengzhong, Editors. 2007, Elsevier. p. 401-404.
17. Selvarani, G., et al., A phenyl-sulfonic acid anchored carbon-supported platinum catalyst for polymer electrolyte fuel cell electrodes. Electrochimica Acta, 2007. **52**(15): p. 4871-4877.
18. Sun, Z.-P., et al., A facile approach towards sulfonate functionalization of multi-walled carbon nanotubes as Pd catalyst support for ethylene glycol electro-oxidation. Journal of Power Sources, 2009. **191**(2): p. 366-370.
19. Sun, Z.-P., et al., A simple approach towards sulfonated multi-walled carbon nanotubes supported by Pd catalysts for methanol electro-oxidation. Journal of Power Sources, 2008. **185**(2): p. 801-806.
20. Sun, Z.-P., et al., Sulfonation of ordered mesoporous carbon supported Pd catalysts for formic acid electrooxidation. Journal of Colloid and Interface Science, 2009. **337**(2): p. 614-618.
21. Tominaka, S., et al., Ionic conductivity improvement in primary pores of fuel cell catalyst layers: Electropolymerization of m-aminobenzenesulfonic acid and its effect on the performance. Journal of Power Sources, 2009. **192**(2): p. 316-323.
22. Yang, S., et al., Pd nanoparticles supported on functionalized multi-walled carbon nanotubes (MWCNTs) and electrooxidation for formic acid. Journal of Power Sources, 2008. **175**(1): p. 26-32.
23. Zhiqiang Xu, Z.Q., and Arthur Kaufmanb, Superior Catalysts for Proton Exchange Membrane Fuel Cells Sulfonation of Carbon-Supported Catalysts Using Sulfate Salts. Electrochemical and Solid-State Letters, 2005. **8**(6): p. A313-A315.
24. Golikand, A., et al., Enhancement of electrocatalytic O2 reduction on carbon nanotube-supported Pt alloys nanoparticles in gas diffusion electrodes. Journal of Applied Electrochemistry, 2009. **39**(9): p. 1443-1449.
25. Golikand, A.N., M. Asgari, and E. Lohrasbi, Study of oxygen reduction reaction kinetics on multi-walled carbon nano-tubes supported Pt–Pd catalysts under various conditions. International Journal of Hydrogen Energy, 2011. **36**(20): p. 13317-13324.

8th Iranian Fuel Cell Seminar
FEBRUARY 25,26
2015

Preparation of Cu/Pt Bimetallic Nanocomposite on the MOF-199 Derived Nanoporous Carbon and its Application for Hydrogen Evolution Reaction

Sakineh Mandegarzad[1], Jahan-Bakhsh Raoof[1]*, Sayed Reza Hosseini[2], Reza Ojani[1]
1 Department of Analytical Chemistry, Faculty of Chemistry, University of Mazandaran, Postal Code: 47416-95447, Babolsar, Iran
2. Nanochemistry Research Laboratory, Faculty of Chemistry, University of Mazandaran, Postal Code: 47416-95447, Babolsar, Iran
** j.raoof@umz.ac.ir*

Abstract
This work is allocated to the preparation of Cu/Pt bimetallic nanocomposite onto glassy carbon electrode modified with MOF-199 derived nanoporous carbon structure (MDNPC), through spontaneous and irreversible reaction via galvanic replacement between $[PtCl_6]^{-2}$ions and Cu particles that it is presented in synthesized nanoporous.The nanoporous carbon is synthesized by direct carbonization of MOF-199 metal organic framework in N_2 atmosphere. The physical characterizations of the solid catalyst were achieved by using X-ray powder diffraction, Energy dispersive X-ray spectroscopy,scanning electron microscopy and nitrogen physisorption measurements. The comparison of the EDX analysis of the electrode surface before and after dipping onto platinum solution confirmed that galvanic replacement is occurred.This behavior can be associated to existence of copper and has been confirmed by XRD pattern, in MDNPC modifier.The electrochemical results have shown that Cu/Pt bimetallic GCE exhibited high current densities and positive potentialin hydrogen evolution reaction.This is attributed to synergetic effect of bimetallic and uniform distribution of the nanoparticle onto modified electrode surface duo to high surface area of nanoporous carbon.

Keywords: MOF-derived nanoporous carbon, MOF-199, Cu/Pt bimetallic nanoparticles, Galvanic replacement, Hydrogen evolution reaction.

Introduction

Growing concerns about global warming and energy securityhave necessitated the realization of renewable sources as a viablealternative to fossil-fuel-based technologies. Because hydrogen isthe cleanest energy source and an ideal energy carrier, several researchers have focused on its production methods [1]. The ideal properties of an electrode used for water electrolysisare (i) large surface area, (ii) good electrical conductivity, (iii) goodstability, (iv) low over-potential, (v) low cost and (vi) ease offabrication [2].Platinum has a high catalytic activity for HER, its limited reserves in the earth and high cost restricts its wide application in industry. Therefore, many efforts are made to find the other materials for HER to replace or reduce the use of Pt [3,4]. Nanoporous carbon (NPC) materials with high surface areas, pore size distribution and high pore volume have attracted attention for use as a template for preparation of electrocatalyst. Another group of nanoporous templates that can used to prepare of carbon nanopore are metal organic frameworks (MOFs) [5, 6]. Liu and coworkers [7] for the first time used porous MOFs for the synthesis of nano carbon materials and checked their hydrogen storage capability as well

as the electrochemical capacitance.Here, we have used $Cu_3(BTC)_2$ as a template to fabricate highly porous carbon by direct carbonizing highly crystalline MOF without any carbon precursors at 900 °C.Nanoporous carbon (NPC) is dispersed in ethanol then it is dropped on the glassy carbon electrode. Galvanic replacement reaction (GRR) is a type of single-stepreaction that utilizes the differences between the standard electrode potentials of various elements, resulting in the deposition ofnobler elements and the dissolution of lesser noble components[8]. Usually, it only requires a beaker and consumes almost zero energy. The electroless nature of GRR affords them the unique andsignificant advantage of simplicity. Recently, it was employed to fabricate several electrocatalysts for various reactions. However, noble metals have been primarily investigated, such as Pt, Pd, Au, and Ag [9-12]. Only a few studies involving catalysts prepared forthe HER have been undertaken. In our study, galvanic replacement between $[PtCl_6]^{-2}$ions and the Cu nanoparticles is occurred and Cu/Pt bimetallic nanocomposite is synthesized through simply dipping of modified electrode in platinum salt solution. The modified glassy carbon electrode was use as electro-catalysis in hydrogen evolution reaction.The result showed that the nanocomposite have a positive effect on the reduction of hydrogen in the acidic media.

2. Experimental

2.1. Materials

Benzenetricarboxylic acid (BTC, 95%) and Hexachloroplatinate (H_2PtCl_6) were acquired from Aldrich and Merck, respectively. the copper nitrate ($Cu(NO_3)_2.3H_2O$, 99.99%) and EtOH as solvent were supplied by Fluka. All reagents were of analytical grade and used without any further purification. Solutions were made with twice distilled water.

2.2. Synthesis of MOF-Derived NanoPorous Carbon (MDNPC)

MOF-199 was prepared by using a hydrothermal method [13]. In the typical synthesis, $Cu(NO_3)_2{\cdot}3H_2O$ (2.327 g) and Benzene-1,3,5-tricarboxylic acid (H_3BTC) (1.414 g) in a 50 mL of solvent consisting of equal parts of ethanol and deionized water and mixed thoroughly until it was completely dissolved. The resultant solution mixture was transferred into a 250 mL teflon-lined stainless steel autoclave. It was kept at 423 K in an isothermal oven for 15 h, yielding light blue crystals. The solid product was filtered and washed by ethanol and water. The MDNPC catalyst was prepared by direct carbonization of the MOF-199 during followed producer as similar to the previous reported [6]. In the typical synthesis, dried MOF-199 was transferred to a ceramic boat in a quartz tube which is fixed in a tube furnace. Air was evacuated by continuous flow of N_2 for 30 min, and temperature of the furnace was raised to 550 °C to decompose the polymeric structure of MOF-199. Further carbonization was performed at 900 °C under N_2 atmosphere for 6 h. The Carbon product was denoted as MDNPC.

2.3.Preparation of modified electrode with Cu/Pt bimetallic nanocomposite

To prepare of working electrode, 1.5 mg of the as-prepared catalyst was suspended in 1 mL of analytical grade ethanol by ultrasonic bath for 15 min. Then, 7 µL of this mixture (without adding any binder and conductive agents) were deposited onto glassy carbon electrode (GCE, 2 mm diameter), which was previously polished with alumina powder (0.3 µm) and cleaned in the pure ethanol sonicately and washed with distillated water.

The modified GC electrode was dipped in H_2PtCl_6 (5.0 mM) for 15 min which is optimum time was achieved voltammetry investigation. This electrode is named Cu/Pt bimetallic/MGCE. In order to investigate the modifier effect on catalysis of HER, bare glassy carbon was dipped in the same solutionand it is named as Pt/GCE.

2.3. Characterization

X-ray powder diffraction patterns were recorded on a Philips 1830 diffractometer using Cu-Kα radiation source, 0.05 step size and 1s step over the range of $4^\circ < 2\theta < 90^\circ$. Surface morphology and percent composition (EDS analysis) of catalyst was examined using a scanning electron

microscope (Philips XL-30) having an energy-dispersive X-ray (EDX) machine attached. The samples were coated with gold in order to increase their conductivity before scanning.

3. Result and discussion

Characterization of (Fig. 1a) exhibits the XRD pattern for MOF-199. The main diffraction peaks at 2θ = 9.4°, 11.62°, 17.4°, 19°, 29.3° and relative diffraction intensities of MOF-199 were found to be the same as previous report [14]. After direct carbonization of this template, as shown in (Fig. 1b), the XRD pattern represents all the main peaks which are attributed to the copper metal, CuO, and Cu_2O with 85.67%, 10.70%, and 23.87% relative intensities, respectively, deriving from the decomposition of the MOF-199 template. Carbon signals with a weak intensity cannot be observed rather than copper signals.

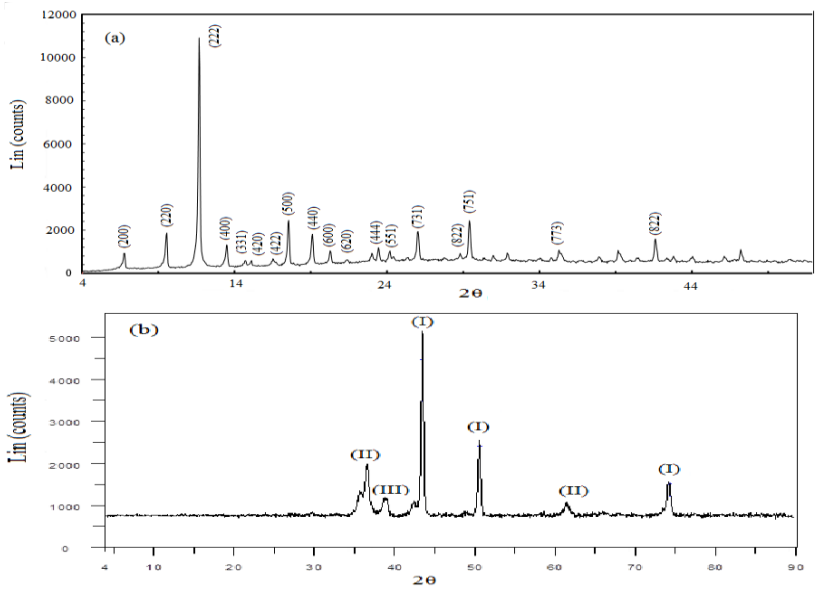

Figure 1.XRD pattern of (a) MOF-199, (b) MDNPC. In the Fig 1b, (I), (II), and (III) indicate the peak position of Cu metal, Cu_2O and CuO, respectively.

The SEM image of bare GCE, MDNPC/GCE, Pt/GCE and Cu/Pt bimetallic/GCE were shown in figure 2. In figure 2A, any particle was not observed in the bare GCE. This is an evidence of the clean surface of BGCE. AS shown in figure 2B, it is confirmed a small amount of platinum is adsorbed on the surface of bare GCE. But as shown in figure 2C, the spherical nanoparticles was observed that was assembled in cauliflower-like structure. In the figure 2D, the Pt nanoparticle is located on the surface of MDNPC. It is suggested that the high external surface area of catalyst was achieved duo to decreasing of particle size in the MDNPC and its catalytic activity was increased.

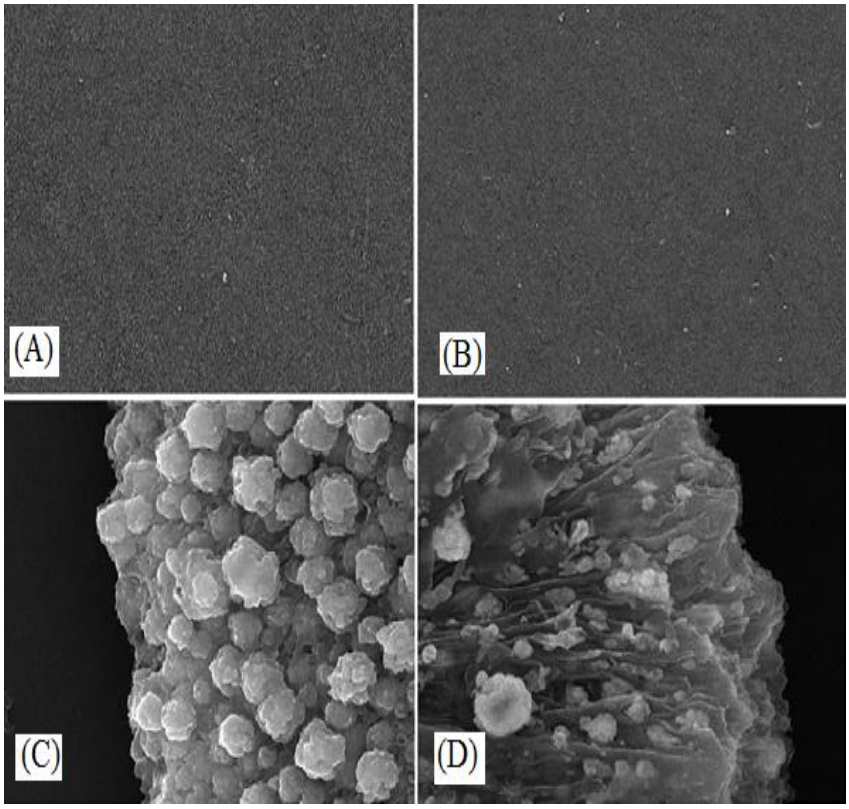

Figure2. SEM images of (A) bare GCE, (B) Pt/GCE, (C) MDNPC/GCE and (D) Cu/Pt bimetallic/GCE.

The EDS experiment for elemental analysis was performed for the three prepared electrode (Figure 3). The EDS gives evidences for the presence of Pt and Cu in the nanocomposite. The obtained results also confirm that the galvanic replacement method is occurred on the modified electrode.

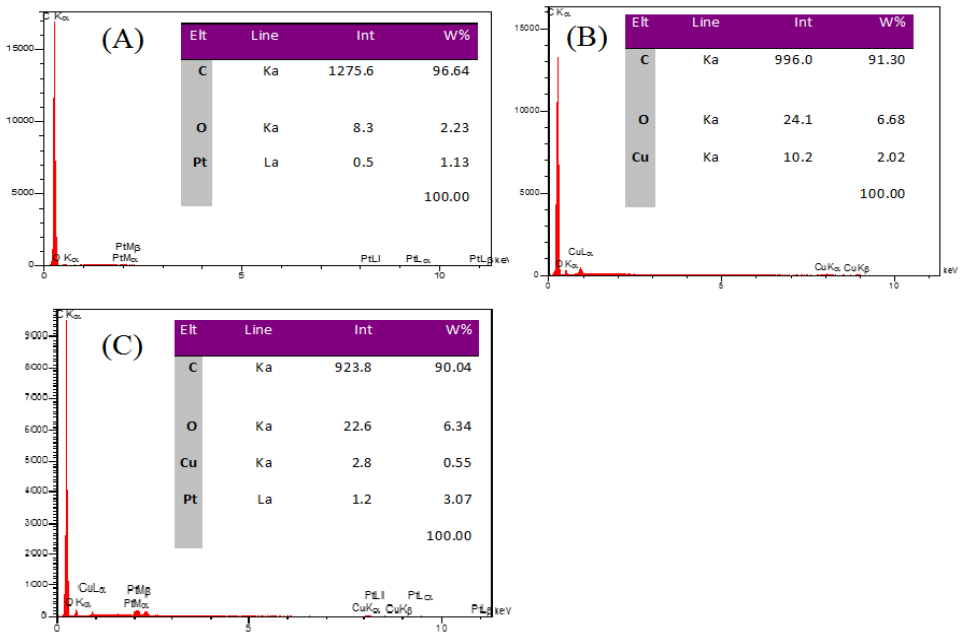

Figure 3**.** EDS spectra for (A) Pt/GCE, (B) MDNPC/GCE and (C) Cu/Pt bimetallic/GCE.

The electrocatalytic activity of the as-fabricated electrode for HER was investigated by LSV technique over the potential range from 0 to -0.7 (V vs Ag | AgCl | KCl (3M)), and results were shown in Figure 4. A comparison of the LSV of HER in 0.5 M H_2SO_4 demonstrates that current at potential of -0.7 V for bare GCE, MDNPC/GCE, Pt/GCE and Cu/Pt bimetallic/GCE are about -30, -74, -253 and -422 µA, respectively. The best performance is related to the Cu/Pt bimetallic /GCE. As can be seen, the slope of current -potential plot for the Cu/Pt bimetallic/GCE is steeper than Pt/GCE and the overpotential of Cu/Pt bimetallic /GC Eat i= -0.7µA is about 20 mV lower than that of Pt/GCE. Furthermore, possessing high surface area and synergism effect of Cu/Pt bimetallic/GCE may be improved HER catalysis in the more positive onset potential and higher current rather than bare Pt/GCE.

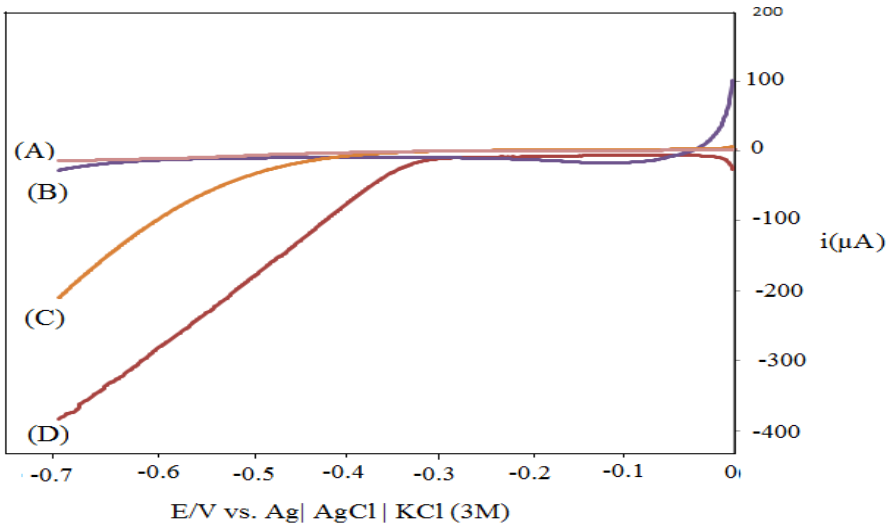

Figure 4. Linear sweep voltammetry of HER on (A) bare GCE, (B) MDNPC/GCE and (C) Pt/GCE and (D) Cu/Pt bimetallic/GCE in 0.5 M H_2SO_4 solution at scan rate 50 mV s^{-1}.

3.1.Parameters affecting the electrode modification

In order to evaluate the effects of various parameters such as H_2PtCl_6 concentration, and replacement time (t_r) on HER, the cathodic peak current at potential of -0.7(V vs Ag | AgCl | KCl (3M)) was monitored as an index for finding an optimum conditions. Results were shown in Figure5 and 6. The data indicate that the peak current increases extensively for H_2PtCl_6 up to 4.0 mM and t_r up to 15 min.

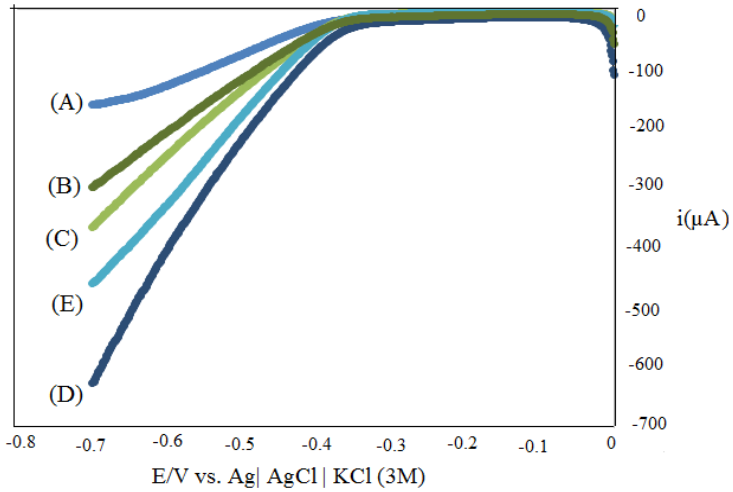

Figure 5. Linear sweep voltammograms of the HER on the Cu/Pt bimetallic/GCE at scan rate 50 mV s^{-1} for various H_2PtCl_6 concentrations: (A) 1, (B) 2, (C) 3, (D) 4 and (E) 5 mM.

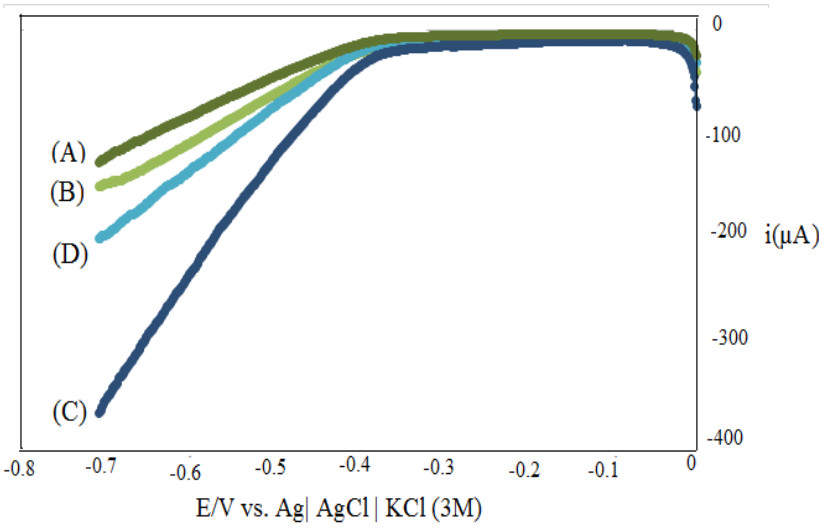

Figure 6. linear sweep voltammograms of the HER on the Cu/Pt bimetallic/GCE at scan rate 50 mV s-1 for various time replacement: (A) 5, (B) 10, (C) 15, and (D) 20min.

Conclusion

In summary, the Cu/Pt bimetallic nanocomposite was synthesized onto modified glassy carbon electrode with MOF-199 derived nanoporous carbon structure (MDNPC), through spontaneous and irreversible reaction via galvanic replacement. Electrochemical measurements of Cu/Pt bimetallic /GCE indicate improvement of HER catalysis in the more positive onset potential and higher current rather than Pt/BGCE. This enhancement is attributed to the synergism effect of bimetallic nanocomposite and high surface area of MDNPC. It is suggested that MOF-199 was probably converted to a nanoporous carbon which was deposited copper metal on the surface that it is replacement with Pt nanoparticle during a simple galvanic reaction.

Reference

1. Z. Yin, F. Chen "A facile electrochemical fabrication of hierarchically structurednickelecopper composite electrodes on nickel foam for hydrogen evolution reaction", Journal of Power Sources, (2014). 265, 273-281

2. Y. G. Li, H. L. Wang, L. M. Xie "MoS_2 Nanoparticles Grown on Graphene: An Advanced Catalyst for the Hydrogen Evolution Reaction", Journal of the American Chemical Society, (2011). 133, 7296-7299

3. R. Ojani, Z. Abkar, E. Hasheminejad, J. B. Raoof "Rapid fabrication of Cu/Pdnano/micro-particlesporous-structured catalyst using hydrogen bubbles dynamic template and their enhanced catalytic performance for formic acid electrooxidation", International Journal of Hydrogen Energy, (2014). 39, 7788-7797

4. C. Xu, Y. Liu, J. Wang,H.Geng,H.Qiu. "Nanoporous PdCualloyfor formic acid electro-oxidation". Journal of Power Sources,(2012).199, 124-131

5. I. Ali Khan, A. Badshah, N. Haider, S. Ullah, D. H. Anjum, M.A.Nadeem"Porous carbon as electrode material in direct ethanol fuel cells (DEFCs) synthesized by the direct carbonization of MOF-5", Journal of Solid State Electrochemistry, (2014).18, 1545-1555.

6. S. J. Yang, T. Kim, J. H. Im, Y.S. Kim, K. Lee, H. Jung,C. R. Park "MOF-Derived Hierarchically Porous Carbon with Exceptional Porosity and Hydrogen Storage Capacity", Chemistry of Materials,(2012). 24, 464−470.

7. B. Liu, H. Shioyama, T. Akita, Q. Xu "Metal-Organic Framework as a Template for Porous Carbon Synthesis", Journal of the American Chemical Society, (2008). 130, 5390–5402.

8. N. M.Sánchez-Padilla, S. M.Montemayor, L. A. Torres, F. J. Rodríguez Varela "Fast synthesis and electrocatalytic activity of M@Pt (M = Ru, Fe_3O_4, Pd) core-shell nanostructures for the oxidation of ethanol and methanol", International Journal of Hydrogen Energy, (2013). 38, 12681-12688.

9. B. Habibi, M. H. Pournaghi-Azar, "Methanol oxidation on the polymer coated and polymer-stabilized Pt nano-particles: A comparative study of permeability and catalyst particle distribution ability of the PANI and its derivatives", International Journal of Hydrogen Energy, (2010). 35, 9318-9328.

10. H.Razmi, E. Habibi "Electrocatalytic oxidation of methanol on carbon ceramic electrode modified by platinum nanoparticles incorporated in poly (*o*-phenylenediamine) film", Journal of Solid State Electrochemistry, (2009). 13,1897-1904.

11. G.P. Jin, X. Peng, Y.F. Ding, W.Q. Liu, J. M. Ye "Electrodeposition of platinum-nickel alloy nanocomposites on polyaniline-multi walled carbon nanotubes for carbon monoxide redox", Journal of Solid State Electrochemistry, (2009). 13, 967-973.

12. F. Jiang, Z. Yao, R. Yue, Y. Du, J. Xu, P. Yang, C. Wang " Electrochemical fabrication of long-term stable Pt-loaded PEDOT/graphene composites for ethanol electrooxidation", International Journal of Hydrogen Energy,(2012). 37, 14085-14093.

13. Z. H. Xiang, D. P. Cao, X. H. Shao, W. C. Wang, J. W. Zhang, W. Z. Wu "Facile preparation of high-capacity hydrogen storage metal organic frameworks: a combination of microwave-assisted solvothermal synthesis and supercritical activation", Chemical Engineering Science, (2010). 65, 3140-3146.

14. S. Loera-Serna, M.A. Oliver-Tolentino, M.D.L. López-Núñez, A. Santana-Cruz, A. Guzmán-Vargas, R. Cabrera-Sierra "Electrochemical behavior of $[Cu_3(BTC)_2]$ metal–organic framework: The effect of the method of synthesis", Journal of Alloys and Compounds, (2012). 540,113–120.

8th Iranian Fuel Cell Seminar
FEBRUARY 25,26
2015

A Complete Research about Synthesizing of PtO in the Form of Octahedral; Some Findings about the Anodic Material of Solid State Oxide Fuel Cells

Kourosh Motevalli[1*], Zahra Yaghoubi[2]
1. Applied Chemistry Department, Basic Sciences Faculty, Islamic Azad University, South Tehran Branch, Tehran, Iran
2. Industrial Engineering Faculty, Islamic Azad University, South Tehran Branch, Tehran, Iran
** k_motevalli@azad.ac.ir*

Abstract
It's known very well that solid oxide fuel cells (SOFCs) consist entirely of metal oxides, PtO, YSZ, and LSM and have advantages of high efficiency and durability without expensive catalysts. In this research, octahedral-shaped PtO particles were synthesized by microwave thermal treatment at 300 watt power for 15 min in a microwave chamber to be used as an anode material in solid oxide fuel cells. SEM image and particle size distribution revealed near-perfect octahedral PtO microparticle with sizes ranging from 7.0~10.0 μm. The anode functional layer (AFL, 60 wt% PtO synthesized: commercial 40 wt% YSZ), electrolyte (commercial Yttria-stabilized zirconia, YSZ), and cathode (commercial La0.8 Sr0.2 MnO_3 , LSM) layers were manufactured using the decalcomania method on a porous anode support, sequentially. The sintered electrolyte at 1470^0 C for 2 h using the decalcomania method was dense and had a thickness of about 10 μm. The cathode was sintered at 1270^0 C for 2 h, and it was porous. Using humidified hydrogen as a fuel, a coin cell with a 15 μm thick anode functional layer exhibited maximum power densities of 0.28, 0.38, and 0.65 W/cm^2 at 700, 750, and 800^0 C, respectively. Otherwise, when a commercial YSZ anode functional layer was used, the maximum power density was 0.65 W/cm^2 at 800^0 C.

Keywords*:* Fuel cell, SOFCs, FE-SEM, Octahedral, Porous.

1. Introduction

controlling the size and shape of the ceramics produced because of many restrictions and complex geometries, is to some extent difficult. For solving this difficulty, many researchers have surveyed the probable ways of maximizing reaction areas by changing stack sizes and developing new materials [1–5]. In many of these fields, SOFC fabrication methods are generally considered as limiting factors based upon considerations of automation [6]. Some SOFC structures are made by using traditional ceramic preparation methods, such as powder pressing, tape casting, screen printing, or conventional spray methods [7]. Other more sophisticated methods, such as plasma spraying [8], vacuum deposition [9], and extrusion-based direct-write methods , have also been reported. In this study, the decalcomania printing method is performed. This method concludes transferring of designs
from specially prepared paper to a wood or glass or metal surface. This method is expected to have some advantages, because it is easy to prepare materials of the desired shape and size, producing is straightforward. On the other hand, PtO/YSZ is widely used as an anode material

for SOFCs because it has sufficient electronic conductivity and a good catalytic reaction for fuel gas at its operating temperature. Generally, anode materials for SOFCs also should be thermally and chemically compatible compared with other component materials at operating and higher temperatures, because SOFCs operate in the temperature range 800~1000^0 C. However, commercial PtO-loaded YSZ anode materials have a serious problem, because they are strongly deactivated during the operations of SOFCs, because of PtO aggregation at high temperature. Research into the synthesis of PtO nanoparticles has increased during the past decade and methods such as, sol-gel, microemulsion precipitation, chemical vapor deposition, and sputtering [5] have been designed. Recently, some researchers [6] have attempted to use advanced microwave treatments using various polymeric or surfactant additives to synthesize various metal materials with special morphologies.

2. Experimental

2.1. Synthesis of Octahedral-Shaped Pt. The PtO was synthesized by the microwave thermal treatment method. The process applied in this way. At first, after adding polystyrene (molecular weight = 10,000, Aldrich, USA) and Pt source ($PtCl_2$ .H_2O, 99.88%) into ethanol, the solution was stirred homogeneously. The mixed solution was then placed in a quartz liner and the solution was microwave heated at 300 W for 15 min. For making anode functional layers, a commercially available YSZ powder, was purchased. For preparing the synthesized PtO (60 wt%)/YSZ (40 wt%) material, a physically mixing method was applied.

2.2. Fabrication of Solid Oxide Fuel Cells Using Decalcomania Method. The decalcomania paper was prepared next. Briefly, two types of commercial and synthesized PtO were each mixed with YSZ powders at a weight ratio 6 : 4 in a mortar for 1 h to obtain anode functional layer (AFL) precursor powder. Mixtures were reduced to unique and fine particles (5~10 μm) using a 3-roll ball mill (EXAKT50, German) and a high speed mixer (Thinky centrifugal mixer, Japan), and then a binder (benzene oil) was dropped into the powder mixture (the weight ratio of powder to benzene oil in paste was 58~66 : 42~34).
$La_{0.7}$ $Sr_{0.3}$ MnO_3 /YSZ paper cathode was fabricated on the YSZ films using the decalcomania method. Finally, the assembled cell was sintered by heating at 1200^0 C for 2 h. Cell 1 was based on commercial PtO anodes (particle size 0.6 μm, Sumitomo, Japan) and PtO anode in cell 2 was synthesized in this study; cell efficiencies were compared. Pt paste (DAD-87, China) was employed as a current collector and a sealing material. After being sealed, cells were tested for power density in an electrical furnace using the four-probe method. The PtO/YSZ anode was reduced in situ at 800^0 C. The anode was fed with hydrogen at a flow rate of 500 mL min^{-1} and the cathode was exposed to an oxygen flow of 1,000 mL min^{-1} .

3. Results and Discussion

Figures 1(a) , 1(b) and also 1(c) show the SEM micrographs of the cells with different anode functional layers after SOFC testing. The pores in the commercial PtO-AFL (cell 1) are submicron in diameter and the large pores are 2~5 micrometers in diameter. The estimated porosity of the commercial AFL is about 35%. However, the pores in the octahedral PtO-AFL (cell 2) were smaller than those in commercial PtO-AFL. Large cracks were clearly discernible at the interface between the AFL and the electrolyte layer in the commercial PtO cell, but no crack was observed in the octahedral PtO cell. The development of cracks at the AFL/electrolyte layer interface was probably caused by the differential sintering shrinkages of the multiple

layers, and thus, the octahedral PtO particles perhaps better matched the YSZ electrolyte particles in this respect. Additionally the grains between octahedral PtO particles were well connected in octahedral PtO-AFL cells.

Fewer cracks at the AFL/electrolyte interface result in a lower ohmic cell ASR. Electrochemical impedance spectroscopy (EIS) measurements in open-circuit conditions were used to evaluate the resistance values with respect to operating temperature for the octahedral PtO-AFL cell. Also, the obtained results show typical Nyquist plots of cells with an octahedral PtO anode functional layer, measured at 700, 750, and 800^0 C. The intercept with the real axis at high frequency represents the ohmic resistance of a cell (Rohmic), which includes its electrolyte and lead wire resistances and some contact resistance associated with interfaces. The low-frequency intercept corresponds to the total resistance of the cell. Therefore, the difference between the high frequency and low frequency represents the total interfacial polarization resistance (R_p) of the cell. The Rohmic of the cell was almost the same (0.78 Ω cm^{-2}) at all temperatures, but R_p was significantly lower at 800^0 C than at 700 and 750^0 C. R_p reduced from 2.85 to 1.21 Ω cm^{-2} , respectively, with increasing temperature from 700 to 850^0 C. Generally, these different resistance values are ascribed to the addition of the anode functional layer, since other parameters, such as electrolyte thickness, cathode material, anode substrate, and sintering temperature, were kept constant. As mentioned above, R_p is mainly due to electrolyte and contact resistance. Therefore, a better contact between electrolyte and anode can decrease contact resistance and reduce total R_p for a given electrolyte thickness. At the anode/electrolyte interface for the cell with anode functional layer, the elimination of macropores led to a better contact between electrolyte and the anode, which reduced contact resistance at the anode/electrolyte interface. In this study, the octahedral PtO-AFL cell provided lower R_p values due to faster electrochemical reactions at the anode/electrolyte interface.

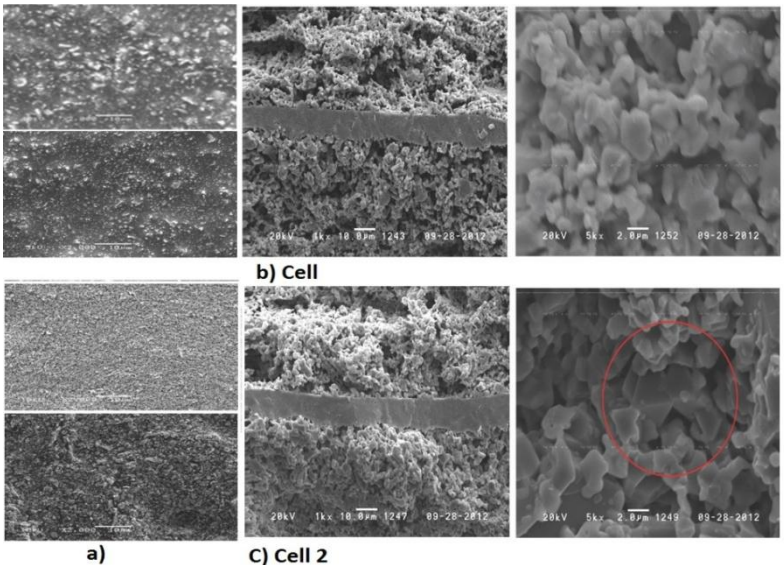

Figure 1: FE-SEM micrographs of cells with different anode functional layers after SOFC testing.

4. Conclusions

This study described the effect of anode functional layer on SOFC performance. Identical single cells, differing only in terms of anode functional layer morphology, were fabricated and tested. Using an octahedral PtO anode functional layer, fuel cell performance was significantly improved by up to a power output of 120 $mWcm^{-2}$ at 879^0C, due to better contact between the electrolyte and anode. These findings demonstrate cell performance is critically dependent on anode microstructure and that microwave thermal treatment provides an effective means of octahedral PtO anode materials.

References

[1] Y. C. Yang, T. H. Chang, Y. C. Wu, and S. F. Wang, "Porous Ni/8YSZ anode of SOFC fabricated by the plasma sprayed method," International Journal of Hydrogen Energy, vol. 37, pp.13746–13754, 2012.

[2] L. R. Pederson, P. Singh, and X. D. Zhou, "Application of vacuum deposition methods to solid oxide fuel cells," Vacuum, vol. 80, no. 10, pp. 1066–1083, 2006.

[3] Y. Du, N. M. Sammes, and G. A. Tompsett, "Optimisation parameters for the extrusion of thin YSZ tubes for SOFC electrolytes," Journal of the European Ceramic Society, vol. 20, no. 7, pp. 959–965, 2000.

[4] Q. Yang, J. Sha, X. Ma, and D. Yang, "Synthesis of PtO nanowires by a sol-gel process," Materials Letters, vol. 59, no. 14-15, pp.1967–1970, 2005.

[5] C. Zhang, J. Zhan, J. Wu, X. Guo, and M. Okido, "Preparation of fibrous nickel oxide particles," Transactions of Nonferrous Metals Society of China, vol. 13, pp. 1441–1445, 2003.

[6] S. M. Tan, S. P. Chai, W. W. Liu, and A. R. Mohamed, "Effects of FeO_x , CoO_x , and PtO catalysts and calcination temperatures on the synthesis of single-walled carbon nanotubes through chemical vapor deposition of methane," Journal of Alloys and Compounds, vol. 477, no. 1-2, pp. 785–788, 2009.

[7] A. M. Reddy, A. S. Reddy, K. S. Lee, and P. S. Reddy, "Growth and characterization of PtO thin films prepared by dc reactive magnetron sputtering," Solid State Sciences, vol. 13, no. 2, pp.314–320, 2011.

[8] C. H. Jung, S. Jalota, and S. B. Bhaduri, "Quantitative effects of fuel on the synthesis of Ni/PtO particles using a microwave-induced solution combustion synthesis in air atmosphere," Materials Letters, vol. 59, no. 19-20, pp. 2426–2432, 2005.

[9] F. Rousseau, S. Awamat, M. Nikravech, D. Morvan, and J.Amouroux, "Deposit of dense YSZ electrolyte and porous PtO- YSZ anode for SOFC device by a low pressure plasma process," Surface and Coatings Technology, vol. 202, no. 4–7, pp. 1226–1230, 2007.

[10] S. Biswas, T. Nithyanantham, S. N. Thangavel, and S. Bandopad- hyay, "High-temperature mechanical properties of reduced PtO-8YSZ anode-supported bi-layer SOFC structures in ambi- ent air and reducing environments," *Ceramics International*, vol. 39, no. 3, pp. 3103–3111, 2013.

[11] D. Y. Han, H. Y. Yang, C. B. Shen, X. Zhou, and F. H. Wang, "Synthesis and size control of PtO nanoparticles by water-in-oil microemulsion," *Powder Technology*, vol. 147, no. 1–3, pp. 113–116, 2004.

[12] N. M. Deraz, M. M. Selim, and M. Ramadan, "Processing and properties of nanocrystalline Ni and PtO catalysts," *Materials Chemistry and Physics*, vol. 113, no. 1, pp. 269–275, 2009.

[13] L. Zhang, S. P. Jiang, W. Wang, Y. Zhang, "PtO/YSZ, anode- supported, thin-electrolyte, solid oxide fuel cells fabricated by gel casting," *Journal of Power Sources*, vol. 170, no. 1, pp. 55–60,2007.

[14] Q. L. Liu, K. A. Khor, and S. H. Chan, "High-performance low- temperature solid oxide fuel cell with novel BSCF cathode," *Journal of Power Sources*, vol. 161, no. 1, pp. 123–128, 2006.

8th Iranian Fuel Cell Seminar
FEBRUARY 25,26
2015

Electrodeposition of Platinum on Glassy Carbon Electrode for Electrooxidation of Glucose in Alkaline Medium

Mehdi khairmand*, Abolfath Eshghi
Fuel Cell Research Laboratory, Department of chemistry, Faculty yasuj University
** kheirmand@yu.ac.ir*

Abstract
his study deals with the glucose oxidation in alkaline medium. For this purpose, first platinum particles were deposited on glassy carbon electrode by using electroplating with cyclic voltammetry. The resulting of glucose oxidation were studied using by cyclic voltammetry (CV) . The results showed higher catalytic activity of the pt/ glassy carbon. Therefore this electrode is a good candidate as an anode for direct glucose fuel cells.

Keywords: Platinum, Glassy carbon electrode (GCE), Direct glucose fuel cell (DGFC).

Introduction:
Glucose is most abundantly found monosaccharide in nature and complete oxidation of glucose produces very high energy (-2.87 □ 10^6 J/mol). To derive useful energy from glucose, direct conversion of chemical energy to electrical energy is the best option. The research work on low temperature direct glucose fuel cell (DGFC) as power source in low power longterm portable devices is under developing stage. [1-3] Studiesthr oughout the last few decades show that noble metal catalysts based on platinum and gold could potentially electrooxidize glucose. Oxidation of glucose was studied at various pH solutions on platinum, gold[4,5] In the present study, the electro-activity of Pt/GCE for electrooxidation of glucose in alkaline medium was studied by different electrochemistry methods.

Materials, methods and Apparatus:
Methanol (Merck, 99.8% purity) and KOH (Merck, 84% purity) were used as received. All other chemicals were of analytical grade and used without further purification. Distilled water was used throughout. The electrochemical experiments were performed in a three-electrode cell arrangement. A platinum sheet was used as counter electrode, while all potentials were measured with respect to Ag/AgClelectrode. Electrochemical experiments were carried out using EG&G PARSTAT 2263 Advanced Electrochemical systems.

Results and discussion

Electrochemical studies of Pt electrodeposition on GCE

Platinum electrochemical growth process on bare GCE was investigated by CV. Fig. 1 illustrates the first cyclovoltammetric scans for a solution of 3 mM H2PtCl6 and 0.5 M H2SO4 at bare GCE. The first scan contains a characteristic “nucleation loop”, which arises from the greater overpotential required for nucleation onto the electrode compared to deposition of metal onto metal [30] a reduction peak of Pt and the oxidation peak of deposited Pt can be seen and the peak at − 0.14 V is related to the reduction of hydrogen ions to hydrogen adatoms [6,7].
A reduction peak of Pt and the oxidation peak of deposited Pt can be seen. The typical peak at − 0.26 V is related to the reduction of hydrogen ions to hydrogen atoms indicate the presence of platinum particles (Fig. 2)

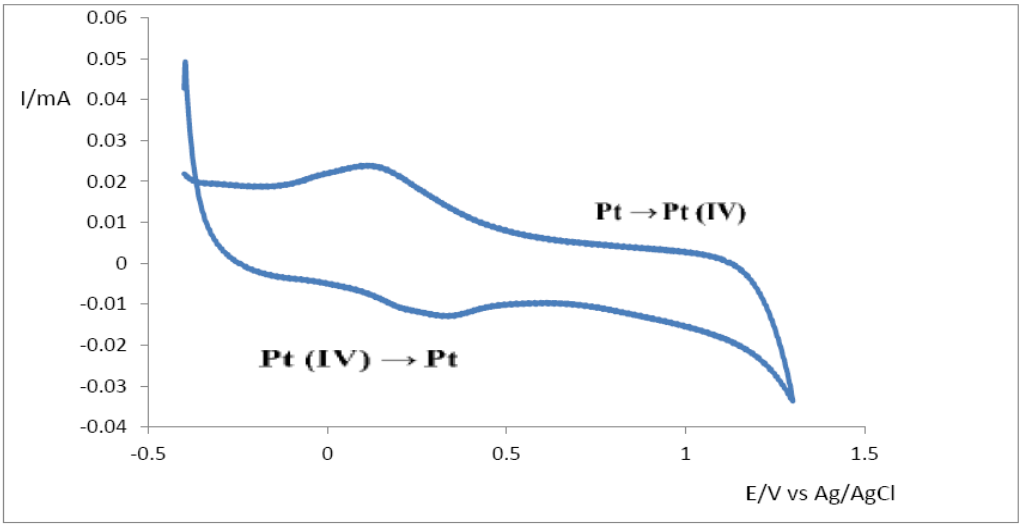

Figure 1

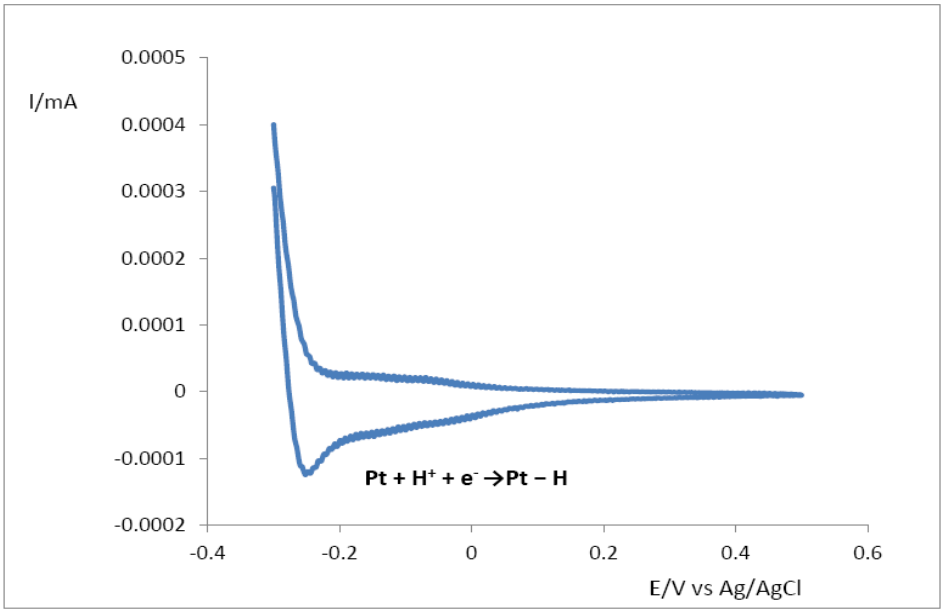

Figure 2
Electro-oxidation of glucose on Pt/GCE

The oxidation of glucose at the modified GC electrode was studied by cyclic voltammetry. Figure 3 shows a glucose oxidation on the Pt/GCE in 0.1M KOH + 10mM glucose at 25ºC with a scan rate of 50 mVS-1 . The oxidation of glucose at the Pt/GCE was occurred at much less potentials, associated with increasing anodic peak current while diminished in the cathodic peak current.

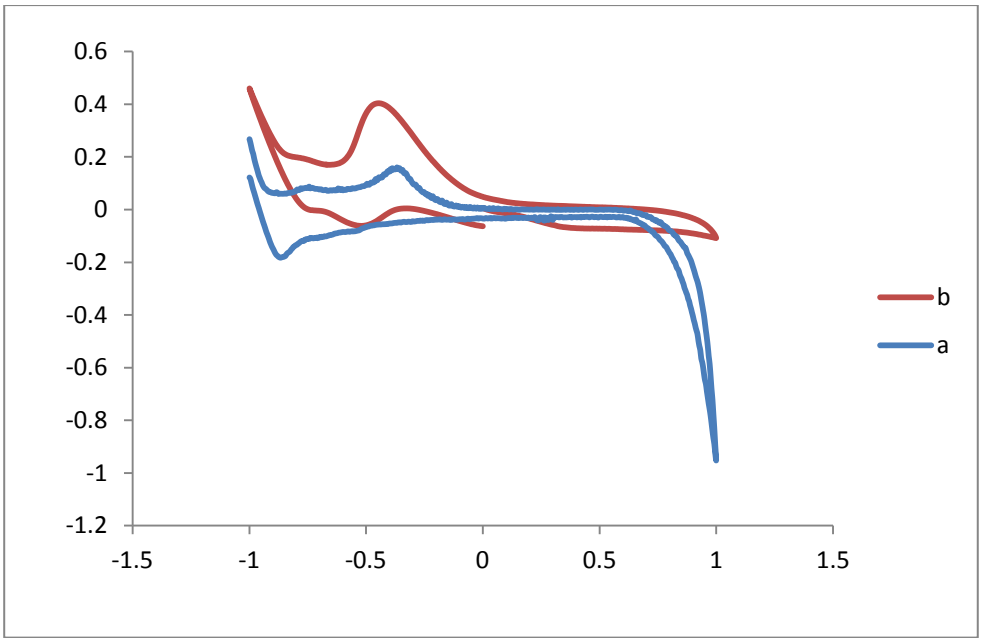

Fig. 3. Cyclic voltammograms obtained for Pt/GCE in 0.1 M KOH in the absence (a) and presence of 10 mM glucose (b). Scan rate, 50 mV s−1.

Conclusion:

Pt /GCE electrode were prepared by electrodeposition method. The electro-catalytic activity of Pt /GCE electrode for electro-oxidation of glucose was evaluated by electrochemical voltammetric measurements and showed high currents for glucose oxidation and good electro-catalytic activity. Therefore, this electrode is a good candidate as an anode for direct glucose fuel cells.

Reference:

[1] Kerzernmacher S, Ducree J, Zengerle R, von Stetten F. An abiotically catalyzed glucose fuel cell for powering medical implants:reconstructed manufacturing protocol and analysis of performance. J Power Sources 2008;182:66e75.

[2] McGinley J, McHale FN, Hughes P, Reid CN, McHale AP. Production of electrical energy from carbohydrate using a transition metal-catalysed liquid alkaline fuel cell. Biotechnol Lett 2004;26:1771e6.

[3] Aoun SB, Bang GS, Koga T, Nonaka Y, Sotomura T, Taniguchi I. Electrocatalytic oxidation of sugars on silver-UPD single crystal gold electrodes in alkaline solutions. Electrochem Commun 2003;5:317e20.

[4] Jin C, Taniguchi I. Electrocatalytic activity of silver modified gold film for glucose oxidation and its potential application to fuel cells. Mater Lett 2006;61:2365e7.

[5] Basu D, Basu S. A study on direct glucose and fructose alkaline fuel cell. Electrochim Acta 2010;55:5775e9.

6. R. Abdullah Mirzaie and A. Eshghi: 'Study of methanol electro-oxidation on Ni and Ni–Pt/carbon paper electrodes for direct methanol fuel cell applications', *Surf. Eng.*, 2014, **30**, 263-267

7. B. Liu, L. R. Liu and X. J. Liu: 'Effects of carbon nanotubes on crystallization in amorphous Ni–Pt electroplating coating', *Surf. Eng.*, 2013,**29,** 190-193

8th Iranian Fuel Cell Seminar
FEBRUARY 25,26
2015

Study of Oxygen Reduction on Pt/ Glassy Carbon Electrode for PEM Fuel Cell Application

Mehdi kheirmand*, Abolfath Eshghi
Fuel Cell Research Laboratory, Department of chemistry, Faculty yasuj University
** kheirmand@yu.ac.ir*

Abstract
This study deals with the oxygen reduction in acidic solution. For this purpose, first platinum particles were deposited on glassy carbon electrode by using electroplating with cyclic voltammetry. The resulting of oxygen reduction were studied using electrochemical method such as cyclic voltammetry (CV) . The results showed higher catalytic activity of the pt/ glassy carbon electrode. Therefore this electrode is a good candidate as a cathode for PEM fuel cells.

Keywords: Platinum, Glassy carbon, Proton Exchange Membrane Fuel Cell (PEMFC).

1- Introduction

Polymer elecrolyte membrane fuel cells (PEMFCs) have long been thought of as a promising clean alternative energy electrochemical device. They have some advantages such as high power density , high efficiency, clean utilization and zero emission for promising green power sources.[1-3]

Oxygen reduction reaction (ORR) is one of the important electrocatalytic reaction due to in particular fuel cells. It is well known that the cell voltages of fuel cells are limited by slow kinetics of ORR at the cathods. Platinum is widely used as the electrocatalyst for ORR due to its high activity and excellent chemical stability. However, pt is expensive and the limited world's supply of platinum poses serious problems to widespread commercialization of the fuel cell technology. Thus, research efforts in the development of cathode electrocatalysts have been focused on decreasing the pt content or replacing it with less expensive materials while maintaining high ORR activity.[4,5]

2.Experimental

KOH (Merck, 84% purity) were used as received. All other chemicals were of analytical grade and used without further purification. Distilled water was used throughout. The electrochemical experiments were performed in a three-electrode cell arrangement. A platinum sheet was used as counter electrode, while all potentials were measured with respect to Ag/AgCl electrode. Electrochemical experiments were carried out using EG&G PARSTAT 2273 Advanced Electrochemical systems.

3. Results and discussion

Electrochemical studies of Pt electrodeposition on GCE

Platinum electrochemical growth process on bare GCE was investigated by CV. Fig. 1 illustrates the first cyclovoltammetric scans for a solution of 3 mM H2PtCl6 and 0.5 M H2SO4 at bare GCE. The first scan contains a characteristic "nucleation loop", which arises from the greater overpotential required for nucleation onto the electrode compared to deposition of metal onto metal [30] a reduction peak of Pt and the oxidation peak of deposited Pt can be seen and the peak at − 0.14 V is related to the reduction of hydrogen ions to hydrogen adatoms [6,7].

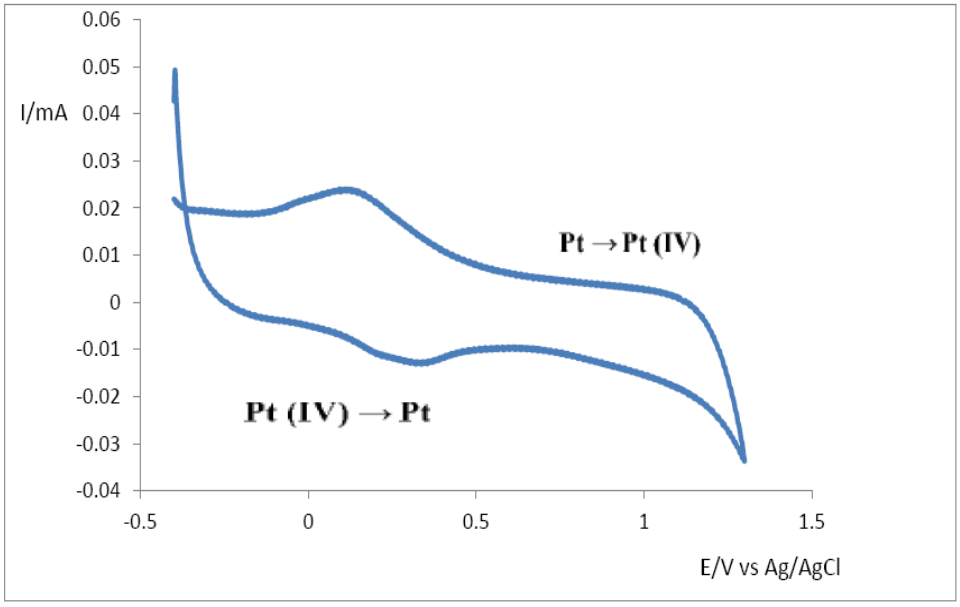

Figure 1

Voltammograms of oxygen reduction at GCE , and Pt/ GCE

Figures 2 Show ORR voltammograms of oxygen reduction on the GCE, and Pt/ GCE in 1M H_2SO_4 at 27 ^oC with a scan rate of 100 mV s^{-1}. There are difference between current density for electrods. The results on Pt/ GCE show that the current density significantly increases.[8,9]

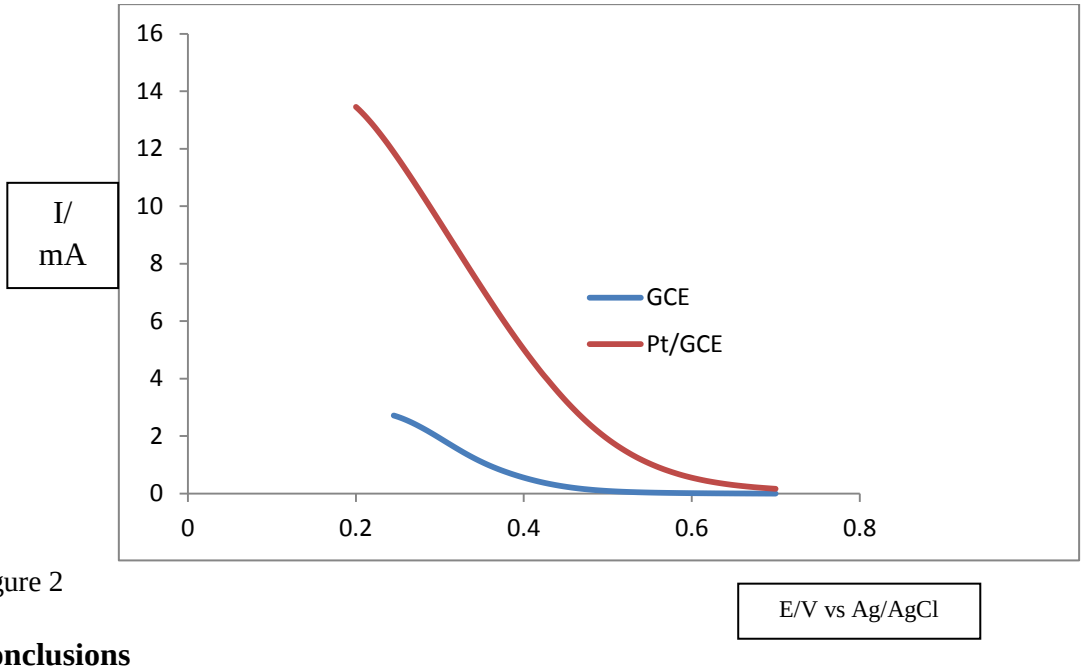

Figure 2

Conclusions

Pt /GCE electrodes were prepared by electrodeposition method. The electro-catalytic activity of Pt /GCE electrode for oxygen reduction was evaluated by electrochemical voltammetric measurements . The Pt /GCE showed extremely higher currents of oxygen reduction than the GCE electrode.

Acknowledgments
The authors would like to acknowledge the support of the Hydrogen and Fuel Cell Research Laboratory, Department of chemistry, Yasouj University.

References

1. H. Zhu, M. Luo, S. Zhang, L. Wei, F. Wang, Z. Wang, Y. Wei and K. Han: 'Combined method to prepare core-shell structured catalyst for proton exchange membrane fuel cells', *Int J Hydrogen Energy*., 2013,**38**,3323-3329
2. V. Mehta and SJ. Cooper: 'Review and analysis of PEM fuel cell design and manufacturing', *J Power Sources*.,2003, **114**, 32-53
3. C.H. Cheng, K. Malek , P.C. Sui and N. Djilali: ' Effect of Pt nano-particle size on the microstructure of PEM fuel cell catalyst layers: Insights from molecular dynamics simulations', *Electrochimica Acta*.,2010, **55**, 1588-1579
4. C. Termpornvithit, N. Chewasatn and M. Hunsom: 'Stability of Pt-Co/C and Pt-Pd/C based oxygen reduction reaction electrocatalysts prepared at a low temperature by a combined impregnation and seeding process in PEM fuel cells', *J Appl Electrochem*., 2012,**42**, 69-78
5. M. Oezaslan, F. Hasche and P. Strasser : 'Oxygen electroreduction on PtCo3, PtCo and Pt3Co alloy nanoparticles for alkaline and acidic PEM fuel cells', *J Electrochem Soc*.,2012,**159:B**, 394-405
6. R. Abdullah Mirzaie and A. Eshghi: 'Study of methanol electro-oxidation on Ni and Ni–Pt/carbon paper electrodes for direct methanol fuel cell applications', *Surf. Eng*., 2014, **30**, 263-267
7. B. Liu, L. R. Liu and X. J. Liu: 'Effects of carbon nanotubes on crystallization in amorphous Ni–Pt electroplating coating', *Surf. Eng*., 2013,**29,** 190-193
8. M. Jafarian, F.Gobal, M.G. Mahjani and M. Hosseini Aliabadi: 'Multistep Reduction of Oxygen on Polycrystalline Silver in Alkaline Solution', *Chinese Journal of Catalysis.*, 2010, **31**, 541–546
9. L.R. Yang, D.S. Tsai,Y.S. Chao,W.H. Chung and D.P. Wilkinson: ' Enhance the oxygen reduction activity of ruthenium selenide pyrite catalyst with nitrogen-doped carbon', *Int J Hydrogen Energy*.,2011,36,7381-7390

8th Iranian Fuel Cell Seminar
FEBRUARY 25,26
2015

Metal Oxide/Pt Based Nanocomposites as Electrocatalysts for Oxygen Reduction Reaction

Tahere Mohammadghasabi*, Nasrin Talebian
Department of Chemistry, Shahreza Branch, Islamic Azad University, Shahrez, Isfahan, Iran
* *t.a.rose2012@gmail.com*

Abstract
Fuel cell is a promising choice for clean energy because of its eco-friendly system, high energy conversion efficiency and high power density. Recently, much of the research work is focused on the system of combining metal oxides to increase the durability and to reduce the cost and with high surface area. In this study, among the various fabrication methods, we used the precipitation method to synthesis composites NiO/SnO2/Pt/C using NaBH4 as a reducing agent. XRD and SEM characterizations were carried out to determine the particle size and distribution of the catalysts. Cyclic voltammetry were recorded to evaluate oxygen reduction reaction (ORR) performance. SEM images revealed that Pt/C and metal oxide nanoparticles were uniformly dispersed in the composite catalyst architecture with smaller particle size for composite/Pt/C catalyst compared to Pt/C catalysts. XRD patterns of samples showed peaks characteristic of Pt and of rutile and cubic phases for SnO2 and NiO, respectively.

Keywords: Fuel cell, Metal Oxide, Precipitation, Oxygen Reduction Reaction.

Introduction

Proton exchange membrane fuel cells (PEMFCs) have received considerable attention in recent years as alternative energy devices for transportation and portable power generation applications [1]. However, two main challenges limit the application of fuel cells in transport [2]: (i) the sluggish kinetics of the oxygen reduction reaction (ORR) on the cathode side due to the formation of –OH species at +0.8 V, which inhibits further reduction of oxygen and hence, results in loss of performance [3] and then, more active catalysts should be used [4]; and (ii) thehigh cost of the whole device limits their commercialization [5]. However, the highest electrocatalytic activity is still gained at Pt and Pt-based alloys.

It has been shown that several factors can diminish the lifetime of PEMFCs including (1) catalyst dissolution, (2) catalyst particle sintering, (3) membrane thinning, and (4) carbon-support corrosion [6, 7].

The cathode performance improvement could be achieved using supported Pt catalysts of higher surface area and lower platinum loading including Pt-based alloys with transition metals such as Sn [8] and Ni [9]. Tin oxide (SnO2), with n-type semiconducting property, high electronic conductivity, and good electrochemical stability, has been proposed as a potential catalyst support material for fuel cell application [10, 11]. In addition, NiO showed an excellent electrochemical performance as an electrode material for lithium ion batteries and fuel cells [12]. These properties recommend consideration of NiO as an alternative catalyst support. However, its low electrical conductivity prevents its use in fuel cells. Carbon (e.g., Vulcan XC-72) is the typical catalyst support material for PEM-based fuel cells due to its large surface area, high electrical conductivity, and well-developed pore structure [13].

The potential of the cathode can reach as high as 1.5 V, causing severe carbon corrosion as indicated by the following reaction [14]:

C + 2H2O → CO2 +4H+ +4e− (Eo = 0.207 Vvs.NHEat25 ◦C) (1)

The electrochemical corrosion of the carbon support causes: (i) agglomeration and sintering of the Pt catalyst particles, resulting in a decreased electrochemical surface area of the catalyst; (ii) electrically isolated Pt particles that are detached from the support. These effects result in a rapid degradation of the Pt catalyst and thus shorten the lifetime of the PEMFC. Therefore, more robust non-carbon support materials, such as metal oxides, are needed. Metal-metal oxide catalysts have been investigated as possible co-catalysts that are believed to operate via the bifunctional mechanism [15].

In this study, Pt catalyst was precipitated on Vulcan XC-72R containing 10 wt. % NiO and SnO_2 using NaBH4 as a reducing agent. XRD and SEM characterizations were carried out to determine the particle size and distribution of the catalysts. Cyclic voltammetry and linear sweep voltammetry were recorded to evaluate oxygen reduction reaction (ORR) performance.

Experimental

Reagents

Vulcan XC-72R carbon black, $K_2Pt(OH)6$, Nafion, $Ni(NO_3)_2{\cdot}6H_2O$, $NaBH_4$, NaOH (98.0%), H_2SO_4, $SnCl_2.2H_2O$ and De-ionized water were used to prepare the solutions.

Pt– SnO2/NiO/C electrocatalystspreparation

Preparation of Pt– SnO2/NiO/C electrocatalysts:Supporting NiO and SnO2 on Vulcan XC-72R carbon black by the precipitation method, followed by the chemical reduction of Pt precursor salt using NaBH4 as the reducing agent. The detailed steps of the catalyst manufacture were as follows: an appropriate amount of Ni(NO3)2·6H2O and $SnCl_2{\cdot}2H_2O$ (10 wt.%) was weighed and dissolved in a suspension of Vulcan XC-72R carbon black in double distilled water. Drops of 1 M NaOH solution were added to the mixture to maintain its pH value at 10 during the constant stirring for 3 h. This induces the formation of small and uniform nanoparticles. The resulting powder was then filtered and washed with double distilled, dried at 80 ◦C. Calcination step at 600◦C was performed in air muffle for 3 h to form SnO_2/NiO/C catalyst. The corresponding volume of KPt(OH)6 (Pt loading 10 wt.%) was added in a suspension of NiO/C powder in double distilled water, sonicated and the reduction step was performed by adding NaBH4 solution slowly with continuous stirring for 3 h. The formed Pt– SnO_2/NiO/C catalyst was then filtered and washed, and drying step was performed in an air oven at 80 ◦C for 6 h.

The electrocatalyst ink was prepared by ultrasonicating 10 mg of electrocatalyst in500 ml of ethanol followed by adding 25 ml of Nafion (5 wt%) and ultasonicated further. 2 ml of the inkwas drop casted over glassycarbon electrode using micropipette. The electrodewas dried in ambient condition.

For material characterization, The X-ray powder diffraction (XRD) pattern of material wascollected on a Bruker, D8 ADVANCE XRD diffractionspectrometer with a Cu K line at 1.5406 A and a Ni filterfor an angle range of 2h = 10–90°for the determination of crystalstructure of composite support as well as their supported catalysts.The morphology of the materials was observed on aPhilips, XL30 scanning electronmicroscope (SEM) with an accelerating voltage of 17 kV.

Electrochemical measurements of the electrocatalysts

Cyclic voltammetry were recorded to evaluate ORR performance.Cyclic voltammograms were obtained in a conventional threeelectrode electrochemical cell. The working electrode used for electrochemical measurement was glassy carbon electrode of diameter 3mmwith a thin layerof electrocatalyst ink drop casted over it. A Pt electrode used as the counter electrode and anAg/AgCl electrode saturated with 1 M KCl was used as the reference electrode.

Results and discussion

Structural characterization

Figure. 1 shows the XRD patterns of synthesized Pt/SnO2/NiO catalyst. The SnO2 peaks at can be respectivelyindexed to the (1 1 0), (1 0 1), (2 0 0), and (2 1 1) reflections of cassiteriteSnO2(JCPDS no. 41-1445). NiO with a cubic structure (bunsenite, NaCl typestructure) was observed ((JCPDS no. 44-1159). The presence of metallic Pt is also clearlyrevealed by the peak at 39.9◦ and 46.2◦ attributed to the Pt [1 1 1]and [2 0 0] reflection, respectively(JCPDS no. 1-1311). The broadening of two peaksindicates the small particle size of Pt.

Morphological analysis

As shown in Figure. 2, SnO2 and NiO nanoparticles are uniformly dispersed on the surface Pt/C support. SEM images revealed that Pt/C and metal oxide nanoparticles were uniformly dispersed in the composite catalyst architecture with smaller particle size for composite/Pt/C catalyst compared to C catalysts.

Cyclic voltammetric technique has proven very useful in obtaining information on the stability in the reaction media and participation of the active sites on the electrode surfaces. The cyclic voltammograms of both Pt/C and Pt/C/SnO2/NiO are presented in Figure. 3. Cyclic voltammogramsof typical Pt features are obtained, with H2adsorption/desorption regions and Pt oxidation/reductionpeaks.The onset potentials for ORR on Pt/C, Pt/C/NiO/SnO2catalysts are 0.28 and 0.21 V, respectively confirming that later has higher activities Pt/C. The onset potential for oxygen reduction is shifted to more positive potential for bjnary metal oxides modified compared to Pt/C. The improved ORR is due to the ready adsorption and easy dissociation of O2 on the NiO-SnO2 modified Pt surface in relation to Pt/C.

These results show that the metal oxide support can affect the activity and stability of the cathode in the polymer electrolyte fuel cell. An enhanced activity for ORR, was observed for all samples with platinum on metal oxide. This could indicate that the platinum surface is less covered by oxides, a hypothesis supported by the postponed oxide formation seen in the cyclic voltammograms of platinum deposited. However, the reason for the improved activity for ORR on the nickel oxide electrodes are not fully understood.

References

[1] H.A. Gasteiger,S.S. Kocha,B. Sompalli,F.T, Wagner “Activity benchmarks and requirements for Pt, Pt-alloy, and non-Pt oxygen reduction catalysts for PEMFCs”, Appl. Catal. B Environ, (2005). 56, 9-35.

[2] T.He, E.Kreidler,L. Xiong,J. Luo,C.J. Zhong “Alloy electrocatalysts”, J. Electrochem. Soc. (2006). 153, A1637-43.

[3] C.C.Liang,A.L.Juliard “The overpotential of oxygen reduction at platinum electrodes”, *J. Electroanal. Chem.*(1965). 9, 390.

[4]T.R. Ralph, M.P. Hogarth “Catalysis for low temperature fuel cells. Part I: the cathode challenges”, Platin Met Rev, (2002). 46, 3-14.

[5] B.C.H.Steele,A.Heinzel “Materials for fuel-cell technologies”, Nature, (2001). 414, 345–352.

[6] S.G.Chalk,J.E,Miller “Key challenges and recentprogress in batteries, fuel cells, and hydrogen storage for clean energy systems”, J. Power Sources, (2006), 159, 73–80.

[7] Z.Siroma,K.Ishii, K.Yasuda, Y. Miyazaki, M. Inaba, A. Tasaka, "Imaging of highly oriented pyrolytic graphite corrosion accelerated by Pt particles", Electrochem. Commun, (2005). 7, 1153–1156.
[8] M.K.Min,J.Cho, K, Cho, H. Kim " Particle size and alloyingeffects of Pt-based alloy catalysts for fuel cell applications", Electrochim. Acta. (2000). 45, 4211.
[9] L.Xiong, A.M. Kannan,A.Manthiram "Pt–M (M¼Fe, Co, Ni and Cu) electrocatalysts synthesized by an aqueous route for proton exchange membrane fuel cells", Electrochemistry Communications, (2002). 4, 898–903
[10]T. Okanishi, T. Matsui, T,Takeguchi, R, Kikuchi, K, Eguchi "Chemical interaction between Pt and SnO2 and influence on adsorptive properties of carbon monoxide", Applied Catalysis A: General, (2006). 298 , 181.
[11]M. Nakada,A,Ishihara,S.Mitsushima, N. Kamiya, K. Ota "Effect of tin oxides on oxide formation and reduction of platinum particles", Electrochemical and Solid-State Letters, (2007), 10, F1.
[12] R.S.Amin, "Pt–NiO/C anode electrocatalysts for direct methanol fuel cells". Electrochim. Acta, (2012). 59, 499-508.
[13] Sheng-Yang Huang, Prabhu Ganesan, Branko N. Popov, "Electrocatalytic activity and stability of niobium-doped titanium oxide supported platinum catalyst for polymer electrolyte membrane fuel cells", Applied Catalysis B: Environmental, (2010). 96, 224–231.
[14] K,Kinoshita "Carbon: Electrochemical and Physicochemical Properties", John Wiley & Sons, New York, (1988).
[15] E.J.McLeod, V.I, Birss "Solegel derived WOx and WOx/Pt films for direct methanol fuel cell catalyst applications", Electrochim Acta, (2005). 51, 684-693.

Tables and figures

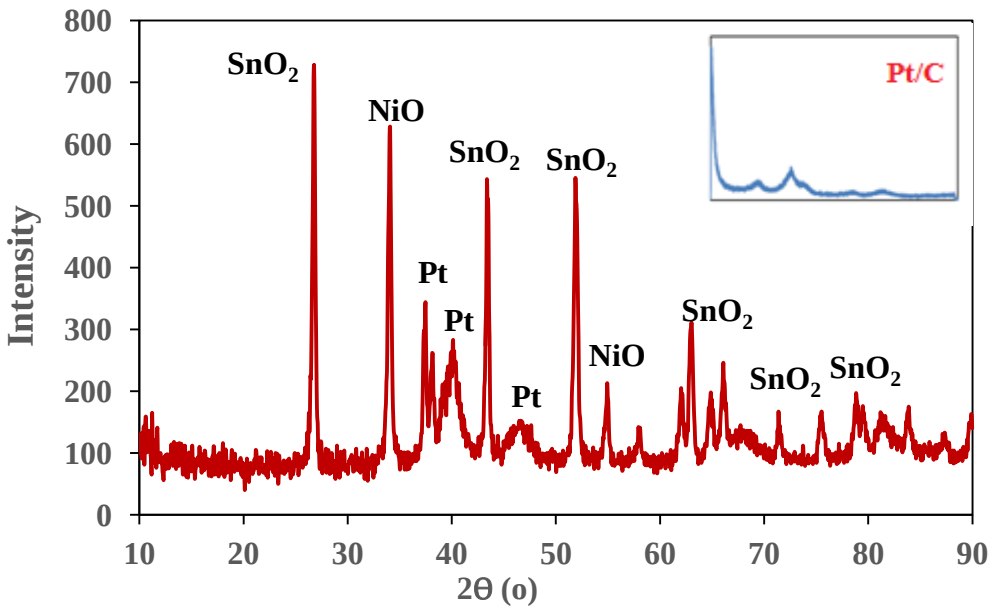

Figure. 1. XRD pattern of Pt/C and Pt–NiO/SnO2 electrocatalysts.

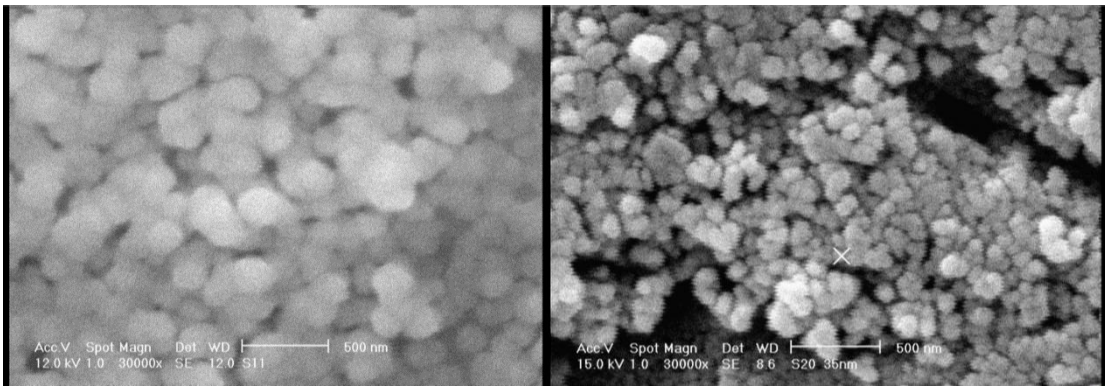

Figure. 2. SEMimages of Pt/C (left) and Pt–NiO/SnO2 electrocatalysts (right).

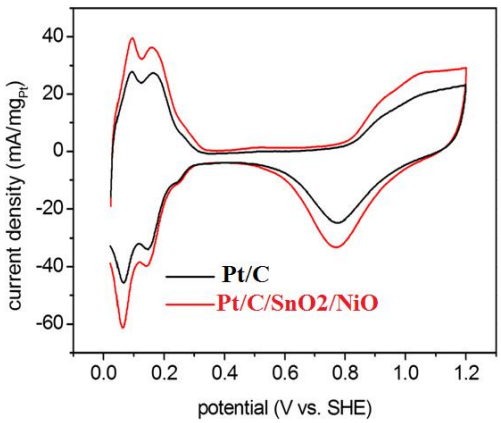

Figure. 3. Cyclic voltammograms of Pt/C andPt/C/SnO2/NiO electrodes in 0.5 M H2SO4.

8th Iranian Fuel Cell Seminar
FEBRUARY 25,26
2015

Performance Comparison of the Two Commercial PEMFC Electrode Substrates: Toray and Ballard Carbon Paper

Mohammad Zhiani*, Mohammad Mohammadi taghiabadi, Ismaeil Mohammadi, Mohsen Keivannejad
Department of Chemistry, Isfahan University Of Technology, Isfahan 84156-83111, Iran
** m_zhiani@cc.iut.ac.ir*

Abstract
In this work, we have compared the performance of two commercial and most common electrode substrates: Toray and Ballard carbon paper. Two electrodes were fabricated with the same structure by these substrates. Then these electrodes were used to make separate MEAs. The performance of these MEAs was investigated in a PEMFC single cell at the same operation conditions. The results show that the Ballard substrate has higher performance at higher humidity. It's because of the special microstructure of Ballard substrate that cause this substrate has a higher resistance to flooding.

Keywords: PEMFC, Electrode substrate, Flooding, Electrode microstructure

Introduction

H_2/O_2 fuel cells based on proton-exchange membranes have many attractive features, including high power density, rapid start-up, high efficiency, which makes them a promising clean energy technology. Great advances have been made in PEM fuel cell development [1]. Catalyst loading has been significantly reduced, power density has been increased, and prototype PEM fuel cell vehicles have been successfully tested on many continents [2-5]. In spite of these successes, there is strong need to enhance the performance of current PEM fuel cells. Several technical obstacles hinder their widespread commercialization for transportation and stationary application sectors.

A problem common to porous electrodes, regardless of the precise application, is to provide the most effective pathway throughout the electrode for each reactant and product involved in the electrochemical reaction, as well as a surface area between the active material and the electrolyte, that is as large as possible. Intuitively, one understands that some of these goals are incompatible; thus the best performing electrode will be the result of a compromise. In fuel cells, a subfamily of porous electrodes is encountered, namely gas diffusion electrodes (GDE), characterized by the reactant or/and the product being a gas (O_2, H_2, CO_2, water vapor). Since gases are transported fastest in the gas phase, GDE are advantageously provided with a pore system that remains free of electrolyte during operation. Thus, in liquid-electrolyte fuel cells, the initial pore system of GDE fulfils two functions; namely to provide space for the gases as well as for the electrolyte. On the contrary, electrodes in polymer electrolyte fuel cells (PEFC) have a fixed interface between the solid phase and the electrolyte owing to the solid nature of the latter. The requisites for PEFC electrodes are thus different.

One of the PEMFC electrodes parts that have a great importance in gas transport is electrode support [6,7]. At the present time, there are two major types of electrode substrate: carbon paper

and carbon cloth. In this work, we have compared the performance of two commercial and most common electrode substrates: Toray and Ballard carbon paper and their performance and tolerance to flooding have been evaluated.

Experimental

Commercially available Toray and Ballard Carbon paper was used for the preparation of the fuel cell electrode. The 20 wt% Pt on Vulcan XC-72 electrocatalyst from Electrochem and 5 wt% Nafion solution supplied by DuPont, were used for catalyst ink preparation.

The catalyst ink was coated on the TGP (from Toray) and Ballard gas diffusion media by a painting method and dried at 80 $^{\circ}$C for 30 min.

Nafion 212 was used as the polymer electrolyte membrane. Prior to use, each membrane was boiled in 3% hydrogen peroxide to remove any organic impurities, washed with water, and then boiled in 1M sulfuric acid to remove any metallic impurities as well as to convert the membrane fully to the H^+ form. Finally, it was boiled in distilled water.

The MEAs was prepared by placing two electrodes, with the same platinum loading on both sides of a Nafion membrane. So, two MEAs were obtained by two different electrode supports.

The MEAs were inserted in a PEMFC single cell (from AHNS Co.) and their electrochemical performance evaluated by a Fuel cell test system.

Results and Discussion

The effects of fuel cell pressure on MEAs performance are shown in figure 1 and figure 2. The operating temperature of cell was fixed at 60 $^{\circ}$C. The higher back-pressure of inlet gases enhances the cell performance. The maximum power density was elevated with the increase in the pressure, according to the Nernst equation. In addition to, the performance of PEMFCs is affected by cathode gas relative humidity. It's observed that by increasing cathode gas RH, the cell performance decreases because of flooding in cathode electrode. This effect is more obvious for the MEA made by TGP substrate.

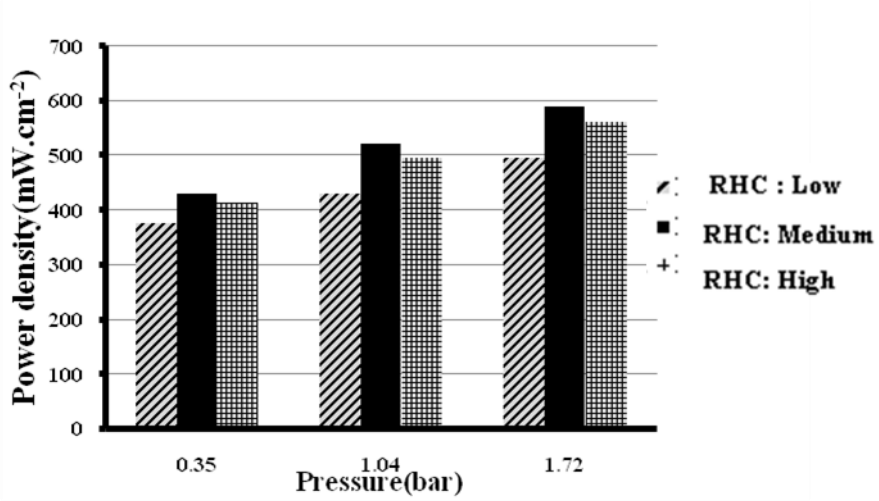

Figure 1: Maximum power density at different pressures and cathode RH for Ballard MEA. T_{cell}: 60°C, Anode RH: fully humidified

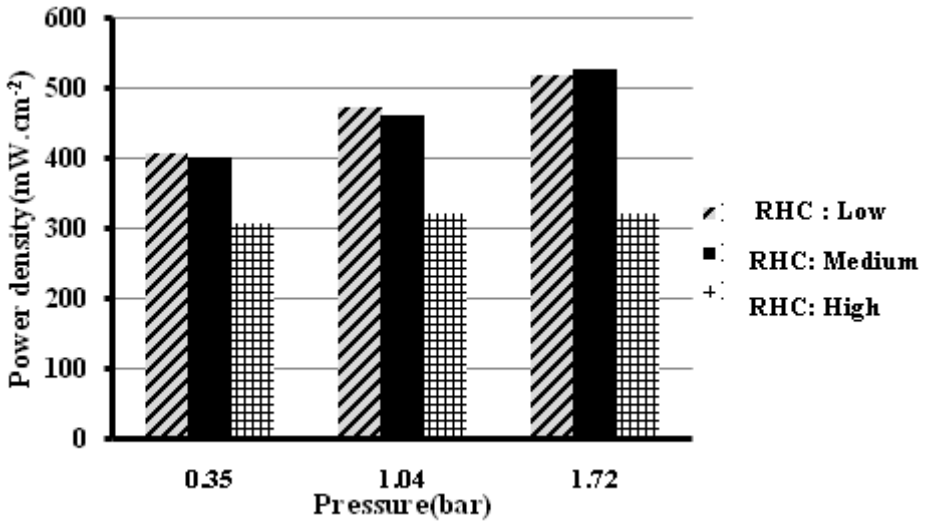

Figure 2: Maximum power density at different pressures and cathode RH for TGP MEA. T_{cell}: 60°C, Anode RH: fully humidified

Figures 3 to 5, shows the performance of TGP and Ballard MEA at different cathode RH. Cathode electrode performance decreases with increasing cathode RH. The reason of this decrease in performance can be found in the structure of electrode substrate. As the cathode RH increase, the flooding phenomena see earlier. With increasing relative humidity, moisture content of the catalyst layer fills the electrode void volumes. So the access of reactants to the catalyst particles is small and the performance decreases.

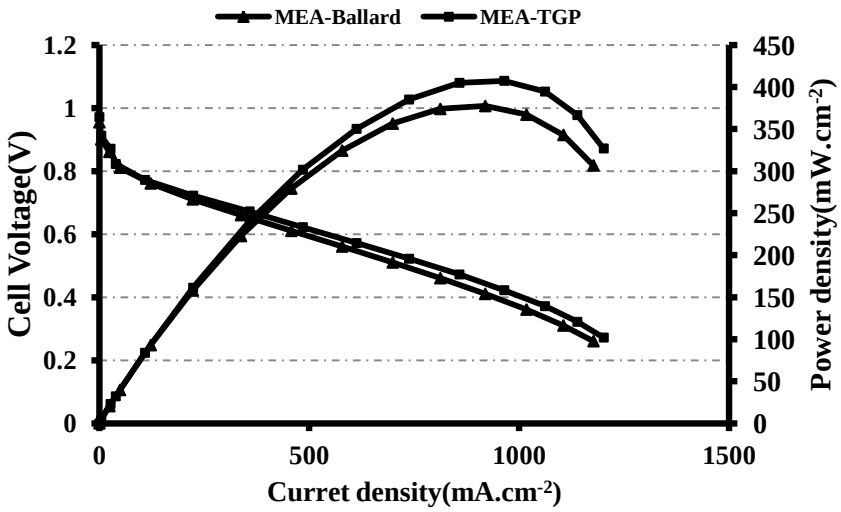

Figure 3: Polarization curve for TGP and Ballard MEAs. T_{cell}: 60°C, Anode RH: fully humidified, Cathode RH: low humidified

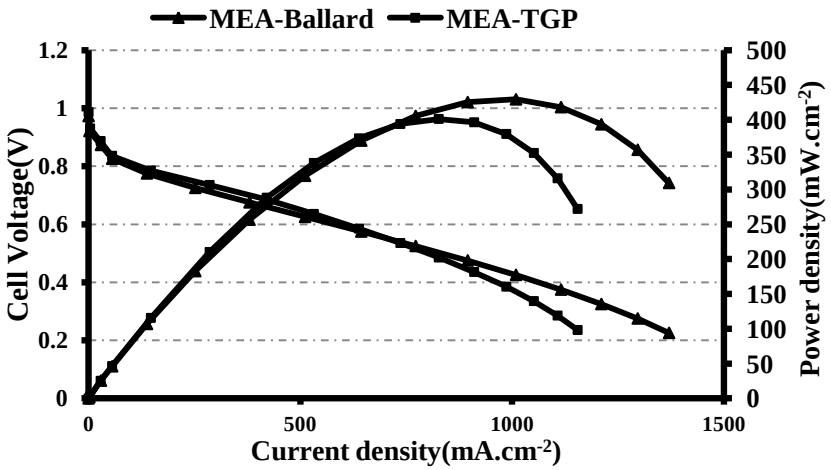

Figure 4: Polarization curve for TGP and Ballard MEAs. T_{cell}: 60°C, Anode RH: fully humidified, Cathode RH: medium humidified

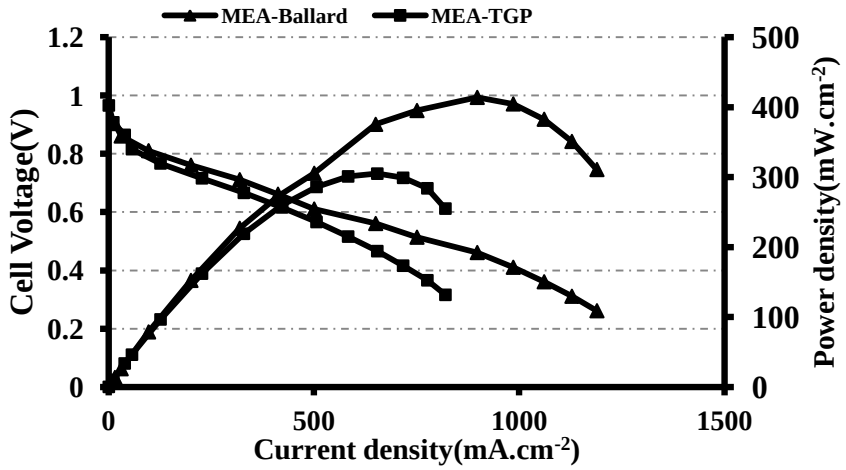

Figure 5: Polarization curve for TGP and Ballard MEAs. T_{cell}: 60°C, Anode RH: fully humidified, Cathode RH: fully humidified

Decrease of performance by increase of cathode RH is more obvious for the MEA made by TGP substrate. This is because of the different microstructure of these substrates. Table 1 shows the physical characteristics of TGP and Ballard substrates.

Table 1: Comparison of physical characteristics of Ballard and TGP carbon paper

Electrode substrate	Thickness (μm)	porosity	Bulk density ($g.cm^{-3}$)
Ballard	200	78%	0.3
TGP	190	78%	0.44

By comparing the values of the bulk density of theses substrates, Ballard substrate pores diameter is larger than the TGP. So by increase of cathode gas RH to 100%, flooding happens earlier for TGP substrate and Ballard substrate has more tolerance to flooding. This structural parameter is more important in higher RH and lower gas pressure.

Conclusion

With performance investigation of two commercial and common electrode substrates, TGP (from Toray) and Ballard carbon paper, we found that Ballard substrate has more performance in higher gas humidity. Ballard substrate pores diameter is larger than the TGP. This causes that the Ballard substrate has more tolerance to flooding. This structural parameter is more important in higher RH and lower gas pressure

References

[1] Shao, Y., Yin, G., Wang, Z., Gao, Y., "Proton exchange membrane fuel cell from low temperature to high temperature□: Material challenges", *Journal of Power Sources*, Vol. 167, pp. 235–242, 2007.

[2] Sasikumar, G., Ihm, J.W., Ryu, H., "Optimum Nafion content in PEM fuel cell electrodes", *Electrochimica Acta*, Vol. 50, pp. 601–605, 2004.

[3] Sasikumar, G., Ihm, J.W., Ryu, H., "Dependence of optimum Nafion content in catalyst layer on platinum loading", *Journal of Power Sources*, Vol. 132, pp. 11–17, 2004.

[4] Escribano, S., Aldebert, P., Pineri, M., "Volumic electrodes of fuel cells with polymer electrolyte membranes□: electrochemical performances and structural analysis by thermoporometry", *Electrochimica Acta*, Vol. 43, pp. 2195–2202, 1998.

[5] Suzuki, T., Tsushima, S., Hirai, S., "Effects of Nafion ionomer and carbon particles on structure formation in a proton-exchange membrane fuel cell catalyst layer fabricated by the decal-transfer method", *International Journal of Hydrogen Energy*, Vol. 36, pp. 12361–12369, 2011.

[6] Gode, P., Jaouen, F., Lindbergh, G., Lundblad, A., et al., "Influence of the composition on the structure and electrochemical characteristics of the PEFC cathode", *Electrochimica Acta*, Vol. 48, pp. 4175–4187, 2003.

[7] Xie, J., More, K.L., Zawodzinski, T.A., Smith, W.H., "Porosimetry of MEAs Made by ‘‘‘ Thin Film Decal ’’’ Method and Its Effect on Performance of PEFCs", *Journal of The Electrochemical Society*, Vol. 151, pp. A1841–A1846, 2004.

8th Iranian Fuel Cell Seminar
FEBRUARY 25,26
2015

Synthesis and Characterization of $PrNiO_3$ Perovskite with Various Ratios of Gelatin as Cathode of Solid Oxide Fuel cell

Bita Roomi*, Ahmad Yazdani
Faculty of Science, Tarbiat Modares University
** bita.roomi@modares.ac.ir*

Abstract
This article focuses on perovskite materials for their application as a cathode material in solid oxide fuel cells(SOFC). Perovskite-type oxides, such as $PrNiO_3$, is one of the material invistigated as a cathode of SOFC. In this study $PrNiO_3$ oxide composition was prepared by using gelatin powder in various ratios of gelatin without using high oxygen pressure and long-time calcination. The obtained powder was calcined at 700℃, 800℃, and 900℃ for 4h and then it was characterized using X-ray diffraction pattern and Fourier Transform Infrared (FTIR) spectroscopy. XRD patterns showed that structure calcined at 900℃ was the best one in tems of the formation of single phase perovskite. FTIR spectra showed that some impurity peaks disappeared whit increasing temperature. A substance which is obtained from this method could create a material ideal for fuel cell applications.

Key words: Solid oxide fuel cell, Peroveskite, Nickel praseodymium oxide

Introduction

The use of Solid Oxide Fuel Cells (SOFCs), which represent the cleanest, most efficient and versatile technologies for chemical-to-electrical energy conversion, could significantly reduce the production of greenhouse gases[1]. Beside the advantages of SOFC such as: internal reforming of the fuel that can increase the efficiency and hence reduces the cost, it has disadvantages like, requiring long-term stability because of its high operating temperatures. So one of the challenge of encountered in commercializing SOFC is to lower its operating temperature [2-4]. Lowering the temperature could lead to a longer lifetime of all components and increase the efficiency (as theory shows) [5, 6]. The cathode is a part of the SOFC system that has to be improved for lowering the operation temperature[5, 7]. Perovskite oxides (like ABO_3) is widely considered as an ideal cathode material for low and intermediate operating temperatures[1, 8]. They have attracted much attention due to their magnetic, electrical, and catalytic properties. These physical properties of perovskite phase materials are related to their phase transitions, which are sensitive to purity, grain size, and sintering conditions [9].

There are several methods for obtaining ceramic oxides with perovskite type structures. Recent studies make use of gelatin as a polymerization agent and this process appears as a new alternative for obtaining materials with high efficiency and low cost [10]. gelatin is used to synthesis compounds without using high oxygen pressure and long-time calcination and a substance obtain from this method creates a porous material[10, 11]. This complex porous structure is ideal for fuel cell applications, as it allows the gaseous fuel and oxygen to flow freely. The material showed good catalytic activity for the oxygen reduction reaction, which is

crucial for fuel cells. As previous works showed $PrNiO_3$ powder is synthesis under condition of long- time calcinations and high oxygen pressure [12-14]. In this study, $PrNiO_3$ was synthesized with gelatin without long- time calcination and oxygen pressure and it was characterized by XRD and FTIR.

Experimental

$PrNiO_3$ powder was synthesized by modified Pechini method using gelatin. The starting materials used to prepare the powder were nickel nitrate(II) hexahydrate ($Ni(NO)_2.6H_2O$,Merck,99%) Praseodymium (III) nitrate pentahydrate ($Pr(NO_3)_3.5H_2O$, Acros, 99.99%), deionized water and commercial gelatin. Nickel nitrate was added to deionized water under constant stirring at 60℃ for 5 min. Praseodymium (III) nitrate hexahydrate was added and the system was homogenized for another 5 min. Gelatin was then added to the solution at 70℃ and stirred about 40 min until it became homogenized. Next, the temperature was increased to 90℃ until it became a resin. After being heat-treated at 350℃ for 2h, the primary composite oxide was calcined at 700 ℃ and for comparison, one of the samples was calcined at 900℃[10]. The mass ratios of gelatin to metal and the grades of gelatin are listed in table 1.

Structural characterization of powder was performed by using a Phillips X-Ray diffractometer using Cu Kα radiation,and the diffraction angles (2θ) were scanned in a range varying between 20° and 90°. Fourier transform infrared absorption spectroscopy (FTIR) was carried out using KBr pellets. The instrument scanned in the range of 4500–400 cm^{-1}.

Table 1 Grade of gelatin and mass ratios of metal/gelatin

Sample	Grade Of Gelatin	Metal:Gelatin Ratio
(a)	Edible	1:2
(b)	Edible	1:3
(c)	Drug	1:3
(d)	Edible-Drug	1:3

Results and Discussion

As Figure 1 shows, sample (a) with its lower metal/gelatin ratio of 1:2 indicated the main $PrNiO_3$ peak along with some secondary phases such as NiO,and Pr_6O_{11}.These results show that the smaller content of gelatin used in the synthesis lead to more secondary phases peaks. The sample (b) with the metal/collagen ratio of 1:3 showed main $PrNiO_3$ peak as well as the high intensity peak related to Pr_6o_{11}. XRD pattern of sample (c) showed similar peaks as (b) with secondary phases attributed to NiO and Pr_6O_{11}. In addition for sample (d) with metal/drug-grade gelatin ratio of 1:3 at700℃, XRD showed main peaks of $PrNiO_3$ and secondary phases of Pr_6O_{11} and NiO . Crystallite size and crystallinity values were calculated by using Deby - Scherrer equation and are listed in Table 1.

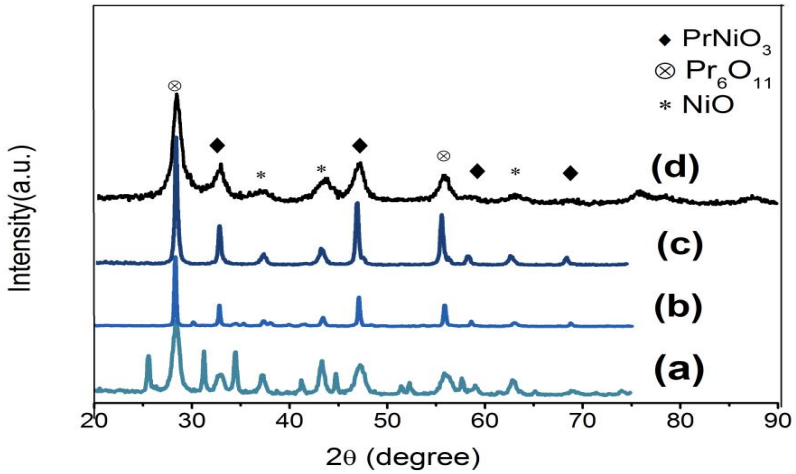

Figure 1 XRD patterns of PrNiO3 perovskite with metal:gelatin ratios of (a) 1:2(edible gelatin), (b) 1:3 (edible gelatin), (c) 1:3 (drug grade gelatin), and (d) 1:3 (edible-drug grade gelatin).

Table 2 Crystallite size and crystallinity of samples.

Sample	Crystallite Size(nm)	Crystallinity (%)
(a)	26	73
(b)	42	76
(c)	28	85
(d)	16	58

Since all samples showed secondary phases, for comparison, calcination temperature of sample(d) was increased to 800℃ and 900℃. In fig 2, XRD pattern showed similar secondary phases at 800℃ while it is the best one in terms of formation of single phase perovskite at 900℃, the peaks related to the secondary phases disappeared with increasing calcination temperature, and perovskite peaks were attributed to orthorombic structure (JSPDS 41-0473). The crystallite size is calculated about 30 nm and 53 nm at 800℃ and 900℃ , respectively.

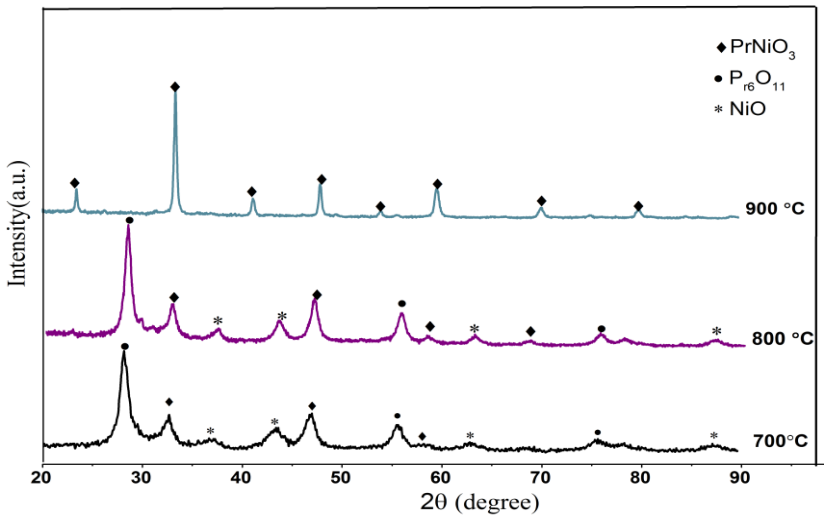

Figure 2 XRD pattern of PrNiO3 at 700°C, 800°C ,and 900°C

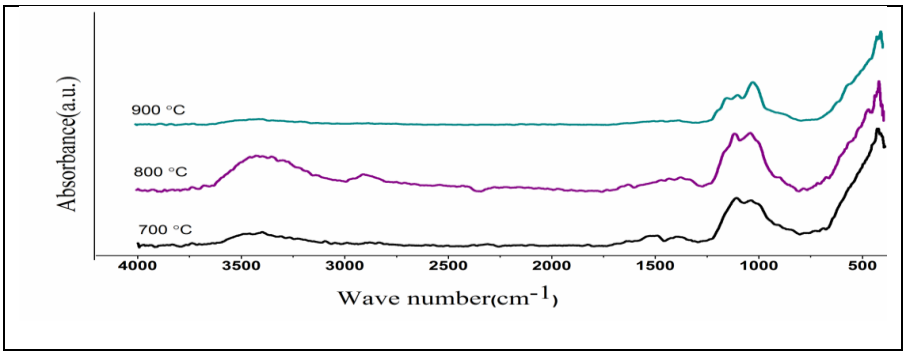

Figure 3 FTIR spectra of PrNiO3 at at 700°C, 800°C ,and 900°C

Figure 3 shows FTIR spectra in the infrared region for the $PrNiO_3$ calcined at 700°C , 800°C, and 900°C. A broad band appearing in the range 3500–3000 cm^{-1} at 700°C and 800°C may be attributed to the O-H stretching vibration of water molecules and disappear at 900°C . The bands over 1500–1400 cm^{-1} is related to the C-H bonds disappear as the temperature increases. The absorption bands below 650 cm^{-1}, are attributable to Ni–O stretching and O–Ni–O deformation in the $PrNiO_3$ perovskite[15, 16]

Conclusions

The obtained results demonstrated that gelatin is an efficient agent to be used in the synthesis of ceramic powders. All samples showed some secondary phases, exception is the sample prepared whit drug-grade gelatin with metal/gelatin ratio of 1:3 at 900°C that formed a single phase material. These facts confirm that oxides with $PrNiO_3$ perovskite-type structure can be obtained by using gelatin at low temperatures without any oxygen pressure, which is a low-cost, organic material and very good chelating agent in the formation of $PrNiO_3$ perovskite structure with nanometric crystallite size. FTIR spectra for the samples calcined at different temperature showed the impurity disappears as the temperature increase.

References

[1] Burnwal, S.K.“ Crystal Structure and Ionic Conductivity Study of Ni- Doped BSCF Cathode for Low Temperature SOFCS”,J. of Industrial Engineering and Management Science, (2013),3(1),20-23.

[2] Ormerod, R.M.“ Solid oxide fuel cells”,J.Chemical Society Reviews”, (2003), 32(1), 17-28

[3] Ishihara, T.“ Perovskite oxide for solid oxide fuel cells”, Springer, (2009).

[4] EG&G technical services. Handbook of Fuel cell,Inc, (2004).

[5] Wackerl, J., et al.“ Correlation of thermal properties and electrical conductivity of $La_{0.7}$ $Sr_{0.3}$ $Cu_{0.2}$ $Fe_{0.8}O_{3-\delta}$ material for solid oxide fuel cells”,J.of Applied Electrochemistry, (2009). 39(8), 1243-1249.

[6] Wachsman, E.D. and K.T. Lee“ Lowering the temperature of solid oxide fuel cells”J. of Science, (2011), 334(6058), 935-939.

[7] Ullmann, H., et al.“Correlation between thermal expansion and oxide ion transport in mixed conducting perovskite-type oxides for SOFC cathodes. Solid State Ionics”, (2000), 138(1), 79-90.

[8] Richter, J., et al.“ Materials design for perovskite SOFC cathodes. Monatshefte für Chemie-Chemical Monthly”, (2009), 140(9), 985-999.

[9] Mao, Y., H. Zhou, and S.S. Wong “Synthesis, Properties, and Applications of Perovskite-Phase Metal Oxide Nanostructure”,J.of Materials Matters, (2010), 5(50), 1-8.

[10] Aquino, F., et al.“Characterization and thermal behavior of $PrMO_3$ (M= Co or Ni) ceramic materials obtained from gelatin”,J. of Materials Research Bulletin, (2012),47(9), 2605-2609.

[11] Oliveira, R., et al. “Microstructural Study of Neodmium Nickelate Doped with Strontium Synthesized by Gelatin Method”. Advances in Materials Science and Engineering, (2013), 2013,1-5.

[12] Lacorre, P., et al.“ Synthesis, crystal structure, and properties of metallic $PrNiO_3$: Comparison with metallic $NdNiO_3$ and semiconducting $SmNiO_3$ ” , J.of Solid State Chemistry, (1991), 91(2), 225-237.

[13] Jaramillo, R., et al.“Origins of bad-metal conductivity and the insulator-metal transition in the rare - earth nickelates”,J. of Nature Physics, (2014). 10(4), 304-307.

[14] Huang, T., et al.“ High-temperature crystal structures of orthorhombic and rhombohedral $PrNiO_3$”,J. of Materials research bulletin, (1990), 25(9), 1091-1098.

[15] Rida, K., et al.“ Effect of calcination temperature on structural properties and catalytic activity in oxidation reactions of $LaNiO_3$ perovskite prepared by Pechini method“, J. of Rare Earths, (2012), 30(3),210-216.

[16] Arockiam, S.I., A.P.P. Regis, and L.J. Berchmans “Synthesis and Characterisation of Nano crystalline Cerium Nickelate (CeNiO3) Powders using Low Temperature Molten Salt Technique. Synthesis”,J. of of ChemTech Research, (2012), 4(2),798-804.

8th Iranian Fuel Cell Seminar
FEBRUARY 25,26
2015

Facile Synthesis of Pd/MWCNT Nanocomposite for Ethanol Fuel Cell

Biuck Habibi*, Soheila Mohammadyari
Electroanalytical Chemistry Laboratory, Faculty of Sciences, Department of Chemistry, Azarbaijan Shahid Madani University, Tabriz, Iran

* *B.Habibi@azaruniv.edu*

Abstract
Pd nanoparticles supported on multi wall carbon nanotube (MWCNT) nanocomposite is prepared by direct deposition method without using any reducing agent. Obtained nanocatalyst (PdNPs/MWCNT) was decorated on the carbon ceramic electrode (CCE) and used as electro catalyst (PdNPs/MWCNT/CCE) for ethanol oxidation in alkaline media. The PdNPs/MWCNT was characterized with X-ray diffraction (XRD), Scanning electron microscopy (SEM) and Energy-dispersive X-ray spectroscopy (EDX) to describe its crystal phases, nanostructure properties and composition. Electrochemical characterization techniques, including cycling voltammetry (CV) and chronoamperometry were used to analyze electrochemical performance of PdNPs/MWCNT/CCE. The obtained results show that the fabricated electrode has satisfactory stability and reproducibility for electrooxidation of ethanol when stored in ambient conditions or continues cycling making it more active for fuel cell applications.

Keywords: Pd nanoparticle, Multi wall carbon nanotube, Carbon ceramic, Ethanol fuel cell

1. Introduction

Direct ethanol fuel cells (DEFCs) are suitable alternative power sources for portable devices and vehicles [1-3]. Liquid fuels such as low molecular weight alcohols compared to pure hydrogen have more advantages, because they have high mass energy density and can be handled, transferred and stored easily. Development of highly efficient electrocatalyst is one of the key steps in the fabrication of fuel cells. Metal platinum (Pt) and palladium (Pd) have been used as electrocatalysts in fuel cells. These two metals are very similar in several properties, but Pd is a better electrocatalyst in direct ethanol fuel cell. Pd nanoparticles are a favorable catalyst in DEFC due to low cost, high catalytic activity and stronger resistance to CO poisoning [4-6]. To decrease the use level of Pd nanoparticles and increase the electrocatalytic activity, the nanoparticles are dispersed by various supports. Carbon materials with several shape and structure, such as carbon black [7], carbon nano fibers [8], mesoporous carbon [9] and carbon nano tubes [10], have been used as support for metal catalysts and can improve the catalytic performance. Carbon supports have low weight, high specific surface area, conductivity and stability. Carbon nanotubes (CNTs) play key role as support of Pd catalyst in fuel cells [11]. In most studies, Pd nanoparticles are chemically deposited on carbon supports via reducing agent. In this study, we synthesized new Pd electrocatalyst deposited on MWCNT support without using any reducing agent. The PdNPs/MWCNT is decorated on CCE and then the PdNPs/MWCNT/CCE electrocatalyst is used in oxidation of ethanol at basic media.

2. Experimental

2.1. Materials

Methyltrimethoxysilane(MTMOS) and palladium chloride were from Sigma Aldrich. Sodium hydroxide, graphite powder, nitric acid, sulfuric acid and ethanol were purchased from Merck, and MWCNT was purchased from US Research Nanomaterials. All solutions were freshly prepared with distilled water.

2.2. Preparation of PdNPs/MWCNT/CCE electrocatalyst

CCE which was used as substrate for supported composite electrocatalyst was fabricated by sol-gel technique according to the following procedure: 0.9 ml MTMOS was mixed with 0.6 ml methanol and 0.6 ml of 0.l M HCl. The mixture was stirred to form clear and homogeneous solution. 0.3 g graphite powder was added to solution and stirred for another 5 min. Then the homogeneous mixture was packed in a Teflon tube (with 3 mm inner diameter and 10 mm length) and dried for at least 24 h at room temperature. To set up an electronic contact, a copper wire was inserted through the end of prepared electrode.

The preparation of PdNPs/MWCNT composite can be describe as follows: MWCNT was functionalized under reflux condition in a boiling solution of mixed acids (H_2SO_4: HNO_3, 1:3, v/v ratio) for 8 h, and then washed with deionized water and dried at 60˚C under vacuum for 10 h. The 40 mg of functionalized MWCNT was dispersed in 100 ml ethanol/water (1:1, v/v ratio) and sonicated for 1h to form a uniform suspension. $PdCl_2$ solution (10 mg of $PdCl_2$ in 5ml water) was added to the suspension dropwise. The suspension was stirred for 5 h to deposit and reduce Pd nanoparticles on support. Then, the suspension was filtered and obtained black solid was washed with deionized water and dried in oven at 70˚ C.

For preparation of the composite modified electrode, CCE was polished with emery paper grade 1500. To load supported electrocatalyst on the CCE, it is necessary to prepare catalyst ink. For preparation of electrocatalyst ink, 5 mg of PdNPS/MWCNT sample was added into 1 ml ethanol. The mixture was ultrasonically dispersed for 1 h to obtain homogeneous ink. Next, 50 µl of ink was uniformly dispersed onto freshly polished CCE and was dried under ambient condition.

2.3. Instrumentation

The electrochemical experiments were carried out using a SAMA (SAMA Co. Iran) instrument (potentiostat/galvanostat) equipped with a USB electrochemical interface. A conventional three electrode cell was used at room temperature: A disc of PdNPs/MWCNT/CCE (with a geometrical surface area of 0.070 cm^2) was used as working electrode, an Ag/AgCl electrode and a platinum wire were used as the reference and auxiliary electrodes, respectively. A LEO1430 vp (Carl Zeiss, Germany) scanning electron microscope (SEM) was used to surfaces and morphology characterization of the PdNPs/MWCNT/CCE. X-ray diffraction (XRD) pattern was recorded with a Bruker AXS model D_8 Advance (Karlsruhe, Germany) instrument with Cu-K_α radiation source (1.54 Å) at 40 kV and 35 mA at room temperature. The 2θ angular regions between 5 and 90 were explored at a scan rate of 5 min^{-1}.

3. Result and discussion

3.1. Catalysts characterization by XRD, SEM and EDX

XRD pattern of PdNPs/MWCNT is shown in Figure 1. In XRD pattern, the first peak, which is located at a 2θ value of ca.26˚, is associated with the graphite plane (002) of MWCNT [12]. In PdNPs/MWCNT XRD pattern there are five characteristic peaks assigned to the face center cubic (fcc) crystalline Pd, corresponding with the planes (111), (200), (220), (311) and (222) at ca.40˚, 47˚, 68˚, 82˚ and 86˚ respectively. The results indicate that the Pd nanoparticles on the surface of MWCNT were metallic state crystals. The average size of Pd nanoparticles was calculated by Deby-Scherrer formula (Eq. (1)) [13].

For calculation of Pd nanoparticles size, the (200) reflection of the Pd face center cubic structure around 2θ=47˚ was used.

$$L=\frac{0.9\,\lambda_{cuk}}{B_{2\theta}\,\cos\theta_{max}} \quad (1)$$

In the Eq. (1), L is the average of particle size, λ_{cuk} is the x-ray wavelength, $B_{2\theta}$ is the full width at half maximum and θ_{max} is the angle of peak maximum. The calculated average particle size for PdNPs/MWCNT is 10 nm.

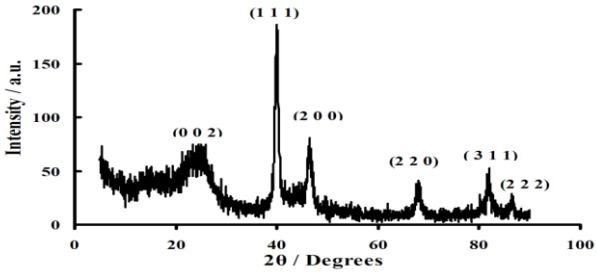

Figure 1. XRD pattern of PdNPs/MWCNT catalyst

SEM analysis was employed to investigate the morphology of PdNPs/MWCNT. Figure 2 (A) shows the typical SEM image of the prepared catalyst. The image shows that the structure attached on the MWCNT has compact and granulated shape. The spots are believed to be Pd nanoparticles sitting on the MWCNT surface. The EDX spectrum of PdNPs/ MWCNT is shown in Figure 2 (B). Three main peaks assigned to C, O and Pd, confirming the existence of Pd nanoparticles in prepared catalyst. It should be noted that, O atoms derived from functional group such as hydroxyl, carboxyl and carbonyl group form on outer walls of the MWCNT during functionalization.

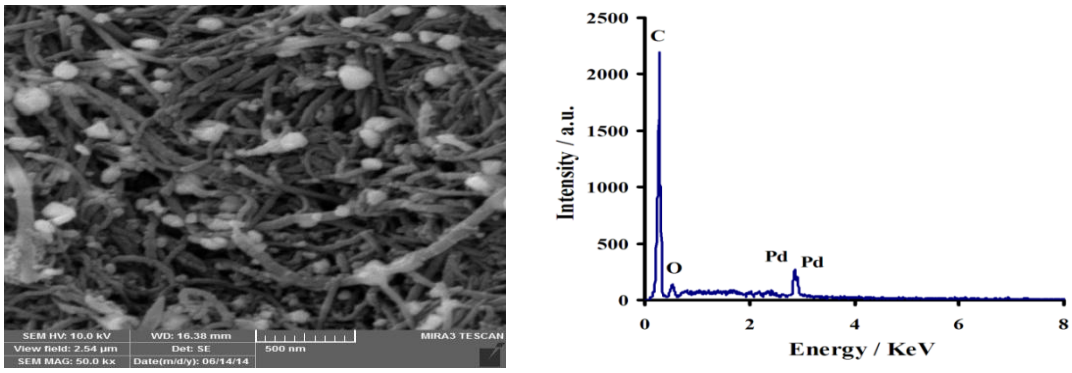

Figure 2. A: SEM image of PdNPs/MWCNT catalyst and B: EDX analysis of PdNPs/MWCNT catalyst.

3.2. Electrocatalytic activity of PdNPs/MWCNT/CCE toward the oxidation of ethanol

The ethanol oxidation reaction on PdNPs/MWCNT/CCE was examined by cyclic voltammetry measurements in alkaline medium. The CVs of PdNPs/MWCNT/CCE was investigated in 0.5 M NaOH solution (inset of Figure 3). In negative scanning, a well-defined peak at -0.5 V is ascribed to reduction peak of the higher valance Pd oxide. The electrochemical active surface area (EASA) of catalyst was calculated by the columbic charge for the reduction of Pd oxide [14], which was observed at the potential region of -0.6 V to -0.4 V [15]. The EASA is estimated using Eq. (2):

$$EASA= Q/Sl \quad (2)$$

Where "*S*" is the proportionality constant used to relate charge with area and "l" is the catalyst loading in "g". The charge required for the reduction of PdO monolayer is assumed as $405 \mu C\, cm^{-2}$ [16]. The EASA based on the columbic charge is $38.7 cm^2$ for PdNPs/MWCNT/CCE.

Figure 3 shows the electrooxidation of 0.5 M ethanol in 0.5 M NaOH on bare CCE (a), MWCNT/CCE (b) and PdNPs/MWCNT/CCE (c). No oxidation peaks are seen in bare CCE and MWCNT/CCE in the potential window used, indicating that nanocarbonic supports are not capable of favoring the oxidation of ethanol. Two oxidation peaks are observed in CV curve corresponding to PdNPs/MWCNT/CCE. The oxidation peak in forward scan is assigned to the oxidation of chemisorbed species coming from adsorbed ethanol. The oxidation peak in backward scanning is associated with removal of carbonaceous species, which are not completely oxidized in the forward scan, rather than chemisorbed species [17].

The electrocatalytic activity of the prepared electrocatalyst for ethanol oxidation can be survived by magnitude of the peak current in forward scan, the ratio of the forward oxidation peak current density (I_f) to backward oxidation peak current density (I_b), (I_f/I_b) is used to determine the tolerance of prepared electrocatalyst to carbonaceous intermediates accumulated on electrode surface [18]. The carbonaceous intermediates generated during ethanol oxidation and adsorb strongly on the surface of Pd [19]. These intermediates can react with OH^- and/or OH_{ads}, which cause to production of CO_2 and reduction of Pd active sites. The higher ratio of I_f/I_b shows the more efficient oxidation of ethanol during the forward scan and less accumulation of carbonaceous residues on the electrode surface. Based on the results in Figure 3, I_f/I_b amount is calculated to be 1.42 for PdNPs/MWCNT/CCE.

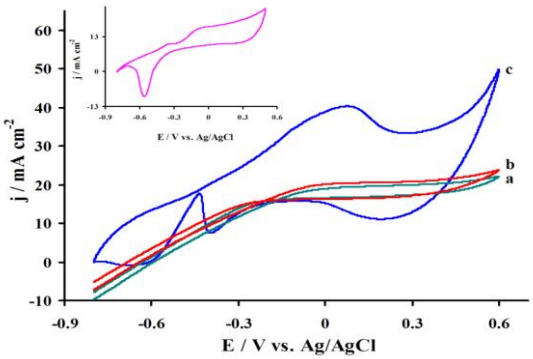

Figure 3. CV curves of ethanol oxidation on bare CCE (curve a), MWCNT/CCE (curve b) and PdNPs/MWCNT/CCE (curve c) in 0.5 M NaOH + 0.5 M ethanol solution. Inset: CV of PdNPs/MWCNT/CCE in 0.5 M NaOH at scan rate of 50 mV s^{-1}.

3.3. Study of various parameter effects on ethanol oxidation

3.3.1. Influence of upper limit potential

By using different ranges of potentials, which formation and dissolution of surface oxide occurs on the electrode, can study the electrochemical behavior of electrodes [20,21]. In order to survey the correlation between ethanol oxidation and Pd oxide species on PdNPs/MWCNT/CCE, the influence of upper limit potential in cyclic potential scanning investigated. Figure 4 shows the ethanol oxidation on PdNPs/MWCNT/CCE for upper limit oxidation of 0.4-0.7 V. As shown in this figure, the anodic current of ethanol oxidation in the positive scanning remains unchanged while anodic peak current density in negative scanning is decreased as increasing the final positive potential limit (Figure 4 inset A). It can be described that in lower potential, the Pd oxides with high valance haven't developed greatly and the effect of these oxides species on ethanol oxidation in backward scanning is approximately small. In addition, by increasing final positive potential limit, the potential of ethanol oxidation peak in positive scanning remains constant while the potential of ethanol oxidation peak in backward scanning shifts negatively (Figure 4 inset B). Increase of final positive potential limit causes to accelerate of Pd to Pd oxides therefore oxidation current is decreased in negative scanning. This demonstrates that ethanol can be oxidized on clean metallic Pd nanoparticles surface [22].

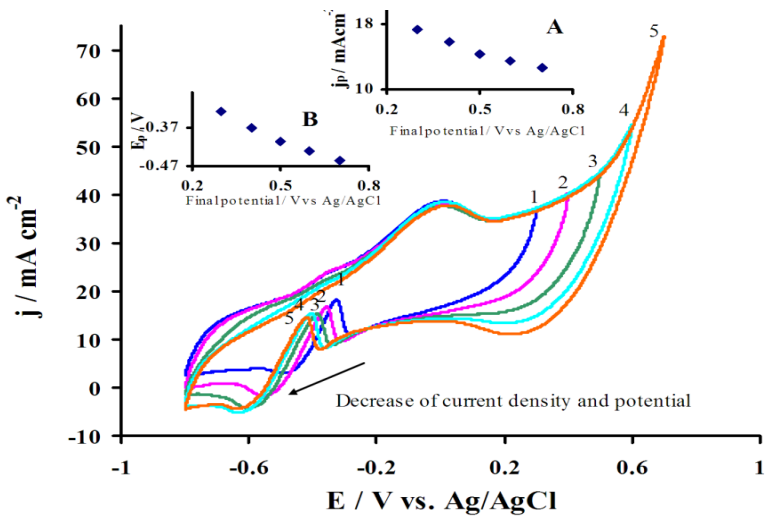

Figure 4. Effect of upper limit potential scanning region on the electrooxidation of 0.5 M ethanol in 0.5 M NaOH on PdNPs/MWCNT/CCE. (1) -0.8-0.3 V (2) -0.8-0.4 V (3) -0.8-0.5 V (4) -0.8-0.6 V (5) -0.8-0.7 V. Scan rate of 50 mv s^{-1}. The insets are anodic peak current (A) and anodic peak potential (B) in the backward scan against limit of final potential.

3.3.2. Effect of scan rate

Investigation of ethanol oxidation for kinetic characterization on PdNPs/MWCNT/CCE can be carried out by study of scan rate effect on ethanol oxidation behavior. CVs of ethanol oxidation on PdNPs/MWCNT/CCE at different scan rates are shown in Figure 5. The results show that the anodic peak current density related to ethanol oxidation in positive scanning increases linearly. The anodic peak current density in positive scan as a function of the square root scan rate are shown in inset A (Figure 6) and it can be resulted that the electrocatalytic reaction is controlled by diffusion [23,24]. In addition the CV curves show that the potential of oxidation peaks vary

with increasing of scan rate. On the other hand, potential of anodic peak in positive scan shifts to positive by increasing the scan rate. There is a linearly relationship between E_p and Log (υ) rate (Figure 5 insets B) which indicates that the oxidation of ethanol is an irreversible electrochemical process [25].

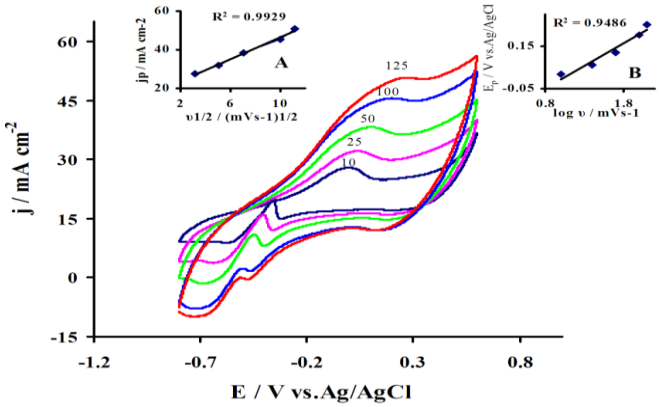

Figure 5. Effect of scan rate on 0.5 M ethanol electrooxidation obtained in 0.5 M NaOH on PdNPs/MWCNT/CCE. Cyclic voltammograms show scan rates. The insets are (A) relationship between forward anodic peak current and square root of scan rates, (B) relationship between forward anodic peak potential and logarithm of scan rates.

3.4. Chronoamperometric study for ethanol oxidation

For more evaluation the activity and stability of PdNPs/MWCNT/CCE catalyst, chronoamperometry tests were conducted in 0.5 M NaOH and 0.5 M ethanol at -0.2 V for 2000 s (Figure 6). As shown in Figure 6, the oxidation current decreases quickly at short times and the decay rate becomes low and low at longer times on composite modified electrode. It can be observed that the current density at 2000 s was 38.7 $mAcm^{-2}$. These results indicate that the current shows less decay on electrocatalyst in ethanol for a long duration. In addition, PdNPs/MWCNT/CCE exhibits a steady-state electrolysis activity for ethanol oxidation [26].

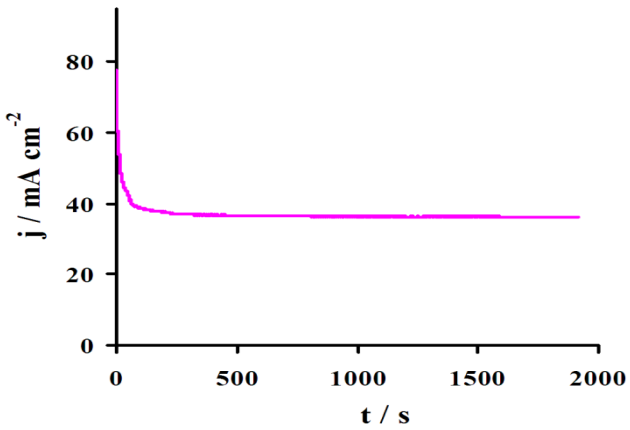

Figure 6. Chronoamperometry curve of PdNPs/MWCNT/CCE in 0.5 M ethanol containing 0.5 M NaOH solution at -0.2 V.

4. Conclusion

Herein, we synthesized an efficient electrocatalyst, i.e., Pd nanoparticles supported on nanostructured functionalized MWCNT (PdNPs/MWCNT/CCE), for ethanol electrooxidation. Physical and electrochemical characterization of the prepared composite electrocatalyst was investigated by XRD, SEM, EDX and electrochemical techniques. The Pd nanoparticles size obtained by this synthesis procedure were around 10 nm and exhibit high catalytic activity toward ethanol electrooxidation. The effect of some factors such as limit of the final potential and scan rate which influence significantly the anodic current density of ethanol oxidation on the PdNPs/MWCNT/CCE was investigated. The present interesting nano-structured electrocatalyst exhibits good and satisfactory stability and reproducibility when stored in ambient conditions and offers potential possibilities of application as an electrocatalyst composite in direct ethanol fuel cells.

Acknowledgment

The authors gratefully acknowledge the research council of Azarbaijan Shahid Madani University for financial support.

References:

[1] U.B.Demirci "Direct liquid-feed fuel cells: thermodynamic and environmental concerns", J. of Power Sources, (2007). 169, 239-246.

[2] L.Huanqiao, S.Gongquan, C.Lei, J.Luhua and X.Qin "Comparison of different promotion effect of PtRu/C and PtSn/C electrocatalysts for ethanol electro-oxidation", Electrochim. Acta, (2007). 52, 6622-6629.

[3] S.Beyhan, J.M.Leger, F.Kadırgan "Pronounced synergetic effect of the nano-sized PtSnNi/C catalyst for ethanol oxidation in direct ethanol fuel cell", Appl. Catal. B-Environ, (2013), 130-131, 305– 313

[4] H.An, L.Pan, H.Cui, B.Li, D.Zhou, J.Zhai and Q.Li "Synthesis and performance of palladium-based catalysts for methanol and ethanol oxidation in alkaline fuel cells", Electrochim. Acta, (2013). 102, 79-87.

[5] C.Xu, L.Cheng, P.K.Shen and Y.Liu "Methanol and ethanol electrooxidation on Pt and Pd supported on carbon microspheres in alkaline media", Electrochem. Commun, (2007). 9, 997-1001.

[6] C.Bianchini and P.K.Shen "Palladium-based electrocatalysts for alcohol oxidation in half cells and in direct alcohol fuel cells", Chem. Rev, (2009).109, 4183 – 4206.

[7] E.Higuchi, K.Miyata, T.Takase and H.Inoue "Ethanol oxidation reaction activity of highly dispersed Pt/SnO2 double nanoparticles on carbon black", J. of Power Sources, (2011). 196, 1730-1737.

[8] T.Maiyalagan and K.Scott "Performance of carbon nanofiber supported Pd-Ni catalysts for electro-oxidation of ethanol in alkaline medium", J. of Power Sources, (2010). 195, 5246-5251.

[9] Z.Yan, H.Meng, L.Shi, Z.Li and P.K.Shen "Synthesis of mesoporous hollow carbon hemispheres as highly efficient Pd electrocatalyst support for ethanol oxidation", Electrochem. Commun, (2010). 12, 689-692.

[10] Z.Xu, J.Lin, V.A.L.Roy, Y.Ou and D.Liao "Catalytic synthesis of carbon nanotubes and carbon spheres using Kaolin supported catalyst" Mater. Sci. Eng. B, (2005). 123, 102-106.

[11] Y.C.Zhao, S.L.Nie, H.W.Wang, J.N.A.Tian, Z.Ning and X.X.Li "Direct synthesis of palladium nanoparticles on Mn_3O_4 modified multi-walled carbon nanotubes: a highly active

catalyst for methanol electro-oxidation in alkaline media", J. of Power Sources (2012). 218, 320-325.
[12] C.Hu, Z.Bai, L.Yang, J.Lv, K.Wang, Y.Guo, Y.Cao and J.Zhou "Preparation of high performance Pd catalysts supported on untreated multi-walled carbon nanotubes for formic acid oxidation". Electrochim. Acta, (2010). 55, 6036-6041.
[13] A.B.Kashyout, A.B.A.Nassr, L.Giorgi, T.Maiyalagan and B.A.B.Youssef "Electrooxidation of methanol on carbon supported Pt-Ru nanocatalysts prepared by ethanol reduction method", Int. J. Electrochem. SC., (2006). 6, 379-386.
[14] R.N.Singh, A.Singh and Anindita "Electrocatalytic activity of binary and ternary composite films of Pd, MWCNT, and Ni, Part II; Methanol electrooxidation in 1 M KOH", Int. J. Hydrogen. Energ., (2009). 34, 2052-2057.
[15] R.N.Singh and R.Awasthi "Graphene support for enhanced electrocatalytic activity of Pd for alcohol oxidation", Catal. Sci. Technol., (2011). 1, 778-783.
[16] Anindita, R.A.wasthi, Madhu and R.N.Singh "Preparation of nanostructured Pd-C-Ru composite electrodes for alcohol electrooxidations. part-II: a study of methanol oxidation by cyclic voltammetry and impedance spectroscopy" T. O. Cat. J ., (2011). 4, 100-106.
[17] K.Ding, G.Yang, S.Wei, P.Mavinakuli and Z.Guo "Cyclic voltammetric preparation of palladium nanoparticles for ethanol oxidation reaction", Ind. Eng. Chem. Res., (2010). 49, 11415–11420.
[18] H.Li, D.Kang, H.Wang and R.Wang "Carbon-supported Pt-RuCo nanoparticles with low-noble metal content and superior catalysis for ethanol oxidization", Int. J. Electrochem. Sci., (2011). 6, 1058 – 1065.
[19] S.Du and Y.Lu "Steinberger-Wilckens R. PtPd nanowire arrays supported on reduced graphene oxide as advanced electrocatalysts for methanol oxidation", Carbon, (2014). 79, 346-353.
[20] R.Pattabiraman "Electrochemical investigations on carbon supported palladium catalysts", Appl. Catal. A-Gen., (1997). 153, 9-20.
[21] S.P.E.Smith, E.C.Rivera and H.D.Abruña "Application of differential electrochemical mass spectrometry to the electrocatalytic oxidation of formic acid at a modified Bi/Pt electrode surface", J. Solid. State. Electrochem., (2003). 7, 582–587.
[22] B.Habibi and N.Delnavaz "Electrocatalytic oxidation of formic acid and formaldehyde on platinum nanoparticles decorated carbon-ceramic substrate" Int. J. Hydrogen. Energ., (2010). 35, 8831-8840.
[23] V.Bambagioni, C.Bianchini, A.Marchionni, J.Filippi, F.Vizza, J.Teddy, P.Serp and M.Zhiani "Pd and Pt–Ru anode electrocatalysts supported on multi-walled carbon nanotubes and their use in passive and active direct alcohol fuel cells with an anion-exchange membrane (alcohol =methanol, ethanol, glycerol)" J. of Power Sources, (2009). 190, 241–251.
[24] A.Nozad Golikand, M.Ghannadi Maragheh, S.Sedaghat Sherehjini, K.M.Taghi-Ganji, and M.Yari "Carbon-supported Pt particles as a catalyst for electrooxidation of methanol and cyclic voltammetry studies under acidic conditions", Electroanalysis, (2006). 9, 911-918.
[25] S.Yang, X.Zhang, H.Mi and X.Ye "Pd nanoparticles supported on functionalized multi-wall carbon nanotubes (MWCNTs) and electrooxidation for formic acid" J. of Power Sources, (2008). 175, 26-32.
[26] P.C.Su, H.S.Chen, T.Y.Chen, C.W.Liu, C.H.Lee, J.F.Lee, T.S.Chan and K.W.Wang "Enhancement of electrochemical properties of Pd/C catalysts toward ethanol oxidation reaction in alkaline solution through Ni and Au alloying" Int. J. Hydrogen. Energ., (2013). 38, 4474-4482.

8th Iranian Fuel Cell Seminar
FEBRUARY 25,26
2015

Investigation of Ethylene Glycol Electrooxidation on Fe_3O_4@Pt Core-Shell Nanoparticles Decorated Carbon-Ceramic Substrate

Biuck Habibi*, Serveh Ghaderi
Electroanalytical Chemistry Laboratory, Department of Chemistry, Faculty of Sciences, Azarbaijan Shahid Madani University, Tabriz
** B.Habibi@azaruniv.edu*

Abstract
In this work, a simple and efficient synthesis method is used to fabricate Fe_3O_4@Pt core-shell nanoparticles. The obtained catalyst is characterized by X-ray diffraction, scanning electron microscopy, energy-dispersive X-ray spectroscopy and transmission electron microscopy. The results show that the size of the Fe_3O_4@Pt nanoparticles, which are uniformly dispersed on carbon-ceramic, are 20-40 nm in diameters. The electrooxidation of the ethylene glycol reaction was studied on Fe_3O_4@Pt core-shell nanoparticles decorated carbon-ceramic substrate by cyclic voltammetry in NaOH solution. The obtained results indicate that the system studied in the present work is the most promising system for use in direct ethylene glycol fuel cells.

Keywords: Fe_3O_4@Pt nanoparticles, Core-shell, Electrooxidation, Ethylene glycol, Fuel cell.

1. Introduction

Direct alcohol fuel cells (DAFCs) are considered as a highly promising future power source due to their high-energy conversion efficiency, low pollutant emission, low operating temperature and economy [1]. As an appealing candidate for fuel cell applications, ethylene glycol has attracted much attention because of its low toxicity, low membrane penetration, while high boiling point and high energy density [2, 3]. The research on the electrochemical kinetics and reaction mechanism shows that the electrooxidation reaction of ethylene glycol displays high activity in alkaline medium and the recent development in alkaline solid membrane electrolyte gives a great potential of using ethylene glycol as a fuel in alkaline fuel cells [4].

It is well-known that platinum nanoparticles are important electrochemical catalysts for proton exchange membrane fuel cells (PEMFCs). However, several drawbacks must be addressed before such catalysts can be commercial applications. The main drawback is the high cost and the scarcity of Pt [5]. In recent years the search for increased activity and reduced catalyst costs has led to intensified research on nanoparticles and especially on core-shell structures. If the particles are stable under working conditions, the advantage is that small particles offer favorable surface-to-volume ratios and hence increased efficiency. On the other hand, core-shell particles with less noble metals in the core are not only more cost-effective but also exhibit superior activity compared to standard Pt systems [6].

In this work, a simple and efficient route to prepare Fe_3O_4@Pt core-shell nanoparticles decorated on carbon-ceramic substrate is demonstrated. The electrocatalytic performance of Fe_3O_4@Pt nanoparticles towards ethylene glycol oxidation was investigated, compared with Pt-alone nanoparticles.

2. Experimental

2.1. Chemicals

$H_2PtCl_6.5H_2O$, $Fe(NO_3)_3.9H_2O$, $NaBH_4$, ethylene glycol and NaOH were obtained from Merck. All solutions were freshly prepared with distilled water.

2.2. Instrumentation

The electrochemical measurements were carried out using an AUTOLAB PGSTAT-100 (potentiostat/galvanostat). A conventional three-electrode system was used accompanied by Carbon ceramic electrode (CCE) with a supported catalyst layer (Pt and Fe_3O_4@Pt nanoparticles) as a working electrode, a platinum wire as an auxiliary electrode, and a saturated calomel electrode (SCE) as a reference electrode. The catalysts were characterized by recording their XRD patterns on a Bruker AXS model D_8 Advance (Karlsruhe, Germany) instrument with Cu-K_α radiation source (1.54 Å) at 40 kV and 35 mA. Scanning electron microscope (SEM) was performed on a LEO1430 vp (Carl Zeiss, Germany) instrument. Transmission electron microscopy (TEM) measurement was carried out on a Carl Zeiss 906 E (Cottingen, Germany) microscope.

2.3. Preparation Fe_3O_4 @Pt nanoparticles decorated carbon-ceramic electrode

The Fe_3O_4@Pt nanoparticles were prepared using $Fe(NO_3)_3.9H_2O$ and $H_2PtCl_6.5H_2O$ as metallic precursors, and $NaBH_4$ as reducing agent. To obtain the Fe_3O_4 cores the metallic salt solution [$Fe(NO_3)_3.9H_2O$, 0.02 M] was added dropwise into the solution containing the reducing agent [$NaBH_4$, 0.01 M] at room temperature and mechanically stirred. The obtained product was washed and separated by centrifugation at 3000 rpm. To obtain the Fe_3O_4@Pt nanoparticles, the cores were suspended on a fresh reducing solution of $NaBH_4$ (0.01 M) and a solution of $H_2PtCl_6.5H_2O$ (0.02 M) was slowly added under mechanically stirring and then the mixture was stirred for 30 min at 25 $^\circ$C. During this period, the color of the mixture gradually turned dark black from orange, indicating that Fe_3O_4@Pt nanoparticles had been formed. Finally, the obtained product was separated by centrifugation at 3000 rpm [7], washed and dried.

Carbon-ceramic electrode (CCE) is used as substrate for supported catalyst. Prior to the surface coating, the CCE surface was polished carefully with 1500 emery paper and was rinsed with distilled water. For preparation of catalyst ink, about 20 mg of Fe_3O_4@Pt nanoparticles was ultrasonically suspended in a 5 ml solution containing distilled water and 5% wt Nafion (50 µL) for about 30 min to obtain homogeneous ink. Next, 5 µL of ink was uniformly dispersed onto freshly polished CCE and dried under ambient condition.

3. Result and discussion

3.1. Physical characterization

XRD measurements were performed in order to evaluate the crystallographic structure of the nanoparticles. The XRD pattern of Fe_3O_4@Pt nanoparticles are shown in Figure 1. The peaks at 39.9, 46.4, 67.6 and 81.7° are attributed to the (111), (200), (220) and (311) of Pt planes respectively [8]. With the presence of Fe_3O_4 into the face centered cubic (fcc) structure of Pt, the Pt reflections are shifted slightly to higher values of 2θ, which show a contraction of the lattice and the formation of Fe_3O_4@Pt core-shell nanoparticles [9].

The morphological characterization of the Fe_3O_4@Pt core-shell nanoparticles was performed with SEM and the corresponding result was shown in Figure 2. It could be seen that the Fe_3O_4@Pt nanoparticles exhibit very well uniform spreading and homogeneously range in size with globular structure. The elemental composition of catalyst was measured by EDX measurement. The corresponding result is shown in the inset of Figure 2.

The fine structures of the core and shell layers were further characterized using transmission electron microscopy. The TEM analyses suggest the formation of the core-shell nanoparticles (Figure 3). The as-prepared Fe_3O_4@Pt nanoparticles have spherical shapes and an average diameter of approximately 20-40 nm which is fairly agreed with the SEM observation.

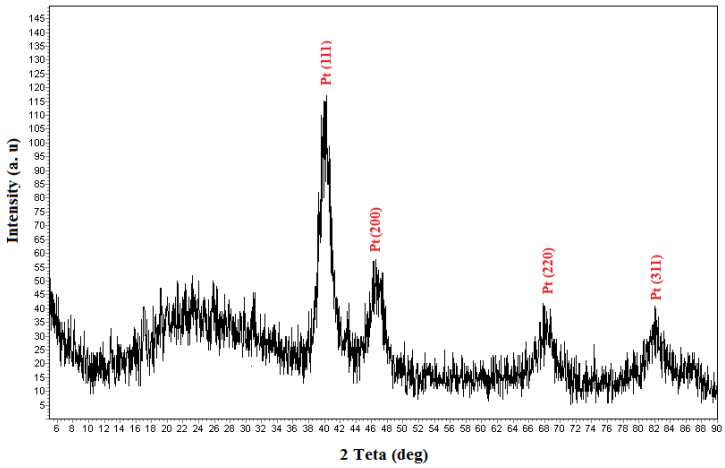

Figure 1: XRD pattern of the Fe_3O_4@Pt core-shell nanoparticles.

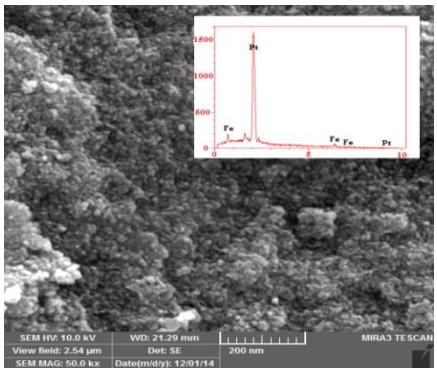

Figure 2: SEM image of Fe_3O_4@Pt core-shell nanoparticles (The inset shows EDX spectrum of Fe_3O_4@Pt nanoparticles).

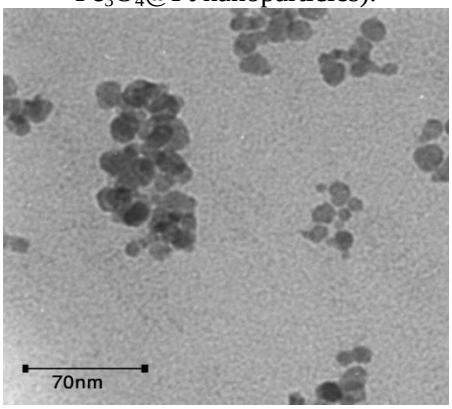

Figure 3: TEM image of Fe_3O_4@Pt core-shell nanoparticles.

3.2. Electrocatalytic activity of the Fe_3O_4@Pt/CCE

The catalytic activity of ethylene glycol electrooxidation on the catalysts (Fe_3O_4@Pt/CCE and Pt/CCE) was measured by cyclic voltammetry (CV) experiments in a 0.5 M ethylene glycol + 0.5 M NaOH solution (Figure 4). There are two oxidation peaks in the forward scan direction and one in the reverse direction. The singular anodic peak in the negative sweep represents oxidation of incompletely oxidized carbonaceous intermediates on the surface of the catalysts left over from the positive sweep. Accumulation of these adsorbed products block active sites on the catalyst, decreasing performance [10].

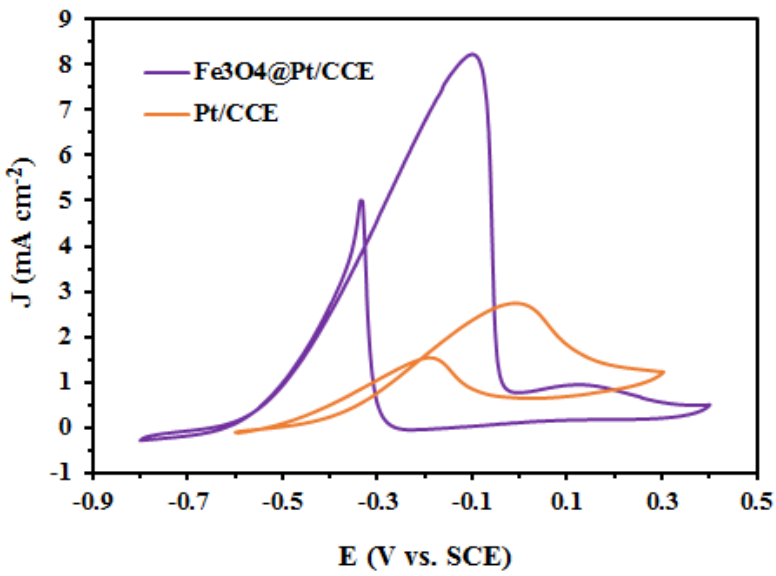

Figure 4: Cyclic voltammograms of the Fe_3O_4@Pt/CCE and Pt/CCE catalysts modified electrodes in 0.5 M ethylene glycol + 0.5 M NaOH at scan rate of 50 mV s^{-1}.

For investigation of the transport characteristics of the ethylene glycol on the Fe_3O_4@Pt/CCE, the influence of the scan rate (v) in the oxidation of ethylene glycol was investigated. Variation of the peak current density as a function of scan rate was given in Figure 5 (a). It can be understood from this observation that the forward oxidation peak current density shifts positively with increasing of scan rates. The anodic peak current density is linearly proportional to the square root of the scan rate, which suggests that the electrocatalytic oxidation of ethylene glycol on the Fe_3O_4@Pt/CCE is a diffusion controlled process [11]. Potential of forward scan peak increases with the increase of scan rate and there is linearly relationship between Ep and ln (v) (Figure 5 (b)). It shows that the oxidation of ethylene glycol is an irreversible electrode process [12]. In order to assess the capacity of the Fe_3O_4@Pt/CCE against ethylene glycol oxidation, the effect of different concentrations on the anodic peak current density was investigated (Figure 6). It can be seen clearly that, by increasing the ethylene glycol concentration, the peak current density increases and drops afterward in concentrations higher than 0.6 M. This effect might be due to the saturation of the Pt active sites by ethylene glycol molecules and also contamination of the catalyst surface which is mainly arisen from the CO_{ads} during the oxidation. In accordance with this result, the optimum concentration to achieve a higher peak current density may be considered as about 0.6 M.

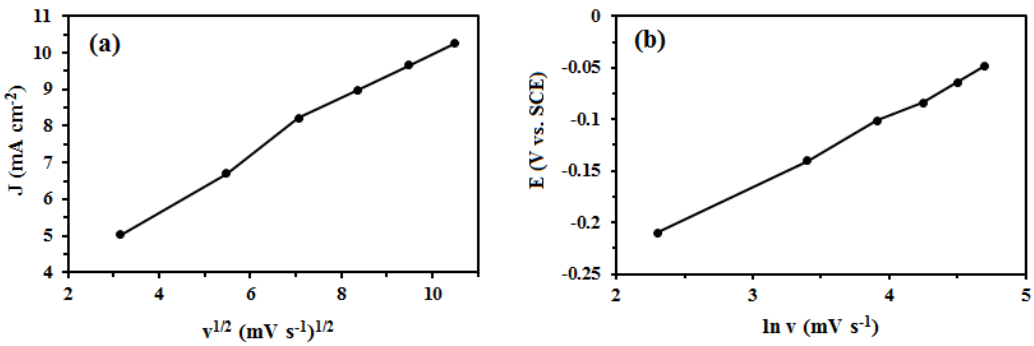

Figure 5: Plot of the peak current density versus the square root of scan rate (a) and plot of E (V vs. SCE) versus the Ln v (mV s^{-1}) (b).

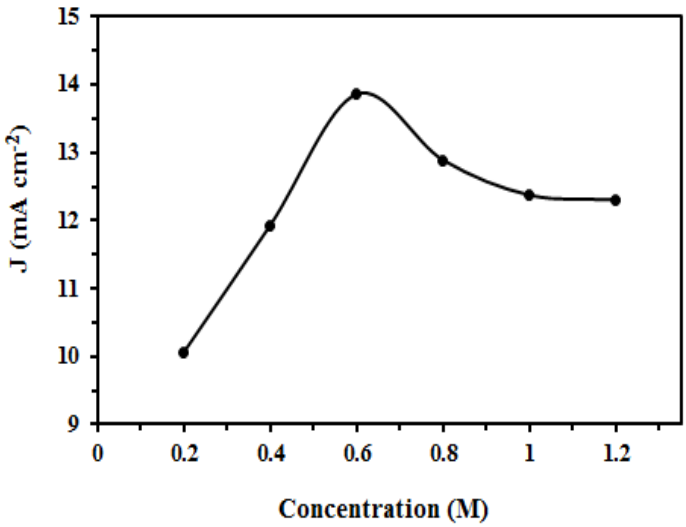

Figure 6: Plot of the peak current density versus concentration of ethylene glycol.

3.3. Long-term stability

To confirm the long-term durability of Fe_3O_4@Pt/CCE and Pt/CCE catalysts toward ethylene glycol oxidation, Chronoamperometric experiments were performed for a duration of 1500 s in 0.5 M ethylene glycol + 0.5 M NaOH solution at -0.09 V. Figure 7 shows the curves for the two catalysts, both electrodes display a current density decay during the initial period because of the formation of intermediate species [1]. The experimental data shows that the Fe_3O_4@Pt/CCE has lesser sensitivity to poisoning by CO_{ads} species which formed during the electrooxidation [12].

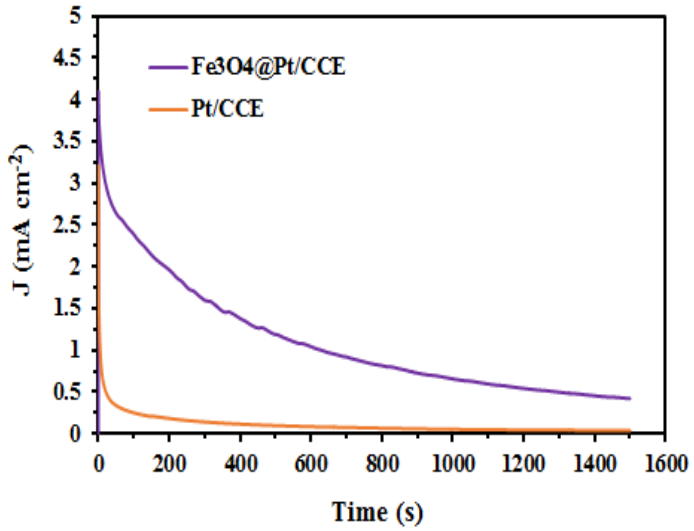

Figure 7: Chronoamperometry curves for Fe_3O_4@Pt/CCE and Pt/CCE recorded in 0.5 M ethylene glycol + 0.5 M NaOH solution at -0.09 V.

4. Conclusion

In conclusion, we synthesized Fe_3O_4@Pt core-shell catalyst for ethylene glycol electrooxidation via a facile method. XRD, SEM, EDX and TEM were applied to characterize the morphology, structure and composition of the catalyst. The electrochemical experiments show excellent properties of the as-prepared catalyst. In addition, the low-cost Fe_3O_4 core helps reduce the Pt dosage. This work could provide new insights into the fabrication of core-shell nanoparticles for ethylene glycol electrooxidation.

Acknowledgment

The authors gratefully acknowledge the Research Council of Azarbaijan Shahid Madani University for financial support.

5. References

[1] Mao H., Li R., Jiang K., Huang T., Yu A., "Facile preparation of Cu@Pt/rGO hybrids and their electrocatalytic activities for methanol oxidation", *Electrochim. Acta, 2013, 107: 419.*

[2] Matsuoka K., Inaba M., Iriyama Y., Abe T., Ogumi Z., Matsuoka M., "Anodic oxidation of polyhydric alcohols on a Pt electrode in alkaline solution", *Fuel Cells, 2002, 2: 35.*

[3] Peled E., Livshits V., Duvdevani T., "High-power direct ethylene glycol fuel cell (DEGFC) based on nanoporous proton-conducting membrane (NP-PCM)", *J. Power Sources, 2002, 106: 245.*

[4] Jin C., Song Y., Chen Z., "A comparative study of the electrocatalytic oxidation of ethylene glycol on PtAu nanocomposite catalysts in alkaline, neutral and acidic media", *Electrochim. Acta, 2009, 54: 4136.*

[5] Zhang H., Yin Y., Hu Y., Li Ch., Wu P., Wei Sh., Cai Ch., "Pd@Pt Core Shell Nanostructures with Controllable Composition Synthesized by a Microwave Method and Their Enhanced Electrocatalytic Activity toward Oxygen Reduction and Methanol Oxidation", *J. Phys. Chem. C, 2010, 114: 11861.*

[6] Kettner M., Schneider W. B., Auer A. A., "Computational Study of Pt/Co Core-Shell

Nanoparticles: Segregation, Adsorbates and Catalyst Activity", *J. Phys. Chem. C, 2012, 116: 15432.*

[7] Sa´nchez-Padilla N. M., Montemayor S. M., Torres L. A., Rodrı´guez Varela F. J., "Fast synthesis and electrocatalytic activity of M@Pt (M [Ru, Fe3O4, Pd]) core-shell nanostructures for the oxidation of ethanol and methanol", *Int. J. Hydrogen Energy, 2013, 38: 12681.*

[8] Li Z., He Ch., Caib M., Kang Sh., Shen P. K., "A strategy for easy synthesis of carbon supported Co@Pt core-shell configuration as highly active catalyst for oxygen reduction reaction", *Int. J. Hydrogen Energy, 2012, 37: 14152.*

[9] Zhang M., Yan Z., Xie J., "Core-shell Ni@Pd nanoparticles supported on MWCNTs at improved electrocatalytic performance for alcohol oxidation in alkaline media", *Electrochim. Acta, 2012, 77: 237.*

[10] Falase A., Main M., Garcia K., Serov A., Lau C., Atanassov P., "Electrooxidation of ethylene glycol and glycerol by platinum-based binary and ternary nano-structured catalysts", *Electrochim. Acta, 2012, 66: 295.*

[11] Yang S., Zhang X., Mi H., Ye X., "Pd nanoparticles supported on functionalized multi-wall carbon nanotubes (MWCNTs) and electrooxidation for formic acid", *J. Power Sources, 2008, 175: 26.*

[12] Wang J. Y., Kang Y. Y., Yang H., Cai W. B., "Boron-doped palladium nanoparticleson carbon black as a superior catalyst for formic acid electro-oxidation", *J. Phys. Chem C, 2009, 113: 8366.*

8th Iranian Fuel Cell Seminar
FEBRUARY 25,26
2015

Synthesis, Characterization and Electrocatalytic Activity of Fe_3O_4@Pt Core-Shell Nanoparticles for Formic Acid Electrooxidation

Biuck Habibi*, Serveh Ghaderi
Electroanalytical Chemistry Laboratory, Department of Chemistry, Faculty of Sciences, Azarbaijan Shahid Madani University, Tabriz
** B.Habibi@azaruniv.edu*

Abstract
In this study, Fe_3O_4@Pt core-shell nanoparticles are synthesized by a fast and simple synthesis method. X-ray diffraction, scanning electron microscopy, transmission electron microscopy and energy dispersive X-ray spectroscopy are used to investigate the crystallinity, surface morphology and chemical structural. The electrocatalytic activity of the Fe_3O_4@Pt nanoparticles towards formic acid oxidation has been investigated by cyclic voltammetry in 0.5 M H_2SO_4 solution. The obtained results indicate that the Fe_3O_4@Pt core-shell nanoparticles show better electrocatalytic performance towards the formic acid oxidation in compared with the Pt-alone nanoparticles.

Keywords: Fe_3O_4@Pt nanoparticles, Core-shell, Electrooxidation, Formic acid**.**

1- Introduction

Nowadays, formic acid oxidation is one of the most studied electrochemical reactions due to its interest in fuel cells. Direct formic acid fuel cell (DFAFC) has attracted great attention because formic acid is less flammable, non-toxic and high power density [1]. In DFAFC, Pt is generally used as an anode catalyst for oxidation reactions. Pt has a wide range of catalysis applications due to its unique chemical and physical characteristic. However, the high cost of Pt is still one of the main disadvantages hindering DFAFC commercialization [2]. At present, the major challenge in this field is to reduce the fuel cell energy cost by developing low cost materials, processes and components, which paves way for the massive introduction of this technology for the common people [3]. To maximize Pt utilization, the ideal structure of a Pt-based catalyst is where the total available Pt atoms are distributed on the electrochemical reaction interface. Following this consideration, the core-shell structure should represent an effective structure model where a monolayer or a few layers of Pt are arranged on inexpensive core materials. More importantly, it is rationally expected that the physical and chemical properties of the Pt shell can be effectively tuned by the underlying core material. This imparts significant area for improvement of the electrocatalytic performance of the Pt shell [4]. Core-shell nanostructure is an effective way to increase the utilization efficiency of precious metal electrocatalysts [5]. By replacing the core of the nanoparticles of electrocatalysts with less expensive or non-precious metals and/or by producing Pt nano sphere shell with high surface-to-volume ratios, the high catalytic activity and utilization efficiency of Pt electrocatalysts and low Pt loading and consequently reduced cost can be achieved [6-8]. In this work, the core- shell of Fe_3O_4 (core) and Pt (shell) was synthesized by the facile synthesis method. The physicochemical properties

of the nanoparticles are investigated. The catalytic activity of the obtained catalyst was tested in the electrooxidation of formic acid in acidic media. It was found that Fe_3O_4@Pt nanoparticles was catalytically more active than Pt-alone nanoparticles.

2- Experimental

2.1. Chemicals

$H_2PtCl_6.5H_2O$, $Fe(NO_3)_3.9H_2O$, $NaBH_4$, Formic acid and H_2SO_4 were obtained from Merck. All solutions were freshly prepared with distilled water.

2.2. Instrumentation

The electrochemical measurements were carried out using an AUTOLAB PGSTAT-100 (potentiostat/galvanostat). A conventional three electrode cell was used at room temperature. Carbon eramic electrod (CCE) with a supported catalyst layer (Pt and Fe_3O_4@Pt nanoparticles) was used as working electrode. A saturated calomel electrode (SCE) and a platinum wire were used as the reference and auxiliary electrodes, respectively. Scanning electron microscope (SEM) was performed on a LEO1430 vp (Carl Zeiss, Germany) instrument. Transmission electron microscopy (TEM) measurements were made on a Carl Zeiss 906 E (Cottingen, Germany) microscope. X-ray diffraction (XRD) pattern was recorded with a Bruker AXS model D_8 Advance (Karlsruhe, Germany) instrument with Cu-K_α radiation source (1.54 Å) at 40 kV and 35 mA.

2.3. Synthesis of the Fe_3O_4@Pt nanoparticles

The Fe_3O_4@Pt nanoparticles were prepared using $Fe(NO_3)_3.9H_2O$ and $H_2PtCl_6.5H_2O$ as metallic precursors, and $NaBH_4$ as reducing agent. To obtain the Fe_3O_4 cores the metallic salt solution [$Fe(NO_3)_3.9H_2O$, 0.02 M] was added dropwise into the solution containing the reducing agent [$NaBH_4$, 0.01 M] at room temperature and mechanically stirred. The obtained product was separated and washed by centrifugation at 3000 rpm. To obtain the Fe_3O_4@Pt nanoparticles, the cores were suspended on a fresh reducing solution of $NaBH_4$ (0.01 M) and a solution of $H_2PtCl_6.5H_2O$ (0.02 M) was slowly added under mechanically stirring and then the mixture was stirred for 30 min at 25 $^\circ$C. During this period, the color of the mixture gradually turned dark brown from orange, indicating that Fe_3O_4@Pt nanoparticles had been formed. Finally, the obtained product was separated by centrifugation at 3000 rpm [9], washed and dried.

2.4. Preparation of electrode

Carbon-ceramic electrode (CCE) is used as substrate for supported catalyst. Before each experiment, the CCE surface was polished with 1500 emery paper and was rinsed with distilled water. For preparation of catalyst ink, about 20 mg of Fe_3O_4@Pt nanoparticles was ultrasonically suspended in a 5 ml solution containing distilled water and 5% wt Nafion (50 µL) for about 30 min to obtain homogeneous ink. Next, 5 µL of ink was uniformly dispersed onto freshly polished CCE and dried under ambient condition.

3. Result and discussion

3.1. Physical characterization

XRD measurements were performed in order to evaluate the crystallographic structure of the nanoparticles. The XRD pattern of Fe_3O_4@Pt nanoparticles are shown in Figure 1. The peaks at 39.9, 46.4, 67.6 and 81.7° are attributed to the (111), (200), (220) and (311) of Pt planes respectively [10]. Presence of Fe_3O_4 into the face centered cubic (fcc) structure of Pt, the Pt reflections are shifted slightly to higher values of 2θ (in comparison with Pt alone), which show a contraction of the lattice and the formation of Fe_3O_4@Pt core-shell nanoparticles [11].

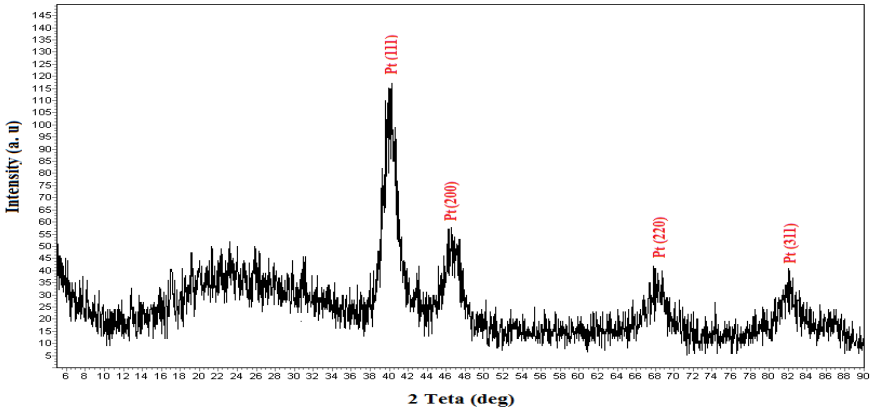

Figure 1: XRD pattern of the Fe_3O_4@Pt nanoparticles.

In order to surface characterization of the Fe_3O_4@Pt nanoparticles, the micrograph of catalyst has been investigated by SEM and the corresponding results were shown in Figure 2. It could be seen that the Fe_3O_4@Pt nanoparticles exhibit very well uniform spreading and homogeneously range in size with globular structure. EDX measurement was performed to identify the elemental composition of catalyst. The corresponding result is shown in the inset of Figure 2.

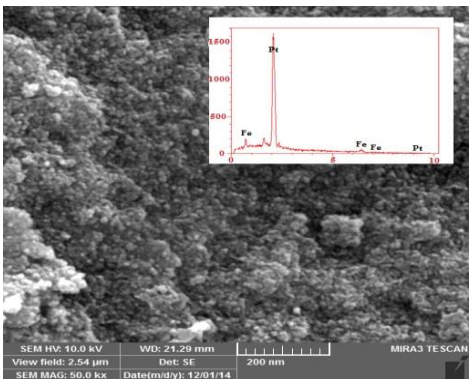

Figure 2: SEM image of Fe_3O_4@Pt nanoparticles (The inset shows EDX spectrum of Fe_3O_4@Pt nanoparticles)

The TEM image suggests the formation of the core-shell nanoparticles (Figure 3). The as-prepared Fe_3O_4@Pt nanoparticles have spherical shapes and an average diameter of approximately 20-30 nm which is fairly agreed with the SEM observation.

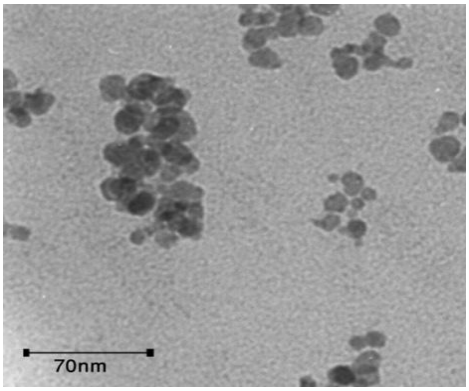

Figure 3: TEM image of Fe_3O_4@Pt core-shell nanoparticles

3.2. Electrochemical characterization

The electrocatalytic activity of the Fe_3O_4@Pt/CCE towards to the oxidation of formic acid was evaluated by using cyclic voltammetry (CV) in 0.5 M formic acid + 0.5 M H_2SO_4 solution at room temperature. The Pt/CCE was also tested under the same conditions for comparison. The electrooxidation of formic acid shows only one main peak both in forward and reverse scan directions and the oxidation current dansities of formic acid on the Fe_3O_4@Pt/CCE are significantly higher than on the Pt/CCE. This large anodic peak in the reverse scan is attributed to the removal of the incompletely oxidized carbonaceous species formed in the forward scan [12].

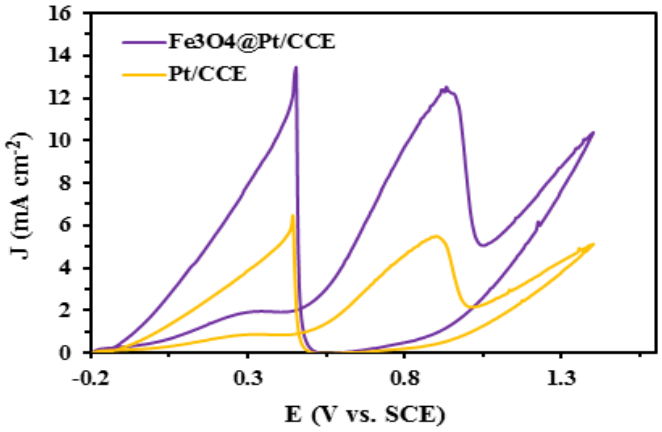

Figure 4: Cyclic voltammograms of the Fe_3O_4@Pt/CCE and Pt/CCE catalysts modified electrodes in 0.5 M H_2SO_4 + 0.5 M formic acid at scan rate of 50 mV s^{-1}.

For investigation of the transport characteristics of the formic acid on the Fe_3O_4@Pt/CCE, the influence of the scan rate (v) in the oxidation of formic acid on the Fe_3O_4@Pt/CCE was investigated. Variation of the peak current density as a function of scan rate was given in Figure 5. It can be understood from this observation that the forward oxidation peak current density shifts positively with increasing of scan rates. The anodic peak current densities are linearly proportional to the square root of the scan rate, which suggests that the electrocatalytic oxidation of formic acid on the Fe_3O_4@Pt/CCE is a diffusion controlled process (the inset of (a) in Figure 5) [13]. Potential of forward scan peaks increases with the increase of scan rate and there is linearly relationship between Ep and ln (v) (the inset of (b) in Figure 5). It shows that the oxidation of formic acid is an irreversible electrode process [14].

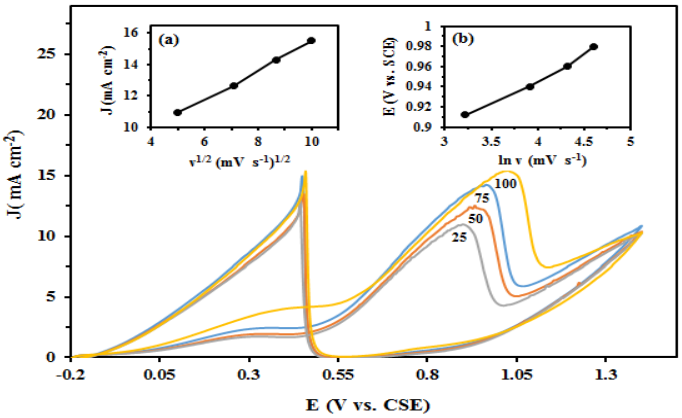

Figure 5: Cyclic voltammograms of Fe_3O_4@Pt/CCE catalyst in 0.5 M formic acid + 0.5 M H_2SO_4 at different scan rates (mV s^{-1}). The inset of (a) shows plot of the peak current density versus the square root of scan rates and the inset of (b) shows E (V vs. SCE) versus the Ln v (mV s^{-1}).

Chronoamperometric experiments were carried out for further evaluation of the catalytic activity and stability of the catalyst under a period of time in continuous operation. Figure 6 shows the chronoamperometric curves of 0.5 M formic acid + 0.5 M H_2SO_4 solution on the Fe_3O_4@Pt/CCE and Pt/CCE electrode at 0.9 V for 1500s, respectively. The experimental data shows that the Fe_3O_4@Pt/CCE has lesser sensitivity to poisoning by CO_{ads} species which formed during the electrooxidation [14].

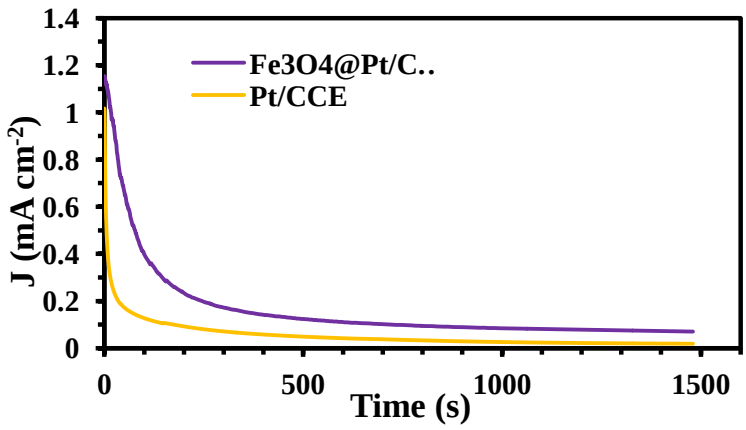

Figure 6: Chronoamperometry curves for Fe_3O_4@Pt/CCE and Pt/CCE recorded in 0.5 M formic acid + 0.5 M H_2SO_4 solution at 0.9 V.

4. Conclusion

In this work, a simple and fast method is used to synthesis of core-shell Fe_3O_4@Pt nanoparticles. XRD, SEM, EDX and TEM were applied to characterize the physicochemical properties of the catalyst. The electrocatalytic activity towards the oxidation of formic acid was measured by cyclic voltammetry and chronoamperometry. Electrochemical results indicated that the Fe_3O_4@Pt nanoparticles had better catalytic performance than that of Pt-alone nanoparticles. These results show that Fe_3O_4@Pt core-shell nanoparticles may have the splendid future as catalysts for DFAFCs.

Acknowledgment
The authors gratefully acknowledge the Research Council of Azarbaijan Shahid Madani University for financial support.

References:

[1] A. Sáez, J. Solla-Gullón, E. Expósito, A. Aldaz, V. Montiel, "Electrochemical analysis of the performance of carbon supported Pd nanoparticles for direct formic acid fuel cells :From gold supported electrodes to catalyst-coated membranes", Int. J. Electrochem. Sci (2013). 8, 7030-7043.
[2] Q. Yuan, D. Duan, Y. Ma, G. Wei, Zh. Zhang, X. Hao, Sh. Liu, "Performance of nano-nickel core wrapped with Pt crystalline thin film for methanol electro-oxidation", J. Power Sources (2014). 245, 886-891.
[3] J. Moreira, P. del Angel, A. L. Ocampo, P. J. Sebastián, J. A. Montoya, R.H. Castellanos, "Synthesis, characterization and application of a Pd/Vulcan and Pd/C catalyst in a PEM fuel cell", Int. J. Hydrogen Energy (2004). 29, 915-920.
[4] X. Zhao, M. Yin, L. Ma, L. Liang, C. Liu, J. Liao, T. Lu and W. Xing, "Recent advances in catalysts for direct methanol fuel cells", Energy Environ. Sci (2011). 4, 2736-2753.
[5] H. Wang, C. Xu, F. Cheng, M. Zhang, S. Wang, S. P. Jiang, "Pd/Pt core–shell nanowire arrays as highly effective electrocatalysts for methanol electrooxidation in direct methanol fuel cells" Electrochem. Commun (2008). 10, 1575-1578.
[6] S. J. Guo, Y. X. Fang, S. J. Dong, E. K. Wang, "High-Efficiency and low-cost hybrid nanomaterial as enhancing electrocatalyst: Spongelike Au/Pt core-shell nanomaterial with hollow cavity", J. Phys. Chem. C (2007). 111, 17104-17109.
[7] J. H. Zeng, J. Yang, J. Y. Lee, W. J. Zhou, "Preparation of carbon-supported core−shell Au−Pt nanoparticles for methanol oxidation reaction: The promotional effect of the Au core" J. Phys. Chem. B (2006).110, 24606-24611.
[8] R. Tena-Zaera, A. Katty, S. Bastide, C. Levy-Clement, "Annealing effects on the physical properties of electrodeposited ,ZnO/CdSe core−shell nanowire arrays", Chem. Mat (2007).19, 1626-1632.
[9] N. M. Sa´nchez-Padilla, S. M. Montemayor, L. A. Torres, F. J. Rodrı´guez Varela, "Fast synthesis and electrocatalytic activity of M@Pt (M [Ru, Fe3O4, Pd) core-shell nanostructures for the oxidation of ethanol and methanol", Int. J. Hydrogen Energy (2013). 38, 12681-12688.
[10] Z. Li, Ch. He, M. Caib, Sh. Kang, P. K. Shen, "A strategy for easy synthesis of carbon supported Co@Pt core-shell configuration as highly active catalyst for oxygen reduction reaction", Int. J. Hydrogen Energy (2012). 37, 14152-14160.
[11] M. Zhang, Z. Yan, J. Xie, "Core/shell Ni@Pd nanoparticles supported on MWCNTs at improved electrocatalytic performance for alcohol oxidation in alkaline media", Electrochim. Acta (2012). 77, 237-243.
[12] Sh. Sh. Li, Y. Y. Hu, J. J. Feng, Z. Y. Lv, J. R. Chen, A. J. Wang, "Rapid room-temperature synthesis of Pd nanodendrites on reduced graphene oxide for catalytic oxidation of ethylene glycol and glycerol", Int. J. Hydrogen Energy (2014). 39, 3730-3738.
[13] S. Yang, X. Zhang, H. Mi, X. Ye, "Pd nanoparticles supported on functionalized multi-wall carbon nanotubes (MWCNTs) and electrooxidation for formic acid", J. Power Sources (2008). 175, 26-32.
[14] J. Y. Wang, Y. Y. Kang, H. Yang, W. B. Cai, "Boron-doped palladium nanoparticleson carbon black as a superior catalyst for formic acid electro-oxidation", J. Phys. Chem C (2009). 113, 8366-8371.

8th Iranian Fuel Cell Seminar
FEBRUARY 25,26
2015

Production of Chromium Oxide Using as Modified Thin Film for Lithium Ion Batteries

Bagher-Aziz kalantari*[1], Mohamad Reza-Talei Bavil Olya[2]
1. Department of Chemistry, Faculty of Science, Karaj Branch, Islamic Azad University, Alborz, Iran
2. Department of Chemistry, Faculty of Science, South Tehran Branch, Islamic Azad University, Tehran, Iran
** b_akalantari@yahoo.com*

Abstract
Disclosed is a method of preparing a pigmentary chromium oxide micro particles having 90 percent particle size more than about 1µm . Highly ordered mesoporous Cr_2O_3 materials with high specific surface area and narrow pore size distribution were successfully prepared by a vacuum assisted impregnation method[1]. in order to method which is used for the production of pigmentary included reaction with sulfur and heating at high temperatures. Thereafter, the solid Cr_2O_3 product was washed twice with distilled water.

Keywords: Component, Litium ion battery, Chromium Oxide, Narrow pore Size.

INTRODUCTION
Among inorganic particles, chromium oxide (Cr_2O_3) have received great attention due to its numerous application domains, including green pigments [2] heterogeneous catalysts [3-5] coating materials for thermal protection [5-6], hydrogen storage [8-10] , digital recording system [10], photonic and electronic devices [12-13]. Various techniques have been developed to synthesize Cr_2O_3 particles such as precipitation, precipitation gelation, sol gel, mechanochemical reaction, oxidation of chromium in oxygen and sonochemical methods[13]. But since either these processes are complex or their reaction apparatus are expensive, most of them have difficulties in being industrialized. Some new methods of preparation should be explored.
In the present study, a simple and original method for the synthesis of chromium oxide Micro particles is described. The surface properties, size, morphology and crystallographic structure of Cr_2O_3 particles are characterized by means of X-ray diffraction (XRD). However for the determination of particle distribution, was used from laser particle sizer (LPS) Fritsch Gmbh, the model of Analysset22 .
Highly ordered mesoporous Cr_2O_3 materials with high specific surface area and narrow pore size distribution were successfully prepared by a vacuum assisted impregnation method. Both 2-dimensional hexagonal and 3-dimensional cubic Cr_2O_3 mesoporous replicas from SBA-15 and KIT-6 templates exhibit enhanced performance for gas sensors and lithium ion batteries, compared to the bulk Cr_2O_3 counterpart Fig.1, [1].

EXPERIMENTAL
All reagents were purchased from Aldrich or Merck and were used without further purification. Experimental procedure for chromium oxide (Cr_2O_3) particles is briefly summarized in Fig.2.

According to the disclosed method potassium dichromate with a grain size of less than 1.5mm is mixed with ammonium sulfate with a grain size of less than 0.25mm and 5% borax into 2% sodium hydroxide solution. Calcinations conditions: 1 Hours in a temperature of about 800ºc and 1 Hours in a temperature of about 1150ºc. The resulting solid, Cr_2O_3, is then separated from the soluble alkali metal compounds under vacuum with twice elution by distilled water.

RESULTS AND DISSCUTION

In this work, chromium oxide (Cr_2O_3) prepared with thermal method. In order to procedures, purity of chromium oxide microparticls are shown with Fig.2. that indicate high purity of the components.

In order to characterize the nature of the Cr_2O_3 microparticls FTIR, XRD and Laser Particle sizer measurements were carried out. Fig.3 shows XRD images of the Cr_2O_3 powder.

The peaks of XRD patterns displayed are evidence for the presence of the crystalline Cr_2O_3 with high purity for both powders.

The FTIR spectrum of chromium oxide nanoparticles is shown in Figure 4. Two sharp peaks displayed at 566 and 626 cm^- attributed to Cr-O stretching modes, are clear evidence for the presence of the crystalline Cr_2O_3.

For the determination of particle distribution, was used from laser particle sizer (LPSA) Fritsch GmbH Nanotech Analysett22 Model.

From results is observed that the particle distribution of chromium oxide is more than 1µm shown in Fig.5.

CONCLUSION

We have described the use of a thermal method for preparation chromium oxide particles that its main advantage is easily controllable conditions with using low cost chromium source is merit to be considered for scaling up by industrial researchers. These particles can used easily as Modified Thin Film for Lithium Ion Batteries.

ACKNOWLEDGMENT

We would like to acknowledge to the Dr.javad Rafeie and Mr. Karvaneh for helping us in this work and we are grateful to department of chemistry Azad University Karaj Branch for financial support of this work.

REFERENCES

[1] Hao Liu,a Xiwen Du,b Xianran Xing,c Guoxiu Wang*d and Shi Zhang Qiao*a, Highly ordered mesoporous Cr2O3 materials with enhanced performance for gas sensors and lithium ion batteries, Chem. Commun., 2012,48, 865-867.

[2] P.M.T. Cavalcante, M. Dondi, G. Guarini,M. Raimondo, G. Baldi, Dyes Pigments, 2009,80, 226-232.

[3] (a) T.V. Malleswara Rao, E.M. Zahidil, A.Sayari, J. Mol. Catal. A. 301 (2009) 159-165. (b)Sh. Deng, H. Li, S. Li, Y. Zhang, Journal of Molecular Catalysis. A, Chemical, 268 (2007)169-175.

[4] (a) G. Dabrilaite-Kudzmiene, S. Kitrys, MATERIALS SCIENCE, 19 (2013) 89-95 (b) T.V. Rao, Y. Yang, A. Sayari, J. Mol. Catal. A.301 (2009) 152-158.

[5] G. Wanga, L. Zhang, J. Deng, H. Dai, H.He, C. Tong, Appl. Catal. A. 355 (2009) 192-201.

[6] X. Pang, K. Gao, F. Luo, Y. Emirov, A.A.Levin, A.A. Volinsky, Thin Solid Films 517(2009) 1922-1927.

[7] X. Hou, K.L. Choy, Thin Solid Films, 516(2008) 8620-8624.

[8] R. Vijay, R. Sundaresan, M.P. Maiya, S.Srinivasa Murthy, J. Alloys Compd. 424 (2006)289-293.
[9] A. Patah, A, Takasaki, J.S. Szmyd, Int. J.Hydrogen Energy 34 (2009) 3032-3037.
[10] J.L. Bobet, S. Desmoulins-Krawiec, E.Grigorova, F. Cansell, B. Chevalier, J. AlloysCompd. 351 (2003) 217-221.
[11] M.D. Bijker, J.J.J. Bastiaens, E.A. Draaisma,L.A.M. Jong, E. Sourty, S.O. Saied, J.L. Sullivan,Tribol. Int. 36 (2003) 227-233.
[12] X. He, D. Antonelli, Angew. Chem. Int. Ed.114 (2002) 222-238.
[13] X. He, D. Antonelli, Angew. Chem. Int. Ed.Engl. 41 (2002) 214-229.

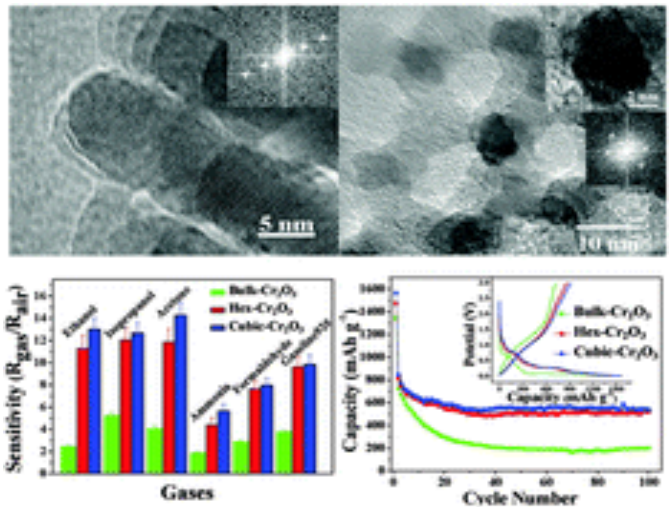

Fig.1.Highly ordered mesoporous Cr_2O_3 materials with high specific surface area and narrow pore size distribution[1]

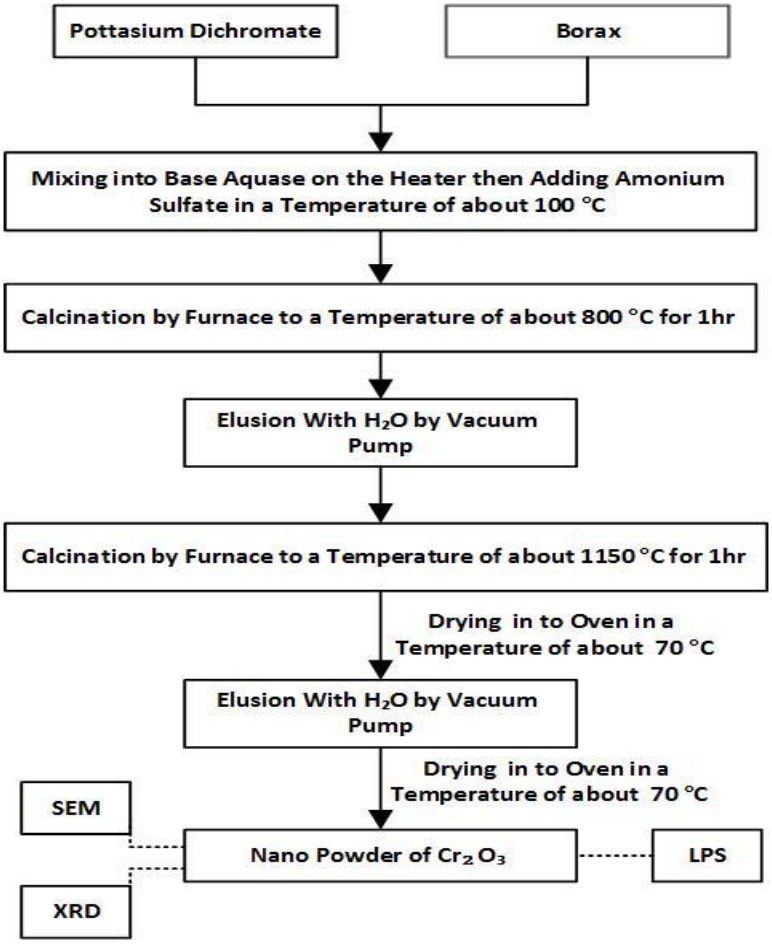

Fig.2. Experimental procedure for the formation of chromium oxide (Cr_2O_3) micro particles

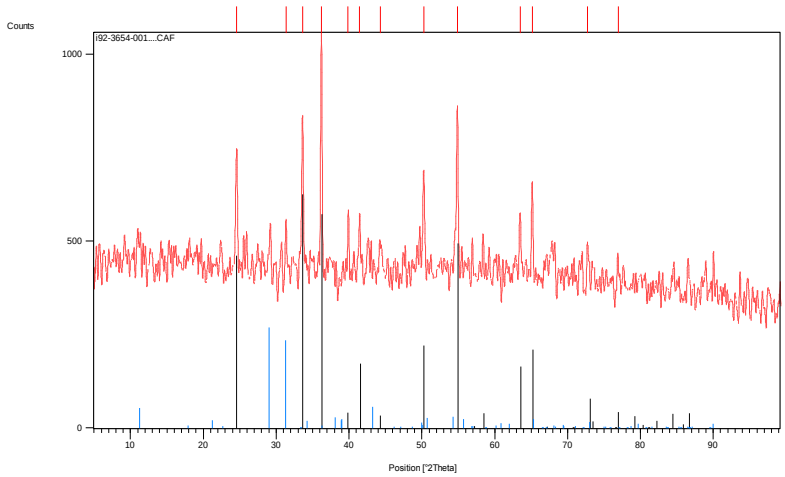

Fig.3. XRD pattern of the Cr_2O_3 micro particles

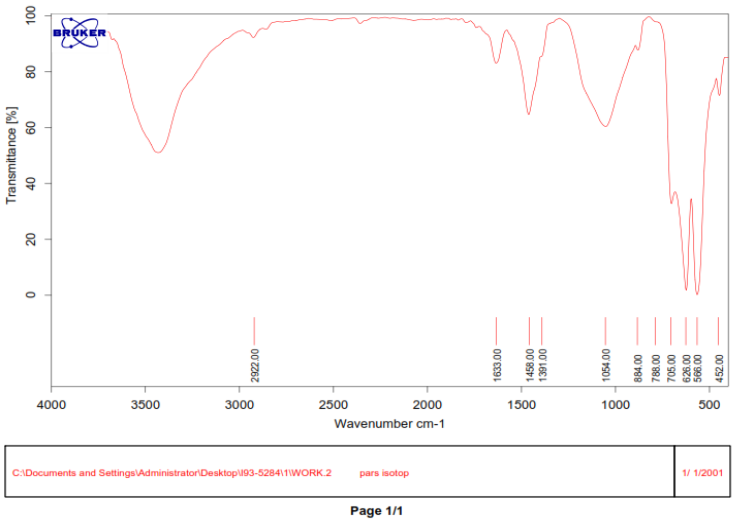

Fig.4. FTIR spectrum of the micro-sized Cr_2O_3

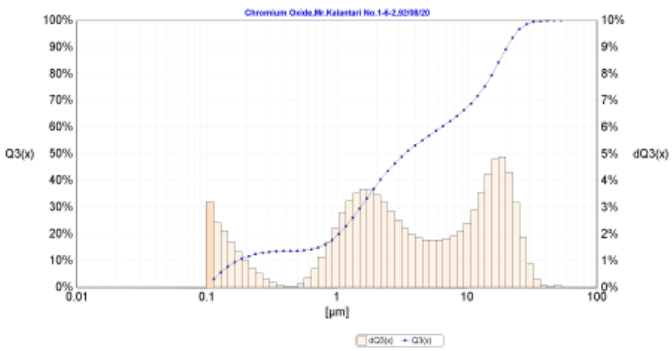

Volume Statistics (Geometric)

Mean	7.63	Variance	68.94
Median	3.31	Coef.	108.86
Mean/Media Ratio	2.31	Skewness	1.14
Mode	0.11	Kurtosis	0.62
Std. Deviation	8.30		

Size Class High [µm]	Q3(x) [%]
0.172	10.000
1.031	20.000
1.517	30.000
2.129	40.000
3.318	50.000
6.366	60.000
11.328	70.000
15.744	80.000
20.328	90.000
45.947	99.900

Fig.5. Particle distribution of Cr_2O_3 micro particles by LPSA

8th Iranian Fuel Cell Seminar
FEBRUARY 25,26
2015

Exploring of the Oxygen Reduction Reaction on the Gas Diffusion Electrode for Zinc Air Fuel Cell

Parisa Akbarian*, Mehdi Kheirmand
Department of Chemistry, Yasouj University, Yasouj, Iran
** Akbarian_parisa@yahoo.com*

Abstract
In this study, a three-layer gas diffusion electrode was made according to the second layer was made of a mixture of carbon black and Teflon with the ratio of 70:30 on a 200µm silver mesh. The third layer that cased of diffusion layer was made of platinum nano-clusters on carbon and Teflon suspension (with the 70:30 ratio). Finally the heat treated electrode was evaluated for oxygen reduction reaction in a three electrode configuration. The performance of electrode was considered in homemade zinc air fuel cell. The results showed that the open circuit voltage of cell was 1.346 V and at the voltage of 0.73 volt; the current density was 166.5 (mA/cm^2).

Keywords: Oxygen reduction reaction, Gas diffusion electrode, Zinc air fuel cell

Introduction

Metal-air fuel cells are electrochemical devices that directly convert the chemical energy stored in metals (e.g., Mg, Al or Zn) into electricity. Compared with hydrogen fuel cells, metal air fuel cells offer many advantages, including facile solid fuel storage, simple system structure and low cost. Due to these intrinsic merits, metal-air fuel cells have gained a great deal of attention and been regarded as promising power sources for application in mobile phones, lights, communication equipments and electric vehicles, etc. [1-5]. Atmospheric oxygen is the oxidant at the cathode of the proton exchange membrane fuel cells (PEMFC) and zinc–air fuel cells (ZAFC) [6-7]. In the most commonly used cathode designs, the oxygen electrode is based on a three-phase reaction zone. Because oxygen is poorly soluble at atmospheric pressure, a three-phase reaction zone is required to provide oxygen in concentrations suitable for higher current densities.

The electrochemical reactions of zinc-air fuel cell can be described as follows [8]:

At the positive (cathode) electrode:

$$O_2 + 2H_2O + 4e^- \rightarrow 4OH^- , E_0 = 0.40V \quad (1)$$

At the negative (anode) electrode:

$$2Zn \rightarrow 2Zn^{2+} + 4e \quad (2)$$

$$2Zn^{2+} + 4OH^- \rightarrow 2Zn(OH)_2 \qquad E_0 = -1.25V \quad (3)$$

$$2Zn(OH)_2 \rightarrow 2ZnO + 2H_2O \quad (4)$$

Overall cell reaction:

$$2Zn + O_2 \rightarrow 2ZnO \qquad E_0 = 1.65V \quad (5)$$

In ZAFC, zinc metal as an anode material is abundantly available, inexpensive, non-toxic, safe, and easy to handle and store. Air is an oxygen source to be supplied at the cathode side, while aqueous alkaline solution is an electrolyte. The advantages of zinc air fuel cell are using

inexpensive materials of catalysts and separators, the high energy density, stable discharge voltage and running at ambient temperature. Theoretical specific energy of zinc air cell based on the molecular weight of ZnO is 1085 Wh/kg and 1.65 volts for the theoretical cell voltage [9]. The Oxygen reduction reaction is one of the most important electrochemical reactions because it is the cathodic reaction in fuel cells and metal air batteries, during aerated media corrosion and in some industrial electrolytic processes. For these reasons, research efforts have been focused on developing a proper catalyst and elucidating the mechanism of this reaction [10-12].

Experimental

2.1. Cell Fabrication

The zinc-air fuel cell wrought of zinc anode, cathode and alkaline electrolyte. This Cell has made non-separator and simple.

2.1.1. Gas diffusion electrode fabrication

The zinc-air fuel cell comprised of zinc anode, alkaline electrolyte, and cathode.

Air electrode were fabricated in three layers, a waterproof diffusion layer on the air side and the active layer on the electrolyte side. The first layer is the gas diffusion layer which was made of carbon Vulcan, PTFE, 2-propanol and glycerin by mixing and was sonicated for 20 min until a homogeneous paste was obtained. Then, the above GDL Was placed in an oven at 80 $^{\circ}$C for 3 h, after it has dried for half an hour left in 80 $^{\circ}$C then put 20 min to 100 $^{\circ}$C and 30 min in 120 ºC. Then mesh up a quarter at 300 ºC and a quarter at 340 $^{\circ}$C has put in the oven to stabilized. The PTFE solution: carbon Vulcan ratio was 30:70.

For each electrode, an active layer (AL) was prepared by mixing 31.5 mg Pt/C, 13.5 mg polytetrafluorethylene powder (PTFE) as the hydrophobic catalyst binder, then 10 mL Millipore water and isopropyl alcohol 1:1. This catalyst ink was sonicated for 20 min to obtain a uniform mixture, which was then painted onto the micro porous side of a paper gas diffusion layer (GDL).

Finally these two layers were mobilized on a silver lace as third layer.

2.1.2. Anode

The metal zinc was used as the fuel anode. Anode was in direct contact with the electrolyte and cathode.

2.2. Zinc-air fuel cell test system

The flowing cell testing is focused on cell performance. Electrolyte applique 1.4 M KOH solution.

Results

The results showed that the open circuit voltage of cell was 1.346 V and at the voltage of 0.73 volt; the current density was 166.5 (mA/cm^2).

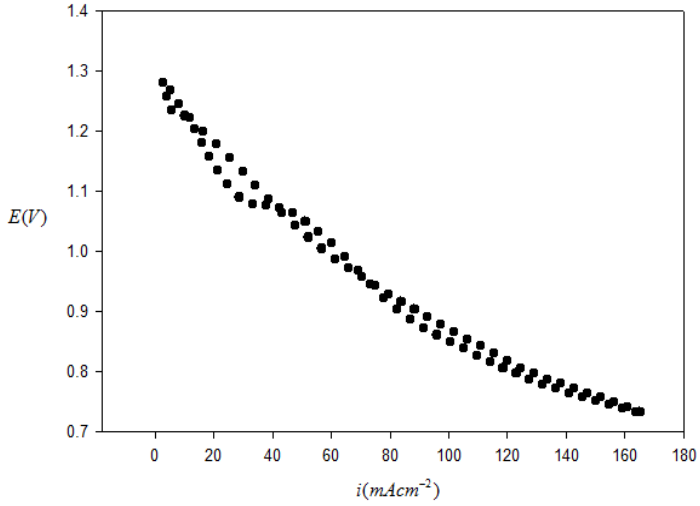

Figure 1. Polarization curve for the zinc-air fuel cell

Conclusions

The experimental study on the improvement of zinc - air fuel cell performance was carried out for non-separator cell. The Cell was made with a good insulation and no leakage was. As you can see from the results of the Cell performance is acceptable.

References

[1] Linden D, Reddy TB. Handbook of batteries. 3rd ed. New York: McGraw-Hill; (2002).
[2] JS. Lee, ST. Kim, RG. Cao, NS. Choi, ML. Liu, KT. Lee, et al. Metal-air batteries with high energy density: Li-air versus Zn-air. Ad Energy Mater, (2011). 1, 34.
[3] Q. Hasvold, H. Henriksen, E. Melvaer, G. Citi, BQ. Johansen, T. Kjqnigsen, et al. Sea-water battery for subsea control systems. J Power Sources. (1997). 65, 253.
[4] MG. Medeiros, RR. Bessette, CM. Deschenes, DW. Atwater. Optimization of the magnesium-solution phase catholyte semi-fuel cell for long duration testing. J Power Sources. (2001). 96, 236.
[5] Q. Hasvold, N. Stqrkersen. Electrochemical power sources for unmanned underwater vehicles used in deep sea survey operations. J Power Sources. (2001). 96, 252.
[6] D.T. Santa Rosa, D.G. Pinto, V.S. Silva, R.A. Silva, C.M. Rangel, High performance PEMFC stack with open-cathode at ambient pressure and temperature conditions, International Journal of Hydrogen Energy. (2007). 32, 4350.
[7] P. Sapkota, H. Kim, Zinc–air fuel cell, a potential candidate for alternative energy, Journal of Industrial and Engineering Chemistry. (2009). 15, 445.
[8] C.K. Yap, T W.C., S.S. Alias, and A.A. Mohamad. Synthesis of zinc oxide by zinc-air system. Journal of Alloys and Compounds. (2009). 484, 934.
[9] R. Othman, W.J. Basirun, A.H. Yahaya, and A.K. Arof. Hydroponics gel as a new electrolyte gelling agent for alkaline zinc air cells. Journal of Power Sources. (2001). 103, 34.
[10] S. Gottsfeld, T.A. Zawodzinski, Advances in Electrochemical science and Engineering. R. C. Alkire, D. M. Kolb, Eds. Vol 5. Wiley-VCH. Weinhim; (1997).
[11] M. R. Tarasevich. Electrokhimiya. (1973). 9, 599.
[12] P. N. Ross. J. Electrochem. Soc. (1979). 126, 78.

8th Iranian Fuel Cell Seminar
FEBRUARY 25,26
2015

Core-Shell Co@Pt Nanoparticles as Highly Active Electrocatalyst for Ethanol Oxidation in Fuel Cells

Biuck Habibi*, Serveh Ghaderi
Electroanalytical Chemistry Laboratory, Department of Chemistry, Faculty of Sciences, Azarbaijan Shahid Madani University, Tabriz, Iran
** B.Habibi@azaruniv.edu*

Absrtact
One of the key objectives in fuel cell technology is to improve activity and reduce Pt loading of the electrocatalysts. This paper describes the facile and fast synthesis method for preparation of Co@Pt nanoparticles and their application for ethanol oxidation in acidic media. The morphology, structure and composition of the as-prepared core-shell nanoparticles were characterized by scanning electron microscopy, transmission electron microscopy, X-ray diffraction and energy dispersive X-ray spectroscopy. Then, the electrocatalytic activity of the Co@Pt nanoparticles toward ethanol oxidation in acidic media was investigated by cyclic voltammetry (CV) and chronoamperometry. Both cyclic voltammetry and chronoamperometry results demonstrate that Co@Pt nanoparticles exhibit significantly high catalytic activity toward the ethanol oxidation reaction in comparison with the Pt-alone nanoparticles.

Keywords: Co@Pt nanoparticles, Core-shell, Electrooxidation, Fuel cell, Ethanol.

1- Introduction

The global energy crisis and various environmental problems have worsened in recent decades [1]. Fuel cell technology has been considered as an effective way to solve the problem of the exhaustion trend for fossil fuel. The fuel cells directly transform the chemical energy to power with high efficiency and potentially zero emission of pollutants. Direct alcohol fuel cells (DAFCs) have attracted increasing interest because of their potential applications in portable electronic devices with high efficiency, low emission, and simple system [2]. It is known that platinum (Pt) is widely used as catalysts in DAFCs due to the rapid kinetics of the oxidation and reduction reactions taking place on its surface and stability. Problem in the fuel cells commercialization is the Pt cost and its scarcity in the earth. A further step in the Pt economy is the reduction of its content by synthesizing core-shell nanoparticles in which Pt is on the surface of a sacrificial metal core [3]. The core-shell nanoparticles can be regarded as a kind of phase separation of an alloy into a core surrounded by the shell composed of a metal. First of all, a core-shell construction can leverage on the use of a low-cost metal core and a noble metal overlayer to greatly reduce the cost of the catalyst. Second, pure Pt deposited on top of non-Pt substrates also showed significantly altered surface catalytic reactivity. This new class of catalysts can be tailored to show significantly enhanced oxidation and reduction reaction kinetics, and at the same time possess improved stability of Pt under typical fuel cell operating conditions [4]. Here, we report the facile synthesis of core-shell nanoparticles with Co as cores and Pt as shells, respectively. The obtained Co@Pt nanoparticles were characterized and then, were applied toward the electrooxidation of ethanol in 0.5 M H_2SO_4 solution by cyclic voltammometric and chronoamperometric measurements. The obtained results were compared with those obtained on the Pt-alone nanoparticles.

2- Experimental

The Co@Pt nanoparticles were prepared using $Co(NO_3)_2.6H_2O$ and $H_2PtCl_6.5H_2O$ as metallic precursors, and $NaBH_4$ as reducing agent. To obtain the Co cores the metallic salt solution [$Co(NO_3)_2.6H_2O$, 0.02 M] was added dropwise into the solution containing the reducing agent [$NaBH_4$, 0.01 M] at room temperature and mechanically stirred. The obtained product was washed and separated by centrifugation at 3000 rpm. To obtain the Co@Pt nanoparticles, the cores were suspended on a fresh reducing solution of $NaBH_4$ (0.01 M) and a solution of $H_2PtCl_6.5H_2O$ (0.02 M) was slowly added under mechanically stirring and then the mixture was stirred for 30 min at 25 ˚C. During this period, the color of the mixture gradually turned dark brown from light green, indicating that Co@Pt nanoparticles had been formed. Finally, the obtained product was separated by centrifugation at 3000 rpm [5], washed and dried overnight. Then, the carbon ceramic electrode (CCE) surface was polished with 1500 emery paper and was rinsed with distilled water. The catalyst layer on the CCE was prepared as follows: About 20 mg of Co@Pt nanoparticles was ultrasonically suspended in a 5 ml solution containing distilled water and 5% wt Nafion (50 µL) for about 30 min to obtain an ink. Then 5 µL of the dispersion was transferred onto the CCE using a micro pipette, and dried.

3. Results and discussion

3. 1. Physicochemical characterization

The surface morphology and chemical structural characterization of Co@Pt nanoparticles were investigated by scanning electron microscopy (SEM). Information on shape and size distribution was obtained with a transmission electron microscope (TEM).The formation, crystallites and lattice parameters of Co@Pt nanoparticles were further characterized using X-ray diffraction (XRD). The chemical composition of the obtained core-sell nanoparticles was determined by energy dispersive X-ray spectroscopy (EDX) (Figure 1). Initially cyclic voltammogram of the Co@Pt/CCE is also presented in Figure 1 (d). The cyclic voltammogram of Co@Pt/CCE was characterized by two regions generally identified as the oxide region in the positive potentials and hydrogen adsorption/desorption region at the negative potentials.

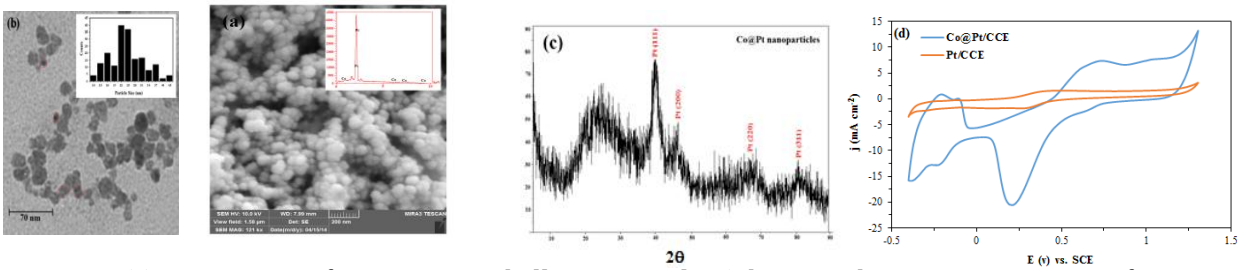

Figure 1: (a) SEM image of Co@Pt core-shell nanoparticles (The inset shows EDX spectrum of Co@Pt core-shell nanoparticles), (b) TEM image of Co@Pt core-shell nanoparticles (The inset shows Particle size distribution from several different regions), (c) XRD pattern of the Co@Pt nanoparticles and (d) CVs of the Co@Pt/CCE (blue line) and Pt/CCE (red line) electrocatalysts in 0.5 M H_2SO_4 electrolyte solution at a scan rate of 50 mV s^{-1}.

3. 2. Electrocatalytic activity toward ethanol electrooxidation

The electrocatalytic activity of the Co@Pt catalyst toward ethanol electrooxidation was characterized by cyclic voltammetry (Figure 2). The electrocatalytic activities are measured in a 0.5 M H_2SO_4 solution containing 0.5 M ethanol with scan rate of 50 mV s^{-1}. During anodic sweep two peaks of ethanol oxidation can be observed. The oxidation peaks appeared in the forward scan related to the oxidation of freshly chemisorbed ethanol species while the reverse oxidation peak is corresponding to removal of carbonaceous species partially oxidized in the

forward scan, rather than caused by newly adsorbed species [6]. The magnitude of the forward peaks current gives the electrocatalytic activity of the Co@Pt catalyst for ethanol oxidation.
The relation between the peak current density and $v^{1/2}$ (square root of scan rate) is plotted in the Figure 3 (a). It can be seen that the oxidation potential and peak current density for ethanol oxidation become larger with increasing scan rate. The peak current densities are linearly proportional to the square root of scan rates, which indicates the electrocatalytic oxidation of ethanol on Co@Pt may be controlled by a diffusion process [7]. In addition, the peak potential (Ep) for the forward scan increases with the increase of scan rate (v). Also a linear relationship can be observed between Ep and ln (v), in Figure 3 (b). It shows that the oxidation of ethanol is an irreversible electrode process [8].

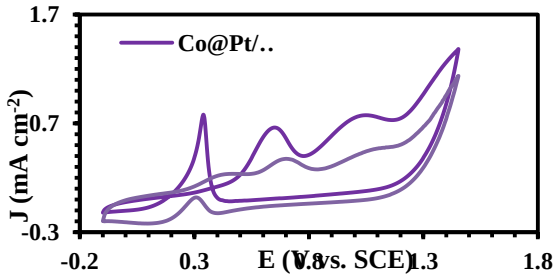

Figure 2: Cyclic voltammograms of the Co@Pt/CCE and Pt/CCE catalysts modified electrodes in 0.5 M H_2SO_4 + 0.5 M ethanol at scan rate of 50 mV s^{-1}.

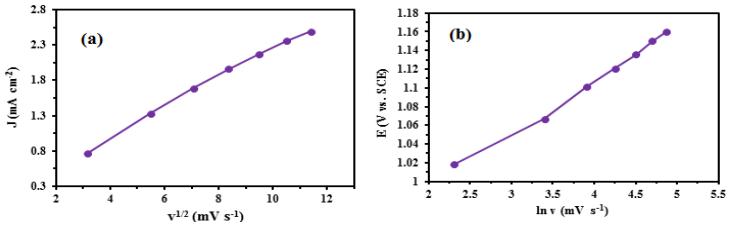

Figure 3: (a) The plot of the peak current density versus the square root of scan rate and (b) The plot of E (V vs. SCE) versus the ln v (mV s^{-1}).

The stability of Co@Pt modified electrode was investigated by chronoamperometry in 0.5 M H_2SO_4 containing 0.5 M ethanol at a potential of 6.5 V for 2500 s (Figure 4), the current density decreases quickly at first because of the poisoning of Co@Pt catalyst by generated species before reaching a stable value. However, Co@Pt modified electrode shows a slower current decay during the measured time, compared with the Pt-alone catalyst. These results showed that Co@Pt catalyst is stable and occupied with robust poisoning tolerance in acidic media [9].

4. Conclusions

In summary, Co@Pt nanoparticles were successfully synthesized by a facile, rapid, and simple method. Co@Pt nanoparticles were characterized using SEM, TEM, XRD and EDX and the results supported the existence of a core-shell structure. The electrocatalytic activity was investigated by electrochemical techniques. The core-shell nanostructure catalyst show improved catalytic activity and stability for ethanol electrooxidation compared to Pt-alone catalyst. The combination of high activity and tolerance to carbonaceous species poisoning makes the Co@Pt nanoparticles a promising catalyst for use in direct alcohol fuel cells.

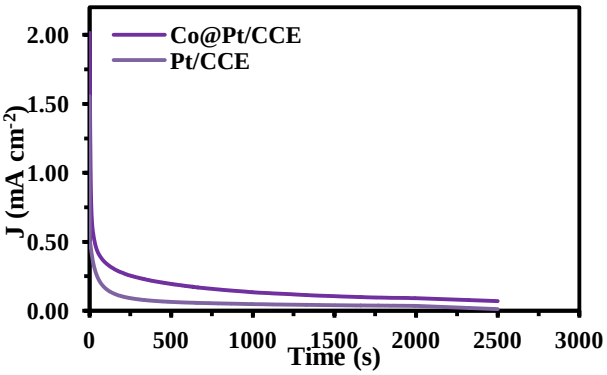

Figure 4: Chronoamperometric curves for the Co@Pt/CCE and Pt/CCE catalysts modified electrodes in 0.5 M H_2SO_4 + 0.5 M ethanol solution (polarization potential: 0.65 V) for 2500 s.

Acknowledgment

The authors gratefully acknowledge the Research Council of Azarbaijan Shahid Madani University for financial support.

References:

[1] X. Lu, F. Luo, H. Song, Sh. Liao, H. Li, "Pulse electrodeposition to prepare core-shell structured AuPt@Pd/C catalyst for formic acid fuel cell application", J. Power Sources (2014) 246, 659-666.

[2] M. Zhang, Z. Yan, J. Xie, "Core/shell Ni@Pd nanoparticles supported on MWCNTs at improved electrocatalytic performance for alcohol oxidation in alkaline media", Electrochim Acta (2012) 77, 237-243.

[3] G. Caballero-Manrique, A. Vel´azquez-Palenzuela, E. Brillas, F. Centellas, A. Garrido-Jos´e, R. M. Rodrı´guez, P. L. Cabot, "Electrochemical synthesis and characterization of carbon-supported Pt and Pt-Ru nanoparticles with Cu cores for CO and methanol oxidation in polymer electrolyte fuel cells", Int J Hydrogen Energy (2014) 39, 12859-12869.

[4] H. Wang, R. Wang, H. Li, Q. Wang, J. Kang, Z. Lei, "Facile synthesis of carbon-supported pseudo-core@shell PdCu@Pt nanoparticles for direct methanol fuel cells", Int J Hydrogen Energy (2011) 36, 839-848.

[5] N. M. Sa´nchez-Padilla, S. M. Montemayor, L. A. Torres, F. J. Rodrı´guez Varela, "Fast synthesis and electrocatalytic activity of M@Pt (M [Ru, Fe3O4, Pd) core-shell nanostructures for the oxidation of ethanol and methanol", Int J Hydrogen Energy (2013) 38, 12681-12688.

[6] N. Kakati, J. Maiti, S.H. Lee, Y.S. Yoon, "Core-shell like behavior of PdMo nanoparticles on multiwall carbon nanotubes and their methanol oxidation activity in alkaline medium", Int J Hydrogen Energy (2012) 37, 19055-19064.

[7] Z-P. Sun, X-G. Zhang, Y-Y. Liang, H- L. Li, "Highly dispersed Pd nanoparticles on covalent functional MWNT surfaces for methanol oxidation in alkaline solution", Electrochem Commun (2009) 11, 557-561.

[8] B. Habibi, E. Dadashpour, Carbon-ceramic supported bimetallic Pt-Ni nanoparticles as an electrocatalyst for electrooxidation of methanol and ethanol in acidic media, Int J Hydrogen Energy (2013) 38, 5425-5434.

[9] M. Etesami, N. Mohamed, "Catalytic Application of Gold Nanoparticles Electrodeposited by Fast Scan Cyclic Voltammetry to Glycerol Electrooxidation in Alkaline Electrolyte", Int. J. Electrochem Sci (2011) 6, 4676-4689.

8th Iranian Fuel Cell Seminar
FEBRUARY 25,26
2015

Electro-Oxidation Ethanol Using Modified Carbon Paste Electrode with MWCNTs and VSB-5 Nanozeolite for Fuel Cell

Mojtaba Gholami-Esfidvajani*, Seyed Karim Hassaninejad-Darzi
Research Laboratory of Analytical & Organic Chemistry, Department of Chemistry, Faculty of Science, Babol University of Technology, Babol, Iran,
** mojtabagholami@stu.nit.ac.ir*

Abstract
In this study, nanoporous nickel phosphate molecular sieve VSB-5 was synthesized and characterized by X-ray diffraction and scanning electronic microscopy (SEM). The electrocatalytic oxidation of ethanol in alkaline medium has been studied using multi-walled carbon nanotubes (MWCNTs) and VSB-5 nanorods modified carbon paste electrode. The electrochemical characterizations were performed using cyclic voltammetry (CV) and chronoamperometry techniques. A sensitive oxidation peak was observed at 0.53 V in 0.1 M NaOH solution for electrocatalytic oxidation of ethanol with EC′ mechanism. The values of catalytic rate constant and diffusion coefficient for ethanol and redox sites were obtained to be 5.76×10^{5} cm^{3} mol^{-1} s^{-1} and 1.49×10^{-7} cm^{2} s^{-1}, respectively. Obtained results from cyclic voltammetry and chronoamperometric techniques specified that the electrode reaction is a diffusion-controlled process. The results show that this electrode is very attractive for application in direct ethanol fuel cell.

Keywords: VSB-5 nanorods, MWCNTs, Electro-oxidation, Ethanol, Fuel cell

Introduction

Direct liquid fuel cells, such as direct alcohol fuel cells (DAFCs), have attracted much attention as one of the most viable candidates to replace batteries as a source of portable power. Among the various liquid fuels, ethanol is less toxic, has the higher energy density and is easier to store and handle than methanol [1]. Also, it can be produced in large quantities from agricultural products or biomass. Therefore, ethanol has received considerable attention over the years as a potential fuel for fuel cells [2, 3]. Therefore, the preparation of high active catalysts for ethanol oxidation is of a great significance. These common efficient catalysts for electro-oxidation of ethanol are noble metals such as Pt [4–6], Pd [6, 7] and their alloys [8–10], but the high price and finite reserves limit their commercial applications. For improving the efficiency of ethanol oxidation on fuel cells, a considerable effort has been devoted to developing nanoscale electrocatalyst. The choice of a suitable supporting material for the nanoparticles is important, which may affect the performance of the supported catalysts.

Carbon nanotubes (CNTs) have appeared to be a promising supporting material for the electrocatalysts owing to their unique one-dimensional nanostructure and excellent mechanical, electrical and surface properties [11]. Recently, there has been great interest to exploit the application of Multi-walled carbon nanotubes (MWCNTs) in the area of catalysts, where nanotubes can function as supports of heterogeneous catalysts [12]. Zeolites constitute a valuable class of advanced crystalline microporous inorganic materials with extraordinary properties making them ideal for molecular sieving, ion-exchange and shape-selective catalytic

processes. They have high surface areas with strongly organized microporous channel systems that exhibits an advantage compared to other classical support materials that are interest for fuel cell technology [13]. Nanoporous nickel phosphates VSB-5 (Versailles Santa Barbara-5) attract great interests, because their structures are thermo-stable and include transitional metal nickels. These materials could be potentially utilized based on their catalytic, spectroscopic, magnetic and electronic properties, which were rarely displayed in traditional zeolites or other porous silicas [14]. Design of modified electrodes for electrocatalysis has been extensively developed because these electrodes provide an excellent way to facilitate (accelerate) charge transfer processes. Modified electrodes decrease the overpotentials, which often required performing electrochemical transformations, as well as increasing the intensity of the corresponding voltammetric responses [15–18].

In this study, Nanoporous VSB-5 was synthesized and characterized by XRD and SEM techniques. Then, this nanozeolite with MWCNTs was applied for modification of CPE and applied for electrocatalytic oxidation of ethanol in the alkaline medium.

Experimental

Reagents and materials

Phosphoric acid (85%), diethyl ether, sodium hydroxide, ethanol, $NiCl_2{\cdot}6H_2O$, potassium ferricyanide ($K_4Fe(CN)_6$) and potassium chloride were purchased from Merck company that were of analytical reagent grade. Triethylamine ($N(C_2H_5)_3$) was obtained from Samchun Korea company. Graphite powder and paraffin oil (d = 0.88 g cm^{-3}) as the binding agent (both from Dayjung company) were used for preparing the pastes. All materials were used without any further purification. Also, all solutions were prepared with deionized water.

Synthesis of VSB-5 nanozeolite

The VSB-5 nanorods were synthesized through using triethylamine as template under hydrothermal conditions. In a typically synthetic, appropriate amount of $NiCl_2{\cdot}6H_2O$ was dissolved in distilled water, followed by adding H_3PO_4 (85%) and triethylamine with stirring. The mixed deep-purple solution (pH = 9.0) was sealed in a 100 mL teflon-lined autoclave. After heated at 180 °C for 3 days under autogenous pressure and quenched in cold water, the VSB-5 crystal nanorods were obtained through centrifuging from the brown solution (pH = 10.1). Then, synthesized material washed with distilled water for five times and calcinated for 10 h at 423 K.

Apparatus

The electrochemical experiments were performed at room temperature using SAMA500 potantiostat galvanostat Electrochemical Analysis System, Iran with a voltammetry cell in a three electrode configuration. The Ag|AgCl|KCl (3M) and platinum wire were used as reference and auxiliary electrodes, respectively. The bare CPE and modified CPE with VSB-5 nanozeolites and MWCNTs (VSB-5–MW/CPE) were used as working electrodes.

Preparation of the electrode

During preparation, diethyl ether was added to a mixture VSB-5 nanozeolites, MWCNTs and graphite powder. After hand mixing with a mortar and pestle, the solvent was evaporated with stirring. Then, paraffin oil (35%) was blended with the mixture in a mortar by hand mixing for 30 min until a uniformly wetted paste was obtained. This paste was packed into the end of a glass tube (ca. 0.35 cm i.d. and 10 cm long) and the copper wire was utilized for electrical contact. A new surface was achieved by pushing an excess of the paste out of the tube and polishing with a weighing paper. Bare CPE were also prepared in the same way in the absence of VSB-5 and MWCNTs.

Results and discussion

Characterization of VSB-5 nanozeolite

Figure 1 displays XRD pattern and SEM image of synthesized nanoporous VSB-5 molecular sieve. On the basis of previous reports [19, 20] VSB-5 has homogeneous morphologies (typically a rod-like shape) and its XRD pattern contains an intense signal at 2θ = 5.7°, also has a signal at 2θ = 11.3° with lower intensity and other weak signals. By considering XRD pattern as well as SEM image of synthesized sample with literature [19, 20], it can be deduced that the synthesized samples have VSB-5 morphology.

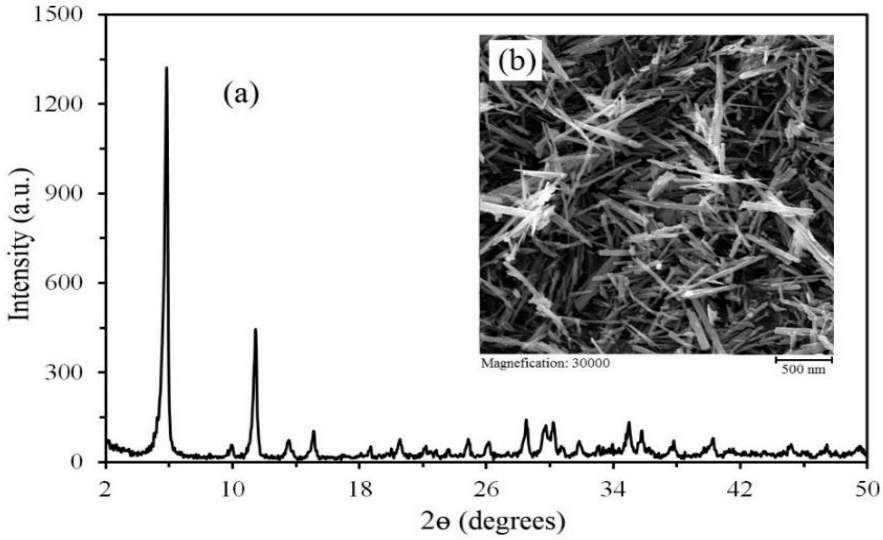

Figure 1: The representation of (a) XRD pattern and (b) SEM image of synthesized nanoporous nickel phosphate VSB-5 molecular sieve.

Electrochemistry of the modified electrode

Cyclic voltammetry (CV) was employed for the investigation of electrochemical properties of the unmodified CPE and modified electrode (VSB-5–MW/CPE) in potassium ferricyanide solution. Figure 2 displays the CVs of the electrochemical oxidation of $K_4Fe(CN)_6$ at the prepared bare CPE and VSB-5–MW/CPE electrodes in the ferricyanide solution. As can be seen in Figure 2, the anodic peak current for VSB-5–MW/CPE is higher than that at bare CPE. This is a quasi- reversible system because the peak separation potential, ΔE_p ($E_{pa} - E_{pc}$), is equal to 100 mV and lower than that for CPE.

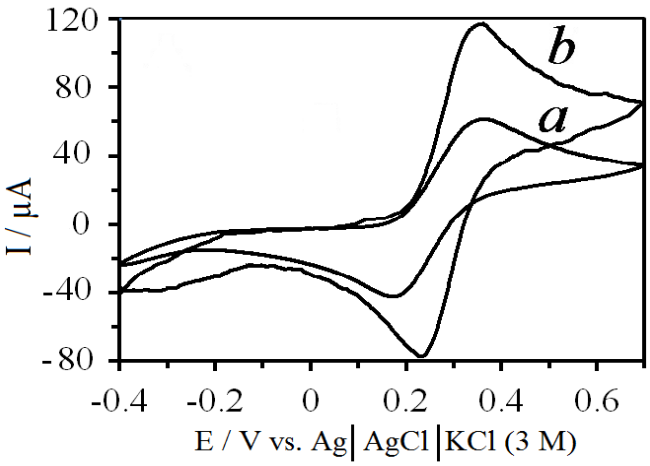

Figure 2: The CVs of (a) bare CPE and (b) VSB-5–MW/CPE in the presence of 10 mM $K_4Fe(CN)_6$ and 0.1 M KCl solution at a scan rate of 20 mV s^{-1} and pH of 7.0.

Electrochemical behavior of electrodes in alkaline media

The bare CPE and modified VSB-5–MW/CPE were immersed in the 0.1 M $NiCl_2$ solution with stirring for 15 min (optimum time) at 200 rpm, and then washed completely with distilled water to remove the surface adsorbed species. Figure 3(a) and 3(c) shows CVs of Ni-CPE and Ni-VSB-5–MW/CPE electrodes in 0.1 M NaOH solution. These redox waves are ascribed to the oxidation of $Ni(OH)_2$ at the VSB-5 nanozeolite/electrolyte interface to NiOOH and reduction of NiOOH to $Ni(OH)_2$ with a peak potential of 0.53 and 0.39 V vs. Ag|AgCl|KCl (3 M), respectively. As can be seen in Figure 3(d), the peak current of $Ni(OH)_2$ oxidation at the surface of Ni–VSB-5–MW/CPE is greater than that at Ni–CPE. These observations can describe clearly the role of the VSB-5 nanozeolite and MWCNTs on improvement of the oxidation currents.

Figure 3(d) exhibits the CV for electrocatalytic oxidation of 0.001 M ethanol in the surface of Ni–VSB-5–MW/CPE in 0.1 M NaOH at scan rate of 20 mV s^{-1}. After addition of ethanol, the peak around 0.53 V corresponding to the $Ni(OH)_2$/NiOOH transformation disappeared; meanwhile, one enhanced oxidation peak appears at around 0.6 V vs. Ag|AgCl|KCl (3 M). Also, cathodic peak current around 0.38 V decreased after addition of ethanol. It can be concluded that the over potential of ethanol electrooxidation was decreased in the surface of modified electrode.

This result specified that the applied modifier in this process participates directly in the electrocatalytic oxidation of ethanol. When ethanol diffuses from the bulk solution to the electrode surface it is quickly oxidized to produce by the NiOOH species on the electrode surface. Therefore, the amount of NiOOH species decreases due to its chemical reaction with ethanol. This behavior is a typical observation expected from the mediated oxidation (EC′ mechanism), illustrated in the following:

$$[(\text{Ni–VSB-5–MW/CPE}) - Ni(OH)_2] + OH^- \rightleftarrows [(\text{Ni–VSB-5–MW/CPE}) - \text{NiOOH}] + H_2O + e^- \quad (E)$$

$$[(\text{Ni–VSB-5–MW/CPE}) - \text{NiOOH}] + \text{EtOH} \rightleftarrows [(\text{Ni–VSB-5–MW/CPE}) - Ni(OH)_2] + \text{product} \quad (C')$$

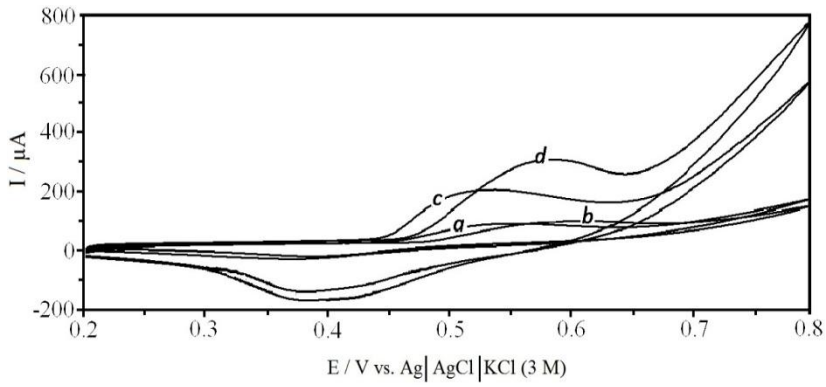

Figure 3: CVs of (a) bare CPE and (c) VSB-5–MW/CPE in the absence of ethanol and (b) bare CPE and (d) VSB-5–MW/CPE in the presence of 0.001 M ethanol at scan rate of 20 mV s^{-1} in the 0.1 M NaOH solution.

The influence of scan rate was also investigated on the electrocatalytic oxidation of 0.001 M ethanol in 0.1 M NaOH at the surface of Ni–VSB-5–MW/CPE. The increase in the peak current with the scan rate can be considered an adsorption or diffusion control of the process. A plot of I_{pa} vs. the scan rate (υ) in the range of 10–300 mV s^{-1} a linear curve (see Figure 4b); meanwhile, a plot of I_{pa} vs. the square root of scan rate ($\upsilon^{1/2}$) was found to be linear with equation of I_{pa} (μA) = 51.756 $\upsilon^{1/2}$ $(mVs^{-1})^{1/2}$ - 20.851 and R^2 = 0.9991 . This observation suggested that this process is diffusion-controlled process rather than surface-controlled process.

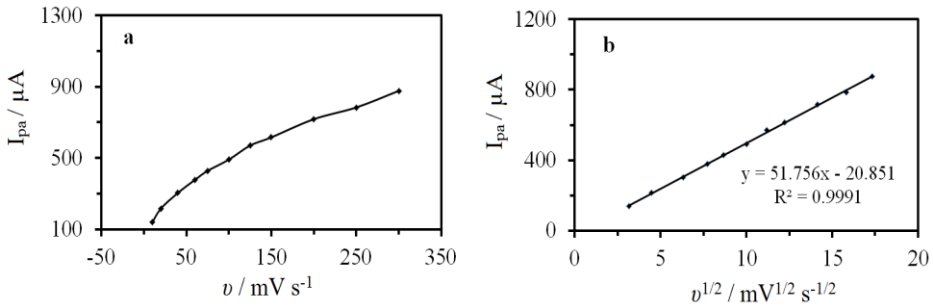

Figure 4: (a) The plot of I_{pa} vs. υ and (b) I_{pa} vs. $\upsilon^{1/2}$ extracted from CVs of the Ni–VSB-5–MW/CPE in the presence of 0.001 M ethanol in 0.1 M NaOH at various scan rates.

Chronoamperometric studies

Figure 5(A) illustrates double-step chronoamperometric measurements at the surface of the Ni–VSB-5–MW/CPE with several concentrations of ethanol such as 0.0, 0.001, 0.005 and 0.01 M. The applied potential steps were 0.65 and 0.35 V vs. Ag|AgCl|KCl (3 M) in the anodic and direction, respectively. It was found that the observed current from chronoamperograms was in good agreement with the detected current from cyclic voltammetry experiment and the current increases as the ethanol concentration increases (curves b, c and d). This result supports our conclusion about the catalytic role of NiOOH for oxidation of ethanol that ethanol oxidation starts directly after the formation of the first amount of NiOOH on the surface of electrode.

Chronoamperometry can be applied for the evaluation of the catalytic rate constant (k_{cat}) between the ethanol and redox sites of electrode according to following equation:

$$\frac{I_{cat}}{I_L} = \pi^{1/2}(k_{cat}C_0t)^{1/2} \quad (1)$$

where I_{cat} and I_L are the currents in the presence and absence of ethanol, respectively. The symbols k_{cat} is the catalytic rate constant ($cm^3\ mol^{-1}\ s^{-1}$), C_0 is the bulk concentration of ethanol ($mol\ cm^{-3}$) and t is the elapsed time (s). Figure 5B shows the plot of I_{cat}/I_L versus $t^{1/2}$ derived from the data of chronoamperograms in the absence (a) and presence of 0.01 M ethanol (d). From the slopes of the I_{cat}/I_L versus $t^{1/2}$ for all concentrations, the mean value of k_{cat} was calculated to be $5.76\times10^5\ cm^3\ mol^{-1}\ s^{-1}$. An exponential behavior of I–t curves shows that a diffusion-controlled process has occurred according to Cottrell equation. From the chronoamperometric study, the diffusion coefficient, D, of ethanol was determined in aqueous solution by using Cottrell equation:

$$I = nFACD^{1/2}.\pi^{-1/2}.t^{-1/2} \quad (2)$$

where F is the Faraday number, A is the area of the electrode, C is the known concentration of ethanol and D is the apparent diffusion coefficient. Figure 5C demonstrates experimental plots of I vs. $t^{-1/2}$ for 0.01 M of ethanol at the surface of Ni–VSB-5–MW/CPE. The same curves were plotted for all concentrations and then the slopes of the resulting straight lines were plotted vs. the ethanol concentration. From the slope of the resulting plots and using the Cottrell equation, the mean value of the D was obtained to be $1.49\times10^{-7}\ cm^2\ s^{-1}$ (with n = 4, F = 96485 $C.mol^{-1}$, and A = 0.0962 cm^2). A linear relationship in the plot I vs. $t^{-1/2}$ indicated that the electrode reaction is a diffusion-controlled process.

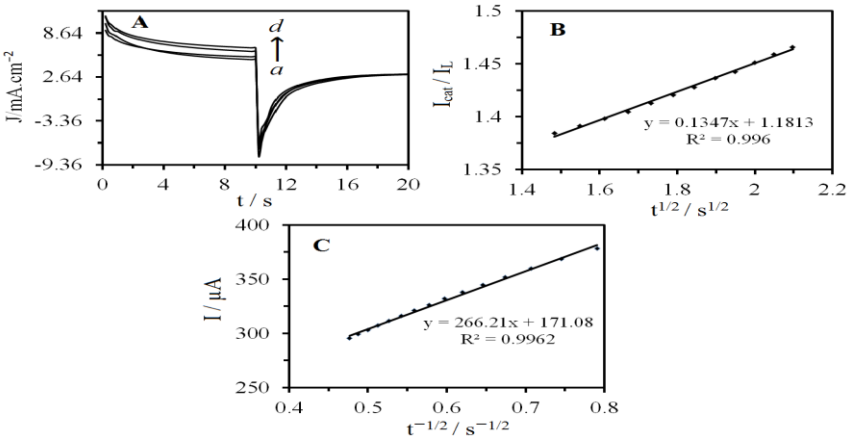

Figure 5: (A) The double-step chronoamperograms of Ni–VSB-5–MW/CPE in 0.1 M NaOH solution in the absence a and presence of b 0.001, c 0.005 and d 0.01 M of ethanol (the potential steps were 0.65 and 0.35 V vs. Ag/AgCl/KCl (3 M)). (B) Dependence of I_{cat}/I_L on $t^{1/2}$, derived from the data of chronoamperograms a and d. (C) Dependence of I on $t^{-1/2}$, derived from the data of chronoamperogram d.

Conclusions

Nickel phosphate VSB-5 nanorods was synthesized in the presence of triethylamine as template. The novel modified carbon paste electrode was prepared by loading nickel ions into VSB-5–MW/CPE modified electrode. The modified electrode can enhance the oxidation of ethanol through a decrease in over potential of ethanol oxidation and overcome the low kinetic of reaction in alkaline solution. Results specified that the NiOOH species formed during the oxidation of Ni-VSB-5–MW/CPE is found to be a good catalyst for oxidation of ethanol. It can be stated from the obtained results that this non-noble catalyst had some advantages such as low cost and stability, ease of preparation and regeneration, stable response and very low ohmic resistance.

References

[1] S.K. Hassaninejad–Darzi, M. Rahimnejad and S.M. Pourali "Preparation of template-free sodalite nanozeolite-chitosan modified carbon paste electrode for electrocatalytic oxidation of ethanol", J. Iran. Chem. Soc., 2014, DOI: 10.1007/s13738-014-0498-3.
[2] S. Nguyen, H. Law, T. Nguyen, N. Kristian, S. Wang and S. Chan "Enhancement effect of Ag for Pd/C towards the ethanol electro-oxidation in alkaline media", Appl. Catal. B Environ, (2009), 91, 507-15.
[3] L. Dai, L. Jiang, E. Abdel-Halim and J. Zhu "The fabrication of palladium hollow sphere array and application as highly active electrocatalysts for the direct oxidation of ethanol", Electrochem. Commun., (2011), 13(12), 1525-1528.
[4] X. Wang, C. Hu, Y. Xiong, H. Liu and G. Du "Carbonnanosphere-supported Pt nanoparticles for methanol and ethanol electro-oxidation in alkaline media", J. Power Sources, (2011), 196, 1904-1908.
[5] S. Lai and M. Koper "Ethanol electro-oxidation on platinum in alkaline media", Phys. Chem. Chem. Phys., (2009), 11, 10446-10456.
[6] P. Su, H. Chen, T. Chen, C. Liu, C. Lee and J. Lee "Enhancement of electrochemical properties of Pd/C catalysts toward ethanol oxidation reaction in alkaline solution through Ni and Au alloying", Int. J. Hydrogen Energy, (2013), 38, 4474-4482.
[7] M. Hasan, S. Newcomb, J. Rohan and K. Razeeb "Ni nanowire supported 3D flower-like Pd nanostructures as an efficient electrocatalyst for electrooxidation of ethanol in alkaline media", J. Power Sources, (2012), 218, 148-156.
[8] Y. Huang, J. Cai, M. Liu Y and Y. Guo "Fabrication of a novel Pt-Pb-Bi/C catalyst for ethanol electro-oxidation in alkaline medium", Electrochim. Acta, (2012), 83, 1-6.
[9] L. Yu and J. Xi "TiO2 nanoparticles promoted Pt/C catalyst for ethanol electro-oxidation", Electrochim. Acta, (2012), 67, 166-171.
[10] Y. Wang, F. Shi, Y. Yang and W. Cai "Carbon supported Pd-Ni-P nanoalloy as an efficient catalyst for ethanol electrooxidation in alkaline media", J. Power Sources, 2013, 243, 369-373.
[11] G. Wu and B.Q. Xu "Carbon nanotube supported Pt electrodes for methanol oxidation: A comparison between multi- and single-walled carbon nanotubes", J. Power Sources (2007), 174, 148-158.
[12] Z. Liu, Z. Li, F. Wang et al. "Synthesis of multi-walled carbon nanotube supported nickel catalysts by hydrazine reduction and their electrocatalytic activity on ethanol electro oxidation", Mater. Lett., (2011), 65, 3396-3398.
[13] A. Samadi–Maybodi, S. K. Hassani Nejad–Darzi, M. R. Ganjali and H. Ilkhani, "Application of nickel phosphate nanoparticles and VSB-5 in the modification of carbon paste electrode for electrocatalytic oxidation of methanol", J. Solid State Electrochem., (2013), 17, 2043-2048.
[14] S.H. Jhung, J.H. Lee, A.K. Cheethan et al. "A shape-selective catalyst for epoxidation of cyclic olefins:The nanoporous nickel phosphate VSB-5", J. catal., (2006), 239, 94-107.
[15] N. Rodthongkuma, N. Ruechab, R. Rangkupana, R.W. Vachetd and O. Chailapakul "Graphene-loaded nanofiber-modified electrodes for the ultrasensitive determination of dopamine", Anal. Chim. Acta, (2013), 804, 84-91.
[16] G. Yildiz, N. Oztekin, A. Orbay and F. Senkal "Voltammetric determination of nitrite in meat products using polyvinylimidazole modified carbon paste electrode", Food Chem., (2014), 152, 245-250.

[17] A. Bobrowski, A. Krolicka, M. Maczuga and J. Zarebski "A novel screen-printed electrode modified with lead film foradsorptive stripping voltammetric determination of cobalt and nickel", Sens. Actuators: B, (2014), 191, 291-297.
[18] M. Mazloum-Ardakani and A. Khoshroo "Nano composite system based on coumarin derivative–titaniumdioxide nanoparticles and ionic liquid: Determination of levodopaand carbidopa in human serum and pharmaceutical formulations", Anal. Chim. Acta, (2013), 798, 25-32.
[19] A. Samadi-Maybodi and S.K. Hassani Nejad-Darzi "Phase-selective crystallization of nickel phosphate VSB-5 with (2-hydroxyethyl) trimethylammonium hydroxide as template", Cryst. Res. Technol, (2011), 46, 383-388.
[20] S.H. Jhung, J.W. Yoon, Y.K. Hwang and J.S. Chang "Morphology control of the nanoporous nickel phosphate VSB-5 from large crystals to nanocrystals", Micropor. Mesopor. Mater. (2006), 89, 9-15.

8th Iranian Fuel Cell Seminar
FEBRUARY 25,26
2015

Evaluation of a Porous Nano Structure Electrode Base on Pt-Free Nano Catalyst for Direct 2-Propanol Fuel Cell

S. Samadinejad*, M. Zhiani
Department of chemistry, Isfahan University of Technology, Isfahan, Iran, 84156-83111
** somayeh.samadi@ch.iut.ac.ir*

Abstract
2-propanol is one of the most promising candidates for direct alcohol fuel cells (DAFCs). 2-Propanol is less toxic than methanol, it is less prone to crossover to the cathode, and it is not poison to the cathode like the methanol. In this project, a porous anode electrode was made based on the Pt-free Hypermec^{TM} (Fe-Co-Ni/C) nanocatalysts for evaluation of 2-propanol electrooxidation in alkaline media. Performances of the mentioned electrode and conventional palladium anode electrode in 2-propanol electrooxidation reaction were compared. The electrochemical behaviors of these electrodes were investigated by cyclic voltammetry techniques.
The chronoamperometry results showed clearly that the Hypermec^{TM} is a better catalyst for 2-propanol oxidation reaction than the Pd/C. The maximum current density value obtained for the Pt-free Hypermec^{TM} was 15 µA μg^{-1}_{metal} and for Pd/C (10% wt) was 11.5 µA μg^{-1}_{metal} . therefore, the Hypermec^{TM} electrocatalyst had a higher catalytic activity than Pd/C (10% wt) electrocatalyst.

Keywords: Non platinum nano catalyst, Pd/C nanocatalysts, Oxidation of 2-propanol.

1. Introduction

Direct alcohol fuel cells (DAFCs) have attracted enormous attention as power sources for portable electronic devices and transportation because liquid alcohol fuels have a higher energy density and are easier to handle and store than hydrogen gas fuel [1]. Direct 2-propanol fuel cells have attracted more and more attention as 2-propanol is the smallest secondary alcohol, less toxic than methanol and its electrochemical oxidation is of great interest due to its particular molecular structure . The direct alcohol fuel cells using 2-propanol as fuel show much higher performance and a much lower crossover current than direct methanol fuel cells[2].

In the present study, we introduce on the first time Pt-free Hypermec^{TM} as anod electrocatalyst, which is high electrocatalytic activity then other non-platinume electrocatalyst for electrooxidation of 2-propanol in alkaline media. Performance of this electrode compared to Pd/C (10% wt) this ability have been done by cyclic voltammetry (CV) and chronoamperometry. Finally, Pt-free Hypermec^{TM} catalyst were incorporated into the passive air breathing direct 2-propanol fuel cell.

2. Experiment

For a comparable reason, both catalyst inks prepared by the same method as follows as: the mixture was prepared by containing 8.0 mg of the catalyst powder, 300 µl of iso-propanol: pure water (80:20) and 1drope of nafion solution (5% wt) was added to the mixture and then it was stirred ultrasonic probe for 2 min to obtain a well-dispersed ink. The catalyst ink transferred onto the surface of the glassy carbon electrode by using micropipette, and finally dried at room temperature.

3. Results and Discussion

3.1 Electrocatalytic activity and stability of Pt-free and Pd/C 10 wt%

Figure 1. is a comparative cyclic voltammograms (CVs) of the different electrocatalysts in 1.0 M KOH and 0.5M 2-Propanol. By considering the onset potential of both catalysts, and peak current density of Pt-free Hypermec^{TM} and Pd/C (10% wt) (15 µA μg^{-1}_{metal} vs 11.5 µA μg^{-1}_{metal}), it could be concluded that the active surface area of Pt-free Hypermec^{TM} is higher than Pd/C (10% wt).

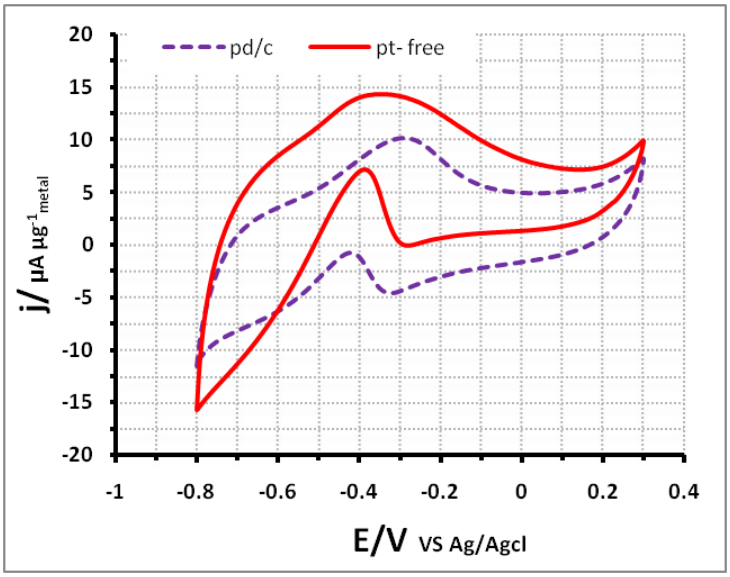

Figure 1.the CVs of 0.5 M 2-Propanol oxidation on different electrocatalysts at20 mV s^{-1} in 1 M KOH at 25 °C.

3.2. The effect of scan rate

The effect of scan rate on the electro-oxidation of 2-propanol on Pt-free Hypermec^{TM} and Pd/C (10% wt) catalysts was shown in Figure 2.In the range of 5-300 mVs^{-1}, the peak current increased with the square root of the scan rates (Figure 3). This result showed that 2-propanol electro-oxidation reaction on Pt-free Hypermec^{TM} and Pd/C (10% wt) catalysts was controlled by diffusion of 2-propanol to the electrode surface. Furthermore, one observed that 2-propanol electro-oxidation peak potential shifted more positive potential by increasing scan rate (Figure 2). This phenomenon could be attributed to irreversible electrode process of 2-propanol electro-oxidation.

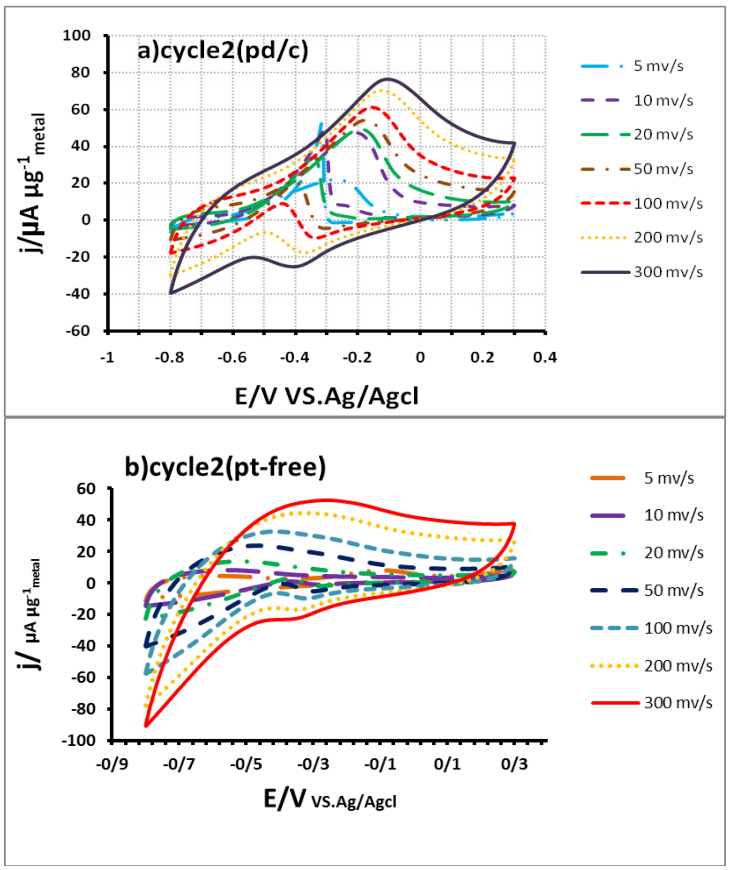

Figure 2- Cyclic voltammograms at varying scan rates in 0.5 M 2-Propanol and 1M KOH

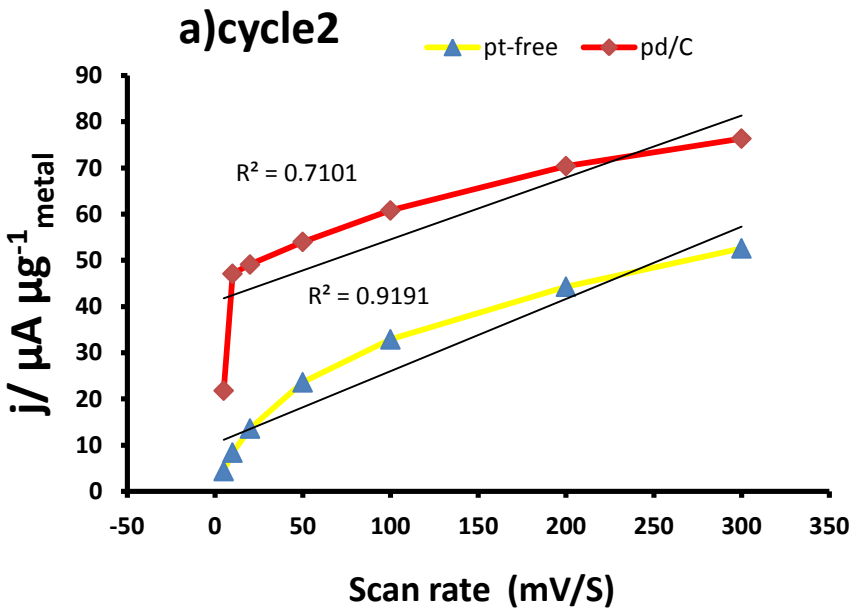

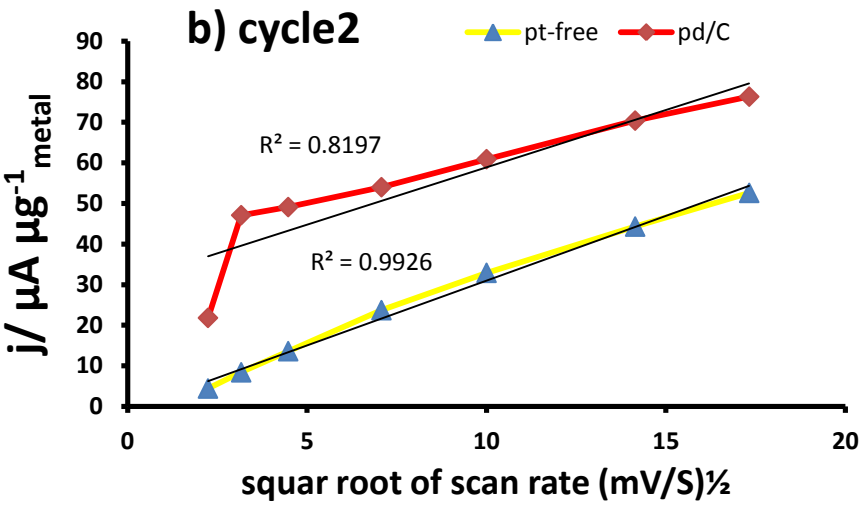

Figure 3 - Plots of currents of 2-Propanol oxidation versus scan rates and versus square root of scan rate.

Acknowledgement

This work was carried out in electrochemical laboratory of Isfahan University of Technology (IUT). The author would like to thanks the research council of IUT. The support of the fuel cell steering committee and Iranian nano technology initiative council are also acknowledged.

References

[1] Y.Liu, Y. Zeng, R. Liu, H.Wu, G.Wang, D. Cao, Poisoning of acetone to Pt and Au electrodes for electrooxidation of 2-propanol in alkaline medium, Electrochimica Acta 76 (2012) 174.

[2] J.Ye , J.Liu a, C. Xu ,S. Ping Jiang, Y.Tong, Electrooxidation of 2-propanol on Pt, Pd and Au in alkaline medium, Electrochemistry Communications 9 (2007) 2760.

8th Iranian Fuel Cell Seminar
FEBRUARY 25,26
2015

Electrocatalytic Activity of Green Synthesized CuO Nanoparticles/Conductive Polymer Composite Film in DMFC

A. Ehsani, M. Ahmadi, A. Rostami-Vartooni
Department of Chemistry, Faculty of science, University of Qom, Qom

Abstract
In this work, CuO NPs was prepared by a simple and green method using Rosarinusofficinalis extract containing phenolic constituents as both the chelating and the stabilizing agents. CuO nanoparticles/ polyorthoaminophenol composite as electro-active electrodes for electro catalytic oxidation of methanol with good uniformity are prepared by electropolymerization. Composite of CuONps/POAP was synthesized by cyclic voltammetry (CV) methods and electrochemical properties of film were investigated by using electrochemical techniques. New composite modified electrode shows a significantly higher response for methanol oxidation.

Keywords: Green synthesis, Nanocomposite, CuO NPs, Impedance, Electrocatalytic

1. Introduction

CuO nanostructures (CuONPs) have been extensively investigated because of their promising applications in various fields such as catalysis, batteries,semiconductors,supercapacitors,solar cells, sensors, nanofluid andphotodetectors [1-5].CuO nanostructures are potential catalysts for oxidation reactions of CO and for substituting noble metal catalysts due to their high catalytic activity, low-cost, and availability. A number of researchers have used thermal decompositions for the preparation ofCuO nanoparticles (NPs.Using the novel compounds or new methods can be useful for preparing nanomaterials to control the size, shape and distribution size. Copper-based and its oxide-based nanomaterials were of great interest for their extensive applications in catalysis, gas sensor, Li ion battery and biosensors for a long time. Herein, we describe a simple strategy dispersing of CuONPs within the conducting polymer matrix by in situ electropolymerization using an ionic surfactant as the supporting electrolyte.

2. Experimental

For green synthesis of CuO NPs, 0.2 M of cupric choridedihydrate$CuCl_2 \cdot 2H_2O$ was dissolved in 100 ml of distilled water under magnetic stirring at 50 $^{\circ}$C temperature. The addition of the Rosarinusofficinalis extract causes the formation of dark brown precipitate which then transforms into CuO by heat treatment. After 30 min, the mixture was centrifuged, washed with distilled water and then dried at 70 $^{\circ}$C for 1 h. Finally, crystalline CuONPs were obtained after calcination at 300 $^{\circ}$C for 3 h in furnace. The CuONPs were first dispersed in an aqueous solution containing an ionic surfactant. Then electroactive monomer (Ty) was added into the above mixture and finally electrochemical reaction was preceded at the surface of the graphite electrode. In the present work CuONPs /POAP composite was synthesized by cyclic

voltammetry methods and electrochemical properties of film were investigated by using electrochemical techniques, viz. CV and electrochemical impedance spectroscopy.

3. Results and discussion

Fig. 1 shows the UV-vis spectra of Rosarinusofficinalis extract. The observed bands are assigned to $\pi \rightarrow \pi^*$ and $n \rightarrow \pi^*$transitions of benzene rings and carbonyl groups in the extract compounds. The constituents of aqueous extract could be adsorbed on the surface of metal nanoparticles, possibly by interaction through π-electrons interaction. Hence, the extract acts as the stabilizeras well as the chelating agents.

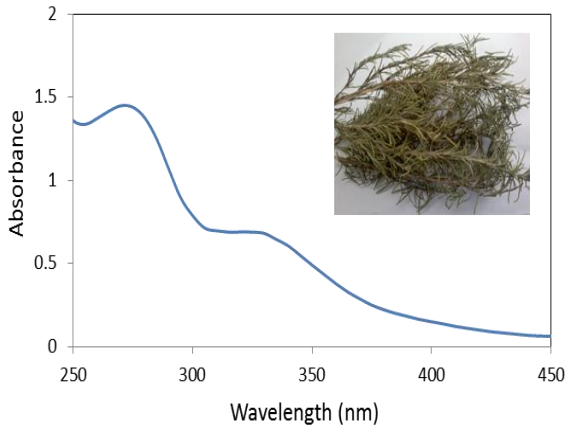

Figurer 1. UV-vis spectrum of Rosarinusofficinalis leaves and roots extract.

Fig. 2 shows the XRD pattern of CuO NPs. All the diffraction peaks could be clearly indexed to monoclinic phase of CuO agreed with the data of the Joint Committee on Powder Diffraction Standards file (JCPDS No.05-0661).

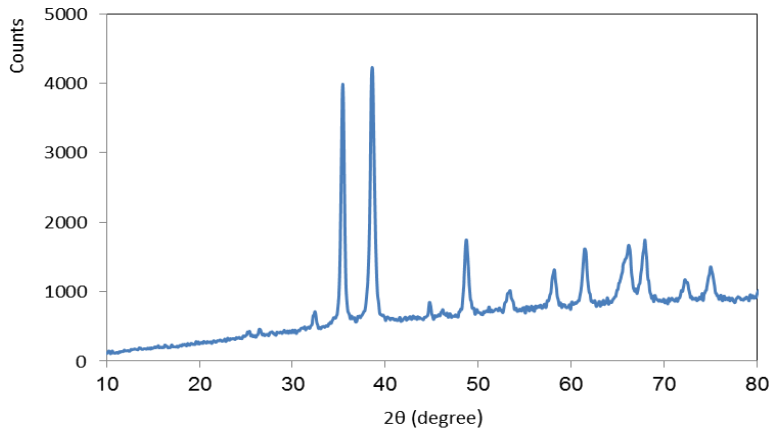

Figure 2.XRD pattern of CuONPs.

Composite films were applied to electrooxidation of methanol in alkaline media.Figure 3 shows cyclic voltammograms of CuONps/POAP/G electrode in 0.1 M NaOH solution in the presence of different concentration of methanol at a potential sweep rate of 10 mV s^{-1}. The larger methanol response at the CuONps/POAP/G respect CuO/G electrode is proposed to be the CuONps/POAP enhances the catalytic properties of copper oxide through fine dispersion of the catalyst particles into the conductive polymer matrix to results in a drastic increase in surface area.

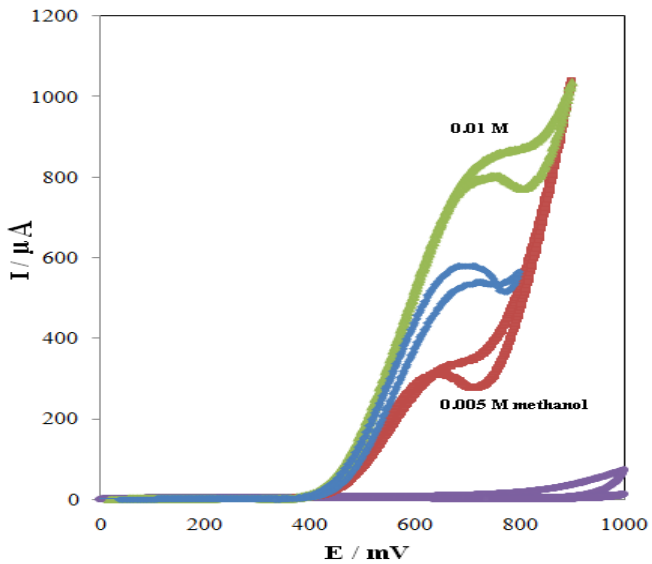

Figure 3. Cyclic voltammograms of CuONps/POAP electrode in 0.1 M NaOH solution in the presence of different concentration of methanol at a potential sweep rate of 10 mV s^{-1}.

At CuONps/POAP/G electrode, oxidation of methanol appeared as a typical electrocatalytic response in alkaline media by $Cu(OH)_2$/CuOOH [6, 7]. The anodic electrochemical reactions can be summarized as follows:

$$Cu^{2+} \rightarrow Cu^{3+} + e^- \quad (1)$$

$$Cu^{3+} + CH_3OH_{ads} \rightarrow Cu^{2+} + intermediate \quad (2)$$

$$Cu^{3+} + intermediate \rightarrow Cu^{2+} + product \quad (3)$$

Figure 4 presents the Nyquist diagrams of CuONps/POAP/G in different concentration of the methanol. In the methanol's concentration range of 0.005-0.02 M a steady decrease of the diameter of the semi-circle is witnessed. Diagrams consist of a small semicircle terminated to depressed capacitive semicircles at low frequency end of the spectrum. The equivalent circuit compatible with the Nyquist diagram recorded in the presence of methanol was depicted in Fig. 4. To obtain a satisfactory impedance simulation of ethanol electro-oxidation, it is necessary to replace the capacitor *C* with a constant phase element (*CPE*) in the equivalent circuit. The most widely accepted explanation for the presence of *CPE* behavior and depressed semicircles on solid electrodes is microscopic roughness, causing an inhomogeneous distribution in the solution resistance as well as in the double-layer capacitance. The parallel combination of charge transfer resistance R_1 and constant phase element CPE_1 accounts for the injection of electrons from the conductive polymer to the back metallic contact. R_2 and CPE_2 represent the methanol oxidation. As increasing methanol concentrations decrease the diameters of semicircle, and charge transfer for methanol electrooxidation on the surface of CuONps/POAP/G is lower than CuO /G.

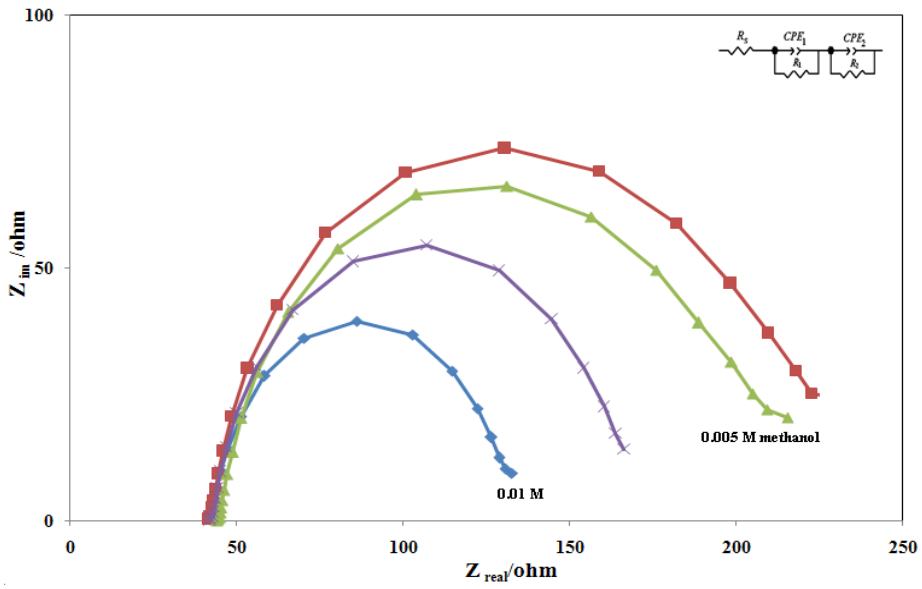

Figure 4. Nyquist diagrams of CuONps/POAP/G electrodes recorded at 600 mV dc-offset in the presence of different concentration of methanol in 0.1 M NaOH solution.

4. Conclusions

CuO NPs was prepared by a simple and green method using Rosarinusofficinalis extract containing phenolic constituents as both the chelating and the stabilizing agents. CuO nanoparticles/ polyorthoaminophenol composite as electro-active electrodes for electro catalytic oxidation of methanol with good uniformity are prepared by electropolymerization. Composite of CuONps/POAP was synthesized by cyclic voltammetry (CV) methods and electrochemical properties of film were investigated by using electrochemical techniques. New composite modified electrode shows a significantly higher response for methanol oxidation.

References

[1] S. Stankovich, D.A. Dikin, G.H.B. Dommett, K.M. Kohlhaas, E.J. Zimney, E.A. Stach, R.D. Pinen, S.T. Nguyen, R.S. Ruoff, Nature 442 (2006) 282 .
[2] S. Guo, S. Dong, E. Wang, ACS Nano 4(2009) 547.
[3] M.D. Stoller, S.J. Park, Y.W. Zhu, J.H. An, R.S. Ruoff, Nano Lett. 8 (2008)3498.
[4] C.S. Shan, H.F. Yang, J.F. Song, D.X. Han, A. Ivaska, L. Niu, Anal.Chem. 81 (2009) 2378.
[5] Y. Wang, Y. Li, L. Tang, J. Lu, J. Li, Electrochem. Commun. 11(2009) 889.
[6] A. Ehsani, B. Jaleh, M. Nasrollahzadeh, J. Power Sources. 257(2014) 300.
[7] AJ. Bard, LR Faulkner. Electrochemical Methods. (Wiley, New York, 2001).

8th Iranian Fuel Cell Seminar
FEBRUARY 25,26
2015

Electrooxidation of Acetaldehyde Using $PtSnO_2$/C and $PtSnO_2$/CNT Catalysts Prepared by Modified Alcohol-Reduction Process

S. Sadeghi*, H. Gharibi, F. Golmohammadi, F. Dehghan
Department of Chemistry, Tarbiat Modares University, Tehran, P.O. Box 14115-175, Iran
** Sadegh.sd@gmail.com*

Abstract
Well-dispersed binary PtSnO2 catalysts with atomic ratio of 75:25 were deposited onto Vulcane XC-72R and CNT using modified alcohol-reduction process for electrochemical oxidation of acetaldehyde. We use CNTs as catalyst support for PtSnO2 catalyst .In this work, we synthesized SnO2 by an ex situ method and made a binary catalyst by adding a tin oxide to Pt supported on CNT and its performance compared with Pt-SnO2/C. The XRD analysis showed the alloy catalyst was synthesized. An electrochemical study in acetaldehyde and acid medium showed that the PtSnO2/CNT catalyst had a better performance compared with the PtSnO2/C catalyst. The CV analysis indicate that the presence of CNT as support increase the activity of catalyst to oxidation of acetaldehyde and have a low onset potential (about 200 mV) for the electrooxidation of adsorbed acetaldehyde than PtSnO2/C. However, for the overall oxidation of acetaldehyde, the PtSnO2/CNT catalyst is favorable for the activation of C-C bond breaking, thereby generating higher current density (mass activity) at higher potentials.

Keywords: CNT, Tin Oxide, Acetaldehyde Oxidation.

Introduction

Acetaldehyde was oxidized to carbon dioxide on various platinum alloy electrodes in the over voltage potential region. Unsuccessfully, the lone reaction product we obtained was acetic acid, which is known to be hard to transform into carbon dioxide.

Electrochemical oxidation of acetaldehyde continues to be an interesting topics because it arouses great investigations in different catalytic application areas. It is an intermediate product in ethanol electrooxidation [1].

However, although it is evidenced that the overall kinetics can be improved by using bimetallic Pt-based electrocatalysts, the incomplete ethanol oxidation also prevails on these binary catalysts.

Adsorbed C2 hydrocarbon residues have been identified as major adsorbed intermediates by means of differential electrochemical mass spectrometry (DEMS) and in situ infrared spectroscopy. Acetaldehyde and acetic acid have been detected as the main by-products. Thus, although there is agreement that PtRu and PtSn are more active for the oxidation of ethanol, the effect of the second metal (Ru and Sn) does not seem to be similar in each case. Further study is necessary to reap the beneficial effects of each metal in improvement of the activity and selectivity for the reaction [2].

Behm et al. showed that on Pt_3Sn/C, PtRu/C and Pt/C atalysts investigated C–C bond breaking is negligible. . The low activity for C–C bond breaking, which is also characteristic for ethanol oxidation, governs acetaldehyde oxidation. Therefore these catalysts will not be able to correct the low selectivities for complete ethanol oxidation observed previously by subsequent complete oxidation of the incomplete oxidation products acetaldehyde and acetic acid [3].
In this work, we synthesized SnO_2 by an ex situ method and made a binary catalyst by adding a tin oxide to Pt. Using CNT and Vulcan for support catalyst results show that the CNT enhanced the ECSA and increase acetaldehyde oxidation in acid environment.

Materials and method

SnO_2 synthesis

The steps involved in the synthesis of SnO_2 were: i) addition of the required $SnCl_4$. $4H_2O$ to 50cc of water ii) add the 2M KOH solution to the mixture until the solution were opaque iii) after 6h the mixture was filtered and washed with water 3 times and drying of the solid at 80 oC for 24 h iv) finally, the solid was heated up to 500 ^oC for 4 h in the stove under ambient gasses to complete oxidation of tin oxide to SnO_2.

Catalyst synthesis

PtSnO2 nanoparticles were deposited on Vulcan XC-72R and CNT by using the modified polyol method. The steps involved in the preparation were: i) incorporation of a predetermined amount of carbon, i.e. Vulcan, to 15 cc of ethylene glycol, and then sonicated the whole mixture for 30 min; ii) addition of the required precursors, i.e. H_2PtCl_6, and SnO_2 to the mixture in the stoichiometric amount required and sonicated for 30min ; iii) 45cc of ethylene glycol was added and sonicated for 30 min;iv)increasing the temperature up to 120 oC, and then keeping it constant for 12 h to allow the nucleation and growth of the alloy metal on the carbon support; v) cooling the suspension down to room temperature; vi) separation of the solid by filtration, subsequent thorough rinsing with water and drying of the solid at 80 ^oC for 24 h in an oven. The atomic ratio of catalysts were $PtSnO_2$ (3:1) with 10% of metal and metal oxide loading.

Electrochemical characterization

For the electrochemical characterization, a conventional three-electrode cell was employed. The working electrode was a glassy carbon of 0.031415 cm^2 geometric area, covered by a thin layer of catalyst imbedded in a Nafion polymer electrolyte film. A Pt foil of 1 cm^2 geometric area was used as counter electrode and a saturated calomel electrode as reference electrode. The electrolyte was a 0.25 M acetaldehyde in 0.5 M H_2SO_4 solution. Most of the electrochemical experiments were carried out at room temperature. The real active electrode area was determined from the CV in acidic media at 50 mV s^{-1} in 0.5 M H_2SO_4.

Results and Discussion

XRD

The XRD patterns were obtained at a scanning rate of 1o/min with a step size in the 2θ scan of 0.02^o in the range $20\text{-}80^o$. Fig.1 Show the tin oxide was synthesized and the sample was pure.

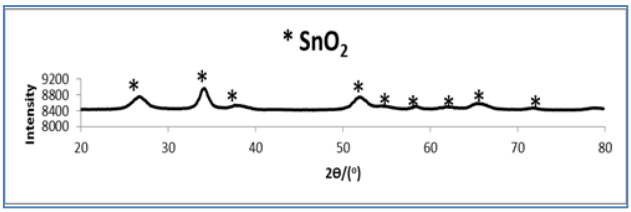

Fig.1. XRD patterns of SnO_2.

Cyclic voltamograms

From the CVs, the electrochemically active surface area (SEAS) is determined by integration of the anodic current corresponding to hydrogen desorption reaction with the correction of double layer region. The SEAS values which can be calculated from Eq. (1) [4]:

$$S_{EAS}(m^2 g^{-1}) = \frac{Q_H(\mu C / cm^2)}{210 \times L(g / m^2)} \quad (1)$$

Where Q_H (μC cm^{-2}) represents the charges corresponding to desorption of hydrogen on the Pt surface, L (g m^{-2}) is the Pt loading on the electrode surface, 210 μC/real cm^2 is the charge required to oxidize a monolayer of hydrogen on the Pt surface. Results from table 1 shows PtSnO2/CNT have a higher EAS than $PtSnO_2$.C. The higher surface of CNT caused the better dispersion of catalyst.

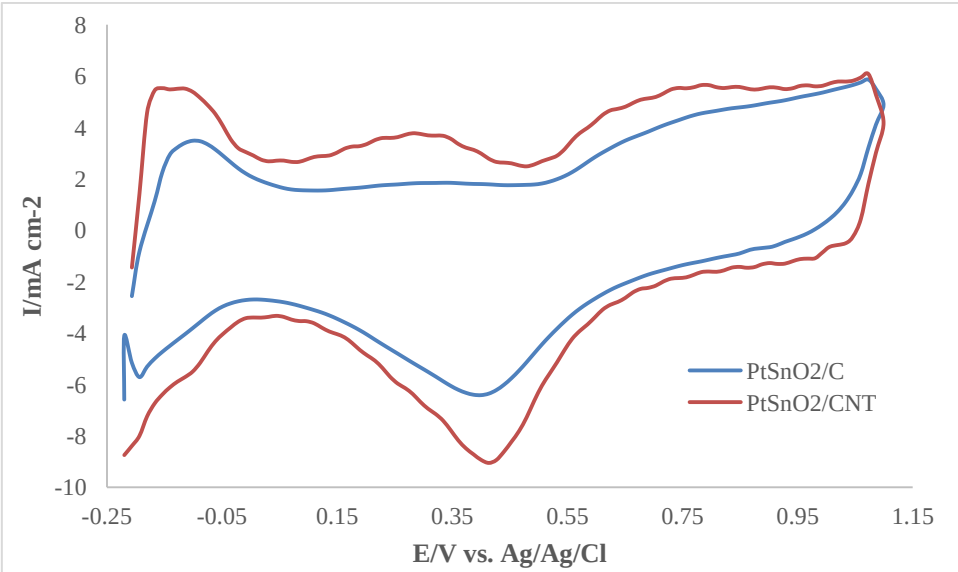

Fig. 3. Cyclic voltamograms of the $PtSnO_2$/C and $PtSnO_2$/CNT in 0.5M H_2SO_4 solution at the 50th cycle with a scan rate of 50mVs^{-1}.

Sample	Q_H(μC)	EAS(m^2/gr)
Pt-SnO2/C	356.8	69.31
Pt-SnO_2/CNT	745.9	14.32

Table1. The EAS values of different catalyst samples determined by hydrogen electroadsorption.

Electrochemical activity of the catalysts for acetaldehyde

The catalytic activities of the carbon-supported $PtSnO_2/C$ and PtSnO2/CNT catalysts for acetaldehyde electrooxidation are investigated at ambient temperature by cyclic voltammetry (CV) at a scan rate of 10 mV s^{-1} in 0.25 M acetaldehyde + 0.5 M H_2SO_4(aq) solution (Fig. 2).

According to the CV curves, the hydrogen adsorption/desorption are greatly depressed by acetaldehyde adsorption onto the catalysts [1]. Highest mass activity and the lowest onset potential were observed on the $PtSnO_2$/CNT. The enhancements toward acetaldehyde oxidation by addition of SnO_2 into Pt are mainly attributed to the effective removal of C2 species and inhibition of poison formation. They do not involve the C-C breaking.

The onset potential on $PtSnO_2$/CNT is about 200 mV less than PtSnO2/C (Fig. 2). Such a significant enhancement in the oxidation current density and reduction of onset potential underline the importance of dispersion of catalyst in the catalytic process. Pt improved by addition of tin oxide that can provide oxygen containing species (i.e., OH) at low potentials for oxidation of poisoning intermediates and reactions which need adsorbed hydroxyl to do such a acetaldehyde oxidation.

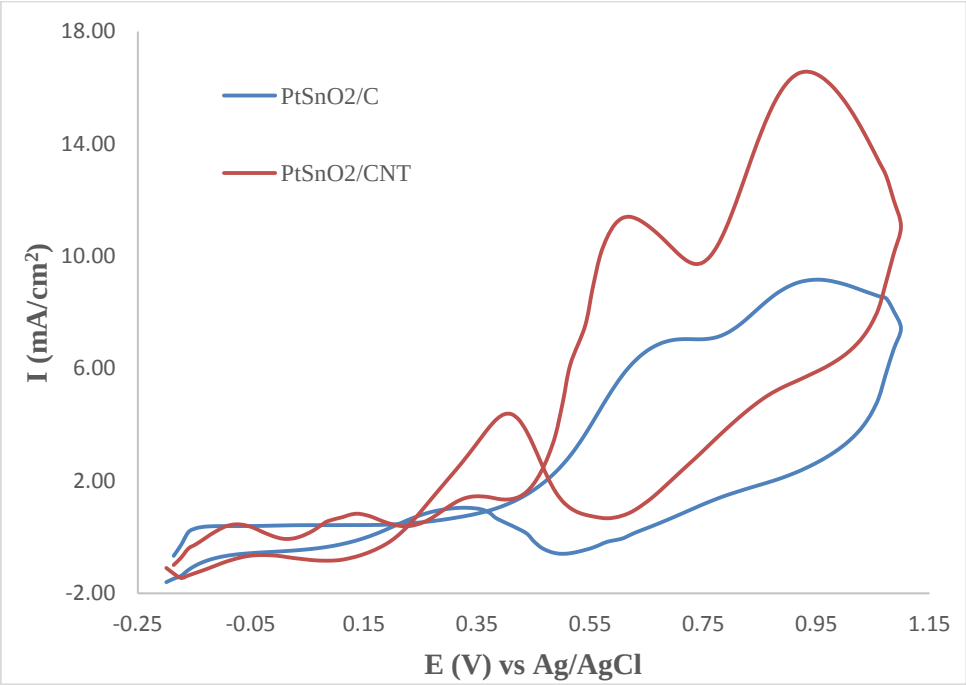

Fig2. Cyclic voltamograms of the $PtSnO_2$ and PtSn in 0.25M acetaldehyde + 0.5M H_2SO_4 solution at the 10th cycle with a scan rate of $10mVs^{-1}$.

References

1. Kokoh, K., et al., Electrocatalytic oxidation of acetaldehyde on Pt alloy electrodes. Electrochimica acta, 2004. **49**(13): p. 2077-2083.

2.Wu, G., R. Swaidan, and G. Cui, Electrooxidations of ethanol, acetaldehyde and acetic acid using PtRuSn/C catalysts prepared by modified alcohol-reduction process. Journal of Power Sources, 2007. **172**(1): p. 180-188.

3.Wang, H., Z. Jusys, and R. Behm, Electrooxidation of acetaldehyde on carbon-supported Pt, PtRu and Pt3Sn and unsupported PtRu0. 2 catalysts: A quantitative DEMS study. Journal of applied electrochemistry, 2006. **36**(11): p. 1187-1198.

4.Zhang, J., PEM fuel cell electrocatalysts and catalyst layers: fundamentals and applications. 2008: Springer.

8th Iranian Fuel Cell Seminar
FEBRUARY 25,26
2015

Preparation and Evaluation of New Anode Electrode Microstructures Based on Iron-Nickel-Cobalt Nano Catalyst for Direct Fuel Cell 1-Propanol

M. Zhiani*, K. Esteghlal
Department of Chemistry, Isfahan University of Technology, Isfahan, Iran
** k.esteghlal@gmail.com*

Abstract
The electro catalytic oxidation of n-propanol was studied on Pt-free Hypermec^{TM} (Fe-Co-Ni) nano catalysts and Pd supported over commercial carbon electrodes in 0.1 M KOH solution at room temperature. Cyclic voltammetry (CV), and chronoamperometry techniques were employed. Scanning electron microscopy (SEM) was also employed to morphological study of the catalyst layer. Performances of the Pt-free electrode and conventional palladium anode electrode in n-propanol electro oxidation reaction were compared. The Pt-free Hypermec^{TM} showed a higher activity toward n-propanol oxidation than the Pd/C (10% wt), in the Cyclic voltammetry measurement. The chronoamperometry results showed clearly that the Hypermec^{TM} is a better catalyst for n-propanol oxidation reaction than the Pd/C (10% wt). The maximum current density value obtained for the Pt-free Hypermec^{TM} was 63 µA µg^{-1} metal and for Pd/C (10% wt) was 48 µA µg^{-1} metal in present the fuel. Therefore, the Hypermec^{TM} electro catalyst had a higher catalytic activity than Pd/C (10% wt) electro catalyst. Moreover, n-propanol oxidation reaction on the tow electrode is diffusion-controlled and represents a good linear correlation with propanol concentration. The results indicate that Pt-free Hypermec^{TM} (Fe-Co-Ni) nanocatalysts is attractive as a promising electro catalyst of alkali-type direct n-propanol fuel cells.

Keywords: Non platinum (Fe-Co-Ni) nano catalysts, Oxidation of n-propanol, Fuel cell.

Introduction

In recent years, direct alcohol fuel cells (DAFCs) have been considered as promising power generators for portable devices [1-2]. The saturated C3-alcohols (1-propanol and 2-propanol) have also been investigated as the fuels for DAFCs due to them are less toxic than methanol [3, 4]. The DAFCs using C3-alcohols as fuel show better performance than DMFCs and a much lower crossover current [5, 6]. As with all organic fuels challenges have to be faced: firstly, reaction kinetics of alcohols are clearly lower compared to hydrogen and therefore the power densities obtained from these cells are moderate. Secondly, only very diluted alcohol solutions can be used due to the severe crossover of the fuels through electrolyte membrane leading to mixed potentials and lower total performance of the cell. It is well known that in alkaline medium alcohol oxidation kinetics is enhanced [15-19]. Unfortunately, the lack of stable anion exchange membrane materials has restricted development of alkaline DAFCs, but in recent years new membranes have been developed and successfully demonstrated in fuel cells [20-28]. With these materials also the alcohol crossover rate is reduced [28, 29] providing a possibility to use more concentrated alcohol solutions that would reduce the complicity and weight of the total

fuel cell system. Currently, alkaline DAFC experiments are often performed with NaOH or KOH introduced to the anode fuel to increase current densities and open circuit voltages (OCV) [27, 28]. In long term experiments, however, this leads to formation of carbonate/bicarbonate if free cations are available that can accumulate to the cell in similar fashion as in alkaline fuel cells (AFC) [30] and therefore in this study alcohol–water mixtures are used as fuels.

A lot of work has been done to study the electro oxidation of 1-propanol on Pt-based catalysts in alkaline medium [7-11]. However, the activity of 1-propanol electro oxidation on Pt-based catalysts is very low and the high price and limited supply of Pt constitute major barriers to the development of DAFCs. Some work on the development of Pt-free electro catalysts for alcohol oxidation has focused on Pd-based catalysts and the results revealed that Pd is a good electro catalyst for ethanol and 1-propanol oxidation in alkaline medium [12-14]. Pd-based electro catalysts have been used for formic acid and hydrazine electro-oxidation in acid medium [31–33] and formaldehyde electro-oxidation in alkaline medium [34]. A novel carbon ceramic electrode is prepared using a Ni-Al LDH nanoparticles and investigation of the electro catalytic properties of a Ni/Al LDH/NMCC electrode toward the oxidation of n-propanol. The electrochemical behavior of n-propanol suggests that Ni/Al LDH/NMCC exhibits obvious electrocatalytic activity to the oxidation of n-propanol, since it greatly enhances the oxidation peak current of n-propanol. Ghasem Karim-Nezhad and et al [35]. Hu and co-workers have also studied the mechanism of the ethanol oxidation on Pd–NiO/C catalyst and have found that the Pd–NiO/C catalyst presents higher electro activity and less CO poisoning for the ethanol oxidation than Pt–NiO/C catalyst [36].

The faster kinetics of the alcohol oxidation and oxygen reduction reactions in alkaline direct alcohol fuel cells (ADAFCs), opening up the possibility of using less expensive metal catalysts, as silver, nickel and palladium, makes the alkaline direct alcohol fuel cell a potentially low cost technology compared to acid direct alcohol fuel cell technology, which employs platinum catalysts. Antolini et al [37].

Experimental

Electrochemical investigation

Deposition of catalysts on glassy carbon

Pt-free Hypermec^{TM} catalyst was purchased from Sigma Aldrich Chemie GmbH. A thin film of catalyst layer on the glassy carbon electrode (with area of 0.0314 cm2) was prepared as follows: a mixture containing 2.0 mg electrocatalyst Pt-free Hypermec^{TM}, 1 ml of 2-propanol (Merck), 1 ml of ultrapure water (MilliQ, Millipore, 18.2 MΩ-cm) and 0.01 ml of 5 wt % Nafion solution (Aldrich) was stirred ultrasonically for 5 min to obtain a well-dispersed ink. The catalyst ink was then quantitatively transferred onto the surface of the glassy carbon electrode by using micropipette, and finally dried in an oven at 60 □C for 15 min to remove the dispersion agent of the catalyst suspension. The catalyst loading on the electrode surface was 0.033 mg cm^{-2}.

CV, EIS and CA measurements

Half-cell electrochemical measurements were carried out with a conventional three-electrode electrochemical cell and an Auto-lab Sama-500 potentiostat/galvanostat at 25 C. The glassy carbon with the surface area of 0.0314 cm2 was used as working electrode. A commercial Ag/AgCl electrode and Pt wire were also chosen as reference and counter electrode, respectively. All electrochemical measurements were carried out in the basic solution containing 10 wt % of KOH and 5 wt% of 1-propanol.

The electrochemical activity and stability of Pt-free Hypermec^{TM} catalyst in 1-propanol oxidation reaction were investigated by CV and CA techniques. CV was carried out by scanning

of the potential between -0.8 and 0.3 V vs. Ag/AgCl with scan rate of 20 mV/s. Chronoamperometry tests were also carried out at potential of -0.2 Volte vs. Ag/AgCl. All potential values in this article have been reported versus Ag/AgCl.

Direct 1-propanol fuel cell preparation and evaluation

The anode electrode was made as follows: catalyst ink comprised of a homogeneous suspension of 95% Pt-free Hypermec^{TM} catalyst with 5 wt% PTFE (Aldrich), isopropyl alcohol (Merck) and water. The ink was homogenized using a sonicator for 20 min and painted on nickel foam support as diffusion medium. The cathode electrodes were prepared by painting the cathode ink on carbon cloth (LT2500W ELAT GDL from BASF) as diffusion medium. Cathode catalyst ink was prepared by mixing of 90 wt% Hypermec ^{TM} (Acta SpA) and 10 wt% PTFE and water as solvent according to reference [38]. Both electrodes were dried at 60 □C for 30 min in the oven. The total cathode and anode catalyst loading (containing catalyst and PTFE) were 3.5 and 5 mg/cm2, respectively. The geometrical surface area of electrodes was 5 cm2. The anode and cathode electrodes and A-006 Tokuyama anion-exchange membrane were sandwiched at room temperature in the cell hardware without using hot press. The MEA was placed in the air breathing DGFC provided by Acta SpA. The DGFC was tested by feeding static alkaline fuel containing 5 wt% glycerol and 10 wt% KOH in the anode side and static air in the cathode side. All tests were conducted on home-made test station at room temperature and ambient pressure. Polarization curve was recorded by measuring the cell voltage at different currents after reaching to steady state.

Results and discussion

Electrocatalytic activity and stability of Pt-free Hypermec^{TM}

In order to study the intrinsic activity, leaching and stability of Pd/C (10% wt) and Pt-free Hypermec^{TM} in alkaline media, CV experiment was carried out in 1 M KOH solution. Fig. 1 indicates the corresponding cyclic voltammograms of 2th and 50th cycles of Pd/C (10% wt) and Pt-free Hypermec^{TM} in 1 MKOH solution at room temperature. As it can be seen in Fig. 1, the position and magnitude of the all peaks (forward and reverse scan) did not change in during 50 cycles, so catalyst did not leach to the solution.

Fig. 2 shows the cyclic voltammogram of the Pt-free Hypermec^{TM} in POR in the solution containing 10 wt% of KOH and 5 wt% of 1-Propanol. By considering of Fig. 1, 1-propanol oxidation peaks can be clearly observed in Fig. 2. The POR on the surface of palladium catalyst is usually characterized by two well defined current peaks on the forward and reverse scans [39]. In the forward scan, the forward anodic peak at -0.144V is corresponding to the oxidation freshly chemisorbed species coming from glycerol adsorption. The reverse anodic peak at -0.3 V is primarily associated with removal of carbonaceous species not completely oxidized in the forward scan than the oxidation of freshly chemisorbed species. The magnitude of the peak current on the forward scan indicates the electro catalytic activity of palladium catalyst in 1-propanol oxidation reaction.

In order to study the tolerate of Pt-free Hypermec^{TM} against POR intermediate products 200 of CV was also recorded in the solution containing 10 wt% of KOH and 5 wt% of 1-propanol. Fig. 3 shows the cyclic voltammograms (1 ft, 20th, 50th, 100th ,150th, 200th cycle) of Pt-free Hypermec^{TM} with the scan rate of 20 mV/s in the potential range -0.8 to 0.3 V. As it can be seen

the anodic peak current of the electrode clearly decreases with increasing of scan number during the initial stages.Decline in the peak current of 1-propanol oxidation is due to catalyst poisoning by POR intermediate products.

The highest peak current for electrode arises during the 1th cycle scan. After this cycle the peak current decreases slowly with successive scans. After 200 CV cycles the 1-propanol oxidation current declines by approximately 82% as it could be understood from the Fig. 1. The reverse anodic peak current density still exists even after 200 cycles. This results show Pt-free Hypermec^{TM} is active in POR even after 200 cycles which can be explained by high tolerate and stability of Pt-free Hypermec^{TM} catalyst against poisoning by POR intermediate products.

Chronoamperometry study of Pt-free Hypermec^{TM} in POR

Fig. 4 shows typical chronoamperograms (after 50th, 100th, 150th and 200th CV cycles) of 1-propanol oxidation on the Pt-free Hypermec^{TM} in the solution containing 10 wt% of KOH and 5 wt% of 1-propanol at potential of 0.2 V versus Ag/AgCl. All of the curves displayed the decay of current during the time which could be related to the remaining of the adsorbed intermediate products of 1-propanol oxidation on the surface of catalyst. As it is shown, the current density of Pt-free Hypermec^{TM} catalyst to 50th cycle behaved with a more gently decreasing trend because the activation of catalyst occurred as it described before. The attenuation behavior of electrode after 50th cycle is determined by the coverage of intermediates and 1-propanol adsorbed on the catalyst active sites.

Direct 1-propanol fuel cell performance

According to the electrochemical results which were conducted in previous sections Pt-free Hypermec^{TM} has comparable activity in the 1-propanol oxidation reaction compared to literature data, so examination of mentioned catalyst in the anode side of alkaline DPFC is reasonable. The test result of MEA made by Pt-free Hypermec^{TM} anode catalyst in alkaline passive air breathing DPFC has been reported in Fig. 5. Cell temperature was 25 □C and cell was fed by static fuel containing 10 wt% of KOH and 5 wt% of propanol. From a perusal of this figure, one readily realizes that the open circuit voltage and maximum power density are 800 mV and 16 mW cm $^{-2}$, respectively. High mass transport issue in high current density region could be attributed to the not optimized electrode structure and thus it means electrode optimizations are required for higher current density.

Conclusions

In this work Pt-free Hypermec^{TM}, was employed as an effective catalyst for 1-Propanol electrooxidation in alkaline media. The activity, leaching and stability of Pt-free Hypermec^{TM} catalyst in POR were investigated in half cell with different electrochemical techniques. Obtained results have highlighted the excellent electrocatalyst activity of Pt-free Hypermec^{TM} in terms of specific peak current density and onset potential. Test results demonstrated that Pt-free Hypermec^{TM} is still active and stable even after 200 cycles. Membrane-electrode assembly (MEA) was made Pt-free Hypermec^{TM} catalyst in the anode side and commercial Hypermec^{TM} cathode catalyst in the cathode side and Tokuyama A-006 anion-exchange membrane as electrolyte and successfully evaluated in alkaline passive air breathing DPFC. By considering the cell peak power density (16 mW/cm^{-2}) obtained at room temperature with static fuel and air breathing condition, one can safely conclude that Pt-free Hypermec^{TM} exhibits acceptable activity for glycerol oxidation in the anode side for alkaline DPFC application.

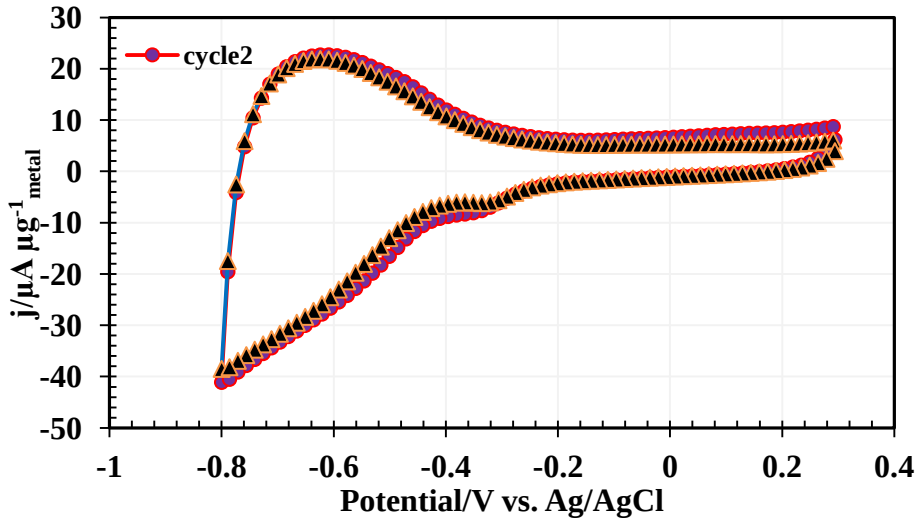

Figure.1- Cyclic voltammogram of Pt-free Hypermec™ in 1 M KOH solution at room temperature with the scan rate of 20 mV/s.

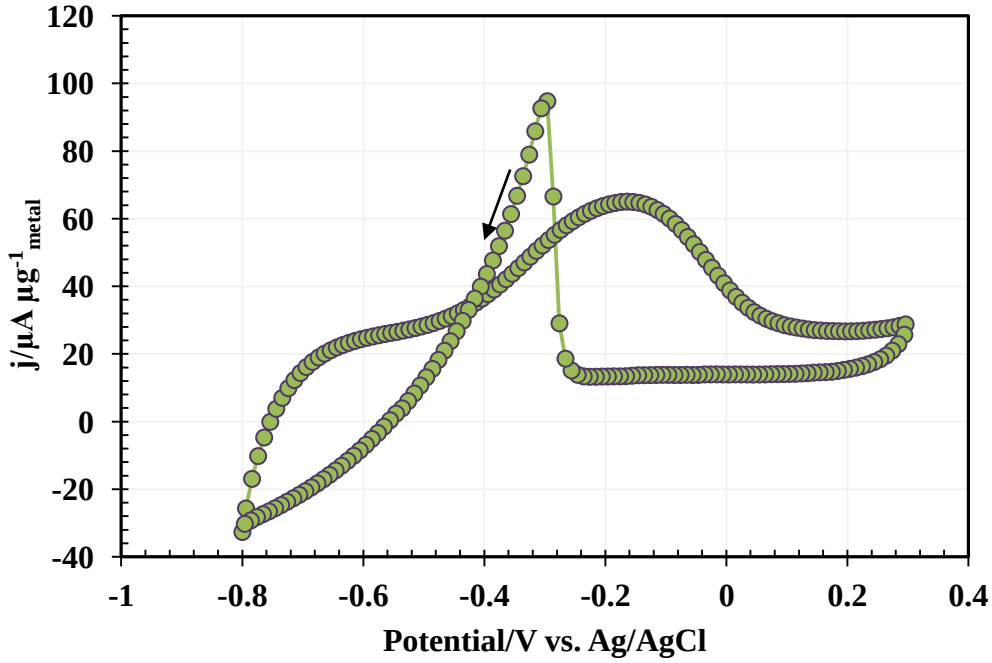

Figure 2-Cyclic voltammogram of Pt-free Hypermec™ in the solution containing 10 wt% of KOH and 5 wt% of glycerol at room temperature with the scan rate of 20 mV/s.

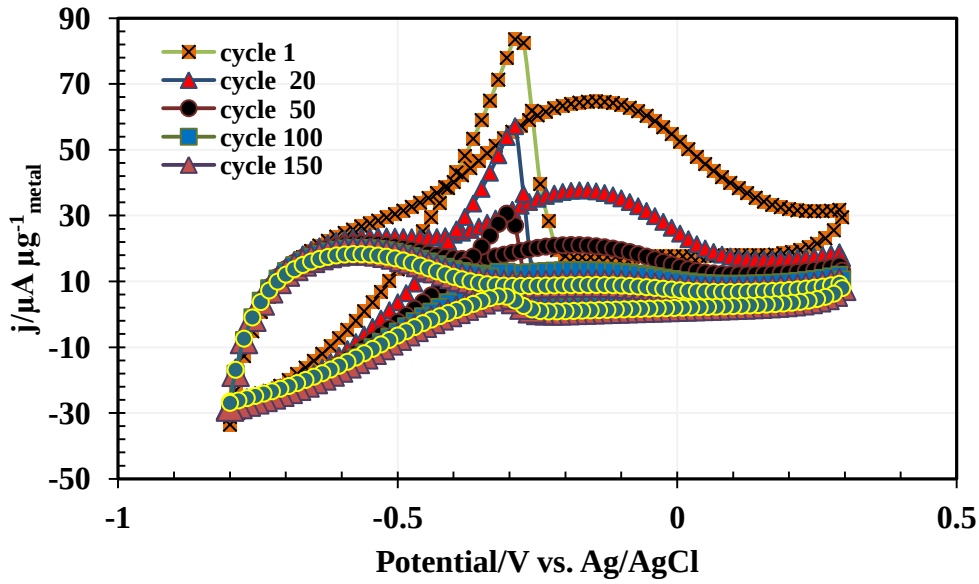

Figure 3-Cyclic voltammograms (1th, 20th, 50th, 100th, 150th and 200th cycle) of Pt-free Hypermec™ in the solution containing 10 wt% of KOH and 5 wt% of 1-propanol at room temperature with the scan rate of 20 mV/s.

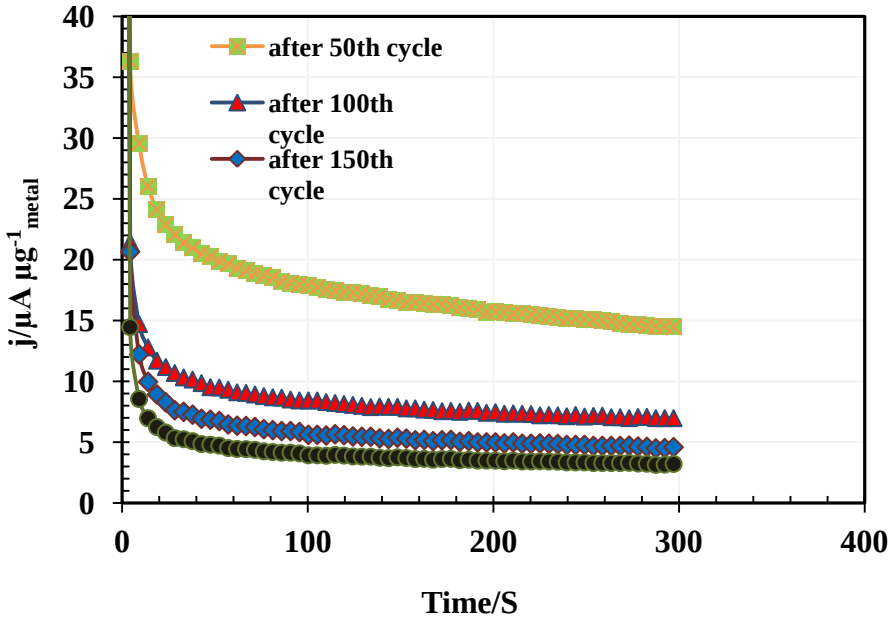

Figure 4-Chronoamperograms (after 50th, 100th, 150th and 200th CV cycle) of Pt-free Hypermec™ catalyst in the solution containing 10 wt% of KOH and 5 wt% of 1-propanol at room temperature, applied potential: -0.2 V

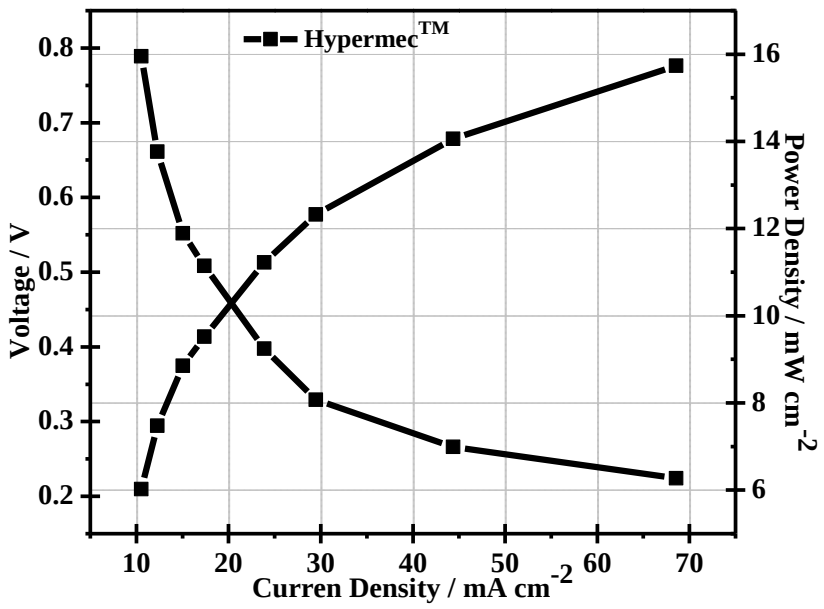

Figure5- I-V and power density curves of alkaline passive air-breathing DPFC made by Pt-free Hypermec™ anode catalyst with the fuel containing 10 wt% of KOH and 5 wt% of 1-Propanol at room temperature.

Acknowledgment

This work was carried out in electrochemical laboratory of Isfahan University of Technology (IUT). The author would like to thanks the research council of IUT. The support of the fuel cell steering committee and Iranian nano technology initiative council are also acknowledged

References

[1] Li Huanqiao, Suna Gongquan, Cao Lei, Jiang Luhua, Xin Qin. Comparison of different promotion effect of Pt Ru/C and PtSn/C electro catalysts for ethanol electro-oxidation. Electrochim Acta 2007; 52:6622e9.
[2] Zhang J, Shen PK. PEM fuel cell electrocatalysts and catalyst layers. 1st ed. Springer; 2008.
[3] J.H. Kim, S.M. Choi, S.H. Nama, M.H. Seo, S.H. Choi and W.B. Kim, Appl. Catal. B, 82 (2008)89
[4] M. Umeda, H. Sugii and I. Uchida, J. Power Sources, 179 (2008) 489
[5] D.X. Cao and S.H. Bergens,J. Power Sources, 124 (2003) 12
[6] J.T. Wang, S. Wasmus and R.F. Savinell, J. Electrochem. Soc., 142 (1995) 4218
[7] S.Y. Wang, X. Wang and S.P. Jiang, Langmuir, 24 (2008) 10505
[8] D.S. Yuan, S.Z. Tan, Y.L. Liu, J.H. Zeng, F.P. Hu, X. Wang and P.K. Shen, Carbon, 46 (2008) 531
[9] J.S. Ye, H.F. Cui, Y. Wen, W.D. Zhang, G.Q. Xu and F.S. Sheu, Microchim. Acta, 152 (2006) 267
[10] C.H. Yen, K. Shimizu, Y.Y. Lin, F. Bailey, I.F. Cheng and C.M. Wai, Energ. Fuel, 21 (2007) 2268
[11] S.H. Seo and C.S. Lee, Energ. Fuel. , 22 (2008) 1204
[12] C.W. Xu, H. Wang, P.K. Shen and S. P. Jiang, Adv. Mater., 19 (2007) 4256
[13] C.W. Xu, Y.L. Liu and D.S. Yuan. Int. J. Electrochem. Sci., 2 (2007) 674
[14] J.P. Liu, J.Q. Ye, C.W. Xu, S.P. Jiang and Y.X. Tong, J. Power Sources, 177 (2008) 67
[15] C. Lamy, J.-M. Leger, S. Srinivasan, in: J.O'M. Bockris, B.E. Conway, R.E. White (Eds.), Modern Aspects of Electrochemistry No. 34, Kluwer Academic/PlenumPublishers, New York, 2001, p. 65.
[16] S.C.S. Lai, M.T.M. Koper, Ethanol electro-oxidation on platinum in alkaline media, Physical Chemistry Chemical Physics 11 (2009) 10446
[17] J.S. Spendelow, A. Wieckowski, Electrocatalysis of oxygen reduction and small alcohol oxidation in alkaline media, Physical Chemistry Chemical Physics 9 (2007) 2654.
[18] G. Cui, S. Song, P.K. Shen, A. Kowal, C. Bianchini, First-Principles Considerations on Catalytic Activity ofPd toward Ethanol Oxidation, Journal of Physical Chemistry C 113 (2009) 15639.
[19] D.F. da Silva, A.N. Geraldes, E.Z. Cardoso, M.M. Tusi, M. Linardi, E.V. Spinacé, A.O. Neto, Preparation ofPtAu/C and PtAuBi/C electrocatalysts using electron beam irradiation for methanol and ethanol electro-oxidation in alkaline medium, International Journal of Electrochemical Science 6 (2011) 3594.
[20] J.R. Varcoe, R.C.T. Slade, An electron-beam-grafted ETFE alkaline anionexchange membrane in metal-cation-free solid-state alkaline fuel cells, Electrochemistry Communications 8 (2006) 839.
[21] J.R. Varcoe, R.C.T. Slade, E.L.H. Yee, S.D. Poynton, D.J. Driscoll, D.C. Apperley, Apperley, Poly(ethylene-co-tetrafluoroethylene)-Derived Radiation-Grafted Anion-Exchange Membrane with Properties Specifically Tailored for Application in Metal-Cation-Free Alkaline Polymer Electrolyte Fuel Cells, Chemistry of Materials 19 (2007) 2686.
[22] A. Santasalo-Aarnio, S. Hietala, T. Rauhama, T. Kallio, In and ex situ characterization of an anion-exchange membrane for alkaline direct methanol fuel cell (ADMFC), Journal of Power Sources 196 (2011) 6153.
[23] H. Bunazawa, Y. Yamazaki, Ultrasonic synthesis and evaluation of nonplatinum catalysts for alkaline direct methanol fuel cells, Journal of Power Sources 190 (2009) 210.

[24] J.R. Varcoe, R.C.T. Slade, Prospects for alkaline anion-exchange membranes in low temperature fuel cells, Fuel Cells 5 (2005) 187.
[25] N. Fujiwara, Z. Siroma, S. Yamazaki, T. Ioroi, H. Senoh, K. Yasuda, Direct ethanol fuel cells using an anion exchange membrane, Journal of Power Sources 185 (2008) 621
[26] Y.S. Li, T.S. Zhao, Z.X. Liang, Effect ofpolymer binders in anode catalyst layer on performance of alkaline direct ethanol fuel cells, Journal of Power Sources 190 (2009) 223.
[27] V. Bambagioni, C. Bianchini, A. Marchionni, J. Filippi, F. Vizza, J. Teddy, P. Serp, M. Zhiani, Pd and Pt–Ru anode electrocatalysts supported on multi-walled carbon nanotubes and their use in passive and active direct alcohol fuel cells with an anion-exchange membrane (alcohol = methanol, ethanol, glycerol), Journal of Power Sources 190 (2009) 241.
[28] A. Santasalo-Aarnio, P. Peljo, E. Aspberg, K. Kontturi, T. Kallio, Methanol, ethanol and iso-propanol performance in alkaline direct alcohol fuel cell (ADAFC), ECS Transactions 33 (2010) 1701.
[29] J.R. Varcoe, R.C.T. Slade, E.L.H. Yee, S.D. Poynton, D.J. Driscoll, Investigations into the ex situ methanol, ethanol and ethylene glycol permeabilities of alkaline polymer electrolyte membranes, Journal of Power Sources 173 (2007) 194.
[30] G.F. McLean, T. Niet, S. Prince-Richard, N. Djilali, An assessment ofalkaline fuel cell technology, International Journal of Hydrogen Energy 27 (2007) 507.
[31] L.L. Zhang, T.H. Lu, J.C. Bao, Y.W. Tang, C. Li, Electrochem. Commun. 8 (2006) 1625.
[32] X.B. Ji, C.E. Banks, W. Xi, S.J. Wilkins, R.G. Compton, J. Phys. Chem. B110 (2006) 22306.
[33] X.B. Ji, C.E. Banks, A.F. Holloway, K. Jurkschat, C.A. Thorogood, G.G. Wildgoose, R.G. Comptona, Electroanalysis 18 (2006) 2481.
[34] G.Y. Gao, D.J. Guo, H.L. Li, J. Power Sources 162 (2006) 1094.
[35] Karim-Nezhad, Ghasem Pashazadeh, Ali Pashazadeh, Sara. J.Anal. Bioanal. Electrochem. Vol. 5, No. 1, 2013, 87 – 98
[36] Hu F, Chen C, Wang Z, Wei G, Shen PK. Mechanistic study of ethanol oxidation on Pd–NiO/C electrocatalyst. Electrochim Acta 2006; 52:1087–91.
[37] E. Antolini, E. Gonzalez, Alkaline direct alcohol fuel cells, Journal of Power Sources, 195 (2010) 3431-3450.
[38] Zhiani M, Gasteiger HA, Piana M, Catanorchi S. Comparative study between platinum supported on carbon and non-noble metal cathode catalyst in alkaline direct ethanol fuel cell (ADEFC). Int J Hydrogen Energy 2011; 36:5110e6.
[39] Xu C, Liu Y, Yuan D. Pt and Pd supported on carbonmicrospheres for alcohol electrooxidation in alkaline media. Int J Electrochem Sci 2007;2:674e80.

8th Iranian Fuel Cell Seminar
FEBRUARY 25,26
2015

Investigation the Performance of Pt-Sn Nanoparticles Supported by Carbon-Polyaniline Composite in a Passive DMFC

Mitra Amani[1*], Hussein Gharibi[2], Mohammad Kazemeini[3], Fereshteh Dehghan[2]

1. Department of Chemical Engineering, Tarbiat Modares University, P.O. Box 14115-175, Tehran, Iran
2. Department of Chemistry, Faculty of Science, Tarbiat Modares University
3. Department of chemical engineering, Sharif University of Technology
** mitra_amani@yahoo.com*

Abstract
Polyaniline fiber (PANI) was synthesized by chemical interfacial method and utilized to fabricate Vulcan-Polyaniline (C-PANI) composite. PtSn(70:30) nanoparticles are reduced on C-PANI composite and the performance of the PtSn(70:30)/C-PANI and commercial PtRu/C, as anode catalysts, are compared in a passive direct methanol fuel cell. The DMFC test results indicate that the membrane electrode assembly (MEA) prepared from PtSn(70:30)/C-PANI anode exhibits better performance in terms of maximum power density and stability. Also the methanol crossover in the presence of PtSn(70:30)/C-PANI has been reduced by 42%. In comparison with the commercial PtRu/C catalyst, the optimal PtSn(70:30)/C-PANI catalyst exhibits superior activity toward methanol oxidation.

Keywords: Polyaniline, Passive direct methanol fuel cell, Methanol crossover

Introduction

The direct methanol fuel cell (DMFC) is one of the alternative candidates for fuel cell vehicles and stationary applications due to its better economics and high theoretical energy density of methanol (6100 Wh kg^{-1} at 25ºC). Nonetheless, various problems including the; contamination of the cathode catalyst by methanol crossover, the high cost and low durability of the electro-catalysts and the poisoning of the Pt anode electro-catalyst prohibited the DMFC from a wider practical usage [1-2]. In order to improve the CO tolerance and decrease the electro-catalyst price, Pt-based bimetallic electro-catalysts have been widely studied, such as PtRu, PtSn, PtPd and etc. Amongst which PtRu and PtSn are the most active ones of binary alloys have previously been widely studied. The PtRu alloy electro-catalyst with a 50% Ru atomic composition is indeed one of the most popular DMFC electro-catalysts utilized to date. However, the CO tolerance of this material at higher CO concentrations is not acceptable; on the other hand, problems with Ru leaching from PtRu anode electro-catalyst, the high price of PtRu and the limited availability of Ru can limit its usage in DMFCs [3]. From an economic viewpoint, the actual cost of the Sn element is much lower than that of the novel Pt or Ru metals. The catalytic activity of PtSn electro-catalyst for methanol oxidation varies considerably depending upon the Pt:Sn molar ratio, the support structure and its synthesis method [4]. Higher catalyst dispersion on a suitable support led toward a decrease in the amount of Pt used in the DMFC active layer without performance loss and decreased the amount of adsorbed linear CO species. In this paper, PANI was synthesized chemically by interfacial method and doped with

para toluene sulfonic acid (PTSA). PtSn nanoparticles with atomic ratio of (70:30) were reduced on a composite of Vulcan (XC-72) and 20% PANI via impregnation method. The performance and methanol crossover of the PtSn (70:30)/C-PANI and commercial PtRu/C as anode catalysts of a passive direct methanol fuel cell were investigated

Experimental section

Polyaniline fibers (PANI) were synthesized under ambient condition by interfacial polymerization. The oxidant solution consisted of APS in H_2SO_4 solution (1M) was carefully added to the organic phase consisted of aniline in chloroform. After 24hr, the aqueous layer was filled with dark green colored emeraldine salt of PANI that was washed repeatedly with distilled water and methanol. The sulfate-ion-doped PANI was converted into emeraldine base form (EB) by treatment with ammonium hydroxide and then PANI (EB) was redoped with PTSA for electro-catalyst synthesis. For the PtSn/C-PANI electro-catalysts synthesis, Vulcan XC-72 (C) and 20wt% PANI were mixed with ethylene glycol ultrasonically for 30 min. The C-PANI composite was impregnated with Pt and Sn particles for a total metal loading of 10 wt%, by the addition of $H_2PtCl_6.6H_2O$ salt in water and $SnCl_2.2H_2O$ to above suspension followed by sonication for 30 min and subsequently the mixture was magnet stirred for 2 h at room temperature. This suspension was mixed ultrasonically with an excess of ethylene glycol and finally was stirred at 130 °C under Ar atmosphere for 16 h. Finally, the resulting mixture was filtered, washed with distilled water several times and then dried in an oven at 80 °C. The in-house prepared oxygen-breathing DMFC with stainless steel (SS316) current collectors used to evaluate the electrochemical performance of the synthesized PtSn(70:30)/C-PANI electro-catalyst in comparison with a commercial PtRu/C (provided by the Electrochem Inc.) A pretreated Nafion 115 membrane with a thickness of 125µm was employed in this work. The pretreatment procedures included boiling of the membrane in 5vol. % H_2O_2, washing in distilled water, boiling in 0.5M H_2SO_4 and washing in distilled water, each step for 1.5h at 80ºC. The pretreated membrane was kept in the distilled water prior to the fabrication of membrane electrode assembly (MEA). Carbon paper used as the backing support of anode and cathode electrodes. The catalyst loading on the cathode electrode of MEA-1 and MEA-2 was $3mg_{Pt}cm^{-2}$ using 20wt. % Pt on Vulcan (XC-72). The catalyst loading on the anode electrode was $4mg_{metal}\,cm^{-2}$ using 20wt. % PtRu on Vulcan (XC-72) for MEA-1 and 20wt. % PtSn (70:30) on C-PANI composite for MEA-2. The membrane-electrode assembly (MEA) was prepared by mechanically pressing anode, cathode and membrane while silicone–rubber gaskets were employed to seal the system.

The Active area of MEAs and the volume of the anode compartment were $4.75cm^2$ and 12.5mL respectively.

Results and discussion

From the practical point of view, the single cell test was the final evaluation criterion for the novel electro-catalytic material developed. Therefore, the only variable parameter in this study namely; the differences in the single cells performance of different anode catalysts depicted to some extent by the activities of these materials investigated. Figure 1 showed the performance of the MEA-1 (PtRu/C as an anode catalyst) and MEA-2 (PtSn(70:30)/C-PANI as another anode catalyst) in a passive DMFC filled with a 2M methanol solution.

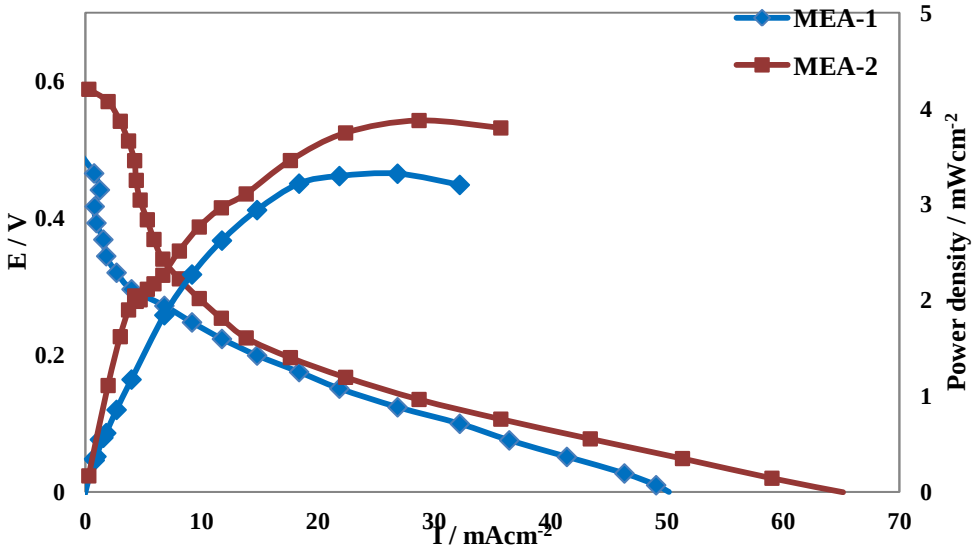

Figure 1. Polarization and power density curves of Passive DMFCs with MEA-1 and MEA-2 at room temperature. Methanol solution 2M (12.5mL).

It was evident that the MEA-2 had a better performance over the entire current density region producing a maximum power density being 20% higher than that of the MEA-1. The cell performance of MEA-2 was satisfyingly comparable to typical passive DMFCs [5-6]. It was observed that, the maximum power density produced by the MEA-2 was analogous to the previously reported ones despite utilizing of more precious metals in both their anode and cathode electrodes. This meant that, more economical power source based upon the PtSn(70:30)/C-PANI anode catalyst for a passive DMFC might be realized compared to the one with the commercial PtRu/C provided by the Electrochem.

The open circuit voltage (OCV) of MEA-2 is significantly higher than the MEA-1 in Figure 1. Since the OCV was related to the concentration of methanol existing at the cathode, its higher value was indicative of lower methanol crossover. Methanol crossover was a process in which un-reacted methanol diffused from the anode to the cathode through Nafion membrane. This caused the mixed potential effect as well as; the poisoning of the Pt electro-catalyst at the cathode. As a result, this process significantly reduced the cell performance and fuel utilization. Therefore, it was essential to reduce methanol crossover to increase the efficiency and stability of the DMFCs.

This higher OCV might be related to the positive effect of the PANI fibers in the anode structure for decreasing the methanol crossover through the Nafion membrane. In order to survey the effect of PANI on MEA open circuit potentials, methanol crossover was measured using an electrochemical technique. Nitrogen was injected into the cathode electrode, and a high positive voltage applied to oxidize the diffused methanol on cathode catalyst surface. Finally, a limiting current was achieved. According to Faraday's law, the methanol crossover rate (n (mol cm^{-2} s^{-1})) might be calculated by $n = i/6F$, where i (mA cm^{-2}) was the crossover current and the number of 6 was the transferred electron number for methanol oxidation [7]. The crossover current density versus applied voltage was shown in Figure 2.

This indicated the presence of PANI in anode electro-catalyst layer of the MEA-2 reduced the methanol crossover by about 30% in comparison with the MEA-1. This might be due to the synergism of carbon Vulcan and PANI as well as; the fast kinetics of methanol oxidation on the surface of the anode catalyst layer of the MEA-2 versus MEA-1.

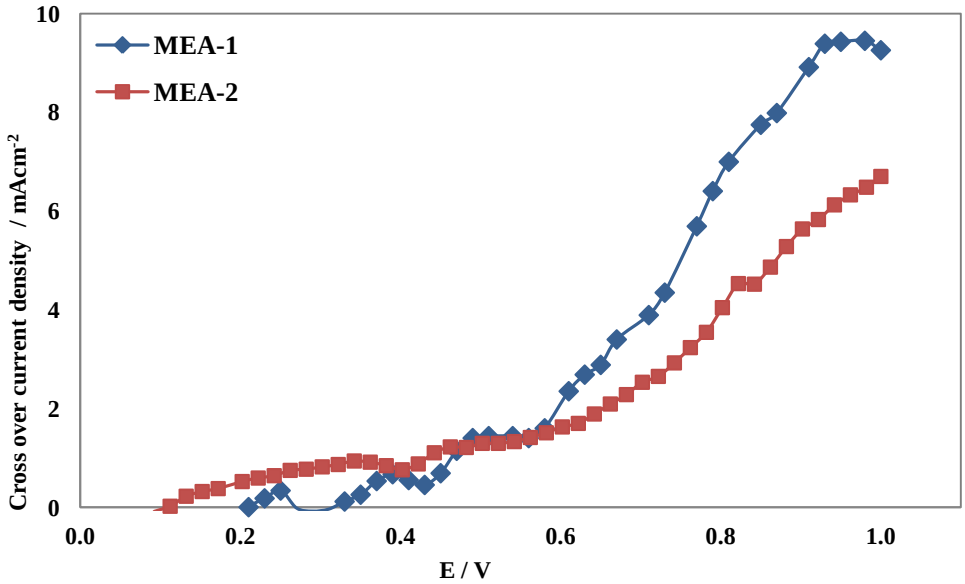

Figure 2. Crossover current density versus potential in the potential range of 0 to 1V, Methanol solution 2M (12.5mL).

To examine the stability of electrocatalytic activity of the MEA-1 and MEA-2, chronoamperometry was employed. Figure 3 showed the variation of the cell current density as a function of time at a constant voltage of 0.2 V for 210 min under a normal operating condition. Both of these MEA's presented a current decay during current–time measurements before a steady condition was attained. This was attributed to the formation of some poisonous intermediate on anode catalyst surface and decreasing of the methanol concentration in the cell reservoir. As evident, the current density and stability of the MEA-2 was significantly better than those of the MEA-1. The observed decrease in the current density measured to be 18% for the MEA-1 whereas it was only 2.5% for the MEA-2. Long term stability of the PtSn(70:30)/C-PANI and diminishing of the methanol crossover in the MEA-2 improved its durability in comparison with that of the MEA-1.

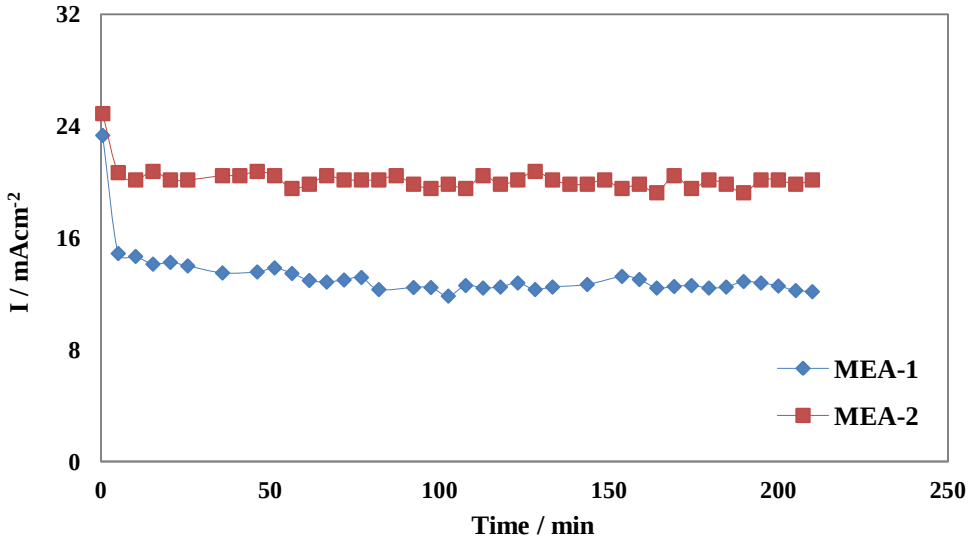

Figure 3. Current density–time behavior of MEA-1 and MEA-2 in a passive DMFC at room.

Conclusion

In summary, PtSn(70:30)/C-PANI electro-catalyst was prepared by impregnation method and its performance compared with the commercial PtRu/C (Electrochem) in a passive DMFC.
Utilization of PtSn(70:30)/C-PANI as anode catalyst in a passive DMFC decreased the methanol crossover by about 30%. Also, the maximum power density of MEA-2 with optimized PtSn catalyst in anode electrode is about 20% more than MEA-1 with commercial one.
The obtained results indicated that the synthesized PtSn(70:30)/C-PANI electro-catalyst displayed a high electrocatalytic activity and stability toward the oxidation of methanol. All of these make this material a good candidate to substitute the commercial PtRu/C.

References

[1]. F. G. Welsch, K. Stöwe and W. F. Maier, Catalysis Today, 2011, 159, 108-119.
[2]. J. R. C. Salgado, J. C. S. Fernandes, A. M. Botelho do Rego, A. M. Ferraria, R. G. Duarte and M. G. S. Ferreira, Electrochimica Acta, 2011, 56, 8509-8518.
[3]. E. Antolini, Journal of Solid State Electrochemistry, 2011, 15, 455-472.
[4]. W.-I. K. Hyun-Joong Kim, Tae-Jin Park, Hyung-Sang Park, Dong Jin Suh, carbon, 2008, 46, 1393-1400.
[5]. S. Yousefi and D. D. Ganji, Electrochimica Acta, 2012, 85, 693-699.
[6]. W. Yuan, Y. Tang, X. Yang and Z. Wan, International Journal of Hydrogen Energy, 2012, 37, 13510-13521.
[7]. J. Zhang, PEM fuel cell electrocatalysts and catalyst layers, 2008.

8th Iranian Fuel Cell Seminar
FEBRUARY 25,26
2015

Investigation of Three Metallic Electrocatalyst Activity for ORR in PEMFC

Masoumeh Javaheri
Ceramic department, Materials and Energy Research Center, Karaj, Iran
** m.javaheri@merc.ac.ir*

Abstract
One series of Ru@Pd-Pt (Ru as core and Pt-Pd as shell) core- shell structures with different molar ratio of metals on Vulcan were prepared by a successive reduction procedure. The effect of Pd-Pt alloy as shell (Ru as core) investigated for oxygen reduction reaction (ORR). The physical properties of the synthesized catalysts are characterized by inductive coupled plasma (ICP) and X-ray diffraction (XRD). The results of half-cell testing indicated that the synthesized catalysts activity for ORR is better than commercial Pt/C. Despite low catalyst loading (0.3 $mg.cm^{-1}$), polarization behavior in the single cell testing also suggests that the Ru@Pd-Pt has a good performance. This good efficiency can be attributed to the effect of Ru on electronic properties of Pt and the positive effect of Pd as alloyed with Pt, increasing adsorption and reduction of O_2 on Pt-Pd.

Keywords: Core- shell, Catalyst, Fuel cell, Ru, Pt, Pd.

1. Introduction

Polymer electrolyte fuel cell (PEMFC) has great potential to be used in both stationary power generation and vehicular power sources [1]. Platinum has a wide range of catalytic applications due to its unique chemical and physical characteristics [2-5]. However, the most critical problem for Pt catalysts is the high cost because of the limited supply. Pt-based electro catalysts are usually employed in PEMFC as cathode electro catalysts for ORR at relatively low temperatures [6].

Bimetallic nanocrystals consisting of two distinct metals such as Pt-Ru, Pt-Pd etc., are attractive for a wide variety of catalytic and electro catalytic applications as they can exhibit not only a combination of the properties associated with both metals, but also enhancement or synergy due to a strong coupling between the two metals [7,8].To maximize the efficiency of Pt particles, the ideal structure of a Pt-based catalyst should consist of the total available Pt atoms distributed on the electrochemical reaction interface. Based on this consideration, the core-shell nanostructure is expected to effectively increase the utilization efficiency of precious metal electro catalysts [9].

Recently, many researches have focused on the synthesis of core-shell catalytic structures to be applied in PEM fuel cells. In 2013, a number of reports were published on the synthesis of Pt as shell on commercial Pd/C with different molar ratios and the ORR on the surface of the catalyst was investigated [10].

L. Zhang et al. [11] studied the anode of PEMFC and reported that the overall performance of core-shell catalyst ($Ru@Pt/Ti_4O_7$) in the presence of CO at various concentrations was significantly higher than that of Pt Ru/C alloy catalyst.
The $Ru@Pt_x Pd_y/C$ core-shell structure were synthesized and applied for formic acid oxidation [12].
Most studies refer to the catalytic activity of Ru on ORR, but fewer on Pt, in acid or alkaline electrolyte [13,14]. Theoretical and experimental research represented the positive effect of Ru on the electronic properties of Pt and consequent enhancement the Pt activity for ORR [15,16]. In addition, Pd can improve the electro catalytic activity of Pt for ORR [17-19].
In this work, core-shell catalyst structures were prepared by the synthesis of 1 series of catalysts included Ru as core and Pt-Pd as the shell through impregnation with hydrothermal method. The effect of molar ratio on the electrode performance for ORR was investigated. A rolling technique was employed to prepare the gas diffusion electrode (GDEs) with three layer structures.

2. Experimental

2.1. Catalyst synthesis

First, adequate amount of Vulcan (cabot) was refluxed in H_2O_2 30% (merck) and HNO_3 10% (merck) at 80°C for 6 h. Carbon powder was removed using centrifugal (ROTINA 46) and washed by distilled water. Then, the pretreated carbon was dried at 80°C for 12 h.
Dispersion of catalyst with core-shell structure was carried out step by step. In the first step, the core seeds were dispersed on Vulcan powder and thereafter the shell was dispersed on the core. To prepare Ru/C, the $RuCl_3.3H_2O$ precursor was dissolved in diluted HCl. Since the molar ratio of Ru and Pt-Pd was different (table 1), the pretreated Vulcan was divided in to 3 parts. Each part was mixed with precise amount of the $RuCl_3$ solution and prepared suspensions were allowed to evaporate in 70°C. Finally, in order to complete reduction of Ru on Vulcan, the powder was heated in furnace at 200°C under H_2 atmosphere. The Ru/C was synthesized with three different molar ratios (table 1).
To prepare Ru@Pt-Pd/C, appropriate amount of $PdCl_2$ and $H_2PtCl_6.6H_2O$ with sodium citrate were dissolved in ethylene glycol and then steered for 1h to completely dissolve sodium citrate. Subsequently, the synthesized Ru/C was added to the mixture and the PH was adjusted up to 10 by drop-wise addition of KOH in ethylene glycol into solution under steering. The mixture was then transferred into a Teflon-lined autoclave and conditioned at 130 ˚C for 6 h, followed by centrifuging, washing, and vacuum drying at 70 ˚C [12].
Hereinafter, the synthesized catalysts were labeled by 3 integers that indicated the molar ratio of Pt, Ru and Pd, respectively (include 211, 231 and 432).

2.2. GDEs fabrication

To fabricate the three-layer GED, the diffusion layer, contained 30 wt% PTFE and 70 wt% Vulcan was rolled onto the carbon paper (TGPH-0120T) (Toray) and dried. Loading of the micro porous layer was fixed at 1 $mg.cm^{-2}$.To prepare the catalyst layer of GDEs, a homogeneous suspension containing the desired amounts of the synthesized catalyst (7 wt.%), Nafion solution (5% from Aldrich), 2-propanol, water, and glycerol was sonicated for 20 min. The suspension was subsequently rolled onto the diffusion layer. The obtained electrode was dried. The catalyst loading was 0.2 $mg.cm^{-2}$ [20, 21].

2.3. Electrode fabrication for single cell

For the single cell, a three-layer electrode was fabricated through the same steps as those used for the fabrication of GDEs (previous section). In this study, the best catalyst of each series was used as the cathode catalyst, while the commercial Pt/C (10%wt) was used as the anode catalyst. The electrode area and catalyst loading value were considered to be 5 cm^2 and 0.3 $mg.cm^{-2}$, respectively.

2.4. Physical properties

The X-ray diffraction (XRD) technique was employed for the synthesized catalysts using a Philips pw3710 diffractometer with a Cu X-ray source operating at 40 kV and 40 mA. The XRD patterns were obtained at a scanning rate of 1°/min with a step size in the 2θ scan of 0.02° in the 20-90° range.

The amount of reduced Ru, Pd and Pt on each support was determined through the application of inductive coupled plasma (ICP) technique (ICP-AES, 314, Switz). In order to conduct these measurements, 5 mg of each sample (synthesized catalyst) was dissolved in a mixture of hydrochloric acid and nitric acid (3/1). These solutions were refluxed at 70°C in advance of being used in the ICP measurements.

2.5. Electrochemical measurement

For electrochemical tests, an EG&G Princeton Applied Research Model 2273 instrument was used to determine the electrochemical properties of the electrodes. The performances of the porous GDEs (geometric exposed area 1 cm^{-2}) in the reduction of oxygen were investigated in 0.5 M H_2SO_4. All measurements were performed at 25°C in a conventional three-electrode cell, with O_2 flowing at 50 $mL.min^{-1}$ for linear sweep voltammetry (LSV), Chronoamperometry, and impedance spectroscopy and Ar flowing for cyclic voltammetry (CV) and ionic resistance measurement. The GDEs were mounted into a Teflon holder containing a graphite disk as current collector and providing oxygen feed from the back of the electrode. An Ag/AgCl reference electrode was placed close to the working electrode surface, while a large area platinum flat electrode was employed as the counter electrode. In order to perform a quantitative evaluation of resistance against the ORR, the AC electrochemical impedance spectroscopy (EIS) method was used.

3. Result and discussion

3.1. Electrocatalyst properties

The electrochemical reaction in GDE occurs in a three-phase zone which includes the reactant (gas phase), electrons (solid phase), and protons (liquid phase). Considering the fact that the reactant gases travel only through voids, the electrode must be sufficiently porous to allow gases travel to the reaction sites. Since the electrons travel through the electrically conductive solids including the catalyst itself, it is important to create electrical connection between the catalyst particles and the substrate. Also since protons travel through the ionomer, the catalyst must also be in intimate contact with the ionomer [22]. Therefore, increasing the triple phase zone improves the electrode quality and consequently the cell performance. It is expected that the core- shell structure of catalyst will increase the triple phase zone.

Table 1. Name and molar ratio of synthesized catalyst

Catalyst No.		1	2	3
name		231	432	211
Pt:Ru:Pd		2:3:1	4:3:2	2:1:1
Precursor	Pt%	32.5	44.5	50
	Ru%	50	33.5	25
	Pd%	17.5	22	25
ICP	Pt%	38	48	53.1
	Ru%	46.2	31.4	25.8
	Pd%	15.8	20.6	21.1

The ICP results indicated that the samples contained 7wt% catalysts. The percentage of catalysts is listed in table1.

The XRD pattern of series 1 and 2 are presented in Fig.1 A and B. The peak centering at 24.5° for all the catalysts could be ascribed to the carbon support. There were four observable peaks at 2θ angles of ca. 40°, 47°, 68°, and 81° for Pt plates (111), (200), (220), and (311), respectively.

The broadening of peaks indicates that the catalyst particles are of nanometer scale (table 2). The averages size of the catalyst particles was calculated from the line broadening of the (111) peak by using the Scherrer equation after background subtraction and found to be nanometer-sized (table 2):

$$d = \frac{0.9\lambda}{B_{2\theta} cos\theta} \qquad (1)$$

Where d is the average particle size, λ is the wavelength of the X-ray (1.54056A), θ is the angle at the maximum of the peak, and $B_{2\theta}$ is the width of the peak at half-height.

If the nanoparticles could be well dispersed on carbon substrate, the triple phase zone could be expanded and the electrode performance could be improved. In contrast with the commercial Pt/C, the XRD pattern of series 1 synthesized catalyst (Ru@Pd-Pt) contains a weak peak at around 43°. This peak is related to Ru (101) and gradually became weaker by reducing the amount of Ru. This phenomenon is attributed to the coverage of Ru particles with Pt-Pd (in series 1), being capable of forming a core- shell structure [10, 23, and 12]. The presence of the Ru (101) peak reveals that Ru has not been alloyed with Pt-Pd. In fact, in case of alloy formation, Ru atoms would enter the fcc structure, while the introduction of Ru into the hcp structure would be eliminated and consequently remove the Ru (101) peak from the XRD pattrn [24]. The XRD results also indicate that the presence of Ru core has affected the position and d-spacing of the Pt peaks where a positive shift appeared and the d-spacing was reduced. For example, the 2θ angles of Pt (111) changed from 39.35° in Pt/C to 39.77° in 231 and d-spacing decreased from 2.3 in Pt/C to 2.26° in 231.

Cyclic voltammetry was employed to measure the electro active surface area (Fig 3 A-C). Also, the columbic charge for hydrogen desorption was used to calculate the electro active surface area (EAS) of each electrode (table 2) [25]:

$$EAS = \frac{Q_h}{0.21 \times [catalyst]} \qquad (2)$$

Where Q_h is the charge for hydrogen desorption ($mC.cm^{-2}$), [catalyst] is the catalyst loading ($mg.cm^{-2}$) and 0.21 ($mC.cm^{-2}$) is the charge required to oxidize a monolayer of H_2 on bright catalyst. The roughness factor (R_f) can then be calculated by using the following equation:

$$R_f = \frac{EAS}{s} \qquad (3)$$

where S is the geometric surface area ($m^2.g^{-1}$). These catalysts demonstrate the adsorption-desorption peak, confirming the activation of the catalyst. The active surface area of catalysts was tabulated in table 2. The achievement of high active surface area could be attributed to the formation of the three-phase zone. According to the EAS results, the performance of GDE for ORR is enhanced due to the expansion of the three-phase zone.

Table 2. Exchange current density, tafel slop, transfer coefficient, current density at 0.3 V, diffusion coefficients, charge transfer resistances, ionic resistances and particle size of all fabricated GDEs

GDE	i0×10-5 (A.cm-2)	b (mV.de-1)	α_c	i at 0.3(V) (mA. mg_{cat}^{-1})	EAS ($m^2.g^{-1}$)	RF	$D^{1/2}\times C^*\times 10^{-8}$ (mol. $Cm^{-2}.s^{-1/2}$)	R_p(ohm)	d(nm)
231	29.12	43.58	1.36	1002.78	174.36	1.430	32.73	0.999	2.4
432	16.51	53.45	1.10	636.90	117.92	1.303	29.33	2.32	2.2
211	14.36	59.40	0.99	639.74	136.45	1.99	28.22	2.10	2.1
Pt/C	7.45	49.12	1.13	653.51	12.7	-	23	4.73	5

The kinetic parameters of GDEs are important to determining the activation of these for ORR. The analysis of the experimental polarization data was performed using the Tafel equation [26]:

$$\eta = E - E_{eq} = -\frac{2.303RT}{nF\alpha} log \frac{i}{i_0} \qquad (4)$$

Where η is the overpotential, E_{eq} is the open-circuit voltage, $\frac{2.303RT}{nF\alpha}$ is the Tafel slope, i is the current density, and i_0 is the exchange current density for the ORR , n is the number of electron, F is the faraday constant and α is the symmetry factor. The kinetic parameters were obtained from I-V curves and equation 4.

The exchange current density, Tafel slope and symmetry factor are regarded as important kinetic parameters. The Tafel slope depends on α and n. The first charge transfer step is an electron transfer reaction the number of electrons involved in which is one [27].

In general, when the Tafel slope increases, the overpotential will increase faster with the current density. Thus, in an electrochemical reaction to obtain a high current at low over potential, the reaction should exhibit a low Tafel slope or large α. Exchanging the current density is an important kinetic parameter representing the electrochemical reaction rate at equilibrium. The exchange current density of an electrochemical reaction depends on the reaction and the electrode surface on which the electrochemical reaction occurs. Therefore, electrode materials or catalysts have a strong effect on ORR kinetics. Different materials can give different exchange current densities. Based on the LSV curve (Fig. 4 A-C), GDE had low Tafel slope, high α, and high exchange current density. Therefore, this electrode had the best performance for ORR (table 2). A comparison between catalysts 231 and commercial Pt/C (Fig. 4C) shows that the activation of this synthesized catalyst for ORR is more efficient than commercial Pt/C. GDE 231 was found to have the best catalytic properties.

By using the chronoamperometry experiment and Cottrell equation the diffusion coefficient of oxygen at GDEs could be calculated [28]:

$$i = nFA(D/\pi t)^{1/2} C^* \qquad (5)$$

Where i is the limiting current (mA), n is the number of electrons, F is the Faraday constant (96485 $Cmol^{-1}$), A is the surface area of the electrode (cm^2), D is the diffusion coefficient ($cm^2 s^{-1}$), t is the time (s), and C* is the concentration of the reactant.

The highest permeability value ($D^{1/2}C^{*}$) in was obtained for GDE 231 (table 2). This result indicated that the diffusion of oxygen in the catalyst layer of GDE 231 was superior to other catalysts, which improves the ORR in the mentioned GDEs. A comparison between this GDE and commercial Pt/C demonstrated that 231 catalyst was more efficient than commercial Pt/C. This result could be attributed to the creation of appropriate substrate for oxygen diffusion to optimize oxygen consumption.

By using the impedance experiment in different condition we were able to determining the polarization and ionic resistance of GDEs. All results reported in table 2.

To gain more information about the GDEs, the AC impedance spectrum of each GDE was obtained. The resulting data was plotted in the Nyquist representation. Although the impedance spectra had similar semi-circular shapes, the diameters of the semi-circles different significantly. As shown in Fig. 5 A-C the charge transfer resistance of GDE 231 had minimum value. This result could be attributed to proper dispersion of catalyst nanoparticles and consequent formation of the three-phase zone in the catalyst layer. When the dispersion of catalyst and then the active surface area was enhanced, the charge transfer and ionic resistance were decreased. The semi-circle shapes of Nyquist plots point out to the equivalent circuit represented in Fig. 5 D.

3.2. Study of Single cell

As previously mentioned, the best catalyst was used as cathode catalyst in the single cell. Polarization curve is the most important characteristic of a fuel cell. The polarization and power density curve of single cell is reported in Fig. 6. The cell were tested under 3 different pressure values and two cathode humidification. Because the membrane requires proton conductivity, both reactant gases must be humidified before entering the cell. Needless to say, the proton was transferred from anode to cathode electrode with water. Water was also produced in the cathode reaction. Therefore, in order to avoided dryness of the membrane in the anode side, the gas (H_2) was 100% humidified. To avoid flooding in the cathode side, the gas humidification should be less than that in the anode side. In this research, 50% and 30% humidity was introduced into the cathode electrode. These results clearly indicated that the cell performance in these two conditions is not different (Fig. 6 A, B). Therefore, it can be concluded that water management in our cells has been successful.

Increasing the gas pressure will enhance access to reactant species, resulting in an increase in the cell potential and performance (table 3). There are two reasons for the improvement of performance by pressure: 1) it helps to remove the produced water from the cell, 2) it keeps the reactant concentration at a sufficiently high level. The power density of this cell is much higher compared with the alloy catalysts shown in other researches [18, 19].

These results confirmed that the presence of Pd as alloy with Pt in shell and Ru in core improved the cell performance for ORR.In general, the electrochemical results indicated that the GDE 231 had maximum and the GDE 211 had minimum performance in ORR. Therefore, it could be concluded that in core- shell structure of Ru@Pt-Pd the 2:3:1 molar ratio with 2.3nm particle size and well dispersion of nanoparticle catalyst could be create vast three-phase zone. About the smaller particle size (2.1 nm in GDE 211) I should mention that the active surface area was low, therefore, the polarization resistance of GDE increased and subsequently the electrode performance decreased (table 2). High ionic resistance of GDE 211 was demonstrated inadequacy of three-phase zone for ORR. In case of larger particles (2.9 nm in GDE 432), the effect of catalyst nanoparticles agglomeration reduced the oxygen diffusion coefficient as well as the electro active surface area (table 2). Consequently, according to the obtained results,

polarization and ionic resistance of this GDE has increased, while the current density is decreased.

4. Conclusion

Because there are three kinds of species, namely gases, electrons and protons, which participate in the electrochemical reaction, the reaction can take place on the catalyst surface where they have access to all three species. The synthesized core-shell catalysts were prepared by using the impregnation and hydrothermal method with different molar ratios of differ metals. The physical properties and electrochemical performance of these electro catalysts were characterized using ICP, XRD and a number of required electrochemical techniques. The ICP results revealed that the applied technique was proper for synthesizing core-shell structures. The XRD pattern illustrate that the catalyst particles were nanometer-sized. The results of electrochemical experiment indicated that molar ratios of metals in the core and shell would affect the GDE performance so that in Ru@Pt-Pd the 2:3:1 for Ru:Pt:Pd had the best performance in ORR. Also, the comparison performance between GDE 231 and commercial catalyst (Pt/C 10%wt.) revealed that the core- shell structure improved the catalytic performance. The single cell results confirmed that the GDE 231 as cathode will improve the performance of PEMFC.

Reference

[1] Thompson SD, Jordan LR, Forsyth M. Platinum electrodeposition for polymer electrolyte membrane fuel cells. Electrochemical acta 2001; 46:1657- 1663.
[2] Li WZ, Sun KQ, Hu Z, Xu BQ. Characteristics of low platinum Pt-BaO catalysts for NO_x storage and reduction. Catal Today 2010;153:103-110.
[3] Liu P, Wang J, Zhang X, Wei R, Ren X. Catalytic performances of dealuminated zeolite supported Pt catalysts doped with Cr in hydroisomerization of n-heptane. Chem. Eng. J. 2008;148:184-190.
[4] Jahel A, Avenier P, Lacombe S, et al. Effect of indium in trimetallicPt/Al_2O_3SnIn-Cl naphtha-reforming catalysts. J. Catal. 2010; 272: 275-286.
[5] Matsumoto T, Komatsu T, Arai K, et al. Reduction of Pt usage in fuel cell electrocatalysts with carbon nanotube electrodes. Chem. Commun. 2004; 7: 840-841.
[6] Liu Z, Ming Gan L, Hong L, Chen W, Lee JY. Carbon-supported Pt nanoparticles as catalysts for proton exchange membrane fuel cells. J. power sources 2005;139: 73-78.
[7] Yang H. Core-Shell and Related Multifunctional Nanostructures of Platinum-Based Electrocatalysts. Angew. Chem., Int. Ed. 2011; 50: 2674-2676.
[8] Wang D and Li Y. Bimetallic nanocrystals: liquid-phase synthesis and catalytic applications. Adv. Mater. 2011; 23: 1044-1060.
[9] Wang H, Xu C, Cheng F, et al. Pd/Pt core–shell nanowire arrays as highly effective electrocatalysts for methanol electrooxidation in direct methanol fuel cells. Electrochemistry Communications 2008; 10: 1575- 1578.
[10] Zhang G, Shao ZG, Lu W. Core–shell Pt modified Pd/C as an active and durable electrocatalyst for the oxygen reduction reaction in PEMFCs. Applied Catalysis B: Environmental 2013;132– 133: 183-194.
[11] Zhang L, Kim J, Zhang J, et al. Ti_4O_7 supported Ru@Pt core–shell catalyst for CO-tolerance in PEM fuel cell hydrogen oxidation reaction. Applied Energy 2013; 103: 507-513.
[12] Gao H, Liao S, Zeng J, et al. Preparation and characterization of core–shell structured catalysts using Pt_xPd_y as active shell and nano-sized Ru as core for potential direct formic acid fuel cell application. Electrochimicaacta 2011; 56: 2024-2030.

[13] Anastasijevic NA, Dimitrijevic ZM, Adzic RR. Oxygen reduction on a ruthenium electrode in acid electrolytes. ElectrochemicaActa 1986; 31: 1125-1130.
[14] Prakash J, Joachin H. Electrocatalytic activity of ruthenium for oxygen reduction in alkaline solution. Electrochim. Acta 2000; 45: 2289-2296.
[15] Lischka M, Mosch C, Gro A. Tuning catalytic properties of bimetallic surfaces: Oxygen adsorption on pseudomorphicPt/Ruoverlayers. ElectrochimicaActa 2007; 52: 2219-2228.
[16] Inoue H, Brankovic SR, Wang JX, Adzic RR. Oxygen reduction on bare and Pt monolayer-modified Ru(0001), Ru(1010)and Ru nanostructured surfaces. ElectrochimicaActa 2002; 47: 3777-3785.
[17] Limpattayanate S, Hunsom M. Electrocatalytic activity of Pt- Pd electrocatalysts for the oxygen reduction reacti on in proton exchange membrane fuel cells: Effect of supports. Renewable Energy 2014; 63: 205-211.
[18] Thanasilp S ,Hunsom M. Effect of Pt: Pd atomic ratio in Pt-Pd/C eletrocatalyst-coated membrane on the electrocatalytic activity of ORR in PEM fuel cells. Renewable Energy 2011; 36: 1795-1801.
[19] Zhang J, Vukmirovic M B, Xu Y,et al. Controlling the Catalytic Activity of Platinum-Monolayer Electrocatalysts for Oxygen Reduction with Different Substrates. Angew. Chem. 2005; 117: 2170-2173.
[20] Gharibi H, Javaheri M, Mirzaie R A. The synergy between multi-wall carbon nanotubes and Vulcan XC72R in microporous layers. International journal of hydrogen energy 2010; 35: 9241-9251.
[21] Gharibi H, Javaheri M, Kheirmand M, Mirzaie RA. Optimization of the amount of Nafion in multi-walled carbon nanotube/Nafion composites as Pt supports in gas diffusionelectrodes for proton exchange membrane fuel cells. International journal of hydrogen energy 2011; 36: 13325-13334.
[22]Barbir F. PEM fuel cells: theory and practice. Elsevier Inc. 2005, p 93.
[23] Zhao H, Li L, Yang J, Zhang Y. Co@Pt–Ru core-shell nanoparticles supported on multiwalled carbon nanotube for methanol oxidation. Electrochem. Commun. 2008; 10: 1527-1529.
[24] Lust E, Härk E, Nerut J, Vaarmets K. Pt and Pt–Ru catalysts for polymer electrolyte fuel cells deposited onto carbide derived carbon supports. Electrochimica Acta 2013; 101: 130-141.
[25] Pozio A, Francesco MD, Cemmi A. Comparison of high surface Pt/C catalysts by cyclic voltammetry. J. Power Sources 2002; 105: 13-19.
[26] Bockris JO'M. Modern electro chemistry. 2nd ed. Plenum 2000, p. 1054.
[27] Beattie PD, Basura V I, Holdcroft S. Temperature and pressure dependence of O_2 reduction at Pt Nafion® 117 and Pt BAM® 407 interfaces. J. Electroanalytical Chemistry 1999; 468:180-192.
[28] Wang J. Analytical electrochemistry. 2nd ed. Wiley 2000, p. 60.

8th Iranian Fuel Cell Seminar
FEBRUARY 25,26
2015

Surface-Enhanced Graphene Supported Pt Nanoparticles for Oxygen Reduction Reaction in PEM Fuel Cells

Monireh Faraji[1], Anil Virkar[1], Hussein Gharibi[1,2]
1. Department of Chemistry, Faculty of Science, Tarbiat Modares University, P.O. Box 14115-175, Tehran, Iran
2. Department of Material Science & Engineering, 122 S Campus Drive, University of Utah, Salt Lake City, UT 84112, United States: E-mail addresses

Abstract
In this work graphene nanosheets (GNSs), which act like both single-layer graphene and highly graphitic carbon reported as a support material for Pt nanoparticles for oxygen reduction in fuel cells. Pt nanoparticles are deposited on graphenes protected by Polyvinyl pyrrolidone (PVP) and acrylamide/β methacryl-oxyethyl-trimethyl-ammonium (Superfloc C-442), and characterized with transmission electron microscopy, X-ray diffraction, Raman spectroscopy, and electrochemical tests. Pt/GNS exhibits greatly enhanced electrochemical performance than commercial (Electro Chem Pt/C). These are attributed to the much graphitized degree of GNS in compared to carbon black and the enhanced Pt-carbon interaction in Pt/GNS.

Keywords: Graphene, PEM fuel cell, Oxygen reduction, Pt nanoparticles.

1. Introduction

Polymer electrolyte fuel cells (PEFCs) are a promising primary power source for the future. Both the anodes and cathodes of PEFCs, however, platinum or its alloys are required as the catalyst, having high activity at low operating temperatures <100°C. For the commercialization of PEFCs, it is very important to reduce the amount of platinum catalyst used while maintaining the durability, since particle size and agglomeration of Pt usually increase with its loading onto supports, synthesis procedures of high-loading Pt catalyst with a narrow size distribution remain an enormous challenge.[1] The morphology and structure of supported Pt are strongly influenced by the synthesis method, metal precursor, support materials.[2]

Besides the modification of the Pt catalyst by incorporating alloying components, the application of appropriate support is another way to improve the performance of the Pt catalyst. In the past decades, carbon materials with diverse morphologies have been tested for this purpose. Although the particular electronic interaction between carbon support and Pt catalyst has been taken into consideration, high specific area, reasonable pore structure, good conductivity and suitable anticorrosion stability are considered to be the most important features for good support.[3]

Graphene is a sp^2 hybridized two dimensional sheet of carbon. Its wide honeycomb structure is the essential building plate of other important allotropes; it can be batched to form three dimensional graphite, trilled to form one dimensional nanotubes, and wrapped to form dimension less fullerenes. Long-range π-conjugation in graphene yields outstanding thermal, mechanical, and electrical properties.[4, 5]

Recently, graphite oxide exfoliation by ultrasonic dispersion or rapid thermal expansion has been one of the worst approaches to obtain graphene oxide (GO) in bulk.[6]Compared to other production methods like micromechanical cleavage, this process is tempting because of its reliability, accountability to large-scale production, and exceptionally low material costs[7].The exfoliation of graphite oxide is practical and results in high yields of single-layered graphene oxide (GO).[8]

Graphen is the candidate to be used as catalyst support in the electrocatalysis area due its high mobility of charge carriers (200,000 cm^2 V^{-1} s^{-1}) and specific surface area (calculated value, 2,630 m^2 g^{-1}).[9]

Recently in several works, use of graphene nanosheets as a support for Pt catalyst has been reported. Seger et al reported the of Pt nanoparticles on reduced graphene oxide sheets and their utilization in proton exchange membrane assembly.[10]Yoo et al prepared a new graphene supported electrocatalyst for methanol oxidation in direct methanol fuel cells.[11]Guo et al synthesized three dimensional Pt-on-Pd bimetallic nanodendrites supported on graphene to utilize as an electrocatalyst for methanol electrooxidation.[12]

Because of the Van der Waals interactions, the as-reduced graphene nanosheets tend to form irreversible agglomerates.[13] In order to obtain water soluble or dispersible graphene as individual sheets, attaching some molecules or polymers onto the sheets is a usable method to prevent aggregation,[8]In order to apply graphene as support for Platinum as a electrocatalyst for PEM fuel cells reactions, physical features like surface area and electrical conductivity of graphene should be optimized.

In this work firstly we prepared three GNS (graphen nanosheets) from GO (graphite oxide) with different reducing methods and investigated their physical properties, then, in another experiment platinum salt in situ has been reduced during GO reduction with different methods. we have reported the preparation of Platinum nanoparticles which is supported on graphene decorated by (Polyvinyl pyrrolidone) PVP, typical capping and structure-directing agent, and, a copolymer of acrylamide and a quaternary ammonium (acrylamide/β methacryl-oxyethyl-trimethyl-ammonium copolymer) known as Superfloc C-442 (Cytec), as the oppositely charged binder,[14] ethylene glycol, reducing agent, synthesized and has been compared with a catalyst prepared with sodium borhydrid and hydrazine as a reducing agent of GO (graphite oxide) and commercial (ElectroChem Pt/C).The aim of this work is the investigation of reducing method impact on graphene physical properties and its role as a catalyst support for platinum nanoparticles as an elctrocatalyst for PEFCs electrodes.

2. Experimental

2.1. Synthesis and exfoliation of GO

GO was synthesized from fine extra pure graphite powder (Merck) by the method of modified Hummers and Offeman.[15, 16] In a typical procedure, 50mL of H_2SO_4 was added into a 500mL flask containing 2g graphite at room temperature. The flask was cooled to 0ºC in an ice bath. Then 6 g potassium permanganate ($KMnO_4$) was added slowly to the above mixture and allowed to warm to room temperature. The suspension was stirred continuously for 2 h at 35ºC. After that, it was cooled in an ice bath, and subsequently, diluted by 350 mL of deionized water. Then H_2O_2 (30 v/V%) was added in order to reduce residual permanganate to soluble manganese ions, until the gas evolution ceased. Finally, the resulting suspension was filtered, washed with water, and dried at 60 ºC for 24 h to obtain graphite oxide. After that, the as-prepared graphite oxides were exfoliated by ultrasonication in a water bath (150 W) for more than 2 h. Finally, a homogeneous graphene oxide aqueous dispersion (0.5 mg/mL) was obtained.

2.2. Synthesis of Graphene Nano sheets

1) Preparation of GNS1 with $NaBH_4$

100 mg of exfoliated Go was added to round bottom and $NaBH_4$ (100cc, 50 mmol) drop wisely added to exfoliated Go. The round bottom refluxed and heated in an oil bath at 120°C under argon atmosphere for 24 h over which the reduced GO gradually precipitated out as a black solid. The product has been washed with water and methanol (100 mL) copiously, and dried in vacuum oven for 48 h in 100°C.[9]

2) *Preparation of GNS2 with Hydrazine hydrate*

100 mg exfoliated Go and Hydrazine hydrate (1.00 mL,32.1mmol) added to the round bottom solution refluxed and heated in an oil bath at 120°C under argon atmosphere for 24 h, the black product washed, filtered and dried in vacuum oven.[17]

3) Preparation of PVP-Capped Graphene(GNS3)

100 mg exfoliated Go, ethylene glycol100 ml (Merck), 600 mg PVP (MW=10000 Aldrich) was added to first round bottom.[18] The mixture was stirred for 24 h at 80°C under argon atmosphere. The oppositely charged (cationic) binder which is used to make a site for negative Pt particle deposition is - acrylamide/β methacryl-oxyethyl-trimethyl-ammonium, SuperflocC-442, (from Cytec company).

According to,[14]the optimum pH which prevents hydrolysis of Superfloc C442to carboxylic group fixed in 4.polyacrylamide solutions (0.8 gL^{-1}) were prepared by adding copolymer powder to a solution containing deionized water and sufficient H_2SO_4 to achieve the desired pH. The graphene/PVP mixture was collected, washed and dispersed in 12 mL of aqueous solution containing 0.625 M potassium chloride and 4.25 mg/mL Superfloc C442. After being mixed well, the mixture was sonicated for 3 h to give a homogeneous black mixture. Excess Superfloc C442was removed by centrifugation, and the composite was rinsed with water four times and dried in vacuum oven.

2.3. Synthesis of Pt/graphene nanosheet (GNS) catalysts

In next step three samples of Pt nanoparticles were deposited on graphene oxide sheets in situ during the graphite oxide reduction process by a chemical reduction of chloroplatinic acid (H_2PtCl_6) during the chemical reduction of GO with hydrazine,$NaBH_4$ and PVP /Superfloc C442 /ethylene glycol. The reduction processes are the same as processes explained for graphite oxide reduction above; the only difference in this step is the presence of the platinum salt.[19, 20]

2.4. Measurements of the physical properties

XRD analysis was carried out operating at 40 kV out for the Graphene and catalysts by using an XPERT MPD Philips diffractometer with a Cu X-ray source and 40 mA. The XRD patterns were obtained at a scanning rate of 1°/min with a step size in the 2θ scan of 0.02° in the range 5-100°.Structural changes in graphite ,Go and graphene were examined by using Almega Thermo Nicolet Dispersive Raman spectrometer with second harmonic @532 nm of Nd:YLF laser.

The N_2 adsorption–desorption isotherms of the GNS samples and commercial carbon black Vulcan XC72r were measured at 77 K using Belsorp mini II in order to determine the specific surface areas. The specific surface area was calculated from the Brunauer–Emmett–Teller (BET) plot of the nitrogen adsorption isotherm obtained on a Digital Instrument Nanoscope. The microstructure of the samples was investigated by a scanning electron microscopy SEM (Model XL30, Philips co,).The Pt content in catalysts was estimated by inductively coupled plasma (ICP) analysis.

2.5. Fabrication of the GDEs

Three layers of gas diffusion electrodes (GDEs) were fabricated to evaluate the electrochemical activity of synthesized catalysts for oxygen reduction reaction in half cell system. The diffusion layer was made from a mixture of 30 wt% PTFE and 70 wt% activated carbon (Vulcan XC-72r,Cabot)in 2-propanol (Merck), water, and glycerol (Merck) which is sonicated for 20 min with a sonicator (Misonix model S-3000) to produce a homogeneous suspension. The suspension was rolled onto the carbon paper (TGPH-0120T) (Toray), and the electrode was dried in air at 120°C for 1 h and then finally sintered at 340 ºC for 30 min. The loading of the diffusion layer was fixed at 1 mg cm^{-2}.To prepare the catalyst layers in gas diffusion electrodes (GDE1-GDE4), a homogeneous suspension containing the desired amounts of the Prepared catalysts (10wt.%), Nafion solution 1mgcm^{-2}, glycerol (Merck), 2-propanol (Merck), and water was sonicated for 20 min. This suspension was rolled onto the diffusion layer; the electrode was then dried at 40^{0}C for 30min and then at 80°C for 30min.The Pt loading was 0.2 mg cm^{-2}.Table 1 shows prepared electrodes ,GDE1-GDE4, catalyst layer features.

2.6. Electrochemical measurements

An EG&G Princeton Applied Research Model 273A instrument and frequency response detector (model 1025) were used to determine the electrochemical properties of electrodes. The performance of the GDEs (geometric exposed area 1 cm^{2}) in the reduction of oxygen was investigated in 0.5MH_2SO_4. All measurements were performed at 25°Cin a conventional three-electrode cell, with O_2 flowing at 50 mL min^{-1}. The GDEs were mounted into a Teflon holder that contained a pyrolytic graphite disk as a current collector and has provision for feeding oxygen from the back of the electrode. A large area platinum flat electrode was used as the counter electrode. An Ag/AgCl reference electrode was placed close to the working electrode surface. A glassy carbon electrode immersed in 0.5 M H_2SO_4 was used to perform cyclic voltammetry. The electrochemical cell was connected to a potentiostat galvanostat (EG&G Model 273A) for IeV polarization measurements and chronoamperometry, for electrochemical impedance spectroscopy. In order to perform a quantitative evaluation of resistance against the ORR, the AC impedance method was used.

2.7 Membrane-electrode assemblies (MEA) preparation for PEMFC

MEAs were prepared by the direct catalyst coated membrane (CCM) method [21], in which the catalyst layers are coated directly on treated 115-Nafion membrane by spray, MEAs were assembled with gas diffusion electrodes. The MEA was placed in 4.5 cm^{2} Paxi-tech single-cell fuel cell for electrochemical testing. The humidification temperatures of the anode and cathode gases were 80 $^{\circ}$C and, with flow rates of 220 mlmin^{-1} hydrogen and 500 mlmin$^{-1,}$ respectively. The cell was kept at 80 $^{\circ}$C, and the gas pressure at the back of the electrodes was 1.5 atm.

3. Results and discussion

3.1. Physical characterizations

3.1.1 XRD analyses of graphite, graphite oxide and graphene.

Fig.1 shows the XRD patterns recorded for graphite, GO and reduced graphene samples, respectively. A characteristic diffraction peak of graphite (002) appears at 26º, and the interspacing between the graphene layers is about 3.37 Å. Strong oxidation/exfoliation of graphite, leads to disruption in the ordering of the graphene layers in graphite and a smaller broader peak at2θ=8.5º appeared for GO which corresponds to water bound intercalated oxidized graphite and oxygen functionality groups indicates the complete oxidation of graphite. The interlayer spacing between the layers is increased from 3.37 to 9 Å.[22] However, the XRD pattern of GNS does not show the diffraction peak at 2θ = 8.5°,the interlayer spacing of GO after

reduction in all GNS samples decreased, which is still a little larger than the d-spacing of well ordered graphite (3.37Aº). The small amount of functional groups and hydrogen remaining might be the main reason for this difference, indicating incomplete reduction of GO sheets to graphene [23].Table 2 shows data obtained from XRD analysis of samples.

As seen in Fig. 1 the (002) diffraction peak broaded in graphene samples which indicates the smaller sheet size of graphene compare to the original graphite powder and GO [24].After reduction the peak at 8.5° in the XRD spectrum is not present and broad peaks were observed between 22-25. GNS1, GNS2 and GNS3 respectively, which is close to, but larger than, the d_{002} spacing of graphite. This indicates that functional groups remove during chemical reduction so layer number increased in Graphene comparing graphite oxide but still is much lower than pristine graphite. The d spacing of GNS3 is greater than that of GNS1and GNS2due to PVP intercalation into the interlayer of the graphene sheets. PVP molecules prevent the GO sheets from aggregating back to graphite, they act as a spacer between graphene sheets.[25]

A recent study has shown that the reduction of graphene oxide by $NaBH_4$ is nominally effective in improving the conductivity of the graphene films. The increase in conductivity is attributed to the increase in the sp^2 hybridization of the carbon network. The increase in sp^2 hybridization further allows π-π interaction between the individual graphene sheets, making the sheets agglomerate in suspension. Hydrazine also is a conventional reducing agent for GO reduction but xps studies exhibited nitrogen atom enters the graphene structure and leads to less conductivity.[11] GNS3 exhibits the higher interlayer spacing among GNS samples ,because PVP prevents graphene sheets agglomeration ,the interaction between PVP and graphene is not a kind of covalent interaction so it does not have any harmful impact on conductivity.[26]

3.1.2. Raman spectroscopy characterization of graphite, graphite oxide and graphene

Fig. 2 shows Raman spectra of samples before and after reduction. In carbonaceous material, the D band and G band correspond to sp^2 and sp^3 carbon stretching modes and their intensity ratio (I_D/I_G) is shows the carbon ratio of sp^2/ sp^3which is the measure of the amount of local defects and disorders.[27] Raman spectrum of the pristine, graphite displays a strong G band at 1579 cm^{-1} a weak D band at 1360 cm^{-1} and a middle D´band at 2700 cm^{-1}[28].In the Raman spectrum of GO the G band is broadened and shifted to 1596 cm^{-1},In addition the D band at 1365 cm^{-1} becomes prominent indicating the reduction in size of the in-plane sp^2 domains possibly due to the extensive oxidation. Oxidation reaction leads to defects in GO structure and increases (I_D/I_G) ratio. After reduction this ratio decreases in graphene sheets indicating a partial restoration of the basal planes in graphene. Table 3 shows the (I_D/I_G) and (I_G)/I_D´) obtained from Raman spectra of samples. The lowest (I_D/I_G) is observed for GNS3 which can be assigned to fewer defects in graphitization by (PVP, EG) the D/G intensity ratio did not change obviously, suggesting that the functionalization of graphene nanosheets did not reduce the size of in-plane sp^2 domains greatly (determining the electrical conductivity of graphene nanosheets).

Raman spectroscopy is also utilized to investigate the single, bi, and multilayer characteristics of graphene and graphene oxide layers. The shape and position of the D´ band are known as key parameters to judge both formation and the layer numbers of the graphene sheets. In this work, the slight shift of the peak position of the G band to lower wave numbers (2 cm^{-1}shift) can be assigned to the presence of multi-layers in prepared samples.[29] When the layer number is smaller than five, the D´ peak becomes more intense than G peak. The increase in the ratio

between the intensity of G and D´ peak, ($I_G/I_{D'}$), indicated an increase in the number of graphene layers, respectively. The highest,($I_G/I_{D'}$), ratio of reduced GO samples demonstrated the largest number of graphene layers.[30]In comparison between GNS1/GNS2/GNS3, GNS3 has the minimum layer number, This is due to the fact that PVP prevents graphene sheets restacking, The (I_D/I_G) is maximum for GNS2 which indicates that hydrazine makes some defects in graphene structure.

3.1.3 BET surface area measurement of Graphene sheets

Table 2shows BET surface area measurement results of graphene sheets with nitrogen gas absorption. Our BET surface areas are significantly lower than the theoretical surface area of 2630m^2/g for individual isolated/separated graphene sheets but these values are much higher than carbon black (250m^2/g) used for commercial Pt/C electrocatalyst (ElectroChem).The Brunauer–Emmett–Teller (BET) nitrogen adsorption/desorption isotherms for graphene samples and activated carbon (Vulcan XC-72r) are shown in Fig. 3. All GNS samples exhibit Type I + Type II behavior and their surface areas are GNS1 (420),GNS2(395) and GNS3(485) m^2g^{-1}.The BET results are confirming XRD and Raman results that GNS3 has the less layer number and the much surface area. Remarkable difference between synthesized GNS samples surface area with single layers graphene which is estimated to have a surface area of 2600 m^2g^{-1}, thereby indicating that all GNS samples consist of more than one layer as indeed found from Raman and other studies.[31]

The pore size distributions obtained from the Barrett–Joyner–Halenda (BJH) method,[32, 33] are shown in Fig. 4 and reveal that GNS1 and GNS2are mesoporous with pores greater than 3 nm while GNS3 has both micropores<3 nm and mesopores>20 nm.[34] The best BET surface area obtained for GNS3 indicated that PVP prevented graphene sheets restacking lead to higher surface area.

3.1.4. XRD Analyses of Pt nanoparticles

XRD pattern of platinumFig.5 shows the XRD patterns of the graphene supported Pt electrocatalysts and Pt/C (ElectroChem) electrocatalyst. The peak at 2θ=26.5°corresponds to the (002) planes of the graphitized graphenes and the peaks at 2θ= 39.8°, 67.5^0, and 46.2°areassociated with the (111), (220), and (200) planes of fcc (face centered cubic) Pt, respectively.[35]These results indicate that Pt has been successfully reduced. The average sizes of the Pt particles were calculated from the line broadening of the (111) peak by using the Scherrer equation,[36] after background subtraction and found to be 2.4, 1.6, 1.9 and 1.2 nm for the four samples, respectively (Table 4). As seen in table 4 the Pt particle size for electrocatalyst which are deposited on graphene sheets are smaller than commercial ElectroChem Pt/C. BET measurements indicate that graphene samples have larger surface area which allow for better distribution of pt particles and prevent their aggregation. The smallest particle size belongs to the catalyst which is supported on GNS3 which has the largest surface area.

3.1.5 Zeta potential measurements of GO,GNS samples, Pt/GNS3 samples

The impact of Superfloc-C442mole ratio on Pt loading on graphene was investigated with zeta potential test and inductively coupled plasma(ICP).[37]The zeta potential is usually used to investigate the potential difference between the dispersion medium and the stationary layer of fluid attached to the dispersed particle.[38] Therefore, in this work, the zeta potential was examined for the samples during the synthesis of graphene oxide(exfoliated GO), GNS1 and GNS2 and Pt/GNS3 in different mole ratio of Superfloc-C442 and the result is shown in Table 4.–Zeta potential and thereby electrostatic interactions are varied by altering Superfloc-C442mole ratio in the (GO/PVP/ Superfloc-C442) suspension. Szabo et al [39] have shown that the surface charge of graphene is negative at pH 7and can be modulated by varying the pH of

the medium. GO had a zeta potential of -66.2 mV, which is attributed to a large number of negatively charged functional groups such as carboxyl groups and hydroxyl groups and these amount of negative charge results repulsion with Pt salt. The surface charge of GNS3 sample is strongly dependent to Superfloc-C442/GO mole ratio, On the other hand Pt nanoparticle deposition loading ,Fig 6, is strongly affected by the surface charges of GNS3 and PVP-Superfloc-C442/GO mole ratio.[40]

In order to obtain maximum Pt loading on GNS3, zeta potential and ICP measuring is carried on samples with varied Superfloc-C442/GO mole ratio which resulted from different loading on. Negative zeta potential of GO shifted to graphene positive zeta potential (+35.5 mV) after modifying by PVP- Superfloc-C442, indicating that the graphene was successfully functionalized by the positively charged PVP- Superfloc-C442.The noncovalent adsorption of PVP- Superfloc-C442 on graphene oxide (GO) not only leads to a highly dense and homogeneous distribution of positive charges on the GO surface, but also preserves the intrinsic properties of the GO. The comparison of surface charge density of GNS1, GNS2 with GNS3 shows that negative charge density in GNS3 surface has been reduced with the incorporation of Superfloc-C442 .These positive charges were used as sites for deposition of Pt nanoparticles on graphene. Therefore, the resultant Pt nanoparticles with small size were uniformly dispersed on and both surfaces of graphene, and its loading density could be controlled with Superfloc-C442/Go mole ratio .By the assembly of negatively charged Pt colloidal nanoparticles, the zeta potential of Pt-GNS3 becomes negative again .The maximum Pt loading is obtained in 30% mole ratio of Superfloc-C442/Go as seen in Fig. 6.

3.2. Morphology analysis by SEM and TEM

3.2.1. SEM characterization

SEM image of pristine graphite flake (Merck) consists of rigid and condensed layers in Fig.7. After the oxidation process; graphite started to crumble forming irregular separated structures and creates expanded and leafy structures of graphite oxide layers. After reduction reaction of GO with three different method graphene sheets made of a few graphene layers could be clearly seen in Fig. 8 Consequently, all the reaction procedures led to the formation of graphene nanosheets which have highly porous and wavy structure. After the reduction by hydrazine and $NaBH_4$, it can be observed that, Fig 9,. GNS1 and GNS2 tend to form very dense agglomerates with layered structure which results from the Van der Waals interactions between the layers of graphene.[4] The introduction of PVP into GNS3 reaction mixture remarkably increased the stability of graphene sheets because of strong hydrophobic interactions between graphene sheets and PVP preventing graphene layers restacking and maintaining high surface area.

3.2.2. TEM characterization

Fig 10a, b, c shows a TEM image of platinum nanoparticles supported on GNS3. In this image, platinum nanoparticles appear as dark dots with a diameter of 2 to 1.5nm on a lighter shaded substrate corresponding to the planar graphene sheet. The nanoparticles cover the graphene sheets with an interparticle distance ranging from several nanometers to several tens of nanometers, occupying only a very small portion of the surface of the graphene sheet. Pt nanoparticles aggregates can be seen only at the graphene edges where abundant amine moieties are available due to the easy adsorption of PVP at defect sites of the graphene edges. This result also indicates a strong interaction between the functionalized graphene support and the Pt nanoparticles. The Pt nanoparticles decorated on the graphene surfaces can act as “spacers” to

prevent the graphene from aggregation and restacking, and both faces of graphene are accessible.

3.3. Electrochemical investigations of prepared catalysts

3.3.1. Electrochemically active surface area

Cyclic voltammetry (CV) is a convenient and efficient tool used to estimate the (electrochemical surface area) ECSA of Pt catalyst on an electrode. The CV curves for different electrocatalysts, in 0.5 M H_2SO_4 solution at a scan rate of 50mV $s^{-1}$are shown in Fig.11.It shows characteristic peaks for the formation and reduction of Pt oxide. In the potential region of 0.2 to 0 V (vs. Ag/AgCl), typical hydrogen adsorption and desorption peaks from polycrystalline Pt were observed using graphene nanosheets as supporting materials. The integrated area under the adsorption peak in the CV curves represents the total charge concerning H^+ adsorption, Q_H, and has been used to determine ECSA by employing the equation.[41]

$$EAS = \frac{Q_h(\mu C / cm^2)}{210(\mu C / cm^2) \times [Pt](mg / cm^2)} \quad (1)$$

Our calculation indicates that Pt/GNS3 has higher ECSA value 135m^2/g than Pt/C (ElectroChem) (45.5m^2/g) (Table 5). It is due to the fact that Pt nanoparticles are smaller and more uniformly dispersed on the surfaces of Pt/graphene sheets, when compared with Pt/C. It is well known that smaller catalyst particles show higher catalytic activity. Furthermore, Pt nanoparticles dispersed on GNS surface will allow for uniform dispersion of the graphene nanosheets by reducing aggregation of the sheets, thereby producing much more accessible Pt sites for efficient catalytic activity in comparison with carbon black used as catalyst support[42] ECSA data is in a good agreement with BET results which indicated that higher carbon surface area lead to better Pt distribution and more active sites for adsorption/desorption of electroactive spices.

3.3.2 potentiostatic-state polarization curves

The polarization curves for the electrodes in conventional three-electrode cells are presented in Fig. 12 The current density values are considerably greater for electrode (GDE3), containing Pt/GNS3, than for the others, the performance of GDE3 is much better than that obtained when using aGDE1containing commercial Pt/C (ElectroChem). The superior performance of GDE3 is attributed to an increase in the size of the three-dimensional reaction zone and to the optimum surface area. As a result, the concentrations of the reactants near the surface of the catalyst are increased, and hence the reaction rate is improved. As seen in polarization curves current densities in mass transfer region is much higher for graphene supported Pt catalyst, especially Pt/GNS3(GDE3), than commercial activated carbon (Vulcan XC72r) supported Pt/C (ElectroChem) which is attributed to the different porous structure of graphene and carbon black. Mesopore sizes in graphene facilitated water transport in electrode which lead to better proton transfer and prevent mass transfer limitation, besides presence of micro pores in graphene structure allow oxygen accessibility to electrode surface. The performance difference between GDE1, GDE2 and GDE3 is attributed to the different micro structures of Pt/GNS1, Pt/GNS2, Pt/GNS3 which results from different reducing methods. These results indicate that carbon supported porous structure highly affects catalyst performance.[43]

The kinetic parameters of the ORR for a GDE can be obtained from the polarization data. Our analysis of the experimental polarization data was performed by using the Tafel equation:[44]

$$E_{\text{rev}} - E = b \log i / i_0 \quad (2)$$

The electrochemical parameters, Table 5, derived from Tafel equation. The best kinetic parameters are observed for GDE3 (Pt/GNS3) catalyst. This result show that surface area and morphology are optimum for GNS3 not only among other prepared graphene samples, but also in comparison with Vulcan XC-72r makes it better catalyst support for Pt to catalyze oxygen reduction reaction.

3.3.3Choronoampermetrye

Choronoamperometry, Fig 13, is employed to determine to the diffusion coefficient of oxygen to the catalyst layer of electrodes. Diffusion coefficient which is seen in Table 5 can be obtained from modified Cottrel equation.

$$i(t) = \left(nFAD^{1/2}C\right)\left(\pi^{1/2}t^{1/2}\right) + {}^{nFADC}/_{r} \quad (3)$$

where r is the diameter of the electrode, i is the limiting current (mA); n is the number of electrons, F is the columbic charge (964850 C mol^{-1}), D is the diffusion coefficient (Cm^2s^{-1}), t is the time (s), and C^* is the saturated concentration of oxygen in sulfuric acid (1.38×10^{-6} mM). GDE3 (Pt/GNS3) exhibits the highest permeability, It is may be due to the modified porous structure of GNS3.The presence of micro pores in GNS3 increased gas permeability and oxygen diffusion toward the catalyst, whereas mesoporous structure of (Vulcan XC-72r) in GDE4 ,GNS1in GDE1and GNS2 in GDE2 act weakly for gas diffusion.

Micropore structure of carbon support which involved with gas has a crucial role in mass transport for liquid face. As a result it seems that the presence of both macropores and micropores in oxygen reduction reaction which occurs in the interface of liquid(proton transport) and gas phase(oxygen permeability) are necessary to enhance the catalyst performance.[45]

3.3.4 Electrochemical Impedance Spectroscopy

The A.C impedance spectrum of GDEs (GDE1-GDE4), each electrode, Fig. 14, was obtained. The resulting data were obtained at 400 mV vs. Ag/AgCl saturated with KCl, and were plotted in the Nyquist representation.

The polarization resistance R_P was found to be lower for GDE3 which contains Pt/GNS3 indicating that interfacial oxygen kinetics is enhanced in the presence of graphene. In another word, more three-phase boundaries (i.e., Pt nanoparticles covered by thin ionomer film through which oxygen diffuses) available for oxygen reduction reaction are formed with the aid of graphene in the catalyst layer, moreover faster charge transfer in Pt/GNS3 in compare with Pt/GNS1 and Pt/GNS2 shows that modification of GNS with PVP-Superfloc C442is non-covalent functionalization and PVP-Superfloc C442 have been removed during the final product washing. If PVP-Superfloc C442 remained in GNS structure, the GNS charge carrier would be disrupted, since the electron transfer has been assumed to mainly originate at edge of plane-like sites of carbon materials, it was to be expected that a material with a high density of edge plane-like sites would have fast charge transfer capability.

The presence of PVP-Superfloc C442in GNS structure may lead to the steric hindrance and the electrostatic interactions which affect density of edge plane like sites than that in Pt/GNS1 and Pt/GNS2. The lower charge transfer resistance for the catalyst has good correlation with the

higher electrocatalytic activity for oxygen reduction, suggesting that the GNSs supported electrocatalysts prepared by our method may be more competitive.

3.4. Single-cell data

Single-cell PEMFC performance examined for MEA1 containing Pt/GNS3 catalyst as cathode and Pt/C10% (ElectroChem) as anode and MEA2 containing ElectroChem commercial 10% Pt/C both cathode and anode were tested. The single-cell performance curves of MEAs are presented in Fig. 15a,b. A comparison of fuel cell performance with the cathode containing different compositions of Pt/GNS3 and Pt/C (ElectroChem) is shown in Table 6. In the present case, as shown in Table 6, MEA1 containing Pt/GNS3 in cathode side has better performance than MEA2 containing commercial catalyst. The Pt nanoparticles may act as spacers to avoid the face-to-face aggregation of graphene sheets and the intrinsic high graphitization degree of GNS leads to enhanced Pt-carbon interaction, which further provides good accessibility to the Pt reaction sites in Pt/GNS thereby improving the electrocatalytic activity of the nanocomposite compared to commercial Pt/C.

Fig. 16 a, b show impedance spectra obtained for MEAs at 0.1 V, which is related to the high current density (HCD) region, and at 0.7 V, which illustrates the behavior in the low current density (LCD) region. For EIS spectra in the LCD region, a semicircle whose diameter is related to the oxygen reduction polarization resistance and a depressed semicircle centered on the x-axis are observed. These depressed semicircles have been explained by a number of phenomena depending on the character of the system being investigated, such as an inhomogeneous electrode surface, the distribution of activation or relaxation processes and concentration. Polarization phenomena Fig. 17 Shows an equivalent circuit for MEAs with R_{el}: membrane resistance (subtracted from the result), R_e electrode intrinsic resistance, R_{ct} charge transfer resistance, R_m mass transfer resistance, and CPE constant phase element.[46]

The values obtained for these parameters are given in Table 6 MEA1 have the minimum charge transfer and mass transfer resistance.

3.4.1. The effects of temperature and relative humidity on the oxygen reduction reaction (ORR) inMEA1 (Pt/GNS3)

The effects of temperature and relative humidity on the oxygen reduction reaction (ORR) in MEA1 (Pt/GNS3) catalyst were investigated using cyclic voltammetry, and Steady-State Potentiostatic Polarization.

Figure 18a, show the steady state cyclic voltammograms of MEA1(Pt/GNS3) at ~60% and 80%RH in Ar atmosphere at 60 ºC and 2.5 atm absolute pressure. Seen in Fig 18a, the hydrogen adsorption/desorption peaks in the voltammogram of the MEA1(Pt/GNS3) are not clearly defined. Different orientations of the polymer chains in different parts of the interface caused to this phenomenon. Integration of the hydrogen adsorption currents in the voltammograms shown in Fig. 18a, reveals that only 78% of the Nafion-covered Pt surface is electrochemically active at 60% RH. A similar comparison based on the platinum oxide reduction at +1.4 V explained even the lower activity of the Nafion covered Pt, getting only 50% at 60% RH. The platinum oxide reduction charge increased, whereas the hydrogen adsorption charge stained almost unchanged or even a little decreased with an increase in temperature [47]. The different temperature effects, as seen in Fig 18b, on platinum oxide and hydrogen adsorption charges made it difficult to unequivocally determine the active fraction of surface area. Based on the platinum oxide reduction, the active fraction of surface area increased with relative humidity and became ~95% at 100% RH and 80°C.

Fig. 19 and Fig. 20 show polarization curves are obtained for MEA1 in different temperatures and relative humidities. The limiting current of ORR was found to depend strongly on both

temperature and relative humidity. The temperature effect on oxygen limiting current results from its positive effect on oxygen diffusion and its negative effect on oxygen solubility in Nafion ionomer.[48] The activation energy for oxygen reduction reaction was obtained from Arrhenius plots based on the following equation:

$$E_a = -2.303R\left[\frac{d\log i_0}{d(1/T)}\right] \quad (4)$$

In addition, a large hysteresis between the forward and reverse scans was frequently observed, The existence of hysteresis phenomenon in the polarization curves during the forward and backward sweeps is because of water generation and distribution within membranes and catalyst layers, or namely the "water reservoir" effect of membranes and catalyst layers were the main reasons accounting for the cross point of the polarization curves. Such cross point strongly depended on the diffusion materials and operation conditions such as flow rates, cell temperatures and the stabilized time at each current density, which in directly showed the evidence for the different water transport mechanism.[49]

As the distortions were increasing with increases in both temperature and relative humidity (Fig. 19), which are known to have opposite effects on Nafion hydration (10), they initially did not seem to be related to membrane hydration. The only two factors that were changing in the same direction with increases in temperature and relative humidity were the water pressure in the gas phase and the membrane permeability to oxygen. As a result, membrane hydration could only be changed with the water pressure changes and, as mentioned above, these were opposite when the water pressure increased due to the temperature and humidity increase. The polarization curve in Fig. 20 demonstrate that full membrane hydration dramatically improves the apparent oxygen reduction kinetics in both forward and reverse scans and that the hysteresis is no longer present. Moreover, the limiting reduction current for the fully hydrated membrane is higher, which shows an enhancement in the membrane permeation to oxygen. The large current density, which indicates that mass transport, is not affected by the electrochemically generated water. This means the "water reservoir" of the graphene as carbon support in catalyst is not completely used at all or the generated water is easier to be carried out of the fuel cell by the reactant gas. The self-inhibition of ORR at the interface between Pt and partially hydrated Nafion membrane reveals that water produced by ORR basically changes the composition of the interface. It can be easily demonstrated that the diffusion flux of product water is not sufficiently high to produce significant changes in the composition of the Pt/Nafion interface unless either (i) small quantities of water induce significant changes in the interfacial structure of Nafion or (ii) water cannot freely diffuse away from the interface.

3.4.2. Effects of relative humidity on proton Conduction in MEA1

RH (relative humidity) has a significant impact on the performance of a single cell. In this study, impedance spectroscopy has been employed to measure the proton Conduction in MEA1 varying with relative humidity. We describe AC impedance experiments to measure membrane resistance and the cathode proton resistance inaH_2 /Ar cell configuration. $R_{membrane}$, C_{cath}, and $R_{H^+,cath}$ in—AC impedance data inH_2/Ar were analyzed by fitting $R_{H^+,cath}$, $R_{membrane}$, C_{cath} to transmission-line model. Table 8 shows parameters obtained from transmission-line model. Fig. 21 shows impedance spectra obtained in OCV potential in different humidities.

In principle, RH decreasing leads to the membrane resistivity increasing. Especially under low RH conditions and high current densities, the proton conduction resistance across the electrode can become rate determination and catalyst utilization limiting factor. Results of this

measurement are compared with work [50] in which the proton resistivity has been investigated for with Ketjen black (KB)] and [Vulcan XC 72r] supported catalyst in the same Ionomer/carbon ratio and we found that Pt/GNS3 has less proton resistivity than Pt/Vulcan and Pt/KB in the same condition.

4. Conclusion

Graphene nanosheets (GNS), which exhibit the advantages of single-layer graphene and highly graphitic carbon, were employed as an alternative support material for Pt nanoparticles for oxygen reduction. Graphene nanosheets were modified by PVP and a polyelectrolyte which leads to greater surface area and better electronic properties in comparison with other conventional reduction methods of GO. Pt nanoparticles were deposited on GNS samples and the activity of prepared catalyst were examined for oxygen reduction reaction, The modified graphene supported catalyst (GNS3) has–better performance than commercial ElectroChem Pt/C and other graphene (GNS2,GNS1) supported catalysts. These results indicate that graphene nanosheets could be a good candidate as a supporting material of catalysts in fuel cells.

Appindex

b	Tafel slope
C*	reactant concentration
CPE	constant phase element
D	diffusion coefficient
$D^{1/2}\times C^*$	permeability
EAS	electroactive surface area
E_{eq}	open-circuit voltage
HCD	high current density
F	faraday constant
GDE	gas diffusion electrode
GNS	graphenenano sheet
GO	Graphite oxide
i	current density
i_o	exchange current density
LCD	low current density
MEA	membrane electrode assembly
n	number of electrons
OCV	open-circuit voltage
ORR	oxygen reduction reaction
R_{ct}	charge transfer resistance
R_i	ionic resistance
R_m	mass transfer resistance
R_s	electrolyte resistance
$R_{internal}$	internal resistance
RH	relative humidity
t	time
Z_{real}	real impedance
Z_{im}	imaginary impedance
η	over-potential
R_{H^+}	Proton resistance
C_{cath}	Cathode capacitance

References

[1] K. Okaya, H. Yano, H. Uchida, M. Watanabe, Control of particle size of Pt and Pt alloy electrocatalysts supported on carbon black by the nanocapsule method ACS Applied Materials and Interfaces, 2 (2010) 888-895.
[2] G. Wu, D. Li, C. Dai, D. Wang, N. Li, Well-dispersed high-loading Pt nanoparticles supported by shell-core nanostructured carbon for methanol electrooxidation Langmuir, 24 (2008) 3566-3575.
[3] A. Wei, Q.J. Wang, X.H. Zhao, S.Y. Zhang, Electronic effect of carbon support on Pt catalyst supported on graphite intercalation compound Chemical Research in Chinese Universities, 26 (2009) 465-471.
[4] M.J. Allen, V.C. Tung, R.B. Kaner, Honeycomb carbon: A review of graphene. Chemical Reviews, 110 (2010) 132-145.
[5] X. Gao, J. Jang, S. Nagase, Hydrazine and thermal reduction of graphene oxide: Reaction mechanisms, product structures, and reaction design Journal of Physical Chemistry C, 114 (2010) 832-842.
[6] J. Shen, Y. Hu, C. Li, C. Qin, M. Shi, M. Ye, Layer-by-layer self-assembly of graphene nanoplatelets Langmuir, 25 (2009) 6122-6128.
[7] C. Soldano, A. Mahmood, E. Dujardin, Production, properties and potential of graphene Carbon, 48 (2010) 2127-2150.
[8] C. Mattevi, G. Eda, S. Agnoli, S. Miller, K.A. Mkhoyan, O. Celik, D. Mastrogiovanni, C. Cranozzi, E. Carfunkel, M. Chhowalla, Evolution of electrical, chemical, and structural properties of transparent and conducting chemically derived craphene thin films Advanced Functional Materials, 19 (2009) 2577-2583.
[9] H.J. Shin, K.K. Kim, A. Benayad, S.M. Yoon, H.K. Park, I.S. Jung, M.H. Jin, H.K. Jeong, J.M. Kim, J.Y. Choi, Y.H. Lee Efficient reduction of graphite oxide by sodium borohydride and its effect on electrical conductance, Advanced Functional Materials 19 (2009) 1987-1992.
[10] B. Seger, P.V. Kamat, Electrocatalytically active graphene-platinum nanocomposites. role of 2-D carbon support in pem fuel cells Journal of Physical Chemistry C, 113 (2009) 7990-7995.
[11] E. Yoo, T. Okata, T. Akita, M. Kohyama, J. Nakamura, I. Honma, Enhanced electrocatalytic activity of Pt subnanoclusters on graphene nanosheet surface Nano Letters, 9 (2009) 2255-2259.
[12] S. Guo, S. Dong, E. Wang, Three-dimensional Pt-on-Pd bimetallic nanodendrites supported on graphene nanosheet: Facile synthesis and used as an advanced nanoelectrocatalyst for methanol oxidation ACS Nano, 4 (2010) 547-555.
[13] S. Stankovich, D.A. Dikin, G.H.B. Dommett, K.M. Kohlhaas, E.J. Zimney, E.A. Stach, R.D. Piner, S.T. Nguyen, R.S. Ruoff, Graphene-based composite materials, Nature 442 (2006) 282-286.
[14] A.P. Angelopoulos, J.B. Benziger, S.P. Wesson, Cationic Polyacrylamide Adsorption on Epoxy Surfaces, Journal of Colloid and Interface Science 185 (1997) 147-156.
[15] W.S. Hummers Jr, R.E. Offeman, Preparation of graphitic oxide, Journal of the American Chemical Society 80 (1958) 1339.
[16] Z.S. Wu, W. Ren, L. Gao, B. Liu, C. Jiang, H.M. Cheng, Synthesis of high-quality graphene with a pre-determined number of layers, Carbon 47 (2009) 493-499.
[17] S. Stankovich, D.A. Dikin, R.D. Piner, K.A. Kohlhaas, A. Kleinhammes, Y. Jia, Y. Wu, S.T. Nguyen, R.S. Ruoff, Synthesis of graphene-based nanosheets via chemical reduction of exfoliated graphite oxide,Carbon 45 (2007) 1558-1565.
[18] G. Carotenuto, G.P. Pepe, L. Nicolais, Preparation and characterization of nano-sized Ag/PVP composites for optical applications, European Physical Journal B 16 (2000) 11-17.
[19] Y. Si, E.T. Samulski, Exfoliated graphene separated by platinum nanoparticles, Chemistry of Materials 20 (2008) 6792-6797.

[20] W. He, H. Jiang, Y. Zhou, S. Yang, X. Xue, Z. Zou, X. Zhang, D.L. Akins, H. Yang, An efficient reduction route for the production of Pd–Pt nanoparticles anchored on graphene nanosheets for use as durable oxygen reduction electrocatalysts, Carbon 50 (2012) 265-274.
[21] M. Prasanna, E.A. Cho, T.H. Lim, I.H. Oh, Effects of MEA fabrication method on durability of polymer electrolyte membrane fuel cells ,Electrochimica Acta 53 (2008) 5434-5441.
[22] H.M. Ju, S.H. Choi, S.H. Huh, X-ray diffraction patterns of thermally-reduced graphenes, Journal of the Korean Physical Society 57 (2010) 1649-1652.
[23] J. Yan, T. Wei, B. Shao, F. Ma, Z. Fan, M. Zhang, C. Zheng, Y. Shang, W. Qian, F. Wei, Electrochemical properties of graphene nanosheet/carbon black composites as electrodes for supercapacitors, Carbon 48 1731-1737.
[24] C.V. Rao, A.L.M. Reddy, Y. Ishikawa, P.M. Ajayan, Synthesis and electrocatalytic oxygen reduction activity of graphene-supported Pt_3Co and Pt_3Cr alloy nanoparticles, Carbon 49 931-936.
[25] J. Yan, T. Wei, B. Shao, F. Ma, Z. Fan, M. Zhang, C. Zheng, Y. Shang, W. Qian, F. Wei, Electrochemical properties of graphene nanosheet/carbon black composites as electrodes for supercapacitors, Carbon 48 (2010) 1731-1737.
[26] S. Yoon, I. In, Role of poly(N-vinyl-2-pyrrolidone) as stabilizer for dispersion of graphene via hydrophobic interaction, Journal of Materials Science 46 (2011) 1316-1321.
[27] Y.H. Ding, P. Zhang, Q. Zhuo, H.M. Ren, Z.M. Yang, Y. Jiang, A green approach to the synthesis of reduced graphene oxide nanosheets under UV irradiation, Nanotechnology 22 (2011).
[28] A.C. Ferrari, Raman spectroscopy of graphene and graphite: Disorder, electron-phonon coupling, doping and nonadiabatic effects, Solid State Communications 143 (2007) 47-57.
[29] O. Akhavan, Graphene nanomesh by ZnO nanorod photocatalysts, ACS Nano 4 (2010) 4174-4180.
[30] B. Saner, F. Okyay, Y. Yî¼rî¼m, Utilization of multiple graphene layers in fuel cells. 1. An improved technique for the exfoliation of graphene-based nanosheets from graphite, Fuel 89 1903-1910.
[31] G. Srinivas, Y. Zhu, R. Piner, N. Skipper, M. Ellerby, R. Ruoff, Synthesis of graphene-like nanosheets and their hydrogen adsorption capacity, Carbon 48 (2010) 630-635.
[32] P.J.M. Carrott, R.A. Roberts, K.S.W. Sing, Adsorption of nitrogen by porous and non-porous carbons, Carbon 25 (1987) 59-68.
[33] K. Kaneko, Determination of pore size and pore size distribution. 1. Adsorbents and catalysts, Journal of Membrane Science 96 (1994) 59-89.
[34] F. Su, C.K. Poh, Z. Tian, G. Xu, G. Koh, Z. Wang, Z. Liu, J. Lin, Electrochemical behavior of pt nanoparticles supported on meso- and microporous carbons for fuel cells. Energy and Fuels, Energy and Fuels 24 (2010) 3727-3732.
[35] H. Huang, H. Chen, D. Sun, X. Wang, Graphene nanoplate-Pt composite as a high performance electrocatalyst for direct methanol fuel cells, Journal of Power Sources 204 (2012) 46-52.
[36] H. Gharibi, M. Javaheri, M. Kheirmand, R.A. Mirzaie, Optimization of the amount of Nafion in multi-walled carbon nanotube/Nafion composites as Pt supports in gas diffusion electrodes for proton exchange membrane fuel cells ,International Journal of Hydrogen Energy In Press, Corrected Proof.
[37] S.-H. Kwak, T.-H. Yang, C.-S. Kim, K.H. Yoon, The effect of platinum loading in the self-humidifying polymer electrolyte membrane on water uptake, Journal of Power Sources 118 (2003) 200-204.
[38] A. Asadzadeh Shahir, S. Javadian, B.B.M. Razavizadeh, H. Gharibi, Comprehensive study of tartrazine/cationic surfactant interaction, Journal of Physical Chemistry B 115 (2011) 14435-14444.
[39] T. Szabó, E. Tombácz, E. Illés, I. Dékány, Enhanced acidity and pH-dependent surface charge characterization of successively oxidized graphite oxides, Carbon, 44 (2006) 537-545.
[40] J. Lu, I. Do, H. Fukushima, I. Lee, L.T. Drzal, Stable aqueous suspension and self-assembly of graphite nanoplatelets coated with various polyelectrolytes, Journal of Nanomaterials 2010 (2010).
[41] A. Pozio, M. De Francesco, A. Cemmi, F. Cardellini, L. Giorgi, Comparison of high surface Pt/C catalysts by cyclic voltammetry, Journal of Power Sources 105 (2002) 13-19.

[42] Y. Li, W. Gao, L. Ci, C. Wang, P.M. Ajayan, Catalytic performance of Pt nanoparticles on reduced graphene oxide for methanol electro-oxidation, Carbon 48 (2009) 1124-1130.
[43] T. Soboleva, K. Malek, Z. Xie, T. Navessin, S. Holdcroft, PEMFC catalyst layers: The role of micropores and mesopores on water sorption and fuel cell activity, ACS Applied Materials and Interfaces 3 (2011) 1827-1837.
[44] J. Zhang, PEM Fuel Cell Electrocatalysts and Catalyst Layers Fundamentals and Applications, Springer-, london, 2008.
[45] Y. Liu, C. Ji, W. Gu, J. Jorne, H.A. Gasteiger, Effects of catalyst carbon support on proton conduction and cathode performance in PEM fuel cells, Journal of the Electrochemical Society, 158 (2011) B614-B621.
[46] N. Fouquet, C. Doulet, C. Nouillant, G. Dauphin-Tanguy, B. Ould-Bouamama, Model based PEM fuel cell state-of-health monitoring via ac impedance measurements, Journal of Power Sources 159 (2006) 905-913.
[47] C.M. Lei Zhang, Sanjeev Mukerjee, Oxygen reduction and transport characteristics at a platinum and alternative proton conducting membrane interface, Journal of Electroanalytical Chemistry, 568 (2004) 273–291.
[48] V.I.B. Paul D. Beattie, Steven Holdcroft, Temperature and pressure dependence of O_2 reduction atPt Nafion® 117 and Pt BAM® 407 interfaces Journal of Electroanalytical Chemistry, Journal of Electroanalytical Chemistry, 468 (1999) 180–192.
[49] J. Hou, A study on polarization hysteresis in PEM fuel cells by galvanostatic step sweep, international journal of hydrogen energy 36 (2011) 7199-7206.

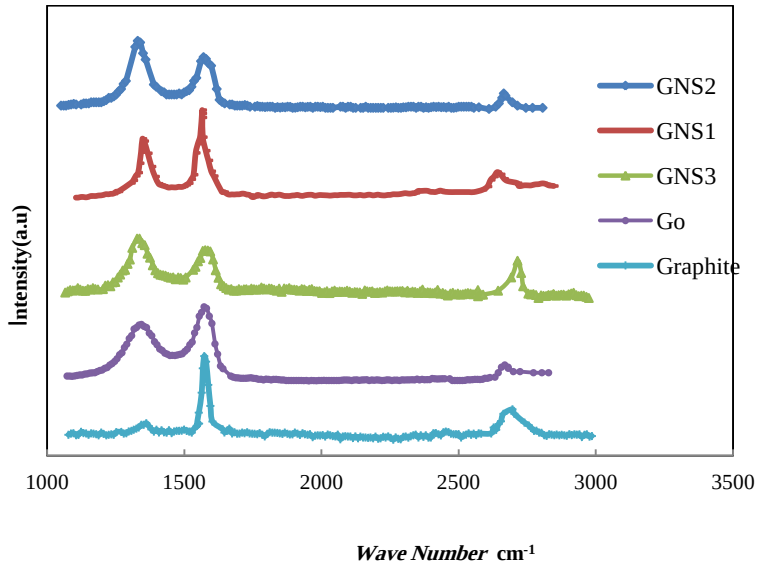

Fig1.XRD patterns Graphite,Go,Graphenenanosheets(GNS)

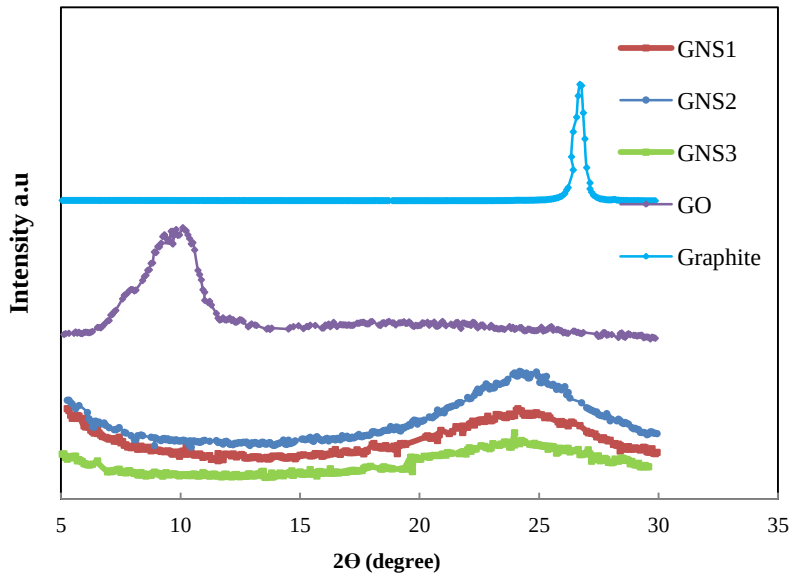

Fig2.Raman spectra of Graphite,Go and Graphenenanosheets

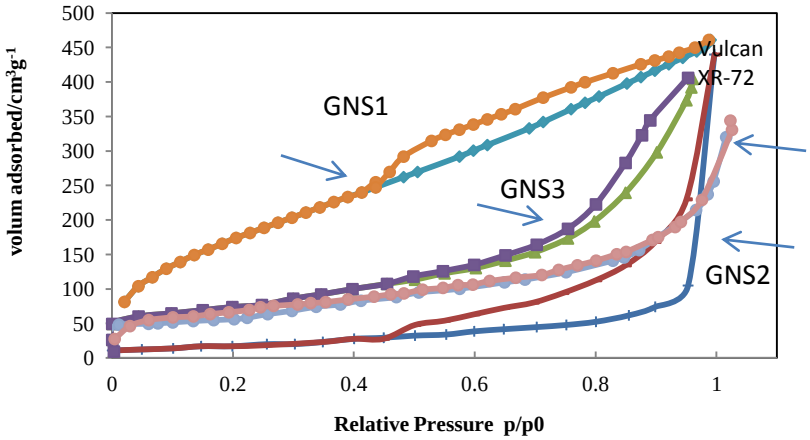

Fig. 3.Nitrogen adsorption/desorption isotherms of GNS samples and activated carbon(VulcanXR72)

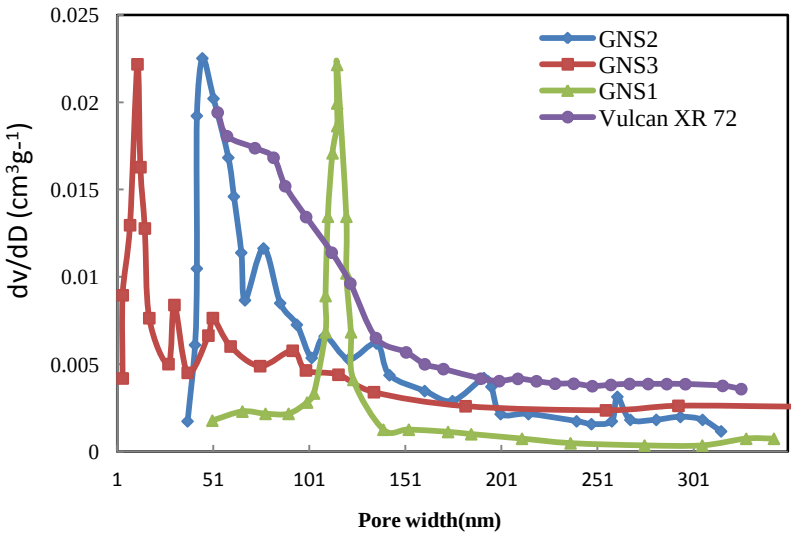

Fig.4.Pore size distribution curves of GNS samples and Vulcan XC 72r

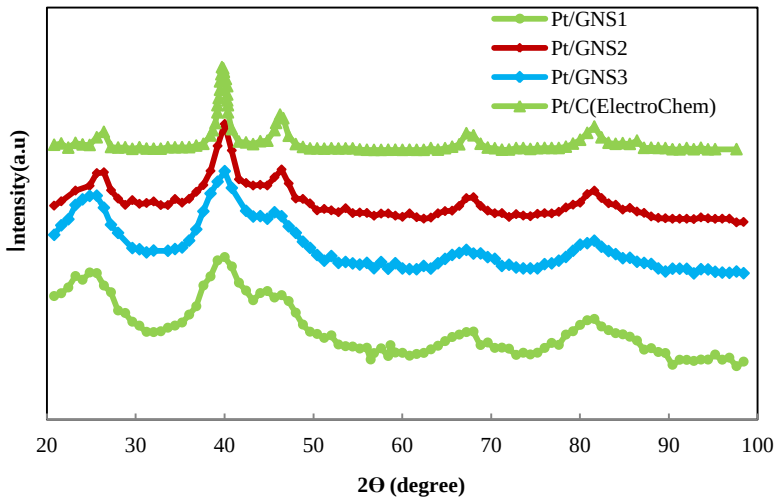

Fig. 5. XRD of patern of Pt/GNS1,Pt/GNS2/Pt/GNS3/Pt/C(ElectroChem)

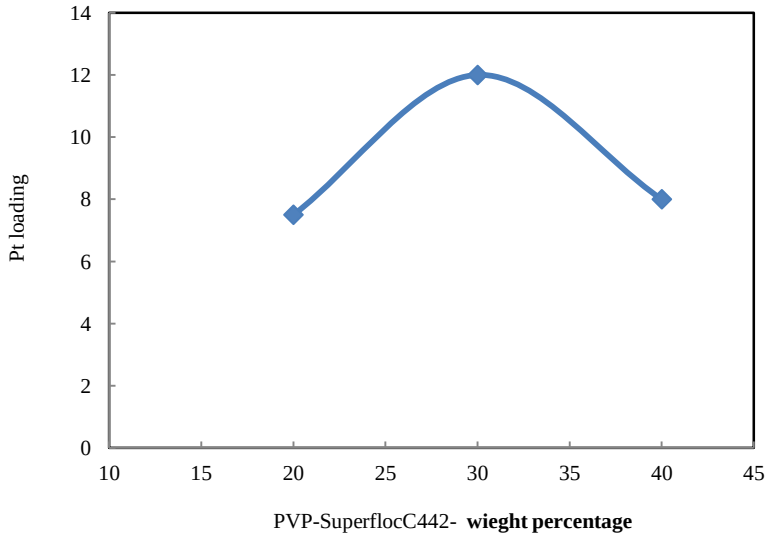

Fig. 6.Pt loading density on GNS3 GO vsPVP-SuperflocC442weight percentage

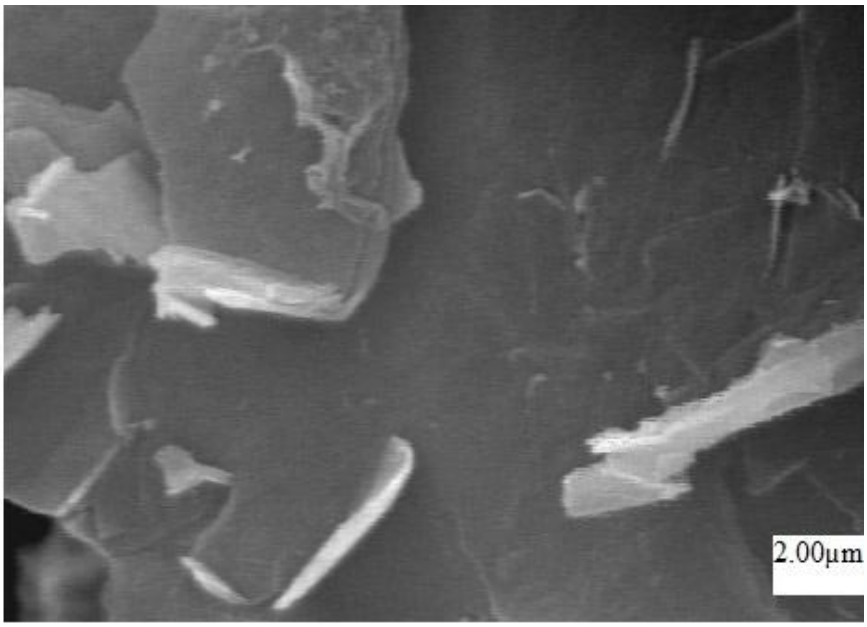

Fig. 7.SEM image of raw graphite flake

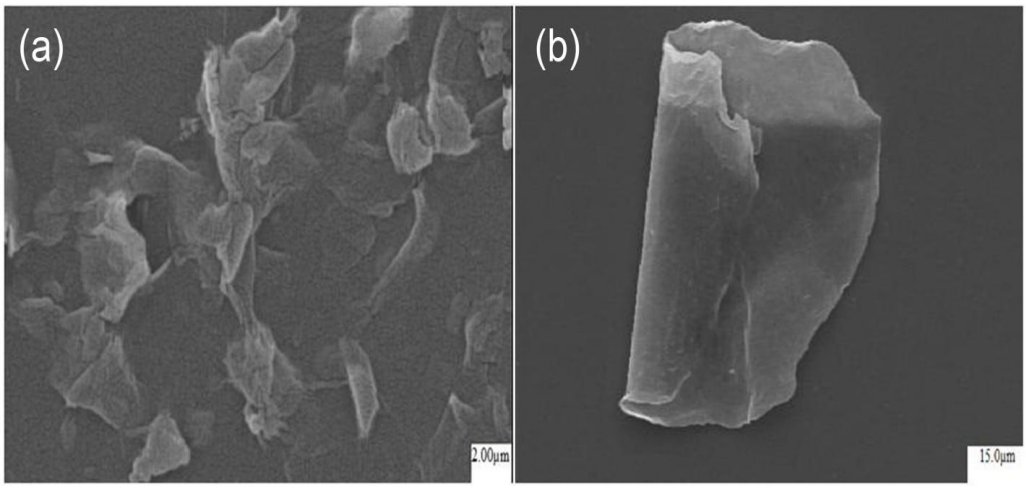

Fig. 8.SEM images (a) and (b) of GO at different magnifications

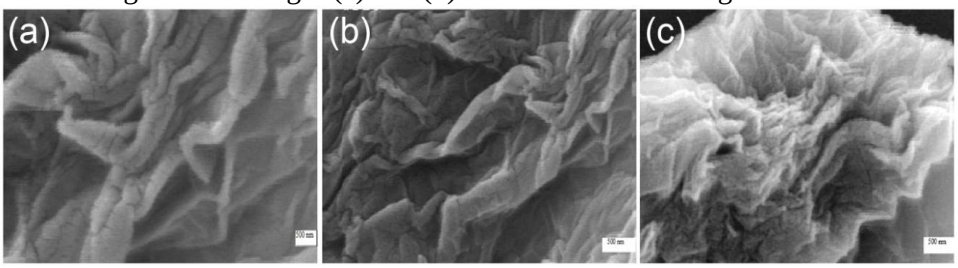

Fig. 9. SEM images (a) GNS1 (b) GNS2 (c) GNS3

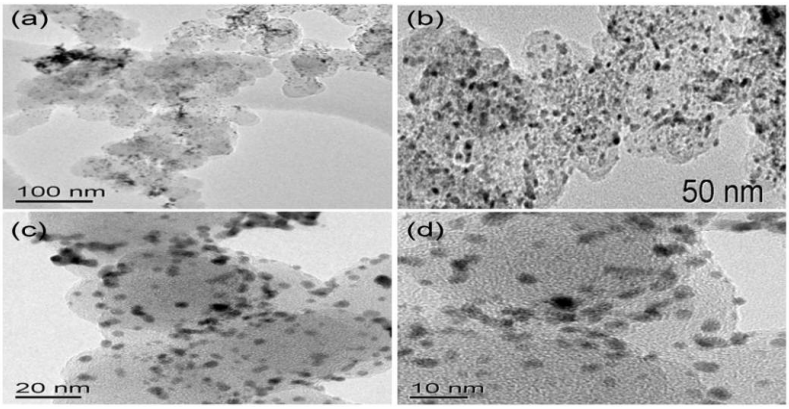

Fig. 10.a, b,c,d TEM images of Pt/GNS3

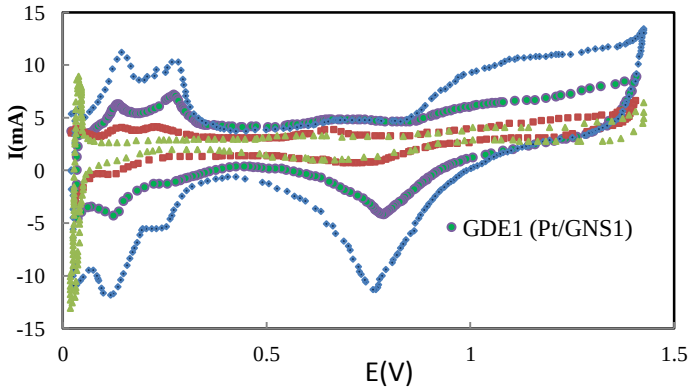

Fig.11.Cyclic voltammetry curves for the GDEs for a scan rate of 50 mV s^{-1} at 25 ºC

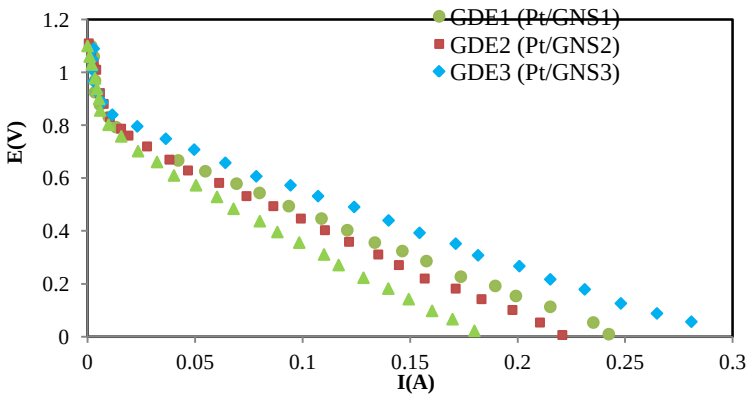

Fig 12IeV curves of the GDEs in the ORR for a scan rate of 1mVs^{-1}at 25 $^{\circ}$C.

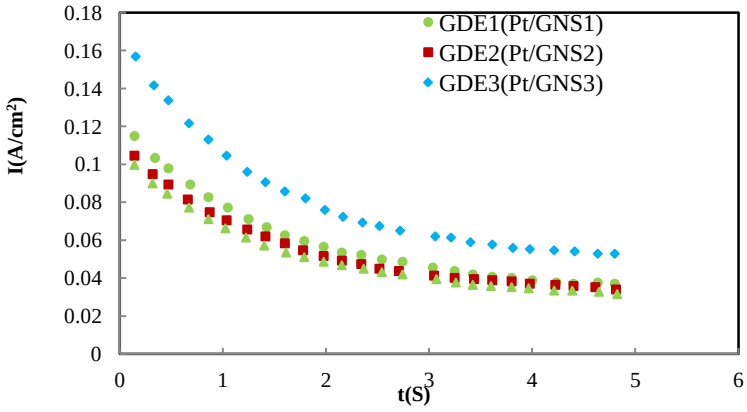

Fig.13.Chronoamperograms of the GDEs in the presenceof O_2, E 0.4 V vs. Ag/AgCl, at 25°C.

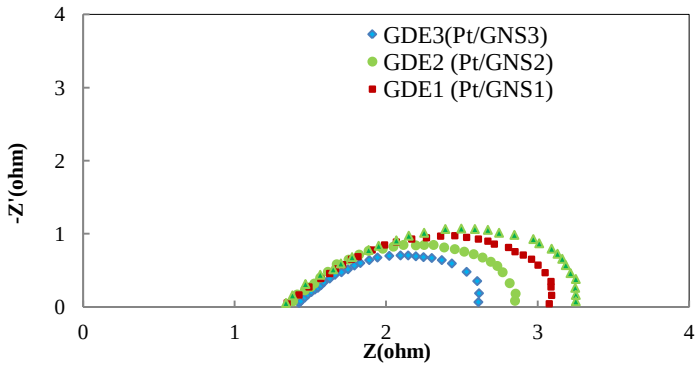

Fig14. Nyquist plots of the impedance responses from 10 kHz to 100 mHz for the GDEs at 400 mV vs. Ag/AgCl, at25°C.

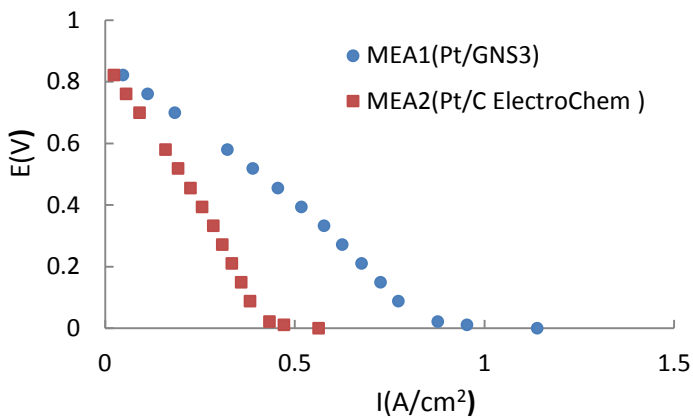

Fig 15. MEA polarization curves relative humidity 100%, with flow rates of 220 $mlmin^{-1}$ hydrogen and 500 $mlmin^{-1}$ oxygen . Humidification temperature 80 °C The cell was kept at 80 °C , and the gas pressure at the back of the electrodes were 1.5 atm. The MEA was placed inPaxi-tech single-cell.

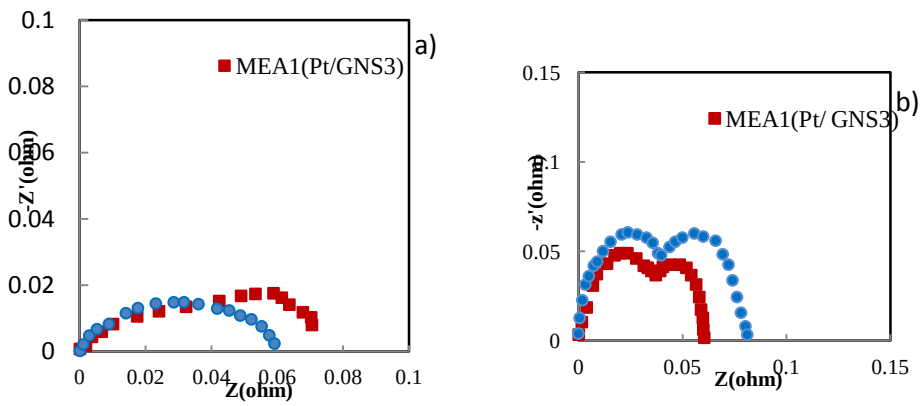

Fig16.Impedance spectra at a) 0.7 V and b) 0.1 V, from 1 mHz to 1000 kHz, 1.5 atm back pressure for the anode and cathode. The relative humidity was 100% for the cathode anode with flow rates of 220 ml/minhydrogen and 500 ml/minoxygen, respectively. The cell was maintained at 80 °C.

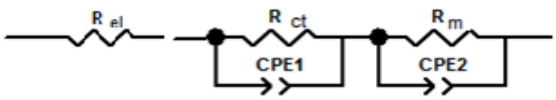

Fig 17.Schematic representation of the equivalent circuit for MEAs with R_{el}: membrane resistance (subtracted from the result), R_{ct}: charge transfer resistance, R_m: mass transfer resistance, and CPE: constant phase element.

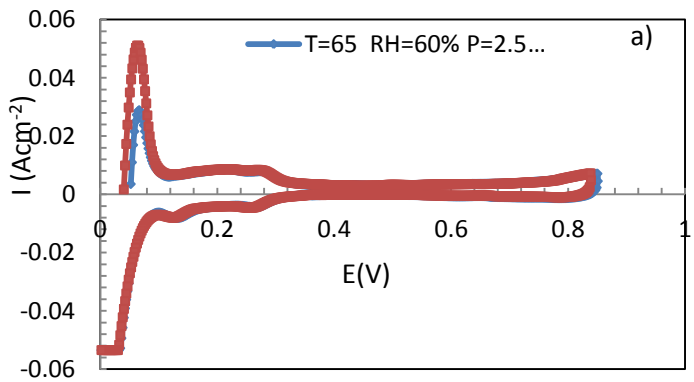

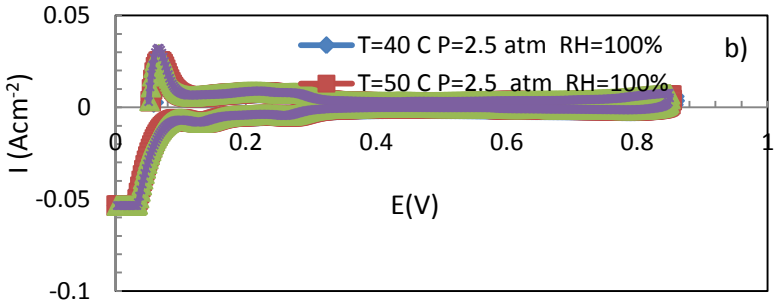

Fig18a,b)cyclicvoltammogram of single cell with MEA1,condition:scan rate=50 mv/s ,cell area:4.25 cm^2,Fuel cell anode/cathode H_2/N_2,anode and cathode absolute back pressure 2.5 atm

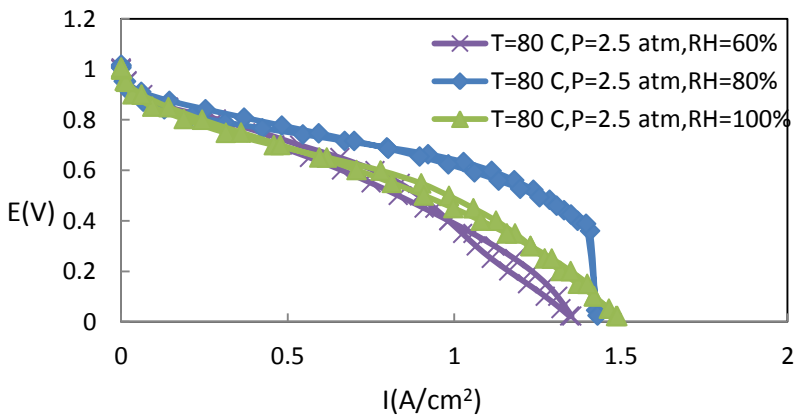

Fig 19 MEA1 polarization curveswith flow rates of 220 $mlmin^{-1}$hydrogen and 500 $mlmin^{-1}$oxygen. In different relative humidites.The cell was kept at 80 °C , and the gas absolute pressure at the back of the electrodes were 2.5 atm.

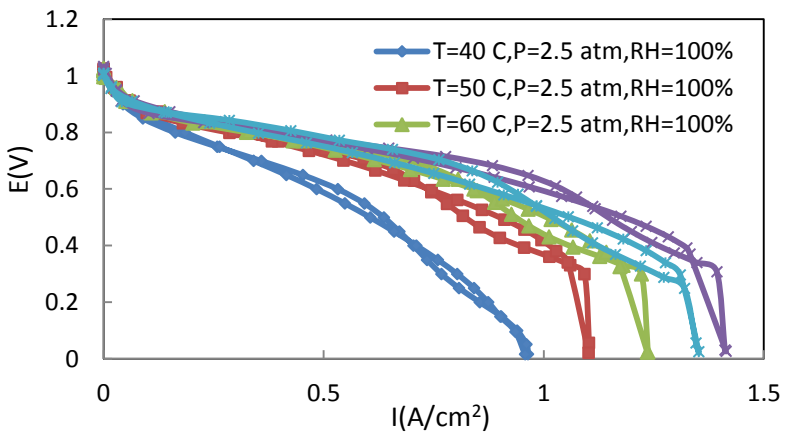

Fig 20 MEA1 polarization curves with flow rates of 220 $mlmin^{-1}$hydrogen and 500 $mlmin^{-1}$oxygen.In different temperatures. The relative humidity as 100%, and the gas absolute pressure at the back of the electrodes were 2.5 atm. The MEA was placed in Paxi-tech single-cell.

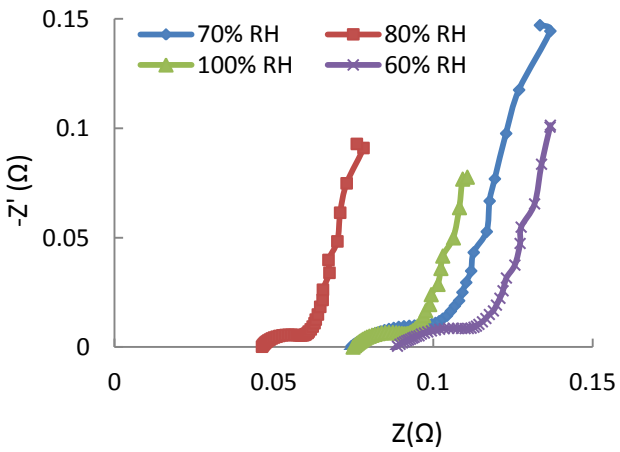

Fig21. Impedance spectra of MEA1 at ocv, from 1 mHz to 1000 kHz,1.5 atm back pressure for the anode and cathode. The relative humidity was 60%, 70%,80%, 100% for the cathode anode with flow rates of 220 ml/minhydrogen and 500 ml/minoxygen, respectively. The cell was maintained at 80 °C.

8th Iranian Fuel Cell Seminar
FEBRUARY 25,26
2015

Study of Process Parameters in Preparing Platinum Nano Electrocatalyst by Cyclic Electrodeposition Method Effect on Glucose Oxidation Reaction in Glucose Alkaline Fuel Cell

Rasol Abdullah Mirzaie[1*], Behnam Moeini[1], Tahereh Gholian Avval[2]
1 Fuel cell Research Laboratory, Dep. Of chemistry, Faculty of science, Shahid Rajaee Teacher Training University, Tehran, Iran.
2 School of Chemistry, College of Science, University of Tehran
** ra.mirzaei@srttu.edu*

Abstract
In this work we analyze the influence of process parameters such as concentration of platinum and number of applied cycles in electrodepositing process on the catalytic activity of nanoplatinum electrocatalyst, fabricated by potentiocyclic electrodeposition to glucose oxidation reaction. Corresponding electrocatalyst were characterized by cyclic voltammetry and the surface texture of electrocatalyst was characterized by scanning electron microscopy, SEM image shows that the platinum elctrocatalyst have a spherical structure in nano scale. Electrodes with high roughness factor are obtained particularly when high platinum ion concentrations (2 mmol L^{-1} Pt, roughness factor 760 cm^2}), and 75 cycles were applied during fabrication. Enhancing the catalytic activity of these electrocatalysts shows that changing the above process parameters reduces the polarization happened in the concentration region.

Keywords: Glucose fuel cell, Platinum, Electrocatalyst, Electrodeposition, Cyclic voltammetry, Glucose oxidation reaction.

1. Introoduction

With an increasing demand of pollution free and cheap energy, investigators are focusing on more easily available, less toxic and safer fuel and this bring the investigator to the very enlightening concept of fuel cell which could run on glucose. Studies on electro-catalytic oxidation of glucose are of high interest to the fuel cell community for various reasons. Glucose is easily available, cheap and non-toxic bio-fuel. No storing problem or explosion hazard is associated like hydrogen in hydrogen-oxygen fuel cell. The studies throughout the last few decades on electro-oxidation of sugars was performed and showed that noble metal catalyst based on platinum and gold in alkaline media improve the rate of electro-oxidation of glucose rather than acidic and neutral [1-7]. In general, glucose-consuming fuel cells can be divided into three main types according to the type of catalyst that is used to enable the electrode reactions: enzymatic, microbial, and abiotic glucose fuel cells enzymatic glucose fuel cells are currently under development [5, 6], the limited stability of enzymes renders their application in a long-term implantable fuel cell power supply difficult. Power-supply systems based on microbial fuel cells are not seriously considered for implantation, due to the infective nature of most known micro-organisms and the associated risks there with an overview about the tentative oxidation pathways and intermediate reaction products of glucose oxidation Theoretically, glucose can be completely oxidized to carbon dioxide and water, releasing 24 electrons per molecule glucose [8]. The corresponding fuel cell reaction and the theoretical Cell voltage U_0 would then be given as: C6H12O6 +6O2→ 6CO2 +18H2O $G_\circ = -2.870\times106$ J mol−1; $U_0 = 1.24$V [17]

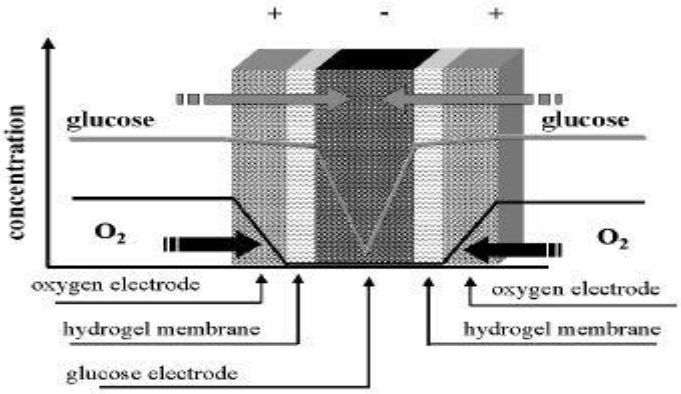

2. Experimental

2.1. Materials

Carbon powder Vulcan XC-72R was used as support and H2PtCl6 and H2SO4 from Merck Company were used as precursor. All aqueous solutions were prepared using ultrapure water during experiments.2-Propanol (>99% purity) (Quailed Fine Chemicals) was used as solvent for preparing Vulcan paste and carbon paper (Toray 90 T) was used as working electrode's-glucose(>99% pure) and KOH (>85% assay, flakes purified) (Merck) were used as fuel and electrolyte, respectively.

2.2. Electrode fabrication

Substrate is fabricated by deposition of 3mg/cm^2 carbon Vulcan paste on carbon paper sheet with 1cm^2 geometric area then it dried by heating in 200 ^{0}C$^{\cdot}$ for 45 minutes.

As-prepared substrate expose to precursor solution included of H_2SO_4 (0.5 M) and H_2PtCl_6 (2mM) (Merck, Germany) then 5, 50, 75,100 and150 CV scans (100 mV.s^{-1}, 1.20 to − 0.60 V vs. Ag/AgCl sat KCl) were performed under N_2 atmosphere to study of cyclic number effect to the catalytic activity of GOR.to study of platinum concentration effect in precursor solution to the catalytic activity of GOR, B1-B7 electrodes were prepared in 0.1,0.2,0.3,0.4,0.5,0.6,0.7,0.8 mM platinum solution in 0.5 M sulphuric acid.

2.3. Electrochemical characterization

Electrochemical experiments were performed in a separator free three-electrode cell. Ag/AgCl saturated with KCl electrode was used as reference electrode and for counter electrode platinum sheet electrode was used. In all experiment glucose and potassium hydroxide concentration was fixed in 0.3 and 0.5 M, respectively.

2.4. Physiochemical characterization

The surface morphology of the deposited platinum nano particles (PNPs) on the modified carbon paper substrate electrode was obtained using a field-emission SEM (KYKY-EM3200

2.5. Determining of Roughness Factor

in this work the charge measurement from stripping of the adsorbed hydrogen upd-H monolayer on the Pt-electrode (QH) was used to evaluate the ECSA for all Pt electrodes [13,14] and expressed as roughness factor (RF) according to RF=QH/Qo.A.Where QH is the measured

charge of the hydrogen desorption, Q0 is the charge of a hydrogen monolayer adsorbed on polycrystalline platinum (210 μC cm-2) and A is the geometric area of the electrode [15].

3. Result and discussion

3.1. Cyclic voltammogram of glucose oxidation in alkaline solution

Figure 2 shows a typical voltammogram of glucose electro oxidation in this work. The cyclic voltammogram from -0.9 to 0.85 V with Ag|AgCl (sat.KCl) reference electrode at 20mVs−1 scan rate and 25 ◦C on Pt electrocatalyst in KOH 0.5 M electrolyte and with 0.3 mol L−3 glucose solution is shown in Fig. 1. Three oxidation peaks (C1, C2, and C3) at −0.75, −0.3 and 0.37V versus Ag|AgCl (sat. KCl), respectively can be seen for glucose oxidation in positive direction scan. The result is in full agreement with glucose electro-oxidation given in the literature [9, 10, 11]. Peaks C1 and C2 appeared due to chemisorption's and dehydrogenation of glucose in the hydrogen wave region of CV. The current density of peak C2 is much lower compared to peak C1 and the peak potential is also slightly higher. The peak C2 appeared at the potential region where the electrode surface is partially covered by adsorbed-OH [9, 10]. In this region, namely double layer region [12, 11], adsorbed-OH catalyst surface can oxidize glucose also [9, 11].

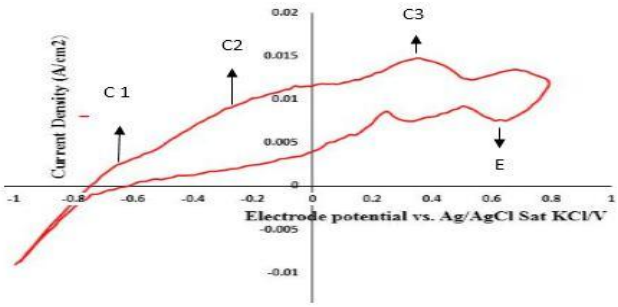

Figure 1, Cyclic voltammogram of Pt electrode at scan rate of 20 mV/s in the presence of 300mM glucose (measurement were performed in 0.5M KOH solution under a nitrogen atmosphere at 25 c).

2, Peak C3 is observed at higher potential on already oxidized platinum surface. Peak E is appeared due to reduction of adsorbed-OH from the catalyst surface [9,11]. Gluconic acid, which was observed by in situ FTIR [13] and HPLC study [9] as main product of glucose electro-oxidation, may be formed due to oxidation of adsorbed dehydrated intermediate directly or from hydrolysis of glucono-γ-lactone, which can be formed from oxidation of adsorbed dehydrogenated intermediate [9,13].

3.2. Dependence of catalytic activity of nanoplatinum electrocatalyst to the number of applied cycles in the platinum electrodeposition process.

Figure 2, shows A1-A5 electrocatalyst's voltammograms which prepared by 5, 50, 75,100,150 cycles respectively. Current density were increased by increasing the number of cycles in preparation of A1-A3 electrocatalysts. But current density in A4 and A5 is decrease.comparison of catalytic activity carry out on the potential of -0.3 V. Correspond to table 1, anodic current density increases with increasing the number of cycles. The Changes which is observed in the anodic current in the range of -0.65 to -0.3 V shows that changing the number of cycles applied

in electrochemical deposition of platinum could achieve a high performance electrocatalyst. Data in table 1 shows that by increasing the number of applied cycles, roughness factors are increased and in A3 is maximized and after that RF are decreased.

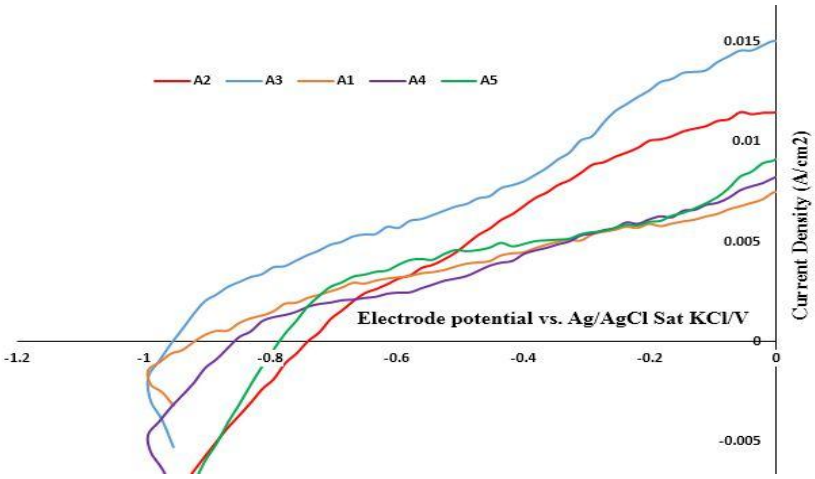

Figure 2, Cyclic voltammogram of A1-A5 electrocatalysts at scan rate of 20 mV/s in the presence of 300mM glucose (measurement were performed in 0.5M KOH solution under a nitrogen atmosphere at 25 c)

Table 1, Open circuit potential & current density data of B1-B7 electrocatalyst

electrocatalyst	A5	A4	A3	A2	A1
Open circuit potential(V)	-0.801	-0.845	-0.985	-0.761	-0.781
Current density(mA/cm^2) at -0.3 V	5.05	4.56	11	8.48	3.92
Roughness Factor(cm^2)	400	450	695	485	328

Comparison of current density in kinetic region shows that by increasing the applied cycles, kinetic over voltage decrease and thus this leads to enhance the GOR rate. These changes can be caused by varing the shape, size and distribution of the platinum particles.

3.3. Dependence of catalytic activity of nanoplatinum electrocatalyst to the concentration of platinum solution in electrodeposition process.

In platinum concentration lower than 0.4mM open circuit potential have very tolerance but after that open circuit potential is fixed to approximately -0.7 V.current density-voltage curves in Figure 3 shows a high open circuit potential in B1 electrocatalyst that illustrates platinum electrodepositing solution with 0.2 mM concentration don’t produce responsible electrocatalyst to GOR. Anodic peaks in B4, B6, B7 shows the polarization in concentration region but with increasing the platinum concentration this polarization is decreased. Data in table 1 shows that by addition of platinum concentration roughness factor of these electrocatalysts increased and in B7 is maximized.

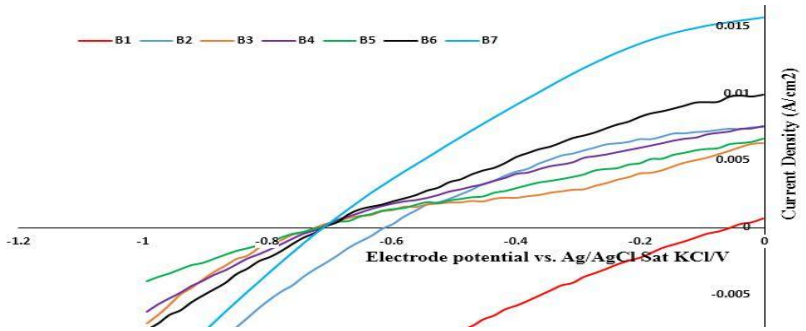

Figure 3, Cyclic voltammogram of B1-B7 prepared in (0.25,0.5,0.75,1,1.25,1.5,1.75 and 2 mM precursor concentration) electrocatalysts at scan rate of 20 mV/s in the presence of 300mM glucose (measurement were performed in 0.5M KOH solution under a nitrogen atmosphere at 25^0c

Table 2, Open circuit potential & current density data of A1-A6 electrocatalyst

electrocatalyst	**B7**	**B6**	**B5**	**B4**	**B3**	**B2**	**B1**
Open circuit potential(V)	-0.705	-0.705	-0.705	-0.705	-0.723	-0.597	-0.039
Current density(mA/cm^2) at -0.3 V	11.44	6.68	3.77	4.84	2.83	5.51	4.01
Roughness Factor(cm2)	760	680	600	550	420	271	250

3.4. SEM characterization

Figure 4, The SEM images taken at 40 KX magnifications indicate the uniformity in size and shape of catalysts. These images show that preparation of electrocatalysts by potentiocyclic electrodeposition method can be produce a large amount of platinum nano particle in electrocatalyst.

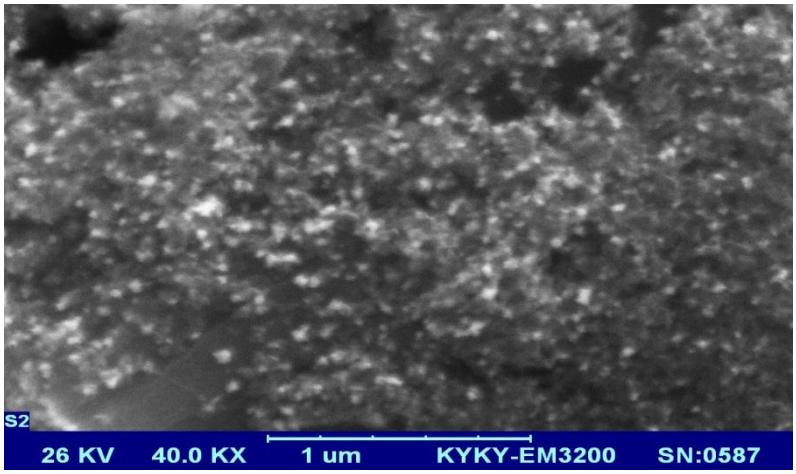

Figure 4, SEM micrographs of platinum electrocatalyst

4. Conclusion

In conclusion, we demonstrated that cyclic electrodeposition of Pt is a versatile method for the fabrication of platinum electrocatalyst with high catalytic activity and high specific surface area & RF. This deposition leads to nanosphere platinum particles in the surface textures of

electrocatalyst. In principle, electrocatalyst with optimized concentration and number of cycles possess higher accessibility to glucose molecules and it has higher mass transport rates in comparison to others. Roughness factors illustrate that changing of precursor solution concentration have more important role in achieving higher RF than the number of applied cycles which leads to enhance the performance of electrocatalysts to GOR.

5. Reference

[1] -S. Roundy, A 2D electret-based resonant micro energy harvester J. Intell. Mater. Syst. Struct. 16 (2005) pp. 809–823.
[2] P.Woias, Proceedings of the Mikrosystemtechnik-Kongress, Freiburg, Germany,
(2005), pp. 405–410.
[3]- G. Gorge, M. Kirstein, R. Erbel, Herz Recent Development of Miniatured Enzymatic Biofuel Cells 26 (2001) pp 64–68.
[4] -C. Watkins, B. Shen, R. Venkatasubramanian, Proceedings of the 24th International Conference on Thermoelectronics (ICT 2005), Clemson, USA, (2005), pp. 265–267.
[5] -F. Davis, S.P.J. Higson, Biofuel cells--recent advances and applications. Biosens. Bioelectron. 22 (2007) 1224–1235.
[6] -A. Heller, Nonenzymatic glucose sensing at rutheniumdioxide–poly(vinyl chloride)–Nafion compositeelectrode Anal. Bioanal. Chem. 385 (2006) 469–473.
[7] -J.R. Rao, G.J. Richter, F. von Sturm, E. Weidlich, BIOFUEL CELLS AS MICRO POWER GENERATORS FOR IMPLANTABLE DEVICES Bioelectrochem. Bioenerg. 3
(1976) 139–150.
[8] -J.R. Rao, in: G. Milazzo, M. Blank (Eds.), Bioelectrochemistry. I. Biological Redox Reactions, Plenum Press, New York, (1983), pp. 283–335.
[9] -L.H.E. Yei, B. Beden, C. Lamy, Nonenzymatic Glucose Sensor Based on Pt-Au-SWCNTs Nanocomposites J. Electroanal. Chem. 246 (1988) pp:349.
[10] - B. Beden, F. Largeaud, K.B. Kokoh, C. Enhancement in Selectivity of Nonenzymatic Glucose Sensors Based on Mesoporous Platinum by A.C. Impedance Lamy, Electrochim. Acta 41 (1996)pp: 701.
[11] -L.H. Li, W.D. Zhang,A Nonenzymatic Amperometric Glucose Sensor Based on a RuO2/Graphene Sheet Composite Electrode J.S. Ye, Electroanalysis 20 (2008)pp: 2212.
[12] -C.P. Wilde, M. Zhang, Oxidation of glucose at electrodeposited platinum J. Chem. Soc., Faraday Trans. 89 (1993) 385.
[13] -B. Beden, F. Largeaud, K.B. Kokoh, C. Lamy, Electrochemical non-enzymatic glucose sensors, Electrochim. Acta 41 (1996) 701.
[14]-W. Vielstich, in Handbook of Fuel Cells, vol. 2, chap 21 andreferences cited therein, ed. by W. Vielstich, A. Lamm, H.A.Gasteiger (Wiley, Chichester, 2003)
[15]-Q.S. Chen, J. Solla-Gullon, S.G. Sun, J.M. Feliu, The potential ofzero total charge of Pt nanoparticles and polycrystalline electrodes with different surface structure. The role of anion adsorption in fundamental electrocatalysis. Electrochim. Acta 55, 7982 (2010)
[16]-B.E. Conway, Electrochemical oxide film formation at noble-metals as a surface-chemical process. Prog. Surf. Sci. 49, 331 (1995)
[17]- J.R. Rao, in: G. Milazzo, M. Blank (Eds.), Bioelectrochemistry. I. Biological Red Reactions, Plenum Press, New York, 1983, pp. 283–335.

8th Iranian Fuel Cell Seminar
FEBRUARY 25,26
2015

Nanosilver/TiO_2 Composite as Photoanode of Water Splitting System under Visible Light Illumination

Maryam Azimzadehirani, Hussein Gharibi*
Department of Chemistry, Tarbiat Modares University, Tehran, 14115-175, Iran.
m.azimzadehirani@modares.ac.ir

Abstract

A thin silver layer deposited on a conducting support of TiO_2, photocatalyzes the oxidation and reduction of water to O_2 and H_2. The light sensitivity in the visible part of the spectrum is due to self-sensitization caused by reduced silver species. To test its water splitting capability, Silver coated-TiO_2 photoanode was employed in the anodic part of a setup for photoelectrochemical water splitting system consisting of platinum plate for cathode and Ag/AgCl as a reference electrode. Illumination of the photoanode led to photoelectrochemical water splitting to O_2 and H_2. Silver coated- TiO_2 photoanode showed more enhanced and increased photocurrent density than the pure TiO_2.

Keywords: Photoelectrochemical water splitting, TiO_2 photoanodes, Silver coating, H_2 production

Introduction

With increased consumption of energy and growing environmental contamination, the development of clean and sustainable energy utilization and environmentally friendly technologies has become a research focus for world-wide scientific researchers. Solar energy from sunlight is widely believed to be the key to solving the future problems of the environment and energy resource because of its clean, sustainable, abundant and economical characteristics. To efficient harvest of solar energy, various kinds of photocatalysts have been explored for applications in splitting water into hydrogen. TiO_2 photocatlysts have been used widely in this field.[١]

However, most of these kind of the photocatalysts were used only under irradiation by ultraviolet (UV) light. Consequently, only 3–5% of the solar energy reaching the earth can be utilized. So the development of an efficient system for visible light energy conversion into chemical energy is one of the urgent subjects for research because sunlight is mostly composed of visible light.[2]

Silver composites with Titanium Dioxide, which exhibit high absorption in the visible region due to the surface plasmon resonance (SPR) of silver nanoparticles, represent a class of highly efficient visible-light-driven photocatalyst .[3]

In this report, a TiO_2 photocatalyst functionalized with silver composites was successfully fabricated and used as an efficient visible-light responsive photoanode for the water splitting system, and the electrochemical test of photocurrent density has been carried out.

Experiment

Titanium P25 (TiO_2; ca. 80% anatase, 20% rutile; BET area, ca. 50 m^2 g^{-1}) was purchased from the Degussa. Silver Nitrate and Ammonium 25% solution and cationic surfactants were provided by Merck. All other chemicals were of analytical grade. Deionized and doubly distilled water was used throughout this study. For anode electrodes we need, FTO glass (1 x 1 cm, 2 slides for 1 cell), Ethanol.

Preparation of the Photoanode

For preparation of Silver composites/ TiO_2 precipitation-deposition method was used.
Photoanodes were synthesized with Dr.Blade method. Thin films of as prepared composites were deposited on the surface of FTO glasses. Figure 1, shows the as synthesized photoandoes.

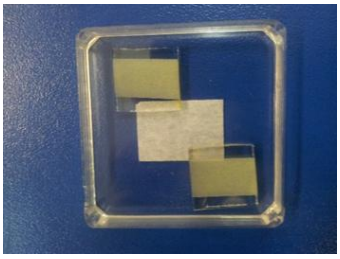

Fig.1. Synthesized Photoanodes on FTO glass

Photoelectrochemical measurement

Photocurrent densities were measured using 300 W Xe was used as a visible light source. Photocurrent densities were measured using an electrochemical interface analysis instrument operated in a standard three-electrode configuration with the as prepared photoanode, (an effective area of 2*2 cm), a Pt foil as the counter electrode, and a saturated Ag/AgCl as the reference electrode. KOH as the electrolyte.

Results and Discussion

XRD measurements has been done for confirmation of presence of Silver particles on the surface of TiO_2 composite. (Fig. 2)(A and R relate to Anatase and Rutile phase of TiO_2). As it has been mentioned before, the role of silver particles for enhancement of photocatlytic effect of TiO_2 is deniable. In a process known as self-sensitization, the photo-activity of Silver compound extends from the UV into the visible light region, which is due to the formation of silver species during the photoreaction. Upon repeated absorption of photons, a cluster of silver atoms can be ultimately formed. [4]

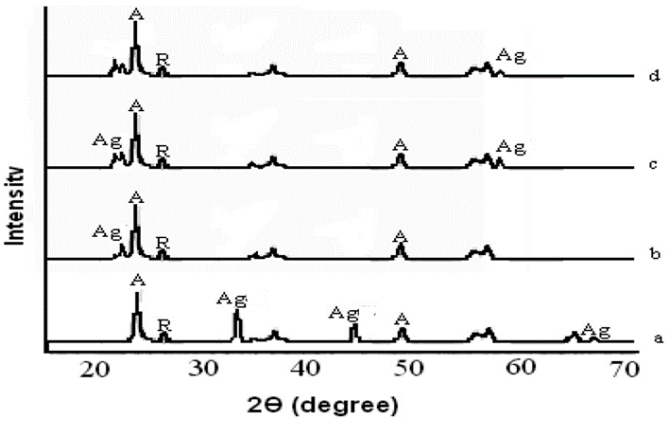

Fig.2 The XRD pattern of synthesized photoanode

The scanning electron microscopy (SEM) images of the composite illustrate the presence of particles with varying size and some pockets of agglomeration (Fig. 3). The SEM patterns also indicate the average sizes of composites are about 70–100 nm.

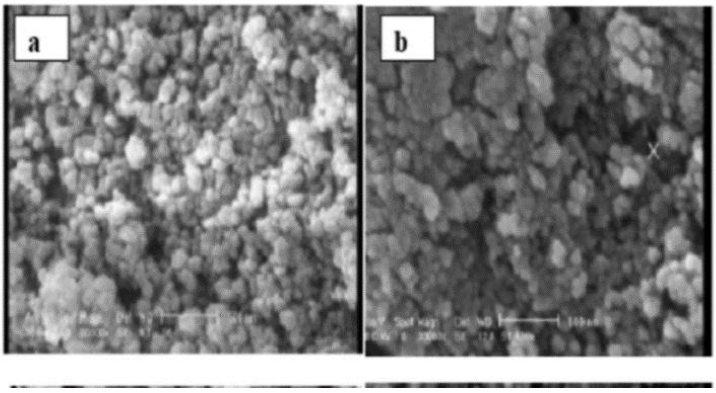

Fig.3 SEM images a) TiO_2 nanopaticles b) Nanosilver/TiO_2 composites

The measurements of Photocurrent versus Time of the compounds are shown in (Fig.٤). This picture shows the increase of current density under illumination by >420 nm for Silver/TiO_2 compounds. Due to this figure, it is clear that the photocurrent of the silver compounds/TiO_2 is more enhanced than the pure TiO_2 under the visible light illuminations.

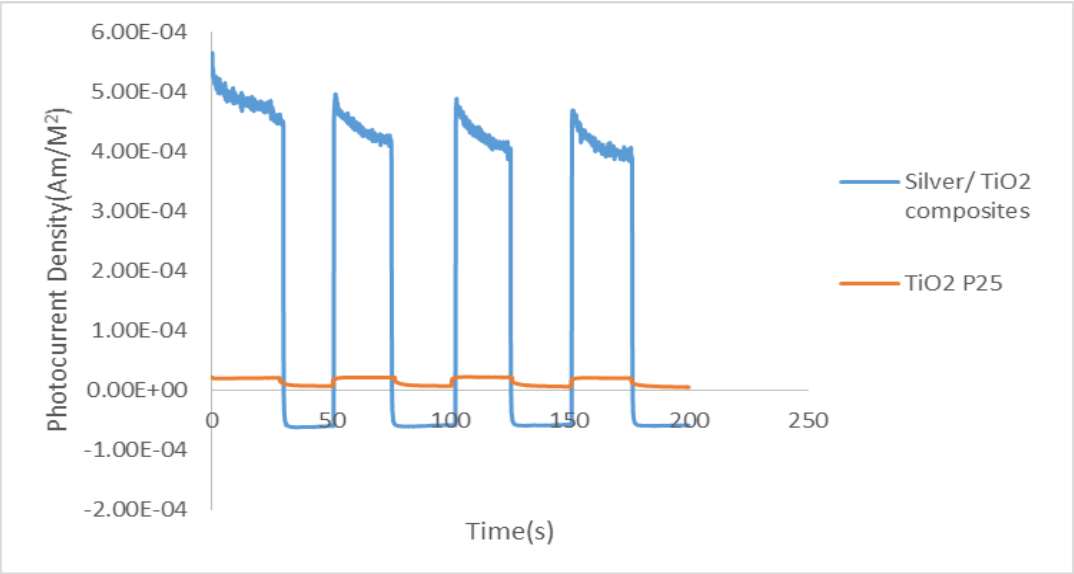

Fig. 4 Photocurrent versus Time of the various compounds

Conclusion

In summary, a Silver/TiO_2 hybrid composite with high visible light photocatalytic activity was successfully prepared by a photoassisted deposition−precipitation. The composite exhibits improved photoelectrochemical performance in the photocurrent density test. This result is due to the metal silver particles that have been produced by visible light on the surface of silver/TiO_2 composite.

Acknowledgment

The support of Tarbiat Modares University is aknowledged.

References

[1] (a) U. Banin, Y. Ben-Shahar and K. Vinokurov, Chem. Mater., 2014, 26, 97–110; (b) C. Chen, W. Ma and J. Zhao, Chem. Soc. Rev., 2010, 39, 4206–4219

[2] X. Lang, X. Chen and J. Zhao, Chem. Soc. Rev., 2014, 43, 473–486;

[3] Yuan, X., Sun, J. C., Wang, H., Li, H., “Accelerated conditioning for a proton exchange membrane fuel cell”, J Power Sources (2012). 205, 340-4.

[4] N. Kakuta, N. Goto, H. Ohkita and T. Mizushima J. Phys. Chem. B, 1999, 103, 5917.

8th Iranian Fuel Cell Seminar
FEBRUARY 25,26
2015

Study of Increasing Reaction Layer Surface Area Effect on Performance of Gas Diffusion Electrode Prepared by Electrocatalyst Electrodeposition Method for Oxygen Reduction Reaction

Rasol Abdullah Mirzaie[*1], Mohammad safi Rahmanifar[2], Narges mohammadkhani[1]
1. Fuel cell Research Laboratory, Dep. Of chemistry, Faculty of science, Shahid Rajaee Teacher Training University, Tehran, Iran
2. Faculty of Basic Science, Shahed University, Tehran, IRAN
** ra.mirzaei@srttu.edu*

Abstract
A simple method for preparing electrodes for proton exchange membrane fuel cell (PEMFC) is proposed, based on the electrodeposition of Platinum on Vulcan XC-72R substare from H_2SO_4 and Na_2SO_4 solution with small amount of H_2PtCl_6. The electrocatalyst support layer was fabricated by applying Vulcan and polytetrafluoroethylene paste (70:30) on carbon paper. charcoal active was added to Vulcan and four electrodes were fabricated with different portion of vulcan/charcoal active to study its result on oxygen reduction reaction. The electrocatalytic activitiy for oxygen reduction reaction (ORR) were determined for the electrode which had no charcoal active and compared with the electrodes with charcoal active addition to the reaction layer. The electrode with no charcoal active addition to reaction layer showed the highest performance among the fabricated electrodes.

Keywords: Electrodeposition, Proton exchange membrane fuel cell, Charcoal active, Platinum electrocatalyst

Introduction

A PEMFC is a device that converts the chemical energy of a fuel directly into electrical energy by electrochemical reactions. When hydrogen is used as the source of the fuel, the byproduct is essentially the pure water. PEMFC has attracted plenty of interest for various applications such as power sources for stationary power generation, transportation, and portable electronic applications. The proton exchange, or polymer electrolyte, membrane fuel cell (PEMFC) combines a series of interesting features such as high energy density, low temperature operation, long stack life and fast startup, which make them suitable for stationary and portable applications. Nevertheless, some economical and technical challenges must be overcome before getting their wide massive commercialization. Among them, the electrodes fabrication constitutes an important factor in the total PEMFC cost. Metal electrodeposition is able to become a simple and cheap method to obtain electrodes with low Pt loadings, having many degrees of freedom originated in the numerous variables that can be manipulated (as electrolytic solution and substrate composition, temperature, type of electrical signal, time of application, etc.) [1-3].

Experimental

Support layer fabrication

A mixture of Vulcan and polytetrafluoroethylene paste (70:30) was prepared. It was put in oven to become a paste and then the paste was applied on carbon paper. It was put in oven for 2 hours in 80 ^{0}C to dry the support layer. Four mixture of Vulcan, charcoal active and polytetrafluoroethylene with different portion of Vulcan/charcoal active were prepared, after putting in oven to become a paste, the pastes were applied on carbon papers, and the support layers dried in oven for 2 hours in 80 ^{0}C

Platinum electrodeposition

A three-electrodes electrochemical cell was used in order to carry out both, the preparation and the subsequent evaluation of the obtained electrodes. It was consisted of Ag/Agcl sat KCl electrode as refrence electrode, platinum electrode as counterelectrode. The as-prepared support layers were put on the top of a holder and it was used as the working electrode. The Pt electrodeposition process was carried out in the following solution: H_2SO_4 (0.03 M), Na_2SO_4 (0.27 mM) and H_2PtC_6 (2 mM). The electrodeposition process was carried out through the application of cyclic voltammetry, where the scan rate was 50 mV/s the potential range was 1.20 to − 0.60 V vs Ag/AgCl sat KCl, and cycles number was 30 [1,4]. The fabricated electrode with no charcoal active in reaction layer named A-30. The fabricated electrodes with 90%vulcan-10% charcola active in support layer named A-30-90%V-10%CA, The fabricated electrodes with 80%vulcan-20% charcoal active in support layer named A-30-80%V-20%CA, The fabricated electrodes with 70%vulcan-30% charcoal active in support layer named A-30-70%V-30%CA and the fabricated electrodes with 60%vulcan-40% charcoal active in support layer named A-30-60%V-40%CA. The electrodes obtained by cyclic voltammetry were characterized electrochemically by linear sweap voltammetry (LSV) and Electrochemical impedance spectroscopy (EIS).

Result and discussion

$i_{0\ LCD}$ and $i_{0\ HCD}$ values of the fabricated electrodes calculated from LSV is shown in table 1

Table 1 - $i_{0\ LCD}$ and $i_{0\ HCD}$ values of the fabricated electrodes calculated from LSV

Electrode	$i_{0\ LCD}$	$i_{0\ HCD}$
A-30-100%V	3.81	17.72
A-30-90%V-10%CA	0.29	0.69
A-30-80%V-20%CA	0.22	0.58
A-30-70%V-30%CA	0.18	0.47
A-30-60%V-40%CA	0.16	0.39

Figure 1 presents impedance spectra of the five fabricated electrodes.

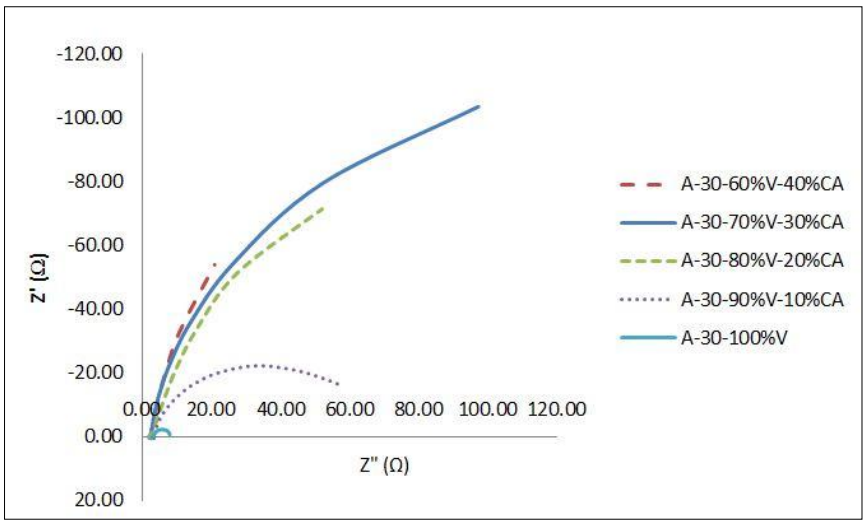

Figure 1 - presents Impedance spectra of the five fabricated electrodes at 0.5 v vs Ag/Agcl sat KCl refrence electrode, at 300 K

R_P, R_{Ct} and $i_{0\ LCD}$ values of the fabricated electrodes calculated from EIS is shown in table 2.

Table 2 – R_P, R_{Ct} and $i_{0\ LCD}$ values of the fabricated electrodes calculated from EIS

electrode	RS	RP	RCt	i0LCD
A-30-100%V	2.61	1.87	5.7	4.3
A-30-90%V-10%CA	2.09	0.22	58	0.44
A-30-80%V-20%CA	2.17	0.26	210	0.12
A-30-70%V-30%CA	1.9	1.27	274	0.11
A-30-60%V-40%CA	2.3	1.1	287.2	0.09

As it was shown above A-30-100%V has the biggest amount of $i_{0\ LCD}$ and $i_{0\ HCD}$ and the lowest amount of R_{Ct}. Therefore addition of charcoal active to support Layer doesn't have positive result on oxygen reduction reaction.

Conclusion

A simple method was developed to produce cheap PEMFC cathode electrodes, consisting in the cyclic voltammetry electrodeposition from Pt diluted precursor solution on Vulcan XC-72R as catalyst support. Charcoal active was added to vulcan and four electrodes were fabricated with different portion of Vulcan/charcoal active to study it's result on oxygen reduction reaction. The electrocatalytic activitiy for Oxygen reduction reaction (ORR) were determined for the electrode which had no charcoal active and compared with the electrodes with charcoal active addition to the reaction layer. The comparison revealed that the electrode with no charcoal active addition to reaction layer had the highest performance among the fabricated electrodes. The highest amount of $i_{o\ LCD}$ and $i_{o\ HCD}$ from linear sweap voltammetry and The highest amount of $i_{o\ LCD}$ and the lowest amount of R_{ct} from Electrochemical impedance spectroscopy belonged to electrode with no charcoal active in it's reaction layer. However, increasing the reaction layer surface area by adding charcoal active has no effect on performance of prepared electrode by electro catalyst electro deposition method.

Refrences

[1] Campagnolo, M.C., C.A. Marozzi, A.C. Chialvo and Gennero de Chialvo. “Preparation and evaluation of the electrocatalyst activity of PEMFC electrodes with highly efficient Pt utilization and without ionomer addition”, Journal of power sources, (2013) . 239:207-216

[2] Baosheng Li and Siew Hwa chan. “PtFeNi tri-metalic alloy nanoparticles as electrocatalyst for oxygen reduction reaaction inprotoncrxchang membrane fuel cells with ultra-low Hydrogen Pt loading”, International journal of Energy, (2013). 38:3338-3348

[3] Zhao, Wenwen, Yong Yang, and Hua zhang. “Electrochemical preparation of highly dispersed Pt/H_xWO_3 composite catalyst for PEMFCs”, Electrochemica Acta, (2013). 99:273-277

[4] Kloke, Arne, Christian kohler, Ramona Gerwig, Roland Zengerle, and Sven Kerzenmacher.. Cyclic electrodeposition of PtCu alloy: Facile fabrication of highly porous platinum electrodes. Germany: Wiley-VCH Verlag GmbH & Co, (2012)

8th Iranian Fuel Cell Seminar
FEBRUARY 25,26
2015

بررسی تاثیر فلز منگنز بر اندرکنش اتانول/الکترود در پیل‌های سوختی غشا پلیمری

محسن رضایتمند*، احسان صائب نوری
دانشکده مهندسی مواد، دانشگاه آزاد اسلامی، واحد نجف آباد، اصفهان، ایران
** Mohsen_Rezayatmand@yahoo.com*

چکیده

امروزه بحران‌های انرژی و آلودگی محیط زیست تبدیل به معضل بزرگی برای بشر شده است. جهت رفع این مشکلات، تلاش‌های گسترده‌ای برای جایگزینی سوخت‌های فسیلی با سایر منابع انرژی پاک نظیر پیل‌های سوختی صورت گرفته است. در یک پیل سوختی، انرژی شیمیایی مربوط به واکنش الکتروشیمیایی یک سوخت با اکسیدکننده مستقیما تبدیل به آب، الکتریسیته و حرارت می‌گردد. در این تحقیق ابتدا به معرفی کلی ساختار و انواع پیل‌های سوختی، پرداخته شده و سپس بررسی اثر الکتروکاتالیستی منگنز بر اندرکنش الکترود/ اتانول برای پیل‌های غشاء پلیمری مورد بحث قرار گرفته است. فلز منگنز به روش لایه نشانی الکترود بر روی زیر لایه نیکل پوشش داده شده است. سطح پوشش توسط میکروسکوپ الکترونی روبشی مورد بررسی قرار گرفته است. جهت تعیین ترکیب شیمیایی سطح پوشش از طیف سنج پراش پرتو ایکس استفاده شده است. برای بررسی واکنش‌های الکتروشیمیایی از روش سیکلیک ولتیمتری استفاده شده است. نتایج حاصل نشان می‌دهد فلز منگنز به بهبود عملکرد پیل سوختی کمک کرده است.

واژه‌های کلیدی: پیل سوختی غشائ پلیمری، منگنز، لایه نشانی الکتریکی، خواص الکتروکاتالیستی، اتانول

مقدمه

ضرورت جایگزین مناسب، ارزان قیمت و تمیز برای سوخت‌های فسیلی آشکار است. از جمله انرژی‌های مطرح، انرژی الکتریکی تولید شده به وسیله پیل سوختی است. سابقه تولید پیل‌های سوختی به سال ۱۸۸۹ بر می‌گردد که اولین پیل توسط لودیک مند[۱] و چارلز لنجر[۲] ساخته شد[۱]. در یک پیل سوختی، انرژی شیمیایی مربوط به واکنش الکتروشیمیایی یک سوخت با اکسیدکننده مستقیما تبدیل به آب، الکتریسیته و حرارت می‌گردد. گاز هیدروژن، متانول، اتانول از جمله سوخت‌های متعارف بکار رفته در پیل‌های سوختی می‌باشند.

پیل سوختی یک سل الکتروشیمیایی است که در آن انرژی شیمیایی سوخت و اکسیدکننده، مستقیما به انرژی الکتریکی

[1] Ludwig Mond
[2] Charles Langer

تبدیل می‌شود. ساختار کلی یک پیل سوختی از یک لایه الکترولیت که در دو طرف آن الکترودهای آند و کاتد متخلخل قرار گرفته، تشکیل شده است. در یک پیل سوختی، سوخت به صورت پیوسته در سمت آند (الکترود منفی) و اکسیدکننده در سمت کاتد (الکترود مثبت) تغذیه می‌شود. در پیل سوختی، سوخت و اکسید کننده گازی بر روی آند و کاتد متخلخل در مجاورت الکترولیت با انجام واکنش اکسید اسیون و احیاء انرژی تولید می‌کنند. در پیل‌های سوختی، معمولا هیدروژن گازی به عنوان سوخت و اکسیژن با هوا به عنوان اکسیدکننده مصرف می‌شوند. در این صورت تنها محصول واکنش پیل سوختی، بخار آب خواهد بود[2].

پیل‌های سوختی از نقطه نظرهای مختلف نظیر نوع سوخت و اکسیدکننده مصرفی، نحوه تبدیل سوخت (مبدل داخلی یا خارجی)، نوع الکترولیت، دمای عملکرد و ... دسته‌بندی می‌شوند. که دسته‌بندی آن‌ها بر حسب نوع الکترولیت به شرح ذیل است[۲].

- پیل سوختی قلیایی (AFC)
- پیل سوختی اسید فسفریک (PAFC)
- پیل سوختی کربنات مذاب (MCFC)
- پیل سوختی اکسید جامد (SOFC)
- **پیل سوختی غشاء پلیمری (PEMFC)**

در بین پیل‌های سوختی، پیل سوختی پلیمری (PEM) به دلیل دانسیته توان بالا، دمای کارکرد پایین و زمان کوتاه راه‌اندازی، مناسب‌ترین گزینه از انواع پیل سوختی می‌باشند. در شکل شماره ۱ اجزاء اولیه یک پیل سوختی نوع (PEM) نشان داده شده است [3].

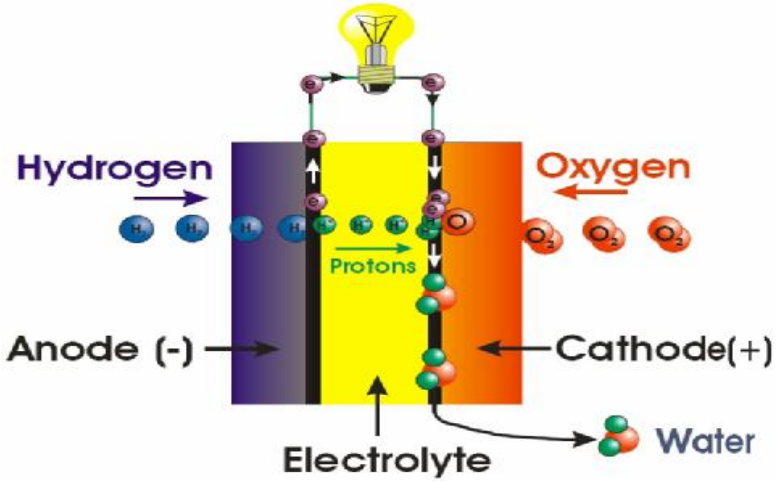

شکل ۱ : شمای ساده‌ای از یک پیل سوختی نوع PEM [2]

در پیل سوختی غشاء پلیمری سوخت مورد استفاده هیدروژن می‌باشد. ملکول هیدروژن در آند به یون‌های پروتون و الکترون یونیزه شده و الکترون‌های آن‌ها جدا می‌شود. یون‌های هیدروژن که شامل بار مثبت هستند (پروتون) به یک سطح غشاء خلل‌دار نفوذ می‌کنند و به سمت کاتد می‌روند. الکترون‌های جدا شده نمی‌توانند از این غشاء عبور کنند بلکه از یک

مدار خارجی عبور کرده و موجب تولید برق می‌شوند. در کاتد الکترون‌ها، پروتون‌های هیدروژن و اکسیژن موجود در هوا با هم ترکیب می‌شوند و آب را تشکیل می‌دهند. واکنش‌ها در الکترودها به شرح ذیل می‌باشند[4].

(۱) واکنش آندی: $H_2 \rightarrow 2H^+{}_{(aq)} + 2e^-$

(۲) واکنش کاتدی: $\frac{1}{2}O_{2(g)} + 2H^+{}_{(aq)} + 2e^- \rightarrow H_2O_{(l)}$

(۳) واکنش کلی: $H_{2(g)} + \frac{1}{2}O_{2(g)} \rightarrow H_2O_{(l)} + Electric\ Energy + Heat$

با توجه به اینکه در ساخت الکترود بایستی ضخامت لایه کاتالیزور تا حد ممکن کاهش یابد لذا از تکنیک‌هایی نظیر روش های برپایه امولسیون تفلون، فیلم نازک، الکتروپاششی، رسوب گیری به کمک بمباران یونی، پلاسما، رسوب گذاری پاششی، کاهش پرتوالکترونی، رسوب گیری به کمک بمباران یونی و پلاسما و لایه نشانی الکتریکی اشاره نمود. رسوب گذاری الکتروشیمیایی با نام آبکاری الکتریکی نیز شناخته می‌شود. در این روش از یک سلول الکترولیز استفاده می‌شود که شامل یک حمام و الکترودهای غوطه‌ور در آن است. در شکل ۲ شمای فرایند لایه نشانی الکتریکی مشاهده می‌گردد.

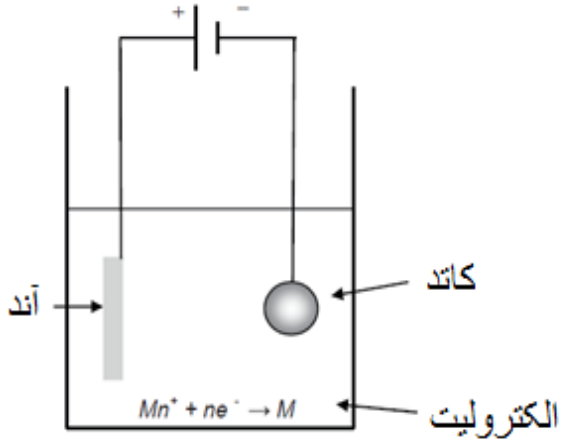

شکل ۲: شماتیک فرایند لایه نشانی الکتریکی **[5]**

فلزی که باید رسوب گذاری شود به شکل یون در حمام الکترولیت وجود دارد. الکترودها به منبع جریان متصل هستند. آن چه به عنوان پوشش باید رسوب گذاری شود به قطب مثبت (آند) متصل می‌گردد و زیر لایه به قطب منفی (کاتد) متصل می‌شود، به جز در مواردی مثل طلا که از آند غیر قابل حل استفاده می‌شود**[5]**.

مواد و روش تحقیق

مواد مورد استفاده شامل اتانول، اسید سولفوریک، اسید بوریک، سولفات منگنز، کلیرید منگنز و نیکل با خلوص ۹۹/۹۹ درصد می‌باشد. تمامی مواد محصول شرکت مرک آلمان می‌باشد. میزان مواد مصرفی به همراه جزئیات حمام پوشش‌دهی در جدول ۱ مشاهده می‌گردد.

جدول ۱: مشخصات حمام مورد استفاده در فرایند پوشش دهی

مشخصات حمام	مقدار
$MnCl_2{\cdot}4H_2O$	۲۰ gr
$MnSO_4{\cdot}4H_2O$	۶۰ gr
آب	۲۰۰ gr
H_3BO_3	۳ gr
PH	۳
T	۲۰ °C
دانسیته جریان (i)	۳۰ $mA.Cm^{-2}$

ورق نیکل به ابعاد ۱×۱cm و ضخامت ۱mm جهت پوشش دهی مانت سرد گردید سپس پولیش شده و توسط استون شستشو و خشک شده است. برای انجام فرایند پوشش دهی از گرافیت استوانه ای به قطر ۵۰mm به عنوان آند استفاده شده است. فلز نیکل به عنوان کاتد در فاصله ۲Cm آند قرار داده شد. پس از اتصال آند و کاتد به منبع جریان فرایند پوشش دهی به مدت ۱۰ دقیقه صورت گرفت.

آزمایشات الکتروشیمیایی در دمای ۲۹۸ °K و توسط یک پیل سه الکترودی با دستگاه پتانسیواستات ساخت شرکت EG&G صورت گرفته است. در این پیل از الکترود گرافیتی و الکترود کالومل (۰/۲۴۱ V-RHE) به عنوان الکترود شمارنده و الکترود مرجع مورد استفاده قرار گرفته است. تصاویر SEM با دستگاه HBO موجود در دانشگاه آزاد نجف آباد گرفته شده است. تصاویر AFM توسط دستگاه AP0100 شرکت Park Scientific Instruments گرفته شده است.

نتایج و بحث

تصاویر SEM پوشش قبل از انجام آزمایشات الکتروشیمیایی در شکل ۳ نشان داده شده است.

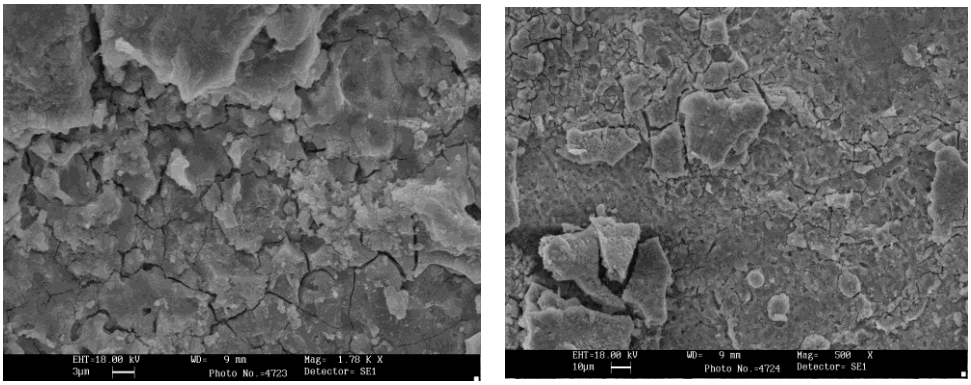

شکل ۳: تصاویر SEM سطح پوشش منگنز

الف: تصویر SEM با بزرگنمایی ۵۰۰ برابر ب: تصویر SEM با بزرگنمایی ۲۰۰۰ برابر

این تصاویر نشان می‌دهد که ذرات پوشش به صورت اشکال هندسی نامنظم تشکیل شده است. که به صورت پرمنفذ و دارای خلل و فرج می باشد. اندازه ذرات بین ۲۰۰nm تا ۳۵۰nm می‌باشد. ترکیب پوشش توسط EDS بررسی شد که وجود پیک منگنز در آنالیز عنصری نشان دهنده وجود این عنصر در ترکیب پوشش می‌باشد. در شکل ۴ نتایج EDS را مشاهده می کنید. بنابراین ذرات منگنز به خوبی بر روی نیکل به روش لایه نشانی الکتریکی تشکیل شده است.

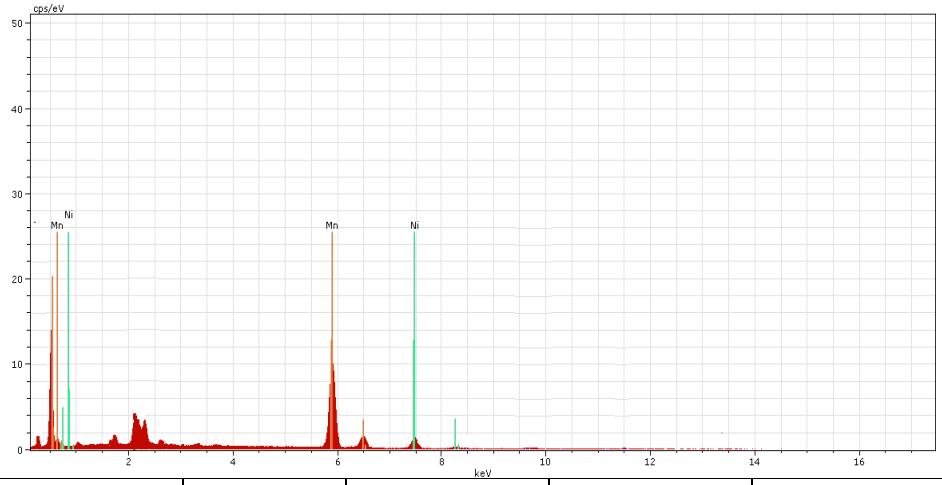

عنصر	series	[wt.%]	[norm. wt.%]	[norm. at.%]
Oxygen	K-series	29.66811	37.52309	67.61511
Manganese	K-series	39.94019	50.51482	26.50909
Nickel	K-series	9.457978	11.96209	5.875795
	Sum:	79.06628	100	100

شکل ۴: نتایج آنالیز عنصری EDS

تصویر AFM گرفته شده از سطح پوشش در شکل ۵ نشان داده شده است.

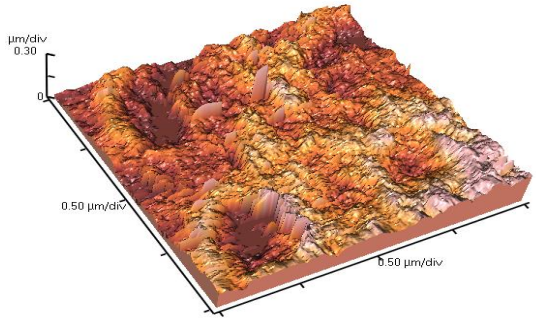

شکل ۵: تصاویر AFM سطح پوشش

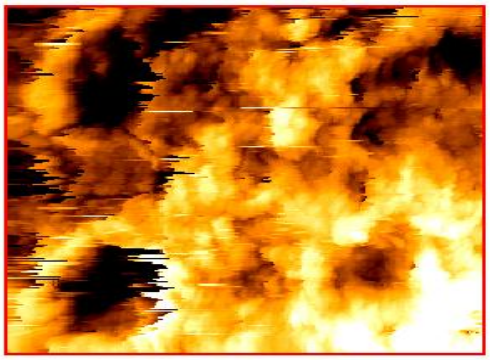

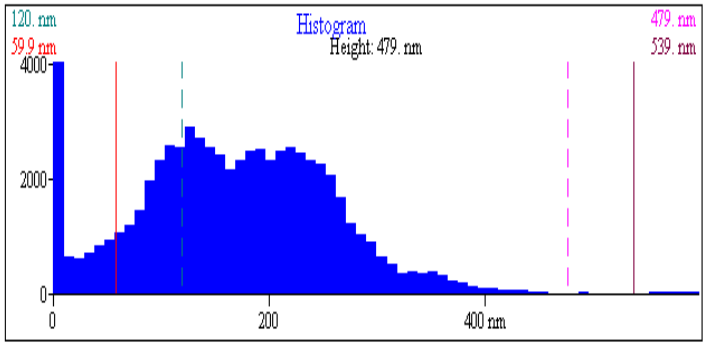

Rp-v	Rms Rough (Rq)	Ave Rough (Ra)	Bearing Ratio	Valley (Rv)	Surface Area	Volume
598.5 nm	87.78 nm	71.51 nm	@80.0% 92.70 nm	-165.5 nm	18.59 µm²	0.6621 µm³

شکل ۶: تصاویر AFM سطح پوشش

این تصاویر نشان می دهد که سطح پوشش دارای پستی و بلندی های مناسب جهت سایت های کاتدی می باشد. در این حالت نمونه دارای زبری متوسط ۷۱/۵۱ و عمق دره آن ۱۶۵/۵ nm- می باشد.

در شکل ۷ نتایج آزمون سیکلیک ولتامتری برای نمونه نیکلی بدون پوشش و نمونه نیکلی پوشش داده شده با منگنز و پلاتین در محلول ۰/۵ M اسید سولفوریک به همراه محلول ۰/۵ M اتانول نشان داده شده است.

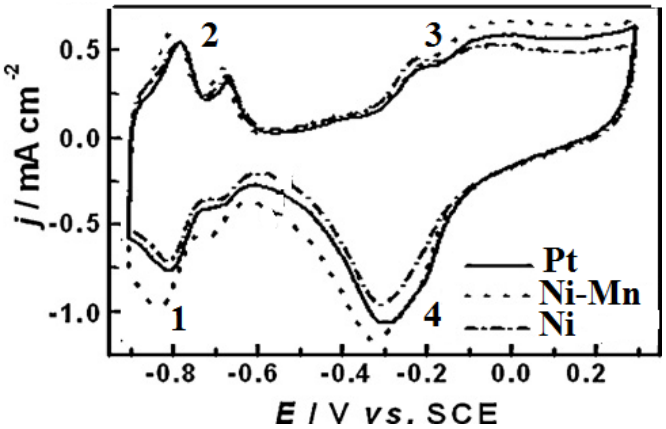

شکل۷: نتایج آزمون سیکلیک ولتامتری، خط مشکی رنگ مربوط به نمونه پلاتین خالص و خط نقطه چین مربوط به نمونه نیکل-منگنز و خط چین مربوط به نمونه نیکل خالص در محلول ۰/۵ M اسید سولفوریک به همراه محلول ۰/۵M اتانول با نرخ روبش ۵۰ mVS^{-1}

همانطور که در شکل ۷ مشاهده می شود پیک های ناحیه ۱ مربوط به جذب الکتریکی هیدروژن بر روی سطح کاتالیزور می‌باشد**[6]**.

$$Mn + H^+ + e^- \rightarrow Mn_H_{ads} \quad (۴)$$

پیک‌های ناحیه ۲ مربوط به ناحیه واجذب الکتریکی هیدروژن می‌باشد**[6]**.

$$Mn_H_{ads} \rightarrow Mn + H^+ + e^- \quad (۵)$$

پیک ناحیه ۳ مربوط به اکسیداسیون سطح منگنز می‌باشد**[6]**.

$$Mn + H_2O \rightarrow Mn_OH + H^+ + e^- \quad (۶)$$

$$Mn_OH + H_2O \rightarrow Mn_(OH)_2 + H^+ + e^- \quad (۷)$$

$$Mn_(OH)_2 \rightarrow MnO + H_2O \quad (۸)$$

و درنهایت پیک ناحیه ۴ مربوط به احیاء اکسید منگنز می‌باشد**[6]**.

$$MnO + 2H^+ + 2e^- \rightarrow Mn + H_2O \quad (۹)$$

بنابراین وجود منگنز در سطح باعث افزایش ناحیه فعال سازی الکتروشیمیایی گردیده است.

نتیجه‌گیری

منگنز به خوبی به روش لایه نشانی الکتریکی بر روی سطح نیکل نشانده شد. ذرات پوشش دارای ساختار شاخه‌ای با میزان تخلخل مناسب جهت انجام واکنش‌های سطحی می‌باشد. بنابراین وجود منگنز در سطح بدلیل دارا بودن جریان تبادلی مناسب باعث افزایش میزان جذب هیدروژن در سطح گردیده است که این امر منجر به افزایش میزان دانسیته جریان پیل می‌گردد.

مراجع

[1] EG&G Services, Parsons.Inc, Science Applications International Corporation. 2000. “Fuel Cell Handbook”, 7th Edition, National Energy Technology Laboratory, Maryland.
[2] Barbir, F. 2012. “PEM Fuel Cells: Theory and Practice”, 2nd Edition, Elsevier, California.
[3] Brault, P. Caillard, A. Thomann, A. L. Mathias, J. Charles, C. Boswell, R.W. Escribano, S. Durand J. and Sauvage, T. 2004. “Plasma sputtering deposition of platinum into porous fuel cell electrodes”, *Journal of Physics D: Applied Physics*, 37, pp. 3419–3423.
[4] Choi, K.H. Kim, H.S. and Lee, T.H. 1998. “Electrode Fabrication for Proton Exchange Membrane Fuel Cells by Pulse Electrodeposition”, *Journal of Power Sources*, 75, pp. 230–235.
[5] Chandrasekar, M.S. Pushpavanam, M. 2008. “Pulse and Pulse Reverse Plating-Conceptual, Advantages and Applications”, *Electrochimica Acta*, 53, pp. 3313–3322.
[6] Zhang, J. 2008. “PEM Fuel Cell Electrocatalysts and Catalyst Layers: Fundamentals and Application”, Springer, Canada.

بررسی پوشش کبالت تولید شده به روش لایه نشانی الکتریکی به عنوان کاتد پیل سوختی غشا پلیمری

امیرحسین آرامی پارچه باف[1]، محمود فاضل نجف آبادی[2]

۱. دانشگاه آزاد اسلامی، واحد نجف آباد، باشگاه پژوهشگران جوان و نخبگان، نجف آباد، اصفهان، ایران

amir.arami@gmail.com

۲. دانشگاه پیام نور، بخش فنی و مهندسی، گروه مهندسی مکانیک، اصفهان، ایران

: fazel.ut@gmail.com

چکیده

امروزه بحران‌هایی نظیر آلودگی هوا و محیط زیست و انرژی از بزرگترین معضل‌های جامعه بشری می‌باشد. برای مقابله با این بحران‌ها تلاش‌های گستردهای برای جایگزینی انرژی‌های سبز و تجدید پذیر نظیر پیل‌های سوختی صورت گرفته است. در این مطالعه به بررسی پوشش کبالت تولید شده به روش لایه نشانی الکتریکی بر روی زیر لایه نیکل به منظور بهره گیری در پیل‌های سوختی غشا پلیمری پرداخته شده است. در ابتدا پوشش کبالت به روش لایه نشانی الکتریکی بر روی زیر لایه‌ای از جنس نیکل رسوب دهی شده است. مرفولوژی و بررسی‌های سطح پوشش توسط میکروسکوپ الکترونی روبشی و میکروسکوپ نیروی اتمی صورت گرفته شد. جهت تعیین ترکیب شیمیایی سطح پوشش از طیف سنج پراش پرتو ایکس استفاده شده است. برای بررسی واکنش های الکتروشیمیایی از روش سیکلیک ولتیمتری استفاده شده است. نتایج نشان می‌دهد که فلز کبالت باعث افزایش ناحیه جذب و واجذب هیدروژن گردیده است بنابراین باعث بهبود عملکرد پیل سوختی گردیده است.

واژه‌های کلیدی: پیل های سوختی پلیمری، لایه نشانی الکتریکی، کبالت، اتانول، خواص الکتروکاتالیستی، AFM، SEM، EDS

مقدمه

پیل سوختی یک پیل الکتروشیمیایی می‌باشد که در آن هیدروژن و اکسیژن واکنش داده و محصول آن آب به همراه الکتریسته می‌باشد بنابراین این موضوع که تنها محصول این فرایند آب می‌باشد باعث شده که پیل‌های سوختی از نقطه نظر زیست محیطی مورد توجه قرار گیرند **[1]**. پیل‌های سوختی براساس نوع الکترولیت به پنج دسته اصلی پیل‌های سوختی غشاء پلیمری[1]، پیل‌های سوختی قلیایی[2]، پیل‌های سوختی اسید فسفریک[3]، پیل‌های سوختی کربنات مذاب[4]، پیل‌های

[1] Polymer Electrolyte Membrane Fuel Cell
[2] Alkaline Fuel Cell
[3] Phosphoric Acid Fuel Cell
[4] Molten Carbonate Fuel Cell

سوختی اکسید جامد[1] تقسیم می‌گردد**[2]**. بجز موارد ذکر شده پیل‌های سوختی دیگری نظیر پیل‌های سوختی میکروبی، هیدرید فلزی و ... نیز وجود دارند که از اهمیت کمتری برخوردارند.

در میان انواع پیل‌های سوختی، پیل‌های سوختی پلیمری به دلیل مزایای بسیاری نظیر دمای عملکرد پایین و رادمان تبدیل انرژی بالا [3]، عدم خوردگی [4]، چگالی جریان بالا برای کاربرد در صنایع خودروسازی [5]، حذف نشت الکترولیت و سادگی طراحی [6]، قیمت پایین و عمر بالای مجموعه [1] مورد توجه محققین قرار گرفته است.

در شکل ۱ اجزای یک پیل سوختی پلیمری به همراه نحوه عملکرد آن نشان داده شده است.

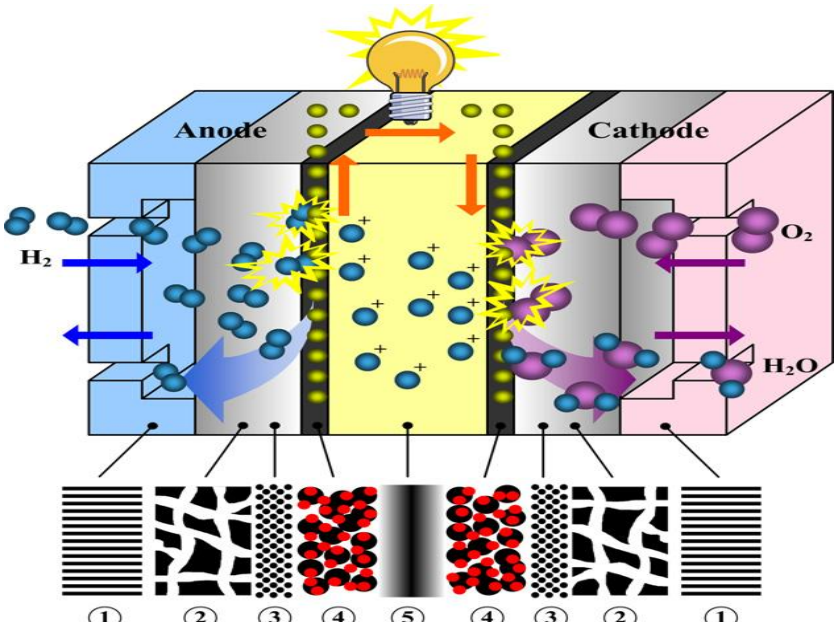

شکل ۱: اجزای یک پیل سوختی پلیمری :

۱) صفحات دوقطبی، ۲) لایه پشتی، ۳) الکترود، ۴) پوشش الکتروکاتالیستی، ۵) غشای پلیمری**[7]**

همانطور که در شکل ۱ مشاهده می‌گردد در یک پیل سوختی هیدروژن به عنوان سوخت در آند و اکسیژن به عنوان اکسیدان در کاتد تزریق می‌شود. هر اتم هیدرژون یک پروتون و یک الکترون دارد که با از دست دادن الکترون در آند به پروتون H^+ تبدیل می‌شود و به این ترتیب قابلیت عبور از الکترلیت را بدست می‌آورد . H^+ از الکترولیت عبور می‌کند و الکترون‌ها از طریق اتصال خارجی به کاتد می‌رسند. در کاتد، الکترون‌ها، پروتون‌های هیدروژن و اکسیژن جذب شده روی کاتد تشکیل آب می‌دهند که خروجی سیستم را تشکیل می‌دهد. معادلات ۱ تا ۳ واکنش‌های موجود در یک پیل سوختی را نشان می‌دهد [1].

(۱۰) واکنش آندی:
$$H_2 \rightarrow 2H^+{}_{(aq)} + 2e^-$$

(۱۱) واکنش کاتدی:
$$\tfrac{1}{2}O_{2_{(g)}} + 2H^+{}_{(aq)} + 2e^- \rightarrow H_2O_{(l)}$$

(۱۲) واکنش کلی:
$$H_{2_{(g)}} + \tfrac{1}{2}O_{2_{(g)}} \rightarrow H_2O_{(l)} + Electric\ Energy + Heat$$

[1] Solid Oxide Fuel Cell

الکترود معمولا ترکیبی از دو لایه، لایه بستر یا وب[1] و لایه کاتالیزور می‌باشند. وظیفه اصلی لایه بستر شامل ایجاد مسیرهایی جهت نفوذ گاز، تامین کننده استحکام مکانیکی، ایجاد یک بستر هادی الکتریکی جهت انتقال الکترون‌ها و ایجاد مسیرهای برای خروج آب تولیدی. بستر معمولا از جنس گرافیت می‌باشد که به صورت پارچه کربنی استفاده می‌شود. در صورتی که الکترولیت پیل سوختی اسیدی نباشد، بستر می‌تواند از توری‌های فلزی نظیر فولاد، تیتایوم و یا نیکل تهیه شود. این لایه باید خواص آب گریزی[2] داشته باشد. بستر توسط یک لایه کاتالیزور پوشش داده می‌شود که معمولا از فلزات فعال با دانسیته جریان تبادلی مناسب تهیه می‌شود. این لایه دارای ویژگی‌های آب دوستی[3] هستند، وجود این خاصیت به منظور ایجاد شبکه انتقال مایع از درون لایه کاتالیزور و انتقال جریان الکترون تولید شده بکار می‌رود [8].

با توجه به اینکه در ساخت الکترود بایستی ضخامت لایه کاتالیزور تا حد ممکن کاهش یابد لذا از تکنیک‌هایی نظیر روش های برپایه امولسیون تفلون، فیلم نازک، الکتروپاششی، رسوب گیری به کمک بمباران یونی، پلاسما، رسوب گذاری پاششی، کاهش پرتوالکترونی، رسوب گیری به کمک بمباران یونی و پلاسما و لایه نشانی الکتریکی اشاره نمود. رسوب گذاری الکتروشیمیایی با نام آبکاری الکتریکی نیز شناخته می‌شود. در این روش از یک سلول الکترولیز استفاده می‌شود که شامل یک حمام و الکترودهای غوطه‌ور در آن است. در شکل ۲ شمای فرایند لایه نشانی الکتریکی مشاهده می‌گردد. فلزی که باید رسوب گذاری شود به شکل یون در حمام الکترولیت وجود دارد. الکترودها به منبع جریان متصل هستند. آن چه به عنوان پوشش باید رسوب گذاری شود به قطب مثبت (آند) متصل می‌گردد و زیر لایه به قطب منفی (کاتد) متصل می‌شود، به جز در مواردی مثل طلا که از آند غیر قابل حل استفاده می‌شود[9]. در فرایند لایه نشانی الکتریکی جریان و زمان به عنوان دو عامل بسیار مهم مطرح است که تاثیر این دو عامل در معادله فاراده مشاهده می‌گردد.

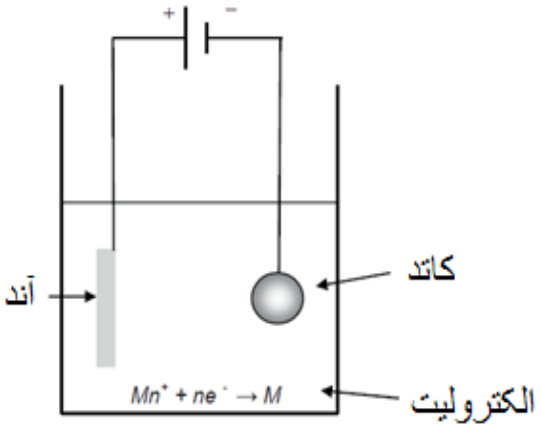

شکل ۲: شماتیک فرایند لایه نشانی الکتریکی **[9]**

$$\mathbf{I.t = \frac{W.n.F}{M}} \qquad (۴)$$

[1] Porous Backing Layer
[2] Hydrophobic
[3] Hydrophilic

در معادله ۴، **I** جریان، **t** زمان، **W** جرم پوشش نشانده شده، **n** تعداد لکترون، **F** عدد فاراده[1] و **M** جرم ملکولی پوشش می‌باشد.

الکل‌ها به عنوان سوخت در پیل‌های سوختی پلیمری مورد استفاده قرار می‌گیرند. اتانول نسبت به سایر الکل‌ها نظیر متانول از سمیت کمتری برخوردار می‌باشد و به راحتی از تخمیر نشاسته قابل فرآوری می‌باشد. از دیگر مزایای اتانول اینست که یک سوخت مایع می‌باشد لذا ذخیره و نگهداری آن بسیار راحتر از هیدروژن می‌باشد[**10**].

مواد و روش تحقیق

مواد مورد استفاده شامل اتانول، اسید سولفوریک، اسید بوریک، سولفات کبالت، کلیرید کبالت و نیکل با خلوص ۹۹/۹۹ درصد می‌باشد. تمامی مواد محصول شرکت مرک آلمان می‌باشد. میزان مواد مصرفی به همراه جزئیات حمام پوشش‌دهی در جدول ۱ مشاهده می‌گردد.

ورق نیکل به ابعاد **۱×۱cm** و ضخامت **۱mm** جهت پوشش دهی مانت سرد گردید سپس پولیش شده و توسط استون شستشو و خشک شده است. برای انجام فرایند پوشش دهی از گرافیت استوانه ای به قطر **۵۰mm** به عنوان آند استفاده شده است. فلز نیکل به عنوان کاتد در فاصله **۲Cm** آند قرار داده شد. پس از اتصال آند و کاتد به منبع جریان فرایند پوشش دهی به مدت ۱۰ دقیقه صورت گرفت.

جدول ۱: مشخصات حمام مورد استفاده در فرایند پوشش دهی

مشخصات حمام	مقدار
$CoCl_2 \cdot 6H_2O$	۲۰ gr
$CoSO_4 \cdot 7H_2O$	۶۰ gr
آب	۲۰۰ gr
H_3BO_3	۳ gr
PH	۳
T	۳۰ °C
دانسیته جریان (i)	۲۰ $mA.Cm^{-2}$

آزمایشات الکتروشیمیایی در دمای **۲۹۸ °K** و توسط یک پیل سه الکترودی با دستگاه پتانسیواستات ساخت شرکت **EG&G** صورت گرفته است. در این پیل از الکترود گرافیتی و الکترود کالومل (**V-RHE** ۰/۲۴۱) به عنوان الکترود شمارنده و الکترود مرجع مورد استفاده قرار گرفته است. تصاویر **SEM** با دستگاه **HBO** موجود در دانشگاه آزاد نجف آباد و تصاویر **AFM** توسط دستگاه **AP0100** شرکت **Park Scientific Instruments** گرفته شده است.

[1] Faraday's Constant (F) = 96485.34 C/mol

نتایج و بحث

تصاویر **SEM** پوشش قبل از انجام آزمایشات الکتروشیمیایی در شکل نشان داده شده است.

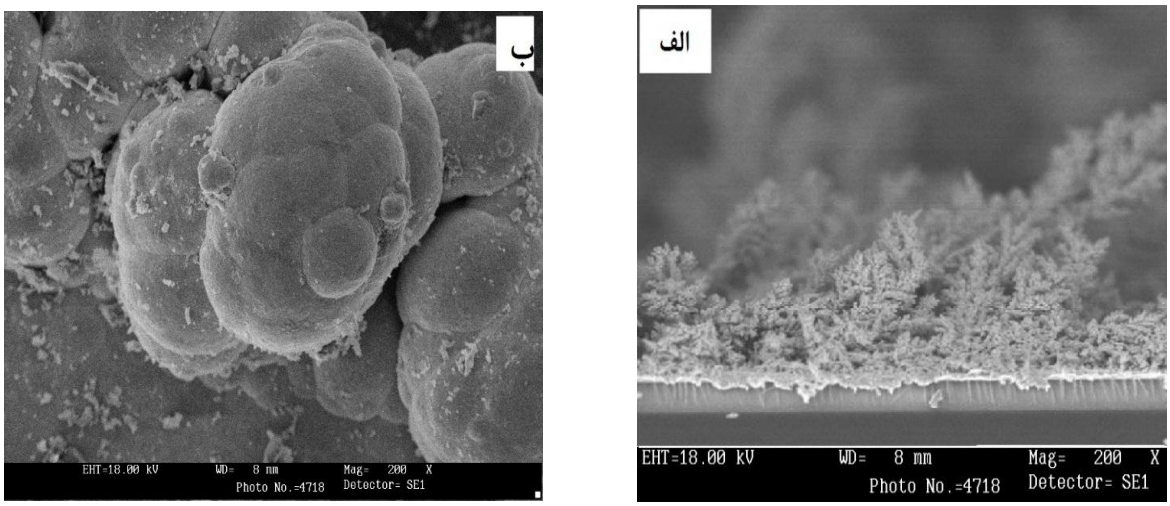

شکل ۳: تصاویر **SEM** سطح پوشش

الف: تصویر **SEM** جانبی از پوشش ب: تصویر **SEM** با بزرگنمایی ۲۰۰۰ برابر از رسوبات کبالت

این تصاویر نشان می‌دهد که ذرات پوشش به صورت شاخه ای رشد نموده است. که به صورت پرمنفذ و دارای خلل و فرج می باشد. اندازه ذرات بین **۱۰۰nm** تا **۲۰۰nm** می‌باشد.

در **شکل ٤** نتایج آنالیز عنصری از سطح پوشش مشاهده می گردد.

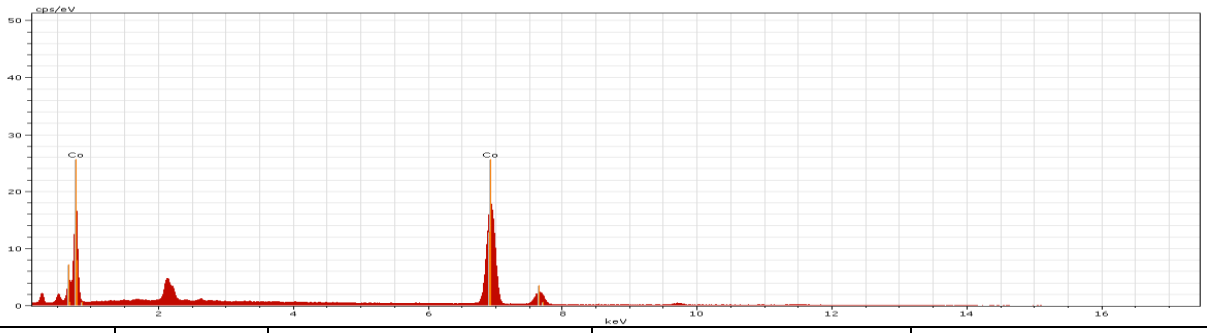

عنصر	series	[wt.%]	[norm. wt.%]	[norm. at.%]
Oxygen	K-series	3.00968225952897	3.45271476701886	11.6395189390211
Cobalt	K-series	84.158892691352	96.5472852329811	88.3604810609789
	Sum:	87.1685749508809	100	100

شکل ۴: تصاویر AFM سطح پوشش

ترکیب پوشش توسط **EDS** بررسی شد که وجود پیک کبالت در آنالیز عنصری نشان دهنده وجود این عنصر در ترکیب پوشش می‌باشد. در بنابراین ذرات کبالت به خوبی بر روی نیکل به روش لایه نشانی الکتریکی تشکیل شده است.
تصاویر **AFM** گرفته شده از سطح پوشش در شکل نشان داده شده است.

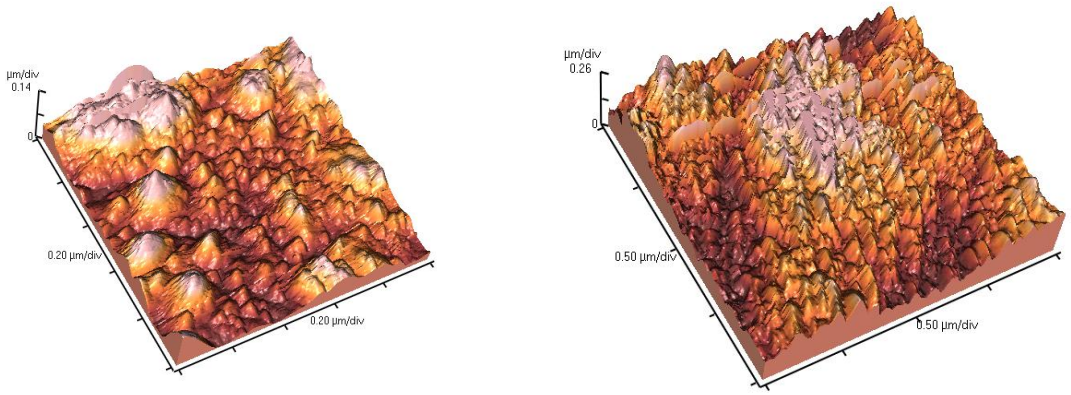

شکل ۵: تصاویر AFM سطح پوشش در سطح **۴ µm²**

مکانیزم ابکاری شامل دو مرحله جوانه زنی و رشد است که مرحله رشد آن شامل سه مرحله: ۱) انتقال یون از داخل محلول به سطح کاتد ۲)انتقال بار و تبدیل یون به اتم فلزی ۳)نفوذ اتم فلزی به داخل شبکه کریستالی فلز و رشد دانه است. با تتوجه به اینکه دانسیته جریان ثابت است لذا با افزایش زمان محل های جوانه زنی است افزایش می یابد. با گذشت زمان یون های بیشتری بر سطح رسوب می کنند و بیشتر به داخل شبکه کریستالی فلز وارد می شوند. و با توجه به این که قرار گیری یون های فلزی بر سطح کاملا ترجیحی است و به دلیل تغییرات موضعی زبری بر سطح قطعه کار، لذا افزایش زبری کاملا مشخص است.

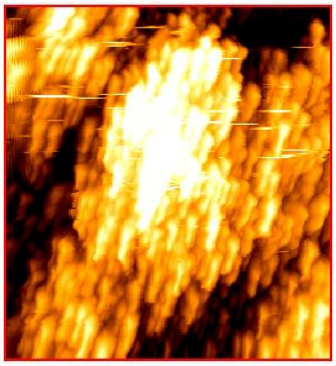

(0,0) x: 0.000 µm y: 0.0000 µm z: 0.2043 µm

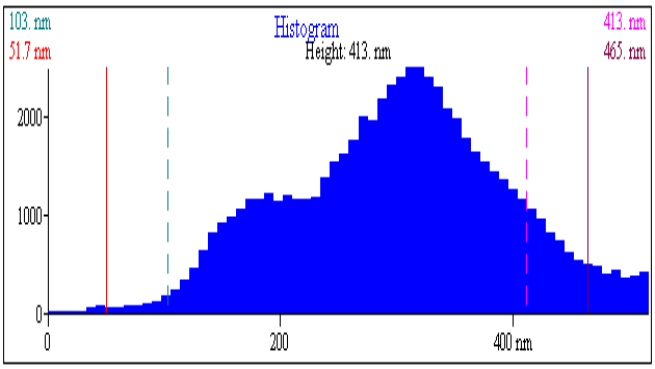

Rp-v	Rms Rough (Rq)	Ave Rough (Ra)	Bearing Ratio	Valley (Rv)	Volume	Surface Area
516.5 nm	96.43 nm	76.96 nm	@80.0% 216.73 nm	-304.1 nm	1.216 µm³	13.58 µm²

شکل ۶: آنالیز **AFM** سطح پوشش

این تصاویر نشان می دهد که سطح پوشش دارای پستی و بلندی های مناسب جهت سایت های کاتدی می باشد. در این حالت نمونه دارای سختی متوسط ۷۶/۹۶ و عمق دره آن **nm** ۳۰۴/۱- می باشد.

معادله ۵ واکنش اکسیداسیون اتانول را در آند نشان می‌دهد:

C (۱۳)

برای محاسبه پتانسیل متناظر آند، با توجه به اطلاعات ترمودینامیکی موجود، ابتدا گرمای تشکیل معادله ۵ را به صورت زیر محاسبه می گردد:

– (۱۴)

–

E

پروتون‌ها تولید شده در واکنش فوق از غشای پلیمری عبور کرده و به سطح کاتد می‌رسند. در اینجا واکنش اکسیژن و هیدروژن طبق معادله ۷ بدست می‌آید:

$\frac{1}{2}$ (۱۵)

E

بنابراین طبق واکنش کلی پیل داریم:

C (۱۶)

Δ

Δ

E

اگر **M** جرم ملکولی اتانول باشد بنابراین انرژی ویژه به صورت زیر محاسبه می گردد:

$$\mathbf{W_e = -\frac{\Delta G^\circ}{3600\times M} = \frac{1325\times 10^3}{3600\times 0.046} \approx 8.00_{KWh/Kg}}$$

و برای محاسبه بازده انرژی برگشت پذیر داریم:

$$\boldsymbol{\varepsilon_{rev} = \frac{\Delta G^\circ}{\Delta H^\circ} = 0.969}$$

این محاسبات در خصوص سایر الکل‌ها نیز انجام گرفته است که اطلاعات مربوط به آن را در جدول ۲ مشاهده می کنید. با توجه به اطلاعات فوق، اتانول دارای بیشترین بازده نسبت به سایر الکل‌ها می‌باشد.

جدول۲: اطلاعات ترمودینامیکی محاسبه شده برای بعضی از الکل‌ها

ε_{rev}	$W_e(KWh/Kg)$	$E^{\circ}_{Cell}(V)$	$\Delta H^{\circ}(Kj/mol)$	$\Delta G^{\circ}(Kj/mol)$	سوخت
0.967	6.09	1.213	-726	-702	CH_3OH
0.969	8.00	1.145	-1367	-1325	C_2H_5OH
0.919	8.58	1.067	-2021	-1853	C_3H_7OH
0.890	8.93	1.029	-2676	-2381	C_4H_9OH

در شکل نتایج آزمون سیکلیک ولتامتری برای نمونه نیکلی بدون پوشش و نمونه نیکلی پوشش داده شده با کبالت در محلول **M** ۰/۵ اسید سولفوریک به همراه محلول **M** ۰/۵ اتانول نشان داده شده است.

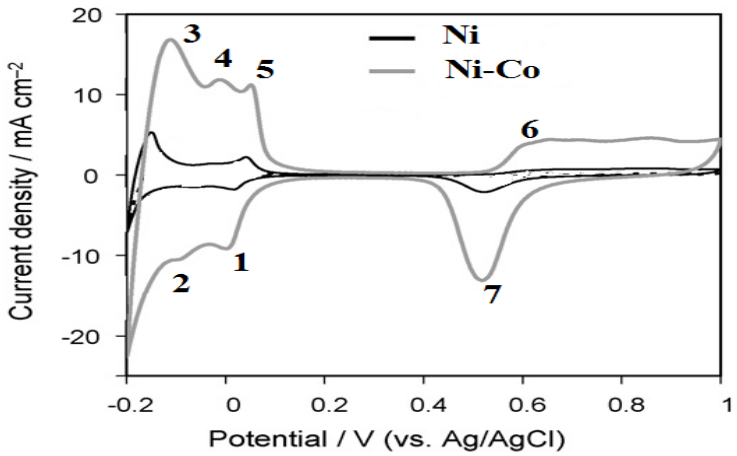

شکل ۷: نتایج آزمون سیکلیک ولتامتری، خط مشکی رنگ مربوط به نمونه نیکل خالص و خط خاکستری رنگ مربوط به نمونه نیکلی با پوشش کبالت در محلول **M** ۰/۵ اسید سولفوریک به همراه محلول **M** ۰/۵ اتانول با نرخ روبش **۵۰ mVS^{-1}**

همانطور که در شکل مشاهده می شود پیک های ۱ و ۲ مربوط به جذب الکتریکی هیدروژن بر روی سطح کاتالیزور می‌باشد[**11**].

C (۱۷)

پیک‌های ۳، ۴ و۵ مربوط به ناحیه واجذب الکتریکی هیدروژن می‌باشد[**11**].

C (۱۸)

پیک ۶ مربوط به اکسیداسیون سطح کبالت می‌باشد[**11**].

C (۱۹)

C (۲۰)

C (۲۱)

و درنهایت پیک ۷ مربوط به احیاء اکسید کبالت می‌باشد[**11**].

C (۲۲)

بنابراین وجود کبالت در سطح باعث افزایش ناحیه فعال سازی الکتروشیمیایی گردیده است.

نتیجه‌گیری

۱) کبالت به خوبی به روش لایه نشانی الکتریکی بر روی نیکل پوشش داده شده است.

۲) ذرات پوشش دارای ساختار شاخه ای بوده است و ساختار دارای تخلخل بالا می باشد نتایج **AFM** نشان می دهد که افزایش میزان زبری منجر به افزایش واکنش پذیری یا به عبارت دیگر افزایش اکتیویته کاتالیستی برای واکنش با اتانول است.

۳) وجود کبالت در سطح تماس الکترولیت و کاتد منجر به افزایش میزان جذب هیدروژن گردیده است که نشان دهده اثر الکتروکاتالیستی پوشش می باشد.

۴) افزایش سایت های فعال جهت انجام واکنش و نیز افزایش دانسیته جریان تبادلی منجر به افزایش و نیز سرعت انجام واکنش اکسیداسیون هیدروژن گردیده که منجر به بالا رفتن راندمان پیل می گردد.

مراجع

1. EG&G Services, Parsons.Inc, Science Applications International Corporation. 2000. “Fuel Cell Handbook”, 7th Edition, National Energy Technology Laboratory, Maryland.Sadasd
2. Barbir, F. 2012. “PEM Fuel Cells: Theory and Practice”, 2nd Edition, Elsevier, California.
3. Brault, P. Caillard, A. Thomann, A. L. Mathias, J. Charles, C. Boswell, R.W. Escribano, S. Durand J. and Sauvage, T. 2004. “Plasma sputtering deposition of platinum into porous fuel cell electrodes”, *Journal of Physics D: Applied Physics*, 37, pp. 3419–3423.
4. Choi, K.H. Kim, H.S. and Lee, T.H. 1998. “Electrode Fabrication for Proton Exchange Membrane Fuel Cells by Pulse Electrodeposition”, *Journal of Power Sources*, 75, pp. 230–235.
5. Caillard, A. Brault, P. Mathias, J. Charles, C. Boswell, R.W. and Sauvage, T. 2005. “Deposition and Diffusion of Platinum Nanoparticles in Porous Carbon Assisted by Plasma Sputtering”, *Surface & Coatings Technology*, 200, pp. 391– 394.
6. Shin, S.J. Lee, J.K. Ha, H.Y. Hong, S.A. Chun, H.S. and Oh, I.H. 2002. “Effect of the Catalytic Ink Preparation Method on the Performance of Polymer Electrolyte Membrane Fuel Cells”, *Journal of Power Sources*, 106, pp. 146–152.
7. Yuan, W. Tang, Y. Yang, X. and Wan, Zh. 2012. “Porous Metal Materials for Polymer Electrolyte Membrane Fuel Cells – A Review”, Applied Energy, 94, pp. 309-329.
8. Litster, S. McLean, G. 2004. “PEM fuel cell electrodes”, *Journal of Power Sources*, 130, pp. 61–76.
9. Chandrasekar, M.S. Pushpavanam, M. 2008. “Pulse and Pulse Reverse Plating-Conceptual, Advantages and Applications”, *Electrochimica Acta*, 53, pp. 3313–3322.

10. Xu, Ch. Su, Y. Tan, L. Liu, Z. Zhang, J. Chen, Sh. Jiang, S.P. 2009. "Electrodeposited PtCo and PtMn Electrocatalysts for Methanol and Ethanol Electro Oxidation of Direct Alcohol Fuel Cells", *Electrochimical Acta*, 54, pp. 6322-9326.

11. Zhang, J. 2008. "PEM Fuel Cell Electrocatalysts and Catalyst Layers: Fundamentals and Application", Springer, Canada.

8th Iranian Fuel Cell Seminar
FEBRUARY 25,26
2015

طراحی سیستم کنترلی تست استیشن پیل سوختی بر اساس برنامه نویسی Labview

بهزاد ارحامی[۱]، عباسعلی ملک برمی[۲]، سیامک توکلی[۳]

۱. پژوهشکده لیزر و اپتیک،پژوهشگاه علوم و فنون هسته ای،تهران، ایران
۲. پژوهشکده مواد، پژوهشگاه علوم و فنون هسته ای، اصفهان، ایران
۳ گروه مپنا،ایران
** behzad_arhami@yahoo.com*

چکیده

سیستم طراحی شده در این مقاله از دو قسمت، نرم افزار و سخت افزار تشکیل شده است. نرم افزار استفاده شده، نرم افزار Labview می‌باشد.از برنامه نویسی گرافیکی جهت کنترل و همچنین مانیتورینگ سیستم برای ارتباط کاربر با برنامه و وارد کردن تنظیمات، استفاده شده است. سخت افزار بکار رفته در این سیستم از کامپیوتر و کارت‌های آنالوگ ورودی، کارت آنالوگ خروجی، کارت دیجیتال ورودی، کارت دیجیتال خروجی و مبدل Rs485/Rs232 تشکیل شده است.از ورودی‌های آنالوگ برای خواندن دمای خروجی رطوبت زن هیدروژن و اکسیژن و دمای و ولتاژ پیل، میزان رطوبت هیدروژن و اکسیژن، فلوی هیدروژن و اکسیژن و فشار هیدروژن و اکسیژن استفاده شده است. همچنین از خروجی های آنالوگ جهت ارسال فرمان کم و زیاد کردن تدریجی شیر برقی هیدروژن و اکسیژن استفاده شده است. از ورودی‌های دیجیتال ، جهت خواندن وضعیت شیرهای برقی هیدروژن، اکسیژن و نیتروژن و وضعیت اضطرار استفاده شده است. همچنین از خروجی‌های دیجیتال، جهت ارسال فرمان تغییر وضعیت رله شیر برقی هیدروژن و اکسیژن و شیرهای نیتروژن و همچنین تغییر وضعیت رله هیتر هیدروژن و اکسیژن و شیر آب خنک کننده استفاده شده است.

واژه‌های کلیدی: تست استیشن؛ پیل سوختی؛ Labview؛ کارت Advantech ؛ کارت آنالوگ و دیجیتال؛

۱- مقدمه

با توسعه کاربرد پیل های سوختی در خودرو سازی، باطری در کامپیوترهای کیفی و کاربردهای الکتریکی بویژه بکارانداختن موتورهای الکتریکی و روشنایی و همچنین استفاده از پیلهای سوختی جهت تأمین همزمان الکتریسیته و حرارت به روش الکتروشیمیایی و راندمانی حدود ۸۰٪ برای سوخت هیدروژن خالص و ۳۰٪ برای گاز متان بعلت عدم تبعیت از سیکل کارنو ، نیاز به سیستمی جهت تست پیل های سوختی با سرمایه کم و هزینه اجرای کم و در عین حال با قابلیت اطمینان بالایی می باشد. بنابراین توسعه و تجهیز دستگاههای فن آوری پیل سوختی ، رسالت مهم این تحقیق می باشد.

در این فرایند، میزان فلوی عبوری گازهای هیدروژن و اکسیژن و وضعیت شیرهای برقی هیدروژن و اکسیژن و نیتروژن کنترل و دمای ، فشارو فلوی گازهای هیدروژن و اکسیژن و دما و ولتاژ پیل مانیتورشده و منحنی آنها نسبت به زمان، بر روی

گراف و میزان رطوبت هیدروژن و اکسیژن بر روی گیج نشان داده می شود. کنترل و مانیتورینگ پارامترهای فوق را می توان با نرم افزار Labview برنامه نویسی کرد و با استفاده از پروتکل ارتباطی modbus و کارت های Advantech با ابزارهای دقیق ارتباط برقرار کرد. نرم افزار Labview که توسط شرکت National Instruments توسعه داده شده است ، یک زبان برنامه نویسی گرافیکی است که از آیکون های بجای خطوط متنی استفاده می شود.در مقایسه با زبان برنامه نویسی متنی که اجرای برنامه را دستورالعمل ها تعیین می کند، Labview از برنامه نویسی جریان داده استفاده می کند بطوریکه اجرای برنامه را جریان داده تعیین می کند[2] .

Rs232 یک استاندارد و روشی برای برقراری ارتباط با PC و ابزار دقیق می باشد. اما RS232 نکات ضعفی از قبیل نرخ انتقال پایین و فاصله انتقال کمتر را دارد که این مشکل توسط RS485 با استفاده از انتقال تفاضلی حل شده است. ماکزیمم نرخ انتقال، Mbps ۱۰ و ماکزیمم فاصله انتقال هم ۱۲۱۹ متر می باشد[3]. در این تحقیق، با ارتباط Rs485 فرامین و مقادیر به کارت ها ارسال می شود و منحنی پارامترها نسبت به زمان انجام فرایند، بکمک کارت Adam 4017 + بر روی یک گراف نشان داده می شود .از آنجایی که اینترفیس کارت ها Rs485 بوده و اینترفیس کامپیوتر هم Rs232 می باشد، لذا باید مبدلی، برای برقراری ارتباط کامپیوتر و کارت ها معرفی شود[2].

۱- معرفی سیستم:

سیستم از ۲عدد کارت آنالوگ ورودیADVANTECH_ADAM4017+ و یک عدد کارت آنالوگ خروجی ADVANTECH_ADAM4020 وکارت دیجیتال ورودی و خروجیADVANTECH_ADAM4055 و مبدل Rs485/Rs232 ADVANTECH_ADAM4520 و کامپیوتر با برنامه Labview جهت کنترل و نمایش پارامترها بر روی گیج و گراف تشکیل شده است. برای برقراری ارتباط بین کامپیوتر و کارت ها و ارسال فرامین از مبدل Rs232/Rs485 استفاده شده است. برای ارسال فرمان به خروجی های آنالوگ و کنترل شیرهای برقی ، می توان با استفاده از نرم افزار Labview زیر برنامه ای را جهت فراخوانی در سطوح مختلف برنامه ، برنامه نویسی کرد.

۲- توصیف Sub-VI و زیر برنامه آماده سازی شیرهای برقی آنالوگ

Sub-Vi یک زیر برنامه در لب ویو است. امکان استفاده از آن در مسیرهای داخلی و با چندین سطح وجود دارد. روش Sub-VI شبیه زبان متنی سنتی است، ممکن است توسط سایر قسمتهای VI استفاده شود[3]. در این تحقیق یک زیربرنامه Sub-VI با عنوان و intial.Vi به منظور وارد کردن و تنظیمات درصد باز و بسته شدن شیر برقی آنالوگ (proportional valve) و آماده سازی مقادیر برای فراخوانی در سطحی دیگر از برنامه، نوشته شده است. این مقادیر ، پس از انجام تنظیمات توسط اپراتور، تحت برنامه ای در یکی از سکانس ها بر روی پورت Com نوشته می شود تا توسط ترانسدیوسر Rs485/Rs232 به خروجی های کارت آنالوگ، ارسال شود. این خروجی ها با اعمال در صدی از سطح سیگنال کنترل (از قبیل Vdc ۱۰-۰ یا mA ۲۰-۴) به شیر برقی آنالوگ، در صدی از آن باز یا بسته می شود. برای کنترل

شیرهای برقی دیجیتال هم باید برنامه ای در دو حالت True و False جهت اعمال فرمان باز یا بسته برنامه نویسی شده است.

۳- ارسال فرمان True یا False به خروجی های دیجیتال

به منظور کنترل باز یا بسته شدن شیرهای برقی دیجیتال گازها و روشن یا خاموش کردن هیتر گرم کننده گازهای هیدروژن و اکسیژن توسط کاربر، از Case structure با دو Case، باز یا روشن (در حالتTrue) و بسته یا خاموش (در حالت False) استفاده شده است. برای ارسال فرمان باز یا روشن شدن شیرها و هیترها ، وضعیتDO را، True و بسته یا خاموش شدن شیرها و هیترها ، وضعیتDO را ، False می کنیم.سپس تحت برنامه ای وضعیت تنظیم شده DO را بر روی پورت Com نوشته می شود تا فرمان از طریق ترانسدیوسر(مبدل Rs485/Rs232) به آدرس و مکان داده ارسال گردد.

٤- پیکربندی و ارتباط با استفاده از کارتADVANTECH_ADAM4017+

برای مانیتور کردن پارامترها از قبیل ولتاژ، دمای بدنه پیل، رطوبت گازها و ... نسبت به زمان بر روی گراف، لازم است از کارت آنالوگ ورودی استفاده شود. برای این منظور، در سکانسی بعد از مراحل فوق ، باید کارت آنالوگ برای برقراری ارتباط، پیکربندی شود شکل(۱).پس از برنامه پیکربندی کارت ورودی آنالوگ، برنامه نمونه برداری از پارامترهای مختلف ، نوشته شده است.

۵- نمونه برداری با استفاده از کارت آنالوگ ورودی

در این حلقه پارامترهای آنالوگ از طریق کارت ADVANTECH_ADAM4017+ و با ایجاد AI Voltage In.Vi بر روی بلوک دیاگرام ، به آرایه ای متشکل از تمام پارامترهای آنالوگ ورودی ، ارسال می گردد شکل(۲).

برای ارسال مقادیر خوانده شده بر روی گراف، باید آرایه حاصل از تمام پارامترها به آرایه دمای خروجی رطوبت زن هیدروژن ، آرایه دمای خروجی رطوبت زن اکسیژن ، آرایه دمای بدنه پیل ، آرایه ولتاژ پیل ، آرایه میزان رطوبت هیدروژن ، آرایه میزان رطوبت اکسیژن، آرایه فلوی هیدروژن، آرایه فلوی اکسیژن ، آرایه فشار هیدروژن و و آرایه فشار اکسیژن تفکیک شود.

٦- تفکیک آرایه ای از تمام پارامترها به چندین آرایه

آرایه ای از مقادیر نمونه برداری شده پارامترهای آنالوگ ورودی ، مطابق جدول (۱) می باشد:

برنامه نوشته شده در هر سیکل کاری سایز گرفته و مقادیر مربوط به هر پارامتر را در یک آرایه ای دیگر و مختص همان پارامتر ، تفکیک می کند. بعنوان مثال اگر از آرایه مربوط به شکل (۱۳) سایز بگیریم ، سایز آرایه تک بعدی فوق برابر ۲۰ خواهد شد. با توجه به اینکه اولین مقدار نمونه برداری در هر سیکل پارامتر ۱ (دمای هیدروژن)و آخرین مقدار نمونه برداری پارامتر۱۰ (فشار اکسیژن) می باشد پس طول آرایه در هر سیکل کاری ۱۰ می باشد لذا اگر از سایز گرفته شده در انتهای هر سیکل کاری عدد ۱۰ را کم کنیم اندیس مربوط پارامتر ۱ و عدد۹ را کم کنیم اندیس مربوط به پارامتر ۲ و عدد ۸ را کم کنیم اندیس مربوط به پارامتر ۳ و عدد ۷ را کم کنیم پارامتر ۴ و عدد۶ را از سایز کم کنیم اندیس مربوط به پارامتر ۵ و ... و عدد ۱ را کم کنیم اندیس مربوط به پارامتر ۱۰ بدست می آید

.(Array Size) در انتهای هر سیکل کاری گرفته شده و با توجه به توضیح بالا و روابط زیر اندیس مربوط به هر پارامتر محاسبه می شود..

Index (Parameter 1) = Array Size – **10** (1)
Index (Parameter 2) = Array Size – **9** (2)
Index (Parameter 3) = Array Size – **8** (3)
Index (Parameter 4) = Array Size – **7** (4)
Index (Parameter 5) = Array Size – **6** (5)
Index (Parameter 6) = Array Size – **5** (6)
Index (Parameter 7) = Array Size – **4** (7)
Index (Parameter 8) = Array Size –**3** (8)
Index (Parameter 9) = Array Size – **2** (9)
Index (Parameter10) = Array Size – **1** (10)

با بدست آمدن اندیس های مربوط به هر پارامتر، با استفاده از تابع Index Array Function مقدار مربوط به هر پارامتر را از آرایه تمام پارامترها، جدا کرده و در آرایه های مختص همان پارامترا قرار داده و همراه با آرایه زمان تست به کمک تابع Bundle Function در یک کلاستر دسته بندی کرده و آرایه حاصل از دسته بندی آرایه های پارامترهای تفکیک شده و زمان را بر روی گراف ارسال می کنیم [1] شکل(3).

برای مطالعه مقادیر نمونه برداری شده جهت پردازش سیگنال، لازم است آیتمی طراحی شود که امکان ذخیره داده ها بر روی فایل به فرمت اکسل را داشته باشیم.

۷- گزارش دهی و ذخیره داده ها بر روی فایل

۷-۱ – گزارش دهی

این آیتم با عنوان Export در Front panel جهت آرشیو و تعیین مسیر ذخیره مقادیر استفاده می شود.

با ایجاد File Dialog Express VI بر روی صفحه بلوک دیاگرام و تعریف نام پیش فرض(test#n) و تعریف پسوند(.xls) و تعریف button label (creat)و تعریف PROMPT یا کاراکتری که توسط کامپیوتر ارائه می شود تا مشخص کند که آماده پذیرفتن ورودی صفحه کلید است(please select a path) و استفاده از تابع Path To String Function و استفاده از تابع Concatenate Strings جهت ترکیب نام فایل و پسوند فایل به فرمت string

و استفاده از تابع String To Path Function جهت تبدیل ورودی به فرمت string به فرمت path و ایجاد File path Indicator بر روی Front panel جهت نمایش مسیر آرشیو ، برنامه Export طبق شکل (۴) تکمیل می شود.
با زدن کلید Export در صفحه Front panel جعبه محاوره شکل(۵) نمایان می شود تا کاربر بتواند مسیر دلخواه خود را تعیین کند، البته در صورت عدم تعریف مسیر هنگامی که نمونه برداری متوقف می شود این جعبه محاوره مجدد نمایش داده می شود.

۷ -۲ - ذخیره بر روی فایل

این قسمت جهت حفاظت مقادیر نمونه برداری شده بعلت عدم تعیین مسیر ذخیره و عدم استفاده از کلید Export طراحی شده است تا بعد از اتمام اجرای برنامه از کاربر نسبت به ذخیره یا عدم ذخیره سازی سئوال می کند. بدین منظور باید آرایه ای از عناوین (Parameter1,.... Paramete10,time) تشکیل داده و آن را به سایز ۱۱×۱ به آرایه دو بعدی شکل دهی و به صفحه گسترده string تبدیل کرد . از طرف دیگر آرایه ای از آرایه های پارامترها و زمان تشکیل داده و ترانهاده آن را بدست آورده و به صفحه گسترده string تبدیل می کنیم. حال برای ارتباط عناوین با مقادیر نمونه برداری و اینکه مقادیر هر کدام از عناوین بطور زنجیروار، زیر همان عنوان لیست شود، باید آرایه ای از خروجی صفحه گسترده string مربوط به عناوین و خروجی صفحه گسترده string مقادیر نمونه برداری تشکیل داده و خروجی آرایه حاصل را تحت صفحه گسترده string به مسیری توسط زیر برنامه write characters to file.vi جهت ذخیره سازی و تعیین مسیر ذخیره فایل ارسال نمود شکل(۶).
کلید مربوط به گزارش دهی و ذخیره بر روی فایل در صفحه front panel در اختیار اپراتور می باشد که با فشردن کلید مسیر ذخیره سازی تعریف می شود.

۸ - توصیف پانل کنترل و نمایش(Front panel)

این صفحه از کلیدهای کنترلی و نمایشی بشکل گراف و گیج تشکیل شده است شکل(۷).
از این لیست که شامل چهارده عدد دکمه یا کلید فشاری میباشد جهت ورود به لایه های مختلف برنامه استفاده می شود.
Sampling Start : با فشردن این دکمه نمونه برداری از کانالهایی که به سنسورهای سیستم متصل شده اند شروع می شود و نتیجه بصورت همزمان روی گراف نمایش می یابد چنانچه مجددا فشرده شود نمونه برداری متوقف و پرسشی مبنی بر اینکه آیا مایلید داده های اخذ شده ذخیره شوند یا خیر مطرح می شود که در صورت تایید در آدرس معین شده ثبت خواهد شد
Import from جهت ورود اطلاعات ذخیره شده تستهای قبلی به هدف بازنمایش استفاده می شود و بعد از فشرده شدن جعبه محاوره ای شکل(۸) آشکار می شود:

نتایج و بحث

- با انجام فرایند و جمع آوری دیتا و ارسال آن به Master ، شاهد کاهش تاثیرات خطای اپراتوری و افزایش بهره وری بودیم.
- استفاده از برخی واحدهای ترکیبی از قبیل ترکیب نرم افزار لب ویو شبکه کردن کارت ها ،موجب شدتا پاسخ زمانی سیستم بطور قابل ملاحظه ای تقلیل یابد.
- میزان حساسیت مجموعه دیتا و مانیتورینگ، بطور قابل ملاحظه ای بهبود یافت.
- با توجه به خطر و قابل انفجار بودن گاز هیدروژن، می توان برنامه ای نوشت که با برنامه نوشته شده برای این سیستم ، از طریق WiFi و تبلت ها یاگوشی های هوشمند، سیستم را کنترل و یا پارامترهای نمایشی را بر روی گوشی مشاهده کرد. همچنین می توان خطاهای سیستم را بر روی گوشی تلفن همراه مشاهده و رفع خطا کرد.

نتیجه‌گیری

۱) با استفاده از نرم افزار Labviw می توان سیستم تست استیشن را کنترل و مانیتور کرد.

۲) با استفاده از شبکه کردن کارت ها می توان پاسخ زمانی سیستم را کاهش داد.

مراجع

۱. ارحامی ب ، اسمعیل نیا م ،.... مقاله" کنترل و مانیتورینگ سرعت و گشتاور چرخاننده بلور و بوته در فرایند رشد بلور بر روی گراف بر اساس برنامه نویسی Labview " ششمین کنفرانس ملی مهندسی برق و الکترونیک ایران دانشگاه آزاد اسلامی واحد گناباد ۲۸-۳۰مرداد ماه۱۳۹۳

2. PENG Wan-huan, XU Gang: RS485 Communication Between Fuji Transducer and Industrial PC Based on LabVIEW,Measurement & Control Technology , (2010) 21-22.

3. Yun Jintian, z Mingle, J Guoguang, L Gang: System on Temperature Control of Hollow Fiber Spinning Machine Based on LabVIEW, Procedia Engineering 29 (2012) 558 – 562

جدول(۱۳) آرایه ای از پارامترهای۱تا۱۰ به ترتیب نمونه برداری و تکرار نمونه برداری پس از اتمام هر سیکل کاری

INDEX	ARRAY OF ALL
INDEX 0	Hydrogen temp.
INDEX 1	Oxygen temp.
INDEX 2	Cell temp.
INDEX 3	Cell voltage
INDEX 4	Hydrogen humidity
INDEX 5	Oxygen humidity
INDEX 6	Hydrogen flow
INDEX 7	Oxygen flow
INDEX 8	Hydrogen press.
INDEX 9	Oxygen press.
INDEX 10	Hydrogen temp.
INDEX 11	Oxygen temp.
INDEX 12	Cell temp.
INDEX 13	Cell voltage
INDEX 14	Hydrogen humidity
INDEX 15	Oxygen humidity
INDEX 16	Hydrogen flow
INDEX 17	Oxygen flow
INDEX 18	Hydrogen press.
INDEX 19	Oxygen press.
INDEX N-1	.....
INDEX N	N TH PARAMETER

1th duty cycle

2th duty cycle

N th duty cycle

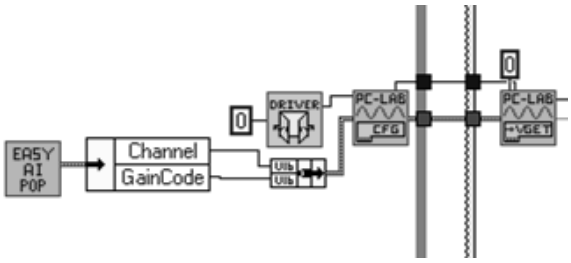

شکل(۱) پیکربندی کارت آنالوگ

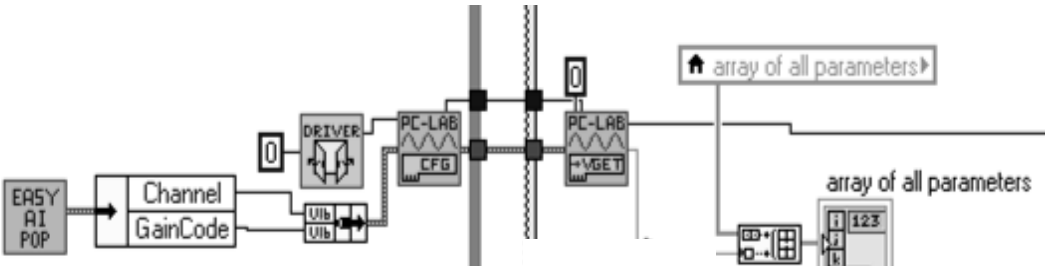

شکل(۲)برنامهء نمونه برداری و خواندن مقدار ورودی های آنالوگ

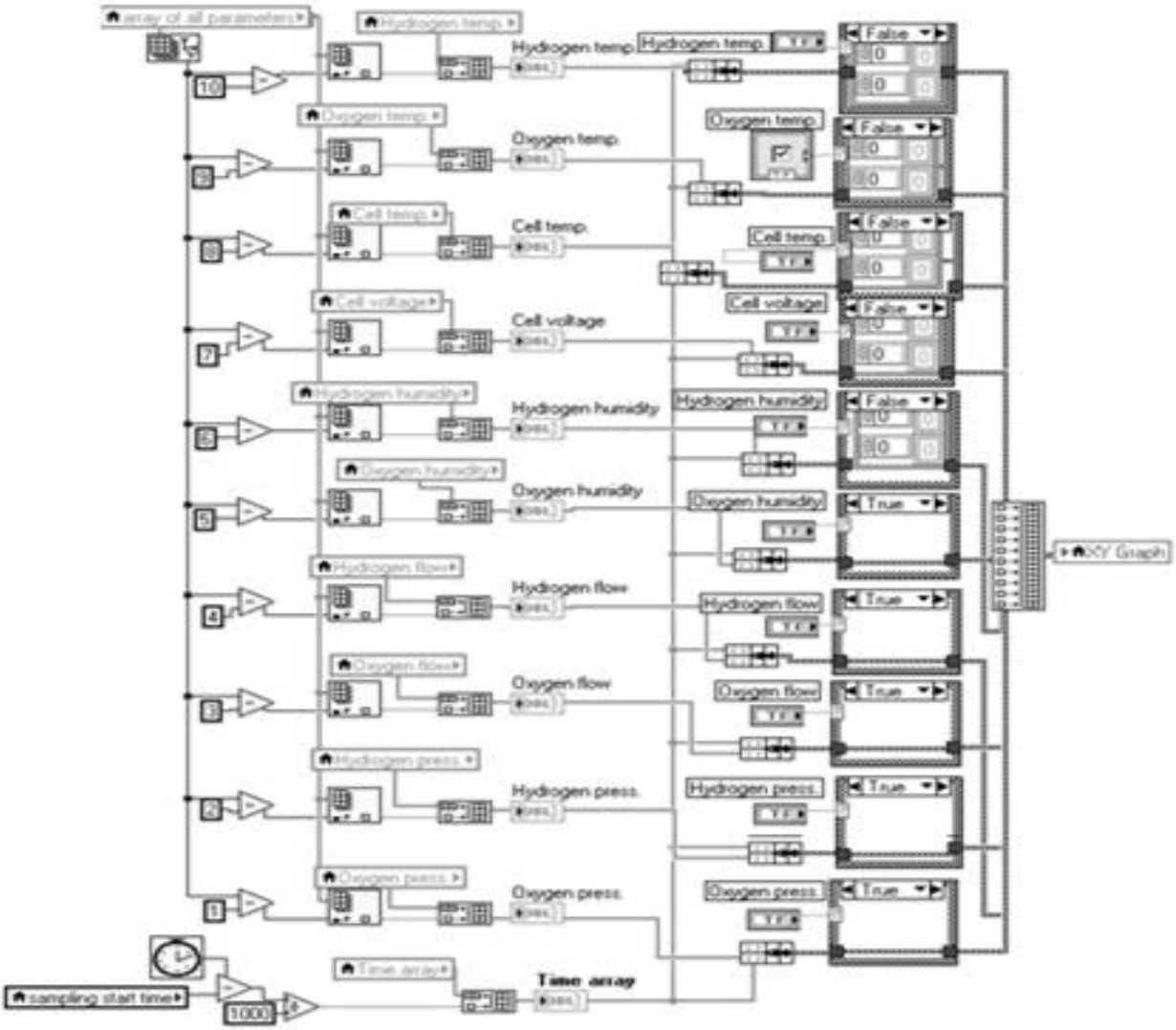

شکل (۳) برنامه تفکیک آرایه تمام پارامترها به آرایه های پارامترهای تفکیک شده و نمایش آنها برروی گراف

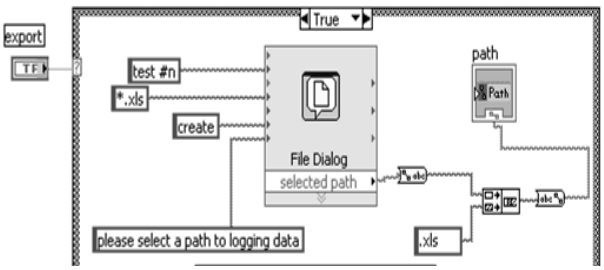

شکل(۴) برنامه Export

شکل(۵) جعبه محاوره تعیین مسیر ذخیره سازی

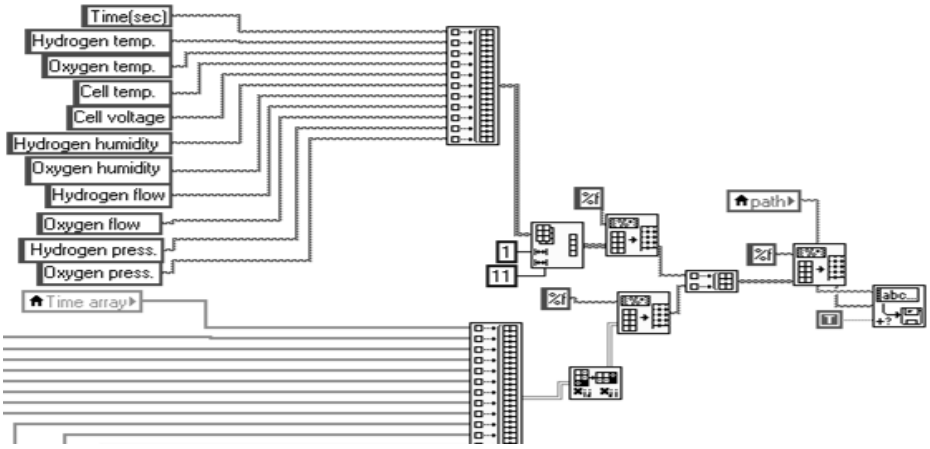

شکل(۶) برنامه ذخیره مقادیر نمونه برداری شده در یک فایل

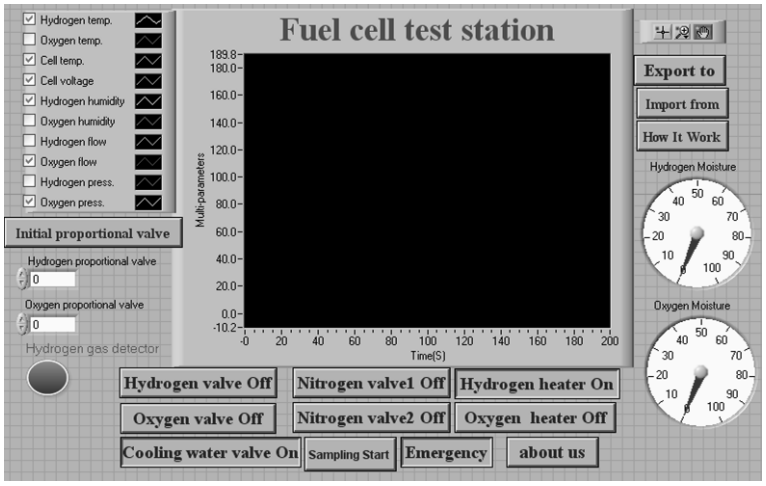

شکل(۷)نمایی از Front panel

ارزیابی رفتار الکتریکی فولاد ضد زنگ Crofer 22 APU مورد استفاده در پیل‌های سوختی اکسید جامد در حضور اسپینل‌های کبالت

هادی ابراهیمی فر، مرتضی زند رحیمی
بخش مهندسی مواد، دانشگاه شهید باهنر کرمان ، ایران

چکیده
آلیازهای کروم دار بهترین مواد برای صفحات اتصال‌دهنده مورد استفاده در پیل‌های سوختی اکسید جامد هستند. به هر حال مشکل کاهش هدایت الکتریکی در طول اکسیداسیون دمای بالا باید حل شود. هدف از این پژوهش مقایسه رفتار الکتریکی فولاد ضد زنگ Crofer 22 APUبدون پوشش و پوشش داده شده با منگنز و کبالت به روش سمانتاسیون فشرده بود. مقاومت سطحی ویژه (ASR) نمونه‌های پوشش داده شده با منگنز و کبالت و نمونه‌های بدون پوشش به عنوان تابعی از دما با آنیل کردن نمونه‌ها از دمای ۴۰۰ تا دمای ۱۰۰۰°C انجام شد. همچنین ASR به عنوان تابعی از زمان اکسیداسیون همدما نیز در دمای ۸۰۰°C مقایسه شد. نتایج نشان داد که افزایش دما موجب افزایش ASR می‌شود. همچنین لایه پوشش منگنز-کبالت در طول فرآیند اکسیداسیون همدما تبدیل به اسپینل‌های $MnCo_2O_4$، $CoCr_2O_4$، $CoFe_2O_4$ و Co_3O_4 شد. اسپینل‌های کبالت مقدار ASR (۲۳/۱۵ $m\Omega\ cm^2$) کمتری را در مقایسه با نمونه بدون پوشش (۳۸/۷۴ $m\Omega\ cm^2$) از خود نشان دادند.

واژه‌های کلیدی: فولاد ضدزنگ Crofer 22 APU، کبالت، منگنز، مقاومت سطحی ویژه (ASR)

مقدمه

فولادهای ضدزنگ مقاوم دربرابرحرارت کاربردگسترده‌ای درصنایع شیمیایی هسته‌ای ونفت دارند که به واسطه مقاومت دمای بالای عالی آنهامی‌باشد. این فولاد ها با ایجاد یک سد اکسیدی جدا کننده، زیر لایه را از اتمسفر احاطه کننده محافظت می کنند. درجه حفاظت تابع ضخامت لایه اکسید، پیوستگی، چسبندگی و نفوذ اکسیژن در اکسید است[۱]. یکی از کاربردهای دیگر فولادهای زنگ نزن استفاده از آنها در پیل های سوختی اکسید جامد (SOFCs) است که این پیل ها انرژی واکنش شیمیایی را به طور مستقیم و بدون احتراق به انرژی الکتریکی تبدیل می کنند. صفحات اتصال دهنده به عنوان یک جز اصلی در پیل های سوختی اکسید جامد در نظر گرفته می شوند (SOFCs) که به طور فیزیکی گازهای سوختی و اکسید کننده را از هم جدا نموده، گازها را در الکترودها توزیع کرده و اتصال الکتریکی بین پیل ها را برقرار می کنند. به دلیل دمای کاری نسبتاً بالای این پیل ها، صفحات اتصال دهنده باید دارای خصوصیاتی مانند، مقاومت به اکسیداسیون در دمای بالا در اتمسفر کاری کاتد و آند، هدایت الکتریکی بالا و تطابق ضریب انبساط حرارتی عالی با سایر اجزا باشند. کاهش دمای کاری سلول های سوختی اکسید جامد به کمتر از ۸۵۰ °C استفاده از آلیاژهای فلزی به عنوان صفحات اتصال

دهنده را مقدور می سازد. مواد فلزی دارای مزیت هایی شامل : سهولت تولید، هزینه کم، هدایت حرارتی و الکتریکی بالا هستند. در میان آلیاژهای فلزی ، فولادهای زنگ نزن فریتی یکی از بهترین مواد برای استفاده در این پیل ها هستند [۴-۲]. به هر حال زیر لایه برهنه به دلیل رشد پیوسته لایه اکسیدی کرومیا و تبخیر Cr(VI) برای مدت طولانی بعد از کارکرد در دمای بالا پایدار نمی ماند که این خود می تواند الکترولیت و کاتد را آلوده نموده و کارکرد پیل سوختی را دچار مشکل کند. یکی از موثرترین اقدامات برای بهبود خصوصیات این صفحات اتصال دهنده استفاده از یک لایه پوششی بر روی زیر لایه به منظور بهبود هدایت الکتریکی، کاهش رشد لایه های اکسیدی و کاهش تبخیر کرم است.

تحقیقات اخیر بر روی ایجاد پوشش های محافظ – رسانا متمرکز شده اند . تکنیک های متعددی برای ایجاد پوشش بر روی فولادهای زنگ نزن فریتی به کار گرفته شده اند. این تکنیک ها شامل شامل آبکاری الکتریکی[۸-۵]، رسوب الکترو شیمیایی آندی [۹]، رسوب الکتروشیمیایی کاتدی و سمانتاسیون فشرده است [۱۳-۱۰]. تکنیک سمانتاسیون فشرده به دلیل هزینه ی کم، چسبندگی خوب رسوب داده شده بر روی زیر لایه و کاربرد گسترده مورد توجه قرار گرفته است.

هدف از این تحقیق مقایسه هدایت الکتریکی فولاد ضدزنگ Crofer 22 APU به عنوان تابعی از دما و زمان بود که در یک مخلوط پایه پودری کبالت ومنگنز پوشش داده شده بود.

مواد و روش تحقیق

در این تحقیق از فولاد ضد زنگ فریتی Crofer 22 APU با ترکیب شیمیایی ۲۲/۷٪ کرم، ۰/۳۸٪ منگنز، ۰/۰۲٪ سیلیسیم، ۰/۰۱٪ کربن و بقیه آهن استفاده شد. به منظور انجام آزمایشات اکسیداسیون دمای بالا ابتدا کبالت توسط عملیات سمانتاسیون فشرده بر روی زیرلایه ضدزنگ فریتی رسوب داده شد. برای ایجاد پوشش از این فولاد قطعاتی به ابعاد mm ۱۰mm×۵mm×۲ با دستگاه کاتر تهیه شد. در مرحله‌ی بعد نمونه ها با کاغذ سنباده SiC تا شماره ۱۲۰۰پولیش و با دستگاه آلتراسونیک در محلول استون و متانول چربی گیری شدند. از پودرهای کبالت، منگنز، اکسیدآلومینیوم و کلرید آمونیوم با دانه بندی ۱، ۱۵۰، ۱۸۰-۷۰ و ۲۴۰ میکرون استفاده شد. بهترین ترکیب پودر بدست آمده توسط محققین برای پوشش دهی کبالت به صورت ۱۰٪ وزنی Co، ۴٪ وزنی NH_4Cl به عنوان فعال کننده و ۸۶٪ وزنی Al_2O_3 است و مناسب ترین دما و زمان برای بدست آوردن بهترین کیفیت پوشش از لحاظ چسبندگی و عدم تخلخل ۸۰۰ ^oC به مدت زمان ۴ ساعت می باشد. همچنین بهترین ترکیب پودر بدست آمده برای پوشش دهی منگنز به صورت ۱۰٪ وزنی Mn، ۵٪ وزنی NH_4Cl به عنوان فعال کننده و ۸۵٪ وزنی Al_2O_3 است و مناسب ترین دما و زمان برای بدست آوردن بهترین کیفیت پوشش از لحاظ چسبندگی و عدم تخلخل ۸۰۰ ^oC به مدت زمان ۳ ساعت می باشد. برای انجام عملیات پوشش دهی از کوره تحت گاز آرگون استفاده شد. برای اندازه‌گیری مقاومت سطحی ویژه (ASR) نمونه‌های پوشش‌دار و بدون پوشش از تجهیزات نشان داده شده در شکل ۱ استفاده شد. سیم های پلاتینی به یک طرف نمونه ها که پولیش داده شده بودند جوش داده شد. به منظور جلوگیری از چسبیدن نمونه‌ها به یکدیگر و آلیاژ شدن و ایجاد نتایج غلط، نمونه‌های جوش داده شده با سیم‌های پلاتینی به مدت ۲۴ ساعت در دمای ۸۰۰ ^oC پیش اکسیداسیون شدند. برای جلوگیری از عدم اتصال

احتمالی نمونه‌ها از اتصالات نگه دارنده نشان داده شده در شکل ۱ استفاده شد. به منظور اندازه‌گیری مقادیر ASR از یک منبع جریان ثابت، با دانسیته‌ی جریان $500\ mA\ cm^{-2}$ استفاده شد و ولتاژ توسط ولتمتر در هر ۳۰ دقیقه اندازه‌گیری شد.با استفاده از قانون اهم و اطلاعات بدست آمده مقادیر ASR محاسبه شد.به منظور به دست‌آوردن مقاومت توزیع شده در اتصالات استفاده شده و سیم‌ها، دو سیم پلاتینی به دو طرف یک نمونه‌ی بدون پوشش جوش داده شدند و نتایج بدست آمده از نتایج تست اصلی کم شد. اندازه‌گیری ASR به عنوان تابعی از دما و زمان در هوای ساکن در کوره الکتریکی انجام شد.

نتایج و بحث

ارزیابی ASR به عنوان تابعی از دما

به منظور بررسی اثر دما بر روی مقاومت سطحی ویژه، ASR در دماهای مختلفی (از دمای ۴۰۰ تا دمای $1000\ ^{o}C$) برای نمونه‌های پوشش‌داده شده با کبالت و منگنز و نمونه های بدون پوشش بعد از پیش اکسیداسیون به مدت ۲۴ ساعت در دمای $800\ ^{o}C$ اندازه گیری شد. شکل ۲ مقادیر ASR را به عنوان تابعی از دما نشان می دهد. با افزایش دما مقادیر ASR افزایش پیدا می کند. این استدلال می تواند به وسیله ی معادله ی زیر اثبات شود [۱۶]. مقاومت سطحی ویژه یک آلیاژ اکسید شده را می توان به وسیله ی معادله ی زیر به دست آورد.

$$ASR = 2\frac{\sqrt{K^{*}t}}{\sigma^{*}}T \quad \exp\left(\frac{-1(1/2)E_0 + E_c}{kT}\right)$$

که K^* و σ^* ثوابت سهمی، E_o انرژی اکتیواسیون برای اکسیداسیون ، E_c انرژی اکتیواسیون برای هدایت، k ثابت بولتزمن و T دما است. بر اساس این معادله، افزایش دما منجر به افزایش مقادیر ASR می شود. همچنین در دماهای بالاتر، ضخامت بیشتری از لایه پوشش و زیر لایه تحت تاثیر واکنش های اکسیداسیون قرار خواهد گرفت و بنابراین ضخامت لایه اکسیدی کرومیا افزایش خواهد یافت و بر اساس معادله ی (۱) ASR افزایش خواهد یافت. در تمامی دماها مقاومت ویژه سطحی نمونه های پوشش دار کمتر از نمونه های بدون پوشش بود.

این به دلیل پوسته ی اکسیدی کرومیا است که در طول اکسیداسیون بر روی نمونه های بدون پوشش تشکیل می شود. هدایت الکتریکی کرومیا به طور چشم گیری کمتر از نمونه های پوشش دار است [۱۷].

ارزیابی ASR به عنوان تابعی از زمان

مقادیر ASR برای نمونه‌های پوشش‌داده شده و نمونه های بدون پوشش به عنوان تابعی از زمان در شکل ۳ نشان داده شده است. مقادیر ASR برای نمونه های بدون پوشش به طور سریع افزایش می یابد و به مقدار $۳۸/۷۴ m\Omega\ cm^2$ بعد از ۴۰۰

ساعت اکسیداسیون همدما می رسد. نمونه‌های پوشش‌داده شده ($23/15\ m\Omega\ cm^2$) مقدار مقاومت کمتری را بعد از زمان اکسیداسیون مشابه در دمای $800\ ^oC$ نشان دادند. شکل ۴ الگوی پراش اشعه ی ایکس نمونه های بدون پوشش (شکل ۴-a) و نمونه های پوشش داده شده را بعد از ۴۰۰ ساعت اکسیداسیون در دمای $800\ ^oC$ نشان می دهد.

در آنالیز XRD نمونه های بدون پوشش اسپینل $(Mn,Cr)_3O_4$، کرومیا و هماتیت مشاهده می شوند. حضور اسپیل $(Mn,Cr)_3O_4$ بر روی نمونه های بدون پوشش مربوط به فولادهای ضد زنگ فریتی است که به طور معمول مقدار کمی منگنز دارند. زمانی که آلیاژ در معرفی رنج دمایی $650-850\ ^oC$ قرار می گیرد لایه اسپینل $(Mn,Cr)_3O_4$ تشکیل می شود که غیر محافظ است [۱۸]. همچنین کرومیا که محافظ است در زیر لایه اسپینل تشکیل می شود [۱۸]. مقادیر ASR صفحات اتصال دهنده فولادی با رشد لایه اکسیدی افزایش پیدا می کند[۱۹].

فاکتورهای متعددی را می توان به افزایش مقاومت الکتریکی صفحات اتصال دهنده نسبت داد. فاکتور اصلی و مهم رشد لایه اکسیدی است [۲۰]. هدایت الکتریکی هر دو لایه اسپینل $(Mn,Cr)_3O_4$ و کرومیا به طور قابل توجهی کمتر از زیر لایه فلزی است [۱۷]. افزایش ضخامت لایه اکسیدی باعث افزایش مقادیر ASR می شود.

تشکیل اسپینل های محافظ $MnCo_2O_4$، $CoCr_2O_4$، $CoFe_2O_4$ و Co_3O_4 در نمونه های پوشش داده شده در طول اکسیداسیون هدایت الکتریکی نمونه های پوشش دار را بهبود داد. هدایت الکتریکی این اسپینل ها به طور چشم گیری بیشتر از هدایت الکتریکی لایه اسپینل $(Mn,Cr)_3O_4$، کرومیا و هماتیت است. فاکتورهای متعددی را می توان به بهبود هدایت الکتریکی نمونه های پوشش دار نسبت داد. این فاکتورها شامل هدایت الکتریکی زیاد لایه اسپینل تشکیل شده بر روی نمونه های پوشش دار و عدم وجود احتمالی حفره های تشکیل شده بر روی سطح نمونه ها است که موجب افزایش سطح تماس و افزایش هدایت الکتریکی می شود [۲۳و۲۲].

نتیجه‌گیری

۱-تشکیل اسپینل $(Mn,Cr)_3O_4$، کرومیا و سیلیکا در طول اکسیداسیون بر روی زیر لایه Crofer 22 APU منجر به افزایش مقادیر ASR شد که این به دلیل هدایت الکتریکی کمتر این ترکیبات نسبت به زیر لایه فلزی است.

۲-استفاده از ترکیبات اسپینل های $MnCo_2O_4$، $CoCr_2O_4$، $CoFe_2O_4$ و Co_3O_4 در نمونه های پوشش داده شده با کبالت و منگنز هدایت الکتریکی فولاد فریتی ضد زنگ مورد استفاده در سلول های سوختی اکسید جامد را افزایش داد.

۳- مقدار مقاومت ویژه سطحی بعد از ۴۰۰ ساعت اکسیداسیون همدما در دمای ^{o}C ۸۰۰ برای نمونه های پوشش داده شده با کبالت و منگنز $m\Omega\ cm^2$ ۲۳/۱۵ و برای نمونه های بدون پوشش $m\Omega\ cm^2$ ۳۸/۷۴ بدست آمد.

تشکر و قدردانی

این پژوهش با همکاری سازمان انرژی های نو ایران (سانا) انجام گرفته است و نویسندگان کمال تقدیر و تشکر را از این سازمان به دلیل حمایت های مالی دارند.

مراجع

[1] J.W. Fergus., "Metallic interconnects for solid oxide fuel cells", Materials Science and Engineering A., Vol. 397, No. 1-2, 271-283, 2005.
[2] P. Huczkowski, N. Christiansen, V. Shemet, J.P. Abellan, L. Singheiser and W.J. Quadakkers., "Oxidation induced lifetime limits of chromia forming ferritic interconnector steels", Journal of Fuel Cell Science and Technology., Vol. 1, No. 1, 30-34, 2004.
[3] W.Z. Zhu and S.C. Deevi., "Development of interconnect materials for solid oxide fuel cells", Materials Science and Engineering A, Vol. 348, No. 1-2, 227-243, 2003.
[4] H. Kurokawa, C.P. Jacobson, L.C. DeJonghe and S.J. Visco., "Chromium vaporization of bare and of coated iron-chromium alloys at 1073 K", Solid State Ionics., Vol. 178, No. 3-4, 287–296, 2007.
[5] X. Chen, P.Y. Hou, C.P. Jacobson, S.J. Visko and L.C. De Jonghe., "Protective coating on stainless steel interconnect for SOFCs: Oxidation kinetics and electrical properties," Solid State Ionics., Vol. 176, No. 5-6, 425–433, 2005.
[6] Z. Yang, G. Xia, S.P. Simner and J.W. Stevenson., "Thermal growth and performance of manganese cobaltite spinel protection layers on ferritic stainless steel SOFC interconnects", Journal of the Electrochemical Society., Vol. 152, No. 9, 1896-1901, 2005.
[7] Z. Yang, G. Xia, X. Li and J.W. Stevenson., "(Mn,Co)3O4 spinel coatings on ferritic stainless steels for SOFC interconnect applications", International Journal of Hydrogen Energy., Vol. 32, No. 16, 3648–3654, 2007.
[8] Z. Yang, G. Xia and J.W. Stevenson., "Mn1.5Co1.5O4 Spinel Protection Layers on Ferritic Stainless Steels for SOFC Interconnect Applications", Electrochemical and Solid-State Letters., Vol. 8, No. 3, A168–A170, 2005.
[9] W. Wei, W. Chen and D.G. Ivey., "Anodic electrodeposition of nanocrystalline coatings in the Mn-Co-O system", Chemistry of Materials., Vol. 19, No. 11, 2816–2822, 2007.

[10] M.R. Bateni, P. Wei, X. Deng and A. Petric., "Spinel coatings for UNS 430 stainless steel interconnects", Surface & Coating Technology., Vol. 201, No. 8, 4677–4684, 2007.
[11] P. Wei, X. Deng, M.R. Bateni and A. Petric., " Oxidation and electrical conductivity behavior of spinel coatings for metallic interconnects of solid oxide fuel cells", Corrosion Vol. 63, No. 6, 529–536, 2007.
[12] X. Deng, P. Wei, M.R. Bateni and A. Petric., "Cobalt plating of high temperature stainless steel interconnects", Journal of Power Sources Vol. 160, No. 2, 1225–1229, 2006.
[13] Y.S. Chou, J.W. Stevenson and P. Singh., "Effect of aluminizing of Cr-containing ferritic alloys on the seal strength of a novel high-temperature solid oxide fuel cell sealing glass", Journal of Power Sources., Vol. 185, No. 2, 1001-1008, 2008.
[14] H. Ebrahimifar and M. Zandrahimi " Pack cementation of SOFC ferritic stainless steel interconnects in a Co-base pack mixture", Int. J. Mater. Sci., Vol. 5, 465-472, 2010.
[15] H. Ebrahimifar and M. Zandrahimi "Coating of SOFCs interconnections with Mn by pack cementation method", J. Metallurgy & Materials Science, 51, 2009, 281-286.

[16] W.Z. Zhu and S.C. Deevi., "Opportunity of metallic interconnects for solid oxide fuel cells: a status on contact resistance", Materials Research Bulletin, Vol. 38, No. 6, 957–972, 2003.
[17] A. Holt and P. Kofstad, "Electrical conductivity and defect structure of Cr2O3. II. Reduced temperatures (<~1000°C) ", Solid State Ionics, Vol. 69, No. 2, 137-143, 1994.
[18] L. Cooper, S. Benhaddad, A. Wood and D.G. Ivey., "The effect of surface treatment on the oxidation of ferritic stainless steels used for solid oxide fuel cell interconnects", J. power sources, Vol. 184, No. 1, 220-228, 2008.
[19] K. Huang, P.Y. Hou and J.B. Goodenough., "Reduced area specific resistance for iron-based metallic interconnects by surface oxide coatings " Mater. Res. Bull, Vol. 36, No. 1-2, 81-95, 2001.
[20] N. Shaigan, D.G. Ivey and W. Chen., "Metal-oxide scale interfacial imperfections and performance of stainless steels utilized as interconnects in solid oxide fuel Cells", J. Electrochem. Soc, Vol. 156, No. 6, B765-B770, 2009.
[21] Ebrahimifar, H., and Zandrahimi, M., 2010, Evaluation of Electrical Resistance Activation energy of Coated Interconnects with Nano spinel, The 2nd national Nano Materials & Nano Technology conference May 4-5, 2010, esfahan, Iran.
[22] N. Shaigan, D.G. Ivey and W. Chen., "Oxidation and electrical behavior of nickel/lanthanum chromite-coated stainless steel interconnects", J. power sources, Vol. 183, No. 2, 651-659, 2008.
[23] N. Shaigan, W. Qu, D.G. Ivey and W. Chen., "A review of recent progress in coatings, surface modifications and alloy developments for solid oxide fuel cell ferritic stainless steel interconnects", J. power sources, Vol. 195, No. 6, 1529-1542, 2010.

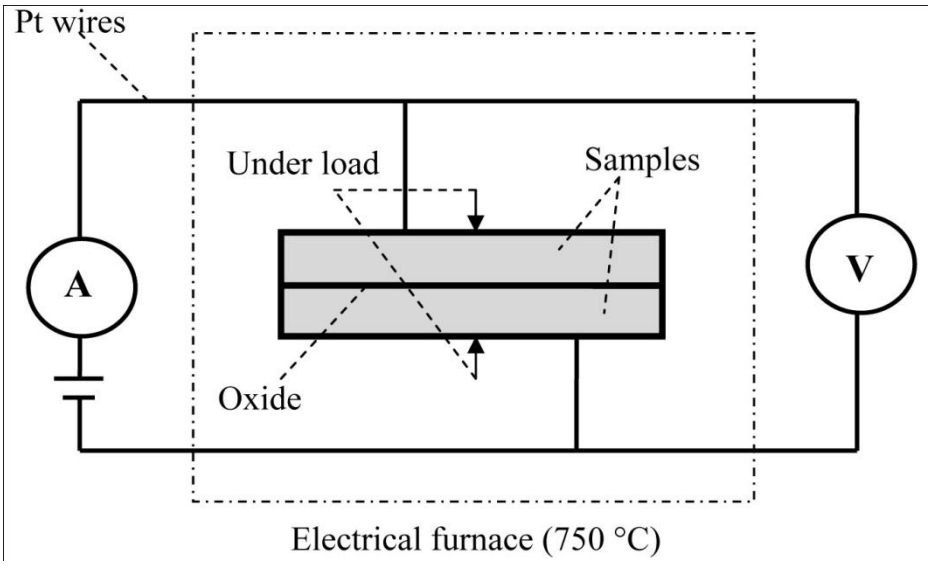

شکل ۱: منبع جریان ثابت، آمپرمتر، ولتمتر و گیره نگه دارنده برای اندازه گیری مقاومت الکتریکی

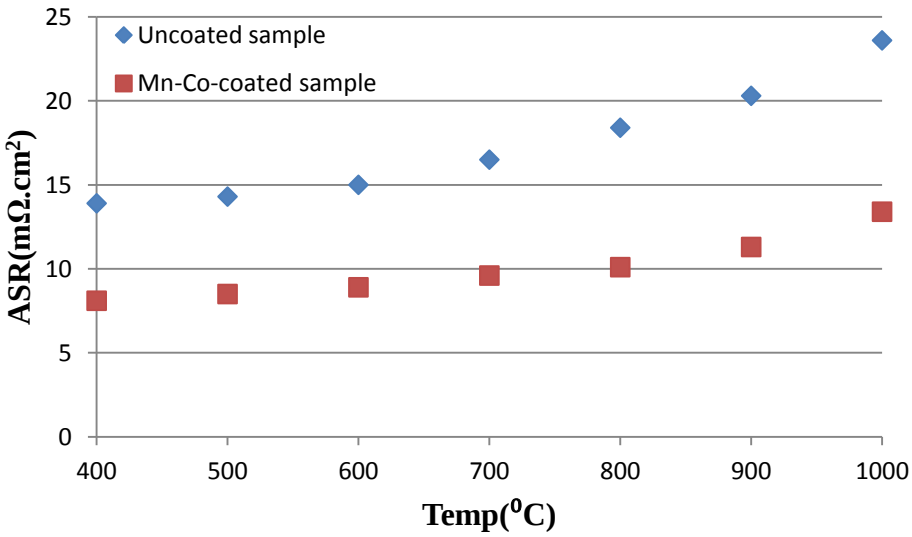

شکل ۲: مقادیر ASR اندازه‌گیری شده برای نمونه‌های پوشش‌داده شده و نمونه های بدون پوشش به عنوان تابعی از دما

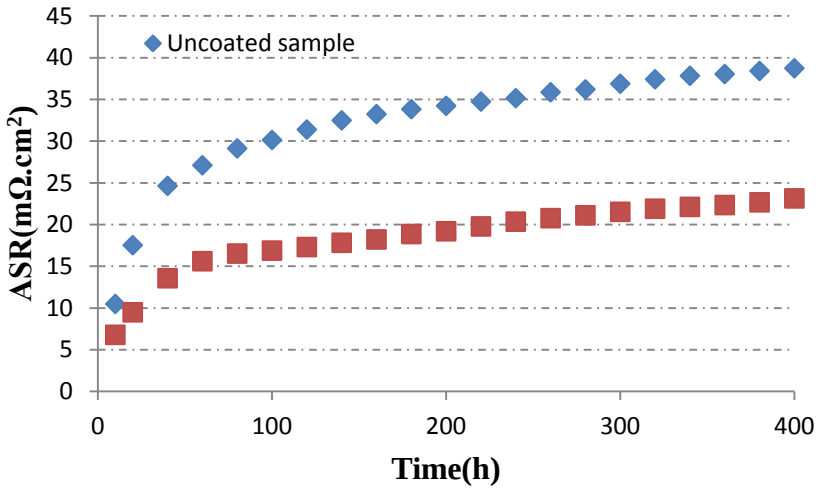

شکل ۳: مقادیر ASR اندازه‌گیری شده برای نمونه‌های پوشش‌داده شده و نمونه های بدون پوشش به عنوان تابعی از زمان اکسیداسیون

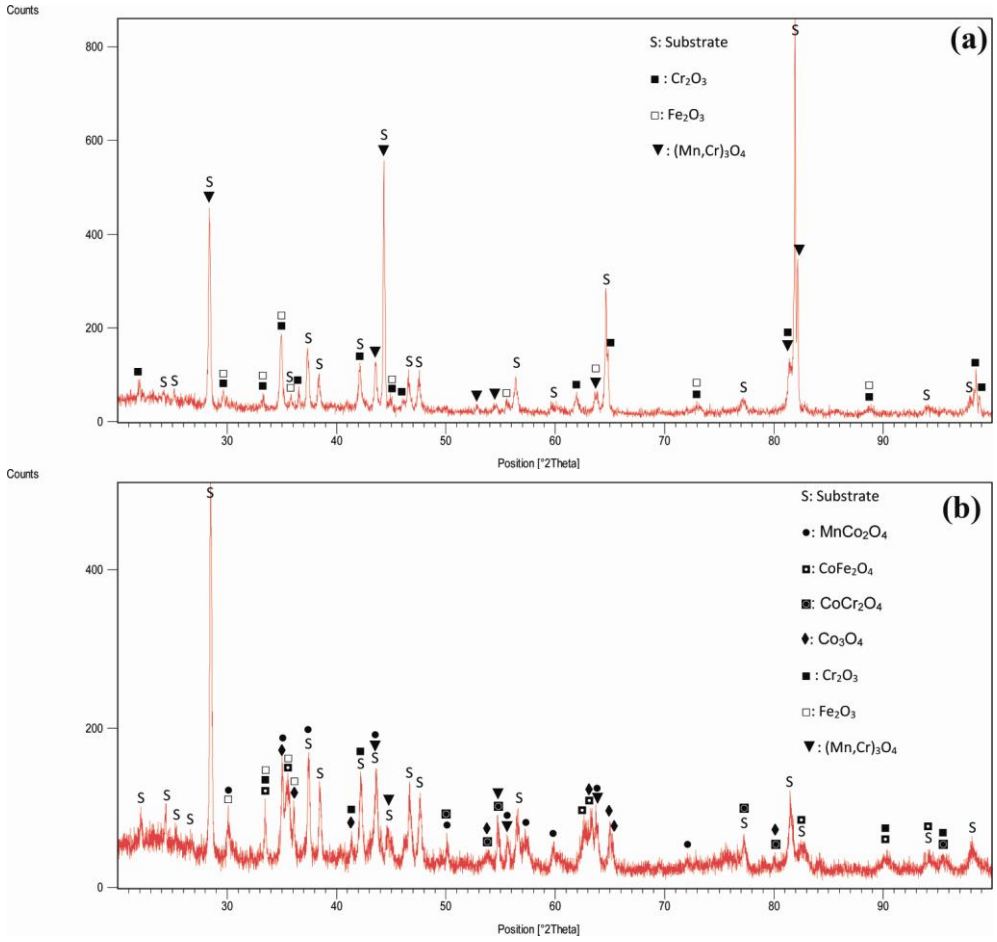

شکل ۴: الگوی XRD نمونه (a) بدون پوشش و (b) پوشش داده شده بعد از ۴۰۰ ساعت اکسیداسیون

تهیه و شناسایی نانوساختارهایFe-Ni- Pd و مطالعه خواص الکتروکاتالیستی آنها در جهت اکسیداسیون سوختهای متداول در پیلهای سوختی

سید سعید میررضی
دانشگاه آزاد واحد فراهان

چکیده

در این پروژه با استفاده از روشهای ترسیب الکتروشیمیایی و ایجاد زیر لایه آهن- نیکل بر روی فلز مس و مجدداً ترسیب الکتروشیمیایی جهت ایجاد پوشش آلیاژی Fe-Ni-Zn بر روی آهن- نیکل و در نهایت استفاده از فرآیند ساده زدایش انتخابی- جایگزینی گالوانیکی، فلزهای نجیب پلاتین و پالادیوم را جایگزین فلز فعال Zn نموده و بدین ترتیب کاتالیستهای Fe-Ni/Fe-Ni-Pd تهیه می¬شوند. زدایش انتخابی Zn و همچنین دوپ شدن نانو ذرات بر روی الکترود متخلخل حاصل به وسیله تکنیک‌های میکروسکوپ روبش الکترونی SEM مورد تایید قرار گرفت. افزایش خاصیت الکتروکاتالیستی الکترودهای تهیه شده به وسیله ولتامتری چرخه‌ای (CV) و تکنیک پلاریزاسیون بررسی شد. در نهایت با استفاده از الکترودهای تهیه شده، الکترو اکسیداسیون الکلهایی چون متانول مورد مطالعه قرار گرفت. نتایج نشان داد که الکترودهای تهیه شده نسبت به الکترود خالص پلاتین خاصیت الکتروکاتالیستی بالایی را در اکسیداسیون و احیای این گونه مواد دارند.

واژه‌های کلیدی: آلیاژ آهن-نیکل-پالادیوم، آبکاری، زدایش انتخابی، نانو ذرات فلزات نجیب، الکترواکسیداسیون، متانول.

۱-۱مقدمه

امروزه جهان در حال مواجه با یکی از مسایل جدی یعنی تخلیه منابع انرژی مرسوم مانند سوختهای فسیلی (ذغال سنگ، نفت و گاز طبیعی) است . از طرفی در هنگام استفاده از این مواد مشکلات زیادی مانند گرم شدن کره زمین، باران های اسیدی، آلودگی و تغییرات آب وهوا موجب پایین آمدن کیفیت زندگی بر روی کره زمین شده است . تحقیقات زیادی در مورد سوختهای جایگزین جهت حل کمبود انرژی انجام شده است ، مهمترین ویژگیهایی که سوختهای جایگزین باید داشته باشند، عبارتند از: تجدیدپذیر بودن ، داشتن دانسیته انرژی بالا به ازای واحد جرم آن ، نداشتن آثار سوء زیست محیطی راحتی در کاربرد و به صرفه بودن از لحاظ تجاری . در همین زمینه استفاده از انرژیهایی مانند انرژی باد، انرژی هسته ای ، انرژی خورشیدی ، انرژی هیدرودینا میکی آب، انرژی گرمایی موجود در زمین و انرژی شیمیایی موجود در مواد پر انرژی مانند سوختهای هیدروژنی و الکلی و.... در کانون توجه دانشمندان قرار گرفته است. در سالهای اخیر استفاده از پیلهای سوختی جهت تولید انرژی از منابع تجدیدپذیری نظیر هیدروژن و ..... اهمیت فراوانی پیدا کرده است.

پیلهای سوختی یک طبقه جالبی از منابع انرژی پایدار و تجدید شدنی را ایجاد کرده اند که جایگزین مناسبی برای منابع انرژی قراردادی مانند نفت، گاز طبیعی و ذغال سنگ است . تولید انرژی از نفت خام و گاز طبیعی با عمل احتراق در موتور گرمائی متناسب با محدودیت چرخه کارنو ذاتاً کافی نبوده و با آلودگی محیط همراه است. در عوض یک پیل سوختی ذاتاً بازده انرژی بالایی دارد ، آلوده کننده نبوده ، بی سروصدا و قابل اعتماد است .

۱ -۲ استفاده از الکلها به عنوان سوخت ها ، الکترواکسیداسیون الکل

از سده ی ۱۸۰۰ تا کنون سوختهای الکلی روز به روز اهمیت بیشتری پیدا میکنند . برای اولین بار در سال ۱۸۹۴ فرانسه و آلمان، از اتانول به عنوان یک سوخت در موتورهای احتراق استفاده کردند . در سال ۱۹۲۵ هنری فورد پیش بینی کرد که اتانول در آینده به عنوان یک سوخت مهم عمل خواهد کر [د ۱۷].

الکلها عمدتا به سه طریق به صورت سوخت استفاده میشوند :

۱ – به عنوان سوخت در موتورهای احتراقی (به جای بنزین)

۲ – به عنوان یک ماده اضافی مخلوط با سوخت اصلی برای افزایش عدد اوکتان

۳ - به عنوان یک سوخت جهت تبدیل مستقیم انرژی شیمیایی به انرژی الکتریکی(در پیلهای سوختی)

الکلها از خانواده ترکیبات اکسیژن دار و هیدروکربنهایی با گروه عاملی هیدروکسی هستند. متانول، اتانول ، پرپانول و بوتانول چهار الکل سادهای هستند که به عنوان سوخت کاربردهای فراوانی یافته اند. هدف از به کار بردن الکل (ها چه در پیلهای سوختی و چه در موتورهای احتراق) اکسایش کامل و تبدیل آنها به دی اکسید کربن و آب و تولید انرژی است . ولی در واقع در حین اکسایش الکلها بر اثر سوختن ناقص محصولات جانبی زیادی از قبیل مونواکسیدکربن، آلدهیدها، کربوکسیلات ها ، و حتی کتونها ایجاد میشوند که این محصولات راندمان انرژی فرایند را کاهش داده و باعث مسمومیت کاتالیستها میشوند .

۲- مواد وروش ها

۲-۱ مواد شیمیای مورد استفاده:

۱- سولفات نیکل ۶ آبه $NiSO_4.6H_2O$, (Merck,99%)

۲- سولفات آهن

۳- سولفات روی

۴- اسید سیتریک

۵- اسید سولفوریکH_2SO_4, (Merck6 %98)

۶- هیدروکسید سدیم NaOH , (Merck)

۷- هیدرواکسید پتاسیم KOH , (Merck)

۸- متانول CH_3OH , (Merck,99%)

۱۱- -کلرید پالادیوم $PdCl_2$, (Merck,99%)

۱۲- رزین پلی استر،کاتالیزور کبالت،سخت کننده (Hardner)

۱۳- کاغذ سمباده

۲-۲ دستگاه های مورد استفاده

۱- منبع تامین کننده مستقیم (DC) ولتاژ(Jps-302D ELECTRONIC AFZAR AZMA)

۲- ترازوی دیجیتالی

۳- همزن مغناطیسی

۴- هیتر ودماسنج

۵- دستگاه پتاسو استات - گالوانو استات (SAMA 500)

۶- الکترود صفحه ای پلاتین

۷- الکترود رفرنس کالومل اشباع

۲-۳ روش انجام تحقیق:

روش انجام این تحقیق کاملاً آزمایشگاهی و عملی بوده که در زیر کارهای مورد نظر برای انجام آزمایشات آورده شده است.

۱- تهیه الکترودهای مس در ابعاد ۱×۱ سانتیمتر مربع به همراه مانت کردن، پولیش زدن، چربیگیری و اسیدشویی

۲- تهیه سیم های به اندازه ۱۲سانتیمتر و قطر ۱,۵سانتیمتر

۳- لحیم کردن سیم ها بر روی الکترودهای مس

۴- مانت کردن الکترود های لحیم شده

۵- پولیش زدن مانت با سمباده های ۸۰-۲۲۰-۸۰۰-۲۵۰۰

۶- چربیگیری و اسیدشویی اکترود مانت شده

۷- انجام آزمایشات اولیه جهت بهینه سازی محلول های آبکاری مختلف.

۸- تهیه الکترودهای Fe-Niاز محلولهایی آبکاری بهینه شده.

۹- تهیه الکترودهای Fe-Ni-zn از محلولهایی آبکاری بهینه شده

۱۰- لیچ کردن وتهیه الکترودهای Fe-Ni-pd

که به این منظور الکترود های Fe-Ni-zn که از پیش آماده کرده بودیم را به مدت ۲۴ ساعت در محلول قلیایی حاوی پلاتین قرار میدهیم تا پالادیوم جایگزین روی شود

۱۲- شناسائی مورفولوژی سطح و ساختار الکترودهای تهیه شده جهت اثبات نانو بودن اندازه ذرات و تعیین درصد وزنی و اتمی عناصر موجود در الکترود

۱۳-انجام مطالعات الکتروشیمیایی در محلولهای قلیایی با استفاده از تکنیکهای مختلف الکتروشیمیایی

۱۴- جمع آوری و ترسیم منحنیها و داده‌های الکتروشیمیایی ثبت شده از دستگاه انجام تستهای الکتروشیمیایی مانند پتانسیواستات- گالوانواستات

۱۵- تجزیه و تحلیل تمام داده‌های حاصل از مطالعات مورفولوژی و الکتروشیمیایی و تعیین مناسبترین الکترود برای اکسیداسیون الکتروشیمیایی متانل و سدیم بوروهیدرید در محلولهای قلیایی

۲-٤ آماده سازی الکترود

۲ -٤-۱ چربی زدایی و اچ کردن مس

ابتدا فویل مس (با ضخامت mm۱) با خلوص بالا (۹۹/ ۹۹٪)با ابعاد ۱× ۱ cm بریده شد و سپس در قالب های خاص، به وسیله ریزین پلی استیرن مانت شد. این نمونه ها به وسیله سمباده به تر تیب از زبر تا نرم (۴۰۰-۲۵۰۰) سمباده شد، تا سطح نمونهٔ مس کاملاً صاف و آینه ای شود پس از شستشو با آب مقطر این نمونه ها برای چربیگیری به مدت ۵ دقیقه در محلول ٪ ۳۰ وزنی سود سوز آور غوطه ور شد. سپس به منظور اچ کردن و زدودن فیلمهای اکسیدی روی سطح مس، مجددا با آب مقطر شستشو داده شد و به مدت یک دقیقه در محلول ٪ ۱۰ وزنی اسید سولفوریک و ٪ ۱۰ وزنی آب اکسیژنه غوطه ور گردید.در نهایت نمونه با آب مقطر شسته شد، تا به طور کلی سطح چربی زدایی و اچ شده و برای آبکاری آماده شود

۳ نتایج

۳-۱ نتایج SEM

تصاویر SEM موجود در شکل ۳-۱ آمده است.

همانگونه که در شکل ۳- ۱ نشان داده شده است پوشش نیکل-روی- آهن پس از آنکه در محلول قلیایی غلیظ به همراه مقدار اندکی نمک پالادیوم کلرید قرار میگیرد حالت متخلخل پیدا میکند. وجود ترک در این شکل کاملا واضح و مشخص است. این میکروترکها سطح موثر الکترود مورد نظر را به میزان قابل توجهی افزایش داده و باعث افزایش خواص الکتروکاتالیتیکی آن میشوند. اما نکته مهم دیگر که در این شکل دیده می شود پراکندگی نسبتا یکنواخت نانوذرات پالادیوم بر روی سطح این الکترود است.

۳ -۲ آنالیز عنصری(EDAX) پوشش های تهیه شده

نتایج آنالیز عنصری برای الکترودهای Ni/Ni-Zn-Pdلیچ شده در شکل۳ - ۲ آمده است

۳-۳ بررســـی خـــواص الکتروکاتالیســـتی الکترودFe/Fe-Ni -pd برای الکترواکسیداسیون متانول و اتانول

یکی از مزایای روش جایگزینی گالوانیکی این است که تمامی ذرات دوپه شده روی سطح مینشینند و به این ترتیب مصرف فلزات گران قیمت نجیب به حداقل ممکن میرسد. در بسیاری از روشهای دیگر چنین چیزی وجود ندارد به عنوان مثال در روش آبکاری آلیاژی فلزات نجیب با نیکل مقداری از فلز نجیب در عمق پوشش قرار گرفته و در فصل مشترک الکترود با محلول قرار نمیگیرد

۳ -۴-۱ نتایج حاصل از ولتامتر ی چرخه ای بـرای الکترواکسیداسـیون متـانول بـر روی الکترود Fe/Fe-Ni -pd

شکل ۳- ۳ مقایسهای بین الکترواکسیداسیون الکلها بر روی سـه الکتـرود Smooth Pd و نیـز Fe/Fe-Ni -pd لیچ شده و Fe/Fe-N در محلول هیدروکسید سدیوم ۱ مولار در دمای ۲۵ درجه سانتی گـراد و در سرعت اسکن ۵۰ میلی ولت بر ثانیه را نشان میدهد.

منحنی a مربوط به الکترود Smooth Pd ، منحنی b مربوط به الکترود Fe/Fe-Ni و منحنـی c مربوط به الکترود Fe/Fe-Ni -Pd لیچ شده است.در این شکل چند نکته قابل توجه است. یکی پیکهای مرسوم نیکل و پلادیوم در محیط قلیایی است که ترتیب افزایش آنها به صورت زیر است:

Fe/Fe-Ni- Pd >Fe/Fe-Ni > smooth Pd

بیشتر بودن دانسیته جریان پیکهای آندی و کاتدی Fe/Fe-Ni نسبت به smooth Pd را میتوان بـه افزایش سطح موثر الکترود Fe/Fe-Ni نسبت داد ، که در بخش گذشته نیز در مورد آن بحث شد. امـا در مـورد افزایش دانسیته جریان الکترود Fe/Fe-Ni- Pdنسبت به الکترود Fe/Fe-Ni چگونه میتوان قضاوت کرد؟

علت این پدیده را میتوان به وجود اثر تزایدی دو فلز نیکـل و پـالادیوم بـر روی یکـدیگر نسـبت داد . همانگونه که خواهیم دید این اثر الکترو اکسیداسیون الکلها را نیـز روی سـطح هـر دوی ایـن فلـزات تسـهیل میکند. اثر تزایدی دو فلز نیکل و پالادیوم را میتوان به صورت زیر توضیح داد:

هنگامی که پالادیوم با نیکل آلیاژ میشود ، انرژی اوربیتالهای d بـرای پـالادیوم کـاهش و بـرای نیکـل افزایش مییابد این امر باعث میشود که جذب گونههای مختلف بر روی سایتهای فعال پالادیوم ضعیف تر و بر روی سایتهای فعال نیکل قویتر گردد . بدین ترتیب جذب گونه Ni3+ بروی سطح الکترود افزایش یافته و هر دو پیک آنـدی و کاتـدی کـه مربـوط بـه زوج ردوکـس Ni2+ / Ni3+ مـی باشـد افـزایش ارتفـاع داشـته باشند. .همانگونه که گفته شد زوج ردوکس Ni2+ / Ni3+ نقش کلیدی را در اکسیداسیون الکلها بازی مـی کنـد لـذا انتظار میرود الکترواکسیداسیون الکلها روی سطح الکترود Fe/Fe-Ni- Pd لیچ شـده نیـز نسـبت بـه الکتـرود Fe/Fe-Ni تسهیل گردد .

شکل۳-۴ ولتاموگرام الکترود پالادیوم خالص با مساحت1cm2 در محلول هیدروکسید سدیم ۱ مولار را در دمای ۲۵ درجه سانتیگراد در سرعت اسکن ۵۰ mV/s نشان میدهد .

همانگونه که در این شکل دیده میشود در این منحنی نیز در حدود V ۰/۴- یک پیک دیده میشود.
این پیک را میتوان به فرایند انتقال الکترون زیر نسبت داد.

$$Pd(OH)_2 + 2e^- \rightarrow Pd + 2OH^-$$ ۱۰-۳

وجود این پیک نیز اثبات کننده ترسیب پالادیوم بر روی سطح الکترودFe/Fe-Ni- Pd است.مقایسه دانسیته جریان پیک مزبور در دو شکل ۳-۴وشکل ۳- ۳ نشان دهنده دانسیته جریان بسیار بیشتر برای الکترودFe/Fe-Ni- Pd است که این امر میتواند ناشی از سطح بسیار بالای نانو ذرات دوپ شده بروی الکترود Fe/Fe-Ni- Pd لیچ شده باشند.
در ۳شکل - ۱۵ در منحنی c یک پیک پهن در محدوده حدودتا V۰/۴-تا V ۰/۰۱- دیده میشود که این پیک مربوط به واجذب هیدروژن جذب شده روی سطح الکترود است . افزایش جریان کاتدی که در این منحنی پس از این پیک دیده میشود، مربوط به واکنش آزادسازی هیدروژن میباشد.
شکل۳ - ۵ نشان دهنده ولتاموگرام الکترودFe/Fe-Ni- Pd لیچ شده در محلول ۱ مولار هیدروکسید سدیم به علاوه ۰/۱ مولار متانول است
ظهور پیکهایی در نواحی V ۰/۲- و V ۰/۵- (پیکهای c و e) نشان دهنده اکسیداسیون متانول بر روی پالادیوم ترسیب شده روی سطح الکترود Fe/Fe-Ni- Pd است[.]۸۳ در واقع پیک c مربوط به اکسیداسیون
متانول بر روی سطح پالادیوم است، در مورد ماهیت پیک e در بین محققین اختلاف نظر وجود دارد [ ].۸۱
بعضی این پیک را مربوط به اکسیداسیون مجدد گونههای جذب شده بر روی سطح پالادیوم و برخی دیگر آن را مربوط به اکسیداسیون مولکولهای متانول موجود در بطن محلول دانسته اند.

۳-۳-۲ اثر افزایش سرعت اسکن بر الکترو اکسیداسیون متانول بر روی الکترود Fe/Fe-Ni- Pd لیچ شده
شکل ۳- ۶ ولتاموگرام محلول ۱ مولار هیدروکسید سدیم به علاوه ۰/۱ مولار متانول بر سطح الکترود Fe/Fe-Ni- Pd لیچ شده را نشان میدهد.
در این شکل در ناحیه روبش آندی (رفت) در پتانسیل حدود -۰/۲ ولت یک پیک دیده می شود .این پیک مربوط به اکسیداسیون متانول بر روی سطح الکترود است و همانگونه که در این شکل دیده میشود با افزایش سرعت اسکن، پتانسیل پیک به سمت مقادیر مثبت جابجا شده و جریان این پیک افزایش مییابد.
۳ -۳-۳ اثر افزایش دما بر الکترواکسیداسیون متانول بر روی الکترود Fe/Fe-Ni- Pd لیچ شده
به منظور بررسی نقش دما در الکترواکسیداسیون متانول بر روی الکترود Fe/Fe-Ni- Pd لیچ شده و همچنین محاسبه انرژی فعال سازی اکسیداسیون متانول ، الکترواکسیداسیون متانول در دماهای مختلف مو رد بررسی قرار گرفت(۳شکل -) ۲۲ همان طور که از شکل دیده می شود، افزایش دما باعث افزایش دانسیتهٔ جریان آندی می شود که نشان دهندهٔ تامین انرژی فعال سازی برای الکترو اکسیداسیون متانول در سطح الکترودFe/Fe-Ni- Pd لیچ شده است. همچنین با افزایش دما همان طور که ملاحظه می شود، پتانسیل پیک به مقادیرمثبت تر جابه جا می شود. این امر احتمالا به این دلیل است که مرحله تعیین کننده سرعت در مکانیزم این واکنش گرماگیر است

٤-١ نتیجه گیری

١ - افزایش سطح فعال یک الکترود، باعث افزایش خاصیت الکتروکاتالیستی الکترود برای الکترواکسیداسیون و احیای گونه های الکتروفعال می شود. افزایش سطح الکترود به وسیلهٔ بستر های مناسب با خلل و فرج فراوان به عنوان پایه برای دوپ فلزات نجیب انجام می گیرد .

٢- روش زدایش انتخابی، روشی بسیار موثر و مفید جهت تولید کاتالیستهای با سطح موثر و در نتیجه خواص الکتروکاتالیستی بالا است .

٣- کوپل کردن روش زدایش انتخابی با روش جایگزینی گالوانیکی برای دوپه کردن نانو ذرات فلزات نجیب بر سطح الکترود نیکل متخلخل ،علاوه بر داشتن مزایایی از قبیل سادگی و مصرف کمتر نمک فلز نجیب، باعث میشود که فعالیت الکتروکاتالیستی الکترود تهیه شده به شدت افزایش یابد .

۴- الکترودهای متخلخل برپایه نیکل به خاطر ویژگی های منحصر به فرد به خصوص به علت داشتن خلل و فرج زیاد در سطح و مساحت فعال زیاد می تواند به عنوان یک بستر برای دوپ انواع فلزات مخصوصاً فلزات نجیب استفاده شود .

۶- دوپ کردن نانوذرات فلزات نجیب پلاتین و پالادیوم به روش گالوانیکی بر روی الکترود آلیاژی Fe- Ni-Zn به روش گالوانیکی به همراه زدایش انتخابی Zn در محلول قلیایی غلیظ به مدت ۲۴ ساعت انجام گرفت . بررسی های مورفولوژی به وسیلهٔ SEM نشان می دهد که نانو ذرات پلاتین با اندازه های در حد نانو(نانومتر) به خوبی بر روی سطح الکترود مورد نظر پخش شده است و این مهم باعث افزایش سطح الکترود و تغییر انرژی اوربیتالی در هر دو فلز می شود که در بالا رفتن خاصیت کاتالیستی و الکتروکاتالیستی الکترود موثر است

٧- نتایج حاصل از ولتامتری چرخهای و طیف سنجی امپدانس الکتروشیمیایی نشان داد که الکترودهای تهیه شده به روش فوق دارای فعالیت الکتروکاتالیستی بسیار بالایی هم برای الکترواکسیداسیون ال کلهایی از قبیل متانول و اتانول و هم برای فرآیند آزادسازی هیدروژن میباشند

منابع

1. Kato T, Kubota M, Kobayashi N, Suzuoki Y, 2005, Effective utilization of by-product oxygen from electrolysis hydrogen production, Energy 30:2580–95.
2. Kai Zeng, Dongke Zhang, 2010, Recent progress in alkaline water electrolysis for hydrogen production and applications, Progress in Energy and Combustion Science 36: 307–326.
3. N.R. Elezovi´ c a, V.D. Jovi´ c a, N.V. Krstaji´c, 2005, , Kinetics of the hydrogen evolution reaction on Fe–Mo film deposited on mild steel support in alkaline solution, Electrochimica Acta .٥٦٠١–٥٥٩٤ :٥٠
4. A. Lasia, 1999, Electrochemical Impedance Spectroscopy and Its Applications, Modern Aspects of Electrochemistry, B. E. Conway, J. Bockris, and R.E. White, Edts., Kluwer Academic/Plenum Publishers, New York, Electrochimica Acta 50: 5594–5601.

5. A. Lasia, 2002 , Modern Aspects Of Electrochemistry , B. E. Conway, J. Bockris, and R.E . White, Edts, Kluwer Academic/Plenum Publishers New York, Vol. 35 p. 13-19.
6. Shelley Minteer , Alcoholic Fuels, Published in 2006 by CRC Press Taylor & Francis Group.
7. S.K. Kamarudina,b, F. Achmada , W.R.W. Dauda, 2009, Overview on the application of direct methanol fuel cell (DMFC) for portable electronic devices, International Journal Of

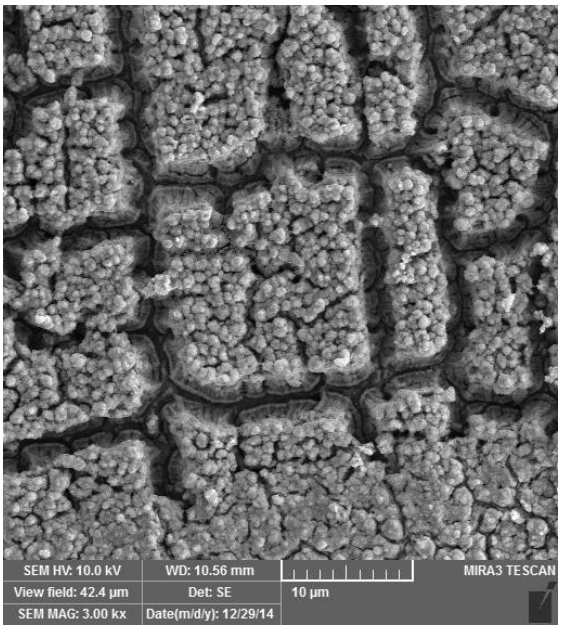

شکل۳-۱ تصاویر SEM الکترود Fe/Fe-Ni- Pd

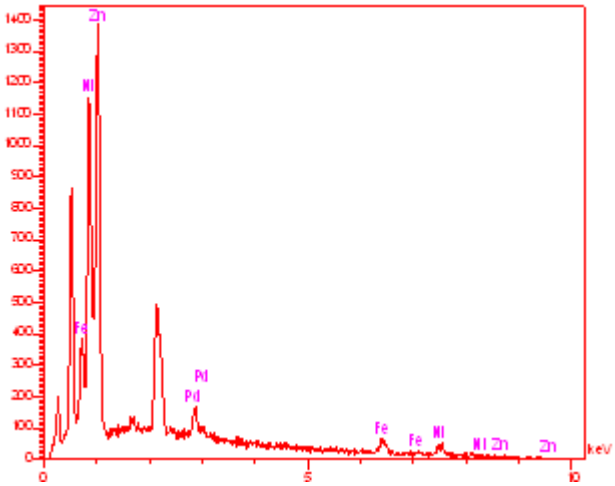

شکل ۳-۲ تصاویر EDAX الکترود Fe/Fe-Ni- Pd

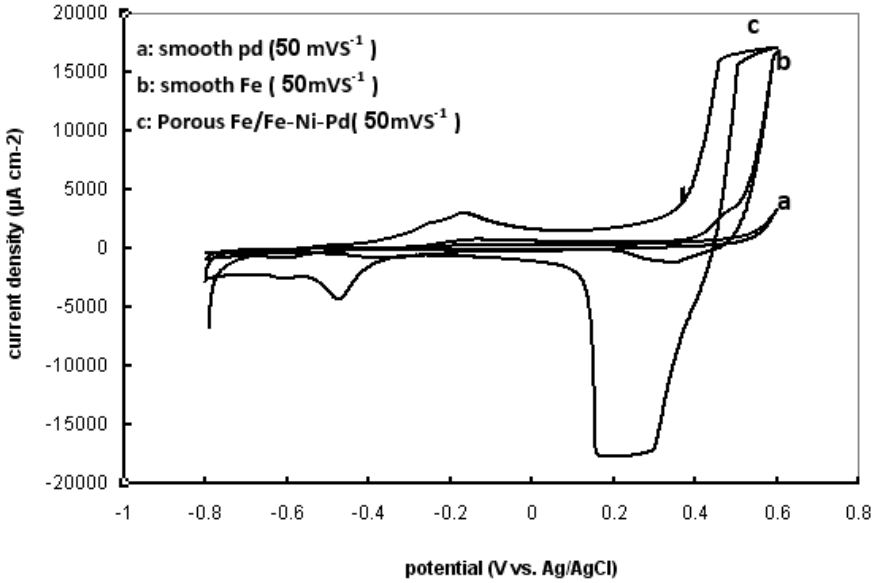

شکل ۳ -۳ مقایسهای بین الکترواکسیداسیون الکلها بر روی سه الکترود Smooth Pdو نیز Fe/Fe-Ni -Pd متخلخل و-Fe/Fe Ni در محلـول هیدروکسید سدیوم ۱ مولار

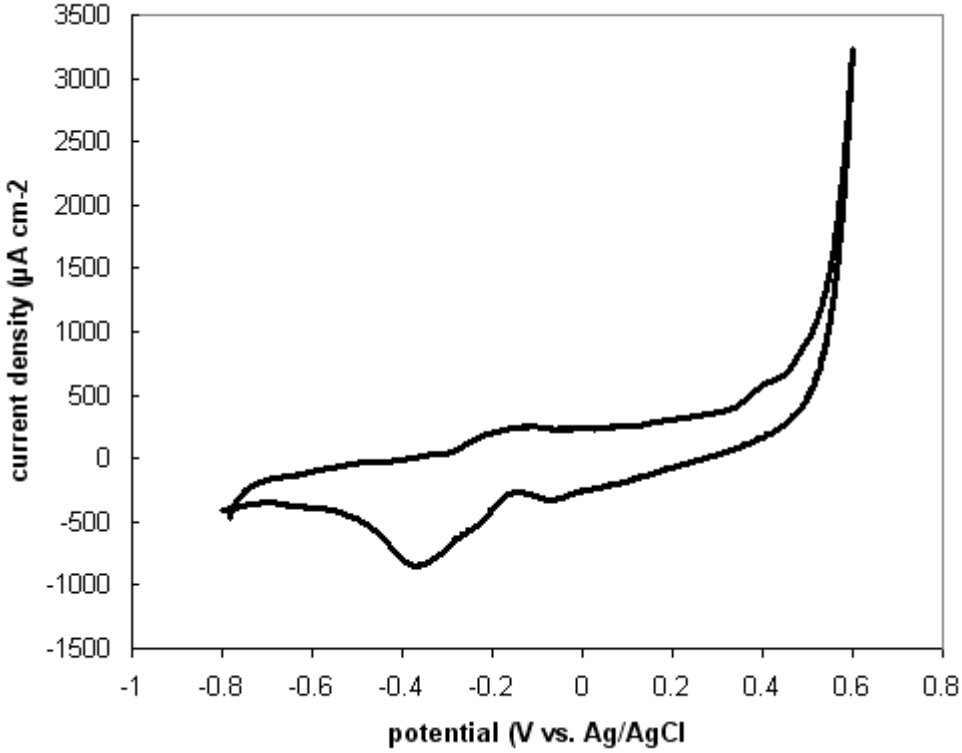

شکل ۳-۴ ولتاموگرام الکترود پالادیوم خالص با مساحت ۱Cm2 در محلول هیدروکسید سدیم ۱ مولار

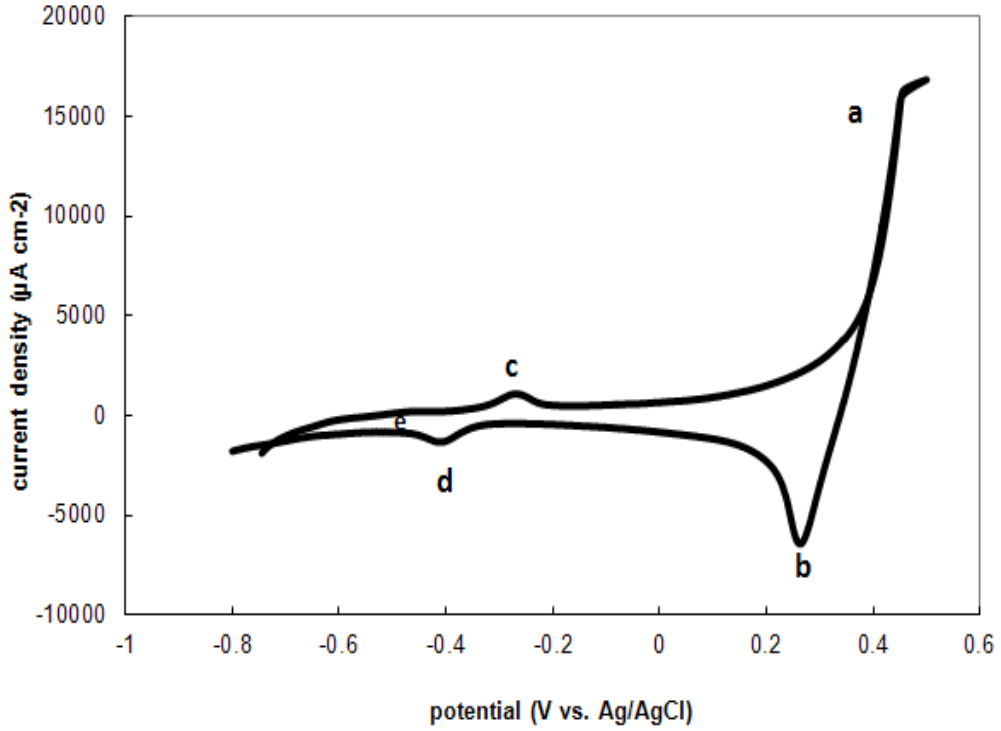

شکل ۳ -۵ ولتاموگرام الکترود Fe/Fe-Ni- Pd در محلول ۱ مولار هیدروکسید سدیم به علاوه ۰/۱ مولار متانول

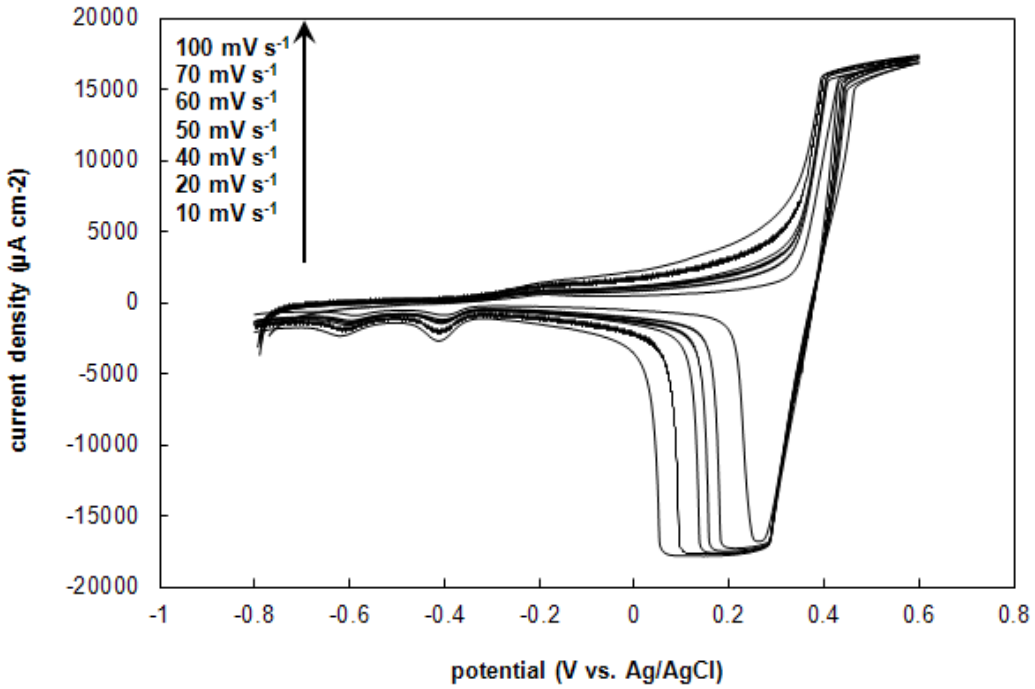

شکل ۳-۶ اثر سرعت اسکن بر ولتاموگرام محلول ۱ مولار هیدروکسید سدیم به علاوه ۰/۱ مولار متانول بر سطح الکترود-Fe/Fe Ni- Pd لیچ شده

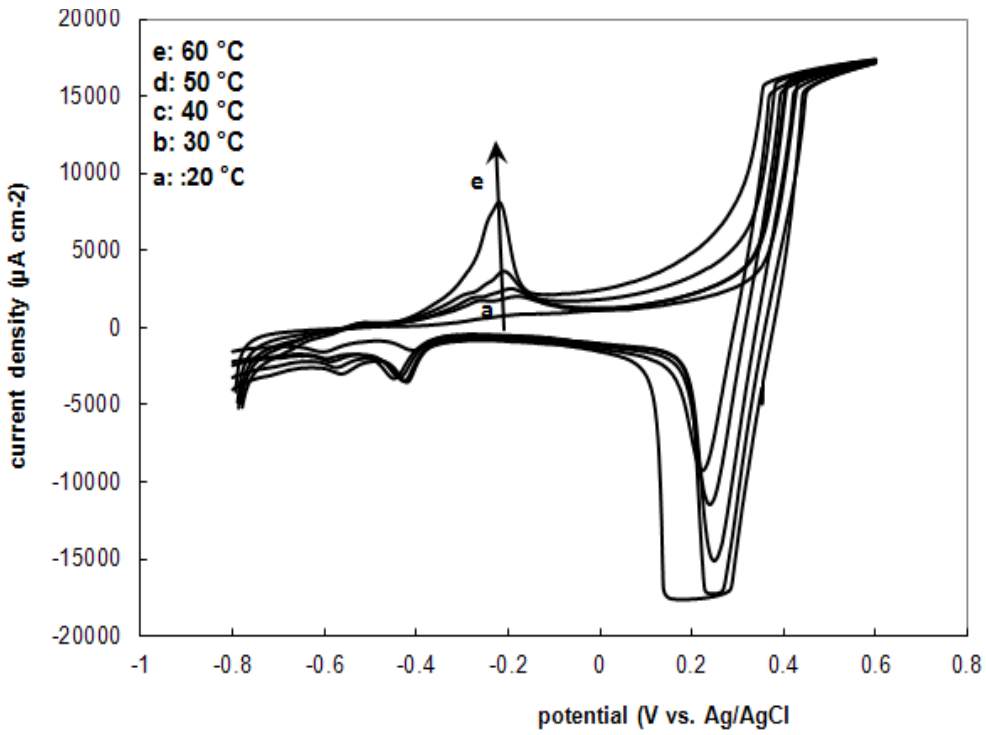

شکل ۳ –۷ تاثیر دما در الکترواکسیداسیون متانول با غلظت ۰/۱ M درسطح الکترود Fe/Fe-Ni- Pd لیچ شده با سرعت اسکن ۵۰ mv/s

استفاده از مواد مختلف پایه کربنی به عنوان الکترود کاتد در پیل سوختی میکروبی

مهرداد مشکور[۱*]، مصطفی رحیم نژاد[۱]، مهدی مشکور[۲]، مریم اصغری[۳]

۱. مرکز تحقیقاتی سوخت‌های زیستی و انرژی‌های تجدید پذیر، دانشکده مهندسی شیمی، دانشگاه صنعتی نوشیروانی بابل، بابل، ایران
۲. دانشکده مهندسی چوب وکاغذ، دانشگاه علوم کشاورزی و منابع طبیعی گرگان، گرگان، ایران
۳ . دانشکده شیمی، دانشگاه مازندران، بابلسر، ایران
** m.mashkour1990@gmail.com*

چکیده

استفاده از پیل‌های سوختی میکروبی به عنوان یکی از منابع تجدید پذیر تامین انرژی مدتی است که مورد مطالعه و بررسی قرار گرفته و امروزه به عنوان یکی از موضوعات مورد علاقه پژوهشگران محسوب می‌شود. قسمت های اصلی یک پیل سوختی میکروبی شامل محفظه های آندی و کاتدی وغشای تبادل پروتون می باشد که ما از این بین محفظه کاتدی را بررسی کردیم. از مواد مختلف پایه کربنی به علت رسانایی خوب آن‌ها به عنوان الکترود کاتد استفاده کردیم. با استفاده ازکاتدهای گوناگون و تغییر شرایط کاتولیت توانستیم الکترود مناسب را از بین الکترودهای موجود که شامل:گرافیت وکربن پارچه‌ای بود، مشخص سازیم.

واژه‌های کلیدی: انرژ ی تجدید پذیر، پیل سوختی میکروبی، الکترود، کاتد،گرافیت، کربن پارچه‌ای.

مقدمه

مصرف منابع ، تولید پساب و تخریب محیط زیست ، به واسطه رشد جمعیت و صنعتی سازی جوامع ، سرعت روزافزونی یافته است و این منجر به افزایش مصرف انرژی ، هم به منظور کاربرد روزانه و هم به منظور تصفیه پساب گشته است. منابع اصلی تامین انرژی همچنان نفت و گاز هستند اما این منابع فسیلی محدودند و در آینده نزدیک گران و کمیاب خواهند شد.همچنین فاجعه‌ی آلودگی زیست‌محیطی ناشی از سوخت های فسیلی، گرم شدن هوا و اثر گلخانه‌ای ، سبب رویکرد محققین به روش‌های جدیدتولید انرژی ازدیگرمنابع باد و ویژگی مهم قابلیت تجدیدپذیری وغیرمخرب بودن برای محیط زیست، شده است.[۱]

از جمله انرژی‌های مطرح شده، انرژی الکتریکی تولید شده به وسیله پیل‌های سوختی میکروبی است، که به دلیل توانایی تبدیل مستقیم سوخت به انرژی الکتریکی به وسیله واکنشهای اکسایش-کاهش مورد توجه زیادی

قرارگرفته است. روند کار به این صورت است که الکترون منجر به تولیدجریان الکتریسیته می شود. پروتون با عبور از غشاء تبادل یونی به سمت کاتد رفته با اکسیژن هوا و الکترون بازگشتی از پیل به آب تبدیل می‌شود.[۲]

ضرورت انتخاب جایگزین مناسب، ارزان قیمت و پاک بجای سوخت‌های فسیلی ضرورتی اجتناب ناپذیر است. و از جمله انرژی‌های مطرح، انرژی الکتریکی تولید شده به وسیلهٔ پیل‌های سوختی می باشد، که به دلیل بازدهی بسیار بالا و عدم آلایندگی محیط‌زیست و نیز مصرف هیدروژن ، متانول،بیومس و... به عنوان سوخت، در حال حاضر راه‌حل مناسبی جهت عبور از تنگنای انرژی و آلودگی محیط‌زیست می‌باشد [۳]. در درون پیل های سوختی انرژی شیمیایی حاصل از یک واکنش شیمیایی به انرژی الکتریکی مفید تبدیل می گردد. لازم به ذکر می باشد که تبدیل انرژی در درون پیل های سوختی تبدیل مستقیم انرژی شیمیایی به انرژی الکتریکی می باشد.عملکرد پیل سوختی مانند باتری نیست که انرژی را ذخیره کند، بلکه در پیل سوختی حالتی از انرژی به حالت دیگر تبدیل می‌شود. تکنولوژی پیل سوختی میکروبی جدیدترین تکنولوژی تولید الکتریسته و بیو الکتریسته است که از بیومس به وسیله باکتریها بدست می آید. در سال ۱۹۱۱ اولین پدیده جریان الکتریسته به کمک میکروارگانیزمها اعم از باکتریها و میکروبها توسط پورت شناسایی شده است. پس از گذشت ۵۵ سال تحولی در توسعه و پیشرفت چشمگیری در کاربری این گونه فرایندها صورت گرفته است.

در یک پیل سوختی بطور پیوسته انرژی شیمیایی به انرژی الکتریکی تا زمانیکه سوخت و اکسیدان در درون سل فراهم باشد تبدیل می گردد. با توجه به بحران های به وجود آمده در زمینه انرژی پیشرفت های زیادی در زمینه پیل های شیمیایی در حال انجام می باشد. بهره دهی بالا از مزایای عمده این نوع از پیل ها می باشد اما هزینه های بالای کاتالیروزها و دمای عملیاتی بالا و خورنده بودن محلول الکترولیت از معایب این نوع از پیل ها می باشد.در این رابطه پیلهای سوختی بیولوژیکی جذاب و امید بخش می باشند[۴].

پیلهای سوختی بیولوژیکی یکی از انواع از پیل های سوختی می باشد که می تواند در دوره طولانی مدت بکار برده شوند. علی رغم پیل های سوختی قدیمی که از هیدروژن اتانول و متانول به عنوان سوخت استفاده می نمودند پیلهای سوختی بیولوژیکی از دهنده های الکترون زنده استفاده می کنند. بر خلاف پیل های سوختی شیمیایی پیل های بیولوژیکی در شرایط ملایمی به عنوان مثال در دما و فشار محیط کار می‌کنند همچنین از الکترولیت های ارزان قیمت استفاده می‌نمایند. در پیل های بیولوژیکی به عنوان نمونه میتوان از آنزیم و یا مخمر نانوایی به عنوان کاتالیست و یا میکروارگانیسم استفاده نمود .

از جمله فواید مهم پیلهای سوختی بیولوژیکی این است که آنها توانایی تبدیل انرژی شیمیایی را از یک محیط بیولوژیکی به جریان الکتریکی دارا می‌باشند و سوخت مورد نیاز را در این سیستمها می‌توان از یک محیط بیولوژیکی و حتی از یک ارگانیزم زنده و یا گیاه گرفت. در طراحی پیلهای سوختی بیولوژیکی برای تبدیل انرژی شیمیایی به انرژی الکتریکی از بیوکاتالیستها استفاده می‌شود[5]. کلا پیل های سوختی بیولوژیکی را به دو دسته

کلی پیل های سوختی میکروبی و آنزیمی طبقه بندی می نمایند.برخلاف سیستمهای میکروبی که از ارگانیزمهای زنده به عنوان منبع کاتالیستی استفاده می‌شود، در سیستم‌های آنزیمی از پروتئینهای آنزیمی خالص برای انجام واکنشهای کاتالیستی خاص استفاده می‌گردد. در مواردی می‌توان چندین آنزیم را با یکدیگر ترکیب نمود تا اکسیداسیون ماده به طور کامل انجام پذیرد. همچنین می‌توان از واحدهای پروتئینی کوچکتر از آنزیمهای کامل به عنوان کاتالیست در پیلهای سوختی استفاده نمود.در پیلهای سوختی آنزیمی، پیل در پتانسیلی، نزدیک به پتانسیل اکسایش- کاهش آنزیم عمل می‌نماید[۶].

از نظر تئوری تولید جریان برق از پیل سوختی میکروبی پدیده جدیدی لحاظ نمی شود بطور حتم روشهای علمی و اجرایی آن برای تولید برق کاملا نوین می باشند. ابزارهایی که از نظر اقتصادی پیل سوختی میکروبی را برای تولید انرژی توجیح نماید نیاز به بررسی دارد اگر هزینه تبدیل انرژی از نفت در سطح پائین حفظ شود. روشهای متنوعی در تکامل و تدوین انرژی نوین شکل گرفته است که فرایندهای رقیب تولید انرژی هستند. پیل سوختی میکروبی روش بسیار جدیدی برای تولید انرژی بوده که تلاش چندانی برای اسکلت و ساخت آن انجام نگرفته است که بتوان اقتصادی بودن آن را توجیح نمود[7].

یکی از قسمت های اصلی در پیل سوختی میکروبی که بر روی بازده آن بسیار موثر است محفظه کاتدی و الکترود کاتد می باشد. که ما در این مطالعه به این موضوع پرداخته ایم.اینگونه که از مواد مختلف به عنوان الکترود کاتد در شرایط گوناگون استفاده کردیم و بهترین الکترود را انتخاب نمودیم.

مواد و روش تحقیق

میکروارگانیسم و محیط کشت: از میکروارگانیزم‌های موجود در پساب بی هوازی به عنوان میکروارگانیسم فعال و مولد بیو الکتریسیته در محفظه آندی استفاده شد. این میکروارگانیزم‌های مورد استفاده از پساب تصفیه‌خانه قائمشهر جمع‌آوری شد. سپس میکروارگانیزم‌ها به محیط کشت MRS تلقیح شد و پس از ۴۸ ساعت به بیشترین میزان رشد خود در شرایط بی هوازی رسید.

در این تحقیق از گلوکز به عنوان منبع قندی استفاده شد .همچنین به محیط کشت مواد دیگری نیز اضافه گردیده که مواد و همچنین ترکیب درصدهای آن در جدول شماره ۱ ارائه شده. تمام مواد شیمیایی و آلی مورد نیاز نیز برای انجام آزمایش از شرکت مرک خریداری گردید. پس از ان به میزان ۵ در صد تلقیح باکتری صورت گرفته و محلول در جای بی هوازی در دمای محیط (26 ∓ ۲ °C) قرار داده شد .

جدول۱- مواد مورد استفاده محیط کشت

ماده	میزان
گلوکز	۳۰ g/l
عصاره مخمر	۳ g/l
پپتون	1 g/l
NH_4Cl	0/5 g/l
$MgSO_4$	0/2 g/l

مشخصات پیل سوختی بیولوژیکی: برای ساخت تک سل پیل سوختی بیولوژیکی از یک پیل دو قسمتی شامل بخش آند بی هوازی و کاتد هوازی مجزا از هم استفاده گردید .جنس محفظه ها از پلکسی گلاس بوده و هر کدام از محفظه ها نیز دارای ظرفیت ۸۲۰ میلی لیتر می باشند.قطر داخلی هر کدام از محفظه ها ۶/۴ سانتیمتر می باشد که توسط یک لوله رابط به قطر ۲/۴ سانتیمتر و طول ۳ سانتیمتر از هم جدا شده اند. دو محفظه آندی وکاتدی بوسیله غشای تبادل پروتون از جنس نفیون ۱۱۷ با یکدیگر در ارتباط بودند. نمای طراحی تک سل بیولوزیکی بصورت تصویری در شکل ۱ آورده شده است. 75 درصد از حجم فوق حجم کاری لحاظ شده است .۶۱۵ لیتر از محیط کشت تهیه شده با مشخصات فوق به قسمت آند اضافه گردید و در سمت کاتد نیز از۶۱۵ میلی لیترآب دیونیزه استفاده شده است که توسط اسپارژی به این محفظه هوادهی نیز صورت گرفته است.

در این کار برای انتقال الکترونهای تولیدی حاصل از فرآیند تخمیر از الکترودهایی از جنس گرافیت و کربن کاغذی استفاده شده است.ابعاد دو الکترود(الکترودهای آند و کاتد) یکسان بوده و ابعاد آنها به اندازهای متفاوت می باشد و جریان حاصل توسط یک سیم مسی به مدار بیرونی منقل گردیده اند.

روش های آنالیز:

اندازه گیری جریان و ولتاژ: برای بدست آوردن جریان از المانهای مقاومتی برای ایجاد مقاومتهای متغیر استفاده شده است. المان مقاومتی معمولی به دلیل اینکه دارای یک مقاومت اهمی ثابت و پایدار (در دمای معمولی) و در ولتاژهای مختلف می باشد. درنتیجه، المان مقاومتی به دلیل نداشتن افت ولتاژ درون المان و نیز صفر بودن جریان نشتی، گزینه مناسبی برای ساخت دستگاه اندازه گیری می باشد.در این روش برای قرار دادن بارهای مختلف مقاومتی روی پیل سوختی از ترکیب یک سیستم رله ای مقاومتی استفاده شده است که می توان با سری کردن مقاومت های مختلف، بارهای مقاومتی دلخواه را ایجاد نمود و با قرار دادن آن روی پیل سوختی، اثر آن را مشاهده نمود.و دستگاهی جهت ثبت نتایج ولتاژ و جریان در پیل سوختی بیولوژیکی ساخته شد.برای ساخت این سیستم مقاومتی و رله ای از ۱۵ مقاومت مختلف و ۱۶ رله استفاده شده است که توانایی گرفتن ۱۸ دیتا را این سیستم ساخته شده دارا می باشد و برنامه مورد استفاده برای ثبت نتایج برنامه MATLAB بوده است.

کمیت های مهم و حائز اهمیت در این مطالعه ولتاژ مدار باز، جریان و توان بودند. جریان تولید شده توسط پیل سوختی میکروبی را مستقیما اندازه‌گیری نکردیم بلکه آن را با اندازه‌گیری افت ولتاژ حاصل از یک مقاومت الکتریکی به صورت $I = E / Rext$ محاسبه نمودیم. توان از ولتاژ و جریان به صورت $P = IE$ محاسبه می گردد. توان خروجی از MFC از ولتاژ اندازه‌گیری شده EMFC در عرض بار الکتریکی و جریان محاسبه می‌گردد:

$$P = IE_{MFC}$$

جریان تولید شده به وسیله MFC در مقیاس آزمایشگاهی با اندازه‌گیری پتانسیل در عرض بار الکتریکی (مقاومت بیرونی Rext) و با استفاده از رابطه $I = EMFC / Rext$ محاسبه می گردد. از این رو داریم:

$$P = E_{MFC}^2 / R_{ext}$$

بر مبنای رابطه $I = EMFC / Rext$ نیز داریم:

$$P = I^2 R_{ext}$$

نتایج و بحث

با توجه به نمودار ۲.الف و ب مشاهده می کنیم که در هر دو حالت با هوادهی و بدون هوادهی بیشترین دانسیته توان مربوط به گرافیت بوده است.این در حالی است که بیشترین دانسیته جریان را الکترود کربن پارچه ای از آن خود ساخته است. در آزمایش انجام شده اندازه الکترود های کاتد متفاوت بوده است وبه همین دلیل اعداد بدست آمده برای جریان و توان را بر اندازه سطح الکترود کاتد تقسیم نموده ایم. علت این کار این است که توان و جریان حاصله از پیل سوختی میکروبی با اندازه سطح الکترود رابطه مستقیم دارد.[۸] با مقایسه دو نمودار ۲.الف و۲.ب وهمچنین نمودار ۱.الف و ب مشاهده شد که هوادهی روی عملکرد پیل بسیار مؤثر می باشد. و این نتیجه دور از انتظار هم نبود. زیرا با توجه به واکنش احیا که در محفظه کاتدی انجام می شود وجود اکسیژن کافی از شرایط لازم برای کامل شدن واکنش و مصرف الکترون های ورودی به کاتد از طریق مدار خارجی است. در بین الکترود های مورد بررسی کربن پارچه ای بیشترین دانسیته توان را دارا بود. که این را می توان به رسانایی خوب و سطح ویژه بالای این ماده نسبت داد.[۹] از شکل ۲ می توان دریافت که الکترود کربن پارچه ای سطح فعال گسترده تری نسبت به اکترود گرافیت دارد. همچنین تأثیر هوادهی بر عملکرد کربن پارچه ای نسبت به گرافیت بیشتر بود و نتایج حاصله نشان داد که دانسیته توان ودانسیته جریان برای کربن پارچه ای بعد از هوادهی بیش از دو برابر شده است. درحالی که این تغییر برای گرافیت تقریبا یک ونیم برابر بود.

نتیجه‌گیری

۱) برای تولید دانسیته جریان بالا در پیل سوختی میکروبی بهتر است از مواد با سطح ویژه بالا همانند کربن پارچه ای استفاده کنیم.

۲) اثر هوادهی در محفظه کاتدی موقعی پر رنگ تر است که سطح ویژه الکترود زیاد بوده که بدین وسیله الکترون های بیشتری می توانند در واکنش احیا در حضور اکسیژن شرکت کنند و بدین وسیله به دانسیته توان و جریان بالاتری دست پیدا خواهیم کرد.

مراجع

1. Rahimnejad, M., et al., A novel microbial fuel cell stack for continuous production of clean energy. International journal of hydrogen energy, 2012. 37(7): p. 5992-6000.

2. Timmers, R.A., et al., Long-term performance of a plant microbial fuel cell with Spartina anglica. Applied microbiology and biotechnology, 2010. 86(3): p. 973-981.

3. Venkata Mohan, S., et al., Bioelectricity generation from chemical wastewater treatment in mediatorless (anode) microbial fuel cell (MFC) using selectively enriched hydrogen producing mixed culture under acidophilic microenvironment. Biochemical Engineering Journal, 2008. 39(1): p. 121-130.

4. Min, B., et al., Electricity generation from swine wastewater using microbial fuel cells. Water research, 2005. 39(20): p. 4961.۴۹۶۸–

5. Huang, L., R.J. Zeng, and I. Angelidaki, Electricity production from xylose using a mediator-less microbial fuel cell. Bioresource technology, 2008. 99(10): p. 4178-4184.

6. Shukla, A., et al., Biological fuel cells and their applications. Current Science, 2004. 87(4): p. 455-468.

7. Rahimnejad, M., et al., Low voltage power generation in abiofuel cell using anaerobic cultures. World Appl Sci J, 2009. 6: p. 1585-1588.

8. Logan, B.E., Microbial fuel cells. 2008: John Wiley & Sons.

9. Tsai, H.-Y ,.et al., Microbial fuel cell performance of multiwall carbon nanotubes on carbon cloth as electrodes. Journal of Power Sources, 2009. 194(1): p. 199-205.

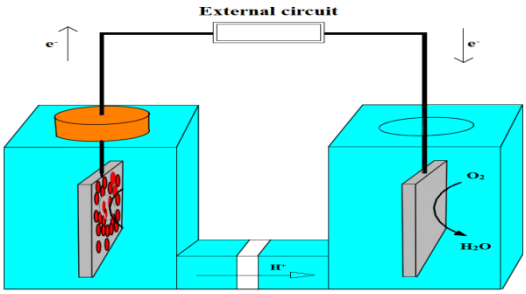

الف

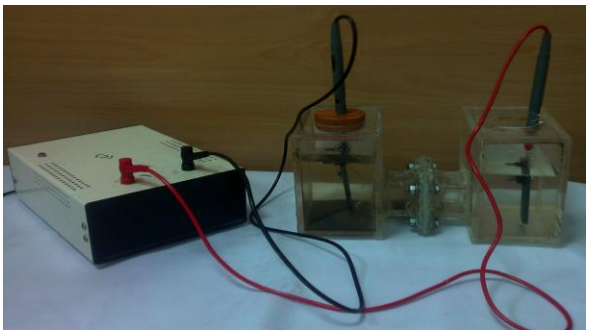

ب

شکل۱: پیل سوختی میکروبی الف) نمای گرافیکی ب) نمای عملیاتی در مقیاس آزمایشگاهی

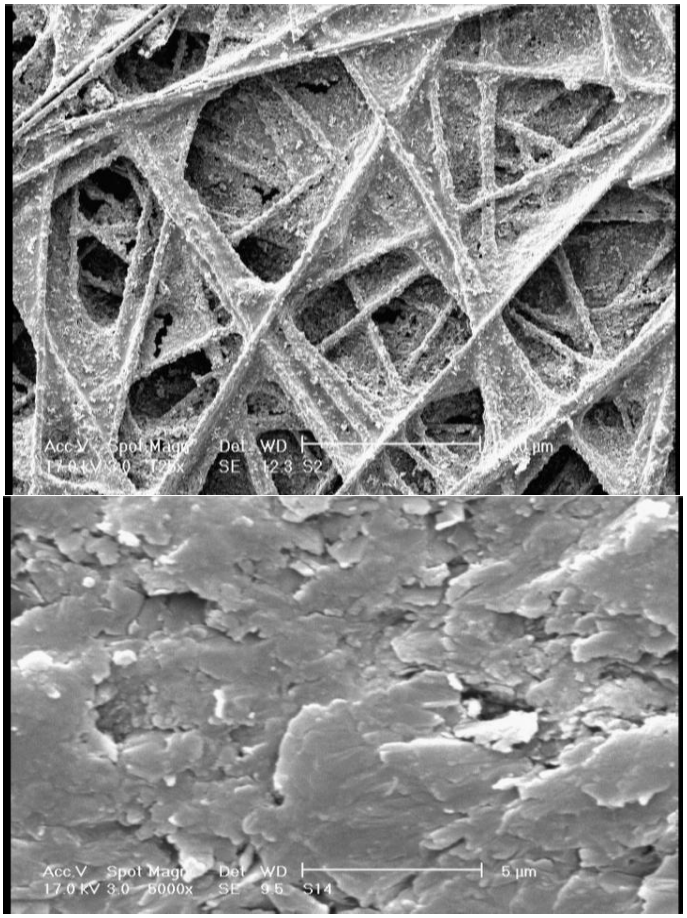

شکل ۲: تصویر میکروسکوپی الکترونی روبشی از الکترود کاتد الف) کربن پارچه ای ب) گرافیت

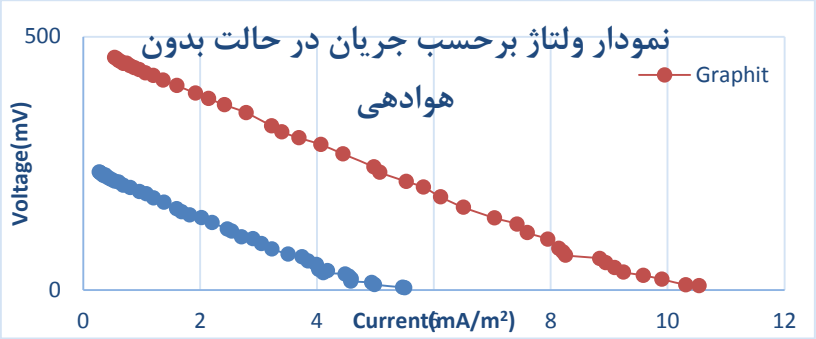

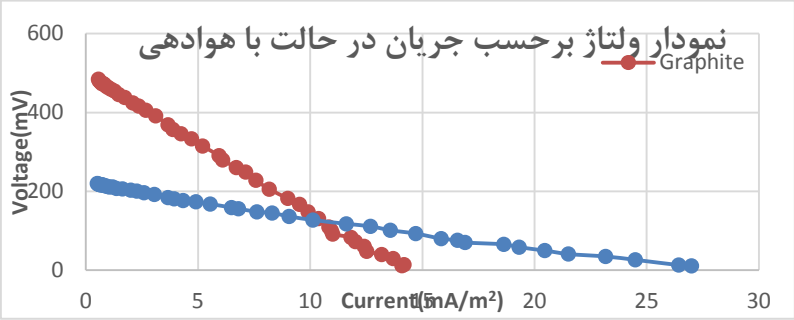

نمودار ۱ : نمودار ولتاژ برحسب جریان در شرایط الف) بدون هوادهی در محفظه کاتدی ب) با هوادهی در محفظه کاتدی

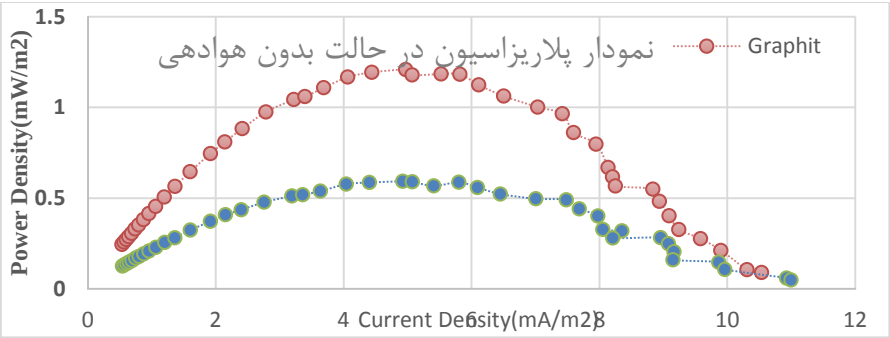

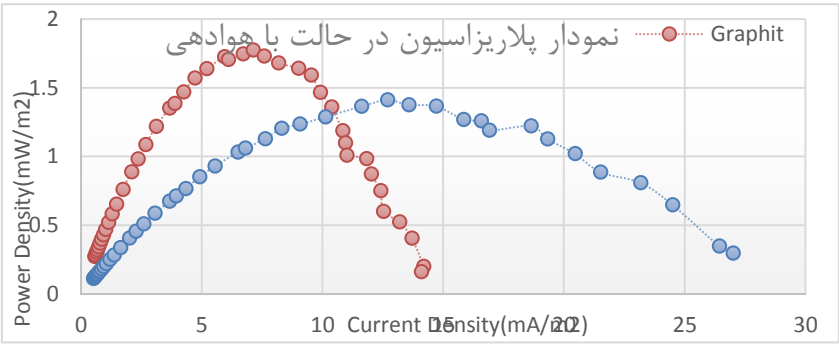

نمودار ۲:نمودارپلاریزاسیون در شرایط الف) بدون هوادهی در محفظه کاتدی ب) با هوادهی در محفظه کاتدی

بررسی تاثیر زمان پوشش‌دهی کبالت و منگنز به روش لایه نشانی الکتریکی در پیل‌های سوختی غشا پلیمری

امیرحسین آرامی پارچه باف، محسن رضایت مند

۱. دانشگاه آزاد اسلامی، واحد نجف آباد، باشگاه پژوهشگران جوان و نخبگان، نجف آباد، اصفهان، ایران

amir.arami@gmail.com

۲. دانشکده مهندسی مواد، دانشگاه آزاد اسلامی، واحد نجف آباد، اصفهان، ایران

Mohsen_Rezayatmand@yahoo.com

چکیده

محدود بودن منابع انرژی و افزایش روز به روز آلودگی‌های محیطی منجر به افزایش تمایل کشورها به استفاده از انرژی‌های تجدید پذیر و پاک گردیده است. پیل‌های سوختی دارای کمترین میزان آلودگی‌های زیست محیطی هستند. در این پژوهش به بررسی تاثیر زمان پوشش دهی کبالت و منگنز به روش لایه نشانی الکتریکی در سطح به منظور استفاده به عنوان کاتد پیل‌های سوختی غشا پلیمری پرداخته شده است. ذرات کبالت و منگنز به خوبی به روش لایه نشانی الکتریکی بر روی زیر لایه نیکل پوشش داده شد. افزایش زمان پوشش دهی منجر به افزایش ناهمواری‌های سطحی و میزان تخلل سطح گردیده است. برای بررسی پوشش‌های تولیدی از میکروسکوپ الکترونی روبشی، میکروسکوپ نیروی اتمی، طیف سنج پراش پرتو ایکس و طیف نگار امپدانس الکتروشیمیایی استفاده شده است.

واژه‌های کلیدی: مهندسی سطح، پیل سوختی غشا پلیمری، لایه نشانی الکتریکی، الکترود، کبالت، منگنز.

مقدمه

پس از بحران انرژی در سال ۱۹۷۳میلادی و احتمال وقوع بحرانی دیگر در اوایل قرن آتی، استفاده از منابع سالم انرژی نظیر انرژی‌های تجدید پذیر خورشیدی، باد، آب، امواج دریا، جزر و مد، استخرهای خورشیدی، هیدروژن، بیوگاز و غیره لازم بوده و نیز ضرورت استفاده از سیستم‌های مبدل انرژی نظیر فتوولتایی، پیل‌های سوختی و فیوژن یا گداخت هسته‌ای را ناگزیر نموده است[۱].

پیل‌های سوختی براساس نوع الکترولیت به پنج دسته اصلی پیل‌های سوختی غشاء پلیمری[۱] ، پیل‌های سوختی قلیایی[۲] ، پیل‌های سوختی اسید فسفریک[۳] ، پیل‌های سوختی کربنات مذاب[۴] ، پیل‌های سوختی اکسید جامد[۱] تقسیم می‌گردد [**2**].

[1] Polymer Electrolyte Membrane Fuel Cell
[2] Alkaline Fuel Cell
[3] Phosphoric Acid Fuel Cell
[4] Molten Carbonate Fuel Cell

بجز موارد ذکر شده پیل‌های سوختی دیگری نظیر پیل‌های سوختی میکروبی، هیدرید فلزی و ... نیز وجود دارند که از اهمیت کمتری برخوردارند. پیل‌های سوختی با الکترولیت پلیمری یکی از انواع اصلی پیل‌های سوختی محسوب می‌شود که به دلیل چگالی جریان مناسب و نیز دمای عملکرد پایین مورد توجه بسیاری از صنایع بویژه صنایع خودرو سازی گردیده است. این پیل‌ها جایگزین مناسبی برای موتورهای احتراقی در صنایع خودرو سازی می‌باشد. از آنجاکه این پیل قادر نیست در دمای بالاتر از C□ ۱۲۰ کار کند، لذا این پیل برای کار با سوخت‌های دارای هیدروژن غنی که فاقد و یا دارای کمی منواکسید کربن است مناسب می‌باشد. منواکسید کربن اگر از حدی بیشتر باشد موجب کاهش واکنش آندی می‌شود و این کاهش با افزایش دمای پیل بیشتر می‌شود[**3**].

در شکل ۱ شمایی از فرایندهای موجود در پیل‌های سوختی پلیمری را مشاهده می‌کنید[**3**].

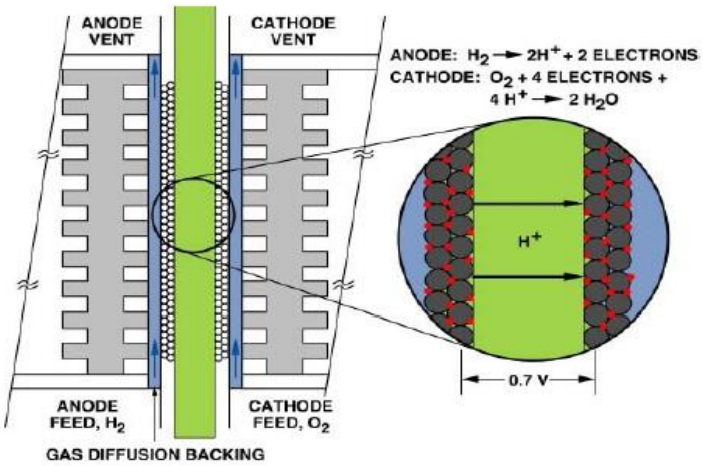

شکل ۱: اساس کار پیل سوختی پلیمری[3]

همانطور که در شکل ۱ مشاهده می شود در پیل سوختی پلیمری یون‌های هیدروژن تولید شده در آند از غشای رسانای یون عبور می‌کنند و به کاتد می‌رسند و الکترون‌های آزاد شده در آند نیز از طریق جریان خارجی به کاتد منتقل می‌شوند. در کاتد اکسیژن با یون‌های هیدروژن و الکترون‌ها ترکیب شده، آب و گرما تولید می‌شود. واکنش های موجود در پیل های سوختی غشا پلیمری را در معادلات ۱ تا ۳ مشاهده می کنید[**3**].

(۱) واکنش آندی: $\boldsymbol{H_2 \rightarrow 2H^+{}_{(aq)} + 2e^-}$

(۲) واکنش کاندی: $\boldsymbol{\frac{1}{2}O_{2_{(g)}} + 2H^+{}_{(aq)} + 2e^- \rightarrow H_2O_{(l)}}$

(۳) واکنش کلی: $\boldsymbol{H_{2(g)} + \frac{1}{2}O_{2(g)} \rightarrow H_2O_{(l)} + Electric\ Energy + Heat}$

برای انجام واکنش‌های الکترو شیمیایی لازم است الکترولیت به داخل الکترود نفوذ کند، از این رو الکترود باید متخلخل و نسبت به گازها نفوذپذیر باشد. علاوه براین الکترود باید غیر قابل سینتر شدن، دارای پایداری در چگالی جریان بالا و طول

[1] Solid Oxide Fuel Cell

عمر بالا باشد. الکترود باید رسانایی الکتریکی داشته باشد[**4**]. معمولا مواد بکار رفته در الکترود به گونه‌ای انتخاب می‌شوند که علاوه بر داشتن خواص ذکر شده، تا حد امکان منافذ سطح الکترود را افزایش دهند. بنابراین به منظور افزایش سرعت واکنش‌ها، مواد تشکیل‌دهنده الکترود باید کاتالیزور، رسانا و دارای خلل و فرج باشند. با توجه به اینکه سرعت انجام واکنش یونیزاسیون با افزایش دما، افزایش پیدا می‌کند اهمیت نقش کاتالیزور در دمای پایین بیشتر از نقش آن در دمای بالا است[**5**].
همچنین الکترود منفذدار نباید مانع نفوذ الکترولیت و گازها باشند ولیکن نفوذ گازها و الکترولیت نباید به حدی باشد که مانع از فعالیت الکترودها شود. چگالی جریان ناشی از الکترودهای صاف و بدون تخلخل معمولا دارای مرتبه کوچکی بر حسب $\mathbf{mAcm^{-2}}$ است، چون سطح موثر برای انجام واکنش بسیار محدود و کوچک می‌باشد، هنگامی جریان قوی با چگالی بالا تولید می‌شود که سطح موثر الکترود نسبت به سطح هندسی آن بیشتر باشد، در این صورت به میزان قابل توجهی سرعت انجام واکنش‌ها افزایش می‌یابد[**3**].
همانطور که در مطالب قبل اشاره شد الکترود معمولا ترکیبی از دو لایه، لایه بستر یا وب و لایه کاتالیزور می‌باشند. وظیفه اصلی لایه بستر شامل ایجاد مسیر هایی جهت نفوذ گاز، تامین کننده استحکام مکانیکی، ایجاد یک بستر هادی الکتریکی جهت انتقال الکترون‌ها و ایجاد مسیرهای برای خروج آب تولیدی. این لایه باید خواص آب گریزی داشته باشد. بستر توسط یک لایه کاتالیزور پوشش داده می‌شود که معمولا از فلزات فعال با دانسیته جریان تبادلی مناسب تهیه می‌شود. این لایه دارای ویژگی‌های آب دوستی هستند، وجود این خاصیت به منظور ایجاد شبکه انتقال مایع از درون لایه کاتالیزور و انتقال جریان الکترون تولید شده بکار می‌رود[**3**].
رسوب گذاری الکتروشیمیایی بانام آبکاری الکتریکی نیز شناخته می شود. در این روش از یک سلول الکترولیز استفاده میشود که شامل یک حمام و الکترودهای غوطه ور در آن است.

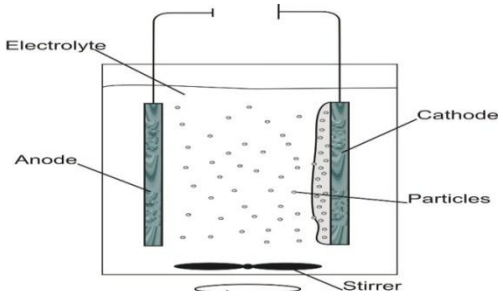

شکل ۲: اساس کار پیل سوختی پلیمری[3]

همانطور که در شکل ۲ مشاهده می شود فلزی که باید رسوب گذاری شود به شکل یون در حمام الکترولیت وجود دارد. الکترودها به منبع جریان متصل هستند. آن چه به عنوان پوشش باید رسوب گذاری شود به قطب مثبت (آند) متصل می‌گردد و زیر لایه به قطب منفی (کاتد) متصل می‌شود، به جز در مواردی مثل طلا که از آند غیر قابل حل استفاده می‌شود[**6**]. در

فرایند لایه نشانی الکتریکی جریان و زمان به عنوان دو عامل بسیار مهم مطرح است که تاثیر این دو عامل در معادله فاراده مشاهده می گردد.

$$\mathbf{I.t = \frac{W.n.F}{M}} \qquad (۴)$$

در معادله ۴، **I** جریان، **t** زمان، **W** جرم پوشش نشانده شده، **n** تعداد الکترون، **F** عدد فاراده[1] و **M** جرم ملکولی پوشش می‌باشد.

مواد و روش تحقیق

مواد مورد استفاده شامل اسید سولفوریک، اسید بوریک، سولفات کبالت، کلیرید کبالت، سولفات منگنز، کلرید منگنز و نیکل با خلوص ۹۹/۹۹ درصد می‌باشد. تمامی مواد محصول شرکت مرک آلمان می‌باشد.

ورق نیکل به ابعاد **۱cm×۱** و ضخامت **۱mm** جهت پوشش دهی مانت سرد گردید سپس پولیش شده و توسط استون شستشو و خشک شده است. برای انجام فرایند پوشش دهی از گرافیت استوانه ای به قطر **۵۰mm** به عنوان آند استفاده شده است. فلز نیکل به عنوان کاتد در فاصله **۲Cm** آند قرار داده شد. پس از اتصال آند و کاتد به منبع جریان فرایند پوشش دهی به مدت ۵، ۱۰، ۱۵ و ۲۵ دقیقه صورت گرفت.

جدول ۱: زمان پوشش دهی نمونه ها

Co-01	Co-02	Co-03	Co-04
Mn-01	Mn-02	Mn-03	Mn-04
5 min	10 min	15 min	25 min

در جدول ۲ جزئیات حمام‌های کبالت و منگنز مورد استفاده مشاهده می‌شود.

جدول ۲: مشخصات حمام های مورد استفاده در فرایند پوشش دهی

حمام کبالت		**حمام منگنز**	
مشخصه	مقدار	مشخصه	مقدار
$CoCl_2 \cdot 6H_2O$	**۲۰ gr**	**$MnCl_2 \cdot 4H_2O$**	**۲۰ gr**
$CoSO_4 \cdot 7H_2O$	**۶۰ gr**	**$MnSO_4 \cdot 4H_2O$**	**۶۰ gr**
آب	**۲۰۰ gr**	**آب**	**۲۰۰ gr**
H_3BO_3	**۳ gr**	**H_3BO_3**	**۳ gr**
PH	**۳**	**PH**	**۳**
T	**۳۰ °C**	**T**	**۲۰ °C**
دانسیته جریان (i)	**۲۰ $mA.Cm^{-2}$**	**دانسیته جریان (i)**	**۳۰ $mA.Cm^{-2}$**

[1] Faraday's Constant (F) = 96485.34 C/mol

آزمایشات الکتروشیمیایی در دمای **۲۹۸ °K** و توسط یک پیل سه الکترودی با دستگاه پتانسیواستات ساخت شرکت **EG&G** صورت گرفته است. در این پیل از الکترود گرافیتی و الکترود کالومل (**V-RHE** ۰/۲۴۱) به عنوان الکترود شمارنده و الکترود مرجع مورد استفاده قرار گرفته است. تصاویر **SEM** با دستگاه **HBO** موجود در دانشگاه آزاد نجف آباد و تصاویر **AFM** توسط دستگاه **AP0100** شرکت **Park Scientific Instruments** گرفته شده است.

نتایج و بحث

مکانیزم لایه نشانی الکتریکی شامل دو مرحله جوانه زنی و رشد است. در مرحله اول که شامل جوانه زنی می باشد دانسیته جریان پارامتر مهم در ایجاد محل های جوانه زنی می باشد. نقاطی که دارای دانسیته جریان بیشتری هستند محل های مناسب تری جهت جوانه زنی می باشند، با توجه به اینکه در اینجا دانسیته جریان ثابت بوده است اما در مقیاس میکرو سطح به طور کامل صاف و صیقلی نمی باشد و جود این ناهمواری های اولیه باعث می گردد نقاط مختلف سطح دارای دانسیته های متفاوتی نسبت به هم باشند بنابراین بعضی از این نقاط نسبت به نقاط دیگر تقدم در جوانه زنی دارند[7].

مرحله رشد شامل سه مرحله: ۱) انتقال یون از داخل محلول به سطح کاتد ۲)انتقال بار و تبدیل یون به اتم فلزی ۳)نفوذ اتم فلزی به داخل شبکه کریستالی فلز و رشد دانه است. بدلیل اینکه در این مرحله مکانیزم فرایند بر پایه نفوذ می باشد لذا زمان پوشش دهی نقش موثری در رشد جوانه ها دارد[7].

در شکل ۳ تصاویر میکروسکوپ الکترونی پوشش کبالت مشاهده می شود.

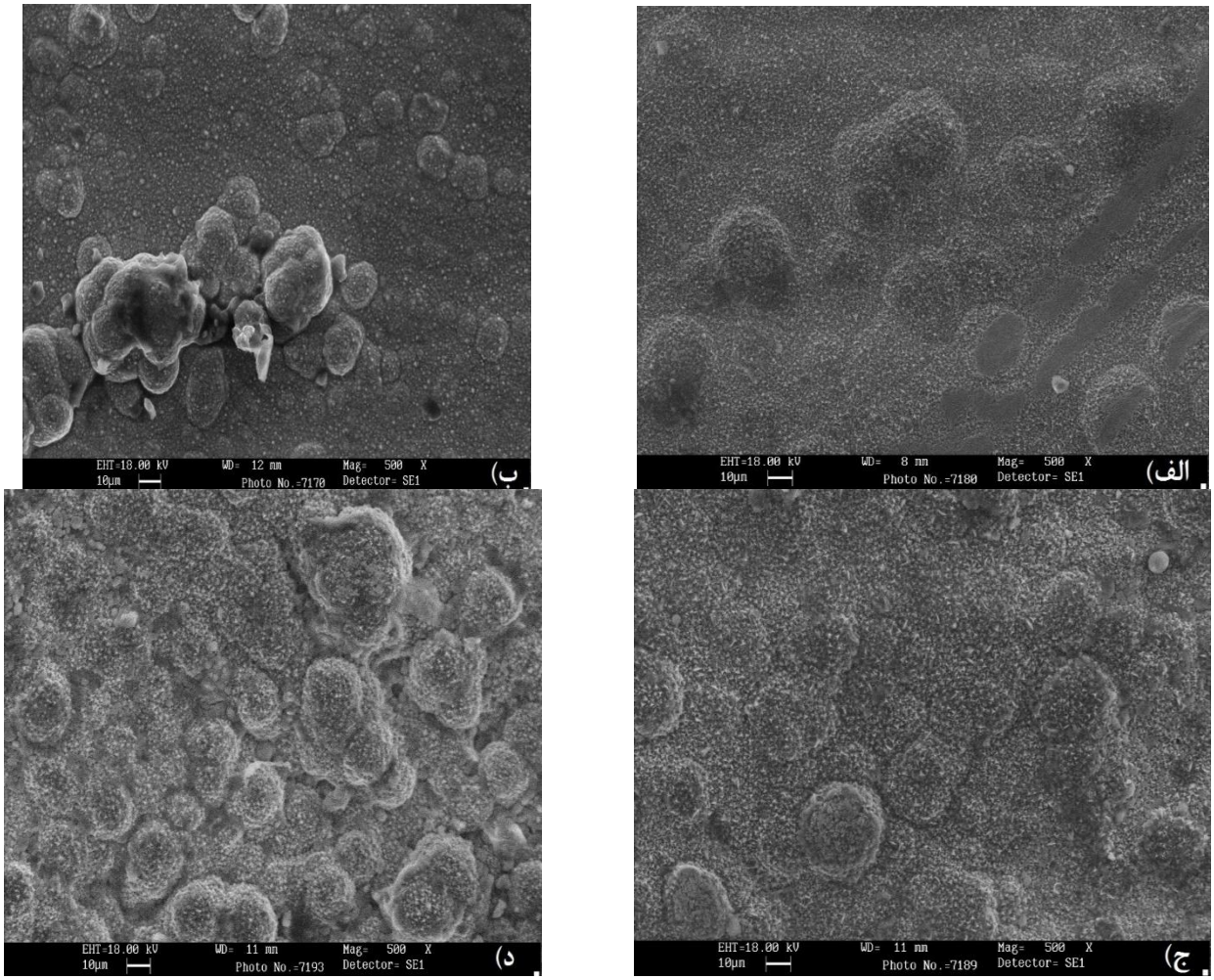

شکل ۳: تصاویر **SEM** پوشش کبالت در بزرگنمایی ۵۰۰ برابر الف) تصویر پوشش نمونه **Co-01** ب) تصویر پوشش نمونه **Co-02** ج) تصویر پوشش نمونه **Co-03** د) تصویر پوشش نمونه **Co-04**

همانطور که در شکل ۳ مشاهده می شود با افزایش زمان پوشش دهی تعداد جوانه های قابل رشد افزایش می یابد که این امر موجب افزایش تراکم دانه های پوشش گردیده است. همچنین افزایش زمان پوشش دهی منجر به افزایش میزان ناهمواری های سطح و در نتیجه افزایش میزان خلل و فرج سطح گردیده است. از طرف دیگرافزایش زمان باعث افزایش تراکم پوشش و در نتیجه کاهش میزان تخلل سطح می گردد.

همانطور که در تصویر الف شکل ۴ مشاهده می شود از لحاظ ریخت شناسی ذرات پوشش به صورت گل کلمی می باشد همچنین آنالیز عنصری این ذرات نشان می دهد که پوشش کبالت به خوبی به روش لایه نشانی الکتریکی برروی زیر لایه نیکل تشکیل شده است. این ذرات تقریبا به صورت کروی می باشد. که از تجمع درات کبالت تشکیل شده است که طبق مکانیزیم گفته شده تشکیل این ذرات منجر به افزایش دانسیته جریان در این نقاط گردیده است.

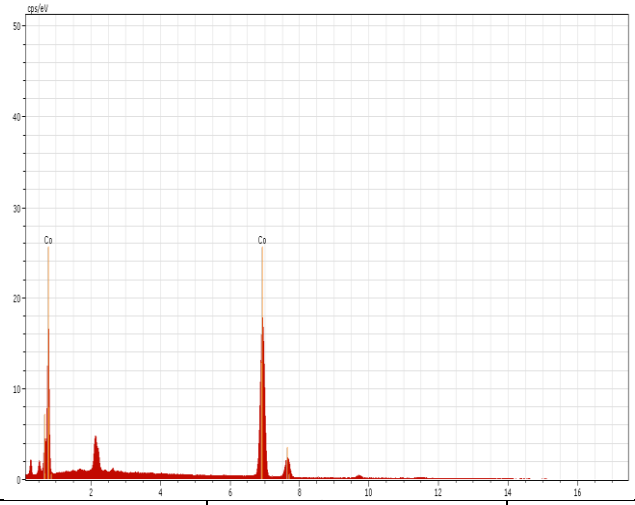

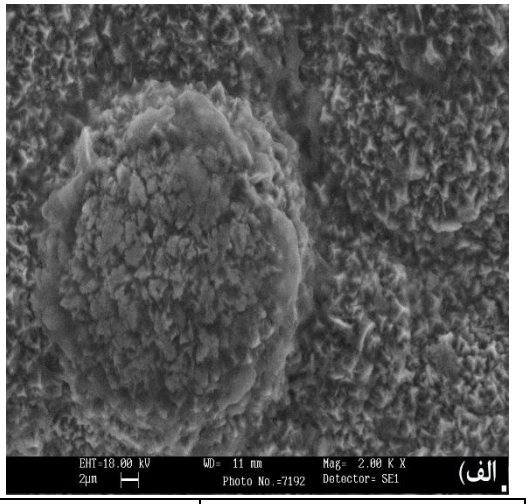

عنصر	series	[wt.%]	[norm. wt.%]	[norm. at.%]
Oxygen	K-series	3.00968225952897	3.45271476701886	11.6395189390211
Cobalt	K-series	84.158892691352	96.5472852329811	88.3604810609789
	Sum:	87.1685749508809	100	100

شکل ۴: الف) ریخت شناسی ذرات کبالت در بزرگنمایی ۲۰۰۰ برابر ب) آنالیز **EDS** ذرات کبالت

برای بررسی دقیق تر سطح پوشش در سه بعد از میکروسکوپ نیروی اتمی استفاده شده است که تصاویر آن در شکل ۵ مشاهده می شود.

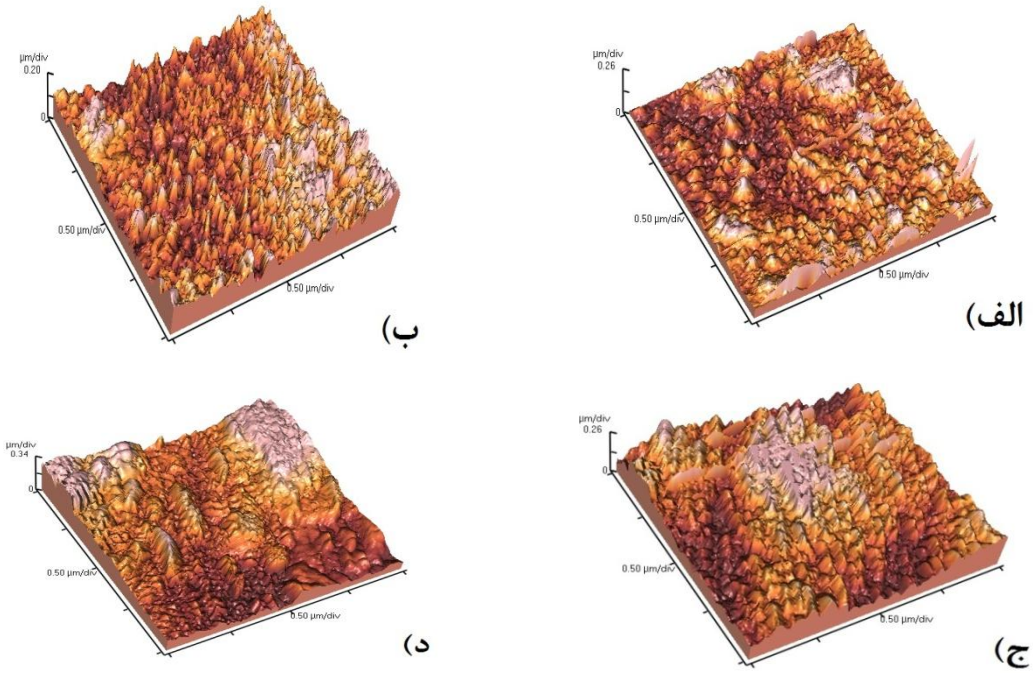

شکل ۵: تصاویر **AFM** سطح پوشش الف) نمونه **Co-01** ب) نمونه **Co-02** ج) نمونه **Co-03** د) نمونه **Co-04**

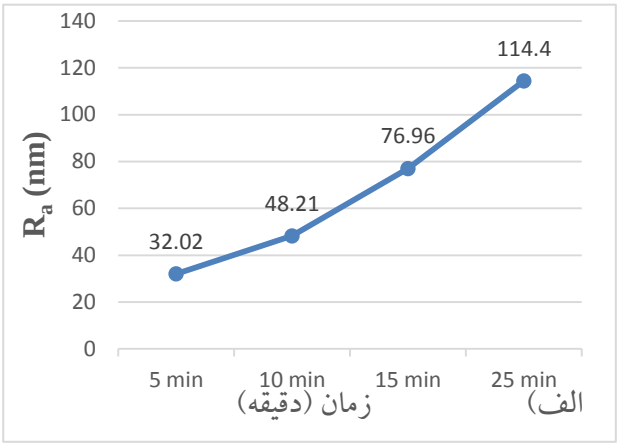

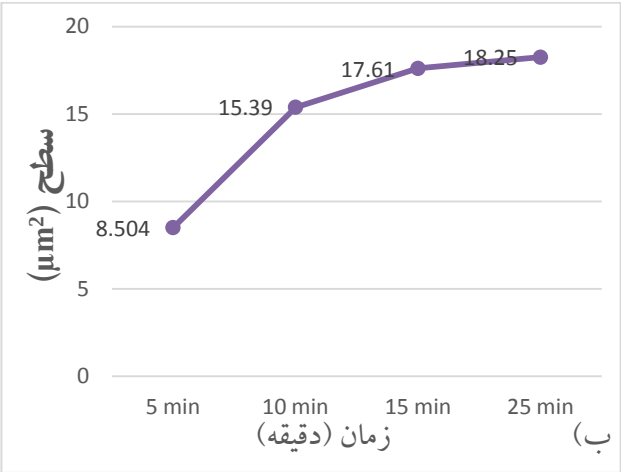

شکل ۶: الف) نمودار تغیرات زبری بر حسب زمان پوشش دهی ب) تغیرات سطح نسبت به زمان پوشش دهی

همانطور که در شکل ۵ مشاهده می شود افزایش زمان پوشش دهی منجر به افزایش میزان زبری سطح گردیده است. در نمودار الف شکل ۶ تغیرات زبری بر اساس زمان پوشش دهی نشان داده شده است با افزایش مدت زمان پوشش دهی چون مکانیزم رشد جوانه ها یک مکانیزم نفوذی می باشد این افزایش زمان باعث می شود جوانه های تشکیل شده فرصت لازم جهت رشد را پیدا نموده لذا زبری سطح افزایش یافته است. این افزایش زبری منجر به افزایش سطح کل در یک مقطع ثابت گردیده است. نمودار ب شکل ۶ نشان می دهد در یک مقطع ثابت سطح کل نسبت به زمان پوشش دهی افزایش یافته است. اما نکته قابل توجه در اینجا اینست که روند تغیرات سطح از نمونه سوم به چهارم دارای شیب کمتری می باشد علت این امر افزایش تراکم سطح و تعداد جوانه های قابل رشد می باشد که منجر به پر شدن خلل و فرج سطحی می گردد.

در شکل ۷ نمودار نایکوئست پوشش کبالت در محلول ۰/۵ مولار اسید سولفوریک از فرکانس **۱۰۰kHz** تا**۱۰۰ mHz** در پتانسیل **۵mV** مشاهده می شود. با افزایش زمان پوشش دهی میزان جذب هیدروژن بر روی سطح افزایش یافته که این امر موجب افزایش میزان انجام پذیری واکنش بین اکسیژن و هیدروژن بر روی سطح این کاتالیست گردیده است. با توجه به نمودارهای نایکوئست بدست آمده از نمونه یک به سمت نمونه چهار میزان پلاریزاسیون اکتیواسیون در حال کاهش می‌باشد. وجود پلاریزاسیون غلظتی در نمونه سه و چهار بیانگر این مسئله می باشد که با افزایش میزان واکنش‌های انجام شده بر روی سطح کاتالیست تشکیل حباب‌های هیدروژن را بر روی این سطح شاهد می‌باشیم که این امر موجب ایجاد پلاریزاسیون غلظتی بر روی سطح نمونه سوم و چهارم گردیده است. در حالت کلی می‌توان گفت با افزایش میزان زبری سطح ما افزایش میزان سطح کل را در یک مقطع ثابت خواهیم داشت که این افزایش سطح منجر به بهبود عملکرد پیل می گردد.

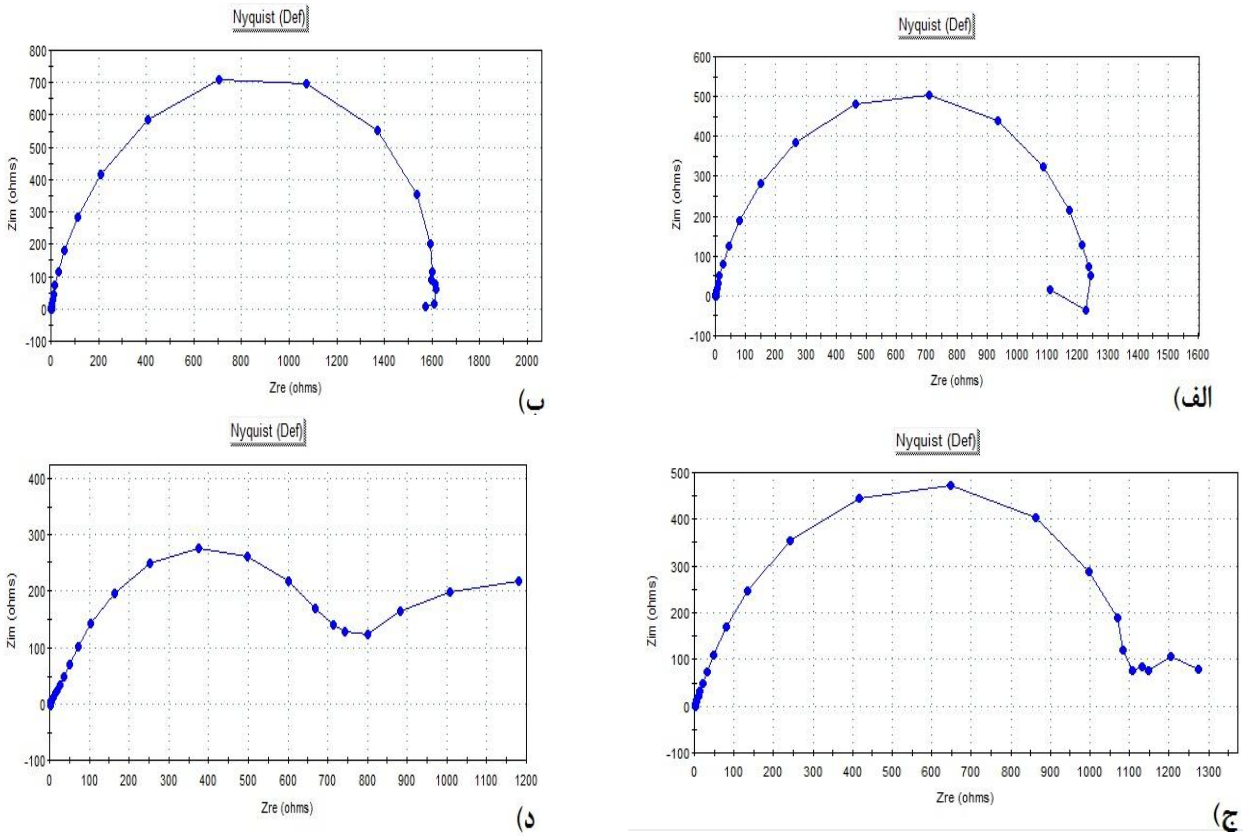

شکل ۷: نمودارهای نایکوئست پوشش کبالت در محلول ۰/۵ مولار اسید سولفوریک از فرکانس **۱۰۰kHz** تا**۱۰۰ mHz** در پتانسیل **۵mV** الف) نمونه **Co-01** ب) نمونه **Co-02** ج) نمونه **Co-03** د) نمونه **Co-04**

در خصوص پوشش منگنز نیز مکانیزم حاکم، مکانیزم جوانه زنی و رشد می باشد. در این حالت نیز دانسیته جریان اعمالی جهت پوشش دهی سطح نیکل مقداری ثابت می باشد اما چون در مقیاس میکرو سطح به صورت صاف و صیقلی نمی باشد و دارای پروفیل سطحی می باشد این امر منجر به این مسله می گردد که در بعضی از نقاط سطح افزایش میزان دانسیته جریان را به صورت موضعی خواهیم داشت بنابراین نقاطی از سطح جهت جوانه زنی دارای ارجعیت می باشد.

در مرحله دوم که مرحله رشد جوانه‌ها می‌باشد طبق مکانیزم فوق، چون فرایند رشد یک فرایندی بر اساس نفوذ می باشد لذا افزایش زمان یک پارامتر موثر در این فرایند می‌باشد. افزایش زمان بایستی منجر به افزایش میزان رشد جوانه‌ها گردد لذا منجر به ایجاد سطحی ناهموار می‌گردد. این ناهمواری سطحی باعث ایجاد سطح متخلخلی می‌گردد که اولا افزایش سطح کل در یک مساحت ثابت را خواهیم داشت ثانیا افزای زبری سطح یک سری مسیرهای مناسب جهت انتقال واکنش دهنده‌ها می‌باشد.

در شکل ۸ تصاویر میکروسکوپ الکترونی روبشی از سطح پوشش منگنز مشاهده می شود.

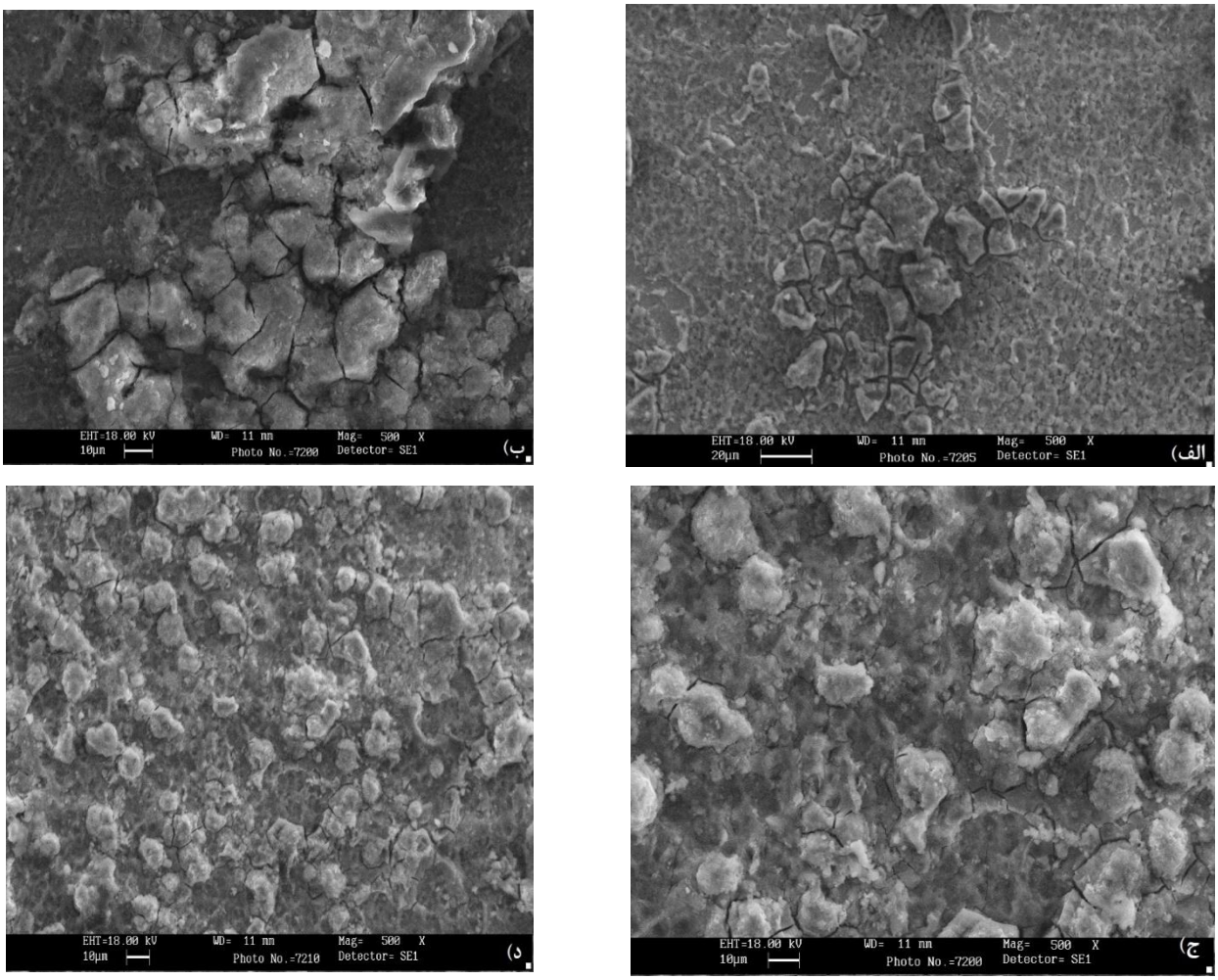

شکل ۸: تصاویر **SEM** پوشش منگنز در بزرگنمایی ۵۰۰ برابر الف) تصویر پوشش نمونه **Mn-01** ب) تصویر پوشش نمونه **Mn-02** ج) تصویر پوشش نمونه **Mn-03** د) تصویر پوشش نمونه **Mn-04**

همانطور که در شکل ۸ مشاهده می شود با افزایش زمان پوشش دهی تعداد جوانه های قابل رشد افزایش می یابد که این امر موجب افزایش تراکم دانه های پوشش گردیده است. همچنین افزایش زمان پوشش دهی منجر به افزایش میزان ناهمواری های سطح و در نتیجه افزایش میزان خلل و فرج سطح گردیده است. از طرف دیگرافزایش بیش از حد زمان باعث افزایش تراکم پوشش و در نتیجه کاهش میزان تخلل سطح می گردد که باعث کاهش توان خروجی پیل می گردد.

همانطور که در تصاویر مشاهده می شود سطح این پوشش دارای ترک های زیادی می باشد که وجود این ترک ها خود باعث افزایش میزان تخلل سطح گردیده است. همانطور که در تصویر الف شکل ۹ مشاهده می شود از لحاظ ریخت شناسی ذرات پوشش به صورت اشکال هندسی نامنظم می باشد همچنین آنالیز عنصری این ذرات نشان می دهد که پوشش منگنز به خوبی به روش لایه نشانی الکتریکی برروی زیر لایه نیکل تشکیل شده است.

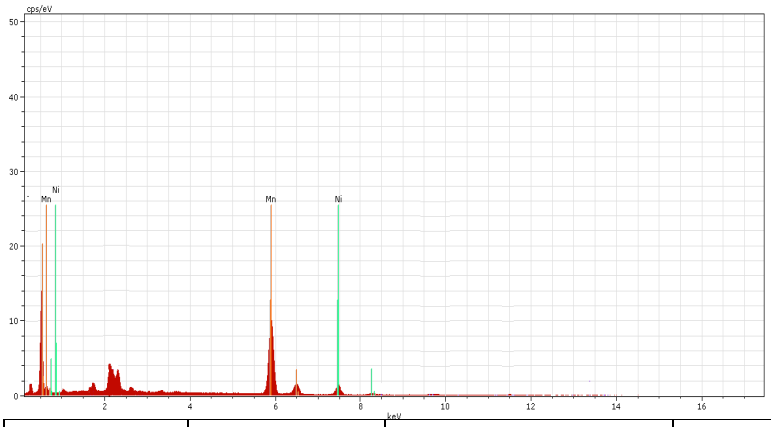

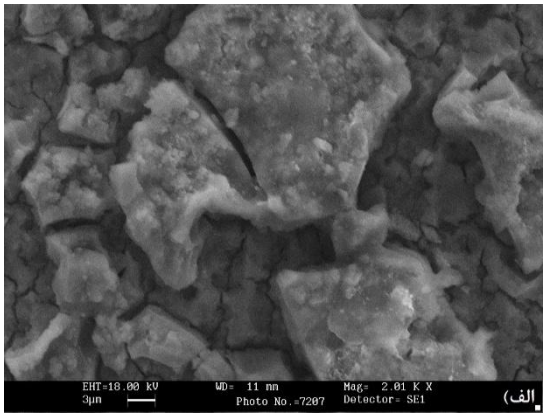

عنصر	series	[wt.%]	[norm. wt.%]	[norm. at.%]
Oxygen	K-series	29.66811	37.52309	67.61511
Manganese	K-series	39.94019	50.51482	26.50909
Nickel	K-series	9.457978	11.96209	5.875795
	Sum:	79.06628	100	100

شکل ۹: الف) ریخت شناسی ذرات منگنز در بزرگنمایی ۲۰۰۰ برابر ب) آنالیز **EDS** ذرات منگنز

در شکل ۱۰ تصاویر سه بعدی سطح مشاهده می گردد.

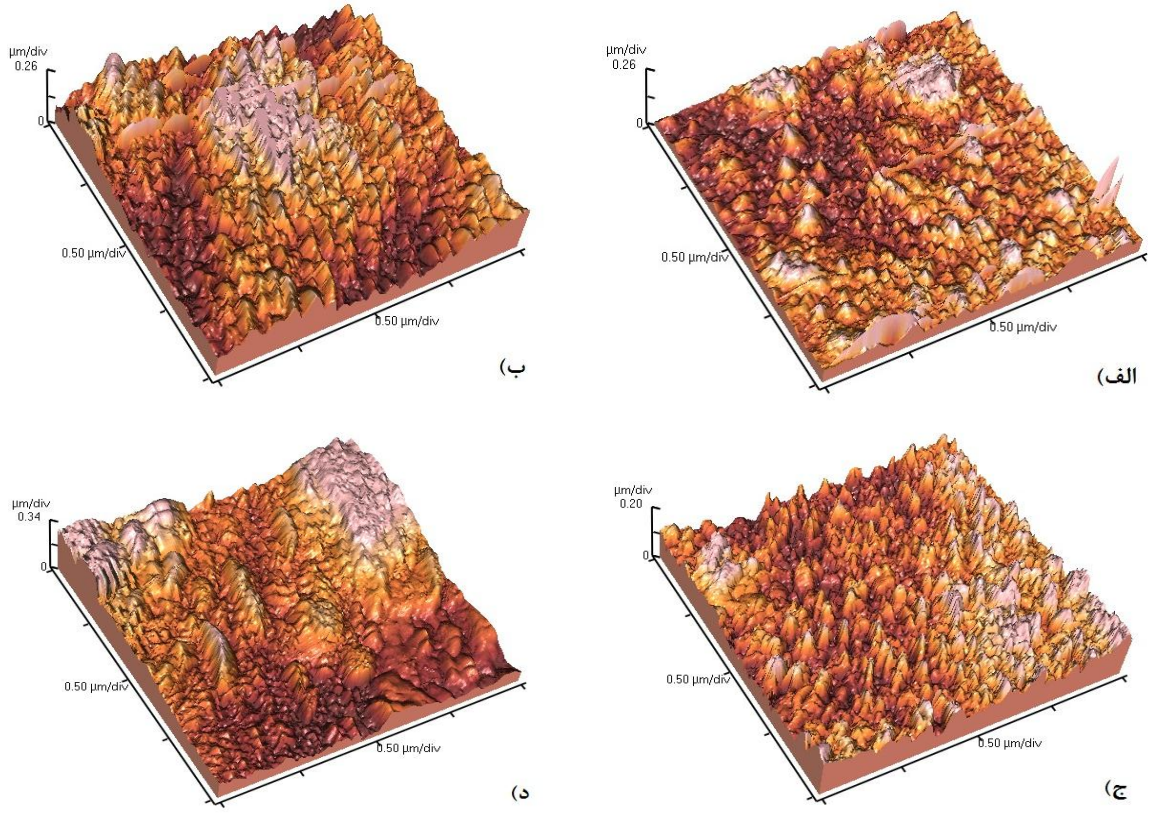

شکل ۱۰: تصاویر **AFM** سطح پوشش الف) نمونه **Mn-01** ب) نمونه **Mn-02** ج) نمونه **Mn-03** د) نمونه **Mn-04**

همانطور که در تصاویر شکل ۱۰ مشاهده می گردد با افزایش زمان پوشش دهی میزان تراکم پوشش افزایش یافته است. افزایش زمان پوشش دهی باعث افزایش زبری سطح شده در نتیجه یک سطح کاملا ناهموار با درصد تخلخل بالا خواهیم داشت.

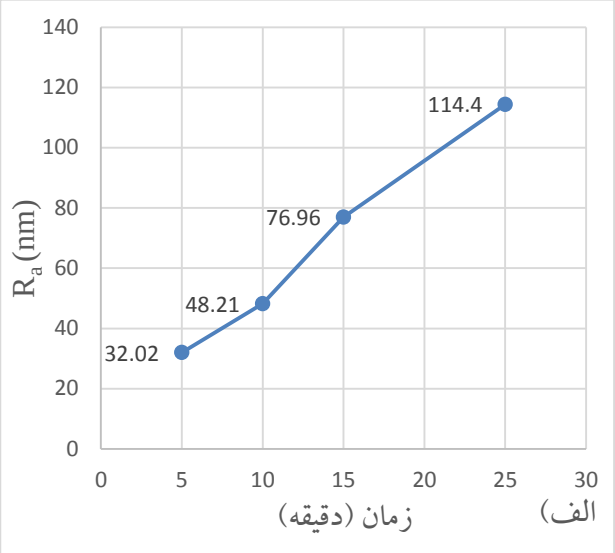

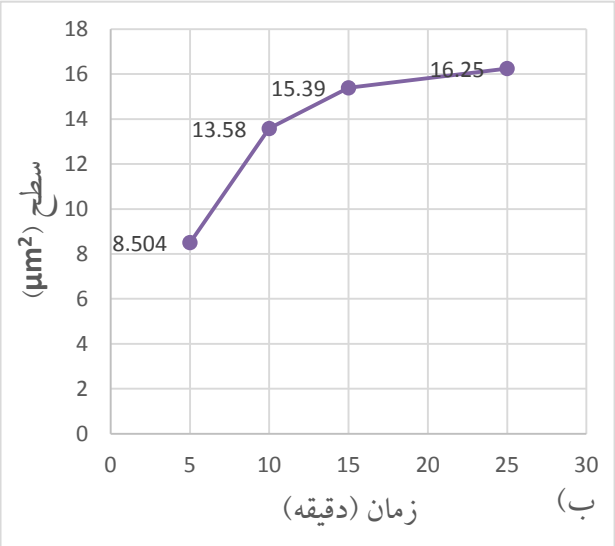

شکل ۱۱: الف) نمودار تغیرات زبری بر حسب زمان پوشش دهی ب) تغیرات سطح نسبت به زمان پوشش دهی

در نمودار الف شکل ۱۱ تغیرات زبری بر اساس زمان پوشش دهی نشان داده شده است با افزایش مدت زمان پوشش دهی چون مکانیزم رشد جوانه ها یک مکانیزم نفوذی می باشد این افزایش زمان باعث می شود جوانه های تشکیل شده فرصت لازم جهت رشد را پیدا نموده لذا زبری سطح افزایش یافته است. این افزایش زبری منجر به افزایش سطح کل در یک مقطع ثابت گردیده است. نمودار ب شکل ۱۱ نشان می دهد در یک مقطع ثابت سطح کل نسبت به زمان پوشش دهی افزایش یافته است. اما نکته قابل توجه در اینجا اینست که روند تغیرات سطح از نمونه سوم به چهارم دارای شیب کمتری می باشد علت این امر افزایش تراکم سطح و تعداد جوانه های قابل رشد می باشد که منجر به پر شدن خلل و فرج سطحی می گردد.

در شکل ۱۲ نمودار نایکوئست پوشش منگنز در محلول ۰/۵ مولار اسید سولفوریک از فرکانس **۱۰۰kHz** تا**۱۰۰ mHz** در پتانسیل **۵mV** مشاهده می شود. با افزایش زمان پوشش دهی میزان جذب هیدروژن بر روی سطح افزایش یافته که این امر موجب افزایش میزان انجام پذیری واکنش بین اکسیژن و هیدروژن بر روی سطح این کاتالیست گردیده است. با توجه به نمودارهای نایکوئست بدست آمده از نمونه یک به سمت نمونه چهار میزان پلاریزاسیون اکتیواسیون در حال کاهش می باشد. وجود پلاریزاسیون غلظتی در نمونه سه بیانگر این مسئله می باشد که با افزایش میزان واکنش های انجام شده بر روی سطح کاتالیست تشکیل حباب های هیدروژن را بر روی این سطح شاهد می باشیم که این امر موجب ایجاد پلاریزاسیون غلظتی بر روی سطح نمونه سوم گردیده است. در نمونه چهار به دلیل افزایش میزان واکنش پذیری میزان مقاومت اکتیواسیون کاهش شدیدی یافته است در حالت کلی می توان گفت با افزایش میزان زبری سطح ما افزایش میزان سطح کل را در یک مقطع ثابت خواهیم داشت که این افزایش سطح منجر به بهبود عملکرد پیل می گردد.

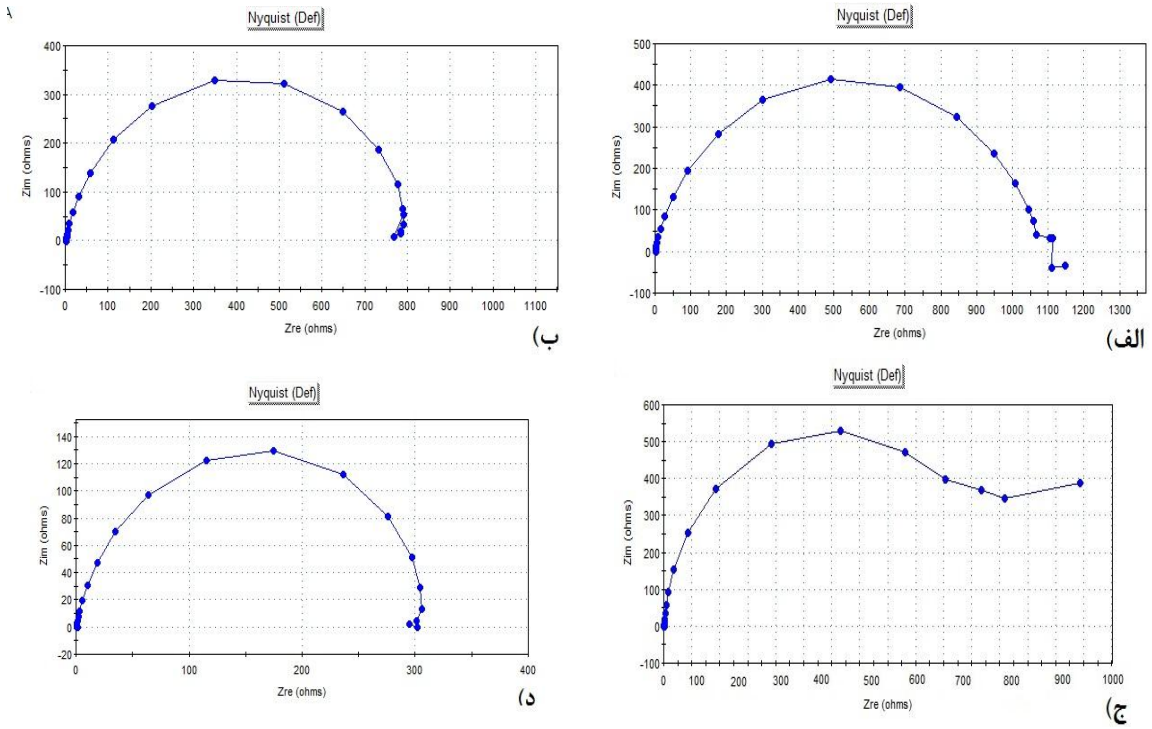

شکل ۱۲: نمودارهای نایکوئست پوشش منگنز در محلول ۰/۵ مولار اسید سولفوریک از فرکانس **۱۰۰kHz** تا**۱۰۰ mHz** در پتانسیل **۵mV** الف) نمونه **Mn-01** ب) نمونه **Mn-02** ج) نمونه **Mn-03** د) نمونه **Mn-04**

نتیجه‌گیری

۱) فرایند لایه نشانی الکتریکی طبق مکانیزم جوانه زنی و رشد، ضخانت لایه پوششی ایجاد شده متناسب با زمان پوشش دهی می باشد.

۲) افزایش زمان پوشش دهی در فرایند لایه نشانی الکتریکی منجر به افزایش زبری و درنتیجه افزایش سطح موثر در یک مقطع ثابت میگردد. افزایش زیاد زمان پوشش دهی باعث افزایش تراکم پوشش در نتیجه کاهش میزان خلل و فرج سطح می گردد.

۳) ایجاد ناهمواری در سطح پوشش منجر به بهبود عملکرد کاتالیست سطحی می گردد.

۴) ذرات پوشش کبالت ایجاد شده از لحاظ ریخت شناسی به صورت گل کلمی می باشد در حالی که ذرات منگنز به صورت اشکال هندسی نامنظم می باشد.

مراجع

۱. الف. ساعی، "هیدروژن، پیل سوختی و محیط زیست"، اولین کنفرانس ملی هیدروژن و پیل های سوختی، تهران، بهمن ۱۳۸۷.

2. Barbir, F. 2012. “PEM Fuel Cells: Theory and Practice”, 2nd Edition, Elsevier, California.

3. EG&G Services, Parsons.Inc, Science Applications International Corporation, Fuel Cell Handbook, 7th Edition, *National Energy Technology Laboratory*, Maryland, 2000.

4. G. Hoogers, Fuel Cell Technology Handbook, *CRC Press LLC*, New York, 2003.

5. W. Yuan, Y. Tang, X. Yang, Zh. Wan, "Porous Metal Materials for Polymer Electrolyte Membrane Fuel Cells – A Review", *Applied Energy*, Vol. 94, pp. 309-329, 2012.

6. M.S. Chandrasekar, M. Pushpavanam, “Pulse and Pulse Reverse Plating-Conceptual, Advantages and Applications”, *Electrochimica Acta*, Vol. 53, pp. 3313–3322, 2008.

7. M.A. Farzaneh, K. Raeissi*, M.A. Golozar, “Effect of current density on deposition process and properties of nanocrystalline Ni–Co–W alloy coatings”, *Journal of Alloys and Compounds*, Vol. 489, pp. 488–492, 2010.

تهیهٔ الکتروکاتالیست Ni-Pt/C و بررسی تاثیر شرایط عملیاتی بر عملکرد پیل‌های سوختی با سوخت مستقیم بورهیدرید

میرقاسم حسینی*، مهدیه صادقی، رعنا محمودی
دانشکده شیمی، دانشگاه تبریز، تبریز، ایران
* mg-hosseini@tabrizu.ac.ir

چکیده

در این مطالعه، کاتالیست کامپوزیتی بر پایهٔ نیکل شامل NiPt روی پارچهٔ کربنی (با نسبت Ni:Pt ۵:۱) آماده شد و در پیل سوختی با سوخت مستقیم بورهیدرید مورد استفاده قرار گرفت. لودینگ کاتالیست $mg.cm^{-2}$ ۲ بود. پراکسید هیدروژن به عنوان اکسیدانت و محلول قلیایی بورهیدرید سدیم به عنوان سوخت در پیل سوختی استفاده شدند. عملکرد پیل سوختی تحت شرایط عملیاتی مختلف از جمله غلظت سوخت و اکسیدانت و دما مطالعه شد. نتایج آزمایش‌ها نشان می‌دهد که با افزایش غلظت سوخت، اکسیدانت و دمای عملیاتی دانسیتهٔ توان نیز افزایش می‌یابد.

واژه‌های کلیدی: پیل سوختی بورهیدرید، کاتالیست NiPt، پراکسید هیدروژن، غلظت بورهیدرید سدیم، غلظت اکسیدانت، دما

مقدمه

پیل های سوختی در پنج دهه اخیر بطور گسترده مورد مطالعه قرار گرفته اند پیل های سوختی باعث شده است تا منابع انرژی جایگزین بیشتری در اختیار باشد. با توسعه سریع در طراحی پیل های سوختی انتظار می رود در یک یک یادو دهه بعد تولید انرژی برای تجهیزات الکترونیک قابل حمل متکی به انرژی حاصل از پیل های سوختی باشد. سوخت هایی مثل گاز طبیعی، پروپان ودیزل مورد توجه قرار گرفته اند اما این سوخت ها باید اصلاح شوند تا هیدروژن تولید کنند [۱]. چند مشکل جدی در این زمینه پیش می آید: قابلیت اعتماد این سیستم ها، امنیت ذخیره این سوخت ها و مشکلات تهیه سوخت قابل اشتعال گازی. بنابراین باید دنبال سوخت جایگزین بود. یک سوخت جایگزین باید مستعد واکنش دهی باشد تا بطور مستقیم بدون اینکه سبب پسیو اسیون آند شود اکسید شود. دستیابی به بعضی سوخت ها مشکل است مخصوصاً اگر از ماکرو مولکول ها استفاده شود. اور ولتاژهای بزرگ آندی نتیجه اکسایش ناقص است. سوخت های هیدرو کربنی می توانند بطور مستقیم در پیل های سوختی اکسید جامد(SOFC) [۲] استفاده شوند، اما اکسایش مستقیم این هیدرو کربن ها چند مرحله مکانیسمی را درگیر می کند و موجب پسیو شدن الکترود می شود[۳،۴]. این نگرانی ها محققان را به استفاده از سوخت های مایع مثل پیل سوختی با سوخت مستقیم متانول (DMFC) وا داشته است. هرچند که در DMFC آند به هنگام اکسایش مسموم می شود و عبور متانول از میان غشا راندمان را کاهش می دهد. پیشرفت های مهمی به بهبود عملکرد DMFC انجامیده است[۷-۵].

اخیراً سدیم بورهیدرید بصورت جامد یا محلول ۳۰ درصد حل شده در محلول غلیظ سدیم هیدروکسید بعنوان بخشی از توسعه های مداوم جایگزین برای پیل های سوختی با دانسیته بالا مورد توجه قرار گرفته است که برای کاربردهای حمل ونقل و ابزارهای زیردریایی بکار می رود. با توجه به اینکه نگه داری هیدروژن در دراز مدت پر خطر است جایگزینی سوخت های دیگر با هیدروژن ضروری است. یون بور هیدرید هم بعنوان محیط ذخیره هیدروژن[۸] و هم بعنوان یک سوخت مورد بررسی قرار گرفت[۹و۱۰]. هردو سیستم مشکلات ظرف های ذخیره پرفشار هیدروژن را کاهش می دهد. بطور ایده آل اکسایش مستقیم یون بور هیدرید درمحیط قلیایی مبادله ۸ الکترون را در پتانسیل تعادلی ۱/۲۴- ولت نسبت به SHE درگیر می کند[۱۱]. واکنش احیای اکسیژن تکمیل کننده واکنش کل است وپتانسیل تعادلی از نظر تئوری ۱/۶۴ ولت است.

$BH_4^- + 8$

$$2O_2 + 4H_2O + 8e \rightarrow 8OH^- \qquad E^\circ = 0.4\,V \quad (2)$$
$$\mathrm{B}H_4^- + 2O_2 \rightarrow BO_2^- + H_2O \qquad E^\circ = 1.64V \ (3)$$

استفاده از هیدروژن پراکسید بجای اکسیژن بعنوان اکسیدانت باعث افزایش پتانسیل پیل می شود. این نوع سیستم با آندهای منیزیم و آلومینیوم در تعدادی از باتری های اولیه و پیل های سوختی بورهیدرید برای وسایل نقلیه زیر دریایی بکار گرفته می شود. هیدروژن پراکسید یک انتخاب مناسب برای این کاربردهاست. در مقایسه با دیگر اکسیدانت ها هیدروژن پراکسید خطر کمتری دارد، در محلول ۳۵٪آبی پایدار است وسمی نیست. معایب این سوخت به قرار زیر است:
انرژی مخصوص آن در مقایسه با اکسیژن کم است و در حضور فلزاتی مثل Pt، Pd و Au استفاده شده در پیل های سوختی تجزیه می شود. بنابراین یک کاتد مناسب باید احیای هیدروژن پر اکسید را بوده و ازتجزیه آن به اکسیژن جلوگیری می کند. واکنش احیای هیدروژن پراکسید در محلول قلیایی بصورت معادله ۴ است :

$4HO_2^- + 4H_2O$

پتانسیل پیل در این حالت ۲/۱۱ ولت است. در حالی که متانول – اکسیژن و هیدروژن – اکسیژن پتانسیل تعادلی به اندازه ۱/۲۱ و ۱/۲۳ ولت تولید می کنند. پتانسیل آند در پیل سوختی با سوخت مستقیم بورهیدرید(DBFC) پتانسیلی مختلط است که تحت تأثیر گونه های ردوکس موجود است. این گونه ها شامل محصولات حاصل از هیدرولیز بورهیدرید و اکسایش آن می باشد. در کاتد نیز دو واکنش احیای مستقیم هیدروژن پراکسید واحیای اکسیژن آزاد شده از تجزیه پراکسید رخ می دهد. احیای هیدروژن پراکسید را در محیط اسیدی به صورت معادلهٔ ۵ است:

$4H_2O_2 + 8e +$

ترکیب این واکنش ها با اکسایش مستقیم بور هیدرید پتانسیل پیلی به اندازه ۳/۰۱ ولت تولید می کند که ۰/۹ ولت بیشتر از احیای هیدروژن پر اکسید در محلول قلیایی است. با وجود همه این چالش ها پیل سوختی بورهیدرید-هیدروژن پر اکسید انرژی بیشتری نسبت به پیل های سوختی متانول – اکسیژن و هیدروژن- اکسیژن تولید می کند.

مواد و روش تحقیق

ابتدا پارچهٔ کربنی به منظور حذف آلودگی‌های سطحی و چربی زدایی در استون، ایزوپروپیل الکل و آب دیونیزه هر کدام به مدت نیم ساعت قرار داده شد. سپس در دمای ۸۰ و۳۰۰ درجهٔ سانتیگراد به مدت نیم ساعت خشک شدند. میزان بار گذاری لایهٔ نفوذ $۲mg.cm^{-2}$ بود. لایهٔ نفوذ از پودر کربن ولکان به همراه محلول تفلونی ۳۰ درصد وزنی و آب و ایزوپروپیل الکل در حمام التراسونیک به مدت ۲ ساعت دیسپرز شده تهیه شد و بر روی ورقه‌های کربنی با روش قلمو اعمال شد. در هر مورد پس از انجام لایه نشانی لایهٔ نفوذ گازی، ورقه‌های کربنی در دماهای ۷۰ و ۳۰۰ درجه سانتیگراد هر کدام به مدت نیم ساعت داخل کوره کاملاً خشک شدند. سپس کاتالیست Ni-Pt/C (با نسبت اتمی ۵:۱) برای نسبت وزنی ۲۰wt.% فلز در پودر کاتالیست و با بارگذاری فلزی $۲ mg\ cm^{-2}$ فلز در سطح تهیه شد.

ابتدا کربن ولکان در مخلوطی از آب و ایزوپروپیل الکل به مدت ۲ ساعت با التراسونیک دیسپرس شد سپس نمکهای مربوطهٔ نیکل و پلاتین به مقدار مناسب اضافه و دوباره به مدت ۲ ساعت دیسپرس شد. سپس pH محلول تا ۸ تنظیم شد و دمای آن به ۸۰ درجهٔ سانتیگراد رسانده شد. در ادامه توسط هیدرازین احیا شد. بعد از سرد شدن مخلوط خشک شد و به منظور حذف یونهای کلر چندین بار با آب مقطر شستشو داده شد و سپس خشک شد.

برای تهیهٔ جوهر کاتالیستی مخلوطی متشکل از ۵ Wt% نافیون، آب و ایزوپروپیل الکل آماده شد و برای یکنواخت شدن جوهر، مخلوط به مدت ۲ ساعت در التراسونیک دیسپرس شد. سپس جوهر کاتالیستی بر روی لایهٔ نفوذ گازی با قلمو به طور یکنواخت اعمال شد.

قبل از استفاده از غشاء نفیون در ترکیب MEA، ابتدا باید کلیه آلودگی‌های احتمالی از آن پاک شود و همچنین پروتونه گردد. برای این منظور ابتدا آن در آب دیونیزه با دمای ۶۰ °C به مدت یک و نیم ساعت قرار داده شد. بعد از آن به مدت یک و نیم ساعت در دمای ۶۰ °C در محلول ۳ wt.% H_2O_2 جوشانده شده تا ناخالصی‌های آلی موجود در آن اکسید شود. پس از این مرحله مجدداً به مدت یک و نیم ساعت در آب دیونیزه با دمای ۶۰ °C قرار داده شد. در مرحله بعد غشا به مدت یک و نیم ساعت در محلول ۰/۵ M H_2SO_4 در دمای ۶۰ °C جوشانده شده و در نهایت غشاء چندین بار با آب دیونیزه شستشو داده شده و تا قبل از اعمال پرس در آن نگهداری می‌شود.

بعد از تهیهٔ آند و کاتد و آماده‌سازی غشا، دو الکترود در دو سمت غشا توسط دستگاه هات پرس تحت دما و فشار بالا، پرس شده و در سلول پیل سوختی مورد استفاده قرار گرفت. در فرآیند تست پیل سوختی با سوخت مستقیم سدیم بوروهیدرید (DBFC) از محلول ۰/۵ M $NaBH_4$ و۱+ ۲ M NaOH به عنوان سوخت در آند و محلول ۱ M H_2O_2 و۰/۵+ M ۰/۵H_2SO_4 بعنوان اکسیدانت در کاتد استفاده شد. تأثیر پارامترهایی چون غلظت سوخت، غلظت اکسیدانت، دمای عمل بر روی راندمان پیل مطالعه شد.

روش فعال سازی این پیلها مشابه بوده و شامل تزریق آب مقطر به آند و کاتد به مدت ۳ ساعت و سپس تزریق محلول ۲M NaOH به مدت ۳ ساعت به آند جهت تبدیل شکل گروه عاملی سولفونیک اسید به Na^+. دلیل این امر این است که کاتیون عبوری از غشا در این دو پیل یون سدیم (Na^+) است نه پروتون (H^+).

نتایج و بحث

اثر دما بر راندمان پیل سوختی $NaBH_4/H_2O_2$

شکل ۱ اثر دما بر روی منحنیهای I-V و I-P پیل سوختی DBFC با لود کاتالیست آندی و کاتدی ۲ mg cm^{-2} نشان می دهد. کاملاً مشخص است که دانسیته توان پیک با افزایش دما افزایش می‌یابد.

با افزایش دما از یک طرف اورولتاژ اکتیواسیون کاهش و از طرف دیگر هدایت‌های غشا و یونها (مانند BH_4^-، Na^+ و OH^-) افزایش می‌یابد. این امر منجر به افزایش راندمان DBFC می‌شود. دماهای خیلی بالا منجر به افزایش سرعت هیدرولیز سدیم بوروهیدرید می‌شود، بنابراین تنظیم دمای عمل مناسب بسیار مهم است.

اثر غلظت سدیم بوروهیدرید بر راندمان پیل سوختی $NaBH_4/H_2O_2$

محلول آندی (سوخت) شامل سدیم بورهیدرید و سدیم هیدروکسید است. مطابق با معادله نرنست[1](معادلهٔ ۶)، ارتباط بین پتانسیل الکترود و محلول الکترولیت به صورت زیر است:

$$E = E^0 = \frac{RT}{8F} \ln \frac{a_{BH_4^-} a_{OH-}^8}{a_{BO_2^-} a_{H_2O}^6} \qquad (۶)$$

بنابراین پتانسیل الکترود با فعالیتهای BH_4^- و OH^- تعیین می‌شود. افزایش غلظت $NaBH_4$، نفوذ سوخت و سینتیک اکسیداسیون را بهبود می‌بخشد و در نتیجه منجر به دانسیته توان بالاتر می‌گردد. هرچند عبور سوخت از غشا و هیدرولیز سدیم بوروهیدرید نیز افزایش می‌یابد که این امر خود منجر به کاهش پتانسیل مدار باز (OCP) در شروع کار می‌شود. بنابراین غلظت سدیم بوروهیدرید برای راندمان بهتر بایستی بهینه شود[۱۲].

تأثیر غلظت سدیم بورهیدرید در دمای ۲۵°C و غلظت ثابت اکسیدانت (۰/۵ M H_2O_2 + ۰/۵ M H_2SO_4) بر روی راندمان پیل‌های سوختی با لودینگ کاتالیست آندی و کاتدی ۲ mg cm^{-2} در شکل ۲ نشان داده شده است. با افزایش غلظت سدیم بورهیدرید از ۰/۵ M به ۱ M، دانسیته توان پیک نیز افزایش داشته است.

اثر غلظت اکسیدانت (H_2O_2) بر راندمان پیل سوختی $NaBH_4/H_2O_2$

برای واکنش دهنده‌های کاتدی مایع، با افزایش غلظت H_2O_2، پتانسیل کاتدی مطابق با واکنش کاتدی و معادله نرنست، افزایش می‌یابد. هرچند مشابه با آنالیز $NaBH_4$، عبور H_2O_2 از غشا برای محلولهای غلیظ‌تر، سریع‌تر است و این امر موجب کاهش ولتاژ در شروع کار می‌شود.

[1] - Nernst

در شکل ۵، تأثیر غلظت هیدروژن پراکسید بر راندمان عملی پیلهای سوختی DBFC با لودهای کاتالیست ۲ mg mg cm^{-2} نشان داده شده است. همانطور که مشاهده می‌شود، با افزایش غلظت H_2O_2 از ۰/۵M به ۱M، دانسیته توان پیک ا افزایش می یابد. لازم به ذکر است که جهت مطالعه تأثیر غلظت هیدروژن پراکسید بر راندمان پیل، ترکیب سوخت، محلول M NaOH ۲+ ۰/۵ M $NaBH_4$ بوده و دمای پیل نیز ۲۵°C تنظیم شده است.

نتیجه‌گیری

۱) افزایش دما دانسیتهٔ توان و دانسیتهٔ جریان را افزایش می‌دهد. ضریب نفوذ واکنش‌دهنده‌ها و هدایت الکترولیت با افزایش دما افزایش می‌یابد. یون‌های بورهیدرید با سرعت بالایی اکسید می‌شوند اما سرعت تولید هیدروژن افزایش می‌یابد.

۲) افزایش غلظت یون‌های بورهیدرید باعث افزایش دانسیتهٔ توان و سرعت تولید هیدروژن و افزایش عبور بورهیدرید از میان غشا می‌شود.

۳) افزایش غلظت پراکسید سدیم باعث افزایش دانسیته جریان و توان پیل سوختی می شود.

مراجع

1. J.D.Holladay, Y.Wang and E.Jones, “review of development in portable hydrogen production using microractor technology”, chemical Reviews,2004,104,4767-4790.
2. S.McIntosh and R.J.Gorte, “Direct Hydrocarbon Solid Oxide fuel cells”, chemical Reviews, 2004,104,4845-4866.
3. M. Mogensen and K. Kammer, “Conversion of hydrogen in solid oxid fuel cells”, Annual Review of Materials Research, 2003,33,321-331.
4. O.A.Marina and M. Mogensen, “High temperature conversion on a composite gadolinia- doped ceria gold electrode”, Applied Catalysis A: General,1999,189, 117-126.
5. F.Maillard, G.-Q.Lu, A.Wieckowski and U.Stimming,“Ru-Decorated Pt surface as Model Fuel Cell Electrocatalysts for co Electro oxidant”, The Journal of Physical Chemistry B, 2005,109, 16230-16243.
6. A.K.Shukla, C.L.Jackson and G.Murgia, “A solid- polymer electrolyte direct methanol fuel cell with amined reactant and air anode”, Journal of Power Sources ,2002,111, 43-51.
7. D.Buttin, M.Dupont, M.Straumann, R.Gille, J.-C. Dubois, R.Ornelas, G.P.Fleba, E.Ramunni,V.Antonucci, A.S.Arico, P.Creti, E.Modica, M.Pham-Thi and J. –P.Ganne, “Adsorption and electrosorption at high –area carbon –felt electrodes for waste-water purification : Systems evaluation with inorganic S-containg anions”, Journal of Applied Electrochemistry , 2001, 31, 275-266.
8. W.Chuan, W.Feng, B.Ying, Y.Baolian and Z.Huamin, “Cobalt boride catalyst for hydrogen generation from alkaline NaBH4- Solution”, Materials Letters , 2005, 59 , 1748-1751.
9. E. Gyenge, M.Itwan and D.Northwood, “Electrocatalysis of Borohudride oxidant on colloidal pt and pt alloys(pt-Ir,pt-Ni,pt-Au) and application for direct borohydride fuel cell anodes”, Journal of The Electrochemical Society, 2006,153, A150- A158.
10. C.Pone de Leon, F.C. Walsh, D.Pletcher, D.J.Browning and J.B. Lakeman, “ Direct borohydride fuel cell”, Journal of Power Sources, 2006, 155, 172-181.
11. L. Wang, C. Ma and X. Mao, “Lm $Ni_{4.78}Mn_{0.22}$ alloy modified with si used as anodic materials in borohydride fuel cells”, Journal of Alloys and Compounds , 2005, 397, 313-316.
۱۲. م. عبدالملکی، پایاننامهٔ دکتری، دانشگاه تبریز، ۱۳۹۲

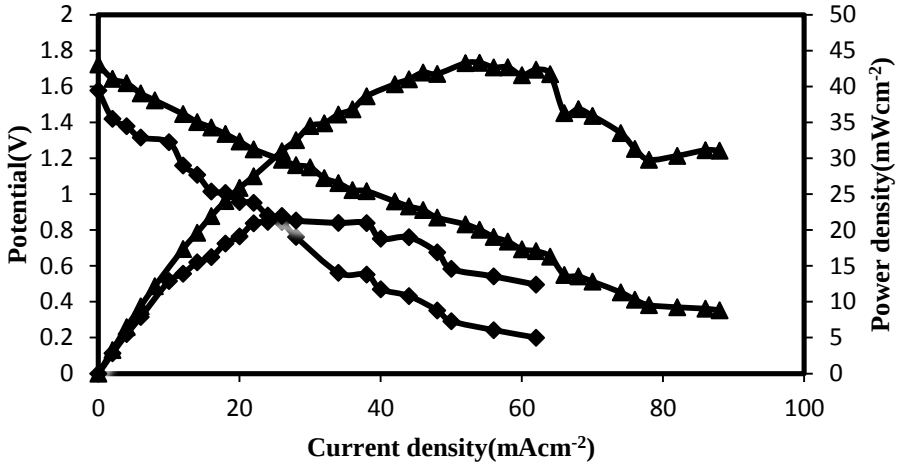

شکل ۱: اثر دما بر روی منحنیهای I-V و I-P، سوخت: محلول ۲ M NaOH + ۱M $NaBH_4$، اکسیدانت: محلول M H_2SO_4 ۰/۵+ ۱ M H_2O_2 (▲ ۴۵ ^oC، ♦) ۲۵ ^oC

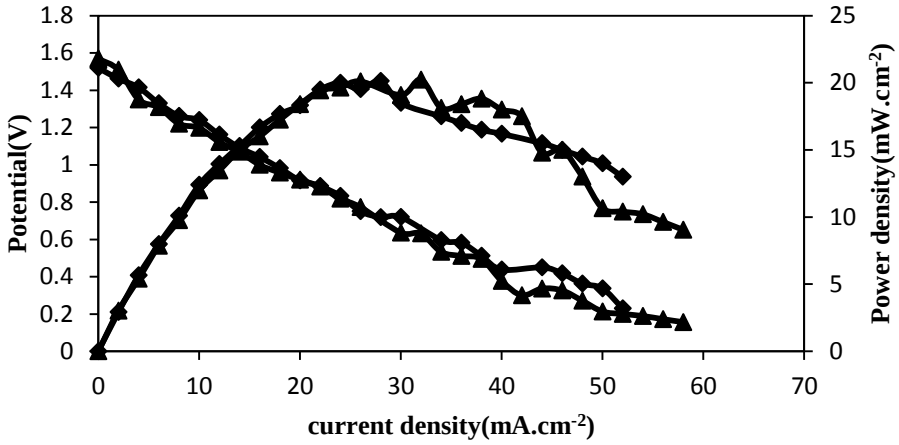

شکل ۲: اثر غلظت سدیم بورهیدرید بر راندمان DBFC، اکسیدانت: محلول ۰/۵M H_2O_2 + ۰/۵M H_2SO_4، دمای ۲۵ °C ▲) سوخت: محلول ۲M NaOH + ۱M $NaBH_4$، ♦) سوخت: محلول ۲M NaOH + M ۰/۵$NaBH_4$

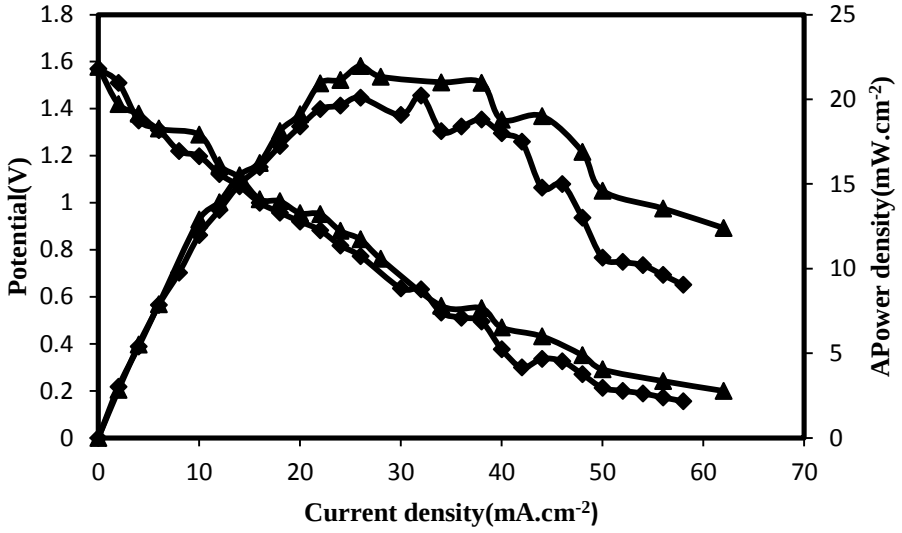

شکل ۳: اثر غلظت هیدروژن پراکسید بر راندمان DBFC، سوخت: محلول ۲M NaOH + ۱M $NaBH_4$، دمای ۲۵ ▲) اکسیدانت: محلول ۰/۵M H_2SO_4 + ۱M H_2O_2، ♦) اکسیدانت: محلول ۰/۵M H_2SO_4 + ۰/۵M H_2O_2

8th Iranian Fuel Cell Seminar
FEBRUARY 25,26
2015

ایجاد پوشش محافظ برای اتصال‌دهنده فلزی پیل سوختی اکسید جامد

زهرا رنجبرنوری، منصور سلطانیه، سعید رستگاری

دانشگاه علم و صنعت ایران-دانشکده مهندسی مواد
** zahra_ranjbar@metaleng.iust.ac.ir*

چکیده

در پژوهش حاضر، به منظور بهبود مشکلات فولاد زنگ‌نزن فریتی AISI-430، به عنوان اتصال‌دهنده پیل سوختی اکسید جامد پوشش محافظ/رسانای اسپینل $(Mn,Cu)_3O_4$ از طریق آبکاری پالسی و اکسیداسیون بعدی ایجاد گردید. به طوریکه ابتدا مس با استفاده از حمام سولفاتی با دانسیته جریان متوسط ۴۸ mA/cm^2 و زمان ۴ دقیقه روی زیرلایه آبکاری شد. سپس برای لایه نشانی منگنز از حمام سولفاتی، دانسیته جریان متوسط ۱۲۵ mA/cm^2 به عنوان دانسیته جریان متوسط بهینه انتخاب شد و زمان رسوب-گذاری ۸ دقیقه بود. در آبکاری پالسی مس و منگنز چرخه کاری ۸۰٪ و فرکانس ۱۰۰ Hz بود. سپس به منظور تبدیل لایه‌های فلزی به اسپینل $(Mn,Cu)_3O_4$ و ارزیابی پایداری پوشش و ممانعت آن از نفوذ کروم به سطح، اکسیداسیون در اتمسفر هوا در دمای ۷۵۰ ^oC به مدت ۱۰۰ ساعت انجام شد. نتایج شناسایی فازی از طریق پراش اشعه ایکس (XRD) تشکیل فاز اسپینل $(Mn,Cu)_3O_4$ را نشان داد. ارزیابی میکروساختاری مقطع عرضی نمونه‌ها توسط میکروسکوپ الکترونی روبشی (SEM) مجهز به EDS نشان داد که پوشش اسپینل $(Mn,Cu)_3O_4$ به طور موثری از نفوذ به بیرون کروم جلوگیری کرد. همچنین لایه پوشش چسبندگی خوبی به زیرلایه داشتند.

واژه‌های کلیدی: پیل سوختی اکسید جامد؛ اتصال‌دهنده؛ فولاد زنگ‌نزن؛ پوشش؛ آبکاری پالسی مس و منگنز ؛ اسپینل $(Mn,Cu)_3O_4$.

مقدمه

اتصال‌دهنده یک جزء بحرانی در پیل‌های سوختی اکسید جامد است. صرف نظر از طراحی صفحه‌ای یا لوله‌ای پیل سوختی اکسید جامد، اتصال‌دهنده نقش دوگانه‌ای را در پیل سوختی ایفا می‌کند. از یک طرف اتصال الکتریکی بین آند یک تک-سلول و کاتد تک‌سلول همسایه برقرار می‌کند، از طرف دیگر یک مانع فیزیکی برای محافظت از مواد الکترود هوا در برابر محیط کاهنده‌ی سوخت و نیز مانع تماس مواد الکترود سوخت با اتمسفر اکسیدکننده است. در واقع گرادیان پتانسیل شیمیایی ناشی از اختلاف فشار جزئی اکسیژن بین محل سوخت و محل اکسیدکننده، یک محدودیت شدید در انتخاب مواد برای اتصال‌دهنده محسوب می‌شود [۱]. لذا برای انجام وظایف خود باید هدایت الکتریکی بالا، پایداری در هر دو اتمسفر

اکسیدکننده و احیاکننده و تطابق ضریب انبساط حرارتی با سایر اجزای پیل سوختی داشته باشد [۲-۴]. اتصال‌دهنده‌های فلزی نسبت به اتصال‌دهنده‌های سرامیکی مزایای زیادی دارند از جمله از پایداری، هدایت الکتریکی و حرارتی، ساخت آسان و هزینه پایین می‌توان نام برد. در بین اتصال‌دهنده‌های فلزی، فولاد زنگ‌نزن فریتی به علت هزینه پایین، تطابق ضریب انبساط حرارتی خوب با سایر اجزای پیل سوختی و مقاومت به اکسیداسیون خوبی که دارد، بهترین گزینه برای استفاده در اتصال‌دهنده است [۵-۹]. با این وجود، استفاده از فولاد زنگ‌نزن فریتی نیز با چالش‌هایی مواجه است که شامل نرخ اکسیداسیون بالا و غیر قابل قبول، کمانش[1] و از هم پاشیدن[2] پوسته‌ی اکسیدی در اثر تنش‌های سیکلی و مسمومیت کاتد در اثر تبخیر کروم است [۳, ۸, ۱۰].

اعمال پوشش محافظ اسپینل اکسیدهای مس و منگنز روشی مناسب برای کاهش نرخ اکسیداسیون اتصال‌دهنده‌های فلزی و ممانعت از تبخیر کروم است [۱۱].

از این رو هدف از این پژوهش بررسی امکان تشکیل پوشش محافظ/رسانای اسپینل $(Mn,Cu)_3O_4$، از طریق آبکاری پالسی لایه‌های فلزی مس و منگنز و اکسیداسیون بعدی در اتمسفر هوا در دمای ۷۵۰°C است.

مواد و روش تحقیق

در این تحقیق از فولاد زنگ‌نزن فریتی AISI-430 با ترکیب شیمیایی ۰/۲۰٪ سیلیسیم، ۰/۴٪ منگنز، ۰/۰۱٪ فسفر، ۰/۵۹٪ نیکل، ۱۵/۵۴٪ کروم و ۸۳/۲۶٪ آهن به عنوان زیرلایه استفاده شد. برای ایجاد پوشش، ورقی از فولاد زنگ‌نزن فریتی AISI-430 با ضخامت ۰/۶ mm به صورت مستطیل‌هایی با ابعاد ۴×۱/۵ cm^2 مورد استفاده قرار گرفت. نمونه‌ها توسط کاغذ سنباده SiC تا شماره ۱۲۰۰ سنباده زده شد. سپس زیرلایه با محلول 10% NaOH در دمای ۸۰°C چربی‌زدایی و در محلول حاوی 20% HNO_3 و 5% HF اسیدشویی انجام شد. نمونه‌ها بلافاصله پس از مرحله اسیدشویی و شست و شو با آب مقطر، از طریق آبکاری پالسی در دمای اتاق پوشش داده شدند و پس از آن در دمای ۷۵۰°C در اتمسفر هوا به مدت ۱۰۰ ساعت اکسید شدند.

آند از جنس پلاتین بود و به همراه الکترود کاری در یک محفظه قرار داشت. ابتدا مس و سپس منگنز روی سطح فولاد زنگ‌نزن با نسبت مولار ۲ به ۳ آبکاری شدند. برای آبکاری مس از حمام سولفات مس حاوی ۱/۵M سولفات مس ($CuSO_4.5H_2O$) و ۰/۸M اسید سولفوریک (H_2SO_4) با pH=۱±۰/۱ استفاده شد [۱۲]. دانسیته جریان متوسط mA/cm^2 ۴۸، فرکانس ۱۰۰ Hz و چرخه‌کاری ۸۰٪ بود.

در مرحله بعد برای آبکاری منگنز از الکترولیتی حاوی ۰/۳M سولفات منگنز ($MnSO_4.H_2O$)، ۱M سولفات آمونیوم ($(NH_4)_2SO_4$) و ۰/۰۳M هیدروکسیل آمین هیدروکلراید ($H_3NO.HCl$) استفاده شد [۱۳]. pH اولیه حمام ۰/۱± ۳/۰ تنظیم شد. فرکانس ۱۰۰ Hz و چرخه کاری ۸۰٪ انتخاب شد. با استفاده از هیدروکسیل آمین هیدروکلراید ضمن آبکاری، از اکسید شدن Mn (II) اطراف آند، حین آبکاری منگنز جلوگیری شد. الکترولیت شفاف باقی ماند و امکان استفاده مجدد از آن میسر شد. اما مشخص شد که در آبکاری منگنز همانطور که زمان آبکاری افزایش می‌یابد، pH به سرعت کاهش

[1] buckling
[2] spallation

می‌یابد. بنابراین باید پس از هر بار آبکاری pH دوباره تنظیم شود. دانسیته جریان متوسط ۱۲۵ mA/cm^2 به عنوان دانسیته جریان بهینه برای لایه نشانی منگنز انتخاب شد. نمونه‌های پوشش داده شده به مدت ۱۰۰ ساعت در کوره با دمای ۷۵۰°C در اتمسفر هوا اکسید شدند. در نهایت توسط میکروسکوپ الکترونی روبشی (SEM) و آنالیز پراش اشعه ایکس (XRD)، مورد ارزیابی‌های ریزساختاری و فازی قرار گرفتند.

نتایج و بحث

از آنجایی که دانسیته جریان در آبکاری منگنز، تاثیر بسزایی روی راندمان جریان، مورفولوژی پوشش، سوختگی لبه‌ها و ساختار پوشش منگنز دارد [۱۴]، آبکاری منگنز در دانسیته جریان‌های مختلف (۲۵۶ mA/cm^2 و ۲۰۰، ۱۷۵، ۱۵۰، ۱۲۵، ۱۰۰) انجام شد تا دانسیته جریان بهینه بدست آید. در دانسیته جریان متوسط ۲۵۶ mA/cm^2 پوشش منگنز به صورت یکنواخت روی سطح نشست اما لبه‌های پوشش لایه‌ای سیاه رنگ ایجاد شد (**Error! Reference source not found.**–ج). در دانسیته جریان‌های بالا، لبه‌های نمونه سیاه‌رنگ می‌شوند. این لایه سیاه، آمورف و ترد است. در نتیجه به راحتی از سطح نمونه جدا می‌شود و حاوی اکسی‌هیدروکسیدها است که از رشد کریستال جلوگیری می‌کنند و راندمان جریان را کاهش می‌دهند [۱۴]. بنابراین دانسیته جریان کمتری (۱۰۰mA/cm^2) انتخاب شد. در این حالت پوشش فقط در لبه‌ها نشست. درحالیکه در وسط نمونه رنگ مس زیرین مشاهده می‌شد (**Error! Reference source not found.**–الف). دانسیته جریان کم منجر به حل شدن منگنز در محلول و در نتیجه کاهش راندمان می‌شود [۱۴]. در نتیجه دانسیته جریان بین این دو مقدار تغییر داده شد تا در نهایت در دانسیته جریان ۱۲۵ mA/cm^2، فلز منگنز به رنگ نقره‌ای- خاکستری سطح زیرلایه را به طور کامل پوشاند (**Error! Reference source not found.**–ب). بنابراین دانسیته جریان ۱۲۵ mA/cm^2 به عنوان دانسیته جریان بهینه برای دستیابی به پوشش منگنز سالم، فشرده و یکنواخت به رنگ نقره‌ای-خاکستری انتخاب شد. نسبت مولی مس و منگنز قبل از عملیات حرارتی روی فازهای تشکیل شده بعد از عملیات حرارتی موثر است. لذا برای رسیدن به نسبت مولی مطلوب برای تشکیل فاز اسپینل $(Mn,Cu)_3O_4$، با دانسیته جریان بهینه‌ی بدست آمده (۱۲۵ mA/cm^2) در سه زمان ۴، ۶ و ۸ دقیقه آبکاری منگنز روی مس انجام شد و زمان ۸ دقیقه برای این منظور مناسب دیده شد. تحت این شرایط پوشش منگنز بدست آمده ضخامتی حدود ۶μm داشت و نسبت مولی منگنز به مس حدود ۳ به ۲ به دست آمد.

در ادامه به منظور تبدیل لایه‌های فلزی به اسپینل، پوشش دو لایه ایجاد شده از طریق آبکاری پالسی، تحت عملیات حرارتی اکسیداسیون در دمای ۷۵۰°C و در اتمسفر هوا قرار گرفت. پوشش روی اتصال‌دهنده فولادی، باید در دمای بالا و زمان کاری طولانی پیل سوختی پایدار باشد. بنابراین برای ارزیابی رفتار پوشش، اکسیداسیون در زمان طولانی یعنی ۱۰۰ ساعت انجام شد. پوشش به دست آمده سالم بود و کیفیت خوبی داشت. شکل ۲ الگوی پراش اشعه ایکس نمونه پوشش‌دار پس از ۱۰۰ ساعت اکسیداسیون در دمای ۷۵۰°C را نشان می‌دهد. آنالیز پراش اشعه ایکس از نمونه‌ی پوشش داده شده بعد از ۱۰۰ ساعت اکسیداسیون حضور اسپینل مکعبی $(Mn,Cu)_3O_4$ روی سطح به عنوان فاز غالب را نشان می‌دهد. سه پیک اصلی این

فاز مربوط به صفحات (۳۱۱)، (۲۲۰) و (۴۴۰) است که به ترتیب در زوایای $۶۳/۳۲^{o}$ و $۳۰/۳۸^{o}$، $۲\theta = ۳۵/۸۶^{o}$ ظاهر شده‌اند. پیک مربوط به اکسید کروم در طیف‌های بدست آمده مشاهده نمی‌شود. بنابراین می‌توان گفت در لایه اکسیدی ایجاد شده در این نمونه، تشکیل فاز اسپینل بر فاز اکسید کروم غلبه کرده است.

شکل ۳ تصویر میکروسکوپی و نقشه توزیع عناصر در مقطع عرضی نمونه با پوشش اسپینلی مس- منگنز پس از ۱۰۰ ساعت اکسیداسیون در $۷۵۰^{o}C$ در اتمسفر هوا با بزرگ‌نمایی ۵۰۰۰ برابر را نشان می‌دهد. پوشش ایجاد شده یکنواختی خوبی در ضخامت داشته و به لایه‌ای چگال تبدیل شده است. همچنین پوشش چسبندگی خوبی به سطح زیرلایه داشته و هیچ گونه جدایش و ناپیوستگی بین زیرلایه و پوشش مشاهده نمی‌شود. با این حال تخلخل‌های بسته‌ای نیز در ساختار آن دیده می‌شود. این تخلخل‌ها در پوشش اسپینلی مس-منگنز ایجاد شده توسط محققان دیگر که با روش‌های مختلف تولید شده‌اند نیز گزارش شده است [۱۲, ۱۵].

نقشه توزیع عناصر در این نمونه نشان می‌دهد که مس و منگنز به خوبی در یکدیگر نفوذ کرده و لایه پوشش یکنواختی خوبی دارد. تصویر میکروسکوپ SEM نشان می‌دهد که ضخامت لایه اکسیدی به حدود ۳۰µm می‌رسد (شکل ۳).

مقادیر جزئی کروم و مقداری آهن نیز در ساختار پوشش مشاهده می‌شود. پوسته اکسیدی تشکیل شده در فصل مشترک پوشش/زیرلایه، عمدتاً از کروم تشکیل شده است. برای بررسی دقیق‌تر آنالیز خطی روی نمونه انجام شد. بر اساس

شکل۴، نمودار مس و منگنز نشان دهنده یکنواختی خوب ترکیب شیمیایی در لایه پوشش است. روند تغییرات آهن و کروم در

شکل نیز تاییدکننده وجود مقداری آهن در پوشش است. اما وجود کروم در آن غیرقابل قبول به نظر می‌رسد. آنالیز خطی کروم در سطح مقطع نمونه پوشش‌دار نشان می‌دهد که کروم در فصل مشترک زیرلایه/ پوشش تجمع کرده است و سپس مقدار آن در پوشش کاهش پیدا می‌کند تا به صفر می‌رسد. با توجه به

شکل می‌توان گفت لایه‌های تشکیل شده روی زیرلایه به ترتیب پوسته اکسیدی نازک غنی از کروم و حاوی مقداری آهن و پوشش اسپینلی مس- منگنز هستند.

به منظور به دست آوردن داده‌های کمی، از نقاط نام‌گذاری شده در

شکل آنالیز نقطه‌ای تهیه شد (**Error! Reference source not found.**۱). آنالیز نقطه ۱ نیز تایید می‌کند که هیچ کرومی به پوشش وارد نشده است در حالی که آهن به لایه پوشش نفوذ کرده است. طبق نتایج EDS نیز کروم به سطح خارجی اسپینل نفوذ نکرده است. روشن است که حضور لایه اسپینل، مانع از نفوذ به بیرون کروم شده است و کروم درون زیرلایه در فصل مشترک زیرلایه/ پوشش تشکیل اکسید می‌دهد.

تصویر الکترون ثانویه با بزرگنمایی ۱۰۰۰۰ برابر از سطح پوشش در شکل ۵، مورفولوژی سطحی پوشش اسپینل اکسیدهای مس و منگنز روی فولاد زنگ‌نزن AISI-430 پس از ۱۰۰ ساعت اکسیداسیون در $۷۵۰^{o}C$ را نشان می‌دهد. مشاهده می‌شود

که سطح با کریستال‌های اکسیدی چگال پوشیده شده است. تصویر SEM از سطح پوشش بعد از اکسیداسیون میکروساختار همگنی را نشان می‌دهد و هیچ ترکی روی سطح پوشش دیده نمی‌شود.

نتیجه‌گیری

پوشش دو لایه مس- منگنز با استفاده از روش آبکاری پالسی روی زیرلایه فولاد زنگ‌نزن فریتی AISI-430 ایجاد شد. پس از آن برای تبدیل لایه‌های فلزی به اسپینل $(Mn,Cu)_3O_4$، اکسیداسیون نمونه‌ها در کوره با دمای ۷۵۰°C در اتمسفر هوا به مدت ۱۰۰ ساعت انجام شد. در نهایت تغییرات ریزساختاری و فازی پوشش‌های بدست آمده بررسی شد. نتایج بدست آمده نشان می‌دهد:

۱) اضافه کردن مقدار کمی (۰/۰۳M) هیدروکسیل آمین هیدروکلراید به عنوان افزودنی به ترکیب حمام سولفاتی آبکاری منگنز، از تشکیل رسوبات حین آبکاری در الکترولیت جلوگیری می‌کند.

۲) دانسیته جریان آبکاری منگنز تاثیر بسزایی در کیفیت پوشش دارد. دانسیته جریان متوسط ۱۲۵ mA/cm^2 برای ایجاد پوششی یکنواخت و سالم مناسب است. دانسیته جریان کمتر از این مقدار منجر به حل شدن منگنز در محلول شده و دانسیته جریان بیشتر، موجب سوختگی لبه‌ها و تشکیل لایه آمورف سیاه‌رنگ در لبه‌ها می‌شود.

۳) روش آبکاری الکتریکی و به دنبال آن اکسیداسیون در دمای بالا روشی مناسب برای ایجاد پوشش اسپینل $(Mn,Cu)_3O_4$ روی فولاد زنگ‌نزن فریتی AISI-430 است و نیز پوشش ایجاد شده چسبندگی خوبی به زیرلایه دارد.

۴) حضور پوشش اسپینلی $(Mn,Cu)_3O_4$ به طور موثری مانع از نفوذ کروم به بیرون در دمای بالا می‌شود و در نتیجه از کاهش عملکرد پیل سوختی ناشی از مسمومیت کاتد با کروم جلوگیری می‌کند.

مراجع

1. W. Z. Zhu and S. C. Deevi, "Development of interconnect materials for solid oxide fuel cells," Materials Science and Engineering: A, 348, 2003, 227-243.

2. J. W. Fergus, "Materials challenges for solid-oxide fuel cells," Jom, 59 ,2007, 56-62.

3. A. L. Prette, M. Cologna, V. Sglavo, and R. Raj, "Flash-sintering of Co2MnO4 spinel for solid oxide fuel cell applications," Journal of Power Sources, 196, 2011, 2061-2065.

4. W. Zhu and S. Deevi, "Opportunity of metallic interconnects for solid oxide fuel cells: a status on contact resistance," Materials Research Bulletin, 38, 2003, 957-972.

5. X. Chen, P. Y. Hou, C. P. Jacobson, S. J. Visco, and L. C. De Jonghe, "Protective coating on stainless steel interconnect for SOFCs: oxidation kinetics and electrical properties," Solid State Ionics, 176, 2005, 425-433.

6. S. Linderoth, "Controlled reactions between chromia and coating on alloy surface," Surface and Coatings Technology, 80, 1996, 185-189.

7. S. Linderoth, P. Hendriksen, M. Mogensen, and N. Langvad, "Investigations of metallic alloys for use as interconnects in solid oxide fuel cell stacks," Journal of materials science, 31, 1996, 5077-5082.

8. J. Wu and X. Liu, "Recent development of SOFC metallic interconnect," Journal of materials science & technology, 26, 2010, 293-305.

9. Z. Yang, K. S. Weil, D. M. Paxton, and J. W. Stevenson, "Selection and evaluation of heat-resistant alloys for SOFC interconnect applications ",Journal of the Electrochemical Society, 150, 2003, A1188-A1201.

10. K. Hilpert, D. Das, M. Miller, D. Peck, and R. Weiss, "Chromium vapor species over solid oxide fuel cell interconnect materials and their potential for degradation processes," Journal of the Electrochemical Society, 143, 1996, 3642-3647.

11. N. Shaigan, W. Qu ,D. G. Ivey, and W. Chen, "A review of recent progress in coatings, surface modifications and alloy developments for solid oxide fuel cell ferritic stainless steel interconnects," Journal of Power Sources, 195, 2010, 1529-1542.

12. M. R. Bateni ,P. Wei, X. Deng, and A. Petric, "Spinel coatings for UNS 430 stainless steel interconnects," Surface and Coatings Technology, 201, 2007, 4677-4684.

13. Y. WANG, "Structure and Electrical Conductivity of Mn-based Spinels Used as Solid Oxide Fuel Cell Interconnect Coatings," Master, Dept. Materials Science and Engineering, McMaster University, Hamilton, Ontario, 2013.

14. J. Gong and G. Zangari, "Electrodeposition and characterization of manganese coatings," Journal of the Electrochemical Society ,149, 2002, C209-C217.

15. N. S. Waluyo, B.-K. Park, S.-B. Lee, T.-H. Lim, S.-J. Park, R.-H. Song, J.-W. Lee, "(Mn,Cu)3O4-based conductive coatings as effective barriers to high-temperature oxidation of metallic interconnects for solid oxide fuel cells," Journal of Solid State Electrochemistry, 18, 2014, 445-452.

جدول ۱: آنالیز نقطه‌ای نمونه با پوشش اسپینل مس-منگنز پس از ۱۰۰ ساعت اکسیداسیون ۷۵۰°C، نقاط در شکل نام‌گذاری شده‌اند.

نقطه	منگنز		مس		کروم		آهن	
	٪اتمی	٪وزنی	٪اتمی	٪وزنی	٪اتمی	٪وزنی	٪اتمی	٪وزنی
۱	۴۳/۵	۴۱/۴	۲۴/۴	۲۶/۹	۰/۰	۰/۰	۳۱/۷	۳۰/۶
۲	۳/۷	۳/۷	۷/۱	۸/۲	۴۷/۳	۴۴/۷	۴۱/۴	۴۲/۰
۳	۰/۰	۰/۰	۰/۲	۰/۲	۱۶/۰	۱۵/۰	۸۳/۵	۸۳/۹

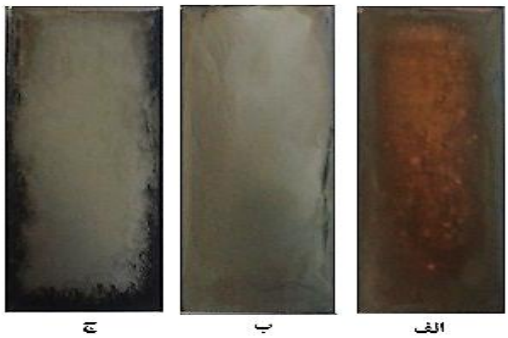

شکل ۱: پوشش حاصل از آبکاری منگنز؛ الف) در دانسیته جریان متوسط mA/cm^2 ۱۰۰ ب) در دانسیته جریان متوسط mA/cm^2 ۱۲۵ ج) در دانسیته جریان متوسط mA/cm^2 ۲۵۶

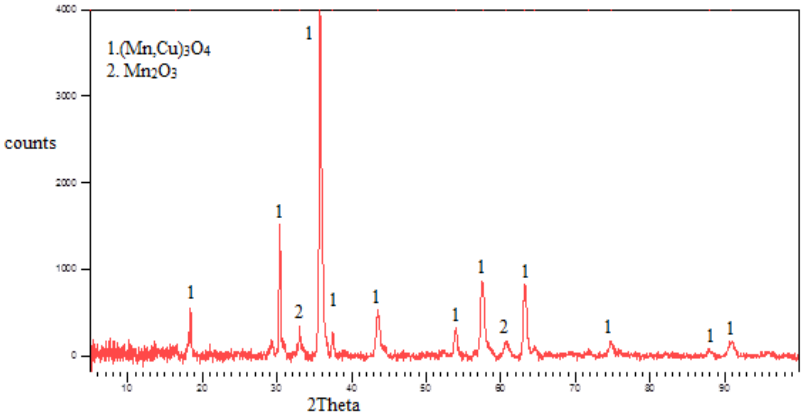

شکل ۲: الگوی پراش اشعه ایکس نمونه با پوشش مس- منگنز پس از ۱۰۰ ساعت اکسیداسیون در $۷۵۰^{o}C$

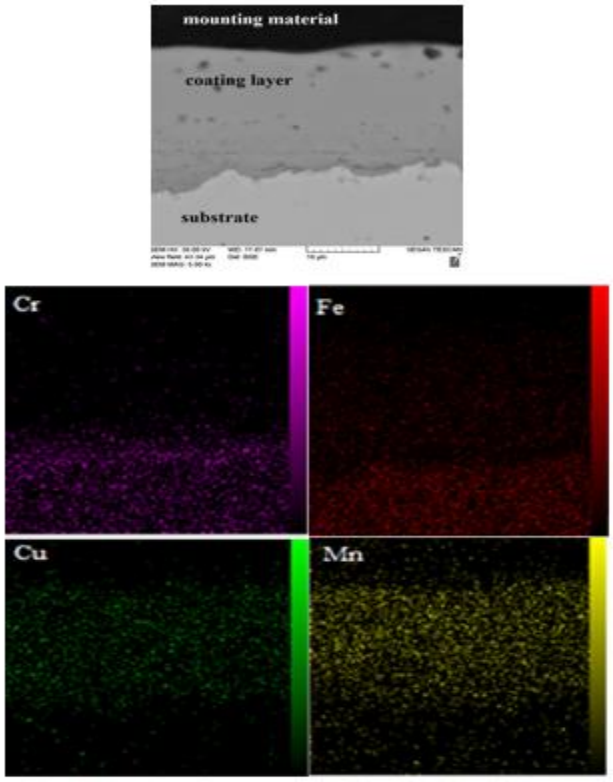

شکل ۳: تصویر میکروسکوپی و نقشه توزیع عناصر در نمونه با پوشش اسپینل مس- منگنز پس از ۱۰۰ ساعت اکسیداسیون در $۷۵۰\ ^{o}C$ با بزرگ‌نمایی ۵۰۰۰ برابر

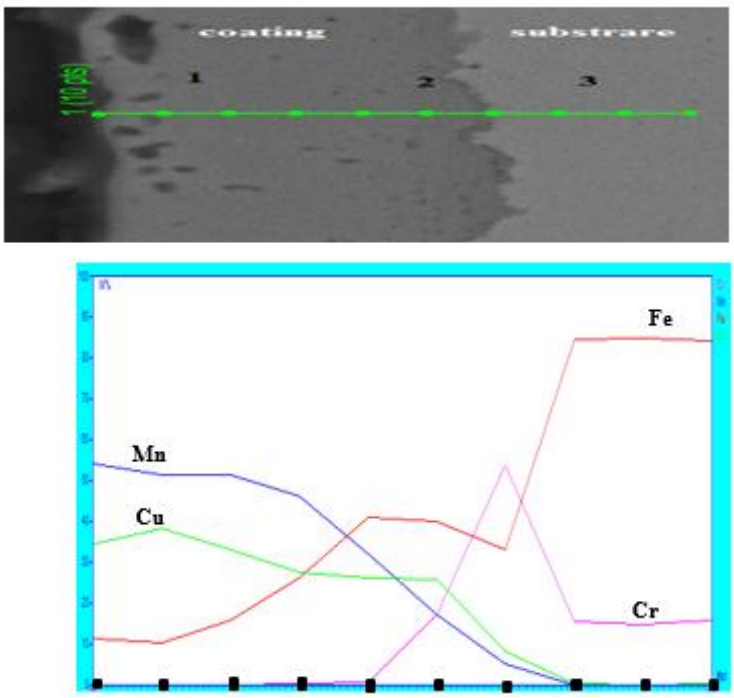

شکل۴: آنالیز خطی نمونه با پوشش مس-منگنز پس از ۱۰۰ ساعت اکسیداسیون

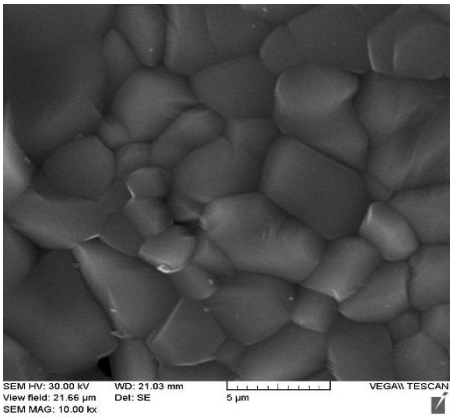

شکل ۵: مورفولوژی سطح پوشش اسپینلی مس- منگنز روی فولاد زنگ‌نزن AISI-430 پس از ۱۰۰ ساعت اکسیداسیون در ۷۵۰^{o}C

بررسی استحکام کششی و ضربه‌ای صفحات دوقطبی تولید شده از پلی استر/دوده

سید احمد مرتضوی[1]، احمد نوزاد گلی کند[2]، اکرم حیدری[1]

۱. دانشکده علوم پایه، دانشگاه آزاد اسلامی، واحد شهرقدس، تهران، ایران

۲. سازمان انرژی اتمی ایران، پژوهشگاه علوم و فنون هسته ای، پژوهشکده مواد

** seyedahmadmortezavi0@gmail.com*

چکیده:

صفحات دوقطبی در پیل سوختی در وزن و حجم و در نتیجه آن در هزینه‌های اقتصادی پیل‌های سوختی بیشترین نقش را ایفا می‌کنند. در ابتدا به دلیل نیاز مبرم پیل‌های سوختی به رسانائی صفحات دوقطبی، از ذرات فلزی و یا از گرافیت استفاده می‌شد. با توجه به پدیده‌های خوردگی و هزینه‌های بالا امروزه با توجه به پیشرفت صنعت پلیمر استفاده از کامپوزیت‌های پایه پلیمری در ساخت این صفحات رایج شده است.

در این مقاله ساخت صفحات دو قطبی توسط کامپوزیت‌های ترموست مورد بررسی قرار گرفته است. در این مقاله از بین پلیمرهای ترموست قابل استفاده برای تولید صفحات دوقطبی از رزین‌های پلی استر (با توجه به خواص مکانیکی بالا و تولید آن در کشور) به عنوان ماتریس پلیمر انتخاب شده است و به دلیل نیارمندی این صفحات به رسانایی از دوده به عنوان پر کننده استفاده شده است. برای نمونه‌های تولید شده خواص مکانیکی آنها از جمله استحکام فشاری و استحکام ضربه‌ای صفحات اندازه گیری شده است.

واژه‌های کلیدی: صفحات دوقطبی، رزین، پلی استر، دوده.

مقدمه

صفحات دوقطبی (Bipolar Plate) از اجزای اصلی تمام انواع پیل سوختی از جمله غشا تبادل پرتون (PEM) می باشد که چندین وظیفه مختلف و کلیدی را در پیل سوختی برعهده دارند. صفحات دوقطبی باید گاز هیدروژن و اکسیژن را در سطح موثر پیل به طور یکنواخت پخش نمایند و جریان الکتریسیته و گرما را از یک واحد به واحد دیگر هدایت کنند. با توجه به اینکه در این نمونه از پیل ها از هیدروژن و اکسیژن جهت تولید الکتریسیته استفاده می شود، این صفحات باید بتوانند مانع نشت گاز به محیط خارج شوند و در عین حال از اختلاط دو گاز هیدروژن و اکسیژن (هوا) جلوگیری نمایند. صفحات دوقطبی همچنین سهم موثری بر کاهش حجم، وزن و هزینه یک مجموعه پیل خواهند داشت. بنابراین تعیین یک جنس مناسب برای صفحات دوقطبی در بازده و قیمت نهایی پیل سوختی تاثیر بسزایی خواهد داشت.

به طور خلاصه وظایف اصلی این صفحات عبارتست از:

- توزیع یکنواخت هیدروژن و اکسیژن در داخل پیل
- تسهیل مدیریت آب در داخل پیل

- هدایت جریان الکتریکی تولیدی در داخل پیل به مدار خارجی
- انتقال گرمای تولید شده در داخل پیل به محیط و به طور کلی مدیریت گرمای پیل

رزین های پلی استر غیر اشباع:

این رزین ها یکی از پرکاربردترین رزین های بکار رفته در صنایع مختلف خصوصا قطعات مورد نیاز در استفاده های روزمره می باشند. این رزین ها از واکنش اسید دوعامله با باز دوعامله آلی بدست می آید. در رزین پلی استر غیر اشباع حداقل دو نوع اسید مصرف می شود. یکی از اسیدها اشباع و دیگری غیر اشباع است. علت استفاده از دو نوع اسید تنظیم میزان غیراشباع بودن رزین یعنی تنظیم میزان توانایی رزین جهت تشکیل پیوندهای عرضی یعنی تنظیم توانایی شبکه ای شدن می باشد. با توجه به استفاده از این دو نوع اسید جهت ساخت رزین، پلی استرهای غیراشباع به دو دسته تجاری با نام های ایزو و اورتو عرضه می گردد. اسید اشباع در نوع ایزو، ایزوفتالیک اسید و اسید اشباع در نوع اورتو، اورتوفتالیک اسید است. اسید غیر اشباع نیز از نوع فوماریک اسید می باشد.

نوع باز مصرفی از نوع پروپیلن گلیکول (یک نوع الکل دو عامله) است. اسیدها می توانند به هر نسبتی با هم مخلوط شوند چرا که از نظر شیمیایی هر دو واکنش یکسانی با عامل الکلی می دهند. نسبت این دو با هم میزان غیراشباع بودن رزین را تعیین می کند.

مواد و روش تحقیق

ابتدا برای ساخت قطعات به صورت دمبلی طبق استاندارد ASTM 638-91 برای انجام تست کشش و همچنین برای ساخت قطعات به صورت میله ای طبق استاندارد ASTM D5941 برای انجام تست ضربه قالب مخصوص آن از جنس سیلیکون RTV تهیه شد. دلیل استفاده از این نوع سیلیکون عدم چسبیدن پلیمرها و صرفا پلی استر به این نوع سیلیکون می باشد.

برای انتخاب نوع رزین از رزین های پلی استر نوع ارتو به دلیل خواص مکانیکی و سفتی و دانسیته بالاتر استفاده شده است. در ابتدا رزین پلی استر به اندازه ۱۰۰ گرم درون ظروف آماده سازی نمونه ریخته شد. پس از آن مقدار ۰/۵ درصد حجمی به آن محلول نفتانات کبالت ۱۰درصد افزوده شد. دلیل استفاده از این محلول آن است که برای رزین های پلی استر پایین آمدن دما تا حد دمای محیط و واکنش خود به خود در دمای محیط تنها با کاتلیزوره امکان پذیر نمی باشد و باید از شتاب دهنده یا کوکاتالیزور استفاده گردد. دلیل عمده استفاده از این محلول ۱) بهبود مقاومت نوری ۲) کاهش تخریب کاتالیز شده فلزی می باشد.

سپس به نمونه آماده شده مقدار ۲، ۳، ۵، ۱۰، ۲۰، ۴۰،۳۰، ۵۰، ۶۰، ۷۰، ۸۰ و ۹۰ درصد دوده در ظروف جداگانه ای افزوده شد و با همزن مکانیکی حدود ۱۵ دقیقه کاملا هم زده شد تا حبابهای رزین کاملا از محلول خارج شود. پس ازآن مقدار ۱/۵ درصد محلول اتیل متیل کتون پروکساید (MEKP) به آن اضافه گردید. این محلول به عنوان کاتالیزور به محلول

اصلی اضافه می گردد تا سرعت انجام واکنش پلیمراسیون را تا حد قابل توجه ای افزایش دهد. نکته مهم در این قسمت آن است که پس از تزریق کاتالیزور به ماتریس (محلول اصلی) سریعا باید محلول تهیه شده را قبل از افزایش ویسکوزیته آن درون قالب RTV ریخت. قالب RTV را قبل از ریختن ماتریس به درون آن باید کاملا با واکس جدا کننده قالب یا روغن سیلیکون کاملا چرب نمود تا قطعه تولید شده به راحتی از قالب خارج گردد. پس از حدود ۲۰ دقیقه نمونه ها را که کاملا به صورت جامد در آمده اند و محکم شده اند از قالب خارج می نماییم و آنها را برای پخت در دمای شکست منطقی کاتالیزور (این دما برای MEKP در حدود ۷۰ الی ۸۰ درجه سانتیگراد می‌باشد) به مدت ۲ ساعت درون آون قرار می دهیم. سپس نمونه ها را به منظور پخت نهایی که برای حذف تنش‌های پسماند و کامل‌شدن پخت زنجیرهای گیرافتاده بین زنجیرهایی که سریعا شبکه‌ای شده‌اند به مدت ۲ ساعت در دمای ۱۰۰ الی ۱۲۰ درجه سانتیگراد قرار می‌دهیم. پس از آن نمونه‌ها را برای پخت ثانویه آماده می نماییم بدین صورت که پس از خنک شدن قطعات تا دمای محیط برای حذف تنش‌های نهایی و افزایش بیشینه خواص مکانیکی، نمونه‌ها را به مدت ۴ الی ۸ ساعت در دمای ۱۲۰ درجه سانتیگراد قرار می‌دهیم. مدت زمان طولانی با دمای بالا زمینه مهاجرت زنجیرها به پایدارترین حالت ممکن و کاهش تنش‌های باقیمانده را فراهم می‌نماید و خواص نهایی قطعات تولید شده بهبود قابل ملاحظه‌ای پیدا می کند. در پایان نمونه‌ها را پس از سرد شدن از آون خارج نموده و پس از سمباده کاری برای انجام تست‌های مکانیکی و مشاهده قطعات توسط میکروسکوپ آماده می کنیم.

نتایج و بحث

هدف از این تحقیق بالا بردن استحکام کششی و ضربه ای صفحات دوقطبی پلیمری با استفاده از دوده نوع N550 در پیل های سوختی می باشد. دلیل این کار رسانا بودن دوده و بالا بردن هدایت الکتریکی صفحات دوقطبی می باشد. جهت این امر از دوده در ۱۲ نوع غلظت مختلف از ۲ درصد تا ۹۰ درصد به منظور بالا بردن استحکام مکانیکی و هدایت الکتریکی در رزین پلی استر استفاده شده است. نتایج استخراج شده از تست های کشش و ضربه به ترتیب در جداول (۱) و (۲) ارائه شده است.

نتیجه‌گیری

با بررسی نتایج بدست آمده از مشخص گردید که افزایش دوده به رزین پلی استر تا غلظت ۵۰ درصد باعث افزایش استحکام کششی می‌گردد اما از غغلظت ۵۰ درصد به بالا این روند افزایشی تغییر نموده به طوریکه در غلظت‌های بالاتر شاهد پایین آمدن استحکام کششی می باشیم. دلیل این پدیده آنست که با افزایش مقدار ویسکوزیته محلول بیشتر شده و این امر مانع خروج حبابهای ایجاد شده در رزین می‌گردد. درنتیجه باقی ماندن حباب در رزین باعث کاهش استحکام آن می‌گردد. همچنین به نظر می‌رسد اگر غلظت دوده در محلول تولید شده بیشتر از ۵۰ درصد باشد به دلیل ازدحام فضایی ایجاد شده مانع تشکیل زنجیره‌های پلیمری و ساختارهای شبکه‌ای منظم و متقارن خواهد شد. نتایج بدست آمده از استحکام ضربه‌ای مؤید آن است که تا غلظت ۷۰ درصد دوده باعث افزایش استحکام شده و غلظت‌های بیشتر باعث کاهش استحکام می‌گردد. بنابراین با توجه به نتایج بدست آمده ار تست‌های استحکام کشش و ضربه ای می توان نتیجه گرفت که

مناسب‌ترین غلظت دوده جهت افزایش استحکام صفحات دوقطبی تولید شده از پلی استر/دوده در حدود ۵۰ درصد بوده و غلظت های بالاتر از آن توصیه نمی گردد.

مراجع

۱. احمد نوزاد گلی کند، پیل های سوختی، انرژی سبز و پاک برای سیاره ما، انتشارات بهشت، ۱۳۸۳.
2. J.S Cooper, J. Power Sources (2004) 18
3. J Huang, D.G Baird, J.E McGrath, J. Power Sources (2005) 10.
4. A Hermann, T Chaudhuri, P Spagnol, J. Power Sources (2005) 6.
5. Narkis et al., US Patent 5 958 303, 1999.
6. Global Recommendation Guide for Conductive Plastics, www.cabot-corp.com
7. Matthew Lee Clingerman, PhD Thesis, Michigan University of Technology, 2001.
8. F Gubbels, S Blacher, E Vanlathem, R Jerome, R Deltour, F Broiers, Ph Teyssie, Macromolecules 28 (1995) 1559.

جدول ۱: نتایج استخراج شده از تست کششی صفحات دوقطبی تولید شده از پلی استر/دوده

ردیف	درصد دوده	درصد کاتالیزور MEKP	درصد شتاب دهنده (نفتانات کبالت)	استحکام کششی (MPa)
۱	۲	۱/۵	۰/۵	۱۳/۸۴
۲	۳	۱/۵	۰/۵	۱۴/۵۲
۳	۵	۱/۵	۰/۵	۱۵/۲۳
۴	۱۰	۱/۵	۰/۵	۲۷/۳۶
۵	۲۰	۱/۵	۰/۵	۳۲/۲۷
۶	۳۰	۱/۵	۰/۵	۳۵/۱۲
۷	۴۰	۱/۵	۰/۵	۳۸/۸۶
۸	۵۰	۱/۵	۰/۵	۴۰/۸۳
۹	۶۰	۱/۵	۰/۵	۲۱/۷۱
۱۰	۷۰	۱/۵	۰/۵	۱۵/۴۵
۱۱	۸۰	۱/۵	۰/۵	۱۳/۲۷
۱۲	۹۰	۱/۵	۰/۵	۱۳/۱۲

جدول ۲: نتایج استخراج شده از تست ضربه ای صفحات دوقطبی تولید شده از پلی استر/دوده

ردیف	درصد دوده	درصد کاتالیزور MEKP	درصد شتاب دهنده (نفتانات کبالت)	استحکام ضربه ای (MPa)
۱	۲	۱/۵	۰/۵	۱۲/۶۶
۲	۳	۱/۵	۰/۵	۱۸/۹۲
۳	۵	۱/۵	۰/۵	۲۴/۳۸
۴	۱۰	۱/۵	۰/۵	۲۹/۴۳
۵	۲۰	۱/۵	۰/۵	۳۲/۱۴
۶	۳۰	۱/۵	۰/۵	۳۷/۶۷
۷	۴۰	۱/۵	۰/۵	۴۳/۱۲
۸	۵۰	۱/۵	۰/۵	۴۸/۱۶
۹	۶۰	۱/۵	۰/۵	۵۴/۷۲
۱۰	۷۰	۱/۵	۰/۵	۵۸/۲۲
۱۱	۸۰	۱/۵	۰/۵	۵۲/۳۰
۱۲	۹۰	۱/۵	۰/۵	۴۸/۳۲

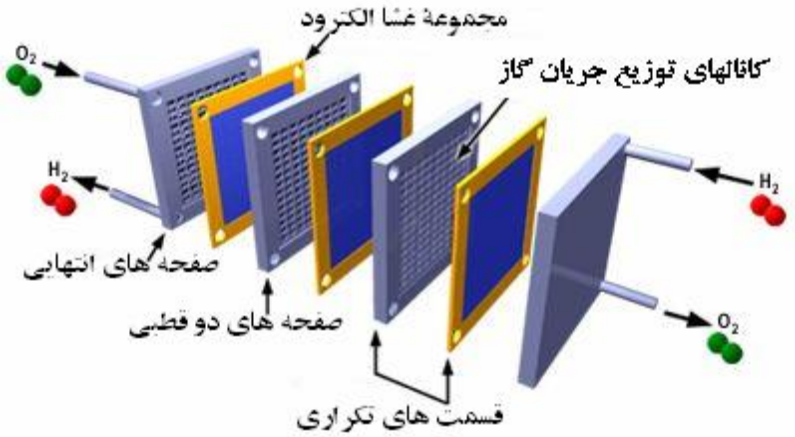

شکل ۱: ساختمان پیل سوختی و جایگاه صفحات دوقطبی [۱]

مطالعه تأثیر ثابت دی الکتریک محلول مورد استفاده در تهیه الکتروکاتالسیت پلاتین به روش الکتروشیمیایی در واکنش کاهش اکسیژن در پیل سوختی پلیمری

رسول عبداله میرزائی، مریم مهدی پور، مهتاب گودرز، صدف دلپذیریان، بهنام معینی

آزمایشگاه تحقیقاتی پیل سوختی، دانشکده علوم ، دانشگاه تربیت دبیر شهید رجایی، تهران، ایران

چکیده

الکتروکاتالیست پلاتین برای تسهیل انجام واکنش اهش اکسیژن در پیل های سوختی به طور گسترده بکار می رود. امروزه تلاش های زیادی برای بهینه سازی عملکرد الکتروکاتالیست پلاتین صورت می گیرد. یکی از فرایندهای تهیه این الکتروکاتالیست استفاده از فرایند ترسیب الکتروشیمیایی می باشد. در این کار سعی شد با مطالعه تغییرات ثابت دی الکتریک محلول مورد استفاده در فرایند الکترودپوزیشن فعالیت الکتروکاتالیستی الکتروکاتالیست های حاصل در واکنش کاهش اکسیژن بررسی شود. الکتروکاتالیست های مورد نظر توسط اعمال پتانسیل چرخه ای تهیه شدند. در این تحقیق تاثیر تغییر میزان قطبیت محلول رسوبگیری پلاتین با بکار بردن مخلوطی از الکل و آب در نسبت های مختلف بررسی شده است که عملکرد الکتروکاتالیست تهیه شده برای واکنش کاهش اکسیژن با روش های الکتروشیمیایی ولتامتری چرخه ای و ولتامتری روبش خطی مورد بررسی قرار گرفت.

واژه های کلیدی: پیل سوختی، کاهش اکسیژن، ترسیب الکتروشیمایی پلاتین، ثابت دی الکتریک

مقدمه:

رشد روزافزون استفاده از منابع تجدیدناپذیر فسیلی، محدودیت این منابع و مشکلات زیست محیطی از قبیل تولید گازهای گلخانه ای توجه محققین را به به کارگیری فناوری های جدید تولید انرژی الکتریکی به خصوص فناوری پیل سوختی جلب کرده است. درواقع پیل های سوختی در ۲۰ سال اخیر به عنوان جایگزین خوبی برای موتورهای احتراق درونی معرفی شده اند [۱] .

پیل های سوختی پلیمری یکی از انواع پیل های سوختی می باشد که به دلیل کارایی بالای این سیستم ها، دانسیته جریان بالا، پاسخ سریع و دمای پایین کارکرد ، کاربردهای فراوانی در مصرف کننده های انرژی الکتریکی دارند[۲]. یکی از موارد محدود کننده کارایی این سیستم ها تمایل پایین اکسیژن برای کاهش می باشد برای رفع این مشکل از الکتروکاتالیست های مختلفی که در راس آن ها الکتروکاتالیست های مبتنی بر پلاتین مورد مطالعه قرار دارند استفاده می شود. لذا مطالعات زیادی برای بهبود عملکرد الکتروکاتالیست پلاتین در این سیستم‌ها در حال انجام است[۷-۳] یکی از روش های تهیه الکتروکاتالیست پلاتین ترسیب الکتروشیمیایی پلاتین روی بستر هایی از جنس های متفاوت می باشد که با کمک تکنیک های مختلف الکتروشیمیایی قابل انجام است. پارامترهای مختلفی بر روی این فرایند تاثیر می گذارند که یکی از این عوامل

می تواند ثابت دی الکتریک محلول ترسیب الکتروشیمیایی باشد.ثابت دی الکتریک توانایی حلال را برای کاهش قدرت میدان الکتریکی اطراف یک ذره باردار که در آن غوطه ور شده است را نشان می دهد[۸].با توجه به ثابت دی الکتریک حلال، حلال ها تقریباً به دو دسته تقسیم شود: قطبی و غیرقطبی، اندازه گیری ثابت دی الکتریک اغلب برای ارزیابی خصوصیات قطبیت مایعات استفاده می شود. حلال های با ثابت دی الکتریک کمتر از ۱۵ به طور کلی غیر قطبی در نظر گرفته می شوند [۹]جدول زیر ثابت دی الکتریک آب واتانول را نشان می دهد:

جدول ۱ مقادیر ثابت دی الکتریک آب واتانول

ماده	اتانول	آب
ثابت دی الکتریک	۲۴/۳	۸۲

در این پژوهش تاثیر ضریب تغییر ضریب دی الکتریک محلول مورد استفاده در فرایند ترسیب الکتروشیمیایی پلاتین با افزودن نسبت های حجمی متفاوتی از اتانول به آب را در فعالیت الکتروکاتالیستی الکتروکاتالیست های تهیه شده در واکنش کاهش اکسیژن در محیط اسیدی بررسی می کنیم.

بخش تجربی

۱-مواد

در این مطالعه از مواد: زغال(cretacolor)، هگزاکلروپلاتنیک اسید(مرک ۴۰٪)، سولفوریک اسید (مرک۹۵-۹۷٪)، اتانول(مرک ۹۶٪) و آب دو بار تقطیر استفاده گردید.

۲-روش کار:

محلول هایی با درصدهای صفر تا ۹۰ درصد اتانول با سولفوریک اسید تهیه گردید. در محلول هگزاکلرو پلاتینیک اسید ۱ میلی مولار ترسیب الکتروشیمیای پلاتین با اعمال ۲۰۰ سیکل توسط روش ولتامتری چرخه ای از پتانسیل ۰/۰۵ تا پتانسیل ۰/۹ولت با سرعت روبش ۱۰۰ میلی ولت بر ثانیه در محلول های با درصد های حجمی مختلف از آب واتانول در دمای محیط انجام گرفت. ترسیب الکتروشیمیایی توسط سیستم سه الکترودی با الکترود مرجع نقره/نقره کلرید والکترود کمکی پلاتین صفحه ای با مساحت ۱سانتی متر مربع والکترود کار که شامل بستر کر بنی مورد استفاده در فرایند ترسیب در نگهدارنده ای از جنس پلی‌تترافلورواتیلن هست انجام شد. ترسیب پلاتین و آنالیز نتایج توسط دستگاه پتانسیواستا – گالوانواستای زاهنر ساخت کشور آلمان انجام شد. به منظور مطالعه فعالیت الکتروکاتالیستی الکتروکاتالیست های تهیه شده در واکنش کاهش اکسیژن از روش ولتامتری روبش خطی (lsv) در محدوده پتانسیل ۱/۲ ولت تا ۰/۲- ولت در محلولی از سولفوریک اسید ۰/۵ مولار و اشباع شده با اکسیژن استفاده شد.

نتایج و بحث

۱-بررسی فعالیت الکتروکاتالیستی نمونه های تهیه شده

منحنی های ولتامتری روبش خطی(LSV) نمونه های A1-A10 فعالیت الکتروکاتالیستی الکتروکاتالیست پلاتین که با تغییرات ثابت دی الکتریک محلول الکترودپوزیشن تهیه شده اند نشان داده شده است.

داده ها نشان میدهد با کاهش ثابت دی الکتریک محلول ناشی از افزایش درصد اتانول در محلول الکترودپوزیشن فعالیت الکتروکاتالیستی ابتدا مقداری افزایش می یابد اما پس از مدتی کاهش می یابد تفاوت مشاهده شده در مقادیر دانسیته جریان الکتروکاتالیست A1 و A10 نشان میدهد با کاهش قطبیت محلول کارایی الکتروکاتالیست در واکنش کاهش اکسیژن کاهش می یابد .

جدول ۱-داده های حاصل از ولتامتری روبش خطی نمونه های A1، A9، A10

نمونه	درصد اتانول	پتانسیل مدار باز برحسب ولت	دانسیته جریان پیشینه بر حسب میلی آمپر
A1	۰	۰/۶۸۳	۲۲۰
A10	٪۹۰	۰/۷۲۲	۱۳۶
A2	۱۰	۰/۷۴۸	۲۵۵

تغییر قطبیت محلول با افزودن مقادیر حداکثر۷۰ درصد اتانول می تواند عملکرد الکتروکاتالیستی نمونه ها را با تغییرات اندکی همراه کند اما زمانی که حضور مولکول های اتانول درصد حجمی بالایی(۹۰ درصد) دارد مطابق آن چه در جدول ۱ نشان داده شده است درA10 دانسیته جریان کاتدی به دلیل پلاریزاسیون غلظتی علی رغم اضافه ولتاژ سینتیکی یکسان با بقیه الکتروکاتالیست ها کاهش می یابد اما در محلول الکترودپوزیشن با مقادیر پایین اتانول کارایی بسیار بهتری مشاهده می شود.

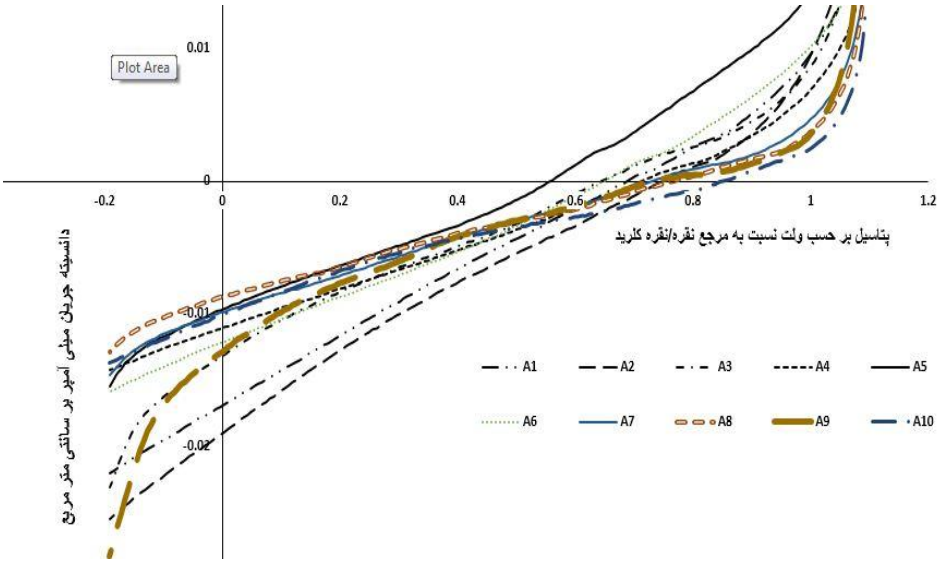

شکل ۱ منحنی روبش خطی الکتروکاتالیست های A1-A10 تهیه شده در درصدهای به ترتیب ۰ ۱۰ ۲۰ ۳۰ ۴۰ ۵۰ ۶۰ ۷۰ ۸۰ ۹۰ در سولفوریک اسید ۰/۵ مولار با سرعت روبش

۲-بررسی منحنی های ترسیب پلاتین بر روی بستر کربنی

نتایج حاصل از منحنی ترسیب الکتروکاتالیست های A1، A2 وa10که در شکل ۲ آورده شده است نشان می دهد در محدوده پتانسیل ۰/۵۵ تا ۰/۰۵ ولت در نمونه A2 دانسیته جریان عبوری هنگام ترسیب پلاتین کمتر از نمونه های A1 و A10 می باشد. اما به رغم عبور دانسیته جریان کمتر از سیستم که می تواند ناشی از بار گذاری پایین تر پلاتین باشد فعالیت الکتروکاتالیستی بالاتری نسبت به واکنش کاهش اکسیژن از خود نشان می دهد.

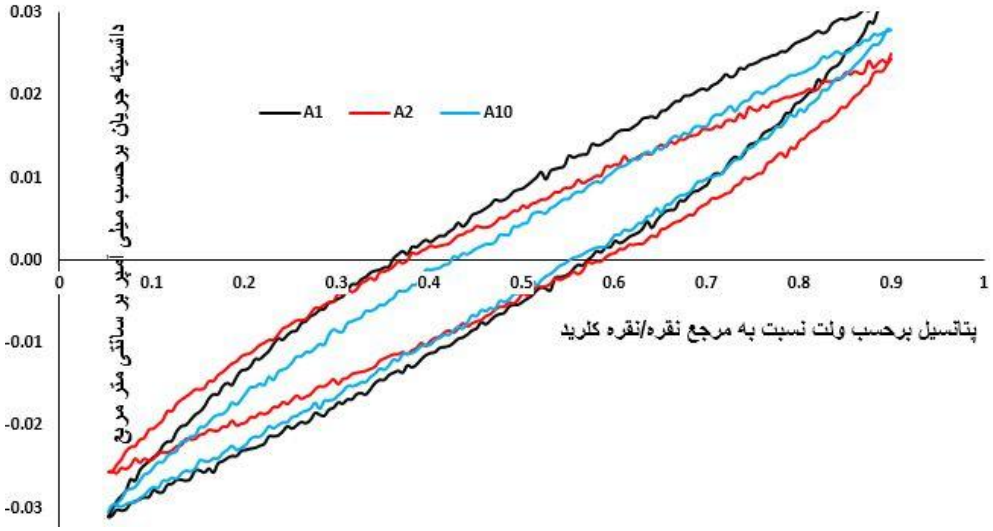

شکل ۲ ولتاموگرام نمونه های A1، A2 و A10ترسیب پلاتین طی اعمال ۲۰۰ سیکل از پتانسیل ۰/۹ تا ۰/۰۵ ولت توسط ولتامتری چرخه ای با سرعت روبش ۱۰۰ میلی ولت بر ثانیه در دمای اتاق.

نتیجه‌گیری

در مطالعه صورت گرفته بر روی واکنش کاهش اکسیژن مشاهده شد با کاهش ثابت دی الکتریک محلول مورد استفاده در فرایند ترسیب الکتروشیمیایی پلاتین فعالیت الکتروکاتالیستی الکتروکاتالیست تهیه شده کاهش می یابد.اما افزودن مقادیر کم اتانول(۱۰دصد) به محلول ترسیب می تواند نتایج بهتری را به دست آورد.

افزودن مقادیر کمی از اتانول می تواند تا حدودی از پلاریزاسیون غلظتی جلوگیری کند که این عامل منجر به عملکرد بهتر الکتروکاتالیست A2 شده است .آنچه از داده های ترسیب برمی آید تفاوت قابل توجهی را نشان نمی دهد بنابراین در مطالعات بعدی سعی بر این است با دنبال کردن مورفولوژی الکتروکاتالیست های تهیه شده تاثیر ثابت دی الکتریک حلال را بر عملکرد الکتروکاتالیستی آن ها نشان دهیم.

مراجع

[1].Chris Rayment,Scott Sherwin, Introduction to Fuel Cell Technology, Notre DameDepartment of Aerospace and Mechanical Engineering University of Notre Dame, U.S.A., 2003.

[2]. Zhuang Xu, Huamin Zhanga, Hexiang Zhong, Qiuhong Lu, Yunfeng Wang, Dangsheng Su, "Effect of particle size on the activity and durability of the Pt/C electrocatalyst for proton exchange membrane fuel cell" , Applied Catalysis B: Environmental , 111-112, 2012, 264

[3]. O. Ikeda, K. Okabayshi, N. Yoshida, H. Tamura, " Spectroelectrochemical study of oxygen reduction at metalloporphyrin-doped polypyrrole film electrodes" , Journal of Electroanalytical Chemistry and Interfacial Electrochemistry, 191, 1985

[4]. A. Elzing, A. Van Der Putten, W. Visscher, E. Barendrecht, " The mechanism of oxygen reduction at iron tetrasulfonato-phthalocyanine incorporated in polypyrrole" , Journal of Electroanalytical Chemistry and Interfacial Electrochemistry, 233, 1987, 113-123

[5]. K-L. Hsueh, H.H. Chang, D-T. Chin, S. Srinivasan, "Electrode kinetics of oxygen reduction on platinum in trifluoromethanesulphonic acid" , Electrochimica Acta, 30, 1985, 1137-1142

[6]. R.C.M. Jakobs, L.J.J. Janssen, E. Barendrecht, " Oxygen reduction at polypyrrole electrodes—II. Experimental results" , Electrochimica Acta, 30 , 1985, 1433-1439
[7]. Jakobs, R.C.M., Janssen, L.J.J., Barendrecht, " Oxygen reduction at polypyrrole electrodes—I. Theory and evaluation of the *rrde* experiments" , Electrochimica Acta, 30, 1985, 1085-1091
[8]. M. Mohsen-Nia and H. Amiri and B. Jazi, " Dielectric Constants of Water, Methanol, Ethanol, Butanol and Acetone: Measurement and Computational Study", *Journal of Solution Chem*, 39, 2010, 701–708
[9]. Lowery, T.H., Richardson, K.S.: Mechanism and Theory in Organic Chemistry, 3d edn. Harper Collins Publishers, New York (1987)

Fuel Cell and Energy

8th Iranian Fuel Cell Seminar
FEBRUARY 25,26
2015

A Nanostructure Magnetic Based Graphene Oxide Electrocatalyst for Methanol Oxidation

R. Sadeghi[1*], H. Karimi-Maleh [2], Necip Atar[3]

1. Department of Physics, Science and Research Branch, Islamic Azad University, Mazandaran, Iran
2. Department of Chemistry, Graduate University of Advanced Technology, Kerman, Iran
3. Department of Chemical Engineering, Pamukkale University, Denizli, Turkey
** h.karimi.maleh@gmail.com*

Abstract
Fuel cells have been attracting more and more attention in recent decades due to high-energy demands, fossil fuel depletions and environmental pollution throughout world. In this study, we report the synthesis of metallic and bimetallic nanoparticles such as spherical iron nanoparticles (sFeNPs), rod iron nanoparticles (rFeNPs) and iron@gold nanoparticles (Fe@AuNPs) involved L-cysteine functionalized reduced graphene oxide nanohybrids (sFeNPs-cis-rGO, rFeNPs-cis-rGO and Fe@Au-cis-rGO) and their applications as an electrocatalyst for methanol electro-oxidation. The nanohybrids have been characterized by transmission electron microscopy (TEM), X-ray photoelectron spectroscopy (XPS) and X-ray diffraction (XRD). Experimental results have demonstrated that reduced graphene oxide-supported bimetallic nanoparticles enhanced electrochemical efficiency for methanol electro-oxidation with regard to diffusion efficiency, oxidation potential and forward oxidation peak current. Fe@Au-cis-rGO, in comparison to sFeNPs-cis-rGO and rFeNPs-cis-rGO, has showed the most efficiency for methanol electro-oxidation.

Keywords: Methanol oxidation, Fuel cell, Reduced graphene oxide, Nanoparticle, Characterization

Introduction

Fuel cells are electrochemical cells used to generate electricity from fuels, and recently have drawn more attention as an alternative method for energy production [1]. One example of these cells is direct methanol fuel cells (DMFCs) which are used for operating portable electronic devices [2]. Methanol is preferred because it has some significant advantages in supply, transport, and storage [3]. More importantly methanol's energy density is higher than gaseous hydrogen, and can integrate into existing energy infrastructure [4]. Many research groups have been investigated the electro-oxidation of methanol in direct methanol fuel cells [5]. Although Pt and Pt-based alloys (with metals such as Ru, Pd, Au, Ni etc.) are the most promising anode catalysts in DMFCs, high cost and limited supply of Pt put some restrictions for large-scale applications [1]. Recently, bimetallic nanoparticles (NPs) have been employed as catalysts in nanotechnology researches [6]. Bimetallic NPs generally show better catalytic properties than their monometallic forms [7]. Use of NPs has some certain advantages [8]. First, bimetallic nanoparticles consist of two different metals which are combined, and this can create a synergetic effect in specific properties such as size dependent optic, electronic and catalytic

properties [9, 10]. Secondly, use of bimetallic nanoparticles allows reducing the amount of expensive catalyst, since a less expensive metal can be employed as the core material. Moreover, because surface area is larger and the majority of atoms can be used at nanoscale, NPs can increase reaction rate and selectivity. Studies showed that the catalytic activity of NPs is determined by some parameters including shape, structure, composition and architecture.

Results and discussion

Characterizations of nanocomposites

The morphologies of the sFeNPs-cis-rGO, rFeNPs-cis-rGO and Fe@Au-cis-rGO nanocomposites were investigated by using the JEOL 2100 HRTEM with an accelerating voltage of 200 keV. A drop of sample solution was deposited on a polymeric grid dried at room temperature under an argon gas stream. Fig 1A shows the transparent, wrinkled and planar sheet like morphology of rGO. In Fig 1B, the TEM image of the sFeNPs-cis-rGO shows that the sizes of the spherical FeNPs are very similar with a mean diameter of 18 to 20 nm on a lighter shaded substrate corresponding to rGO sheet. Fig. 1C shows the size of the rFeNPs-cis-rGO around 7-10 nm on the lighter shaded rGO sheets.

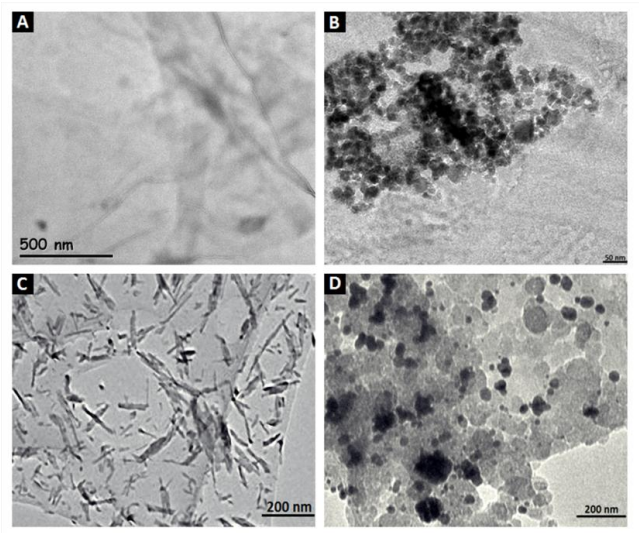

Figure 1. TEM image of (A) rGO, (B) sFeNPs-cis-rGO, (C) rFeNPs-cis-rGO and (D) Fe@Au-cis-rGO.

Fig 1D is the last TEM image that is corresponded to Fe@Au-cis-rGO and shows that the Fe@Au bimetallic nanoparticles have been seen as dark dots with a mean diameter of 12 to 15 nm on rGO sheets.

The electrocatalytic activities of sFeNPs-cis-rGO, rFeNPs-cis-rGO and Fe@Au-cis-rGO modified GCE were investigated by CV at 100 mV s^{-1} in a 0.1 mol L^{-1} HClO4 solution. Fig 2A shows the voltammograms of L-cysteine functionalized rGO, spherical FeNPs and sFeNPs-cis-rGO, respectively. The peak current of 0.5 mol L^{-1} methanol on sFeNPs-cis-rGO modified GCE increases slowly at lower potentials and then quickly increases at potentials higher than 500 mV. The current density is directly proportional to the amount of methanol oxidized at the electrode. The observed current density on sFeNPs-cis-rGO modified GCE is much higher than spherical FeNPs and cis-rGO modified GC electrodes. Fig. 2B shows the voltammograms of L-cysteine functionalized rGO, rod FeNPs and rod FeNPs-cis-rGO, respectively and Fig 2C shows the voltammograms of L-cysteine functionalized rGO, Fe@AuNPs and Fe@Au-cis-rGO, respectively.

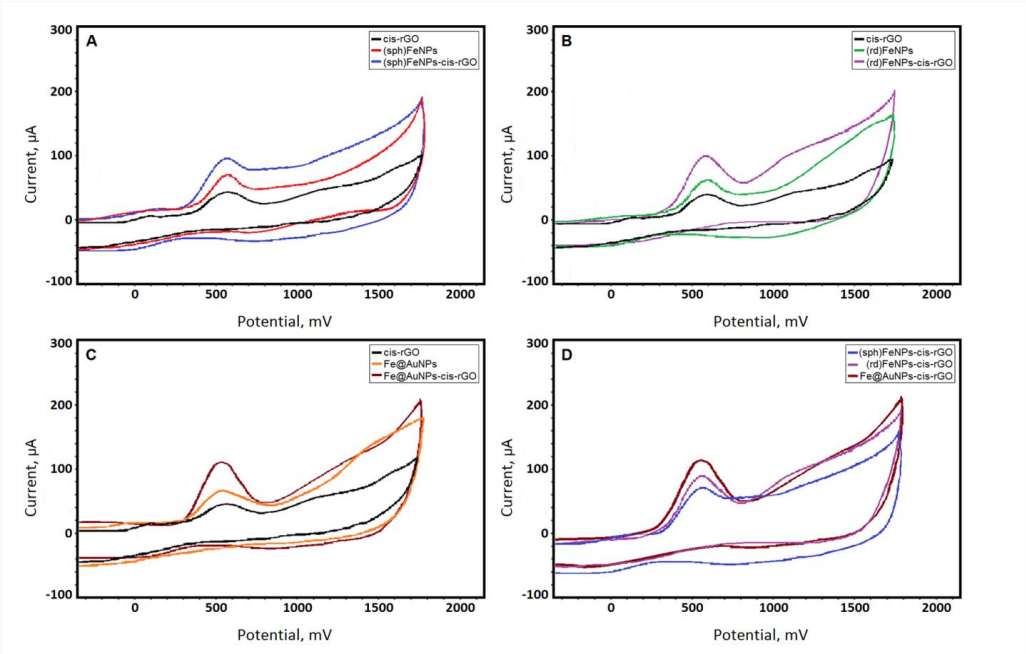

Figure 2. The electrocatalytic activities of (A) cis-rGO, sFeNPs and sFeNPs-cis-rGO, (B) cis-rGO, rFeNPs and rFeNPs-cis-rGO, (C) cis-rGO, Fe@AuNPs and Fe@AuNPs-cis-rGO and (D) sFeNPs-cis-rGO, rFeNPs-cis-rGO and Fe@Au-cis-rGO.

Fig. 2B and 2C are similar to Fig. 2A and shows that the current densities on sFeNPs-cis-rGO (Fig. 2B) and Fe@Au-cis-rGO (Fig. 2C) modified GC electrodes are much higher than rod FeNPs (Fig. 2B) and Fe@AuNPs (Fig. 2C) and cis-rGO (both Fig. 2B and 2C) modified GC electrodes, which confirms that reduced graphene oxide-supported spherical FeNPs (Fig. 2A), rod FeNPs (Fig. 2B) and Fe@AuNPs (Fig. 2C) generate more complete oxidation of methanol to carbon dioxide.

The efficiencies of the sFeNPs-cis-rGO, rFeNPs-cis-rGO and Fe@Au-cis-rGO on methanol oxidation were compared with regard to oxidation potential and current densities in Table 1. As shown in Table 1, the oxidation peak potential of methanol for Fe@Au-cis-rGO was 554 mV, compared with an oxidation potential of 559 mV for (sph)FeNPs-cis-rGO and an oxidation potential of 562 mV for (rd)FeNPs-cis-rGO. This observation shows that the Fe@Au-cis-rGO catalyst can significantly decrease the barrier to methanol oxidation and perform better than the other reduced graphene oxide-supported catalysts in Fig 2D.

Table 1. Comparison of electrocatalytic activity of methanol oxidation on bare GCE, rGO, (sph)FeNPs-cis-rGO, (rd)FeNPs-cis-rGO and Fe@Au-cis-rGO (scan rate: 100 mV s^{-1}).

GC Electrode	Peak Current Density (mA cm^{-2})	E (mV)
(sph)FeNPs-cis-rGO	4.91 ± 0.1	559
(rd)FeNPs-cis-rGO	6.23 ± 0.3	562
Fe@Au-cis-rGO	14.67 ± 0.2	554
rGO	0.64 ± 0.4	567
GCE	-	-

References

[1] V.K. Gupta, M.L. Yola, N. Atar, Z. Üstündağ, A.O. Solak, Journal of Molecular Liquids, 191 (2014) 172-176.
[2] K. Ahn, M. Kim, K. Kim, H. Ju, I. Oh, J. Kim, Journal of Power Sources, 276 (2015) 309-319.
[3] H. Wu, Y. Cao, Z. Li, G. He, Z. Jiang, Journal of Power Sources, 273 (2014) 544-553.
[5] Y. Ma, H. Li, H. Wang, X. Mao, V. Linkov, S. Ji, O.U. Gcilitshana, R. Wang, Journal of Power Sources, 268 (2014) 498-507.
[6] Y. Huang, H. Huang, Q. Gao, C. Gan, Y. Liu, Y. Fang, Electrochimica Acta, 149 (2014) 34-41.
[7] M.L. Yola, T. Eren, N. Atar, Biosensors and Bioelectronics, 60 (2014) 277-285.
[8] V.K. Gupta, M.L. Yola, T. Eren, F. Kartal, M.O. Çağlayan, N. Atar, Journal of Molecular Liquids, 190 (2014) 133-138.
[9] V.K. Gupta, N. Atar, M.L. Yola, M. Eryilmaz, H. Torul, U. Tamer, T.H. Boyaci, Z. Üstündağ, Journal of Colloid and Interface Science, 406 (2013) 231-237.
[10] H. Karimi-Maleh, A.L. Sanati, V.K. Gupta, M. Yoosefian, M. Asif, A. Bahari, Sensors and Actuators, B: Chemical, 204 (2014) 647-654.

8th Iranian Fuel Cell Seminar
FEBRUARY 25,26
2015

GrapheneNanosheets/CarbonNanotube/Pt/PoLyaniline Nanocompositeas Electrode Material for Supercapacitor

Mojtaba Bagherzadeh[*1], Zeinab Shirazi[2], Ahmad Nozad[1], Vahid Esfahdani[1]
1. Material Research School, NSTRI, 81465-1589, Isfahan, I.R. IRAN
2. Malek Ashtar University of Technology of Shahinshahr (MAUTS).
** mjmo123@yahoo.com*

Abstract
Graphene nanosheets/carbon nanotube/Pt/polyaniline nanocomposite (GNS/CNT/Pt/PANI) is synthesized via in situ polymerization. The PANI nanofibers homogeneously coating on the surface of GNS greatly improve the charge transfer reaction. Electrochemical properties were characterized by cyclicvoltammetry (CV), electrochemical impedance spectroscopy (EIS) and galvanostatic charge/discharge. This analysis showed that the GNS/CNT/Pt/PANI composites exhibit remarkable specific capacitance than the pure individual components.

Keywords: Supercapacitor, Pt nanoparticles, Polyaniline.

1. Introduction

Electrochemical capacitors (ECs), known as supercapacitors, have attracted great interest as promising energy storage devices due to their high power energy density and long cycle performance than conventional dielectric capacitors [1,2]. Flexible supercapacitors have played an increasingly important role in power source applications, since they combine the advantages of high power of conventional capacitors and the high specific energy of batteries [3]. Supercapacitors are based on electrostatic charge accommodation at the electrical double-layer and the occurrence of superficial Faradaic reaction [4]. The capacitance of a redox supercapacitor consisting of electroactive materials with several oxidation states or structures (e.g. transition metal oxides and conducting polymers) is expected to be higher than that of a double-layer capacitors [5,6]. Hence, the conducting polymers such as polyaniline (PANI) have advantageous properties with respect to low cost, ease of synthesis, good stability in air as well as relatively high conductivity [7]. However, PANI is susceptible to rapid degradation in performance upon repetitive cycles (charge/discharge process) because of its swelling and shrinkage. In order to alleviate this limitation, the combination of PANI with carbon materials has been proved to reinforce the stability of PANI as well as maximize the capacitance value [8,9]. Due to the intriguing properties of graphene and the advantages of PANI, composites of graphene and PANI have exhibited great promise as supercapacitors electrode materials due to the conductivity, high surface area and the ability to store energy via two charge storage mechanisms. Recently, several researches have been reported on incorporating graphene into PANI matrices to produce nanocomposites for supercapacitors electrode [10]. In addition owing to much unique structural, mechanical, electronic properties and high stability [11], carbon nanotubes (CNTs) show high surface area, excellent electrical conductivity and interconnectivity. So CNTs have been predicted as excellent filler for polymer on improving the electric conductivity as well as the mechanical properties [12].

Herein, we reported a simple process to synthesis a composite of GNS/CNT/Pt/PANI via *in-situ* polymerization. Percentage of materials together was optimized. Then prepared nanocomposite was characterized by using chemical and physical methods like, XRD, SEM, TEM and FTIR. Performance of the prepared nanocomposite for supercapacitor application was evaluated by using cyclic voltammetry (CV), electrochemical impedance spectroscopy (EIS) and galvanostatic charge/discharge. Obtained results are presented and will be discussed here.

2. Experimental

2.1. Synthesis of GNS/CNT/Pt/PANI composites

All the chemicals were of analytical grade and were used without further purification. The as-prepared MWNTs were treated using a 3:1 mixture of concentrated H_2SO_4:HNO_3, as reported by Liu et al [13]. Which produced carboxylic acid groups at the defect sites and thus improved the solubility of the MWNTs that contained carboxylic groups (designated as c-MWNTs) in HCl solution. GNS was prepared by reduction of graphene oxide with glucose as described elsewhere [14].Suspension were made with a certain amount of GNS, H_2PtCl_6 solution and treatment CNT and sonicated for 2 h. Then aniline monomers (solvent: 1 M HCl) were added into GNS/CNT/Pt^{4+} suspension and sonicated for 30 min. platinum ions was reduced with $NaBH_4$ salt. Afterwards, an equal volume of 0.25 M ammonium per sulfate (APS) solution was added into the above mixture and kept at 0–4°C for 4 h. Finally, GNS/CNT/Pt/PANI composite was washed with distilled water and ethanol, dried in a vacuum oven at 80°C for 12 h.

2.2. Preparation of electrodes and electrochemical measurements

A glassy carbon electrode (GCE, ϕ 4 mm) was used as the substrate to prepare the modified electrodes. Typically, 1 mg of the nanocopmosite (GNS/CNT/Pt/PANI) was dispersed in 10 mL of ethanol containing 10 μL of nafion (5 wt% in ethanol) by ultrasonication for 10 min. 10μL of the treated suspension was dripped on to the GCE surface, naturally dried at room temperature to form the modified GCE electrode (GCE/GNS/CNT/Pt/PANI). The electrochemical tests were carried out in H_2SO_4 aqueous (1M) electrolyte solution at room temperature. A three-electrode system was used, consisting of the GCE/GNS/CNT/Pt/PANI as the working electrode, platinum as the counter electrode, and Ag/AgCl as the reference electrode.

3. Results and discussion

3.1. Characterizations

The results confirmed the successful synthesis of the GNS/CNT/Pt/PANI composite.

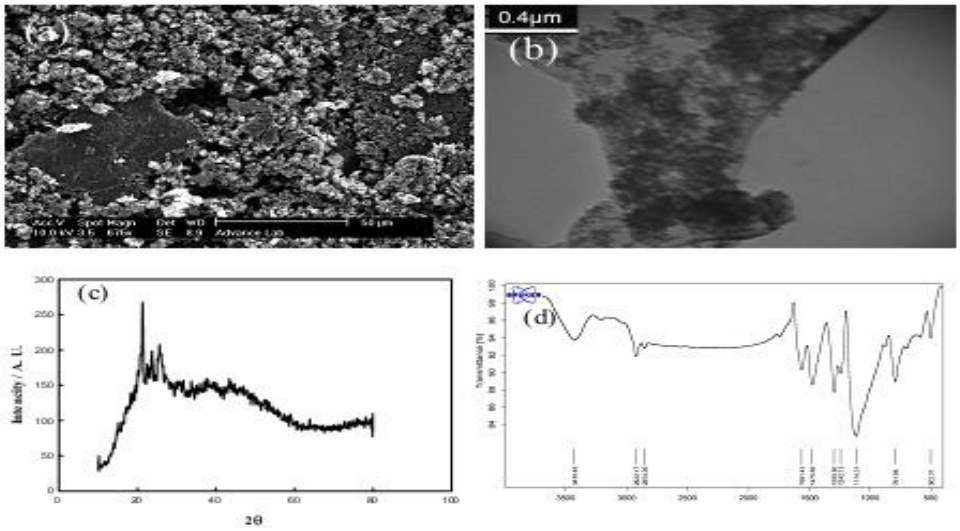

Figure 1. (a) SEM image, (b) TEM image, (c) XRD pattern and (d) FT-IR of GNS/CNT/Pt/PANI composite.

3.2. Electrochemical behavior

The cyclic voltammetry (CV) and electrochemical impedance spectroscopy (EIS) showed that the GNS/CNT/Pt/PANI composites exhibit remarkable specific capacitance than the pure individual components.

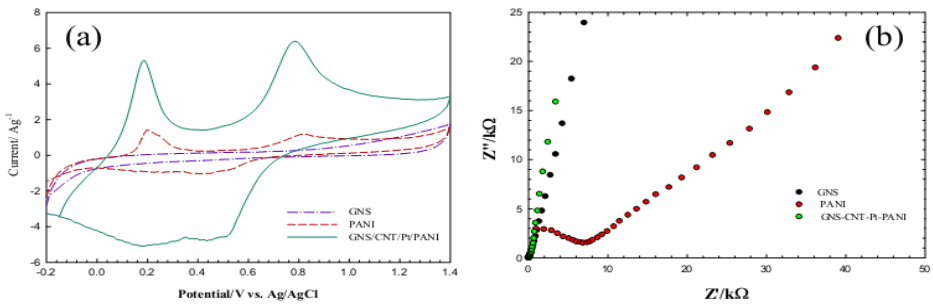

Figure 2. (a) CV curvesand (b) EIS of pure PANI, GNS and GNS/CNT/Pt/PANI composite at 5 mV s^{-1}.

Also the galvanostatic charge/discharge curves were recorded for all materials that will be present in conference.

3. Conclusions

In this paper, GNS/CNT/Pt/PANI composite was synthesized via in situ polymerization. GNS are used as support materials for deposition of PANI particles, CNTs as conductive wires interconnected among GNS/PANI particles and also Pt nanoparticles as an extender surface area. CNTs can not only provide highly conductive path resulting in the improvement of conductivity of composite, but also maintain the mechanical strength. Therefore, the intriguing GNS/CNT/Pt/PANI composite is quite a suitable and promising electrode material for supercapacitors. Obtained results will be present.

5. Reference

1. B.E. Conway. "Transition from “Supercapacitor” to “Battery” Behavior in Electrochemical Energy Storage", J. Electrochem. Soc, 138, (1991), 1539–1548.
2. B. Dong, B-L, He, C, Xu, H-L, Li. "Preparation and electrochemical characterization of polyaniline/multi-walled carbon nanotubes composites for supercapacitor", Mater. Sci. Eng. B, 143, (2007), 7–13.
3. Y. Horng, et al. "Flexible supercapacitor based on polyaniline nanowires/carbon cloth with both high gravimetric and area-normalized capacitance", J. Power Sources 195 (2010), 4418–4422.
4. K. Kim, S. Park. "Influence of multi-walled carbon nanotubes on the electrochemical performance of graphene nanocomposites for supercapacitor electrodes", Electrochim. Acta 56, (2011), 1629–1635.
5. A. Sumboja, J. Yan. "Nanoarchitectured current collector for high rate capability of polyaniline based supercapacitor electrode", Electrochim. Acta 65 (2012) 190– 195.
6. S-B. Yoon, E-H. Yoon. "Electrochemical properties of leucoemeraldine, emeraldine, and pernigraniline forms of polyaniline/multi-wall carbon nanotube nanocomposites for supercapacitor applications", J. Power Sources 196, (2011), 10791– 10797.
7. M. Zhong, et al. "Effect of reduced graphene oxide on the properties of an activated carbon cloth/polyaniline flexible electrode for supercapacitor application", J. Power Sources 217 (2012) 6 e12.
8. Y. Zhou, Z. Qin, et al. "Polyaniline/multi-walled carbon nanotube composites with core-shell structures as supercapacitor electrode materials", Electrochim. Acta, 55, (2010), 3904–3908.
9. R.B. Rakhi, H.N. Alshareef. "Enhancement of the energy storage properties of supercapacitors using grapheme nanosheets dispersed with metal oxide-loaded carbon nanotubes", J. Power Sources, 196, (2011), 8858– 8865.
10. H. Liu, et al. "Three-dimensional graphene/polyaniline composite material for high-performance supercapacitor applications", Materials Science and Engineering B, (2012), MSB 13279 1–6.
11. W. Chen, T. Wen. "Polyaniline-deposited porous carbon electrode for supercapacitor", Eelectrochem. Acta, 48, (2003), 641-649.
12. Q. Liu, O. Nayfeh, S-T. Yau. "Flexible supercapacito r sheets based on hybrid nanocomposite materials", Nano Energy, (2012), 1221-1226.
13. T-M. Wu, Y-W.Lin, Ch-Sh. Liao. "Preparation and characterization of polyaniline/multi-walled carbon nanotube composites", Carbon 43 (2005) 734–740.
14. C. Zhu, S. Guo, Y. Fang, S. Dong. "Reducing sugar: new functional molecules for the green synthesis of graphenenanosheets", ACS Nano, (2010), 4, 2429.

8th Iranian Fuel Cell Seminar
FEBRUARY 25,26
2015

Effect of Noncovalan Attachment of Magnetic Nanoparticles on Supercapacitive Performance of Reduced Graphene Oxide Nanosheets

Mojtaba Bagherzadeh[*1], Vahid Esfahdani[1], Mahdi Jabouri-Abassi[2]
1. Material Research School, NSTRI, 81465-1589, Isfahan, I.R. IRAN
2. Islamic Azad University, Shahreza Branch, Shahreza, 86145-311, I.R. IRAN, Iran
** mjmo123@yahoo.com*

Abstract
Magnetic nanoparticles of Fe_3O_4 (MNP) was noncovalently attached to reduced graphene oxide nanosheets (RGO) to produce RGO/MNP nanocomposites and characterized by XRD, SEM, TEM and VSM techniques. Electrochemical properties of prepared nanocomposite materials were characterized by cyclic voltammetry, galvanostatic charge/discharge and electrochemical impedance spectroscopy in 1 M Na_2SO_4 electrolyte solution, in comparison to RGO nanosheets. Supercapacitive performance of RGO/MNP nanocomposites was also investigated. Our results demonstrated that the RGO nanosheets, RGO/MNP (1:1), RGO/MNP (1:20) nonocomposites deliver an initial specific capacitance at current density of 6 Ag^{-1} as 112, 105 and 69 Fg^{-1}, respectively. After 1000 cycle the specific capacitance of these materials decreased to 63, 73 and 51 Fg^{-1}, respectively. Consequently, RGO/MNP (1:1) nanocomposite has higher capacitive retention than other, after 1000 cycle.

Keywords: Supercapacitor, Graphene, Magnetic Nanoparticle, Composite.

1. Introduction

Climate change and the decreasing availability of fossil fuels call for not only urgent development of sustainable, renewable resources and emission control of global warming gases, but also more advanced energy storage and management devices worldwide [1-3]. Supercapacitors have drawn tremendous attention as an energy storage device for their high power density, good rate performance and long cycling life [4]. If the energy capacity can be further increased, it can be used in much wider array of fields such as hybrid electric vehicle [5], fuel cell, battery [6], and alternation power source, engine starting system, electric actuator, and telecommunication [7-8]. Supercapacitors are usually defined into electrochemical double layer capacitors (EDLCs) and pseudo-capacitors based on their different energy storage mechanisms. Generally, the carbon based porous materials, including graphene, activated carbon and carbon nanotubes that offer high surface areas and readily accessible mesopores are widely used for EDLCs, where the charge storage process in non-faradic and energy storage is electrostatic. At the same time, the capacitance of pseudo-capacitor is mainly from faradic redox reaction. In recent years transition metal oxides such as MnO_2, Co_3O_4 have been drown extensive attentions for psedudo-capacitors [9-10]. In this paper, the effect of Fe_3O_4 as a magnetic nanoparticle (MNP) on supercapacitive performance of RGO was studied. Electrochemical experiments showed that the RGO/MNP (1:1) composite electrode deliver greater specific capacitance than other electrodes after 1000 cycle.

2. Experimental

Graphene oxide was synthesized from natural graphite by a modified Hummers method [11]. As-synthesized GO was suspended in water to give a brown dispersion, which was subjected to dialysis to completely remove residual salts and acids. The purified GO were then dispersed in water to make a 10 mg/mL suspension. Exfoliation of GO was achieved by ultrasonication using an ultrasonic bath. Reduction of GO was performed via Fe^{2+} ion for the first time. Finally, the resulting RGOs was collected with filtration, washed with pure water and ethanol several times, and dried at 80 °C for 12 h in an oven. Magnetic nanoparticles of Fe_3O_4 (MNP) were noncovalently attached to reduced graphene oxide nanosheets (RGO) to produce RGO/MNP nanocomposites via coprecipitation method.

All electrochemical measurements were done in conventional three electrode setup: glassy carbon (1 cm^2) coated with electroactive materials as the working electrode, platinum wire and Ag/AgCl (3 M KCl) electrode as the counter and reference electrodes. The working electrodes were prepared by mixing electroactive materials, carbon black and poly(tetrafluoroethylene) with mass ratio of 80:10:10 and dispersed in ethanol. Then the resulting mixture was coated on the glassy carbon electrode. The weight of active material was 6.25µg. The electrochemical properties of the supercapacitores were studied through cyclic voltammetry (CV), electrochemical impedance spectroscopy (EIS) and galvanostatic charge/discharge methods. 1M Na_2SO_4 solution was used as the electrolyte. CV tests were done between -0.2 and 1 V at scan rate of 100 mVs^{-1}. Galvanostatic charge/discharge curves were measured at current density of 6 Ag^{-1} and EIS measurments were also carried out in the frequency range from 100 kHz to 100 mHz at open circuit potential with an ac perturbation of 5 mV.

3. Results and discussion

The capacitive performance of electrodes were evaluated using CV and galvanostatic charge/discharge techniques in 1 M Na_2SO_4 electrolyte solution at ambient temperature. The cyclic voltammograms of MNP, RGO, RGO/MNP (1:1) and RGO/MNP (1:20) nanocomposite electrodes at 100 mVs^{-1} are shown in Fig. 1. Obviously, all of voltammograms show a semi rectangular and symmetrical shape due to the capacitance C ($C=i/m\upsilon$, i is the current, and m is the mass of active material) would keep constant at a linear charge/discharging rate ($\upsilon=dE/dt$ that is constant, E is the potential window of charge/discharge, and t is the time of charge/discharge) [2]. It could be found that the area surrounded by cyclic voltammogram for RGO electrode is apparently larger than of other electrodes (Area surrounded: RGO > RGO/MNP (1:1) nanocomposite > RGO/MNP (1:20) nanocomposite > MNP), implying the higher specific capacitance of RGO electrode.

The specific capacitance of RGO in 1 M Na_2SO_4 solution could be attributed to the nature of the electrolyte, providing a double-capacitance. In composite electrodes, both RGO and Fe_3O_4 nanoparticles can make electrochemical contributions to the specific capacitance. But, unexpectedly areas surrounded of composite electrodes are smaller than of RGO electrode. Which may be due to agglomeration of active materials and decreasing the possible surface for electrochemical reaction. The energy storage mechanism of Fe_3O_4 electrode has been accepted as the proton-electron mechanism [10].

In addition, the rate performance of electrode materials is also crucial for supercapacitors. Galvanostatic charge-discharge curves of MNP, RGO, RGO/MNP (1:1) and RGO/MNP (1:20) nanocomposite at current 6 Ag^{-1} are shown in Fig. 2. The specific capacitance of samples is calculated from the galvanostatic charge-discharging function according to the following equation:

$$C = \frac{I \times \Delta t}{m \times \Delta V} \quad (1)$$

Where C is the specific capacitance, I is the current, Δt is the discharging time, m is the mass of electroactive materials, and ΔV is the potential window. Therefore, the value of specific capacitance at 6 Ag^{-1} is 112, 105, 69 and 66 Fg^{-1} for RGO, RGO/MNP (1:1) and RGO/MNP (1:20) nanocomposites, and MNP, respectively, which are well agree with the results of CV measurement.

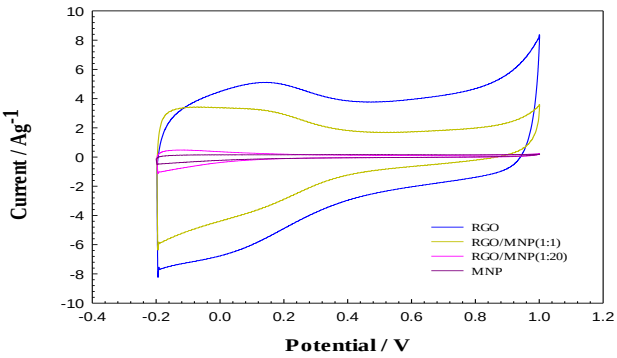

Figure 1: Cyclic voltammograms of RGO,MNP, and RGO/MNP composite in 1M Na_2SO_4 solution

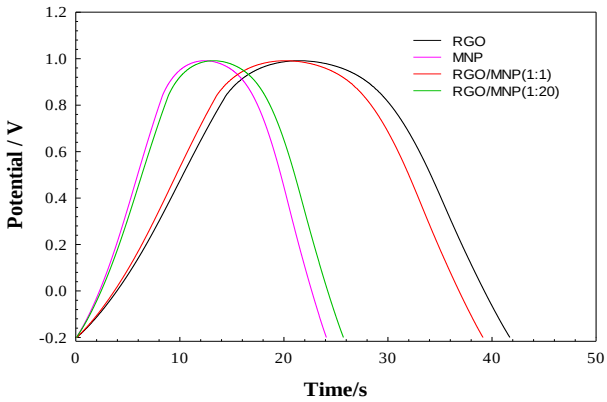

Figure 2: Charge-discharge curves of RGO, MNP and RGO/MNP composites

Long cycle life of supercapacitors is a crucial parameter for their practical applications. A galvanostatic charging-discharging test was conducted at 6 Ag^{-1} for 1000 cycles, which the results have been depicted in Fig. 3. The capacitive retention for RGO, RGO/MNP (1:1) , RGO/MNP (1:20) nanocomposites, and MNP is 57%, 74%, 69% and 77% after 1000 cycle, respectively. It is interesting to note that RGO electrode deliver a high initial specific capacitance than of RGO/MNP (1:1), but the specific capacitance for RGO fall down after nearly 100 cycles to the values lower to the value was obtained for RGO/MNP(1:1) nanocomposite electrode. Attachment of the MNP by ratio of 1:1 on the surfaces RGO nanosheets resulted in enhanced mechanical strength of the material and prevents them from agglomeration and therefore long charging/discharging cycling ability was obtained, while RGO/MNP(1:20) nanocomposite deliver smaller specific capacitance than of RGO/MNP(1:1) nanocomposite.

The EIS analysis has been recognized as one of the principal methods examining the fundamental behavior of electrode materials for supercapacitor. Complex plane plots of all

materials are presented in Fig. 4. As can be see all plots had semicircle shape at high and intermediated frequencies, followed by a relatively linear response at the low frequencies. The initial non-zero intercept in high frequency region at the beginning of the semicircle is identical in all the curves which are resulted of the electrical resistance of the electrolyte (R_s). In addition, it also finds that charge transfer resistance value was RGO < RGO/MNP (1:1) nanocomposite < RGO/MNP (1:20) nanocomposite < MNP. Evidently, it indicates that the conductivity of RGO is greater than of other materials. Obtained results will be present and discussed.

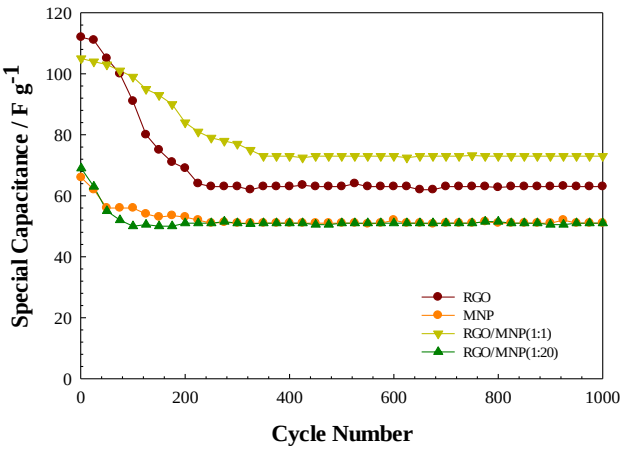

Figure 3: Cycling performance of RGO, MNP, and RGO/MNP composite

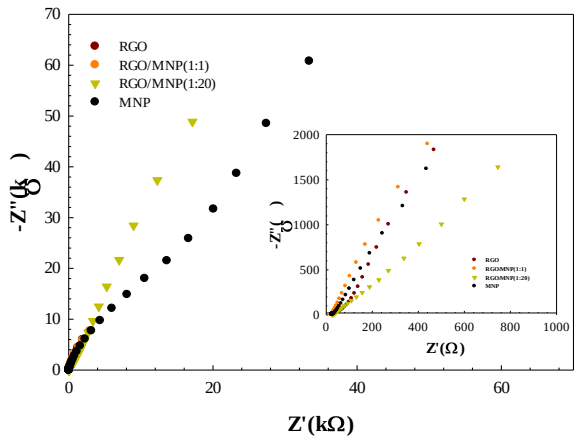

Figure 4: Nyquist plots of RGO, MNP, and RGO/MNP composite

4. Conclusions

In Summary, we investigated the supercapacitive properties of RGO and RGO/MNP nanocomposites in the Na_2SO_4 solution by electrochemical methods. The results show that the RGO deliver maximum specific capacitance in initial cycles than of other electrodes, but after nearly 100 cycles specific capacitace of RGO/MNP(1:1) nanocomposite is greater than of other electrodes.

References

[1] P.Simon, Y. Gogotsi, Materials for electrochemical capacitors, Nat. Mater. 7 (2008) 845.
[2] J. Yan, T. Wei, W. Qiao, B. Shao, Q. Zhao, L. Zhang, Z. Fan, Rapid microwave-assisted synthesis of grapheme nanosheet/Co_3O_4 composite for supercapacitors, Electrochem. Acta 55 (2010) 6973.
[3] T. –Y. Wei, C. –H. Chen, H. –C. Chien, S. –Y. Lu, C. –C. Hu, A cost-effective supercapacitor material of ultrahigh specific capacitances: Spinel nickel cobaltite aerogels from an epoxide-driven sol-gel process, Adv. Mater. 22 (2009) 347.
[4] W. H. Shi, J.X. Zhu, D. H. Sim, Y. Y. Tay, Z. Y. Lu, X. J. Zhang, Y. Sharma, M. Srinivasan, H. Zhang, H. H. Hng, Q. Y. Yan, Achieveving highspecific charge capacitences in Fe_3O_4/reduced grapheme oxide nanocomposites, J. Mater. Chem. 21 (2011) 3422.
[5] A. Burke, Why, how, and where is the technology, J. Power Sources 91 (2000) 37.
[6] P.Thounthong, S. Rael, B. Davat, Energy management of fuel cell battery/supercapacitor for hybrid power source for vehicle application, J. Power Sources 193 (2009) 376.
[7] S. Zhang, Y. Li, N. Pan, Graphene based supercapacitor fabricated by vacuum filtration deposition, J. Power Sources 206 (2012) 476.
[8] R. Kotz, M.carlen, Principles and applications of electrochemical capacitors, Electrochim. Acta 45 (2000) 3498.
[9] C. Liu, Z.Yu, D. Neff, A. Zhamu, B. Z. Jang, Graphene-based supercapacitor with an ultrahigh energy density, Nano Letters 10 (2010) 4863.
[10] Y. Wu, S. Liu, H. Wang, X.Wang, X.Zhang, G. Jin, A novel solvothermal synthesis of Mn_3O_4/graphene composites for supercapacitors, Electrochem. Acta 90 (2013) 210.
[11] W.S. Hummers, R.E. Offeman, “Preparation of Graphitic Oxide” J. Am. Chem. Soc. 80 (1958) 1339.

8th Iranian Fuel Cell Seminar
FEBRUARY 25,26
2015

Effect of Titanium Foil Surface in Anodized Titanium Oxide Nanotubes as Electrode for Lithium-Ion Batteries

Hamideh Kashani, Hussein Gharibi*
Department of Chemistry, Tarbiat Modares University, Tehran 14115-175, Iran
Hykashani@Modares.ac.ir

Abstract
Titanium oxide nanotubes were synthesized by anodizing method in four different degree of sleek surfaces and study as anode of Li ion battery. The results show if the surface of titanium foil as substrate is sleeker, the cyclability and the capacity of Titanium oxide nanotube as anode of Li ion battery is increased and decreased respectively. Ti foil samples polished with abrasive paper in grit size 1000 and 5000.

Keywords: Li Ion Battery, Anode, Titanium foil, Nanotube Titanium Oxide, Anodize

Introduction
TiO2 is of great interest as a promising anode material for Li-ion batteries because it offers enhanced safety, low self-discharge, and good capacity retention on cycling. Because of its high operation potential (varying between 1.45 and 1.80 V for different phases) vs. Li^+/Li, the electrode avoids formation of an unstable solid-electrolyte interface (SEI) on the electrode surface and thus eliminates the risk of short circuit caused by dendrites formed in overcharging. The SEI-free interface also allows rapid charging and power release. In addition, the small volume change (<4%) of TiO2 under Li^+ insertion provides high structural stability and potentially good cycling life. Anodic self-aligned TiO2 nanotube arrays (NTs) mitigate the rate-limiting effects of sluggish electron kinetics and mass transport, taking advantage of the large surface area, short diffusion lengths, and orthogonal electron transport paths [1]
The advantage of TiO2 nanotubes produced by anodizing is that they have been effectively immobilized on a titanium surface during preparation. As the result, these nanotubes have several possible applications. It has recently been found that the electro conductivity of TiO2 nanotube films increases by several orders of magnitude in the presence of gaseous hydrogen, making this a promising material for hydrogen sensing. Similar TiO2 nanotubes have also shown promise for use as photo catalytic, self-cleaning surfaces, as photoanodes for water splitting or in dye-sensitized solar cells (where the efficiency of the photoanodic response depends on the nanotube wall thickness, and the current collection efficiency is a function of the quality of the nanotube–electrode contact)
The growth of nanotubes by anodizing titanium can be described as a selective etching, and the method can be related to a top down approach. In the simplest approach, such nanotube growth can be described in terms of a competition between several electrochemical and chemical reactions, including: anodic oxide formation [2, 3].
$Ti + 2H_2O \rightarrow TiO_2 + 4H^+ + 4e^-$
chemical dissolution of the titanium oxide as soluble fluoride complexes, e.g.:
$TiO_2 + 6F^- + 4H^+ \rightarrow [TiF6]^{2-} + 2H_2O$
and direct complexation of Ti ions migrating through the film [1-5].:
$Ti^{4+} + 6F^- \rightarrow [TiF_6]^{2-}$

Experiment

Synthesis of TNAs TiO_2 nanotube arrays were synthesized by electrochemical anodization of Ti foil at room temperature. Prior to anodization, a Ti foil with a thickness of 0.5 mm was polished with abrasive paper in grit size 1000, 5000 and then successively cleaned with aceton, ethanol, 2-propanol and deionized (DI) water in an ultrasonic bath for 30 min. Then it was subjected to potentiostatic anodization for 4 h in a two-electrode electrochemical cell with a Cupper foil as the counter electrode. A constant voltage of 50V was employed for the anodization and the electrolyte used is 0.3% M NH_4F in a 2: 98 (w/w) mixture of DI water ethylene glycol (EG). After reaction, the anodized Ti foil was ultrasonically rinsed with DI water several times and annealed at 500 C for 3 h with a ramp rate of 1 □ C/min to obtain crystalline TNAs on the Ti foil.

Results and Discussion

Fig 1. Compares the top and cross-sectional morphology of titanium nanotube without treatment (TNAWT), titanium nanotube polished abrasive paper in grit size 1000 (TNA1000) and 5000 (TNA5000), the TNA5000 have a much larger tube diameter (OD: 300-400 nm) than the TNTWT (OD: 100-200). The morphological characteristics of TNAs are characterized using a Field-emission scanning electron microscope (FESEM) Fig 1.

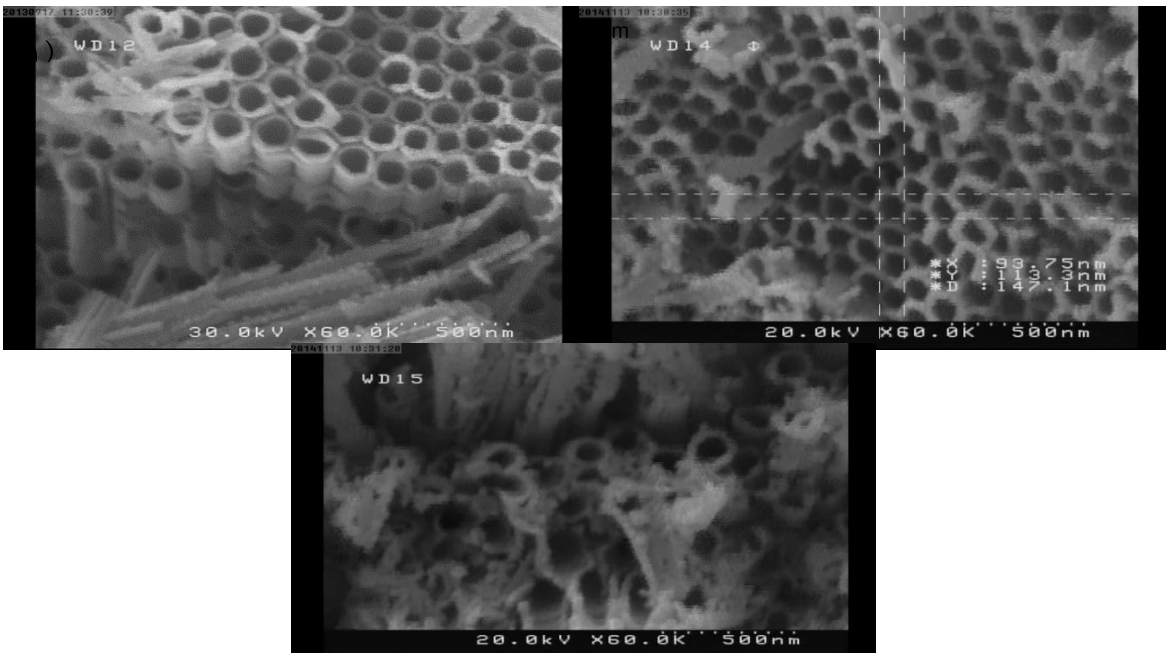

Fig. 1) Field Emission SEM a) TNA5000 b) TNA1000 c)TNAWT

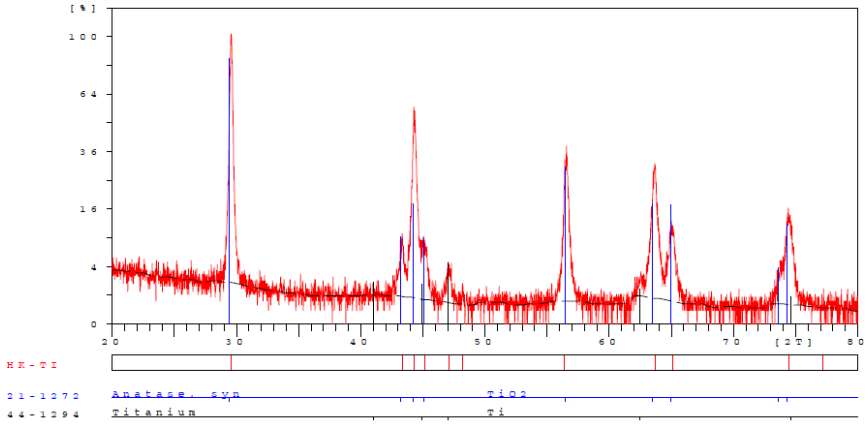

Fig. 2 X-ray diffraction pattern TiO2 nanotube. The vertical lines show the peak positions (h k l lines) of the anatas phase.

Crystal structure of the tubes studied by XRD. The XRD patterns of TiO2 nanotubes are shown Fig. 2. The patterns were indexed as anatase phase.

Galvanostatic discharge–charge cycling plots shows the first discharge capacity are 2000, 1500, and 1000 for TNA5000 to TNAWT but cyclability has inverse significant. Cycled in the potential range, 1.0–2.6V vs. Li. During the first discharge, both TiO2 nanoparticles and nanofibers show a reduction plateau at ~1.75V (Fig. 2) [4] and during charge cycle a oxidation plateau was ~1.8–2.0 V. The different plateaus are observed during Li-intercalation/de-intercalation in to TiO2 with different particle. Lower discharge capacity of TNA5000 is most likely due to crystallinity of perfect tubes compared to that of the TNA1000 or TNAWT. The crystallinity of TNA5000 results in an enhanced density of surface defects and therefore, results in poor electrical conductivity and lower diffusion of Li-ions. Interestingly, the capacity fading for 2–50 cycles (Fig. 3) was ~25% for TNA5000 which is nearly half of that of corresponding TNAWT (~63%). The reduced capacity fading could have resulted from the peculiar structure defects of the TNA5000[5, 6]

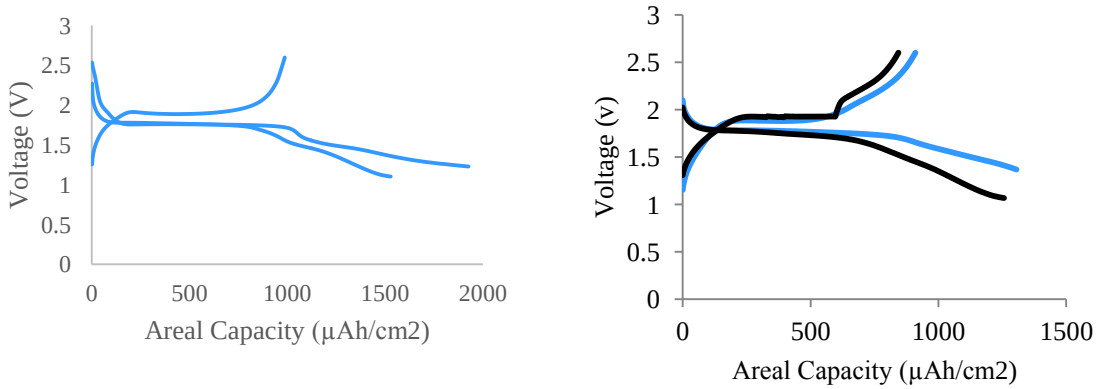

Fig 2. Galvanostatic first discharge–charge plot at current density of 33.5mA/g (0.1 C) a) TNAWT b) TNA1000.

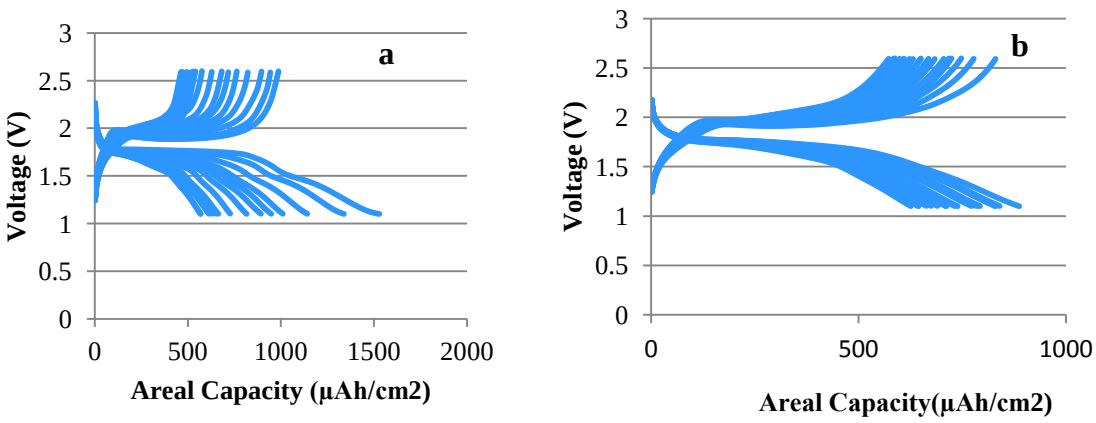

Fig. 3 Galvanostatic discharge–charge cycling plots at current density of 33.5mA/g (0.1 C) a) TNTWT, b) TNT1000 respectively.

Conclusion

In summary, The TiO2 nanotubes prepared by anodizing method showed higher specific capacity compared to the other. However, the electrochemical cycling stability (current rate of 0.1 C) was better for TNA5000. The capacity fading for 2–50 cycles was ~23% for TNA1000 which for the TNAWT was ~63%.

References

[1] H. Li, S. K. Martha, R. R. Unocic, H. Luo, S. Dai, J. Qu, Journal of Power Sources 218 (2012) 88-92

[2] D. V. Bavykin and F. C. Walsh "Titanate and Titania Nanotubes Synthesis, Properties and Applications" (2010) chapter2 page 40.

[3] N. A. Kyerematenga, C. Lebouinb, P. Knauthb, T. Djenizian, Electrochimica Acta 88 (2013) 814– 820.

[4] M.V. Reddy, R. Joseb, T.H. Tengb, B.V.R. Chowdaria,∗, S. Ramakrishna, Electrochimica Acta 55 (2010) 3109–3117

[5] N. A. Kyerematenga, C. Lebouinb, P. Knauthb, T. Djenizian, Electrochimica Acta 88 (2013) 814– 820.

[6] H. Li, J. Qu, Q. Cui, H. Xu, H. Luo, M. Chi, R. A. Meisner, W. Wang, and S. Dai, J. Mater. Chem. 21 (2011) 9487-9490.

8th Iranian Fuel Cell Seminar
FEBRUARY 25,26
2015

Evaluation of the Activity of Binary PtM/C Alloy Catalysts Towards the (HOR) for PEMFC$_S$

S. Ordoukhani [*1], A. Nozad Golikand[2]

1. Department of chemistry, Islamic Azad University,Shahre Gods branch, Tehran, Iran
2. material research school, NSTRI, Tehran ,Iran
** Samineh.Ordoukhani@Yahoo.com*

Abstract
A comprehensive study of the investigations performed in search for development of electrocatalysts with enhanced catalytic activity and stability for low temperature polymer electrolyte membrane (PEM) fuel cells are presented. we evaluated the activity of binary PtM/C (M = Ni,Mo,Ru,Co,Sn,W,Fe,….) alloy catalysts towards the Hydrogen oxidation reaction (HOR) .The comparison is done based on the potential difference in HOR. While the HOR kinetics on high surface area Pt catalyst is still sluggish, intensive researches have focused on the Pt alloyed catalysts, such as Pt-Co, Pt-W, Pt-Ru and Pt-Sn. It has been established that by alloying Pt with non-precious transition metals, the kinetics of the HOR can be significantly improved and the expense of catalyst can be reduced as well. The enhanced activity of the Pt alloys has been attributed to the electronic structure change and the geometric effects that facilitate the adsorption/desorption of the HOR intermediates The enhanced CO tolerance of the developed catalysts is strongly dependent on the type, composition and atomic ratios of the added elements/groups, and type and structure of the support materials.

Keywords: PEM fuel cells, Binary alloys, Hydrogen oxidation reaction, Geometric effects

Introduction:

Polymer electrolyte membrane fuel cells (PEMFCs) are attractive power generators for vehicles, electronic devices, and stationary generators on account of their low operating temperature and high efficiency of energy conversion [1-2]. On the other hand, the commercialization of PEMFCs will require an increase in the lifespan of the membrane electrode assembly (MEA) on the PEMFC as well as a decrease in manufacturing cost [3-4]. The synthesis of Pt alloy catalysts, development of non Pt catalysts, and the reduced use of Pt catalysts through optimization of the catalyst layer structure to a three-phase boundary are effective ways of reducing the MEA cost [5-6] because electrocatalysts, such as carbonsupported Pt (Pt/C), demand a large fraction of material costs. The use of cathode catalysts for the oxygen reduction reaction (ORR) has been studied extensively to minimize the use of Pt in the MEA because the ORR is considered the kinetic limit for PEMFCs. For instance, Pt based metal alloy catalysts with transition metals such as PtCo/C, PtNi/C, PtCr/C, and PtFe/C were employed to improve the ORR activity [7-8]. In addition, Pd-based metal alloy catalysts such as PdPt/C, PdCo/C, PdFe/C, PdNi/C, and PdPtNi/C have been studied as substitutes for Pt [10-12]. On the other hand, the amount of Pt in anodes is almost half of that in the cathodes. Therefore, to reduce the cost of MEA, it is important to reduce the use of Pt in the anode also is necessary [9-11].

The presence of carbon monoxide (CO) as the most common impurity in the hydrogen stream degrades the performance of polymer electrolyte membrane fuel cells (PEMFC's) [13–14]. It is well-known that one of the greatest obstacles in commercialization of PEMFC's is the high cost of the electrocatalysts and their susceptibility to impurities. Thus, a remarkable number of studies have focused on the synthesis and development of catalysts for PEM fuel cells with enhanced CO tolerance to be used in the anode. In a conventional approach, Pt is alloyed with another element such as Ru to form Pt–Ru catalyst enhancing the CO tolerance of the catalyst. Another advantage of inclusion of a second or third element in the catalyst structure is that these novel materials reduce the high loading of Pt thus lower cost than Pt/C.
The high reformate tolerance of these electrocatalysts is usually attributed to the electronic [15–16,17] and bifunctional mechanisms [14,10]. In the former, the electronic effects argue that the added element modifies the Pt electronic structure in a way that either the Pt CO bond is weakened facilitating the CO oxidation by nearby OH groups, or the Pt–H_2O activation is improved making it possible for CO molecules to be directly oxidized on the Pt sites. The electronic structure modification of Pt is related to the electron donation or back-donation of the added element. This modification reduces the impurities coverage leaving more vacant Pt sites for hydrogen oxidation. In the latter, the bifunctional mechanism, the electro-oxidation of CO is promoted through the formation of OH groups on oxophilic sites:

$$M + H_2O \rightarrow M\text{-}OH + e^- + H^+$$

And then the spillover process of CO molecules to the vicinity of the sites occupied by OH species and CO oxidation:

$$M\text{-}OH + Pt\text{–}CO \rightarrow Pt + M + CO_2 + e^- + H^+$$

The composition, morphology, size and structure of the catalyst particles affect the interactions formed between the reactants (H_2O, CO and H_2) and the catalyst, determining the activity of the catalyst particles [18–20]. Furthermore, these factors influence the stability of the catalyst [21–19].

1- Composition of the catalysts :

The crystalline structure of catalysts with ordered intermetallic architectures is well-defined and normally possesses high enthalpies of formation, which increases the stability of these materials compared to that of alloys. In addition, the cluster size and morphology can influence the catalytic activity of the electrocatalysts towards CO electrooxidation. For instance, the morphology and size of the clusters and Ru islands play a critical part in the relative importance of the mentioned mechanisms. Controlling the catalysts structure and morphology and understanding the structure–activity correlations are of great importance in designing novel CO tolerant electrocatalysts with superior performance.
It is observed that formation of an alloy is not a necessary condition for attaining effective CO oxidation activity. It is possible to enhance the CO electro-oxidation of the Pt-based electrocatalysts by decorating the catalysts surface by other metals or groups. The role of the added metal/group is to promote the catalytic activity. In addition, it is a must for the promoter to be in the vicinity of Pt sites in order to be effective for the CO electro-oxidation.
Fig. 1 illustrating the M - O bond energies for elements from different groups [49], enables one to prepare catalysts via including suitable oxophilic elements into the catalysts structure. Theoretically, the M-O bond energy should be around that of Pt - CO bond energy, which is

~590 kJ/mol. Therefore, Mo, Ru, Os, Sn, and Re are suggested to be appropriate elements to be added to the active surface phase of a catalyst. The reformate tolerance of some binary and ternary catalysts including Pt–M (M = Ru, Mo, Fe, Co, Ni) electrocatalysts was investigated in a comprehensive research [29].

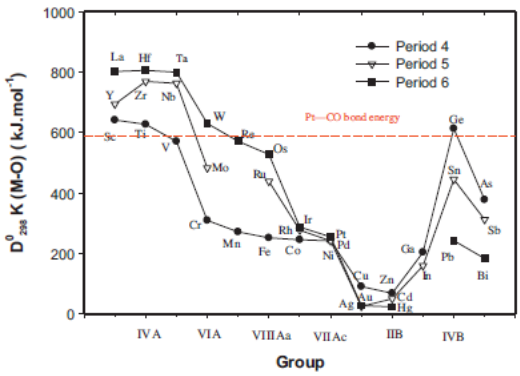

Fig. 1. The metal oxygen bond dissociation energy in diatomic molecules as a function of group in the period

Table 1 shows the electrocatalysts developed so far to enhance the CO tolerance of the deployed catalysts in PEM fuel cells operating at low temperatures. These include carbon supported Pt-based binary alloys Development of non-Pt electrocatalysts is of great interest because if the catalytic performance can be comparable with that of Pt-based electrocatalysts, significant economic impacts will be achieved .

Hammer and Norskov [21,22] have developed a simple model stating that the overall binding energy of simple adsorbates such as H, O, and CO on a transition metal surface is weakened/strengthened by downshift/ upshift of the d-band centre of the metal. Kitchin et al. using DFT calculations declared that the ligand effects between Pt (1 1 1) and subsurface 3d elements downshift the Pt surface d-band centre additive to the concurrent compressive-strain effects [23].

Table 1 List of the electrocatalysts developed for enhanced CO tolerance and the electrochemical tests carried out to characterize the performance.

Catalyst formula	Electrochemical tests performed	Results and mechanisms	Ref's.
Pt–Ru/C	PEM fuel cell operation at 85 ◦C with H_2/x ppm CO	Pt–Ru/C exhibits significant CO and CO_2 tolerance compared to Pt/C due to both electronic and bifunctional mechanisms	[13- 15,24,25]
Pt–W/C	PEM fuel cell operation at 85 ◦C with H_2/100 ppm CO PEM fuel cell operation at 85 ◦C with H_2/x ppm CO	Tungsten exhibits a co-catalytic activity for hydrogen oxidation in the presence of CO, although the effect is not as effective as that of Ru	[13,26,27]
Pt–Sn/C	Test in 1 M H_2SO_4 in a stream of H_2/x ppm CO PEM fuel cell operation at 85 ◦C with H_2/x ppm CO	Pt–Sn/C exhibits enhanced CO tolerance compared to Pt–Ru/C due to the electronic and bifunctional mechanisms. Stability is an issue	[17,30–32]
Pt–Co/C	Test in 0.5 M H_2SO_4 in a stream of H_2/x ppm CO Tests under PEMFC operating conditions	Cobalt shifts the CO oxidation onset potential negatively. Stability is an issue	[28,29,33]
Pt–Mo/C	Test in 1 M H_2SO_4 in a stream of H_2/x ppm CO PEM fuel cell operation at 85 ◦C with H_2/x ppm CO	Pt–Mo/C performs much better (3–4 folds) than Pt–Ru/C. The dominating mechanism is the bifunctional mechanism. Stability is an issue	[14,34,35,36]
Pt–Fe/C	Test in 0.5 M H_2SO_4 in a stream of H_2/x ppm CO PEM fuel cell operation at 85 ◦C with H_2/x ppm CO	Superior CO tolerance is observed due to formation of Pt-skin and electronic effect	[13,33,34]
Pt–Ni/C	Test in 0.5 M H_2SO_4 in a stream of H_2/x ppm CO Test in 0.5 M $HClO_4$	Superior CO tolerance is observed compared to Pt/C	[35,29]

2- Structure :

The catalytic activities of electrocatalysts for PEM fuel cell applications are significantly affected by the structure and morphology of the catalysts. Depending on the preparation conditions, different molecular structures form including alloys, intermetallic phases, core–shell structures and oxidative agents decorated Pt/C.

The enthalpies of formation of alloys are very small values, thus they can be unstable [41]. Electrochemical conditions such as high current densities can change the structure and composition of the top layer of a PtRu alloy catalyst significantly [43]. Incontrast, the crystalline structure of catalysts with ordered intermetallic structures are well-defined and normally possess high enthalpies of formation, which increases the stability of these materials compared to that of alloys [30,41,42]. The atomic scale electronic and geometric structures of intermetallic compounds can be well controlled and preserved. Furthermore, these structures have been reported to exhibit excellent electrocatalytic performance towards CO oxidation of [30,44]. However, according to results of electrochemical experiments, intermetallic structures including non-noble elements such as Bi or Pb may not be stable at the electrode potentials as high as +0.80 V or beyond [45].

3-Atomic ratio of the elements :

The atomic ratio of the elements plays an important role in the catalytic activity. It is concluded that for bimetallic electrocatalysts such as PtRu, PtFe and PtW the maximum activity and the most superior CO tolerance is exhibited by those with atomic ratio of 1:1. In the case of oxidative agents modified Pt-based electrocatalysts, the activity of the catalysts are strongly dependent on the content of the promoter. An optimum content of the promoter must be added to the Pt/C to effectively enhance the CO oxidation. In fact, adding too much of the oxidative agent would block a large portion of the Pt active sites.

The atomic ratio of the constituent elements can affect the catalytic activity of the catalysts towards CO oxidation. Ianniello et al. [46] studied the CO oxidation on catalysts with different Ru contents through in situ infrared (FTIR) spectroscopy and differential electrochemical mass spectrometry (DEMS). According to their results, the CO oxidation onset potential remains the same for all the samples. However, the peak potential for CO oxidation decreases by increasing Ru content. PtRu (1:1) has the lowest peak potential presenting the optimal composition which has been also reported in the research by Wasmus and Kuver [47].

Fig. 2 gives the cyclic voltammograms (CVs) for various Pt–W/C and Pt/C (20 wt%, Johnson-Matthey) catalysts in electrolyte solution saturated with inert gas, which show typical Pt features for the underpotential deposition (UPD) adsorption/desorption of hydrogen, indicating the surface enrichment of Pt in these Pt–W/C catalysts even in Pt-lean PtW_2/C catalyst. In fact, the surface enrichment of Pt in these catalysts was also implied by the results of the angular-resolved XPS measurements. By deconvoluting the XPS spectra in binding energy region between 68 eV and 80 Ev into components of Pt_{4f} and W_{5s} through Gauss-Lorentzian fitting and correcting the sensitivity of each element, the Pt/W atom ratios in the near surface region were estimated to be 4.2:1, 3.6:1, 4.2:1 and 2.5:1 for the Pt_3W/C, Pt_2W/C, PtW/C and PtW_2/C respectively [48], which are much higher than the corresponding nominal compositions. The estimation performed with the W_{4f} spectra in the binding energy region between 31 eV and 40 eV gave very similar results.

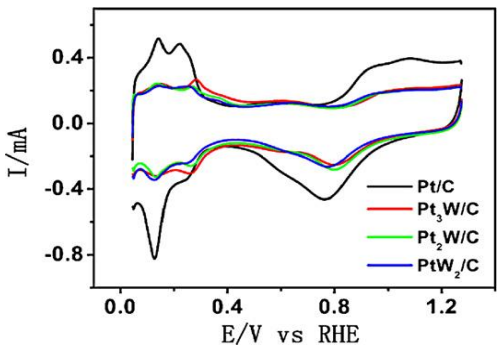

Fig. 2. CVs in Ar-saturated 0.5 M H2SO4 for the prepared Pt–W/C and the JM Pt/Ccatalysts. Potential scanning rates: 50 mV/s. The total metal loadings: 51 μg cm−2.

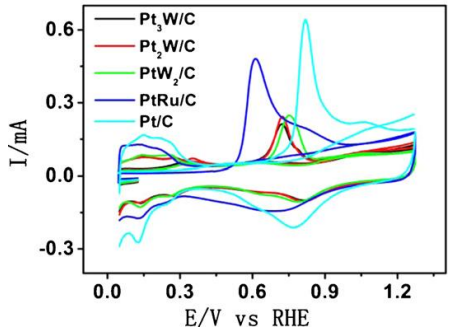

Fig. 3. CO stripping curves in Ar-saturated solution for the prepared Pt–W/C, the JM Pt/C and JM PtRu/C catalysts. Scanning rates: 20 mV/s Total metal loadings: 51 µg cm-2

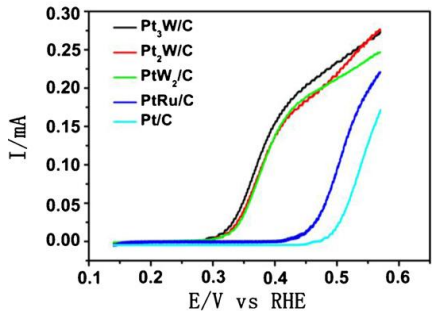

Fig. 4. Steady-state HOR polarization curves in H2/CO-saturated solution for the prepared Pt–W/C, the JM Pt/C and JM PtRu/C catalysts. Scanning rates: 5 mV/s. Total metal loadings: 20 µg cm−2.

Fig. 4 When the HOR-CO polarization curves are compared, the Pt–W/C catalysts exhibit HOR onset potentials about 150 mV and 200 mV more negative than that on the Pt–Ru/C and Pt/C respectively, suggesting that the Pt–W alloy catalysts are more CO tolerant for HOR than Pt/C and PtRu/C. The enhanced CO tolerance of Pt–W/C catalysts over Pt/C is in consistence with their more negative CO stripping potentials than Pt/C. The better CO tolerance of Pt–W/C catalysts than PtRu/C, however, contradicts with their more positive CO stripping potentials than PtRu/C. This suggests that the mechanism of CO-tolerant oxidation of H_2 on Pt–W alloys differs from that on Pt–Ru alloys.

4- Catalytic activity of the catalysts towards CO oxidation :

To compare the catalytic activity of the electrocatalysts investigated by other researchers, the results from rotating disc electrode and single PEM fuel cell polarization curves measurement and cyclic voltammetry experiments are used, which is the most common technique applied to determine the catalytic activity towards hydrogen and carbon monoxide oxidation in acidic media. CO oxidation onset potential and current density at a certain potential measured from CV and polarization measurements are listed in Tables 2 illustrating the electrocatalysts kinetic parameters for CO oxidation.

Table 2: Kinetics parameters of CO electro-oxidation under fuel cell operating conditions.

Electrocatalyst	i (A cm^{-2})@ E	E_{onset}	Refs.
Pt/C	0.16@0.7 V	0.4	[14]
Pt–Ru/C[a]	0.21@0.7 V	0.25	[15]
Pt–Mo/C[a]	0.35@0.7 V	0.05	[15]
Pt–Sn/C[b]	0.05@0.7 V	0.25	[26,40]
Pt–Fe/C[a]	0.19@0.7 V	0.42	[13]
Pt–Ni/C[a]	0.19@0.7 V	0.41	[29]
Pt–W/C[a]	0.36@0.7 V	0.41	[13]
Pt–Co/C[a]	0.2@0.7 V	0.41	[29]

[a] 85 °C, 100 ppm CO/H_2–O_2, 0.3 MPa.
[b] H_2/150 ppm CO.

Comparing the information presented in Tables 2, it is observed that the catalytic activity of Pt/C is enhanced significantly by adding the transition metals.

Conclusions:

It is essential to add appropriate amounts of elements to Pt/C or PtRu/C which enhance the catalytic activity through the bifunctional mechanism and electronic effects. Mo, Ru, Os, Sn, and Re are suggested to be appropriate elements which create oxophilic groups on the catalyst surface facilitating the CO electrooxidation through bifunctional mechanism. In addition, all transition metals change the electronic properties of the electrocatalysts nanoparticles via electron transfer between the Pt and the added element in a way that the Pt CO bond weakens leading to a decrease in CO coverage, and thereby enhancing the catalytic performance.

Stability of the electrocatalysts is essential for PEM fuel cell's long term operation. Anode materials with ordered intermetallic structure and those including metals with chemical stability in acidic media such as tungsten, cerium and iron are promising candidates offering improved CO tolerance and superior performance compared to PtRu/C.

Acknowledgement

Here is necessary to know the Dear professor Doctor Nozad Golikand for their valuable advice will be appreciated.

References:

1. Carrette L, Friedrich KA, Stimming U. Fuel cells: principles, types, fuels, and applications. ChemPhysChem 2000;1:163-93.
2. Ticianelli EA, Derouin CR, Redondo A, Srinivasan S. Methods to advance technology of proton exchange membrane fuel cells. J Electrochem Soc 1988;135:2209-14
3. Hommura S, Kawahara K, Shimohira T, Teraoka Y. Development of a method for clarifying the perfluorosulfonated membrane degradation mechanism in a fuel cell environment. J Eletrochem Soc 2008;155:A29-33.
4. Wilson MS, Valerio JA, Gottesfeld SJ. Low platinum loading electrodes for polymer electrolyte fuel cells fabricated using thermoplastic ionomers. Electrochim Acta 1995;40:35563.

5. Gasteiger HA, Kocha SS, Sompalli B, Wagner FT. Activity benchmarks and requirements for Pt, Pt-alloy, and non-Pt oxygen reduction catalysts for PEMFCs. Appl Catal B Environ 2005;56:9-35.
6. Zhong H, Zhang H, Liu G, Liang Y, Hu J, Yi B. A novel nonnoble electrocatalysts for PEM fuel cell based on molybdenum nitride. Electrochem Commun 2006;8:707-12
7. Toda T, Igarashi H, Uchida H, Watanabe M. Enhancement of the electroreduction of oxygen on Pt alloys with Fe, Ni, and Co. J Electrochem Soc 1999;146:3750-6.
8. Yang H, Alonso-Vante N, Leger JM, Lamy C. Tailoring, structure, and activity of carbon-supported nanosized Pt-Cr alloy electrocatalysts for oxygen reduction in pure and methanol-containing electrolytes. J Phys Chem B 2004;108:1938-47.
9. Grigoriev SA, Lyutikova EK, Martemianov S, Fateev VN. On the possibility of eplacement of Pt by Pd in a hydrogen electrode of PEM fuel cells. Int J Hydrogen Energy 2007;32:4438- 42
10. Zhao J, Jarvis K, Ferreira P, Manthiram A. Performance and stability of Pd-Pt-Ni nanoalloy electrocatalysts in proton exchange membrane fuel cells. J Power Sources 2011;196: 4515-23
11. Yoo SJ, Park HY, Jeon TY, Park IS, Cho YH, Sung YE. Promotional effect of palladium on the hydrogen oxidation reaction at a PtPd alloy electrode. Angew Chem Int Ed 2008;47:9307-10.
12. Fernandez JL, Walsh DA, Bard AJ. Thermodynamic guidelines for the design of bimetallic catalysts for oxygen electroreduction and rapid screening by scanning electrochemical miscroscopy. MeCo (M: Pd, Ag, Au). J Am Chem Soc 2005;127:357-65.
13 L.G.S. Pereira, V.A. Paganin, E.A. Ticianelli, Investigation of the CO tolerance mechanism at several Pt-based bimetallic anode electrocatalysts in a PEM fuel cell, Electrochimica Acta 54 (2009) 1992.
14. R.C. Urian, A.F. Gulla, S. Mukerjee, Electrocatalysis of reformate tolerance in proton exchange membranes fuel cells: Part I, Journal of Electroanalytical Chemistry 554/555 (2003) 307.
15. T.R. Ralph, M.P. Hogarth, Catalysis for low temperature fuel cells, Platinum Metals Review 46 (2002) 117.
16. P.P. Lopes, K.S. Freitas, E.A. Ticianelli, CO tolerance of PEMFC anodes: mechanisms and electrode designs, Electrocatalysis 1 (2010) 200.
17. E. Antolini, Platinum-based ternary catalysts for low temperature fuel cells. Part II, Applied Catalysis B: Environmental 74 (2007) 337.
18. F.J. Scott, S. Mukerjee, D.E. Ramaker, CO coverage/oxidation correlated with PtRu electrocatalyst particle morphology in 0.3 M methanol by in situ XAS, Journal of the Electrochemical Society 154 (2007) A396.
19. X. Yu, S. Ye, Recent advances in activity and durability enhancement of Pt/C catalytic cathode in PEMFC. Part II: degradation mechanism and durability enhancement of carbon supported platinum catalyst, Journal of Power Sources 172 (2007) 145.
20. Y. Liang, H. Zhang, Z. Tian, X. Zhu, X. Wang, B. Yi, Synthesis and structureactivity relationship exploration of carbon-supported PtRuNi nanocomposite as a CO-tolerant electrocatalyst for proton exchange membrane fuel cells, Journal of Physical Chemistry B 110 (2006) 7828.
21. N.P. Lebedeva, G.J.M. Janssen, On the preparation and stability of bimetallic PtMo/C anodes for proton-exchange membrane fuel cells, Electrochimica Acta 51 (2005) 29.
21. B. Hammer, J.K. Nřskov, Electronic factors determining the reactivity of metal surfaces, Surface Science 343 (1995) 211.
22. B. Hammer, J.K. Norskov, Why gold is the noblest of all the metals, Nature 376 (1995) 238.

[23. J.R. Kitchin, J.K. Norskov, M.A. Barteau, J.G. Chen, Modification of the surface electronic and chemical properties of Pt(1 1 1) by subsurface 3d transition metals, Journal of Chemical Physics 120 (2004) 10240.
24. A.E. Russell, S.C. Ball, S. Maniguet, D. Thompsett, Unravelling the complexities of CO_2 tolerance at PtRu/C and PtMo/C, Journal of Power Sources 171 (2007) 72.
25. S. Ball, A. Hodgkinson, G. Hoogers, S. Maniguet, D. Thompsett, B. Wong, The proton exchange membrane fuel cell performance of a carbon supported PtMo catalyst operating on reformate, Electrochemical and Solid-State Letters 5 (2002) A31.
26. M. Gotz, H. Wendt, Binary and ternary anode catalyst formulations including the elements W, Sn and Mo for PEMFCs operated on methanol or reformate gas, Electrochimica Acta 43 (1998) 3637.
27. P.K. Shen, A.C.C. Tseung, Anodic oxidation of methanol on Pt/WO_3 in acidic media, Journal of the Electrochemical Society 141 (1994) 3082.
28. M.D. Obradovi´ c, A.V. Tripkovi´ c, S.L. Gojkovi´ c, Oxidation of carbon monoxide and formic acid on bulk and nanosized Pt-Co alloys, Journal of Solid State Electrochemistry 16 (2012) 587.
29. S.M. Mousavi Ehteshami, Q. Jia, S.H. Chan, S. Mukerjee, The role of electronic properties of Pt and Pt alloys for enhanced reformate electrooxidation in polymer electrolyte membrane fuel cells, Unpublished results.
30. Z. Liu, G.S. Jackson, B.W. Eichhorn, PtSn intermetallic, core-shell, and alloy nanoparticles as CO-tolerant electrocatalysts for H_2 oxidation, Angewandte Chemie – International Edition 49 (2010) 3173.
32. J. McBreen, S. Mukerjee, In situ X-ray absorption studies of a Pt-Ru electrocatalyst, Journal of the Electrochemical Society 142 (1995) 3399.
33. M. Wakisaka, S. Mitsui, Y. Hirose, K. Kawashima, H. Uchida, M. Watanabe, Electronic structures of Pt-Co and Pt-Ru alloys for CO-tolerant anode catalysts in polymer electrolyte fuel cells studied by EC-XPS, Journal of Physical Chemistry B 110 (2006) 23489.
34. E.I. Santiago, G.A. Camara, E.A. Ticianelli, CO tolerance on PtMo/C electrocatalysts prepared by the formic acid method, Electrochimica Acta 48 (2003) 3527.
35. Z. Liu, J.E. Hu, Q. Wang, K. Gaskell, A.I. Frenkel, G.S. Jackson, B. Eichhorn, PtMo alloy and MoOx@Pt core-shell nanoparticles as highly CO-tolerant electrocatalysts, Journal of the American Chemical Society 131 (2009) 6924.
36. F. Maillard, G.Q. Lu, A. Wieckowski, U. Stimming, Ru-decorated Pt surfaces as model fuel cell electrocatalysts for CO electrooxidation, Journal of Physical ChemistryB 109 (2005) 16230.
37. H. Igarashi, T. Fujino, Y. Zhu, H. Uchida, M. Watanabe, CO tolerance of Pt alloy electrocatalysts for polymer electrolyte fuel cells and the detoxification mechanism, Physical Chemistry Chemical Physics 3 (2001) 306.
38. Z. Liu, G.S. Jackson, B.W. Eichhorn, Tuning the CO-tolerance of Pt-Fe bimetallic nanoparticle electrocatalysts through architectural control, Energy and Environmental Science 4 (2011) 1900.
39. M.V. Martيnez-Huerta, S. Rojas, J.L. Gḿez de la Fuente, P. Terreros, M.A. Pe˜na, J.L.G. Fierro, Effect of Ni addition over PtRu/C based electrocatalysts for fuel cell applications, Applied Catalysis B: Environmental 69 (2006) 75.

40. D.H. Lim, D.H. Choi, W.D. Lee, H.I. Lee, A new synthesis of a highly dispersed and CO tolerant PtSn/C electrocatalyst for low-temperature fuel cell; its electrocatalytic activity and long-term durability, Applied Catalysis B:Environmental 89 (2009) 484.
41. N. de-los-Santos-ءlvarez, L.R. Alden, E. Rus, H. Wang, F.J. DiSalvo, H.D. Abru˜na, CO tolerance of ordered intermetallic phases, Journal of Electroanalytical Chemistry 626 (2009) 14.
42 C. Ranjan, R. Hoffmann, F.J. DiSalvo, H.D. Abru˜na, Electronic effects in CO chemisorption on Pt-Pb intermetallic surfaces: a theoretical study, Journal of Physical Chemistry C 111 (2007) 17357.
43. S. Stoupin, E.H. Chung, S. Chattopadhyay, C.U. Segre, E.S. Smotkin, Pt and Ru X-ray absorption spectroscopy of PtRu anode catalysts in operating direct methanol fuel cells, Journal of Physical Chemistry B 110 (2006) 9932.
44. E. Casado-Rivera, D.J. Volpe, L. Alden, C. Lind, C. Downie, T. Vلzquez-Alvarez, A.C.D. Angelo, F.J. DiSalvo, H.D. Abru˜na, Electrocatalytic activity of ordered intermetallic phases for fuel cell applications, Journal of the American Chemical Society 126 (2004) 4043.
45. Y. Liu, H. Abe, H.M. Edvenson, T. Ghosh, F.J. Disalvo, H.D. Abru˜na, Fabrication and surface characterization of single crystal PtBi and PtPb (1 0 0) and (0 0 1) surfaces, Physical Chemistry Chemical Physics 12 (2010) 12978.
46. R. Ianniello, V.M. Schmidt, U. Stimming, J. Stumper, A. Wallau, CO adsorption and oxidation on Pt and PtRu alloys: dependence on substrate composition, Electrochimica Acta 39 (1994) 1863.
47. S. Wasmus, A. Küver, Methanol oxidation and direct methanol fuel cells: a selective review, Journal of Electroanalytical Chemistry 461 (1999) 14.
48. R.F. De Morais, D. Loffreda, P. Sautet, A.A. Franco, Towards a multiscale modeling methodology for the prediction of the electro-activity of PEM fuel cell catalysts, ECS Transactions 25 (2010) 167.
49. K.L. Ley, R. Liu, C. Pu, Q. Fan, N. Leyarovska, C. Segre, E.S. Smotkin, Methanol oxidation on single-phase Pt-Ru-Os ternary alloys, Journal of the Electrochemical Society 144 (1997) 1543.

8th Iranian Fuel Cell Seminar
FEBRUARY 25,26
2015

Palladium-Based Catalysts for Oxygen Reduction Reaction in Fuel Cells

Fereshteh Dehghani sanij*, Hussein Gharibi and Farhad Golmohammadi
Department of Chemistry, Tarbiat Modares University, Tehran, Iran.
** Dehghan82@gmail.com*

Abstract
Fuel cells, especially low temperature fuel cells are clean energy devices that are expected to help address the energy and environmental problems that have become prevalent in our society. Platinum-based catalysts are usually used as the catalysts for cathode (oxygen reduction) reactions. The high cost and limited resources of this precious metal hinder the commercialization of fuel cells. Pt alone does not present satisfactory activity for the oxygen reduction reaction when used as cathode material. For all these reasons, non-platinum-based catalysts have been tested as electrode materials for low temperature fuel cells. Palladium and platinum have very similar properties because they belong to the same group in the periodic table. Recent efforts have focused on the discovery of palladium-based catalysts with little or no platinum for oxygen reduction reaction (ORR).

Keywords: Palladium, Catalysts, Fuel cells, Platinum, Cathode, Oxygen reduction reaction.

1. Introduction

Fuel cells, and especially low temperature fuel cells such as proton exchange membrane fuel cells (PEMFCs), direct alcohol fuel cells (DAFCs) and alkaline fuel cells (AFCs), are widely considered to be a sustainable energy conversion system and are a key technology for the development of a hydrogen economy.

At the cathode of the fuel cell, the oxygen is reduced, leading to formation of water. The cathodic reactions require catalysts to reduce the overpotentials and increase reaction rates. Pt-based materials are usually used as the catalysts for both the reactions. Because catalysis is a surface effect, the catalyst needs to have the highest possible surface area. So, the active phase is dispersed on a conductive support such as high surface area carbon powders. Generally the particle size of carbon supported metals increases going from Pt to Pd, independently of the preparation method. However, the elevated price and limited resources of Pt are hindering the commercialization of fuel cells. Moreover, Pt alone does not present satisfactory activity for the oxygen reduction reaction (ORR) when used as cathode material.

With the exception of Pt, the catalytic activity of Pd is one of the highest among the pure metals for ORR. Pt and Pd have very similar properties (same group of the periodic table, same fcc crystal structure, similar atomic size). Pd is interesting as it is at least fifty times more abundant on the earth than Pt. This, combined with the fact that the cost of Pd is lower than that of Pt, makes it an attractive alternative[1]. While Pd is less expensive than Pt, the electrocatalytic activities of pure Pd for ORR are at least five times lower than that of Pt, which prevents it from being used directly in fuel cells. Great efforts have been dedicated to improve the activity of Pd by surface modification and alloying[1,2]. This paper attempts to summarize the recent progress of catalysts containing Pd for ORR.

2. Oxygen reduction reaction (ORR)

2.1 ORR in acidic solutions

The ORR activity of Pd/C is generally five times lower than that of Pt/C in perchlorate acid due to the stronger binding energy of oxygen containing species on the surface of the former.

For the Pd–Fe systems, an optimized composition of Pd:Fe = 3:1 was found by several groups[3,4]. The ORR activity of Pd_3Fe/C was comparable to or higher than that of Pt/C. A comparison between Pd_3Fe/C and Pd_2Co/C in Figure 1 reveals that the former has a slightly higher ORR activity[3].

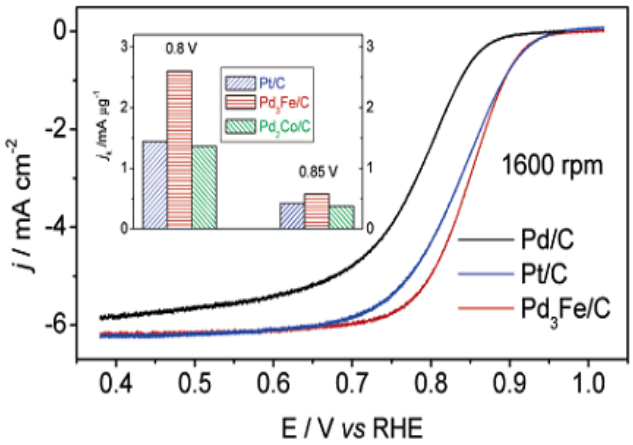

Figure 1: Comparison of polarization curves for the ORR on Pd/C (ETEK), Pt/C (ETEK) and Pd_3Fe/C nanoparticles in 0.1 M $HClO_4$. Sweep rate 10 mV s^{-1}; room temperature. Insert: comparison of noble metal mass activity for Pt/C (ETEK), Pd_3Fe/C and Pd_2Co/C at 0.8 V and 0.85 V[3].

2.2 Alcohol tolerance

Due to kinetic limitations of ORR, the cathodic overpotential losses amount to 0.3–0.4 V under typical PEMFC operating conditions. The development of more active oxygen reduction catalysts than Pt has been the subject of extensive research.

Regarding direct alcohol fuel cells, one of the major problems is of alcohol crossover through the polymer electrolyte. The problem of alcohol crossover could be solved either by using electrolytes with lower alcohol permeability or by developing new cathode electrocatalysts with higher alcohol tolerance than Pt. Among various metals, Pd and Pd–M catalysts present very important selectivity for ORR in acid medium in the presence of alcohol. By alloying with Pd, the methanol tolerance of Pt-based catalysts can be improved by diluting the Pt–Pt bonds, which are required for dissociative adsorption of alcohol on the surface of the catalyst.

Shao et al. found no evidence of methanol oxidation on Pd_2Co/C in nitrogen-saturated $HClO_4$ solution containing 0.1 M methanol (Figure 2a). For the ORR, the half-wave potential drops ca.20 mV with 0.1 M methanol in solution, compared to the same catalyst without methanol. The loss of 20 mV might reflect the blocking of some active sites for oxygen reduction by the adsorbed methanol or its intermediates from oxidation. A somewhat higher methanol oxidation activity was observed by the same research group on a Pd_3Fe/C catalyst in the same electrolyte, as several small oxidation current peaks corresponding to methanol oxidation appeared (Figure 2b) [5].

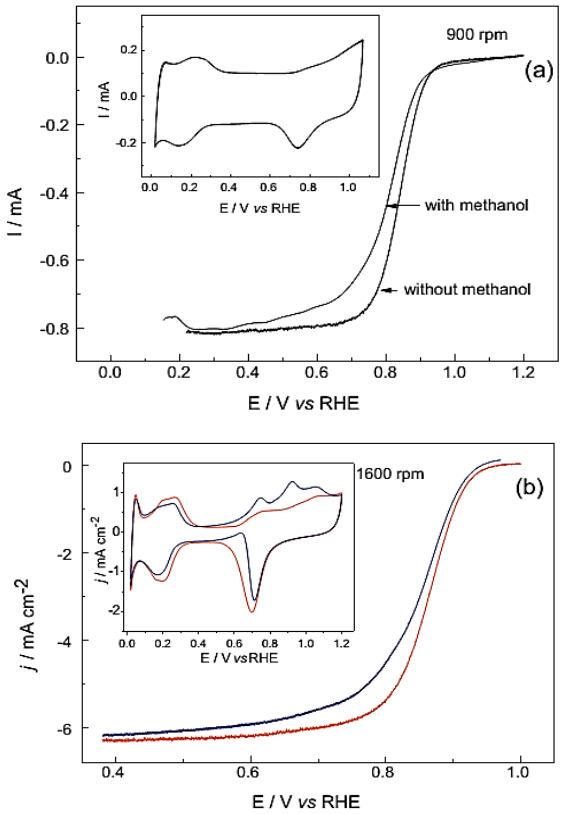

Figure 2: (a) Comparison of polarization curves for ORR on Pd_2Co/C in oxygen saturated 0.1 M $HClO_4$ solution with and without 0.1 M methanol; rotation rate 900 rpm; sweep rate 10 mV s^{-1} . The insert is the cyclic voltammetry of Pd_2Co/C nanoparticles in nitrogen saturated 0.1 M $HClO_4$+ 0.1 M methanol solutions; sweep rates 20 mV s^{-1} . (b) Comparison of polarization curves for the ORR on Pd_3Fe/C nanoparticles in 0.1 M $HClO_4$with (blue line) and without (red line) 0.1 M methanol. Sweep rate 10 mV s^{-1}; room temperature. The insert is the cyclic voltammetries of Pd_3Fe/C in nitrogen saturated 0.1 M $HClO_4$ solution with (blue line) and without (red line) 0.1 M methanol)[5].

3. Conclusions

Pd-based catalysts may play a role to replace or partially replace costly Pt in cathode of low temperature fuel cells. Generally, Pd-based catalysts present larger particle size than Pt-based catalysts, and they have a lower active surface area than Pt-based catalysts, which decreases their catalytic activity. So, systematic studies of the effects of synthesis methods, particle size, alloy degree, and composition on ORR activity and stability are crucial for optimization of Pd-based catalysts. The long term durability of Pd-based catalysts is one of the unavoidable issues for PEM fuel cell applications.

Reference

[1] S.Q. Song, Y. Wang, P. Tsiakaras and P.K. Shen "Direct alcohol fuel cells: A novel non-platinum and alcohol inert ORR electrocatalyst", Appl. Catal. B: Environ. (2008) 78, 381–387.
[2] N.A. Karim, S.K. Kamarudin "An overview on non-platinum cathode catalysts for direct methanol fuel cell", Applied Energy (2013) 103, 212–220.
[3] M.H. Shao, K. Sasaki and R.R. Adzic "Pd-Fe Nanoparticles as Electrocatalysts for Oxygen Reduction", J. Am. Chem. Soc. (2006) 128, 3526-3527.
[4] M.R. Tarasevich, G.V. Zhutaeva, V.A. Bogdanovskaya, M.V. Radina, M.R. Ehrenburg and A.E. Chalykh "Oxygen kinetics and mechanism at electrocatalysts on the base of palladium–iron system", Electrochim. Acta (2007) 52, 5108–5118.
[5] M.H. Shao, T. Huang, P. Liu, J. Zhang, K. Sasaki, M.B. Vukmirovic and R.R. Adzic "Palladium Monolayer and Palladium Alloy Electrocatalysts for Oxygen Reduction", Langmuir (2006) 22, 10409–10415.

8th Iranian Fuel Cell Seminar
FEBRUARY 25,26
2015

Biomass, Resources and Technology for Use in PEMFC

Akram Heidari[1*], Ahmad Nozad Golikand[1,2] , Seyed Ahmad Mortazavi[1], Maryam Heidari[3]

1. Department of chemistry, Shahr-e-Qods Branch, Islamic Azad University, Tehran, Iran
2. Material Research School, NSTRI, Tehran, Iran.
3. Department of Agricultural biotechnology, science & research branch, Islamic Azad University, Tehran, Iran.

heidari654@yahoo.com

Abstract

Bioenergy is renewable energy derived from living biological material, or biomass. Biomass comprises all biological material derived from living, or recently living organisms. Technology conversion of biomass are: thermal, chemical, biochemical. Biofuel is a form of renewable energy that can be produced from various biomass. One of the main biofuel is bioethanol. Bio-ethanol, is a clean and renewable fuel. The conversion pathways for the production of bio-ethanol are fermentation, catalytic conversion of syngas and fermentation of syngas. Fuel cell is an electrochemical device in which the chemical energy is directly converted into electrical energy. Among the various fuels which can be converted into hydrogen to be used in fuel cells, ethanol, is very promising candidate because it is easily decomposed in the presence of water and generate an H_2-rich mixture suitable for feeding fuel cells. In the present study, biomass, resources and technology for use in PEMFC have been investigated.

Keyword: Biomass, Bioenergy, Ethanol production, PEMFC

1. Introduction

1.1. Bioenergy

Bioenergy is renewable energy derived from living biological material, or biomass. Bioenergy is the energy contained in biomass is energy from the sun captured through natural processes of photosynthesis [1]. The bio-energy resources are classified into two main categories. One is agro-fuels and the other is bio-fuels. Bio-fuels are biomass- derived fuels designed to replace petroleum and used mainly in the transport sector. An agro-fuel, is a type of bio-fuel, consisting of crops and/or trees grown on a large scale. Forms of bioenergy include power, heat, and solid, liquid, and gas fuels. Uses of these various forms of bioenergy include industrial, residential, and commercial applications (Figure 1). Renewable energy sources can be a good substitute of the fossil fuel which Bioenergy produce are being terminated fast [2].

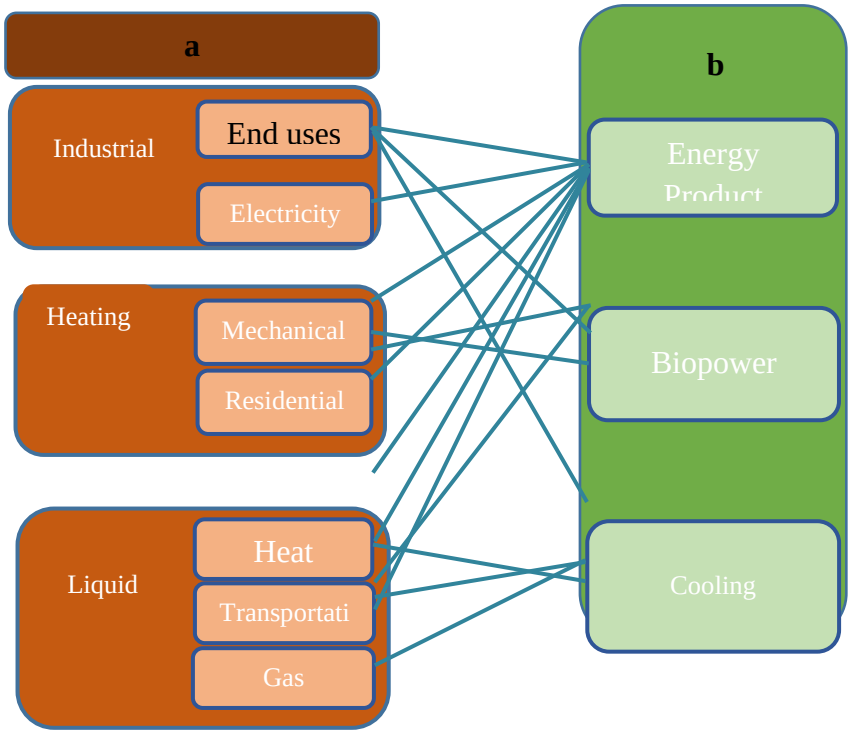

Figure1: Energy product and their uses.

1.2. Biomass

Biomass is fourth largest primary energy resource in the word and it is one of the most promising renewable energy, that is available in the worldwide [2]. Biomass comprises all biological material derived from living, or recently living organisms. Biomass can be burnt directly or it can be converted into solid, gaseous and liquid fuels using conversion technologies [4]. Unlike fossil fuels, biomass is renewable in the sense that only a short period of time is needed to replace what is used as an energy resource [3]. For three main reasons: First, it is a renewable resource that could be sustainably developed in the future. Second, it has positive environmental properties resulting in no net releases of carbon dioxide and very low sulfur content. Third, it appears to have significant economic potential provided that fossil fuel prices increase in the future. Biomass has the unique advantage among the rest of the renewable resource energy, to be able to provide solid, liquid and gaseous fuels that can be stored, transported and utilized, far away from the point of origin [5].

1.2.1 BIOMASS FEEDSTOCKS AND SOURCES

There are three main types of biomass materials from which bioenergy feedstocks are derived: lipids, sugars/starches [6], and cellulose/lignocellulose (Figure 2). Lipids are energy-rich, water-insoluble molecules such as fats, oils, and waxes. Lipids are a feedstock source derived from nonwoody plants and algae. Soybean, oil palm, and various seed crops such as sunflower are common agricultural sources of oils for biodiesel production. Sugars and starches are the carbohydrates typically found in the edible portions of food crops, such as corn grain and sugarcane. Cellulosic/lignocellulosic biomass is composed of complex carbohydrates and noncarbohydrate molecules typically found in the leaves and stems of plants. Cellulose/lignocellulose has no food value to humans [1]. lignocellulosic materials are abundant

in nature and does not compete with food, Lignocellulosic materials such as, forest residues, municipal solid waste, waste paper, could produce up to 442 billion liters per year of bioethanol therefor this materials are promising materials to production of ethanol. Lignocellulose, wich is a component of plant cell walls, is mainly composed of cellulose, hemicellulose, and lignin. Cellulose is a polymer consist in ß-glucose monomers. Hemicellulose can be xyloglucans or xylans depending on the types of plants. Lignins are phenolic compounds wich are formed by polymerization of three types of monomers (p-coumaryl, coniferyl and synapyl phenols) [7, 8].

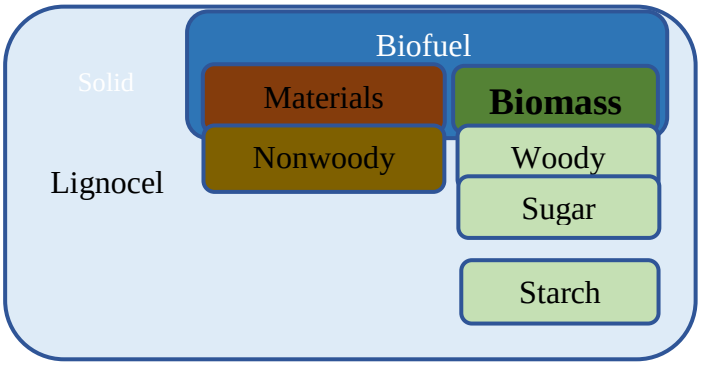

Figure 2: Types of biomass derived from woody and nonwoody.

There are two broad categories of plants, that they are woody and nonwoody (Figure 2). The majority of biomass for bioenergy feedstocks comes from three sources: forests, agriculture, and waste. Woody biomass from forests is the original source of bioenergy. It is the most important source of fuel for cooking and space heating throughout the world, particularly among subsistence cultures. Forest residues are comprised of biomass remaining after forest thinning and harvesting operations, and thus do not directly compete with pulp-and-paper, lumber, composite panel furnish, and other commodity timber products [9]. Agriculture is a source of sugars, starches, lipids, nonwoody cellulosic materials, and woody materials (i.e., lignocellulosic biomass) [6]. Agriculture-based biomass comes from crops grown specifically for bioenergy production, as well as agricultural residues. Agricultural residues are nonedible, cellulosic materials that remain after harvest of edible portions of crops. Agricultural residues include plant leaves and stems. Waste-based biomass includes organic materials leftover from industrial processes, agricultural liquid and solid wastes (e.g., manure), municipal solid wastes, and construction [4]. The major sources of nonwoody wastes include waste paper, liquid leftover from paper production (i.e., black liquor), and textile manufacturing [1].

1.3 OVERVIEW OF CONVERSION TECHNOLOGIES

To make use of the energy available in biomass, it is necessary to use technology to either release the energy directly, as in direct combustion for heat, or to transform it into other forms such as solid, liquid, or gaseous fuel. There are three main types of conversion technologies currently available: thermal, chemical, and biochemical (Figure 3). These technologies may also be used in combination. Thermal conversion processes use predominantly heat to convert biomass into other forms. Thermal conversion processes include combustion, pyrolysis, torrefaction, and gasification [1].

Traditionally, biomass had been utilized through direct combustion. Burning biomass produces pollutants including dust and the acid rain gases such as sulfur dioxide and nitrogen oxides but the sulfur dioxide produced is 90% less than that is produced by burning coal. The combustion process is started by heating the fuel above its ignition temperature in the presence of oxygen or air. Under the influence of heat, the chemical bonds of the fuel are cleaved [2].

Pyrolysis is the decomposition of biomass at high temperatures in the absence of oxygen. fast pyrolysis becomes a promising option for the thermo-chemical conversion of lignocellulosic biomass into liquid fuels because of its higher yield and quality of liquid oil compared to other techniques. For fast pyrolysis process, a bubbling fluidized bed reactor has been widely used at bench-scale and pilot-scale plants due to its high heat transfer rate [10]. Torrefaction is pyrolysis at low temperature [1]. Torrefaction is a thermal process performed in an inert atmosphere at temperatures between 200 and 300 □C, with residence times lower than 60 min and heating rates lower than 20 □C/min. Its aim is to improve biomass as a solid fuel. In this processing, the lignocellulosic components are degraded (hemicellulose and cellulose are more degraded than lignin), having as result a biomass with a predominant amount of lignin [11]. Gasification is the conversion of solid biomass into various gases using heat and varying amounts of oxygen [1]. Promising routes to convert biomass into liquid are by means of gasification followed by syngas conversion. All biomass compounds hemicellulose, cellulose and lignin can be converted into a H2/CO rich syngas. [6].

During a gasification process, biomass is directly converted to synthesis gas (syngas) in a gasifier under a controlled amount of air. Syngas can be used in internal combustion (IC) engine to produce heat, or in a cogeneration system to produce heat and electricity. The gasification step involves reacting biomass with air, oxygen, or steam to produce a gaseous mixture of CO, CO2, H2, CH4, and N2 either known as producer gas or synthesis or syngas, depending on the relative proportions of the component gases [2]. Chemical conversion involves the use of chemical agents to convert biomass into liquid fuels. [1]. Biochemical conversion involves the use of enzymes of bacteria or other microorganisms to break down biomass. There are three routes for biochemical conversion: Digestion (aerobic, anaerobic), Fermentation, Enzymatic or acid hydrolysis [12].

Aerobic digestion, is a biochemical breakdown of biomass, that it takes place in the presence of oxygen. It uses different types of microorganisms that access oxygen from the air, producing carbon dioxide, heat, and a solid digestate. Anaerobic digestion is an attractive waste treatment practice in which both pollution control and energy recovery can be achieved. Many agricultural and industrial wastes are ideal candidates for anaerobic digestion because they contain high levels of easily biodegradable materials. The inhibitors commonly present in anaerobic digesters include ammonia, sulfide, light metal ions, heavy metals, and organics [2]. Fermentation can be performed as a batch, fed-batch or continuous process. Batch culture is a closed culture system which contains an initial, limited amount of nutrient, and microorganisms, which allow the fermentation. The major advantage of fed-batch, comparing to batch, is the ability to increase maximum viable cell concentration, and product accumulation to a higher concentration. In the

continuous process, feed, which contains substrate, culture medium and other required nutrients, is pumped continuously into an agitated vessel where the microorganisms are active. The product, which is taken from the top of the bioreactor, contains bioethanol, cells, and residual sugar [8]. lignocellulosic materials should converted to simple sugars before fermentation, through a process called hydrolysis. The most commonly applied methods include: chemical hydrolysis (dilute and concentrated acid hydrolysis) and enzymatic hydrolysis. When hydrolysis is catalyzed by such enzymes, the process is known as enzymatic hydrolysis. By enzymatic method, conversion of cellulose to glucose is selective and degradation products like tars are not produced. Enzymatic hydrolysis of lignocellulosic materials is a very slow process because cellulose hydrolysis is hindered by structural parameters of the substrate, such as lignin and hemicellulose content, surface area, and cellulose crystallinity [7].

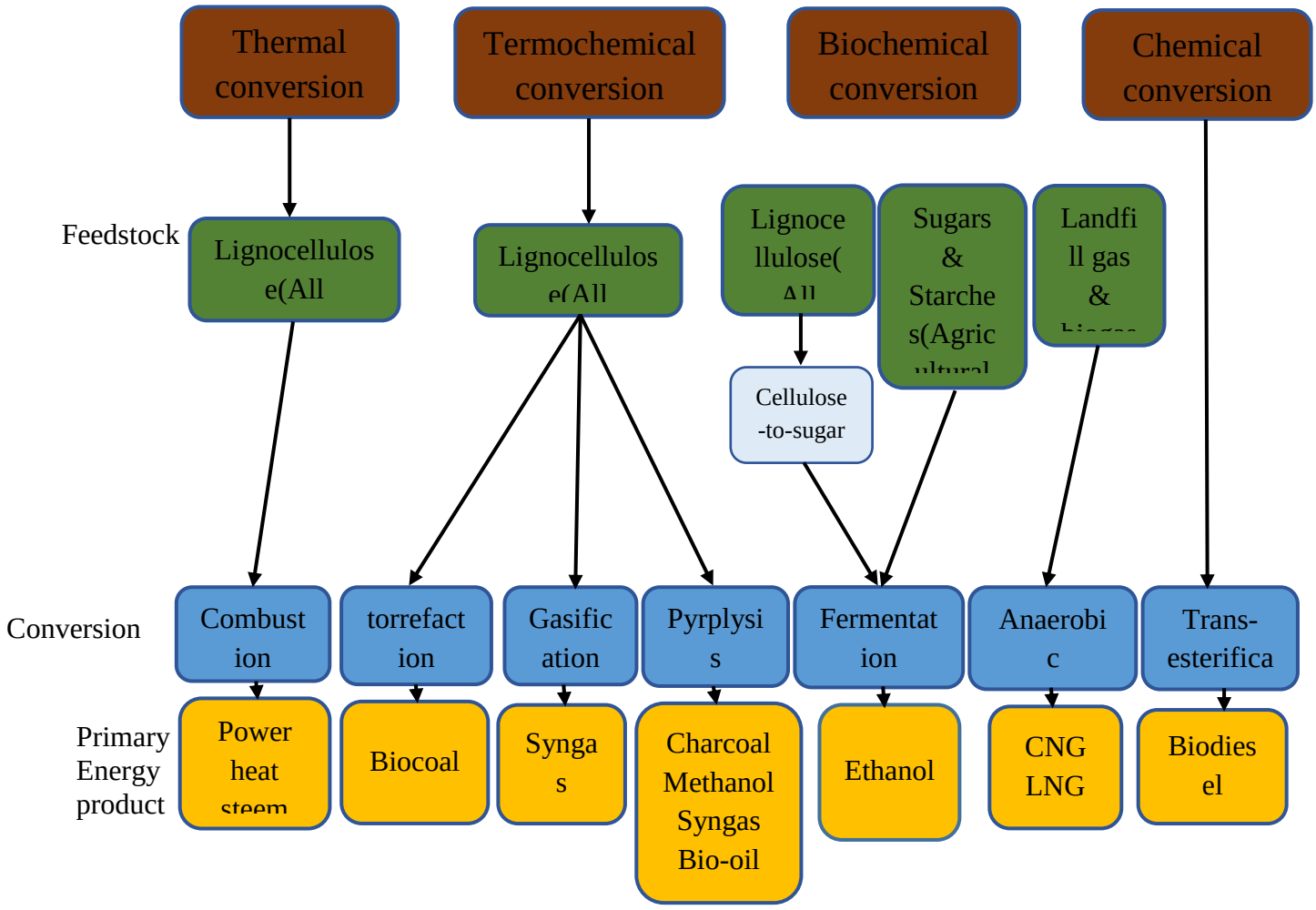

Figure 3: Conversion pathways.

1.4 Biofuel

Biofuel is a form of renewable energy that can be produced from various biomass resources including agricultural feedstocks [13]. The term biofuel is referred to as liquid or gaseous fuels for the transport sector that are predominantly produced from biomass. A variety of fuels can be produced from biomass resources including liquid fuels, such as ethanol, methanol, biodiesel, Fischer-Tropsch, and gaseous fuels, such as hydrogen and methane. Liquid biofuels are primarily used to fuel vehicles, but can also fuel engines or fuel cells for electricity generation. There are several reasons for biofuels to be considered as relevant technologies by both developing and industrialized countries include energy security reasons, environmental concerns, foreign exchange savings, and socioeconomic issues related to the rural sector. Advantages of biofuels are the following: (a) biofuels are easily available from common sources, (b) they are represent a carbon dioxide-cycle in combustion, (c) biofuels have a considerable environmentally friendly potential, (d) there are many benefits the environment, economy and consumers in using biofuels, and (e) they are biodegradable and contribute to sustainability. The biggest difference between biofuels and petroleum feedstocks is oxygen content. Biofuels have oxygen levels from 10% to 45% while petroleum has essentially none making the chemical properties of biofuels very different from petroleum. All have very low sulfur levels and many have low nitrogen levels. Liquid biofuels being considered world over all into the following categories: (a) bioalcohols; (b) vegetable oils and biodiesels; and (c) biocrude and bio-synthetic oils. They may be pure (100%) biofuels for dedicated vehicles or blend fuels in such a proportion that they can substitute conventional motor fuels without affecting car performance. For example, ethanol can be blended with gasoline without problems with as much as 15–20% alcohol by volume (E15-20) [5].

1.4.1 Bioethanol

One of the main biofuel is bioethanol. Bio-ethanol, as a clean and renewable fuel, is gaining increasing attention, mostly through its major environmental benefits. It can be produced from different kinds of renewable feedstock. On the basis of the raw material used for its production, bioethanol is divided into first, second and third generation bioethanol. First generation include; sucrose-containing feedstocks (sugar can, sugar beet) and starchy materials (wheat, corn). Second generation include; lignocellulosic biomass (wood, straw,), and third generation include algal biomass [16]. using bio-ethanol as fuel have several advantages such as: (i) its use as renewable energy to partially substitute oil and increase security of supply; (ii) its use as octane enhancer in unleaded gasoline to replace metyl-tert-butylether (MTBE); (iii) its use as oxygenated compound for clean combustion of the gasoline, thus reducing the tailpipe emissions and improving the ambient air quality and (iv) its use as renewable fuel to reduce CO2 emissions and its contribution to a reduced effect on climate change [15] .The conversion pathways for the production of bio-ethanol are:

a. Ethanol synthesis from gasification of biomass
b. Ethanol production from fermentation of biomass
c. Ethanol production from fermentation of syngas

1.4.1.1 Ethanol synthesis from gasification of biomass

Synthesis gas (or syngas) is ultimately produced, which is a mixture of carbon monoxide, carbon dioxide, and hydrogen. Syngas can then undergo a water-gas shift reaction in order to produce hydrogen, as follows:

$CO + H_2O \rightarrow CO_2 + H_2$ [17]

The chemical formula of the direct synthesis of ethanol from syngas is described in Eq. (1).

$$2CO + 4H_2 = C_2H_5OH + H_2 \qquad (1)$$

Four kinds of catalysts have been reported for the direct synthesis of ethanol from syngas: Modified F–T synthesis (Fe-based or Co-based, which hydrocarbons as the main products), catalysts modified Cu-based catalysts (produceC1–C6 alcohols mixtures in which methanol and isobutanol are the main products) , sulfide Mo-based catalysts (produce methanol and ethanol as the main oxygenates but also form large amounts of methane and CO2 as by-products) and Rh-based catalysts (have the highest selectivity for ethanol among various catalysts but the selectivity for methane is still large (>30%). Rh-based catalysts [19]. Studies have shown, The CuZn+Al catalyst exhibited high ethanol selectivity in production of ethanol from syngas [18]. Rhodium catalysts loaded on silica modified by various transition metal oxides were investigated for the conversion of syngas to ethanol. In gasification, all kind of biomass, convert to syngas [20].

1.4.1.2Ethanol production from fermentation of biomass

Bio-ethanol can be produced from a large variety of carbohydrates (mono-, di-, polysaccharides) [15]. Sugarcane is the primary feedstock in Brazil, and corn grain is the primary feedstock in the United States [1]. In the biological conversion of lignocellulosic feedstocks, pretreatment is required. Pretreatments break down cellulose and hemicellulose into sugars and separate lignin and other plant constituents from fermentable materials. Pretreatment technologies are physical, biological, and combinatorial; the form of pretreatment used will depend on the nature of the feedstock. Physical pretreatment includes gamma-ray exposure; chemical pretreatment methods include the use of acids, alkali, and ionic liquids; and biological methods include use of microorganisms to degrade lignin and hemicellulose [12, 21]. lignocellulosic materials should converted to simple sugars before fermentation, through a process called hydrolysis. The supernatant from enzymatic hydrolysis of lignocelluloses can contain both six-carbon (hexoses) and five-carbon (pentoses) sugars (if both cellulose and hemicellulose are hydrolyzed). Microorganisms can be used to ferment all lignocellulose-derived sugars to bioethanol. The performance parameters of fermentation are: temperature range, pH range, alcohol tolerance, growth rate, productivity, osmotic tolerance, specificity, yield, genetic stability, and inhibitor tolerance. If, fermentation products are more volatile than water, recovery by distillation is often the technology of choice. Distillation technologies that will allow the economic recovery of dilute volatile products from streams containing a variety of impurities have been developed and commercially demonstrated. A distillation system separates the bioethanol from water in the liquid mixture.The first step is to recover the bioethanol in a distillation or beer column. The product (37% bioethanol) is then concentrated in a rectifying column to a concentration just below the azeotrope (95%). The remaining bottoms product is fed to the stripping column to remove additional water and finally bioethanol 99.6% is produced. After the first effect, solids are separated using a centrifuge and dried in a rotary dryer [7]

1.4.1.3 Ethanol production from fermentation of syngas

Conversion of synthesis gas to ethanol by C. ljungdahlii has been developed into a commercial process that combines cellulose gasification, synthesis gas fermentation, and recovery of ethanol from the reaction products by distillation. The limited solubilities in water at about 37 □C of carbon monoxide (0.03 g/kg) and hydrogen (0.0014 g/kg) limit conversion rates and a high degree of agitation and increased pressure are necessary to stimulate gas/liquid mass transfer

rates. Continuous stirred tank reactors (CSTRs) with high impeller speeds are used to reduce bubble size and so improve interfacial contact and, consequently, reaction rate. A variety of trickle bed reactors have been considered, and these have been more efficient than either CSTRs or bubble column reactors. Elevated pressures are obviously desirable for bacteria that can withstand pressures of 4050Mpa. Although higher fermentation temperatures should lead to improved rates of reaction, they have the downside effect of lowering the solubility of the synthesis gas. Fermentation of synthesis gas offers a more narrowly defined product slate than chemical conversion where ethanol, isobutanol, acetates, and butyrates are the primary products. Synthesis gas fermentation also proceeds at lower temperatures and pressures than an analogous FT process, and is apparently independent of a specific ratio of carbon monoxide to hydrogen [22].

1.4.1.2 Ethanol as fuel of fuel cell

The utilization of alternative fuels such as ethanol for generation of electrical power in fuel cells may be considered as a long-term policy capable of providing significant economic and environmental benefits [23]. Fuel cell is an electrochemical device in which the chemical energy is directly converted into electrical energy [24]. Fuel cell has an electrolyte in contact with an anode (negative electrode) and a cathode (positive electrode) [26]. The polymer electrolyte membrane or proton exchange membrane fuel cell (PEMFC) with hydrogen as fuel, is considered to be the one of the most promising portable power sources due to its fast start-up, high power density, quick load following, and ease of electrolyte handling, zero-pollution, high output density, low corrosion and system robustness. The purity of the hydrogen (H_2) should be relatively high to achieve high efficiency, power density and long life there are difficulties in hydrogen supply infrastructure or fuel reforming technology with the clean-up of impurities such as carbon monoxide and sulfur compounds [25].

In recent years a lot of research in the field of proton exchange membrane (PEM) fuel cells is focused on direct ethanol fuel cells (DEFCs) due to ethanol's intrinsic advantages. Among the various fuels which can be converted into hydrogen to be used in fuel cells for automotive and stationary applications, alcohols, in particular, methanol and ethanol, are very promising candidates because they are easily decomposed in the presence of water and generate an H_2-rich mixture suitable for feeding fuel cells. Methanol has been thoroughly studied in recent years but the main drawbacks are its high toxicity and its production based essentially on non-renewable fossil fuel. In contrast, ethanol has advantage such as its non-toxicity, less volatility than methanol and renewability with high energy density (8.0 kWh/kg). Furthermore its easy production in large quantities by fermentation from sugar containing agricultural wastes adds up to its advantages [26]. The basic difference of ethanol in comparison with methanol and other alternative fuels, is the feasibility of its production from biomass with biochemical processes. Therefore, methanol does not address the goal of reducing neither the dependence on fossil fuels nor the emissions of greenhouse gases, such as CO_2. In general, technologies for the production of hydrogen from liquid and gaseous fuels are based on one of the following processes:

Steam reforming (SR).

Partial oxidation (POX).

Autothermal reforming (ATR). [27].

Ethanol reforming consists on an interesting alternative for the renewable production of hydrogen, not only as a chemical feedstock for the industry, but also for the production of electricity in selected applications using fuel cells [28]. Daniel G. Lopes et al. presents a technical and economic analysis of a power supply system based on a 5 kW Proton Exchange Membrane Fuel Cell (PEMFC) fed with hydrogen produced by the auto-thermal reforming of

ethanol. The results point out that the cost of the hydrogen produced by the ethanol reformer prototype is lower than the hydrogen prices in the Brazilian market, and that the cost of the electricity produced by that hydrogen in a PEMFC is lower than other alternative sources of energy, except when compared to the electricity available in grid-connected power system in Brazil [26]

Conclusions

Bioenergy produced from biomass is a promising solution to environmental challenges and a driver of economic development from local to global levels. Biofuel is recognised as an important renewable and sustainable energy source to substitute fossil fuel [14]. Due to its environmental merits, the share of biofuel in the automotive fuel market will grow fast in the next decade. Biofuels stand for liquid or gaseous fuel for transport produced from biomass. Ethanol as a clean and renewable fuel can be produced from biomass, therefor, ethanol feedstocks are available in the world. For reasons, low pollution, no toxicity, safe storage and handling, high energy density, capability reformation to hydrogen, and different methods for production, ethanol is favorable fuel for PEMFCs.

References

[1] Carol L. Williams, et al. Bioenergy: Biomass to Biofuels, Elsevier Inc, (2015) pp. 5-37

[2] Mukrimin Sevket Guney "Utilization of hazelnut husk as biomass", Sustainable Energy Technologies and Assessments, (2013). 4, 72–77

[3] Justo José Roberts, Agnelo Marotta Cassula, et al. "Assessment of dry residual biomass potential for use as alternative energy source in the party of General Pueyrredón, Argentina", Renewable and Sustainable Energy Reviews, (2015). 41, 568–583

[4] Mustafa Ozcan, Semra Oztürk and Yuksel Oguz "Potential evaluation of biomass-based energy sources for Turkey", Engineering Science and Technology, an International Journal, (2014) 1-7

[5] Ayhan Demirbas, "Biofuels sources, biofuel policy, biofuel economy and global biofuel projections", Energy Conversion and Management, (2008). 49, 2106–2116

[6] Philippe Girard, Abigaïl Fallot, "Review of existing and emerging technologies for the production of biofuels in developing countries", Energy for Sustainable Development, (2006). 2, 92-108

[7]. Mustafa Balat," Production of bioethanol from lignocellulosic materials via the biochemical pathway: A review", Energy Conversion and Management, (2011). 52, 858–875

[8].Edgard Gnansono, Arnaud Dauriat, "Ethanol fuel from biomass:A review", J.Scientific & Industrial Research,(2005). 64, 809-821

[9] James A. Marciano, Robert J. Lilieholm, et al. "Factorsaffectingpublicsupportforforest-basedbiorefineries: A comparisonofmilltownsandthegeneralpublicinMaine,USA", Energy Policy, (2014). 75, 301–311

[10] Binh M.Q. Phan, Long T. Duong, et al. "Evaluation of the production potential of bio-oil from Vietnamese biomass resources by fast pyrolysis", b i oma s s and b i o energy, (2014). 62, 74-81

[11] D.A. Granados, H.I. Vel_asquez and F. Chejne "Energetic and exergetic evaluation of residual biomass in a torrefaction process", Energy, (2014). 74, 181-189

[12] Mahmoud Karimi, Bryan Jenkins and Pieter Stroeve "Ultrasound irradiation in the production of ethanol from biomass", Renewable and Sustainable Energy Reviews, (2014). 40,400–421
[13] Long Wu, Yuan Li, et al. "Efficient conversion of sugarcane stalks into ethanol employing low temperature alkali pretreatment method", Bioresource Technology, (2011). 102, 11183–11188
[14] Weng Hui Liew, Mimi H. Hassim and Denny K. S. Ng "REVIEW OF EVOLUTION, TECHNOLOGY AND SUSTAINABILITY ASSESSMENTS OF BIOFUEL PRODUCTION", Journal of Cleaner Production (2014). 71, 11-29
[15] Jan Baeyens, Qian Kang, et al. "Challenges and opportunities in improving the production of bio-ethanol", Progress in Energy and Combustion Science (2015). 47, 60-88
[16].Ping Wei, Li-HuaCheng '' A review of membrane technology for bioethanol production", Renewable and Sustainable Energy Reviews, (2014). 30, 388–400
[17].M.Yazdanie, F.Noembrini, L.Dossetto, K,Boulouchos "A comparative analysis of well-to-wheel primary energy demand and greenhouse gas emissions for the operation of alternative and conventional vehicles in Switzerland, considering various energy carrier production pathways" , J. of Power Sources, (2014). 249, 333-348
[18]. Zhi-Jun Zuo, Le Wang, et al." The effect of CuO–ZnO–Al2O3 catalyst structure on the ethanol synthesis from syngas", Catalysis Communications, (2013). 34, 69-72
[19]. Yanyong Liu, Kazuhisa Murata, et al. "Synthesis of ethanol from methanol and syngas through an indirect route containing methanol dehydrogenation, DME carbonylation, and methyl acetate hydrogenolysis", Fuel Processing Technology, (2013). 110, 206–213
[20]. Jingjuan Wang, Qinghong Zhang, Ye Wang," Rh-catalyzed syngas conversion to ethanol: Studies on the promoting effect of FeOx", Catalysis Today, (2011). 171, 257– 265
[21] Renu Singh, Ashish Shukla, et al. "A review on delignification of lignocellulosic biomass for enhancement of ethanol production potential", Renewable and Sustainable Energy Reviews, (2014). 32, 713-728
[22] Arthur M. Brownstein, "Synthesis Gas-Based Fuels", Renewable Motor Fuels, (2015). 33-46
[23] Shuqin Song, Savvas Douvartzides and Panagiotis Tsiakaras " Exergy analysis of an ethanol fuelled proton exchange membrane
(PEM) fuel cell system for automobile applications", Journal of Power Sources (2005). 145, 502–514
[24] Umberto Lucia "Overview on fuel cells", Renewable and Sustainable Energy Reviews (2014). 30, 164–169
[25].S. Song, G. Wang, W. Zhoua, et al. "The effect of the MEA preparation procedure on both ethanol crossover and DEFC performance" J.of Power Sources, (2005). 140, 103–110
[26].Jyoti Tayal, Bhuvnesh Rawat, et al. "Effect of addition of rhenium to Pt-based anode catalysts in electro-oxidation of ethanol in direct ethanol PEM fuel cell" international journal of hydrogen energy'', (2012). 37, 4597-4605
[27].A. Perna "Hydrogen from ethanol: "Theoretical optimization of a PEMFC system integrated with a steam reforming processor" International Journal of Hydrogen Energy, (2007). 32, 1811 – 1819
[28]. D.G. Lopes, E.P. da Silva ,C.S. Pinto,N.P. Neves Jr, J.C. Camargo , P.F.P. Ferreira, A.L. Furlan, D.G. Lopes "Technical and economic analysis of a power supply system based on ethanol reforming and PEMFC" Renewable Energy, (2012). 45, 205-212

8th Iranian Fuel Cell Seminar
FEBRUARY 25,26
2015

Synthesis of Fe:Pt Nanoalloy and Application of it in Preparation of Modified Carbon Paste Electrode in Methanol Oxidation

Hassan Karimi-Maleh[1*], Sahebe Khosravi[2]

1. Department of Chemistry, Graduate University of Advanced Technology, Kerman, Iran
2. Department of nanophysics, Institute of Science and High Technology and Environmental Sciences, Graduate University of Advanced Technology
** h.karimi.maleh@gmail.com*

Abstract
A catalyst for methanol oxidation, PtCo nano alloy, has been synthesized and its electrochemical activity for methanol oxidation has been investigated. X-ray diffraction depicts a good crystallinity of the supported Pt nanoparticles in the composites and reveals the formation of PtCo alloy .Structural characterizations with transmission electron microscopy (TEM) and X-ray powder diffraction (XRD) revealed that PtCo nanoparticles possess an interesting dendritic morphology with excellent structural continuity and integrity. The results show that the PtCo nano alloy modified carbon paste electrode exhibits large electrochemical capacitance for methanol electrooxidation.

Keywords: Methanol oxidation, Pt:Co nano alloy, Modified electrode

Introduction

Nanoparticles (NPs) are a subject of constantly growing interest inmany research areas such asmicroelectronic devices, photocatalysis, electrocatalysis, and biosensors [1]. Electrodeposition is one of the most efficient methods for the formation and synthesis of nanoparticles since it is rapid and facile, allowing easy control of the nucleation and growth of metal nanoparticles [2,3]. The electrodeposition is simple and the composition of the nanoparticles can be controlled by changing the electrodeposition parameters. Electrode surfaces are exquisitely sensitive to any redox active species that are able to diffuse to the electrode/electrolyte interface during an electrochemical experiment [4]. Compton et al. [4] introduced a new concept of “diffusional protection” of an underlying electrode surface, using chemical microarchitectures to create a designer interface. Various types of nanoparticles supported on electrode substrate were developed [5–9]. The ordered porous particles have high surface area for the electrocatalytic reactions. Direct alcohol fuel cells (DAFCs) based on liquid fuels have attracted much attention as power sources for portable electronic devices and fuel-cell vehicles due to themuchhigher energy density of liquid fuels than gaseous fuels such as hydrogen [10–13]. Among the different possible alcohols, methanol is the most promising organic fuel because its use as a fuel has several advantages in aqueous electrolytes, liquid fuel available at low cost, easily handled, transported and stored, high theoretical density of energy comparable to that of gasoline.

Results and discussion

Characterizations of nanocomposites

The morphologies of the Fe:Co nano alloy was investigated by using the XRD and TEM methods. Fig. 1a shows a typical TEM image of Pt:Co nanoparticles. The dark spots correspond to Pt:Co nanoparticles.

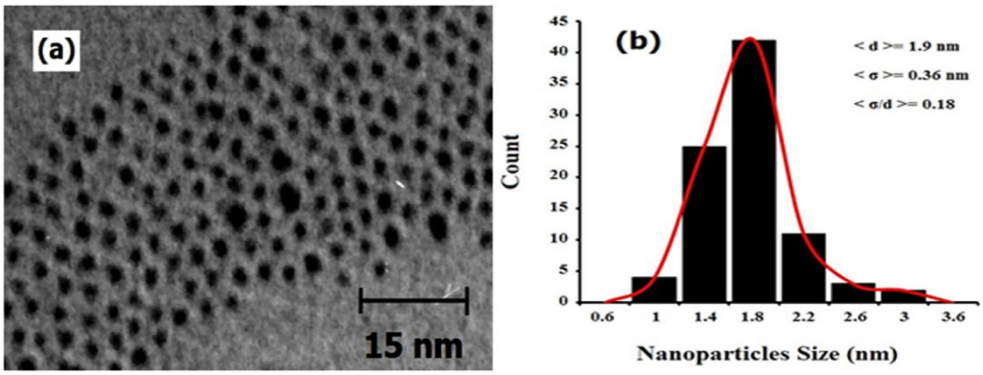

Figure 1: (a) TEM image of Pt:Co NPs deposited. (b) Histograms of size distribution of Pt:Co NPs.

Bimetallic Pt:Co nanoparticles with near spherical shapes, were synthesized. Fig. 1b is the histogram of Pt:Co nanoparticles size distribution based on log-normal fitting. Histogram graph shows that the particles have a single size with an average diameter (<d>) about 1.9 nm and standard deviation (s) of about 0.36, indicate narrow size distribution
(s/<d>) of 0.18.

The XRD patterns of the Pt:Co nanostructure showed diffraction peaks absorbed at 2θ values (Fig. 2).

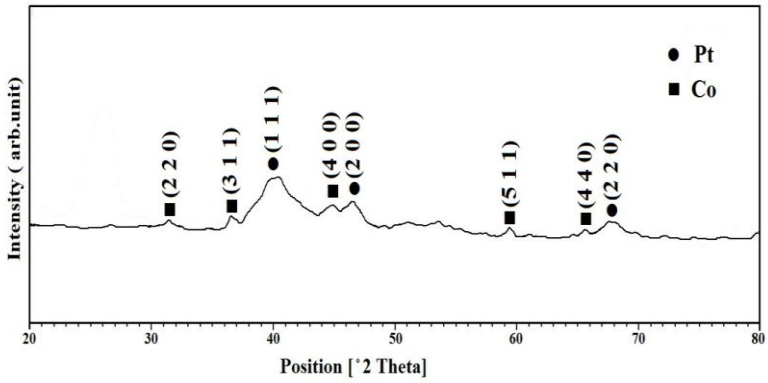

Figure 2: XRD pattern of synthesis nanoalloy

Figure 3 shows cyclic voltammogram Pt:Co modified carbon paste electrode in the absence (a) and in the presence of 1.0 mM methanol. As can be seen in the presence of methanol oxidation signal increase and confirm electrocatalytic process.

.

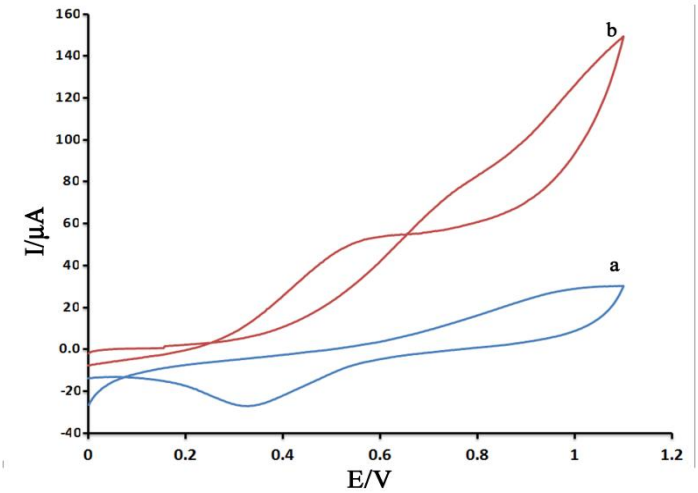

Figure 3. cyclic voltammogram Pt:Co modified carbon paste electrode in the absence (a) and in the presence of 1.0 mM methanol.

References

[1] E. Scavetta, S. Stipa, D. Tonelli, Electrochem. Commun. 9 (2007) 2838.
[2] C.M.Welch, R.G. Compton, Anal. Biochem. 384 (2006) 601.
[3] P. Liu, X.A. Guo, H. Huang, Q.Q. Yang, Y.X. Tong, G.A. Hope, Adv. Mater. 18 (2006) 1873.
[4] G.G. Wildgoose, F.G. Chevallier, L. Xiao, C.A. Thorogood, S.J. Wilkins, A. Crossley, L. Jiang, T.T.G. Jones, J.H. Jones, R.G. Compton, J. Mater. Chem. 16 (2006) 4103.
[5] I. Streeter, R.G. Compton, J. Phys. Chem. C 111 (2007) 18049.
[6] X. Dai, G.G. Wildgoose, C. Salter, A. Crossley, R.G. Compton, Anal. Chem. 78 (2006) 6102.
[7] L.Wang, S.J. Guo, J.F. Zhai, X.G. Hu, S.J. Dong, Electrochim. Acta 53 (2008) 2776.
[8] F. Ye, L. Chen, J.J. Li, J.L. Li, X.D.Wang, Electrochem. Commun. 10 (2008) 476.
[9] Y.H. Xu, X.Q. Lin, J. Power Sources 170 (2007) 13.
[10] H.L. Tang, S.L. Wang, M. Pan, S.P. Jiang, Y.Z. Ruan, Electrochim. Acta 52 (2007) 3714.
[11] S.Q. Song, W.J. Zhou, Z.X. Liang, R. Cai, G.Q. Sun, Q. Xin, V. Stergiopoulos, P. Tsiakaras, Appl. Catal. B 55 (2005) 65.
[12] S. Rousseau, C. Coutanceau, C. Lamy, J.M. Léger, J. Power Sources 158 (2006) 18.
[13] G.C. Li, P.G. Pickup, J. Power Sources 161 (2006) 256.

پیل‌های سوختی با سوخت مستقیم بورهیدرید و تاثیر شرایط عملیاتی بر عملکرد پیل‌های سوختی

میرقاسم حسینی*، رعنا محمودی

دانشکده شیمی، دانشگاه تبریز، تبریز، ایران
** mg-hosseini@tabrizu.ac.ir*

چکیده

طی ۲۰ سال گذشته، علاقهٔ زیادی به تحقیق در زمینهٔ پیل‌های سوختی با سوخت مستقیم بورهیدرید وجود داشته است تا شرایط بهینهٔ عملکرد آنها بدست آید. استفاده از سدیم بورهیدرید به عنوان سوخت در پیل سوختی به این دلیل است که ولتاژ مدار باز بالاتر و در نتیجه توان بالاتری در مقایسه با پیل های سوختی الکلی دارند. مشکل اصلی، هیدرولیز یونهای بورهیدرید است که تولید هیدروژن می‌کند و باعث کاهش بازده انرژی و دانسیتهٔ توان آنها می‌شود. الکترونهای آزاد شده در طول اکسیداسیون بورهیدرید، اختلاف پتانسیل سل و توان خروجی به شدت تحت تاثیر آند و کاتد انتخابی، ترکیب الکترولیت و شرایط عملیاتی از قبیل دما است. بررسی-های وسیعی روی الکتروکاتالیست‌های آندی مختلف و تاثیر آنها روی اکسیداسیون، هیدرولیز و همچنین در مورد کاتالیستهای کاتدی و تاثیر آن روی عملکرد کلی پیل سوختی انجام شده است.

واژه‌های کلیدی: پیل سوختی، بورهیدرید، عوامل موثر بر عملکرد پیل

۱- مقدمه

پیل های سوختی ابزارهای الکتروشیمیایی‌اند که به طور مستقیم انرژی شیمیایی را به انرژی الکتریکی تبدیل می کنند. پیل های سوختی به دلیل تولید انرژی تمیزتر مورد توجه قرار گرفته اند [۱] و معمولا بر اساس الکترولیت مورد استفاده در آن طبقه بندی می‌شوند . پیل های سوختی استفاده شده در کاربردهای حمل و نقل باید در شرایط محیطی با کمترین امکانات، با دانسیته توان بالا کار کنند. این شرایط در صورت استفاده از سوخت های مایع قابل حصول است و دلیل آن ظرفیت بالای این سوخت ها و هزینه های کم آن هاست. متانول به صورت گسترده به عنوان منبع انرژی برای کاربردهای حمل و نقل کوچک به کار می‌رود. با این حال پیل سوختی با سوخت مستقیم متانول (DMFC) معمولا ولتاژ مدار باز پایین و دانسیتهٔ‌توان کم از خود نشان می‌دهد و دلیل آن فعالیت الکتروشیمیایی پایین متانول و عبور متانول است. برای افزایش دانسیتهٔ توان، به لودینگ فلزات گرانی مثل Pt یا آلیاژهای Pt – Pu نیاز است[۲]. پیش زمینه‌هایی از این قبیل دربارهٔDMFC محققان را به یافتن سوخت های جایگزین وادار می‌کند. بور هیدریدیکی از این سوخت های جایگزین است. پیل سوختی با سوخت مستقیم بور هیدرید (DBFC) به دلیل استفاده از الکترولیت غشایی، شبیه پیل سوختی مبادله پروتون (PEMFC) و DMFC

است و به دلیل استفاده از یک محیط قلیا به (AFC)شباهت دارد. نبود مشکلات ذخیرهٔ هیدروژن و استفاده از سوخت مایع ایمن، عبور کم سوخت به سمت کاتد، ولتاژ تئوری بالا (1064 mV) و دانسیتهٔ توان تئوری بالا (۹/۳KW/Kg) از مزایای DBFC است . در حالت تئوری یک یون BH_4^- می تواند هشت الکترون تولید کند. در حالی که تعداد الکترون های مبادله شده درحالت عملی به دلیل آزاد شدن هیدروژن در آند و عبور سوخت، کمتر از این تعداد است. آزاد سازی هیدروژن به دلیل واکنش هیدرولیز بور هیدرید می‌باشد که نه تنها عملکرد پیل را دچار مشکل می‌کند بلکه در طراحی سیستم نیز مشکلاتی به وجود می‌آورد . علاوه بر این، عبور BH_4^- ، انباشتگی NaOH در کاتد و انباشتگی $NaBO_2$ در آند مشکلات دیگری هستند که باید حل شوند [۳]. واکنش آندی در DBFC اکسایش مستقیم بور هیدرید در محیط قلیایی به صورت معادلهٔ ۱ است :

$$[BH_4^- + 8\,OH^- \rightarrow Bo_2^- + 6\,H_2O + 8e \qquad E^\circ{}_{anode} = -۱/۲۴\ \text{V} \qquad (۱)$$

و واکنش کاتدی با اکسیژن به عنوان اکسیدانت به صورت معادلهٔ ۲ است :

$$O_2 + 2\,H_2O + 4\,e \rightarrow 4\,OH^- \qquad E^\circ{}_{cathode} = ۰/۴\ \text{V} \qquad (۲)$$

ولتاژ تئوری پیل۱/۶۴Vاست. برخلاف DMFC، هیدروژن پراکسید یک اکسیدانت مناسب علاوه بر اکسیژن برای DBFC است [۴]. ولتاژ احیا در کاتد با هیدروژن پر اکسید به صورت معادلهٔ۳ است :

$$4H_2O_2 + 8\,e \rightarrow 8\,OH^- \qquad E^\circ{}_{cathode} = ۰/۸۷\ \text{V} \qquad (۳)$$

ولتاژ تئوری پیل در این حالت ۲/۱۱V است. پارامترهای عملی تاثیر به سزایی روی عملکرد DBFC دارند. غلظت سدیم بور هیدرید یکی از این پارامتر هاست که بسیار پر اهمیت است و مطالعات زیادی دربارهٔ تاثیر بورهیدرید بر اکسایش الکتروشیمیایی آن انجام شده است [۸-۵ و ۲]. پتانسیل پیل یک پیل سوختی از مقدار پتانسیل مدار باز در نتیجهٔ ۳ عامل تغییر می‌کندکه در شکل ۱ نشان داده شده است:

۱) پلاریزاسیون اکتیواسیون در الکترودها که یک سد انرژی در مقابل واکنش‌های انتقال بار نشان می‌دهد.

۲) مقاومت‌های اهمی در الکترولیت، غشا، الکترودها و صفحات جمع‌کنندهٔ جریان و مقاومت‌های حاصل از تماس‌های نادرست بین لایه‌ها.

۳) پلاریزاسیون غلظتی حاصل از محدودیت انتقال واکنشدهنده‌ها به سایت‌های واکنش(سطح کاتالیست). پتانسیل پیل می-تواندبه صورت معادلهٔ ۴ نشان داده شود[۹]:

$$E_{Cell} = E^o_{Cell} - |\eta^a_{act}| - |\eta^c_{act}| - |\eta^a_{Conc}| - |\eta^c_{Conc}| - \sum_K (IR)_K \qquad (۴)$$

استفاده از سدیم بورهیدرید مزایای زیادی دارد:

۱) در محلول قلیایی قوی پایدار بوده و نیمهٔ عمر آندرpH=۱۴تقریبا ۴۳۰ روز می‌باشد و به صورت جامد و محلول ۳۰Wt% موجود است[۱۰].

۲) حاوی غلظت جرمی بالایی از هیدروژن است(۱۰/۶Wt%) که به فرم سالم و بی ضرر نگهداری می‌شود[۱۱].

۳) از نظر تئوری ۸ الکترون به ازای هر یون بورهیدرید در پتانسیل‌های خیلی پایین(-۱/۲۴ vs SHE) آزاد میشود و قادر است تا توان بالایی را با مقادیر پایینی از سوخت ایجاد کند[۱۲].

۴) بر عکس اتانول و متانول، کربن دی اکسید درپیلهای سوختی ایجاد نمی‌شود[۱۳].

۵) محصول اکسیداسیون آن، متابورات است که از نظر محیط زیست قابل دسترسی بوده و می‌تواند دوباره به سدیم بورهیدرید تبدیل شود[۱۴].

شمای کلی پیل سوختی با سوخت مستقیم بورهیدرید در شکل ۲ نشان داده شده است.سوختهایی همچونبورهیدرید می‌تواند مستقیما در آند اکسید شوند.بهترین دانسیتهٔ توان حاصل از DBFC در حدود۳۶W است که توسط میلی [۲۱]و همکارانش با استفاده از $۲۵cm^2$ ($۱/۴۴W.cm^{-2}$) $NaBH_4/H_2O_2$ با آند Pd/C و کاتد Au با غشای نافیونی ۱۱۲ بدست آمده است[۱۵].

۲- عملکرد پیل و تاثیر متغییرهای عملیاتی

۲-۱- تاثیر دما روی عملکرد پیل سوختی بورهیدرید

مزیت پیل های سوختی بورهیدرید توانایی آنها در تولید انرژی در دمای اتاق است که آنها را برای کاربردهای خاص مستعد می‌سازد. به عبارت دیگر عملکرد آنها با افزایش دما بهبود می‌یابد. دانسیتهٔ جریان و توان با افزایش دما افزایش می‌یابد. افزایش دما باعث بهبود فرایند انتقال جرم واکنش‌دهنده‌ها، تسریع سنتیک الکترواکسیداسیون بورهیدرید و افزایش هدایت یونی غشا/الکترولیت می‌شود البته دماهای خیلی بالا، سرعت عبور یون از میان غشا و هیدرولیز BH_4^- را بالا می‌برد. مشکل دیگر دماهای بالا، افزایش دهیدراتاسیون غشا است که مقاومت غشا را بالا می‌برد.

ما [۲۲]و همکارانش [۱۶]، آزمایشهایی را در پیل‌های سوختی بورهیدرید با نافیون ۲۱۲و آند Ni+Pd/C و کاتد $۱mg.cm^{-2}$ Pt/Cانجام دادند. سوخت شامل محلول ۵Wt% بورهیدرید ($۱/۳۲mol.dm^{-3}$) و ۱۰Wt% NaOH($۲/۵mol.dm^{-3}$) بود و سرعت عبور سوخت $۵dm^3/min$ بود. اکسیدانت اکسیژن مرطوب با سرعت $۰/۱۵\ dm^3.min^{-1}$ بود. دانسیتهٔ توان با افزایش دما از ۲۸^oC به ۶۰^oC از $۷۷mW.cm^{-2}$ به $۱۶۷mW.cm^{-2}$ افزایش یافت.

هاجون [۲۳]و همکارانش[۱۷] تاثیر دما را بررسی کردند و مشاهده کردند که در پیل سوختی $NaBH_4/H_2O_2$ با نافیون ۱۱۷، آند Pt/C ($۴mg.cm^{-2}$)، کاتد MnO_2 ($۴mg.cm^{-2}$)، سوخت$۰/۵M\ NaBH_4$+۲M NaOH و اکسیدانت ۶M H_2O_2 با افزایش دما از۲۰^oC به ۸۰^oC دانسیتهٔ توان از $۳۰mW.cm^{-2}$ به $۷۳mW.cm^{-2}$ افزایش می‌یابد.

چنگ[۲۴]و همکارانش [۱۸] نشان دادند که با افزایش دما از ۲۵^oCبه ۸۵^oC در پیل سوختی $NaBH_4/H_2O_2$ با نافیون ۱۱۷، آندAu/C($۲mg.cm^{-2}$)،کاتدPt/C ($۲mg.cm^{-2}$)، سوخت ۵ Wt% $NaBH_4$ در ۱۰ Wt% NaOHو اکسیدانت O_2 دانسیتهٔ توان $۱۵mW.cm^{-2}$ به $۷۵mW.cm^{-2}$ افزایش می‌یابد.

[21]Miley
[22]Ma
[23]w. Haijun
[24]H. Cheng

حسینی و همکارانش[۱۹و۲۷و۲۸] نشان دادند که با افزایش دما از ۲۵^oC به ۵۵^oC در پیل سوختی $NaBH_4/H_2O_2$ با نافیون ۱۱۷، آند($Pt/C(۲mg.cm^{-2})$، کاتد($Ni/C(۲mg.cm^{-2})$، سوخت $۱ M$ $NaBH_4$ در $۲ M$ NaOH و اکسیدانت $۰/۵ M$ H_2SO_4 + $۲H_2O_2$ دانسیتهٔ توان از $۶۰mW.cm^{-2}$ به $۱۵۰mW.cm^{-2}$ افزایش می‌یابد(مطابق شکل ۳).

۲-۲- تاثیر غلظت $NaBH_4$ روی عملکرد پیل سوختی بورهیدرید

مطابق با معادلهٔ نرنست انتظار می‌رود که OCP با افزایش غلظت BH_4^- افزایش یابد. آزمایش‌ها نشان دادند که افزایش غلظت $NaBH_4$، عملکرد آند را افزایش می‌دهد اما همچنین پلاریزاسیون کاتدی را نیز افزایش می‌دهد[۲۰]. سرعتی که پلاریزاسیون کاتدی افزایش می‌یابد با افزایش غلظت یون‌های بورهیدرید کاهش می‌یابد. چنگ و اسکات[۲۵][۱۸] آزمایش‌هایی در پیل سوختی $NaBH_4/O_2$ با نافیون ۱۱۷، آند ($Au/C(۲ mg.cm^{-2})$، کاتد ($Pt/C(۲mg.cm^{-2})$ در محلولهایی حاوی غلظتهای۳Wt%، ۵، ۸ و ۱۰ (۰/۷۹، ۱/۳۲، ۲/۱و ۲/۶۴ $mol.dm^{-3}$) در ۱۰Wt% NaOH($۲/۵mol.dm^{-3}$)انجام دادند و مشاهده کردند که دانسیتهٔ توان ۳۰% افزایش می‌یابد وقتی غلظت بورهیدرید از ۳Wt% به ۵Wt% افزایش می‌یابد اما با افزایش بیشتر غلظت دیگر تقریبا افزایش نمی‌یابد.

هاجون[۲۶] و همکارانش [۱۷] در پیل سوختی $NaBH_4/H_2O_2$ با نافیون ۱۱۷ و آند($Pt/C(۲mg.cm^{-2})$، کاتد $mg.cm^{-}$ ($MnO_2(۲^2)$، اکسیدانت $۶M$ H_2O_2 در دمای ۸۰^oC مشاهده کردند که با افزایش غلظت بورهیدرید از ۰/۵M به ۲/۵M دانسیتهٔ توان از $۱۰۰mW.cm^{-2}$ به $۱۳۰mW.cm^{-2}$ افزایش می‌یابد.

چلیک[۲۷] و همکارانش [۲۱] در پیل سوختی $NaBH_4/H_2O_2$ با نافیون ۱۱۷ و آند $mg.cm^{-}$ ($Pd/C(۰/۳^2)$، کاتد($Pt/C(۰/۳mg.cm^{-2})$ در دمای ۲۵^oC مشاهده کردند که با افزایش غلظت بورهیدرید از ۰/۵M به ۱/۵M دانسیتهٔ تواناز $۶mW.cm^{-2}$ به $۱۲mW.cm^{-2}$ افزایش می‌یابد.

حسینی و همکارانش[۱۹و۲۷و ۲۸] نشان دادند که با افزایش غلظت بورهیدرید از ۱M به ۲M در دمای $۴۵ ^oC$ در پیل سوختی $NaBH_4/H_2O_2$ با نافیون ۱۱۷، آند($Pt/C (۲mg.cm^{-2})$، کاتد ($Ni/C(۲mg.cm^{-2})$، ۲M NaOH و اکسیدانت $۰/۵ M$ H_2SO_4 + $۲H_2O_2$ دانسیتهٔ توان از $۹۰mW.cm^{-2}$ به $۱۱۱/۱۳mW.cm^{-2}$ افزایش می‌یابد.

۲-۳- تاثیر غلظت اکسیدانت روی عملکرد پیل سوختی بورهیدرید

برای واکنش‌دهندهٔ کاتدی مایع با افزایش غلظت H_2O_2، پتانسیل کاتد مطابق با معادلهٔ نرنست افزایش می‌یابد. اما همانند بورهیدرید، عبور H_2O_2 از میان غشا با افزایش بیش از حد غلظت افزایش یافته و منجر به کاهش پتانسیل می‌شود. بنابراین در پیل سوختی $NaBH_4/H_2O_2$ با نافیون ۱۱۷ و آند($Pt/C(۴mg.cm^{-2})$، کاتد ($MnO_2(۲mg.cm^{-2})$، ۰/۵M $NaBH_4$+۲M NaOH در دمای ۸۰^oC با افزایش غلظت H_2O_2 از ۱M به ۸M تا ۶M پیک دانسیتهٔ توان از $۳۰ mW.cm^{-2}$ به $۷۰ mW.cm^{-2}$ افزایش می‌یابد و سپس شروع به کاهش می‌کند بنابراین غلظت بهینهٔ H_2O_2، ۶M است[۱۷].

[25] Scott
[26] W. Haijun
[27] Celik

حسینی و همکارانش[۱۹و۲۷و ۲۸] نشان دادند که با افزایش غلظت H_2O_2 از ۱M به ۳M در پیل سوختی $NaBH_4/H_2O_2$ با نافیون ۱۱۷، آند($Pt/C(۰/۵mg.cm^{-2})$، کاتد ($۰/۵Ni/Cmg.cm^{-2}$)، ۱M $NaBH_4$+۲MNaOH ، دانسیتهٔ توان از $mW.cm^{-2}$ ۳۲/۴۷ به $mW.cm^{-2}$۱۰۱/۵۶ افزایش می‌یابد.

۲-٤- تاثیر سرعت فلو روی عملکرد پیل سوختی بورهیدرید

سرعت فلوی سوخت و اکسیدانت فاکتور دیگری است که پیل سوختی DBFC را تحت تاثیر قرار می‌دهد. سرعت‌های فلوی ۱۰، ۲۰، ۹۰ و $۱۵۰cm^3.min^{-1}$ توسط چلیک و همکارانش[۲۲] با استفاده از یک سل $۲۵cm^2$ شامل آند Pd/C و کاتد Pt/C و نافیون۱۱۷انجام شد. منحنی‌ها نشان می‌دهد که افزایش سرعت عبور اکسیدانت منجر به افزایش کمی در دانسیتهٔ توان ($۸/۵mW.cm^{-2}$و۱۰/۱ به ترتیب در $۱۰cm^3.min^{-1}$ و ۱۵۰) می‌شود.

کیم [۲۸]و همکارانش [۲۳] دانسیتهٔ توان را ۲۱% با افزایش سرعت فلوی اکسیدانت از $dm^3.min^{-1}$ ۵ به ۱۰افزایش دادند.

۳- تبدیل محصول متابورات سدیم به واکنش‌دهندهٔ سدیم بورهیدرید

اکسیداسیون بورهیدرید یک واکنش برگشت پذیر است که محصول یک مخلوط کمپلکس از بوراتها و متابوراتها است. روش‌های شیمیایی مختلفی برای بازیافت بورهیدرید وجود دارد. کجیما[۲۹]و هاگا[۳۰][۲۴]، واکنش $NaBO_2$ باMgH_2 را بررسی کردند که بازده بین ۴/۸و ۹۷% برای فشار بین ۰/۵و ۷MPaو دمای ۵۵۰^oC دارد. محققان دریافتند که راندمان بازیافت $NaBO_2$ از واکنش ۵ با افزایش دما و فشار افزایش می‌یابد اما مستقل از زمان واکنش است.

$$NaBO_2 + 2MgH_2 \rightarrow NaBH_4 + 2MgO \quad (۵)$$

$NaBH_4$همچنین می‌تواند از $NaBO_2$با استفاده از MgSi تحت فشار بالای H_2 ایجاد شود (واکنش‌های ۵ و ۶). راندمان ۹۸% در ۵۵۰^oC تحت فشار ۷MPa است و با افزایش دما افزایش می‌یابد.

$$NaBO_2 + 2Mg + Si + 2H_2 \rightarrow NaBH_4 + 2MgSi + 2H_2 \quad (۶)$$

$$NaBO_2 + Mg_2\mathrm{Si} + 2H_2 \rightarrow NaBH_4 + 2\mathrm{MgO} + \mathrm{Si} \quad (۷)$$

کک همانطوریکه در واکنش ۸ نشان داده شده است یا متان در واکنش ۹ می‌توانند برای بازیافت $NaBH_4$ از $NaBO_2$ استفاده شوند. متان یک عامل کاهندهٔ ارزان است و منجر به تولید $NaBH_4$ از $NaBO_2$ طی فرایند یک مرحله‌ای می‌شود واکنش ۹ [۲۵].

$$NaBO_2 + 2C + 2H_2O \rightarrow NaBH_4 + 2CO_2 \quad (۸)$$

$$NaBO_2 + 2CH_4 + 2H_2O \rightarrow NaBH_4 + 2CO_2 + 4H_2 \quad (۹)$$

[28]Kim
[29]Kojima
[30]Haga

سانلی [31] و همکارانش[۲۶] از عامل کاهندهٔ H_2 برای ایجاد $NaBH_4$ استفاده کردند و نشان دادند که ولتامتری چرخه‌ای از محلول حاوی $NaBO_2$ ۰/۱ $mol.dm^{-3}$ در $NaOH$ ۱$mol.dm^{-3}$ روی الکترود Ag پیک کاهشی در 0.5 V vs SCE نشان می‌دهد. الکترولیز تحت پتانسیل ثابت منجر به سنتز بورهیدرید از طریق مکانیسم زیر می‌شود(واکنش‌های ۱۲،۱۱،۱۰)

$$BO_2^- + 4H_2 \rightarrow BH_4^- + 2H_2O \quad (۱۰)$$

$$2H_2O + 2e^- \leftrightarrow 2OH^- + H_2 \quad (۱۱)$$

$$2OH^- + 2H^+ \leftrightarrow 2H_2O \quad (۱۲)$$

بعد از الکترولیز، یک پیک جدید در ۰/۲V vs SCE- در منحنی CV یافت شد که ارتفاع پیک با زمان الکترولیز افزایش می‌یابد که مربوط به تشکیل $NaBH_4$ از $NaBO_2$ است.

نتیجه‌گیری

DBFC یک منبع توان است اما پارامترهای ساختاری و عملیاتی زیادی باید مد نظر قرار گیرد.

۱) افزایش دما دانسیتهٔ توان و دانسیتهٔ جریان را افزایش می‌دهد. ضریب نفوذ واکنش‌دهنده‌ها و هدایت الکترولیت با افزایش دما افزایش می‌یابد. یون‌های بورهیدرید با سرعت بالایی اکسید می‌شوند اما سرعت تولید هیدروژن افزایش می‌یابد.

۲) افزایش غلظت یون‌های بورهیدرید باعث افزایش دانسیتهٔ توان و سرعت تولید هیدروژن و افزایش عبور بورهیدرید از میان غشا می‌شود. افزایش غلظت یونهای هیدروکسید سرعت عبور بورهیدرید از میان غشا را کاهش می‌دهد اما ویسکوزیتهٔ محلول را افزایش می‌دهد و باعث کاهش سرعت نفوذ واکنش‌دهنده و افزایش افت اهمی در الکترولیت می‌شود.

۳) افزایش سرعت فلو عملکرد پیل را با بهبود انتقال واکنش‌دهنده‌ها در الکترودها و کاهش بلوکه شدن کانال‌ها در نتیجهٔ تشکیل محصولات بهبود می‌بخشد.

مراجع

1. R. x. Feng, H. Dong, Y. D. Wang, X. p. Ai, Y. L. cao and H . x. Yang,"A simple and high efficient direct borohydride fuel cell with MnO_2-catalyzed cathode", Electrochemistry Communications, 7 ,2005 , 449 – 452
2. B. H. Liu, Z. P. Li and S. Suda, "Electrocatalysts for the anodic oxidation of borohydrides", ElectrochimicaActa, 49, 2004, 3097 – 3105.
3. K. T. Park, U. Ho. Jung, S. U. Jeong and S. H. Kim, "Influence of anode diffusion layer properties on performance of direct borohydride fuel cell" Journal of **Power Sources,**162, 2006, 192 – 197.
4. J. Ma, N. A. Choudhury and Y. sahai, "A comprehensive review of direct borohydride fuel cells", Renewable and **Sustainable Energy** Reviews, 14, 2010, 183 – 199.
5. H. chengand K. scott, "Determination of kinetic parameters for borohydride oxidation on a rotating Au disk electrode"ElectrochimicaActa, 51, 2006, 3429-3433.
6. E. Gyenge, M– Atwan and D. Nothwood ,"Electrocatalysis of Borohydride Oxidation on Colloidal Pt and Pt-Alloys (Pt-Ir, Pt-Ni, and Pt-Au) and Application for Direct Borohydride Fuel Cell Anodes",Journal of The **Electrochemical Society,** 153, 2006, A150 – A158.

[31] Sanli

7. J. H. Kim, H. S. Kim, Y. M. Kang and J. Y. Lee, “Carbon-supported and unsupported Pt anodes for direct borohydride liquid fuel cells”, Journal of the electrochemical society, 151, 2004, A1039 – A1043.
8. Z. P. Li, B. H. Liu, K. Arai, K. Asaba and S – Suda, “Evaluation of alkaline borohydride solutions as the fuel for fuel cell”, Journal of power sources, 126, 2004, 28 – 33.
9. D. Pletcher, AFirst Course in Electrode Processes, RSC, Cambridge, UK, 2009.
10. C. Ponce de Leon, F.C. Walsh, D. Pletcher, D.J. Browning and J.B. Lakeman, “Direct borohydride fuel cells”, Journal of Power Sources, 155, 2006, 172-181.
11. J.I. Martins, M.C. Nunes, R. Koch, L. Martins and M. Bazzaoui,“Electrochemical oxidation of borohydride on platinum electrodes: The influence of thiourea in direct fuel cells□Electrochimica Acta,52, 2007,6443-6449.
chimicaActa
12. D.A. Finkelstein, N.D. Mota, J.L. Cohen and H.c.D. Abruna, “Rotating Disk Electrode (RDE) Investigation of BH_4^- and BH_3OH^- Electro-oxidation at Pt and Au: Implications for BH_4^- Fuel Cells□, Journal of Physical Chemistry C, 113, 2009, 19700-19712.
13. U.B. Demirci, “Direct borohydride fuel cell: Main issues met by the membrane–electrodes-assembly and potential solutions”, Journal of Power Sources, 172, 2007, 676-687.
14. Y. Kojima and T. Haga, “Recycling process of sodium metaborate to sodium borohydride□,**International Journal of Hydrogen Energy**, 28, 2003, 989-993.
15. G.H. Miley, N. Luo, J. Mather, R. Burton, G. Hawkins, L. Gu, E. Byrd, R. Gimlin,P.J. Shrestha, G. Benavides, J. Laystrom and D. Carroll, “Direct $NaBH_4/H_2O_2$ fuel cells”, Journal of Power Sources, 165, 2007, 509-516.
16. J. Ma, Y. Sahai and R.G. Buchheit, “Direct borohydride fuel cell using Ni-based composite anodes□, Journal of Power Sources, 195, 2010, 4709-4713.
17. W.Haijuna, W. Cheng, L.ZhixiangandM.Zongqiang, “Influence of operation conditions on direct $NaBH_4/H_2O_2$fuelcell performance”, International Journal of Hydrogen Energy, 35, 2010, 2648–2651.
18. H. Cheng and K. Scott, “Influence of operation conditions on direct borohydridefuel cell performance”, Journal of Power Sources, 160, 2006, 407–412.
۱۹. م. عبدالملکی، پایاننامهٔ دکتری، دانشگاه تبریز، ۱۳۹۲.
20. Z.P. Li, B.H. Liu, K. Arai, K. Asaba and S. Suda, “Evaluation of alkaline borohydride solutions as the fuel for fuel cell□, Journal of Power Sources, 126, 2004, 28-33.
21. C.Celik, F. G.B.San and H. I.Sarac, “Influences of sodium borohydride concentration on direct borohydridefuel cell performance”,Journal of Power Sources, 195, 2010, 2599–2603.
22. C. Celik, F.G. Boyaci San and H.I. Sarac, “Effects of operation conditions on direct borohydride fuel cell performance”, Journal of Power Sources, 185, 2008, 197-201.
23. C. Kim, K.-J. Kim and M.Y. Ha, “Performance enhancement of a direct borohydridefuel cell in practical running conditions”, Journal of Power Sources, 180, 2008, 154-161.
24. Y. Wu, M.T. Kelly and J.V. Ortega, Review of Chemical Processes for the Synthesisof Sodium Borohydride, Millenium Cell Inc, 2004.
25. A.E. Sanli, i. Kayacan, B.Z. Uysal and M.L. Aksu, “Recovery of borohydride from metaborate solution using a silver catalyst for application of direct rechargableborohydride/peroxide fuel cells□,Journal of Power Sources, 195, 2010, 2604-2607.
26. F. Walsh, A First Course in Electrochemical Engineering, RSC Publishing,Cambridge, UK, 1993.

27. M. G. Hosseini and M. Abdolmaleki, “Synthesis and characterization of porous nanostructured Ni/PdNi electrode towards electrooxidation of borohydride”, International Journalof Hydrogen Energy XXX, 2012, 1-8.
28. M. G. Hosseini, M. Abdolmaleki and S. Ashrafpoor, “Electrocatalytic Oxidation of sodium borohydrid on a nanoporous Ni/Zn-Ni electrode”, Chinese Journal of Catalysis, 33, 2012, 1-0.

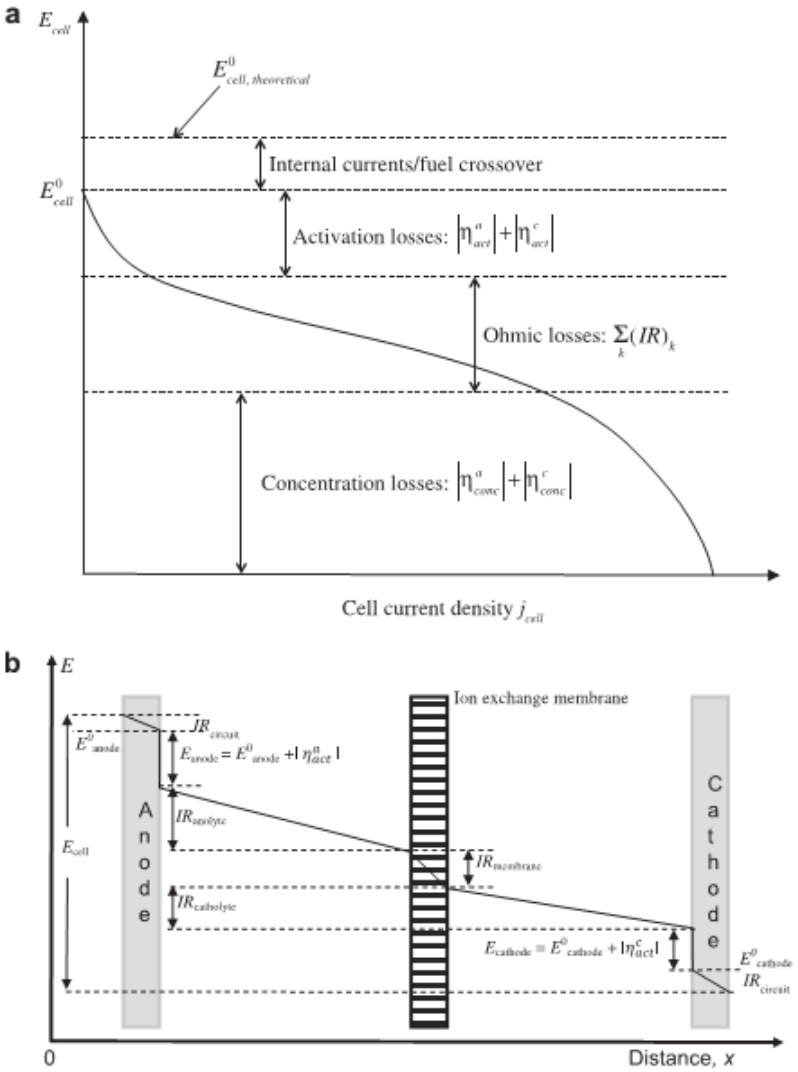

شکل ۱: a) عواملی که در افت پتانسیل کل پیل دخالت دارند، b) پتانسیل در امتداد الکترودها، الکترولیتها و غشا بر حسب فاصلهٔ بین دو الکترود در پیل[۲۷]

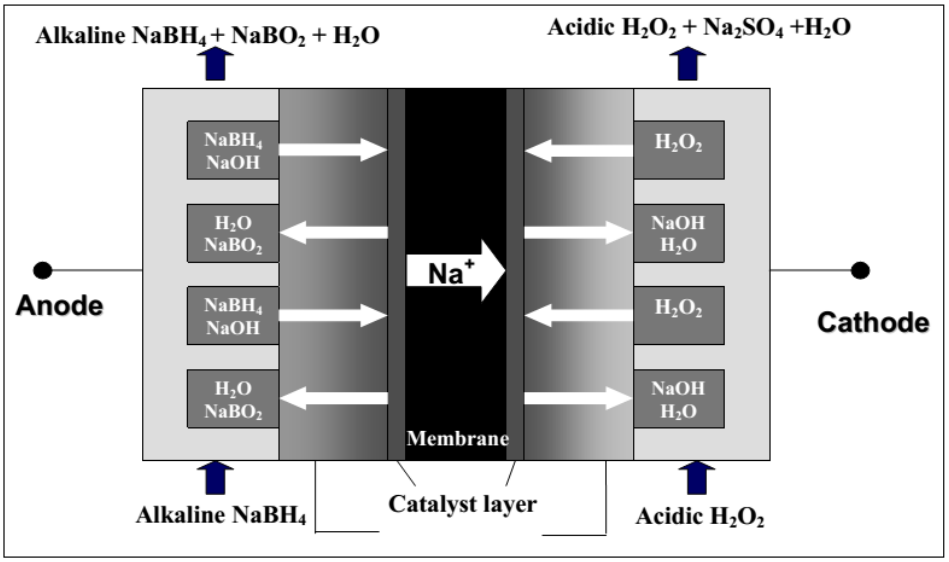

شکل ۲: اصول عملیاتی پیل سوختی بورهیدرید

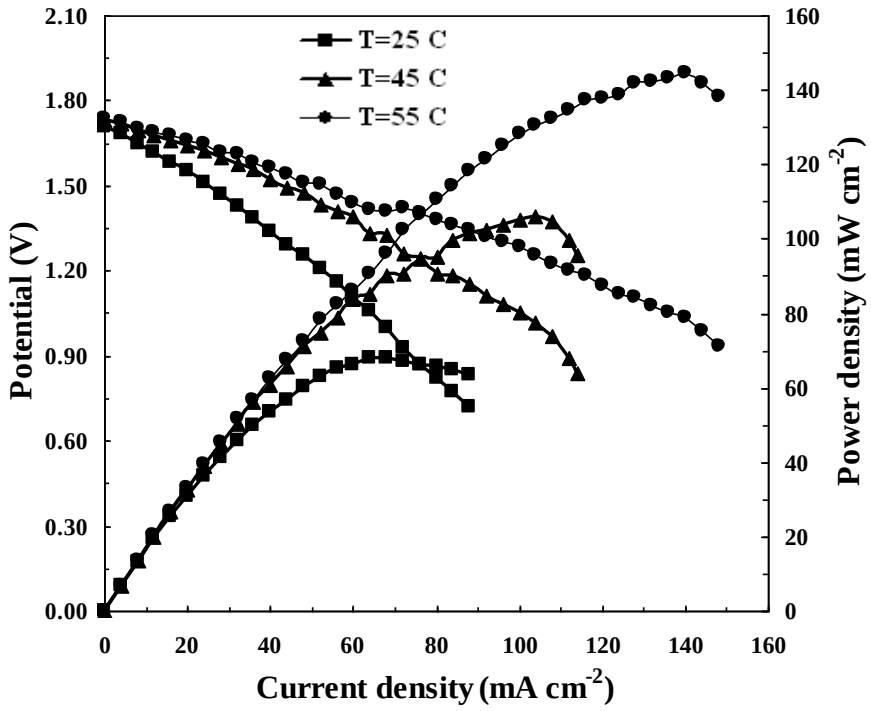

شکل ۳: اثر دما بر روی منحنیهای I-V و I-P، سوخت: محلول ۲M NaOH + ۱M $NaBH_4$، اکسیدانت: محلول ۰/۵M H_2SO_4 + M ۲H_2O_2 و لودینگ کاتالیست آندی ۲ mg cm^{-2}[۱۹].

Simulation and Computational Methods

8th Iranian Fuel Cell Seminar
FEBRUARY 25,26
2015

High Performance Nanocomposite Proton-exchange Membranes for Fuel Cell Applications

Ghasem Bahlakeh
Department of Engineering and Technology, Golestan University, Aliabad Katool, Iran
gh.bahlakeh@gu.ac.ir

Abstract
Nanocomposite proton-exchange membranes of Nafion and hydroxyapatite were studied by using classical all-atom molecular dynamics simulations methods to examine the structural behavior of Nafion in its nanocomposite membranes used for fuel cells. Evaluation of radial distribution function of sulfur atoms of sulfonic acid group with respect to each other showed the presence of strong correlations between sulfur atoms implying the significant localization of sulfonic acid groups near each other in nanocomposite membrane compared to unmodified Nafion membrane. Additionally, from the concentration profile analysis of sulfur atoms, it was found that Nafion chains has moved towards the hydroxyapatite surface because of the strong interactions between the Nafion side chain and hydroxyapatite surface atoms.

Keywords: Nafion Ionomer, Nanocomposite Membrane, Hydroxyapatite, Molecular Dynamics Simulation

1 Introduction

Over the past years, proton conduction polymeric membranes have been subject of extensive research studies because of their uses in proton-exchange membrane fuel cells (PEMFCs) [1]. Performance of these polymer based materials when employed as membrane in fuel cells highly depends upon their properties. Nafion membrane, which is a perfluorosulfonic ionomer containing a tetrafluoroethylene backbone and a sulfonic acid group in side chain position, is the first and frequently used polymer, stemming from the fact that Nafion demonstrates high proton conductivity and good chemical and mechanical stability [2]. However, drawbacks associated with Nafion application in PEMFC, that is, high methanol permeability occurred in direct methanol fuel cells (DMFCs), very high production cost of membrane as well as low conductivity at higher operating temperatures, have limited Nafion applications and motivated research efforts toward the development of new membranes [3-5].

Molecular dynamics (MD) simulations methods are useful tools that are able to provide new information about characteristics of PEM materials. These Methods have been recently applied to examine membrane features associated with its proton conductivity in Nafion [6-14] and alternative pure hydrocarbons ones [15-23]. However, theoretical investigations using MD simulation have not been carried out for nanocomposite membranes. Therefore, we aim to study the behavior of nanocomposite membranes made of Nafion (shown in Figure 1) and hydroxyapatite by means of classical simulation tools.

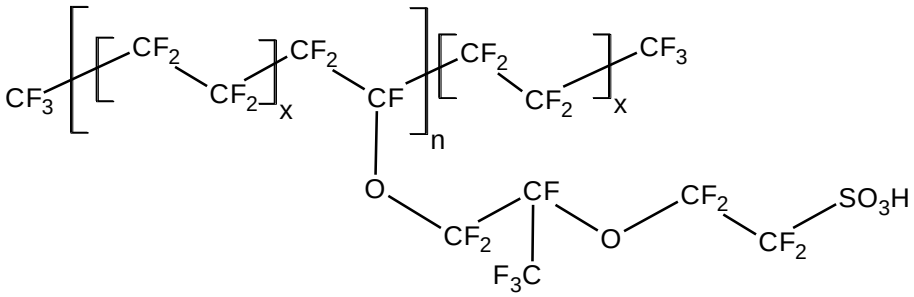

Figure 1: Chemical structure of Nafion.

2 Simulation Details

MD simulations were conducted on 3-D cells representing hydrated pure Nafion and Nafion/HA composite membranes at room temperature. For pure Nafion membrane, a cell containing 107 water molecules, 10 hydronium ions ($H3O^+$) and single Nafion chain with 10 monomer units was constructed at low initial density of approximately 0.7 g cm^{-3} using Amorphous Cell builder module of Materials Studio software package. It should be noted that the number of water molecules used for simulation was determined on the basis of experimentally obtained membrane water uptake values. During simulations, it was assumed that all the sulfonic acid groups in Nafion chain are dissociated and thus the same number of hydronium ions as the number of sulfonic acid groups was applied for amorphous cell to get electrically neutral system. The obtained amorphous cell was first minimized by Smart minimizer method for 1000 steps which was followed by NPT MD simulation over 200 ps at 1 atm to fully equilibrate the simulation cell. The equilibrated average density was 1.88 g cm^{-3} which agreed well with reported density for hydrated Nafion membranes.

In the case of Nafion/HA composite 3D simulation cell, the crystallographic HA surface was selected to study the interfacial interactions between HA nanoparticle surface and hydrated Nafion. For this purpose, HA structure implemented in Materials Studio was used. The HA surface with thickness of 12.5169 Å was built by cleaving the HA unit cell and then minimized for 1000 steps using Smart minimizer algorithm. In order to ensure appropriate interactions of HA surface with water molecules, hydronium ions and Nafion chain, its surface area were increased to 34.395 Å × 48.9685 Å. The constructed surface was then converted to 3D periodic cell with a vacuum space of thickness 120 Å above the surface. Afterwards, water molecules, hydronium ions and Nafion chain in equilibrated cell corresponding to hydrated pure Nafion membrane were all placed above the HA surface at a location more than 10 Å apart from the surface, as displayed in Figure 2. The vacuum slab was applied to limit the interaction of water molecules, hydronium ions and Nafion chain to only one side of the HA surface. Equilibration run of 1000-step optimization followed by 200 ps NVT MD simulation was conducted on resultant hydrated Nafion/HA cell to bring the cell to the equilibrium conditions.

After reaching the cells equilibration, production simulations were performed for 200 ps under NVT conditions for both pure hydrated Nafion and hydrated Nafion/HA cells. All were carried out using Discover module of Materials Studio software at 300 K. Partial atomic charges for water, hydronium ion, Nafion chain and HA surface were all assigned by using charge equilibration (QEq) method developed by Rappe et al. COMPASS (Condensed-Phase Optimized Molecular Potentials for Atomistic Simulation Studies) force field parameters were applied for all the molecules and HA surface atoms. Non-bonded van der Waals (vdW) and coulomb interactions were taken into account using Ewald summation method where accuracy level and update width parameters were set to 0.01 kcal/mol and 1 Å, respectively. Velocity Verlet integration algorithm was chosen to solve the Newton’s equation of motion with a time

step of o.5 fs. Andersen thermostat and barostat was used to control the temperature and pressure during NVT and NPT dynamics simulations. Periodic boundary conditions (PBC) were imposed in all three directions. In the case of hydrated Nafion/HA composite model cell, position of all atoms in the HA surface were kept fixed during all MD simulations.

3 Results and discussion

In order to better examine the presence of hydroxyapatite fillers on various structural properties of Nafion/HA nanocomposite membrane, the results obtained from MD simulations of pure Nafion as well as Nafion/HA systems were analyzed in terms of radial distribution function (also called pair correlation function) (RDF, g(r)), and concentration profile. RDF analysis was specifically carried out to examine the behavior of Nafion chains with respect to themselves, in particular sulfonic groups in side chain, and concentration investigation was done to explore Nafion behavior with regards to hydroxyapatite surface.

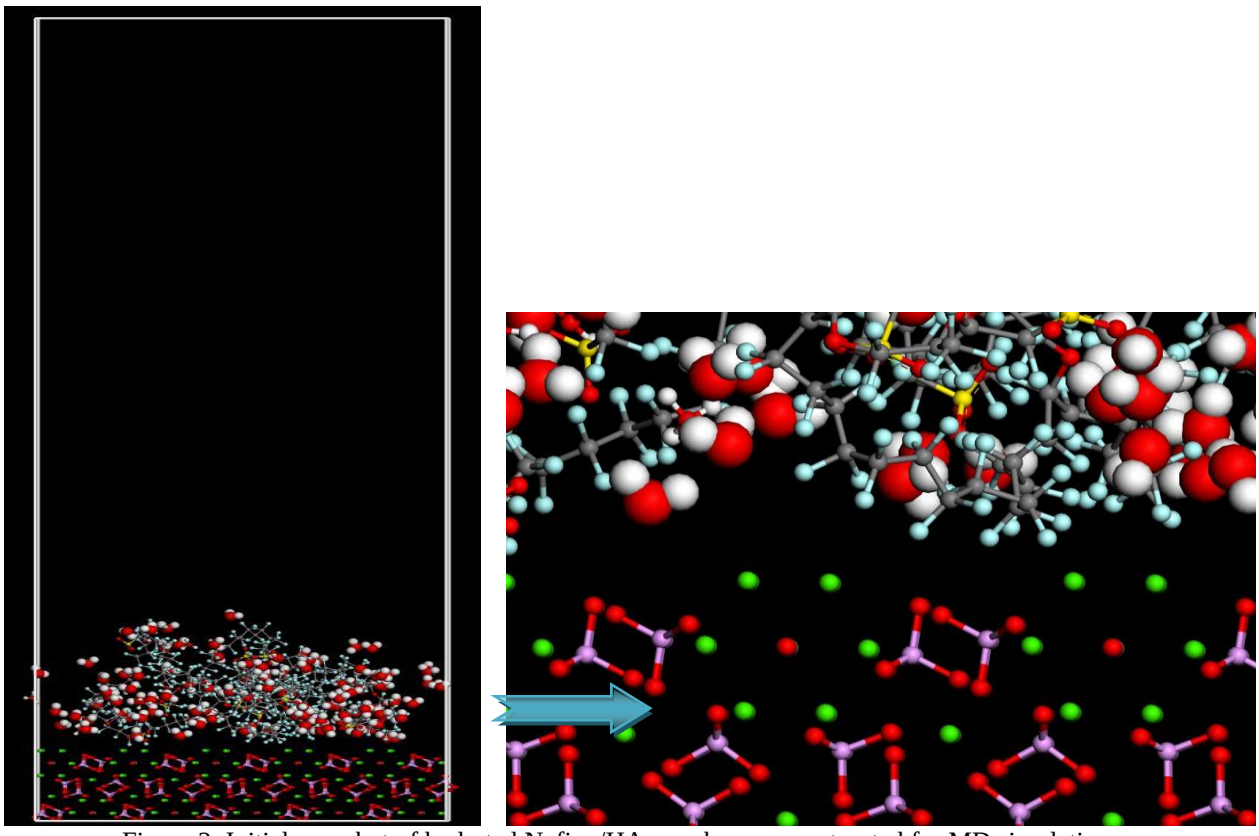

Figure 2: Initial snapshot of hydrated Nafion/HA membranes constructed for MD simulations.

Figure 3 displays the radial distribution function of sulfonic acid sulfur to sulfonic acid sulfur atomic pairs (S–S) in hydrated pure Nafion and Nafion-hydroxyapatite nanocomposite membranes as a function of distance. As clear in this figure, S-S RDFs indicate two very sharp peaks in nanocomposite membrane as compared to pure Nafion membrane. Appearance of these dominant peaks means that sulfonic acid groups have strong correlations, and are closer to each other in nanocomposite system. This behavior for sulfonic acid groups implies that addition of hydroxyapatite to Nafion could assist proton hopping between sulfonic acid groups via reducing the distance between neighboring sulfonic acid groups, although it also impedes methanol permeation through membrane and thereby reduces methanol permeability in nanocomposite membrane relative to unmodified Nafion system.

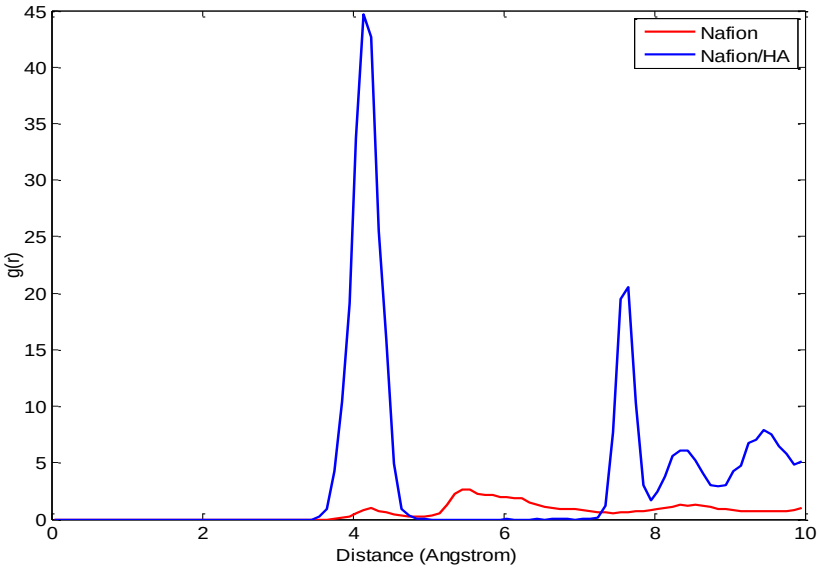

Figure 3: RDFs of sulfur-sulfur (sulfonic acid group) in the hydrated pure Nafion and hydrated Nafion/HA composite membrane.

Figure 4 exhibits the concentration profile of sulfur atoms in sulfonic acid group of Nafion in direction normal to the hydroxyapatite surface in two different simulation times of before and after MD simulations. As demonstrated in Figure 4, sulfur concentration profile before MD simulation initiates at about 12 Å from the HA surface, which is in agreement with the initial distance between HA and Nafion polymers. In addition, as it is clear from this figure, in comparison with the initial sulfur concentration, profile of sulfur concentration at the end of simulation has shifted towards the HA nanocomposite surface with an intensified peak at a distance smaller than 5 Å accompanied by gradual reduction in peak height. This trend in concentration profile of sulfur atoms compared to that in unmodified Nafion indicates the migration of Nafion chains against HA surface owing to the strong interactions of Nafion especially its sulfonic side chain with surface atoms of HA nanocomposite.

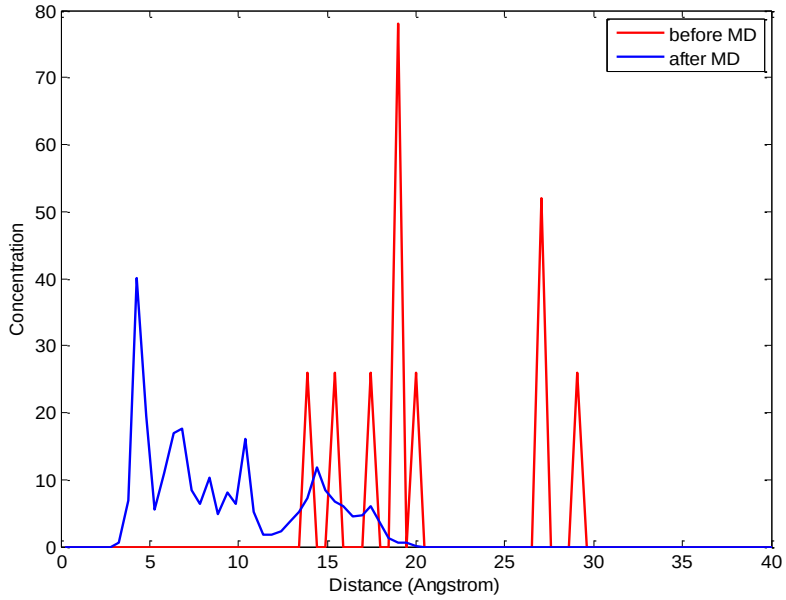

Figure 4: Concentration profile of sulfur atoms of sulfonic acid group in direction normal to the HA surface before and after the MD simulations.

Conclusions

In the current research, classical all-atom MD simulation tools were employed to study the various structural properties of nanocomposite membranes made of Nafion and hydroxyapatite. The results obtained from MD simulations were analyzed in terms of radial distribution function and concentration profile of sulfur atoms in sulfonic acid side chain groups. From RDF results for sulfonic acid sulfur atoms, it was understood that sulfonic acid groups are closer to each other in Nafion chains interacting with hydroxyapatite in comparison with unmodified Nafion membranes, which could enhance ionic conductivity of ionomer via assisting proton hopping between neighboring sulfonic acid groups. Moreover, analysis of concentration profile for sulfonic acid sulfur atoms revealed that within MD simulations, Nafion chains has moved significantly toward the HA surface.

Acknowledgment

The authors gratefully acknowledge the use of School of Computer Science, Institute for Research in Fundamental Science (IPM).

References

[1] Carrette, L., Friedrich, K. A., Stimming, U., Fuel Cells – Fundamentals and Applications, Fuel Cells, 1 (2001) 5-39.

[2] Mauritz, K. A., Moore, R. B., State of Understanding of Nafion, Chem. Rev., 104 (2004) 4535-4586.

[3] Rikukawa, M., Sanui, K., Proton-conducting polymer electrolyte membranes based on hydrocarbon polymers, Prog Polym Sci, 25 (2000) 1463-1502.

[4] Ahmad, H., Kamarudin, S. K., Hasran, U. A., Daud, W. R. W., Overview of hybrid membranes for direct-methanol fuel-cell applications, Int. J. Hydrogen Energy, 35 (2010) 2160-2175.

[5] Hasani-Sadrabadi, M. M., Mokarram, N., Azami, M., Dashtimoghadam, E., Majedi, F. S., Jacob, K. I., Preparation and characterization of nanocomposite polyelectrolyte membranes based on Nafion® ionomer and nanocrystalline hydroxyapatite, Polymer, 52 (2011) 1286-1296.

[6] Vishnyakov, A., Neimark, A. V., Molecular dynamics simulation of microstructure and molecular mobilities in swollen Nafion membranes, J Phys Chem B, 105 (2001) 9586-9594.

[7] Jang, S. S., Molinero, V., Cagin, T., Goddard, W. A., Nanophase-Segregation and Transport in Nafion 117 from Molecular Dynamics Simulations: Effect of Monomeric Sequence, J Phys Chem B, 108 (2004) 3149-3157.

[8] Urata, S., Irisawa, J., Takada, A., Shinoda, W., Tsuzuki, S., Mikami, M., Molecular Dynamics Simulation of Swollen Membrane of Perfluorinated Ionomer, J Phys Chem B, 109 (2005) 4269-4278.

[9] Cui, S., Liu, J., Selvan, M. E., Keffer, D. J., Edwards, B. J., Steele, W. V., A Molecular Dynamics Study of a Nafion Polyelectrolyte Membrane and the Aqueous Phase Structure for Proton Transport, J Phys Chem B, 111 (2007) 2208-2218.

[10] Devanathan, R., Venkatnathan, A., Dupuis, M., Atomistic Simulation of Nafion Membrane: I. Effect of Hydration on Membrane Nanostructure, J Phys Chem B, 111 (2007) 8069-8079.

[11] Cheng, C. H., Chen, P. Y., Hong, C. W., Atomistic Analysis of Hydration and Thermal Effects on Proton Dynamics in the Nafion Membrane, J Electrochem Soc, 155 (2008) B435-B442.

[12] Karo, J., Aabloo, A., Thomas, J. O., Brandell, D., Molecular Dynamics Modeling of Proton Transport in Nafion and Hyflon Nanostructures, J Phys Chem B, 114 (2010) 6056-6064.
[13] Abroshan, H., Akbarzadeh, H., Taherkhani, F., Parsafar, G., Effect of water–methanol content on the structure of Nafion in the sandwich model and solvent dynamics in nano-channels; a molecular dynamics study, Mol Phys, 109 (2011) 709-724.
[14] Knox, C. K., Voth, G. A., Probing Selected Morphological Models of Hydrated Nafion Using Large-Scale Molecular Dynamics Simulations, J Phys Chem B, 114 (2010) 3205-3218.
[15] Brunello, G., Lee, S. G., Jang, S. S., Qi, Y., A molecular dynamics simulation study of hydrated sulfonated poly(ether ether ketone) for application to polymer electrolyte membrane fuel cells: Effect of water content, J. Renewable Sustainable Energy, 1 (2009) 033101-033114.
[16] Mahajan, C. V., Ganesan, V., Atomistic Simulations of Structure of Solvated Sulfonated Poly(ether ether ketone) Membranes and Their Comparisons to Nafion: I. Nanophase Segregation and Hydrophilic Domains, J Phys Chem B, 114 (2010) 8357-8366.
[17] Lins, R. D., Devanathan, R., Dupuis, M., Modeling the nanophase structural dynamics of phenylated sulfonated poly ether ether ketone ketone (Ph-SPEEKK) membranes as a function of hydration, J Phys Chem B, 115 (2011) 1817-1824.
[18] Ohkubo, T., Kidena, K., Takimoto, N., Ohira, A., Molecular dynamics simulations of Nafion and sulfonated polyether sulfone membranes. I. Effect of hydration on aqueous phase structure, J Mol Model, 17 (2011) 739-755.
[19] Zhu, S., Yan, L., Zhang, D., Feng, Q., Molecular dynamics simulation of microscopic structure and hydrogen bond network of the pristine and phosphoric acid doped polybenzimidazole, Polymer, 52 (2011) 881-892.
[20] Pozuelo, J., Riande, E., Saiz, E., Compañ, V., Molecular Dynamics Simulations of Proton Conduction in Sulfonated Poly(phenyl sulfone)s, Macromolecules, 39 (2006) 8862-8866.
[21] Chen, P. Y., Chiu, C. P., Hong, C. W., Molecular structure and transport dynamics in Nafion and sulfonated poly(ether ether ketone ketone) membranes, J Power Sources, 194 (2009) 746-752.
[22] Bahlakeh, G., Nikazar, M., Hafezi, M.-J., Dashtimoghadam, E., Hasani-Sadrabadi, M. M., Molecular dynamics simulation study of proton diffusion in polymer electrolyte membranes based on sulfonated poly (ether ether ketone), Int. J. Hydrogen Energy, 37 (2012) 10256-10264.
[23] Bahlakeh, G., Nikazar, M., Molecular dynamics simulation analysis of hydration effects on microstructure and transport dynamics in sulfonated poly(2,6-dimethyl-1,4-phenylene oxide) fuel cell membranes, Int. J. Hydrogen Energy.

8th Iranian Fuel Cell Seminar
FEBRUARY 25,26
2015

Investigation of Characteristics of Hybrid PEMs from Atomistic Molecular Dynamics Simulations

Ghasem Bahlakeh
Department of Engineering and Technology, Golestan University, Aliabad Katool, Iran
gh.bahlakeh@gu.ac.ir

Abstract
Molecular dynamics simulations were employed to study the morphological characteristics of hybrid fuel cell membranes based on sulfonated poly(ether ether ketone) (SPEEK) and sulfonated poly(phenylene oxide) (SPPO) under varied hydration levels. Obtained simulation results showed that by increasing the hydration level of solvated membrane, the sulfonic acid groups attached to polymeric backbones become farther apart and their interactions with positively charged hydronium ions were decreased owing to the stronger solvation of sulfonic acid groups at higher hydration levels.

Keywords: Hybrid Membrane, Sulfonated poly (ether ether ketone), Sulfonated poly(phenylene oxide), Molecular Dynamics Simulation

1 Introduction

Polymer electrolyte membranes (PEMs) have been subject of many researches thanks to their usages in both polymer electrolyte membranes fuel cells (PEMFCs) and direct methanol fuel cells (DMFCs) [1-2]. PEMs are one of the vital components in PEMFCs and DMFCs as fuel cell performance greatly depends on their properties. Due to their good conductivity, Nafion-based PEMs are the most widely used membranes in these fuel cells [3-4]. However, high production cost and high methanol permeability of Nafion limited their usages and give rise to the development of new PEMs such as sulfonated poly(2,6–dimethyl–1,4–phenylene oxide) (SPPO), sulfonated poly(ether ether ketone) (SPEEK), and etc. [5-9], which have been applied in different forms like hybrid. Hybrid acid-acid membranes in which an acidic material (e.g., Nafion) is blended with another one have been studied in recent works as potential PEMs.
Molecular dynamics (MD) simulations methods are highly useful tools that are able to provide molecular level information regarding characteristics of PEM materials that could not be easily attained using experimental studies. During the recent years, these techniques have been successfully applied to probe the molecular structure and transport of proton and water in perflourinated Nafion membranes [10-18] and alternative pure membranes [19-27]. Despite the significant experimental attempts performed for hybrid membranes, MD simulation study of these membranes have not been implemented in previous efforts. Therefore, in this work, it is intended to investigate the properties of hybrid membranes consisting of SPEEK and SPPO under various hydration conditions by employing atomistic MD simulation methods.

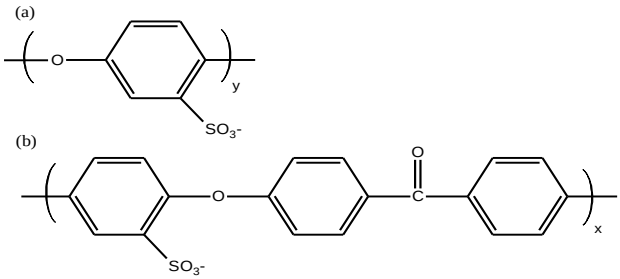

Figure 1: Chemical structure of ionized sulfonated (a) PPO and (b) PEEK monomers used for MD simulations.

2 Simulation Details

MD simulations were performed for a range of water content values of membrane. Water content was expressed by a parameter λ (which is defined as the ratio of weight of number of water molecules to the number of fixed sulfonic acid groups in structure of SPPO and SPEEK polymers (Figure 1)). Three different water content levels of λ = 3, 6 and 12 are selected for hybrid membrane, for which three three–dimensional (3D) cubic cells containing SPEEK and SPPO chains, hydronium ions (H_3O^+), and varying number of water molecules (H_2O) were constructed. For SPEEK and SPPO polymers, DREIDING force field was employed [28]. Partial charges for SPEEK and SPPO were taken from charge equilibration (QEq) method [29]. Flexible 3–centered (F3C) force field [30] was selected for water molecules and for hydronium ions, partial charges and potentials were chosen from the work carried out by Jang et al. [11].

All MD simulations were performed by means of LAMMPS (large–scale atomic/molecular massively parallel simulator) open-source simulation code [31]. A cutoff radius of 12 Å was used to treat the non–bonded interactions, and long–range electrostatic interactions were evaluated by using Particle–Particle Particle–Mesh (PPPM) summation method [32]. Velocity Verlet algorithm was applied to solve Newton's equation of motion [33]. Time step was set to be 1 fs for all MD simulations. During simulations, the temperature and pressure were maintained constant using Nose–Hoover thermostat and barostat with 0.1 and 1 ps coupling parameters, respectively [34-36].

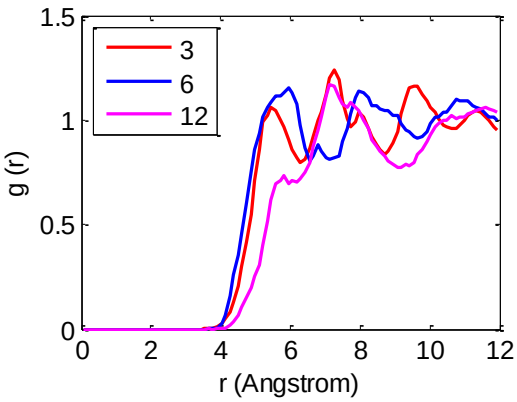

Figure 2: RDFs for sulfur–sulfur atoms of sulfonic acid group for hydration levels of λ = 3, 6 and 12

3 Results and discussion

Figure 2 displays the radial distribution function (RDF) of sulfonic acid sulfur to sulfonic acid sulfur atomic pairs (S–S) for all hydration degrees in order to examine the correlations between anionic sulfonic acid groups as a function of hydration level. As shown, with an increase in the

hydration degree of the hybrid membrane, position of the first dominant peak will be shifted to farther distances, which means that the distance between neighboring sulfonic acid groups has increased, and they have become more separated from each other as the level of hydration has increased. This observation can be rationalized by higher hydration of hydrophilic sulfonic acid groups at increased water uptakes of SPEEK–SPPO hybrid membrane.

Figure 3 (a) and (b) exhibit the sulfonic acid sulfur to water oxygen (S–Ow), and sulfonic acid sulfur to hydronium oxygen (S–Oh) RDFs, respectively, for λ = 3, 6 and 12 water contents. Appearance of the high peak in these RDFs suggests that water molecules and hydronium ions have tendency to be located close to the negatively charged sulfonic acid groups. As shown, the intensity of the observed peak decreases by increasing hydration of hybrid system in both S–Ow and S–Oh RDFs, which is due to the fact that enhancing the membrane water content improves solvent effect of water molecules on water molecules and hydronium ions, and reduces their interactions with sulfur atoms.

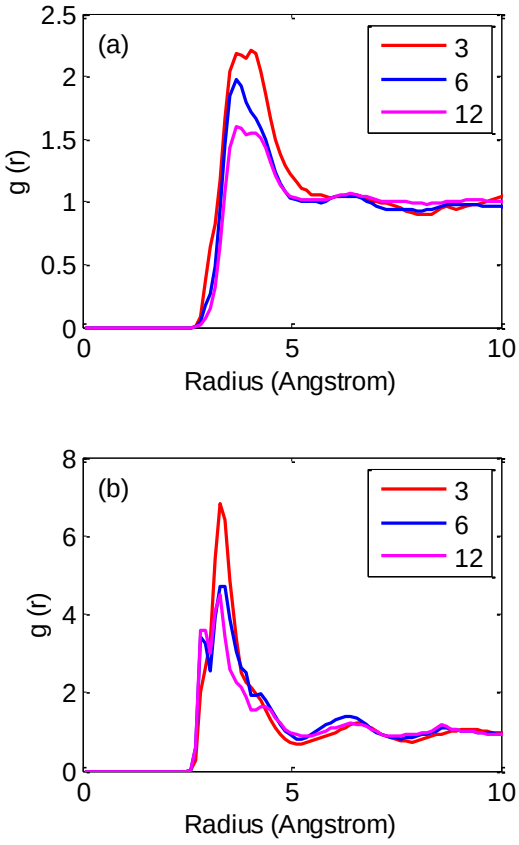

Figure 3: RDFs of (a) sulfur (sulfonic acid group)– oxygen (water molecules) and (b) sulfur (sulfonic acid group)– oxygen (hydronium ions) for hydration levels of λ = 3, 6 and 12

Figure 4 (a) and (b) illustrate the calculated average coordination numbers for water and hydronium ions around sulfonic acid sulfur atoms as a function of hydration level. It is clearly seen that with changing water content from λ = 3 to λ = 12, water coordination number around sulfur atoms increases, whereas hydronium ion coordination number reduces. Therefore, increasing membrane water content will result in gathering of higher number of water molecules in the vicinity of negatively charged sulfonic acid groups, and decreases the sulfonic acid–

hydronium ion electrostatic interactions. So, pushes hydronium ions to a greater distance from sulfonic acid groups.

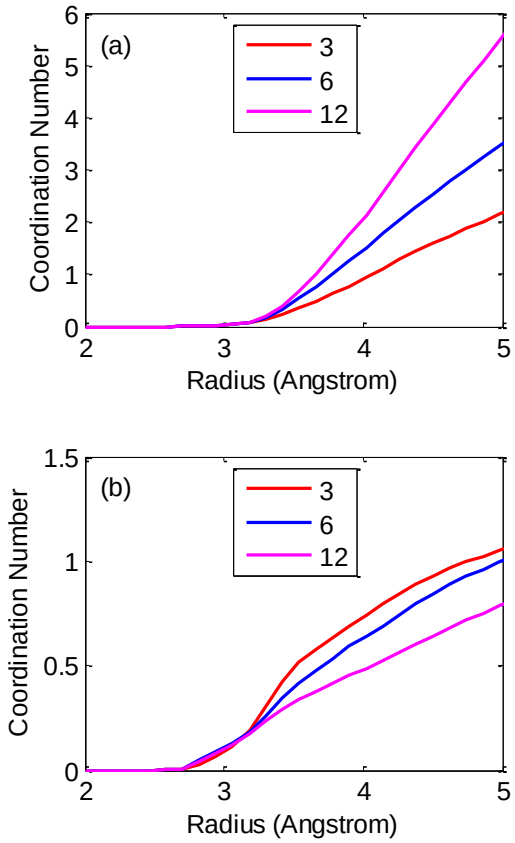

Figure 4: Average coordination number for (a) water molecules and (b) hydronium ions around sulfur atoms of sulfonic acid groups for hydration levels of λ = 3, 6 and 12

Conclusions

In the current study, classical all-atom MD simulations were employed to investigate the structural behavior of water-solvated polymeric acid–acid hybrid membranes based on the SPEEK and SPPO materials at different water content values (λ = 3, 6 and 12) and 300 K.

In order to investigate the correlation of different atoms in hydrophilic domain of hydrated membrane, radial distribution function and coordination number were evaluated for sulfonic acid groups, water molecules and hydronium ions. It was found that by changing water content of the membrane from λ = 3 to λ = 12, more water molecules solvate the sulfonic acid groups, and thereby the average separation between sulfur atoms in neighboring sulfonic acid groups intensifies. Moreover, with increase in hydration, hydronium ions less localized near the sulfonic acid groups, and their coordination number for sulfur and oxygen atoms in sulfonic acid reduce.

Acknowledgment

The authors gratefully acknowledge the use of School of Computer Science, Institute for Research in Fundamental Science (IPM).

References

[1] Carrette, L., Friedrich, K. A., Stimming, U., Fuel Cells – Fundamentals and Applications, Fuel Cells, 1 (2001) 5-39.
[2] Kamarudin, S. K., Achmad, F., Daud, W. R. W., Overview on the application of direct methanol fuel cell (DMFC) for portable electronic devices, Int. J. Hydrogen Energy, 34 (2009) 6902-6916.
[3] Mauritz, K. A., Moore, R. B., State of Understanding of Nafion, Chem. Rev., 104 (2004) 4535-4586.
[4] Alberti, G., Casciola, M., Solid state protonic conductors, present main applications and future prospects, Solid State Ion, 145 (2001) 3-16.
[5] Rikukawa, M., Sanui, K., Proton-conducting polymer electrolyte membranes based on hydrocarbon polymers, Prog Polym Sci, 25 (2000) 1463-1502.
[6] Gil, M., Ji, X., Li, X., Na, H., Hampsey, J. E., Lu, Y., Direct synthesis of sulfonated aromatic poly(ether ether ketone) proton exchange membranes for fuel cell applications, J Membr Sci, 234 (2004) 75-81.
[7] Xu, T., Wu, D., Wu, L., Poly (2, 6-dimethyl-1, 4-phenylene oxide)(PPO)--A versatile starting polymer for proton conductive membranes (PCMs), Prog Polym Sci, 33 (2008) 894-915.
[8] Ahmad, H., Kamarudin, S. K., Hasran, U. A., Daud, W. R. W., Overview of hybrid membranes for direct-methanol fuel-cell applications, Int. J. Hydrogen Energy, 35 (2010) 2160-2175.
[9] Saarinen, V., Kreuer, K. D., Schuster, M., Merkle, R., Maier, J., On the swelling properties of proton conducting membranes for direct methanol fuel cells, Solid State Ion, 178 (2007) 533-537.
[10] Vishnyakov, A., Neimark, A. V., Molecular dynamics simulation of microstructure and molecular mobilities in swollen Nafion membranes, J Phys Chem B, 105 (2001) 9586-9594.
[11] Jang, S. S., Molinero, V., Cagin, T., Goddard, W. A., Nanophase-Segregation and Transport in Nafion 117 from Molecular Dynamics Simulations: Effect of Monomeric Sequence, J Phys Chem B, 108 (2004) 3149-3157.
[12] Urata, S., Irisawa, J., Takada, A., Shinoda, W., Tsuzuki, S., Mikami, M., Molecular Dynamics Simulation of Swollen Membrane of Perfluorinated Ionomer, J Phys Chem B, 109 (2005) 4269-4278.
[13] Cui, S., Liu, J., Selvan, M. E., Keffer, D. J., Edwards, B. J., Steele, W. V., A Molecular Dynamics Study of a Nafion Polyelectrolyte Membrane and the Aqueous Phase Structure for Proton Transport, J Phys Chem B, 111 (2007) 2208-2218.
[14] Devanathan, R., Venkatnathan, A., Dupuis, M., Atomistic Simulation of Nafion Membrane: I. Effect of Hydration on Membrane Nanostructure, J Phys Chem B, 111 (2007) 8069-8079.
[15] Cheng, C. H., Chen, P. Y., Hong, C. W., Atomistic Analysis of Hydration and Thermal Effects on Proton Dynamics in the Nafion Membrane, J Electrochem Soc, 155 (2008) B435-B442.
[16] Karo, J., Aabloo, A., Thomas, J. O., Brandell, D., Molecular Dynamics Modeling of Proton Transport in Nafion and Hyflon Nanostructures, J Phys Chem B, 114 (2010) 6056-6064.
[17] Abroshan, H., Akbarzadeh, H., Taherkhani, F., Parsafar, G., Effect of water–methanol content on the structure of Nafion in the sandwich model and solvent dynamics in nano-channels; a molecular dynamics study, Mol Phys, 109 (2011) 709-724.

[18] Knox, C. K., Voth, G. A., Probing Selected Morphological Models of Hydrated Nafion Using Large-Scale Molecular Dynamics Simulations, J Phys Chem B, 114 (2010) 3205-3218.
[19] Brunello, G., Lee, S. G., Jang, S. S., Qi, Y., A molecular dynamics simulation study of hydrated sulfonated poly(ether ether ketone) for application to polymer electrolyte membrane fuel cells: Effect of water content, J. Renewable Sustainable Energy, 1 (2009) 033101-033114.
[20] Mahajan, C. V., Ganesan, V., Atomistic Simulations of Structure of Solvated Sulfonated Poly(ether ether ketone) Membranes and Their Comparisons to Nafion: I. Nanophase Segregation and Hydrophilic Domains, J Phys Chem B, 114 (2010) 8357-8366.
[21] Lins, R. D., Devanathan, R., Dupuis, M., Modeling the nanophase structural dynamics of phenylated sulfonated poly ether ether ketone ketone (Ph-SPEEKK) membranes as a function of hydration, J Phys Chem B, 115 (2011) 1817-1824.
[22] Ohkubo, T., Kidena, K., Takimoto, N., Ohira, A., Molecular dynamics simulations of Nafion and sulfonated polyether sulfone membranes. I. Effect of hydration on aqueous phase structure, J Mol Model, 17 (2011) 739-755.
[23] Zhu, S., Yan, L., Zhang, D., Feng, Q., Molecular dynamics simulation of microscopic structure and hydrogen bond network of the pristine and phosphoric acid doped polybenzimidazole, Polymer, 52 (2011) 881-892.
[24] Pozuelo, J., Riande, E., Saiz, E., Compañ, V., Molecular Dynamics Simulations of Proton Conduction in Sulfonated Poly(phenyl sulfone)s, Macromolecules, 39 (2006) 8862-8866.
[25] Chen, P. Y., Chiu, C. P., Hong, C. W., Molecular structure and transport dynamics in Nafion and sulfonated poly(ether ether ketone ketone) membranes, J Power Sources, 194 (2009) 746-752.
[26] Bahlakeh, G., Nikazar, M., Hafezi, M.-J., Dashtimoghadam, E., Hasani-Sadrabadi, M. M., Molecular dynamics simulation study of proton diffusion in polymer electrolyte membranes based on sulfonated poly (ether ether ketone), Int. J. Hydrogen Energy, 37 (2012) 10256-10264.
[27] Bahlakeh, G., Nikazar, M., Molecular dynamics simulation analysis of hydration effects on microstructure and transport dynamics in sulfonated poly(2,6-dimethyl-1,4-phenylene oxide) fuel cell membranes, Int. J. Hydrogen Energy.
[28] Mayo, S. L., Olafson, B. D., Goddard, W. A., DREIDING: a generic force field for molecular simulations, J Phys Chem, 94 (1990) 8897-8909.
[29] Rappe, A. K., Goddard, W. A., Charge equilibration for molecular dynamics simulations, J Phys Chem, 95 (1991) 3358-3363.
[30] Levitt, M., Hirshberg, M., Sharon, R., Laidig, K. E., Daggett, V., Calibration and Testing of a Water Model for Simulation of the Molecular Dynamics of Proteins and Nucleic Acids in Solution, J Phys Chem B, 101 (1997) 5051-5061.
[31] Plimpton, S. J., Fast Parallel Algorithms for Short-Range Molecular Dynamics, J Comput Phys, 117 (1995) 1-19.
[32] Hockney, R. W., Eastwood, J. W., Computer Simulation Using Particles, McGraw-Hill, New York, 1981.
[33] Swope, W. C., Andersen, H. C., Berens, P. H., Wilson, K. R., A computer simulation method for the calculation of equilibrium constants for the formation of physical clusters of molecules: Application to small water clusters, J Chem Phys, 76 (1982) 637-649.
[34] Nose, S., A unified formulation of the constant temperature molecular dynamics methods, J Chem Phys, 81 (1984) 511-519.
[35] Nose, S., A molecular dynamics method for simulations in the canonical ensemble, Mol Phys, 52 (1984) 255-268.
[36] Nose, S., An extension of the canonical ensemble molecular dynamics method, Mol Phys, 57 (1986) 187-191.

شبیه‌سازی سیستم الکترونیکی برای اندازه‌گیری اختلاف فاز متناظر با ضریب شکست مایع پیل سوختی

زهرا دشتبان، سعید علیائی*
آزمایشگاه تحقیقاتی نانوفوتونیک و اپتوالکترونیک، دانشگاه تربیت دبیر شهید رجائی، لویزان، تهران، ایران.
* *s_olyaee@srttu.eud*

چکیده

تداخل‌سنج هترودایِن یک سیستم اندازه‌گیری با حساسیت بالا است که اختلاف وضوح ضریب شکست با تغییر مقدار رطوبت در غشای پیل سوختی را اندازه‌گیری می‌کند. این سیستم، تغییرات درصد رطوبت غشای پیل سوختی را با استفاده از اندازه‌گیری اختلاف مسیر نوری که توسط ضریب شکست آب باعث شده است، تعیین می‌کند. هنگامی که درصد رطوبت غشا تغییر می‌کند، ضخامت و ضریب شکست غشا مطابق با آن تغییر خواهد کرد. با اندازه‌گیری اختلاف فازی که ناشی از اختلاف مسیر نوری ایجاد شده است، می‌توان ضریب شکست پیل سوختی را اندازه گرفت. در این مقاله بخش الکترونیک تداخل سنج هترودایِن سه مود توسعه یافته به منظور اندازه‌گیری اختلاف فاز متناظر با ضریب شکست شبیه‌سازی شده است. این بخش‌ها شامل تقویت‌کننده، فیلتر، مخلوط‌کننده، نوسان‌ساز و بخش اندازه‌گیری فاز است. در نهایت نمودار تغییرات اختلاف فاز به ازای ضریب شکست مایع پیل سوختی برای چند اختلاف مسیر نوری شبیه‌سازی شده است و با مقایسه آن با تداخل‌سنج دومود معمولی نشان داده‌ایم که قابلیت تفکیک‌پذیری دراین سیستم افزایش یافته است.

واژه‌های کلیدی: پیل سوختی، ضریب شکست، تداخل‌سنج لیزری، اختلاف مسیر نوری

مقدمه

پیل سوختی دستگاهی است الکتروشیمیایی که انرژی حاصل از واکنش شیمیایی را به انرژی الکتریکی مفید تبدیل می‌کند. تبدیل انرژی در پیل سوختی، تبدیل مستقیم انرژی شیمیایی به انرژی الکتریکی است [۲-۱]. رشد و توسعه فناوری پیل سوختی از طرفی به دلیل بازده بالا، عدم آلودگی محیط زیست و سهولت نحوه بهره‌برداری می‌باشد و از طرف دیگر ناشی از این امر است که انواع پیل‌های سوختی در موارد بسیار وسیعی از جمله در نیروگاه‌ها، شاتل‌های فضایی، زیر دریایی‌ها، خودروها و .... کاربرد دارد، به طوری که می‌توان گفت امروزه رقیب اکثر فناوری‌های فعلی تولید انرژی الکتریکی و حتی گرمایی محسوب می‌گردد. پیل سوختی با غشای پروتونی PEM به‌طور گسترده‌ای به عنوان منبع انرژی استفاده می‌شود. عملکرد پیل سوختی بستگی مستقیم به میزان آب موجود در غشای آن دارد. رطوبت بالا باعث افزایش بازده‌ی پیل سوختی می‌شود اما چنانچه میزان رطوبت بیش از حد شود مشکلاتی از جمله باد کردن، فشار مکانیکی و خرابی غشای پیل سوختی پدیدار می‌شوند. از آن‌جایی‌که درصد رطوبت و ضریب شکست در غشا در هر نقطه باهم متناسب هستند، پس با تخمین‌زدن نمایه ضریب شکست، می‌توان به‌درستی تغییر در میزان آب غشای پیل سوختی را اندازه‌گیری کرد. روش‌های تداخل‌سنجی برای اندازه‌گیری ضریب شکست به صورت تحقیقات خیلی پرطرفدار و جذاب در سال‌های اخیر تبدیل شده‌اند که این به

دلیل دقت، ویژگی‌های غیرمخرب و اندازه‌گیری سریع و تنظیم نسبتا آسان سیستم نوری و آزمایشگاهی آن‌هاست. هر چه قابلیت تفکیک پذیری تداخل سنج بهتر باشد اندازه‌گیری ضریب شکست با دقت بیشتری همراه خواهد بود.

به منظور افزایش قابلیت تفکیک‌پذیری، تداخل‌سنج سوپرهترودواین در سال ۲۰۰۱ توسط Yokoyama و همکارانش [۳] ارائه شد. تنها عیب این تداخل‌سنج دارا بودن خطای بیشتر نسبت به دو مود است. با توجه به نیاز صنعت به افزایش قابلیت تفکیک‌پذیری، نوعی از تداخل‌سنج‌های سوپر هترودواین در سال ۲۰۱۰ توسط علیایی و همکارانش ارائه شد [۴] که این تداخل‌سنج دارای قابلیت تفکیک‌پذیری چهار برابر نسبت به تداخل‌سنج هترودواین دو مود و دو برابر نسبت به تداخل‌سنج سوپرهترودواین معرفی شده در سال ۲۰۰۱ است. آرایش نوری این تداخل‌سنج مشابه با تداخل‌سنج دو مود ارائه شده توسط Guo و همکارانش (۲۰۰۰) است [۵]، با این تفاوت که به جای منبع نور دو مود از لیزر سه مود برای افزایش قابلیت تفکیک-پذیری استفاده شده است.

استفاده از روش‌های الکترونیک با دقت بالا برای اندازه‌گیری مستقیم اختلاف فاز متناظر با ضریب شکست ظاهر شده در طرح‌های تداخلی مورد استفاده قرار گرفته است. از قدیمی‌ترین روش‌هایی که برای آشکارسازی فتوالکتریک استفاده می-شود روش نول است. در این روش اصلی‌ترین عامل محدودیت دقت این است که در عمل با لیزر دقت اندازه‌گیری محدود می‌شود. روش دیگر اندازه‌گیری فاز روش شمارش فریز الکترونیکی است [۶]. روش‌های متفاوت دیگری موجود است که در مرجع [۶] به تفکیک بیان شده است. روشی که در این مقاله به آن پرداخته‌ایم، روش تداخل‌سنجی هترودواین است. در این روش یک جابه‌جایی فرکانس کوچک در پرتو تداخل‌سنج ظاهر می‌شود که با روش هترودواین آشکار می‌شود. در روش سوپرهترودواین، دو سیگنال دریافت شده از مسیرهای مبنا و اندازه‌گیری، ابتدا تقویت شده و سپس با مخلوط شدن در خود به فرکانس پایین‌تر تبدیل می‌شوند و در نهایت اختلاف فاز بین این دو سیگنال که متناظر با جابه‌جایی و با ثابت بودن جابجایی متناظر با ضریب شکست مایع پیل سوختی است توسط اندازه‌گیر فاز اندازه‌گیری می‌شود.

در این مقاله بخش الکترونیک سامانه تداخل سنجی به منظور اندازه‌گیری جابجایی متناظر با ضریب شکست مایع پیل سوختی شبیه سازی شده است. همان طور که بیان شد تغییرات رطوبت غشای پیل سوختی باعث تغییر اختلاف مسیر نوری و در نهایت اختلاف فاز می‌گردد. پس ما می‌توانیم با طراحی سیستمی که می‌تواند اختلاف فاز را به طور دقیق اندازه بگیرد، به تغییرات ضریب شکست و در نهایت به تغییر رطوبت پی برد. این بخش‌ها شامل تقویت‌کننده، فیلتر، مخلوط‌کننده، نوسان-ساز و بخش اندازه‌گیری فاز است.در قسمت اول به یک تقویت‌کننده با بهره بزرگتر از ۱۵ دسی‌بل، پهنای‌باند ۵۰۰ مگاهرتز و عدد نویز کمتر از ۲/۵ دسی‌بل نیاز است. این مشخصات به این دلیل انتخاب شده است که سطح جریان دریافتی از بخش نوری تداخل‌سنج در محدوده میکروآمپر و محدوده‌ی فرکانسی آن در رنج ۵۰۰ مگاهرتز است. یک تقویت‌کننده کم نویز با فناوری CMOS 0.5μm از نوع کاسکود را طراحی و شبیه‌سازی کرده‌ایم که به بهره ۱۹/۱ دسی‌بل و عدد نویز ۲/۵ دسی-بل در فرکانس ۵۰۰ مگاهرتز دست یافته‌ایم. در قسمت دوم یک فیلتر میان‌گذر از نوع بسل با فرکانس مرکزی ۵۰۰ مگاهرتز شبیه‌سازی شده است. پس از این قسمت، یک مخلوط‌کننده متعادل دوگانه سلول گیلبرت طراحی و شبیه‌سازی شده است که به بهره تبدیل ۷/۵۱۱ دسی‌بل با ورودی RF برابر با ۵۰۰ مگاهرتز، ورودی LO برابر با ۵۰۰/۳ مگاهرتز و خروجی IF برابر با ۳۰۰ کیلوهرتز رسیده‌ایم. فیلتر پایین‌گذری از نوع بسل با فرکانس قطع ۳۰۰ کیلوهرتز برای عبور هارمونیک با

فرکانس تداخلی ثانویه بعد از مخلوط‌کننده لازم است قرار داده شود که شبیه‌سازی شده است. در نهایت دو سیگنال آنالوگ بازسازی شده به یک مقایسه‌گر سرعت بالا داده می‌شود و پس از تبدیل شدن به پالس دیجیتال به بخش اندازه‌گیر فاز فرستاده می‌شود. در عمل، بخش اصلی اندازه‌گیرفاز یک شمارنده سرعت بالا با قابلیت تفکیک‌پذیری ۱ نانوثانیه است که TDC-GP1 نام دارد. این شمارنده فواصل زمانی را به مقادیر دیجیتالی تبدیل می‌کند و تعداد شمارش با رابطه‌ای که با فاز دارد، توسط میکروکنترولر بر روی LCD نمایش داده می‌شود. به این ترتیب فاز متناظر با ضریب شکست مایع پیل سوختی آشکار می‌شود.

اساس کار تداخل سنج سه مود بهبود یافته

شکل ۱ سامانه تداخل سنجی سه مود بهبود یافته را نشان می دهد. در این سیستم، میدان‌های الکتریکی خروجی لیزر سه مود عبارتند از:

$$E_{v_1}=\begin{bmatrix}1\\ \alpha\end{bmatrix}e^{i(2\Pi v_1 t)},E_{v_2}=\begin{bmatrix}\beta\\ 1\end{bmatrix}e^{i(2\Pi v_2 t)},E_{v_3}=\begin{bmatrix}1\\ \alpha\end{bmatrix}e^{i(2\Pi v3 t)} \qquad (۱)$$

در این معادله v_1,v_2,v_3 فرکانس‌های نوری منبع لیزر هستند و $\alpha=|\alpha|e^{i\phi_\alpha}$ و $\beta=|\beta|e^{i\phi_\beta}$ به دلیل قطبش بیضوی به وجود آمده است. ابتدا نور خروجی لیزر سهمود توسط شکافنده‌ی پرتو[۳۲] (BS) به دو مسیر هدف و مرجع فرستاده می‌شود، سپس بازتاب آن‌ها، بر اساس قطبش، به وسیله‌ی شکافنده- قطبنده پرتو جدا می‌شود و به سمت آشکارسازهای D_1, D_2 می‌روند. در مسیر مرجع یک صفحه تاخیر ربع طول موج با زاویه ۴۵ درجه قرار داده شده است تا جهت قطبش‌ها را عوض کند. همان طور که مشاهده می کنید پیل سوختی در مسیر هدف قرار داده شده است که این باعث تولید اختلاف فاز می گردد. که این اختلاف فاز پس از تبدیل شدن سیگنال نوری توسط آشکارسازهای D_1, D_2 به سیگنال جریانی، قابل رویت است. جریان خروجی آشکارساز که با هم اختلاف فاز دارند و به سیستم الکترونیکی جهت آشکارسازی فاز متناسب با ضریب شکست پیل سوختی فرستاده می شود عبارت است از:

$$i_{m_1}=\frac{1}{2}\cos[(2\Pi f_b)t+2\Delta\phi+\psi] \qquad (۲)$$

$$i_{m_2}=\frac{1}{2}\cos[(2\Pi f_b)t-2\Delta\phi+\psi] \qquad (۳)$$

در این روابط، f_b فرکانس تداخلی ثانویه و ψ خطای غیرخطی ناشی از بخش نوری است و در نهایت اختلاف فاز بین سیگنال‌های اندازه‌گیری و مرجع ($\Delta\Phi$) به صورت معادله (۴) است:

$$\Delta\Phi=4\Delta\varphi+\psi_{nl}=(16n\pi/\lambda)\Delta z+\psi \qquad (۴)$$

جمله دوم خطای غیرخطی است که در مرجع [۴] تعریف شده است.

[32] Beam Splitter

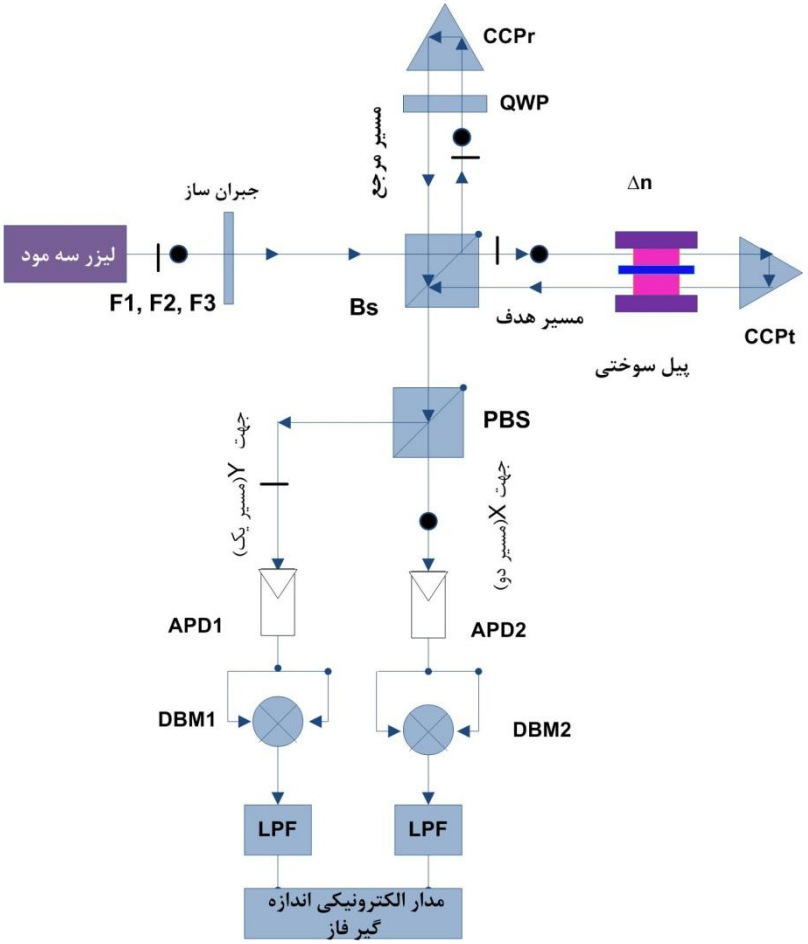

شکل ۱ تداخل‌سنج سه‌مود توسعه یافته برای اندازه‌گیری ضریب شکست مایع پیل سوختی.

طراحی بخش های اساسی سامانه الکترونیک

در این بخش به منظور آشکارسازی اختلاف فاز متناظر با ضریب شکست بخش های اصلی سامانه تداخل سنجی را طراحی کرده ایم. این بخش‌ها شامل تقویت‌کننده، فیلتر، مخلوط‌کننده، نوسان‌ساز و بخش اندازه‌گیری فاز است. شماتیک تقویت-کننده‌ی شبیه‌سازی شده در شکل (۲) نشان داده شده است. در این طراحی از فناوری Agilent CMOS 0.5 µm استفاده کرده‌ایم، که در این فرآیند کوچک‌ترین طول گیت 0.6µm است. منحنی بهره شبیه‌سازی شده در شکل (۳) نشان داده شده است.

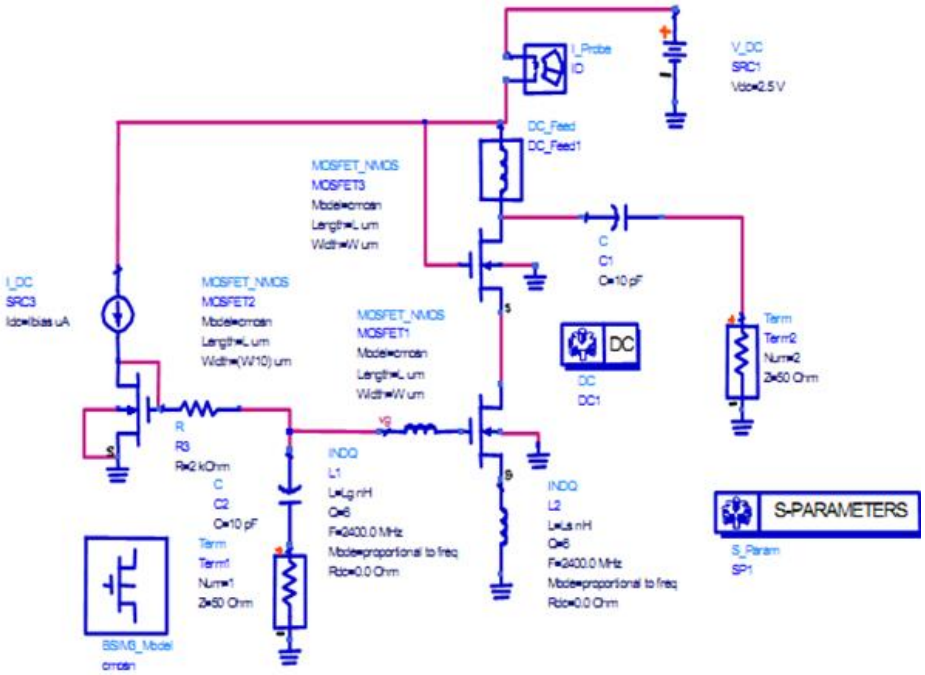

شکل ۲ شماتیک تقویت‌کننده‌ی کم نویز کاسکود

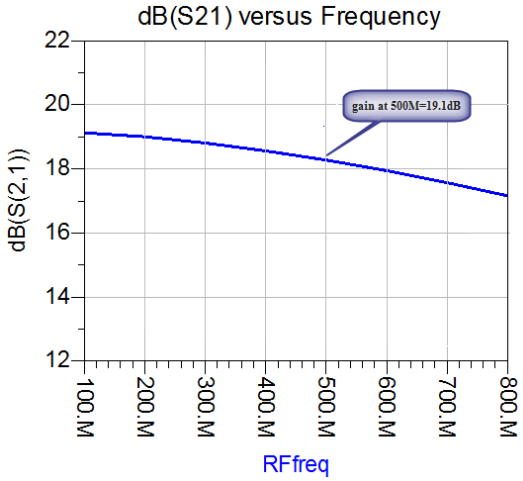

شکل ۳ منحنی بهره (منحنی سمت چپ) نسبت به فرکانس مدار تقویت‌کننده کم نویز کاسکود

مشاهده می‌شود که بهره در فرکانس ۵۰۰ مگاهرتز برابر با 19.1dB است که این مقدار بهره، بهره‌ی مطلوبی است. به طور خلاصه مشخصات شبیه‌سازی شده‌ی مدار کاسکود در جدول (۱) آورده شده است.

جدول ۱ مشخصات حاصل از شبیه‌سازی مدار تقویت‌کننده مورد نیاز

پارامتر	مشخصه	واحد
فرکانس	۵۰۰	مگاهرتز (MHz)
عدد نویز	۲/۸	دسی بل (dB)
بهره	۱۹/۱	دسی بل (dB)
توان مصرفی	۳۰	میلی وات (mw)
امپدانس منبع/ بار	۵۰	اهم (Ω)
عرض گیت ماسفت	۵۰۰	میکرومتر(µm)
مقدار سلف سورس(Ls)	۱	نانو هانری(nH)
مقدار سلف گیت(Lg)	۴/۲	نانو هانری(nH)
منبع تغذیه	۲/۵	ولت(v)
جریان بایاس	۱۱	میلی آمپر(mA)

اکنون فیلتر میان‌گذر با فرکانس مرکزی ۵۰۰ مگاهرتز و پهنای باند 400KHz جهت عبور سیگنال با فرکانس تداخلی اولیه با استفاده از نرم‌افزار Filter Solution شبیه‌سازی شده است. شماتیک فیلتر میان‌گذر طراحی شده در شکل (۴) نشان داده شده است. فیلتر نشان داده شده در شکل (۴) یک فیلتر میان‌گذر مرتبه سه از نوع بسل است. این فیلتر دارای فرکانس مرکزی 500MHz و پهنای باند 400KHz است در نتیجه فقط سیگنال‌هایی با فرکانس تداخلی اولیه را از خود عبور می‌دهد. منحنی شبیه‌سازی شده‌ی پاسخ فرکانسی فیلتر در شکل (۵) نشان داده شده است. بخش بعدی مخلوط کننده است. جدول (۲) خلاصه‌ای از مشخصات مورد انتظار برای مخلوط‌کننده‌ی بخش الکترونیکی سامانه‌ی اندازه‌گیری نانومتری را برای طراحی نشان می‌دهد. اکنون شبیه‌سازی را مطابق با فرضیات جدول (۲) انجام می‌دهیم. جدول (۳) خلاصه ای از طراحی انجام شده از این بخش را نشان می‌دهد. شکل (۶) شماتیک مخلوط‌کننده سلول گیلبرت مطابق با داده‌های طراحی شده جدول (۳)، که در محیط نرم‌افزار ADS رسم شده است را نشان می‌دهد.

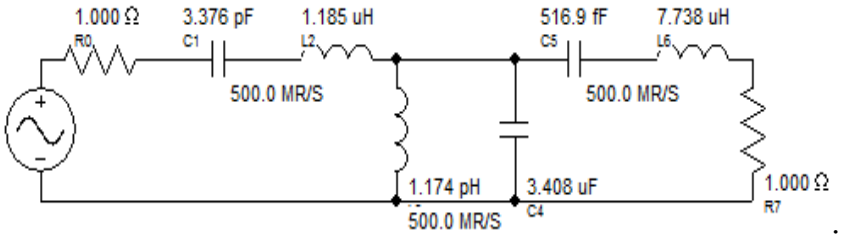

شکل ۴ فیلتر میان‌گذر مرتبه سه از نوع بسل

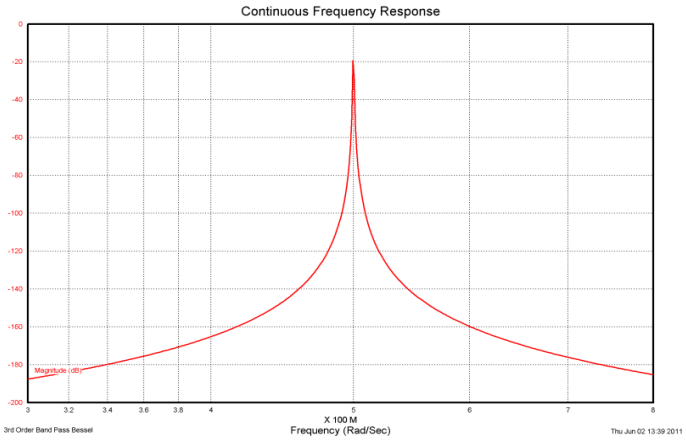

شکل ۵ پاسخ فرکانسی فیلتر میان‌گذر طراحی شده

جدول ۲ مشخصات مورد انتظار برای مخلوط‌کننده‌ی مناسب جهت بخش الکترونیکی تداخل‌سنج هترودایِن سه مود

پارامتر	مشخصات	واحد
فرکانس	۳۰۰-۷۰۰	مگاهرتز (MHZ)
عددنویزدوطرفه (DSB)	۱۰>	دسی‌بل (dB)
بهره ولتاژ	۸<	دسی‌بل (dB)
توان مصرفی	۱۰۰>	میلی وات (mW)
امپدانس منبع	۵۰	اهم (Ω)
امپدانس بار	۵۰۰	اهم (Ω)
اعوجاج مرتبه ۳ ورودی (IIP3)	۲۰<	دسی‌بل (dBm)
منبع ولتاژ	±۲,۵	ولت (v)

جدول ۳ فرضیات طراحی شده برای شبیه‌سازی مخلوط‌کننده سلول گیلبرت

جریان دنباله[۳۳]	6mA
مقومت‌های دیژنراسیون سورس	10Ω
عرض گیت ماسفت‌ها	233µm
طول گیت ماسفت‌ها	0.6µm
مقاومت بار	500Ω
منبع تغذیه	2.5 V

[33] Tail current

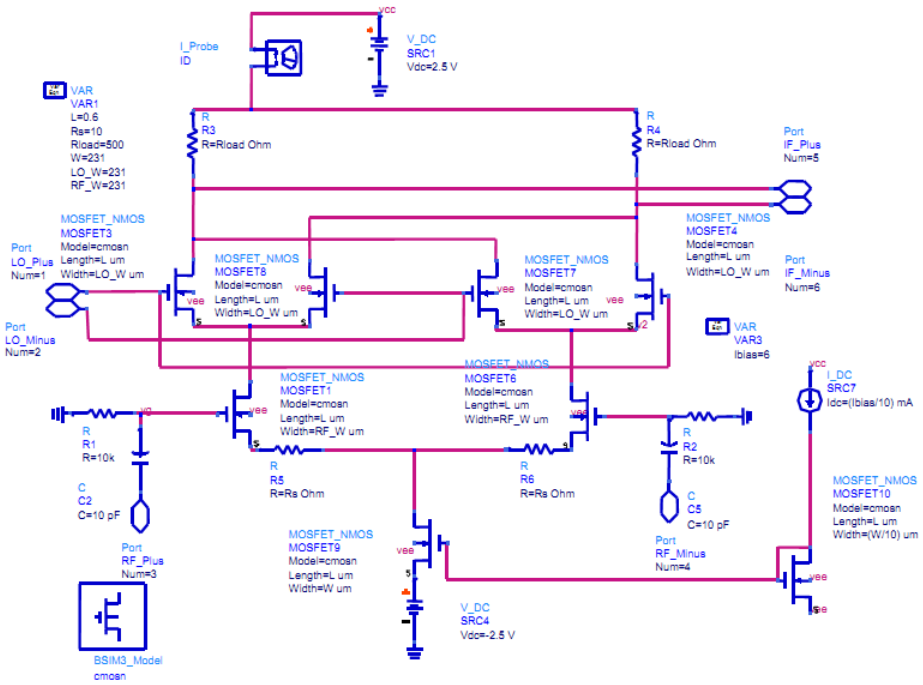

شکل ۶ شماتیک مداری شبیه‌سازی شده‌ی سلول گیلبرت

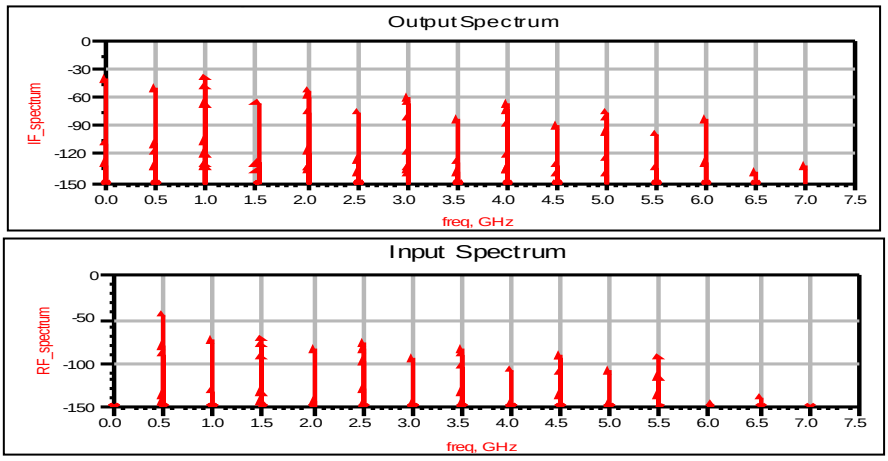

شکل ۷ طیف فرکانسی ورودی و خروجی مخلوط کننده سلول گیلبرت

طیف فرکانسی RF و IF شبیه‌سازی شده که از خروجی مدار فوق گرفته شده است در شکل (۷) نشان داده شده است. منحنی طیف فرکانسی از فرکانس 0 تا 7GHz در شکل (۷) نشان داده شده است که می‌بایست توسط فیلتر پایین‌گذری که در بخش بعد شبیه‌سازی شده است سیگنال با فرکانس 300KHz که سیگنال مورد نظر ما است را از بین این هارمونیک‌ها دریافت کرد. توجه شود به دلیل درجه‌بندی وسیع نمودار هارمونیک با فرکانس ۳۰۰ کیلوهرتز در شکل مشاهده نمی شود.

در این بخش فیلتر پایین‌گذری طراحی شده است که بتواند سیگنال سینوسی که دارای فرکانس تداخلی ثانویه (۳۰۰ کیلوهرتز) است را از خروجی مخلوط‌کننده دریافت کند. شماتیک مداری فیلتر در شکل (۸) رسم شده است.

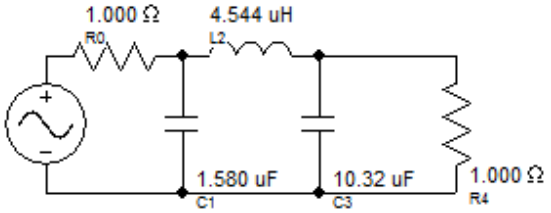

شکل ۸ شماتیک مداری فیلتر پایین‌گذر مرتبه سه از نوع بسل.

شکل (۸) فیلتری از نوع بسل مرتبه سه را نشان می‌دهد که دارای فرکانس قطع 300KHz است. تابع تبدیل این فیلتر برابر است با:

$$\frac{2.7\times10^{16}}{S^3+7.299\times10^{0.05}\times S^2+11S+2.7\times10^{16}} \qquad (۵)$$

سیگنالی که بعد از این فیلتر مشاهده می‌شود همان سیگنالی است که توسط تقویت‌کننده، تقویت شده و توسط مخلوط-کننده به فرکانس پایین‌تر (فرکانس تداخلی ثانویه) منتقل شده است. این دو سیگنال اختلاف فاز کمی نسبت به یکدیگر دارند.

ابتدا این دو سیگنال سینوسی به منظور اندازه‌گیری اختلاف فاز موجود بین آن‌ها، توسط یک مقایسه‌گر سرعت بالا به دیجیتال تبدیل شده و به مدارات اندازه‌گیری فاز اعمال می‌شوند.آخرین بخش سیستم الکتریکی تداخل‌سنج‌های سوپر هترودایِن، بخش اندازه‌گیری فاز است. سیگنال دریافت شده از آشکارساز پس از بازسازی توسط یک مقایسه‌گر سرعت بالا به دیجیتال تبدیل می‌شود و به این بخش فرستاده می‌شوند. دو پالس با فرکانس 300KHz که با هم اختلاف‌فاز دارند و از مسیرهای مبنا و اندازه‌گیری آمده‌اند به منظور اندازه‌گیری اختلاف فاز به روشی که در بخش آینده گفته خواهد شد، به این بلوک وارد شده است.

با توجه به رابطه‌ی بین اختلاف فاز و ضریب شکست، با اندازه‌گیری اختلاف فاز، ضریب شکست اندازه‌گیری خواهد شد. شکل (۹) بخش دیجیتال سیستم اندزه‌گیری جابه‌جایی را نشان می‌دهد.

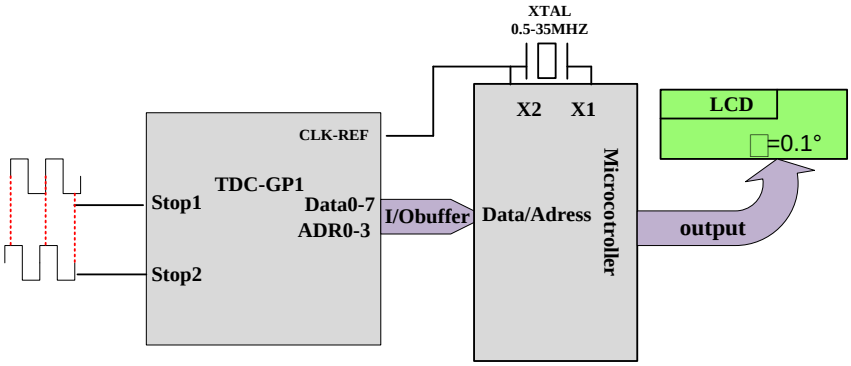

شکل ۹ شماتیک بخش دیجیتال سیستم اندازه‌گیری جابه‌جایی نانومتری

دو پالس که در بخش قبل تولید شد و با هم اختلاف فاز کمی دارند به یک شمارنده سرعت بالا اعمال می‌شوند. این شمارنده یک مبدل زمان به دیجیتال است (TDC-GP1) که فواصل زمانی را به مقادیر دیجیتالی با سرعت بالا تبدیل می‌کند. این شمارنده برای تبدیل‌هایی با قابلیت تفکیک‌پذیری کمتر از 1ns است. شکل ۱۰ تغییرات اختلاف فاز به ازای ضریب شکست مایع پیل سوختی برای چهار اختلاف مسیر نوری ثابت در دونوع تداخل‌سنج سه مود بهبود یافته و دو مود معمولی را نشان می دهد. با توجه به شکل مشاهده می‌شود که با اندازه‌گیری دقیق اختلاف فاز توسط بخش دیجیتال می‌توان تغییرات ضریب شکست مایع پیل سوختی را محاسبه کرد. با مقایسه دو تداخل سنج، نشان داده‌ایم که تداخل سنج سه مود توسعه یافته دارای قابلیت تفکیک‌پذیری بهتری نسبت به دو مود می‌باشد. شکل ۱۰ تغییرات اختلاف فاز به ازای ضریب شکست مایع پیل سوختی برای چهار جابه‌جایی در دو سیستم تداخل سنجی دو مود و سه مود بهبودیافته را نشان می‌دهد.

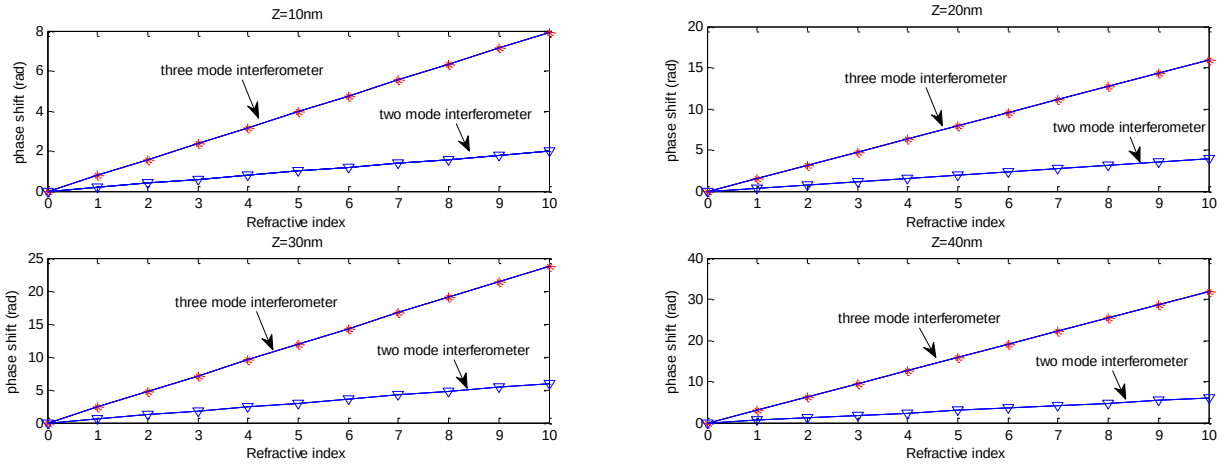

شکل ۱۰ تغییرات اختلاف فاز به ازای ضریب شکست مایع پیل سوختی برای چهار جابه‌جایی در دو سیستم تداخل سنجی دو مود و سه مود بهبودیافته

نتیجه‌گیری

روش‌های تداخل‌سنجی برای اندازه‌گیری ضریب شکست به دلیل دقت، ویژگی‌های غیرمخرب و اندازه‌گیری سریع و تنظیم نسبتا آسان سیستم نوری و آزمایشگاهی آن‌ها مورد استفاده قرار گرفت. در این مقاله بخش‌های مورد نیاز جهت اندازه گیری اختلاف فاز متناظر با ضریب شکست پیل سوختی طراحی و شبیه‌سازی شد. این بخش‌ها شامل تقویت کننده، فیلتر، مخلوط کننده، نوسان‌ساز و بخش اندازه‌گیری فاز بود در نهایت به تقویت‌کننده کم نویز کاسکود با بهره 19.1dB و عدد نویز 2.8dB معادل با نوع عملی ADL5536 با بهره 19.41dB و عددنویز 2.7dB در فرکانس 500MHz و مخلوط‌کننده متعادل دوگانه با بهره تبدیل 7.5dB در فرکانس 500MHz و محدوده LO/RF برابر با فرکانس تداخلی اولیه (500MHz) و محدوده IF برابر با 300KHz و اعوجاج هارمونیکی مرتبه سوم 24dBm معادل با نوع عملی ADL5801 با نقطه فشردگی 28.5dBm و اعوجاج هارمونیکی مرتبه سوم برابر با 28.5dBm دست یافتیم. در بخش آخر یک اندازه‌گیر فاز با قابلیت تفکیک‌پذیری یک نانو ثانیه با استفاده از شمارنده سرعت بالای TDC-GP1 ساخته شد. درنهایت تغییرات اختلاف فاز به

ازای ضریب شکست مایع پیل سوختی برای چهار اختلاف مسیر نوری ثابت (z=10nm,20nm,30nm,40nm) در دو نوع تداخل‌سنج سه مود بهبود یافته و دو مود معمولی رسم کردیم و نشان دادیم علاوه بر داشتن قابلیت‌تفکیک‌پذیری بالاتر در تداخل سنج سه مود می‌توان تغییرات اختلاف فاز را نسبت به ضریب شکست مایع پیل سوختی مشاهده کرد.

مراجع

[1] A. Kirubakaran and Jain R.K., "A review on fuel cell technologies and power electronic interface", Renewable and Sustainable Energy Reviews, 2009, 13: 2430.

[2] S. Thomas and Zalbowitz M., Fuel Cells – Green Power Hand Book. U.S. Department of Energy, Office of Transportation Technologies, 2010

[3] T. Yokoyama, T. Araki, Sh. Yokoyama and N. Suzuki. 2001. A subnanometre heterodyne interferometric system with improved phase sensitivity using a three-longitudinal-mode He–Ne laser. Meas. Sci. Technol. Vol. 12, No. 2, pp. 157–162.

[4] S. Olyaee and S. Hamedi. 2010. A low-nonlinearity laser heterodyne interferometer with quadrupled resolution in the displacement measurement.The Arabian Journal for Science and Engineering, Vol. 36, No. 2, pp. 279-286.

[5] J. Guo, Y. Zhang and S. Shen. 2000. Compensation of nonlinearity in a new optical heterodyne interferometer with doubled measurement resolution. Optics Communications, Vol. 184, Issue 1-4, pp. 49-55.

[6] P. Hariharan. 2003. Optical Interferometry, School of physics university of Sydney, Australia, Academic press, ISBN 0-12-311630-9, chapter 6.

Applications

8th Iranian Fuel Cell Seminar
FEBRUARY 25,26
2015

A Total Research about Quick Synthesis of Ultrafine NiPd Bimetallic Nanoparticles and Their High Performance in Relation with Methanol Electrooxidation

Kourosh Motevalli[1*], Zahra Yaghoubi[2]
1 Applied Chemistry Department, Basic Sciences Faculty, Islamic Azad University, South Tehran Branch, Tehran, Iran
2 Industrial Engineering Faculty, Islamic Azad University, South Tehran Branch, Tehran, Iran
** k_motevalli@azad.ac.ir*

Abstract
In this research, uniform and sub-10 nm size bimetallic NiPd nanoparticles (NPs) have been synthesized via a simple and facile method without using any surfactants at an ambient temperature. The morphology, composition, and structure of NiPd NPs had been characterized by transmission electron microscopy (TEM), field emission high resolution transmission electron microscopy (FE-HRTEM), energy dispersive spectroscopy (EDS), X-ray diffraction (XRD), and X-ray photoelectron spectroscope (XPS). Comparing with both the monometallic Ni and Pd, the being prepared alloy nanoparticles exhibit superior electrocatalytic activity and better tolerance against poisoning by intermediates generated during methanol electrooxidation, which makes them a promising electrocatalysts for direct methanol fuel cells (DMFCs). Meanwhile, the green and simple approach could be easily extended to the manufacture of bimetallic or trimetallic alloy nanomaterials.

Keywords*:* Nanomaterials, Bimetallic, EDS, TEM, Electrocatalytic activity

1. Introduction

Alongwith the increasing depletion of fossil energy and the severity of environmental pollution, people pay great attention to develop a renewable, clean, and effective energy. A lot of research has been carried out extensively on the direct methanol fuel cells (DMFCs) due to their unique advantages, such as its high specific energy, environmental-friendly, and portability. The selection of anodic catalyst is extremely crucial for the performance of the DMFCs. Considering high catalytic activity and stabilized chemical properties, nickel is the most primary catalyst for the electrooxidation of low carbon-chain aliphatic alcohol such as methanol and ethanol in DMFCs [1, 2]. Unfortunately, the application of Ni-based catalysts in DMFCs is severely hindered in commercial market because of the poor natural content of Ni and poisoning effect with CO-like intermediates of the methanol electrooxidation [3]. Therefore, exploitation of new anodic catalysts in DMFCs is very important for improving the cell performance. It was verified that alloying Ni with inexpensive metals especially the transition metals can not only substantially reduce the cost of the electrocatalyst but also alter the geometrical and electronic effect to yield a more active catalytic surface [4]. Therefore, the research of bimetallic , trimetallic ,or multimetallic alloy nanomaterials has become a focal point in anodic electrocatalyst of DMFCs. [5–10]. Palladium, is considered as an ideal substitution for the growth of the Ni-based bimetallic nanocatalysts owning to only 0.77% lattice mismatch with Ni. NiPd alloy nanomaterials exhibit a similar catalytic performance as

well as a higher intermediate poison resistance compared with Ni during methanol electrooxidation [11, 12]. Therefore, bimetallic NiPd nanocatalysts are expected to be a promising substitute for Ni catalysts in DMFCs.
In this research, we have developed a simple and fast way for gaining the uniform and ultrafine NiPd NPs. The experiments were carried out in aqueous solution with any organic solvents or surfactant agents at an ambient temperature. It is worth noting that ascorbic acid is served as the reductant to reduce K_2NiCl_4 and K_2PdCl_4 simultaneously[11-13].
The morphology and structure of the prepared NiPd nano particles were characterized by various techniques, including TEM, XRD, and XPS. Therefore, we examined and compared the electrocatalytic activity and tolerance of carbon black (Vulcan XC-72) supported bimetallic nanoparticles (NiPd NPs/V) with carbon black supported monometallic Ni and Pd NPs (Ni NPs/V, Pd NPs/V) toward methanol oxidation. The further electrochemical characterizations indicate superior electrocatalytic activity and poison tolerance of the prepared NiPd NPs/V for methanol oxidation compared with Ni NPs/V and Pd NPs/V, which indicates potential use of NiPd NPs/V as a new anode catalyst in DMFCs.

2. Materials and Methods

2.1. Instruments. XRD analysis of the synthesized samples was recorded on D8-advance diffractometer (Bruker, Germany) with a CuKα radiation source (λ = 0.15418 nm). TEM and FE-HRTEM were employed to characterize the morphology and sizes of the samples. EDS was performed for determining the chemical composition of the catalysts. All electrochemical measurements were conducted using a 550 electrochemical workstation at room temperature in a conventional three-electrode system which consisted of a Ni counter electrode and an Ag/AgCl reference electrode. For removing dissolved oxygen, pure nitrogen gas was bubbled through the solution at the beginning of each experiment.
2.2. Preparation of Working Electrode. The procedure of preparing modified working electrodes consulted some previous reports . At first, the glassy carbon (GC) electrode must ensure being polished to a mirror finish by using slurry of 1, 0.3, and 0.05 μm alumina powers, washing via ultrasonic in ethanol and ultrapure water for 3 minutes, and then drying under nitrogen steam. Afterwards, 2 mg of the nanocatalysts loaded Vulcan XC-72 was distributed into a mixture of ultrapure water (0.9 mL) and 0.1 mL of Nafion (5 wt.%) and then using ultrasonic treatment to form a homogeneous black suspension. Finally, 5 μL of the uniform suspension was laid on the surface of the GC electrode and dried at an ambient temperature.

3. Results and Discussion

3.1. Morphology and Structural Characterization of NiPd NPs/V. For investigating the alloy nature and crystalline structure, the synthesized NiPd NPs/V, Ni NPs/V, and Pd NPs/V were characterized by XRD measurements. The obtained data shows that the crystal structures of monometallic catalysts are face-centered cubic structure (fcc). Similarly, the peaks at the 2 θ value of 39.92^0 , 46.22^0 , and 67.74^0 in the pattern of NiPd NPs/V are attributed to (111), (200), and (220) crystal planes for the fcc structure of NiPd. All the peak positions of NiPd NPs/V are found to be slightly shifted to high diffraction angles compared with that of Ni NPs/V. Taking an example of the (111) plane diffraction peak, the 2 θ value of NiPd NPs/V planes (39.92^0) is between those of Ni NPs/V (39.82^0) and Pd NPs/V (40^0). These results were attributed to the addition of Pd to the Ni for the difference in atomic size (Pd < Ni). Therefore, it is an indication that NiPd alloy nanoparticles have been successfully synthesized.
The TEM and HRTEM images of the bimetallic NiPd nanoparticles before and after loading on Vulcan XC-72 are shown in Figure 1. Figures 1(a) and 1(b) are the images of NiPd alloy

nanoparticles before loading on Vulcan XC-72 at different magnification. Well-dispersed NiPd alloy nanoparticles were observed with the average size 7 nm through the statistics of TEM image. No visible aggregation was found. For NiPd NPs/V (Figure 1(c)), the NiPd nanoparticles are uniformly dispersed on Vulcan XC-72 and the original morphology of nanoparticles basically remained.

The HRTEM image of NiPd NPs/V (Figure 1(d)) shows well- resolved continuous fringes in the same direction. The interval between the two lattice fringes was found to be 0.225 nm, which is between 0.2265 and 0.2246 nm, corresponding to the (111) interplanar distance of fcc Ni and Pd, respectively, indicating the formation of NiPd alloy nanostructures. These TEM results showed that well-dispersed NiPd alloy nanoparticles have been successfully synthesized and could be loaded onto carbon black for further application in DMFC.

For more characterize the alloy nature of the synthesized nanocrystals, NiPd nanoparticles were investigated by EDS, revealing the presence of C, Ni, and Pd. The bulk composition estimates the ratio of Ni and Pd is 4 : 3 which is deviated from the nominal ratio (Ni : Pd 4 : 1).

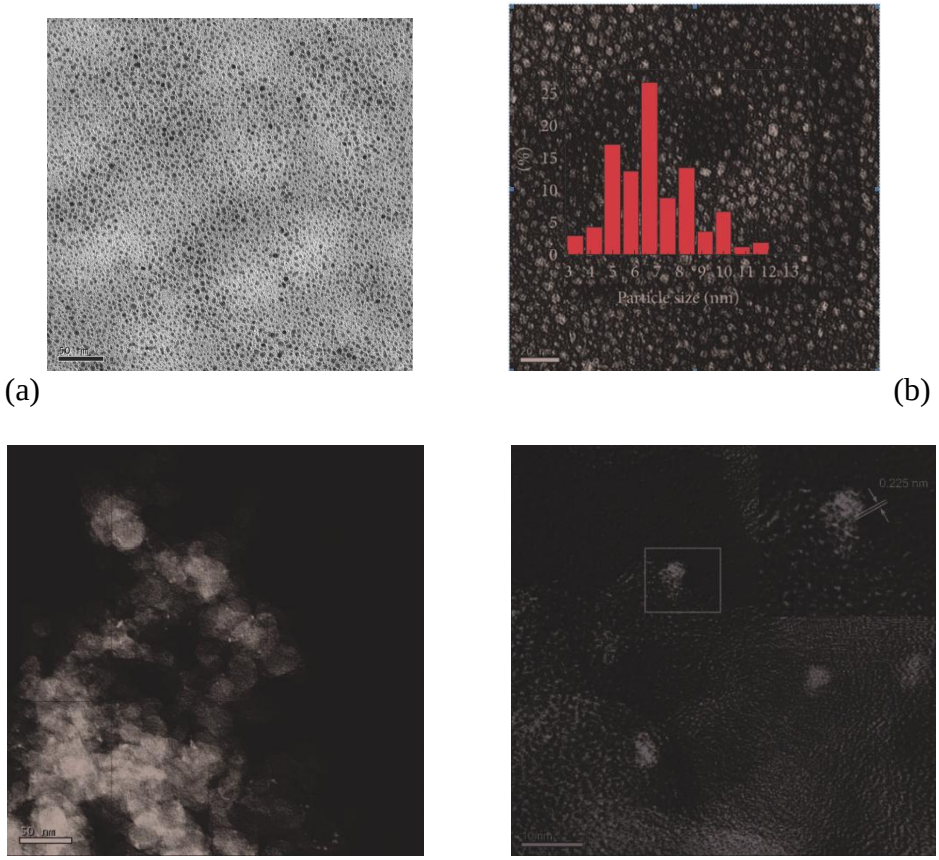

(a) (b)

(c) (d)

Figure 1: TEM images of NiPd NPs ((a), (b)) and NiPd NPs/V (c); the inset in (b) is the distribution of particle size; HRTEM image of NiPd NPs/V (d); the inset in (d) is the enlarged figure of the selected area. The scale bars are 50 nm (a), 20 nm (b), 50 nm (c), and 10 nm (d).

This result should be able to consider the different banding energy of Ni and Pd relative to the supports.

4. Conclusion

In this research, we successfully fabricated uniform and sub-10 nm bimetallic NiPd nanocrystals by a clean and facile method in aqueous solution at ambient temperature, in which ascorbic acid act as soft and green reductant. The synthesized NiPd NPs/V shows great catalytic activity and super poisoning tolerance for MOR in alkaline media than those of monometallic Ni NPs/V and Pd NPs/V. This facile method is also versatile for preparing the other bimetallic or trimetallic alloy nanoparticles as new electrocatalyst for the application in fuel cell.

References

[1] P. Zhou, Z. Dai, M. Fang, X. Huang, J. Bao, J. Gong, "Novel palladium nanostructure and its application in biosensing," Journal of Physical Chemistry C, vol. 111, no. 34, pp. 12609–12616, 2007.

[2] S. Kim, G.H. Jeong, D. Choi et al., "Synthesis of noble metal/graphene nanocomposites without surfactants by one-step reduction of metal salt and graphene oxide," Journal of Colloid and Interface Science, vol. 389, no. 1, pp. 85–90, 2013.

[3] G. Fu, K. Wu, J. Lin et al., "One-pot water-based synthesis of Pt- Pd alloy nanoflowers and their superior electrocatalytic activity for the oxygen reduction reaction and remarkable methanol- tolerant ability in acid media," The Journal of Physical Chemistry C, vol. 117, no. 19, pp. 9826–9834, 2013.

[4] Y. Piao, Y. Jang, M. Shokouhimehr, I. S. Lee, T. Hyeon, "Facile aqueous-phase synthesis of uniform palladium nanoparticles of various shapes and sizes," Small, vol. 3, no. 2, pp. 255–260, 2007.

[5] R. Yue, C. Wang, F. Jiang et al., "Electrocatalytic oxidation of formic acid on Pt –Pd decorated polyfluorenes with hydroxyl and carboxyl substitution," International Journal of Hydrogen Energy, vol. 38, no. 29, pp. 12755–12766, 2013.

[6] J. Datta, A. Dutta, and S. Mukherjee, "The beneficial role of the cometals Pd and Au in the carbon-supported NiPdAu catalyst toward promoting ethanol oxidation kinetics in alkaline fuel cells: temperature effect and reaction mechanism," The Journal of Physical Chemistry C, vol. 115, no. 31, pp. 15324–15334, 2011.

[7] W. He, H. Jiang, Y. Zhou et al., "An efficient reduction route for the production of Pd-Pt nanoparticles anchored on graphene nanosheets for use as durable oxygen reduction electrocatalysts," Carbon, vol. 50, no. 1, pp. 265–274, 2012.

[8] H. Li, G. Sun, N. Li, S. Sun, D. Su, and Q. Xin, "Design and preparation of highly active Pt-Pd/C catalyst for the oxygen reduction reaction," The Journal of Physical Chemistry C, vol. 111, no. 15, pp. 5605–5617, 2007.

[9] J. Russell, P. Zapol, P. Kra´l, and L. A. Curtiss, "Methane bond activation by Pt and Pd subnanometer clusters supported on graphene and carbon nanotubes," Chemical Physics Letters, vol. 536, pp. 9–13, 2012.

[10] G. Fu, L. Tao, M. Zhang et al., "One-pot, water-based and high-yield synthesis of tetrahedral palladium nanocrystal decorated graphene," Nanoscale, vol. 5, no. 17, pp. 8007–8014, 2013.

[11] S. S. Mahapatra, A. Dutta, and J. Datta, "Temperature dependence on methanol oxidation and product formation on Pt and Pd modified Pt electrodes in alkaline medium," International Journal of Hydrogen Energy, vol. 36, no. 22, pp. 14873–14883, 2011.

[12] N.V. Long, T.D. Hien, T. Asaka, M. Ohtaki, M. Nogami, "Synthesis and characterization of Pt-Pd alloy and core-shell bimetallic nanoparticles for direct methanol fuel cells (DM- FCs): enhanced electrocatalytic properties of well-shaped core-shell morphologies and nanostructures," International Journal of Hydrogen Energy, vol. 36, no. 14, pp. 8478–8491, 2011.

[13] M. Shao, J.H. Odell, S. Choi, Y. Xia, "Electrochemical surface area measurements of nickel- and palladium-based nanoparticles," Electrochemistry Communications, vol. 31, pp.46–48, 2013.

Study and Fabrication of Monocell and Stack Fuel Cell

8th Iranian Fuel Cell Seminar
FEBRUARY 25,26
2015

Synthesis, Studing and Performance Comparing of Membrane Electrode Assembly Fabricated by Pt/N-rGO with Pt/Vulcane

Ahmad Heydari*, Hussein Gharibi, Fatemah Yasi

Department of chemistry, faculty of basic sciences tarbiat modares university
** ahmad.heydari1@gmail.com*

Abstract
Proton exchange membrane fuel cells (PEMFCs) are one of the most promising clean energy conversion devices due to their high conversion efficiency, low/zero emission, and high power/energy densities. Nitrogen doping has been an effective way to tailor the properties of graphene and render its potential use for various applications. We developed a simple chemical method to obtain bulk quantities of N-doped, reduced grapheme oxide (GO) powder through thermal annealing of GO in ammonia and hydrazine. Oxygen reduction and nitrogen doping were achieved simultaneously under the hydrothermal reaction. Electrochemical measurements and MEA performance show that the nitrogen doped graphene support has the better activity than Vulcan.

Keywords: PEMFC, Graphene, N-doped, Pt nano particle

Introduction
Polymer electrolyte fuel cells (PEFCs) are promising power sources for automotive and stationary applications due to their low pollutant emission and high energy-conversion efficiency. PEFCs have been intensively developed for decades to their performance, but a longer lifetime is still needed before extensive commercialization is possible. Cathode catalysts are mainly composed of platinum nanoparticles on a carbon support, and catalyst degradation is one of the main factors that reduce the lifetime of PEMFCs. One of main causes of catalyst degradation is loss of the platinum surface area due to corrosion of the carbon supports and subsequent agglomeration of platinum nanoparticles . Carbon supports, such as carbon black, are thermodynamically unstable and may corrode at the high potentials typical of PEMFC cathodes. In addition, the carbon corrosion is accelerated by the catalytic effect of platinum nanoparticles on the carbon support. Therefore, an alternate support material is needed to improve the stability of the cathode catalyst. Graphene and nitrogen doped graphene have been reported to demonstrate high oxidation resistance . This material is thought to show higher electrical conductivity than Vulcan support. These supports is additionally expected to have a large surface area. Furthermore, in this work the graphene support was active for ethanol and hydrogen oxidation alone.

Experimental section
Synthesis of graphene oxide:
Graphene oxide (GO) was made by a modified Hummers method. using expandable graphite flake as starting material. Expandable graphite flake (3 g) was ground with NaNO3 (50 g) for 30

min. $NaNO_3$ was dissolved in water and removed by filtration (~15% carbon was lost during this step). The remaining ground expandable graphite flake (~2.55 g) was stirred in 98% H_2SO_4 (70 mL) for 28 h. $KMnO_4$ (15 g) was gradually added while keeping the temperature <5 °C. The mixture was then stirred at 35–40 °C for 60 min, and then at 65–80 °C for 90 min. Next, water (200 mL) was added and the mixture heated at 98–105 °C for 15h. The reaction was terminated by addition of distilled water (520 mL) and 30% H_2O_2 solution (50 mL). The mixture was washed by repeated centrifugation and filtration, first with 5% HCl aqueous solution, and then distilled water. Water (480 mL) was added to the final product and vortexed well to make a uniform suspension for storage.

Synthesis of nitrogen doped graphene:

The graphite oxide was first synthesized using Hummer's method. Next, 0.1 g of graphite oxide was dispersed in 100 ml of 1 M HCl solution with the assistance of 30 min of ultrasonication.
Then, 5 ml of the aniline monomer was added to the graphite oxide solution with constant stirring. Finally, 100 ml of the APS (2.5 g) solution was dropped into the above solution for 30 min to initiate polymerization. The reaction was continued for 6 h at 0–5 ◦C. Then, the final product was washed using water and methanol. The washed powder was dried in a vacuum oven at 80 ◦C for 24 h. The N-doped carbon/graphene core/shell structure was obtained by carbonization of the graphite oxide/PANI in two steps. First, stabilization was carried out at 250 ◦C in air for 2 h. Second, carbonization was carried out at 850 ◦C under N_2 gas for 2 h with the heating rate of 5 ◦C/min and an N_2 flow rate of 200 ml/min.

Preparation of Pt/Support:

In this work we used graphene, nitrogen doped graphene and Vulcan as support and pt ion solution in the form of H_2PtCl_6. we mixed support and ion platinum with methanol:water (1:1) solution and then ultrasonicated them in 20min. The mixture refluxed in 90 C in Ar atmosphere and ethylene glycol reducing agent was aded to mixture to reduce pt ion .after 24h, the mixture was filtered and washed with distilled water and dried in vacuum aven.

Electrochemical characterization:

For determination of the electrochemical performance and stability of supports and catalysts, a conventional three-electrode electrochemical cell was employed. All the electrochemical measurements were carried out in 0.5M H_2SO_4 solution at 25 ◦C, and ultra-pure N_2 (Air Products) was passed through a 0.5M H_2SO_4 solution and 0.5M ethanol + 0.5 M H_2SO_4 solution for 30 min before the electrochemical measurements, a platinum electrode was the counter electrode, and a Ag/AgCl(KCl(sat)) electrode was the reference electrode. For convenience, all potentials measured are referred to as the normal hydrogen electrode (NHE). A polished glassy carbon disk electrode (3mm diameter) was used as the substrate for the supported catalysts (or supports). The working electrode was fabricated as follows : 5mg of the catalysts (or supports) was dispersed in 2mL of deionized water: isopropyl alcohol (1:2) and then mixed with 17.65mg of 5 wt.% Nafion solution. The mixture was sonicated for 6min to obtain an ink like slurry. 10 µl of this slurry was spread onto the flat surface of the glassy carbon disk using Hamilton; and then glassy carbon was dried in oven.

Results and discussion

Raman spectroscopy and XRD technique for GO identify

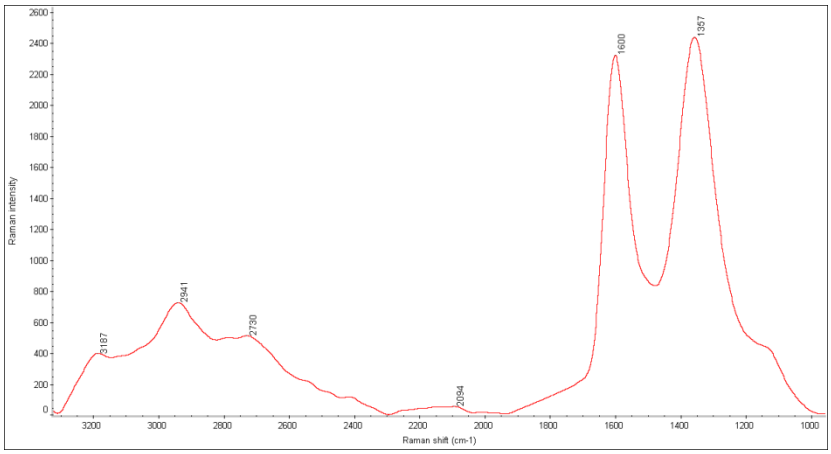

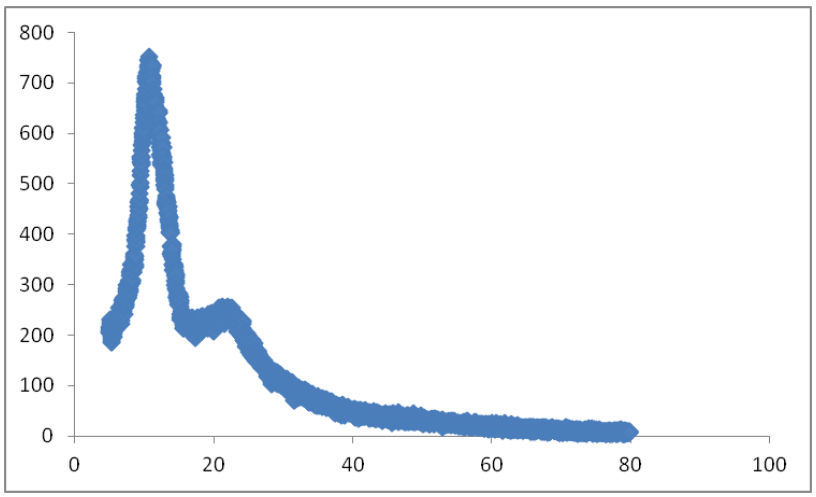

These results show that graphene oxide was synthesized successfully.

Raman spectroscopy of nitrogen doped graphene

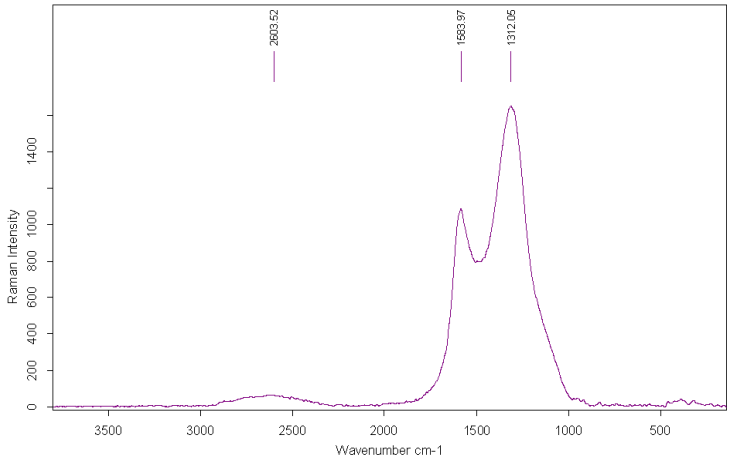

In N-doped Graphene, a down shift in G-band occur (1583.97 vs. 1590.85 cm-1 (GO)) and 2D band in broad.

Below figures show TEM results for Pt/N-rGO and Pt/rgo.these result show that GO was synthesized successfully and platinum nano particles was dispersed good. **Pt/rGO**

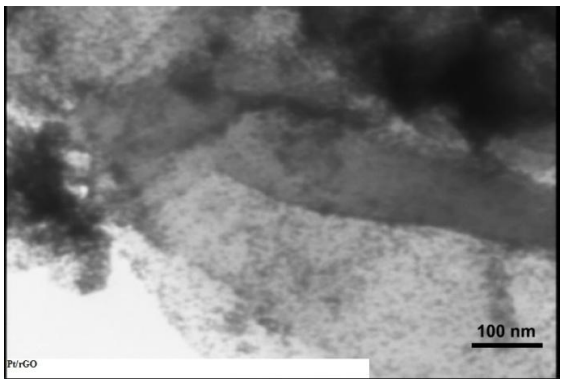

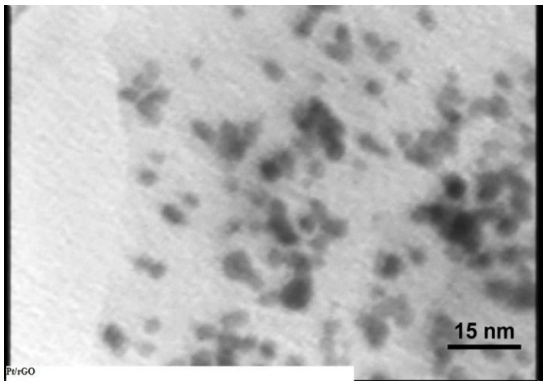

Electrochemical measurement results

The impedance spectroscopy of membrane electrode assembly in open circuit voltage and other potential show that Pt/nitrogen doped graphene has lower ionic resistance than Pt/Vulcan.

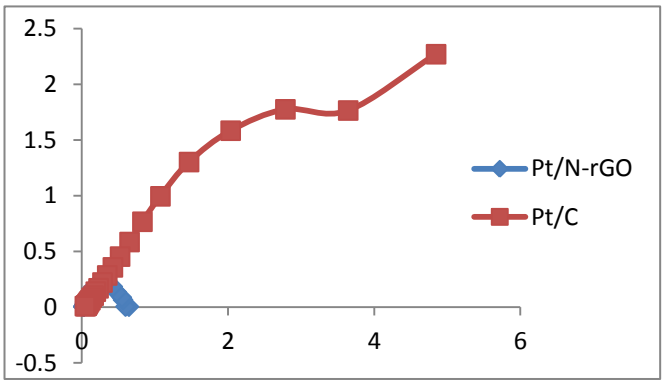

Cyclic voltametry results

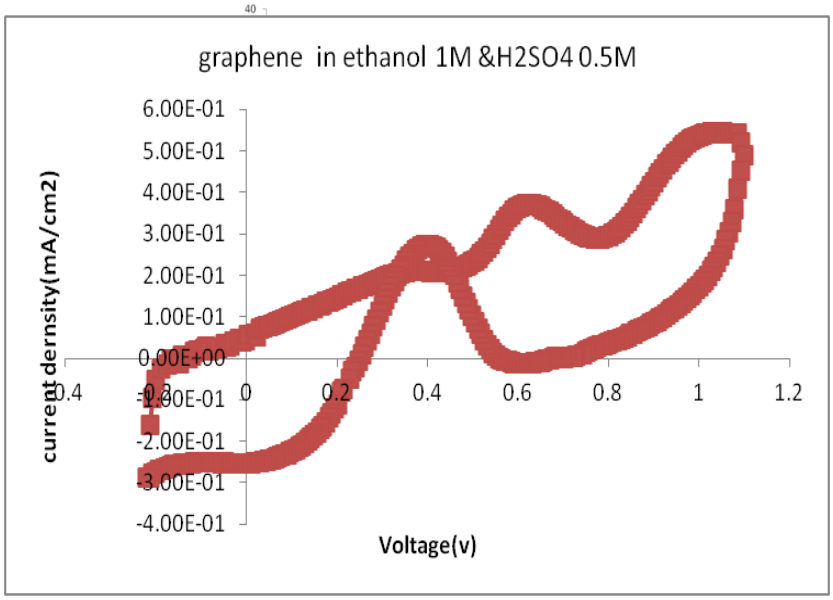

Electrode	Δ Q	ECSA (m2/gr Pt)
Pt- sp5	4.318 mc	327.26
Pt-GO	2.428 mc	184.02
Pt/vulcan	0.939 mc	71.2

References

[1] Haibo Wang, Thandavarayan Maiyalagan, and Xin Wang. ACS Catal. 2012, 2, 781−794
[2] Zhengzong Sun, Dustin K. James, and James M. Tour. J. Phys. Chem. Lett. 2011, 2, 2425–2432
[3] C. Jeyabharathia, P. Venkateshkumarb, M. Sankara Raoa, J. Mathiyarasua, K.L.N. Phania Electrochimica Acta 74 (2012) 171– 175
[4] Jincheng Bai a,b, Qianqian Zhu a, Zhexin Lv a, Hongzhou Dong a, Jianhua Yu a, Lifeng Dong. International journal of hydrogen energy 38(2013) 1413 -1418

8th Iranian Fuel Cell Seminar
FEBRUARY 25,26
2015

Electrochemical Analysis of Anodic Catalysts in Direct Borohydride Fuel Cell

M. Zhiani[1*], I. Mohammadi[1], M.M. Taghiabadi[2]
1. Department of Chemistry, Isfahan University of Technology, Isfahan, Iran
2. Asian Hydrogen New Science Co., No. 5, Crystal Building, Sheikh Bahaei Science and Technology Park. Isfahan Science and Technology Town, Isfahan, Iran
** Mohammad.zhiani@gmail.com*

Abstract
The electrochemical oxidation of BH_4^- in 2M KOH on palladium decorated (>> 1 wt. % palladium) Ni/C (PD Ni/C) and 10 wt. % Pd/C has been studied by polarization and electrochemical Impedance spectroscopy technique. Electrochemical measurements reveal that the Direct Borohydride Fuel Cell (DBFC) equipped with both catalyst 3D anode produced excellent catalytic performance. However, higher open circuit voltage and peak power density obtained on Pd/C compared to the PD Ni/C, 1010 mV vs 990 mV and 138 mW cm^{-2} vs. 125.8 mW cm^{-2} respectively at 45 °C and ambient pressure. These values are close and among the highest open circuit voltages and peak power densities reported for any air breathing passive low temperature direct borohydride fuel cells. Therefore, palladium decorated (> 1 wt. %) Ni/C can be promising catalyst for DBFCs.

Keywords: Direct Borohydride Fuel Cell, Polarization, Electrochemical Impedance Spectroscopy, Catalyst

Introduction
It is now well admitted that using a liquid fuel to replace hydrogen for feeding fuel cell anodes would have many advantages in term of fuel cell system simplicity, mass and volume, as well as for safety reasons [1], which is mandatory for portable electronic devices. Amendola first showed the interest of the tetrahydroborate anion (BH_4^-) direct oxidation in a fuel cell anode instead of hydrogen [2]. Sodium borohydride (BH_4^-) offers a number of advantages as an interesting alternative fuel for fuel cells, including high hydrogen contents (10.6 wt. %), and high specific capacity (5668 Ah kg^{-1}), safe handling, superior storage properties, and low pollution [3-5]. Direct borohydride fuel cells (DBFCs) have received considerable attention over the past decade due to their high power density, high open circuit voltage, high number of transferred electron and avoidance of CO poisoning [5].The reactions in borohydride fuel cells are:
Anode reaction is the electro-oxidation of borohydride ion to release $8e^-$ according to the following reaction:

$$BH_4^- + 8OH^- \rightarrow BO_2^- + 6H_2O + 8e^- \quad \text{(Eq. 1)}$$

Cathode:

$$2O_2 + 4H_2O + 8e^- \rightarrow 8OH^- \quad \text{(Eq. 2)}$$

Overall:

$$BH_4^- + 2O_2 \rightarrow BO_2^- + 2H_2O + 8e^- \quad \text{(Eq. 3)}$$

However, heterogeneous hydrolysis of the BH_4^- anion that produces H_2 gas (Eq. (2)) and the incomplete electrooxidation of $NaBH_4$ in alkaline solution proceed in parallel with Eq. (1), lead consequently to significant reduction in the utilization of $NaBH_4$[6].

$BH_4^- + H_2O \rightarrow BH_3OH^- + H_2$ (Eq. 4)

Therefore, the anode electrocatalyst is one of the key components in DBFC in order to achieve the maximum utilization of $NaBH_4$ by minimizing hydrolysis and complete oxidation of BH_4^- [7-14].

In this study, we demonstrate a low-cost (very low-precious metal) catalysts for the DBFC anode (borohydride oxidation reaction). Fuel cell experiments was performed in detail to analyze and compare the performance of DBFC using very low-precious metal and Pd/C catalysts.

Experimental Method

The two anode pastes were prepared in the same way by thoroughly blending the low-precious metal catalyst (Acta SpA) or 10 wt. % Pd/C (E-TEK) with ultrapure water, isopropyl alcohol, recast Nafion® ionomer (5% Nafion® suspension DuPont) to form paste−like slurry. An appropriate amount of the anode paste was painted onto the substrate and then dried at 60ºC for 30 min to obtain the anode catalyst loadings of approximately 5 mg cm^{-2}. Identical cathode was prepared by mixing of Fe-Co/C, with ultrapure water, isopropyl alcohol, 10 wt. % PTFE and finally sprayed onto a piece of hydrophobic carbon cloth (E−TEK) to obtain the cathode catalyst loadings of approximately 4 $mgcm^{-2}$.

Two membrane electrode assemblies (MEAs) were prepared and assembled in passive DBFC with a surface area of 4.5 cm^2; one with a the low-precious metal anode catalyst denoted as MEA-LPMC and the other with a 10 wt. % Pd/C cathode catalyst represented by MEA-Pd.

Single cell tests were conducted in a passive air breathing DBFC using a static alkaline solution containing 1, 3, 5 and 8 wt. % $NaBH_4$ (denoted as SBH, purity 99%, Merck) and 10 wt. % KOH.

Result and discussion

The cell with the MEA-Pd anode exhibits a higher open-circuit voltage than the cells with MEA-LPMC anode; 1010 mV vs. 992 mV. Although, the open cell voltage (OCV) in both cells are lower than the theoretical OCV of DBFC (1.64 V). The deviation is mainly due to the formation of the mixed potentials at open voltage caused by fuel cross-over to cathode and simultaneous oxidation of BH_4^- ions and hydrogen at the anode side. As shown in Figure 1, the MEA-Pd and MEA-LPMC generate approximately 224 and 200 mA cm^{-2} at 0.5 V and a maximum power density of 138 mW cm^{-2} and 125.8 mW cm^{-2} respectively. Although power density of MEA-LPMC is less than that obtained on the MEA-Pd, however PD Ni/C catalyst has very low palladium (> 1% metal) in its structure. Therefore, it can be concluded that PD Ni/C catalyst is promising candidates for anode in direct borohydride fuel cells.

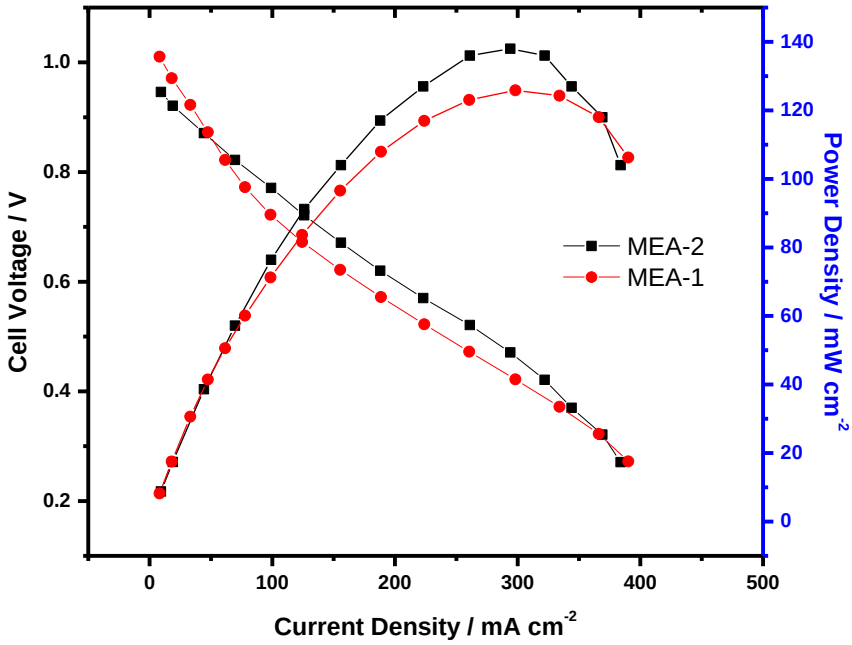

Figure 8: Comparison between cell polarization curves of MEA 1 and 2 in DBFCs fueled with 3 wt% of SBH

PD Ni/C performance was investigated in different fuel concentration. Figure 2 shows the effect of borohydride concentrations on the air breathing passive DBFC performance. The OCV increased with increasing borohydride concentrations from 1 to 3 wt. % SBH, which is determined by the Nernst's equation. The maximum power density of DBFC was also increased from 51 to 125.8 mW cm^{-2} when the borohydride concentration was increased from 1 to 3 wt. % SBH. It can probably be attributed to the improved mass transfer of the fuel and kinetics of borohydride oxidation. However, further increase in sodium borohydride concentration to 5 wt% caused a decrease in the power density due to the enhancement of the fuel crossover and borohydride hydrolysis by increasing borohydride concentration. As the hydrolysis reaction proceeds, not only hydrogen bubbles are generated from catalyst surface, but also borate is formed. Hydrogen bubbles destruct the catalyst layer and mass transport of the reactant is substantially hindered by borate molecules.

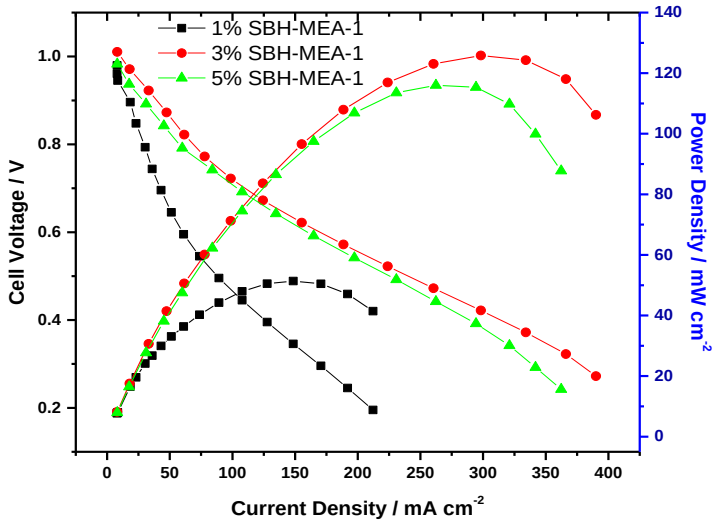

Figure 9: Cell polarization curves of MEA-1 in DBFCs fueled by solution containing 1, 3 and 5 wt% of SBH

Figure 3 shows the electrochemical impedance spectra of the MEA-LPMC and the MEA-Pd at operating dc voltage of 0.3 (high current densities region). The results demonstrated that MEA-LPMC had lower, but close charge and mass transport resistance.

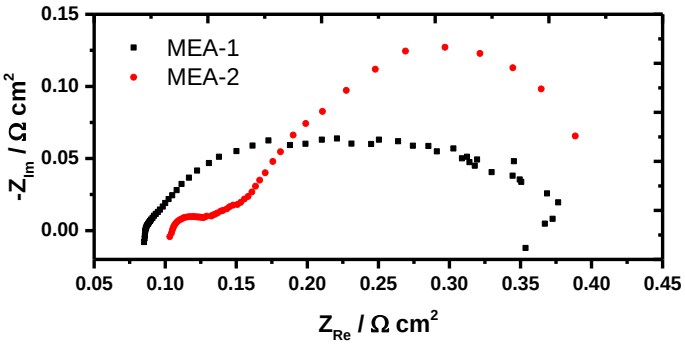

Figure 10: Comparison between Nyquest spectra of MEA 1 and 2 in DBFCs fueled with 3 wt% SBH at 0.3

Conclusion

This work demonstrated that the PD Ni/C catalyst which has very low Pd metal (<1 wt. %) exhibited a close electrocatalytic activity for $NaBH_4$ electrooxidation compared to the 10 wt. % Pd/C catalyst. The BOR activity of the catalysts is evaluated using single cell polarization and EIS test.

According to single-cell results, Pd/C catalyst showed an higher performance compare to PD Ni/C in air breathing passive DBFC; maximum power density of 138 $mWcm^{-2}$ Vs. 126 mW cm^{-2} at room temperature. However, higher OCV (1010 mV) was obtained using PD Ni/C which is lower, but close when compared to that obtained for 10 wt. % Pd/C (1010 mV) in the same fuel concentration.

It can be concluded that PD Ni/C catalyst is promising candidates for anode in direct borohydride fuel cells.

Reference

[1] Vielstich W, Lamm A, Gasteiger HA. Handbook of Fuel Cells: Fundamentals, Technology, and Applications: Wiley; 2009.
[2] Amendola SC, Onnerud P, Kelly MT, Petillo PJ, Sharp-Goldman SL, Binder M. A novel high power density borohydride-air cell. Journal of Power Sources. 1999;84:130-3.
[3] Rees N, Compton R. Sustainable energy: a review of formic acid electrochemical fuel cells. J Solid State Electrochem. 2011;15:2095-100.
[4] Demirci UB, Miele P. Sodium borohydride versus ammonia borane, in hydrogen storage and direct fuel cell applications. Energy & Environmental Science. 2009;2:627-37.
[5] Ma J, Choudhury NA, Sahai Y. A comprehensive review of direct borohydride fuel cells. Renewable and Sustainable Energy Reviews. 2010;14:183-99.
[6] Finkelstein DA, Mota ND, Cohen JL, Abruña HD. Rotating Disk Electrode (RDE) Investigation of BH4− and BH3OH− Electro-oxidation at Pt and Au: Implications for BH4− Fuel Cells. The Journal of Physical Chemistry C. 2009;113:19700-12.
[7] Chatenet M, Micoud F, Roche I, Chainet E. Kinetics of sodium borohydride direct oxidation and oxygen reduction in sodium hydroxide electrolyte: Part I. BH4− electro-oxidation on Au and Ag catalysts. Electrochimica Acta. 2006;51:5459-67.
[8] Cheng H, Scott K. Determination of kinetic parameters for borohydride oxidation on a rotating Au disk electrode. Electrochimica Acta. 2006;51:3429-33.
[9] Coowar FA, Vitins G, Mepsted GO, Waring SC, Horsfall JA. Electrochemical oxidation of borohydride at nano-gold-based electrodes: Application in direct borohydride fuel cells. Journal of Power Sources. 2008;175:317-24.
[10] Demirci UB. Commentary about the number of electrons, really involved in the direct oxidation of borohydride catalysed by Ag and Ag-alloys, determined by Gyenge and co-authors. International Journal of Hydrogen Energy. 2008;33:2123-4.
[11] Dong H, Feng R, Ai X, Cao Y, Yang H, Cha C. Electrooxidation Mechanisms and Discharge Characteristics of Borohydride on Different Catalytic Metal Surfaces. The Journal of Physical Chemistry B. 2005;109:10896-901.
[12] Gyenge E. Electrooxidation of borohydride on platinum and gold electrodes: implications for direct borohydride fuel cells. Electrochimica Acta. 2004;49:965-78.
[13] Krishnan P, Yang T-H, Advani SG, Prasad AK. Rotating ring-disc electrode (RRDE) investigation of borohydride electro-oxidation. Journal of Power Sources. 2008;182:106-11.
[14] Mirkin MV, Yang H, Bard AJ. Borohydride Oxidation at a Gold Electrode. Journal of The Electrochemical Society. 1992;139:2212-7.

8th Iranian Fuel Cell Seminar
FEBRUARY 25,26
2015

Effect of Potential Cyclic and External Humidity Injection on Proton Exchange Membrane Fuel Cell Performance

M. Zhiani[1*], I. Mohammadi [1], M.M. Taghiabadi[2]

1. Department of Chemistry, Isfahan University of Technology, Isfahan, Iran
2. Asian Hydrogen New Science Co., No. 5, Crystal Building, Sheikh Bahaei Science and Technology Park. Isfahan Science and Technology Town, Isfahan, Iran
** Mohammad.zhiani@gmail.com*

Abstract
In this work, effect of two membrane-electrode assembly (MEA) pre-conditioning procedures of potential cyclic and external humidity injection on the final cell performance and electrochemical impedance spectroscopy (EIS) response was studied under conditions. Obtained results under steady state condition proposed that humidity injection have a better effect on MEA in order to reach to the maximum performance of MEA compared to potential cyclic under different operation conditions. From the impedance experiments of MEA affected by potential cyclic it was observed that the ohmic, charge transfer and mass transfer resistances of MEA is higher than MEA affected by external humidity injection. Moreover, the polarization technique results show that MEA affected by external humidity injection has higher power density compared with that affected by potential cyclic; 1448mW cm^{-2}vs. 1090mW cm^{-2}.

Keywords: Polymer electrolyte membrane fuel cell, Potential cyclic, Polarization, Electrochemical Impedance Spectroscopy

Introduction
The fuel cells are devices that convert the chemical energy of fuels such as hydrogen, directly into electrical energy. Due to its low emissions, fast start-up, small size, low operation temperature, and high power density, polymer electrolyte membrane fuel cells (PEMFCs) are considered as promising technology for power sources in transportation, stationary, and mobile applications[1].The performance of PEMFC is known to be affected by many structural and operational parameters such as: catalyst layer composition[2, 3], diffusion medium properties[4], electrode preparation[5, 6], membrane characteristics[7, 8], Method of manufacturing membrane electrode assembly[9, 10] and reactants pressure, temperature and relative humidity[11-13].
A large amount of research has been directed towards improving the performance of proton exchange membrane fuel cells (PEMFCs) while keeping the Pt loading as low as possible.It is clear that increasing the catalyst utilization is the key factor in achieving a good performance. It found that even after an electrode is made, the catalyst utilization can be increased by simply treating the electrode in different ways[14].
In this work, we studied the effects of potential cyclic and external humidity injection procedures on the MEA performance and its EIS response after reaching steady state and under different operation conditions.

Experimental

Membrane electrode assembly and cell hardware

The catalyst ink was consisted of Pt/C (20 wt. % Pt, BASF) that was directly mixed with a solvent and Nafion solution (5 wt. % solution, EW1000, Aldrich), deposited on the surface of GDL. In this work, applied MEA in the home made PEM fuel cell was consisted of Nafion 212 (Fuel Cell store) was used to prepare the gas diffusion layer (GDL). The catalyst loading of 0.4 $mg_{Pt}cm^{-2}$ was used in both the anode and cathode electrode. The serpentine pattern graphite flow field was used for the anode and the cathode (Asian Hydrogen New Science Co.).

The first MEA denoted by MEA-1 is affected by the potential cyclic and the second MEA denoted MEA-2 is affected by the humidity injection.

Electrochemical measurements

The performance of the MEAs was characterized by polarization curves and electrochemical impedance spectroscopy under different conditions: low and medium RH cell pressure .All tests were repeated twice but the last results were presented.

Result and discussion

The influence of RH on the performance and EIS response of MEAs

Relative humidity is important parameter for both performance and durability due to its effect on MEA water management. Therefore, can be reflected by i-V and EIS spectra measurements. Figures 1 and 2 indicate the performance and EIS response of MEA-1 and MEA-2 under low and medium relative humidity.

Figure 1 indicates that at medium RH, both MEAs show higher power density compared to low RH. The MPD of the MEAs has been reported in table 1.

The best performance in both low and medium RH is related to MEA-2, which was affected by external humidity injection procedure.

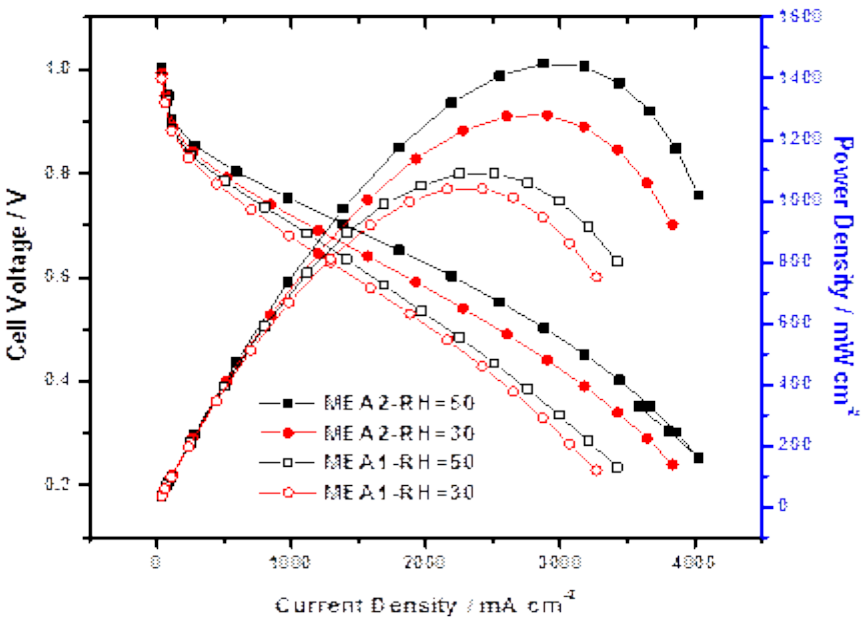

Figure 11: Polarization curves of MEA 1 and 2 under 30% and 50% of RH and 25 psi pressure of gases.

Table 1: Maximum power densities and OCV of MEA 1 and 2 under different operation relative humidity of gases, gas pressure 25 psi.

RH	MEA	MPD / mW cm^{-2}	OCV / mV
50%	1	1448	1003
50%	2	1090	985
30%	1	1279	992
30%	2	1040	983

Better understanding of the electrochemical processes involved in the performance of MEAs is provided by the EIS method at 0.5V. As shown in figure 3, EIS spectrum of both MEA consist of two arcs in medium and low frequency which is attributed to charge and mass transfer limitations, respectively. Moreover, the intersection of the imaginary impedance with the real impedance reflects the ohmic resistance (Rs).

As can be seen, at both medium and low RH, MEA-2 show lower Rs as compared to MEA-1. It could be related to higher water generation during external humidity injection of MEA-2. Moreover, this figure indicates that with increasing RH, lower Rct values can be observed. Also, at both medium and low RH, MEA-2 show lower Rmt as compared to MEA-1.

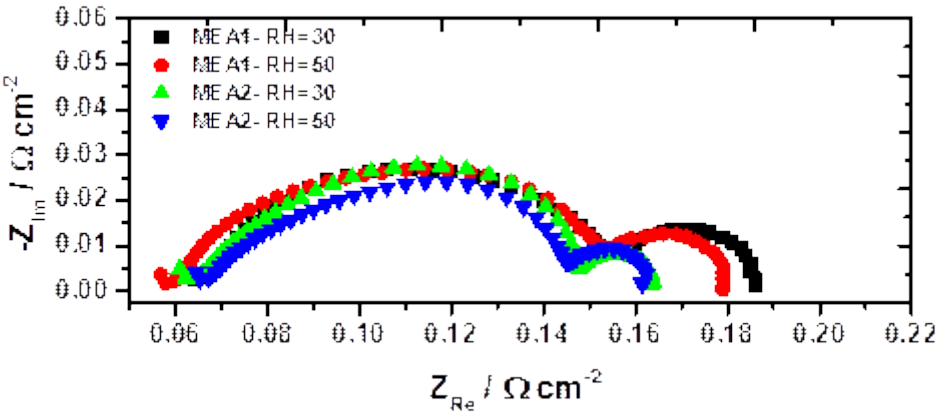

Figure 2: Nyquist plots of MEA 1 and 2 at 0.5 V under 30% and 50% of RH and 25 psi pressure of gases.

Since all MEAs have an identical structure, their performance difference is mainly related to the procedure applied for them. Therefore, it can be concluded that applied procedures to MEA have a very important effect on the MEA performance and EIS response.

The influence of RH on the performance and EIS response of MEAs

In order to study the influence of the operating pressure on the performance and EIS response of the three activated MEAs, the pressure of gases was increased.

Figure 3 represents polarization curves of MEAs at different pressure of reactants. Given that the structure of two MEAs was identical at the beginning, it could be concluded that the both potential cyclic and external humidity injection procedure had an irreversible effect on the MEA interfacial structure which could not be corrected even at high pressure of gases. Polarization curves results show that in both high and medium operating pressure and, MEA-2 had the higher performance. The MPD of the MEAs has been reported in table 2.

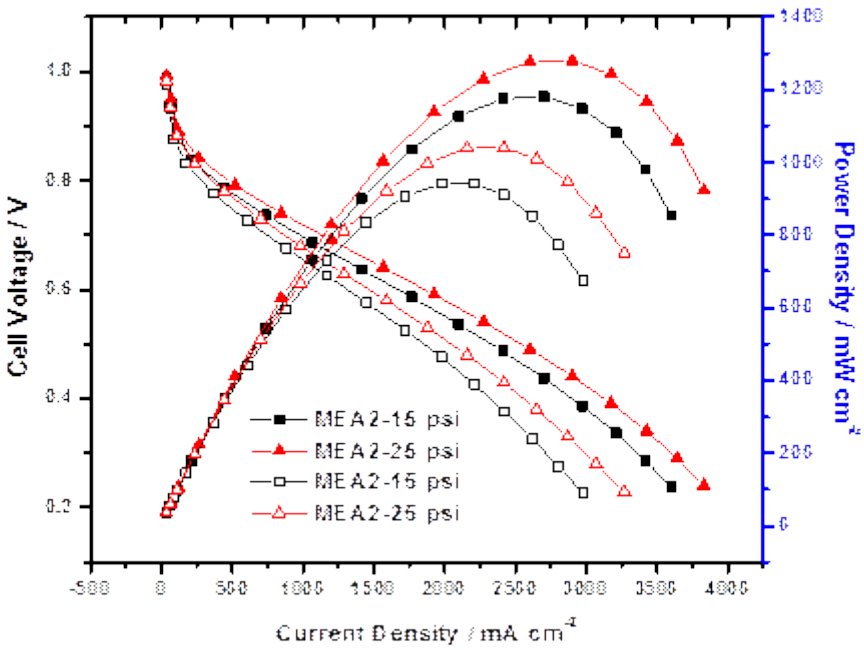

Figure 3: Polarization curves of MEA 1 and 2 under 15 psi and 25 psi pressure of gases and 30% of RH.

Table 2: Maximum power densities and OCV of MEA 1 and 2 under different operation pressures of gases, RH 30%.

Pressure / psi	MEA	MPD / mW cm^{-2}	OCV / mV
15	1	1181	987
15	2	942	977
25	1	1279	992
25	2	1040	983

Figure4 indicates the Nyquist plots of the two MEAs at 0.5 V under high and medium operating pressure, consistent with polarization curves results. This figure indicates that by increasing the gases pressure from 15 psi and 25 psi, Rs of both MEAs was increased; this may be related to the enhancement of the contact resistance between diffusion medium and flow field plates in the anode and cathode sides. Rct of MEAs was reduced at high operation pressure when compared to low pressure of gases. It can also be seen from this figure that the amounts of Rmt of both MEA-1 and MEA-2 have been enhanced with the increase of the operating pressure from 15 psi to 25 psi. This problem is most likely due to more water covering active catalyst surface, which fills the pores and blocks gas channels.

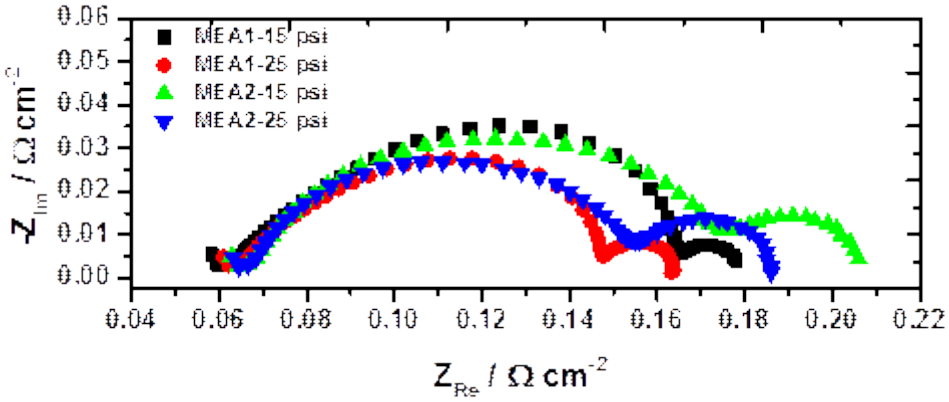

Figure 4: Nyquist plots of MEA 1 and 2 at 0.5 V under 15 psi and 25 psi pressure of gases and 30% of RH.

Conclusion

Two identical MEAs were affected by using two techniques: potential cyclic, external humidity injection protocol. The performance and EIS response of the both MEAs were evaluated under two operation conditions: 15 psi and 25psi pressure, 30% and 50% relative humidity.

Different pre-conditioning methods create different MEA performance and EIS response in H_2/O_2 mode.

Different pre-conditioning methods not only create irreversible effect but also caused different MEA performance and EIS response in H_2/O_2.

Potential cyclic is not an effective procedure compared to external humidity injection to reach to the maximum performance of MEA.

Reference

[1] Dincer I. Technical, environmental and exergetic aspects of hydrogen energy systems. International Journal of Hydrogen Energy. 2002;27:265-85.

[2] Khajeh-Hosseini-Dalasm N, Kermani MJ, Moghaddam DG, Stockie JM. A parametric study of cathode catalyst layer structural parameters on the performance of a PEM fuel cell. International Journal of Hydrogen Energy. 2010;35:2417-27.

[3] Parrondo J, Mijangos F, Rambabu B. Platinum/tin oxide/carbon cathode catalyst for high temperature PEM fuel cell. Journal of Power Sources. 2010;195:3977-83.

[4] Park S, Lee J-W, Popov BN. A review of gas diffusion layer in PEM fuel cells: Materials and designs. International Journal of Hydrogen Energy. 2012;37:5850-65.

[5] Mitzel J, Arena F, Natter H, Walter T, Batzer M, Stefener M, et al. Electrodeposition of PEM fuel cell catalysts by the use of a hydrogen depolarized anode. International Journal of Hydrogen Energy. 2012;37:6261-7.

[6] Huang T-H, Shen H-L, Jao T-C, Weng F-B, Su A. Ultra-low Pt loading for proton exchange membrane fuel cells by catalyst coating technique with ultrasonic spray coating machine. International Journal of Hydrogen Energy. 2012;37:13872-9.

[7] Mollá S, Compañ V, Gimenez E, Blazquez A, Urdanpilleta I. Novel ultrathin composite membranes of Nafion/PVA for PEMFCs. International Journal of Hydrogen Energy. 2011;36:9886-95.
[8] Akbarian-Feizi L, Mehdipour-Ataei S, Yeganeh H. Survey of sulfonated polyimide membrane as a good candidate for nafion substitution in fuel cell. International Journal of Hydrogen Energy. 2010;35:9385-97.
[9] Bonifácio RN, Paschoal JOA, Linardi M, Cuenca R. Catalyst layer optimization by surface tension control during ink formulation of membrane electrode assemblies in proton exchange membrane fuel cell. Journal of Power Sources. 2011;196:4680-5.
[10] Bose AB, Shaik R, Mawdsley J. Optimization of the performance of polymer electrolyte fuel cell membrane-electrode assemblies: Roles of curing parameters on the catalyst and ionomer structures and morphology. Journal of Power Sources. 2008;182:61-5.
[11] Wang L, Husar A, Zhou T, Liu H. A parametric study of PEM fuel cell performances. International Journal of Hydrogen Energy. 2003;28:1263-72.
[12] Yan X, Hou M, Sun L, Liang D, Shen Q, Xu H, et al. AC impedance characteristics of a 2 kW PEM fuel cell stack under different operating conditions and load changes. International Journal of Hydrogen Energy. 2007;32:4358-64.
[13] Wasterlain S, Candusso D, Hissel D, Harel F, Bergman P, Menard P, et al. Study of temperature, air dew point temperature and reactant flow effects on proton exchange membrane fuel cell performances using electrochemical spectroscopy and voltammetry techniques. Journal of Power Sources. 2010;195:984-93.
[14] Qi Z, Kaufman A. Enhancement of PEM fuel cell performance by steaming or boiling the electrode. Journal of Power Sources. 2002;109:227-9.

8th Iranian Fuel Cell Seminar
FEBRUARY 25,26
2015

Performance of Membrane-Electrode Assembly in the PEMFC under the Constant Voltage Procedure

Somayeh Majidi*, Hussein Gharibi
Department of Chemistry, Tarbiat Modarres University, P.O. Box 14155-4838, Tehran, Iran
** s.majidi@ch.iut.ac.ir*

Abstract
The present study aims at obtaining a better understanding on the changes that the membrane electrode assembly (MEA) of a proton exchange membrane fuel cell (PEMFC) experiences along time under voltage control procedure. Constant voltage 0.6 V was set-up at 55 ^{o}C. After every hour, the electrochemical characterization was performed using polarization curves, and electrochemical impedance spectroscopy (EIS). Polarization curves showed an effective increase of the MEA performance along time, with the maximum power density increasing from 1141 mW to 1481 mW. From the impedance experiments it was observed that the proton exchange membrane (PEM) and the charge transfer resistances decrease with time.

Keywords: Constant voltage procedure, Membrane-electrode assembly, PEM fuel cell

Introduction

Among the various types of fuel cells, polymer electrolyte membrane fuel cells (PEMFCs) are in the forefront stage, drawing much attention in both fundamental research and industrial applications in recent years [1]. The key component that determines the performance of a PEMFC is its membrane electrode assembly (MEA). One very effective procedure to enhance performance is to activate the MEA. Not only humidification of the proton exchange membrane occurs with time, but also transport channels creates for electrons, protons, gases and water. During time also the electrode structure is optimized [2] and the activity and utilization of the catalyst is improved by opening “dead” regions in this layer [3]. As a result, the performance of a newly fabricated PEMFC greatly increases to its maximal value and guarantees its reproducibility. Various approaches have been investigated to maximize fuel cell performance and shorten the time. Techniques explored include current control [4,5], potential control [6,7]. Murthy et al. [8] recommended monitoring a fuel cell’s output current density at 0.6 V and recording it as a function of time during the application of a given conditioning procedure. Silva et al. applied a procedure setup considering six loading cycles [9]. After each loading cycle, the electrochemical characterization was performed using polarization curves, linear sweep voltammetry, cyclic voltammetry, and electrochemical impedance spectroscopy (EIS). In this study, we present a systematic investigation of the MEA performance with time. Constant voltage procedure at 0.6 V was chosen [10] and applied to the MEA. The performance of the PEMFC was investigated with time by electrochemical techniques such as polarization curves and EIS.

Experiment

The MEAs consisted of a Nafion 212 membrane and two gas diffusion electrodes. Anode and cathode gas diffusion medium were constructed using 30 wt.% PTFE and 70 wt.% carbon

particles (Vulcan XC72R) in 2-propanol (Merck) and water. The mixture was sonicated for 20 min by using a sonicator (Misonix Model S-3000) to prepare a homogeneous suspension [26,27]. The suspension was then deposited onto teflonized carbon paper TGPH-060T (Toray), and the electrode was dried in air at 120 ^{o}C for 1 h and finally sintered at 350 ^{o}C for 30 min. The amount of MPL in each electrode was fixed at 1 mg/cm^{2}. The anode and cathode catalyst ink were prepared by directly mixing Pt/C (20% wt. Pt) with a required amount of solvent and Nafion solution (5% wt. solution, Electrochem Inc.). The catalyst ink was deposited on the surface of the membrane. The Pt loadings on both the anode and cathode were 0.4 mg cm^{-2}. Active area of MEAs was 4 cm^{-2}.

All experiments were conducted on a fuel cell test station (Fuel Cell Test System Model150s). Polarization curve was obtained by scanning of the cell voltage from OCV to 250 mV. Impedance spectra were also recorded over the frequency range from 10 kHz to 10 mHz. The Nyquist plots were recorded at 0.7, 0.5, and 0.3 V every 1-h along the time.

Pure and fully humidified hydrogen and oxygen were used in anode and cathode sides. Cell temperature was 55 °C. The cathode and anode gas pressure were 34 kPa.

Results and Discussion

Polarization curves provide a good insight about the evolution and quantification of the fuel cell performance. Current densities at 0.9 V, 0.6 V and 0.3 V of the MEA at different instants of constant voltage procedure were extracted from polarization curves and listed in table 1. Constant voltage procedure was stopped after 9 hours because changes in the polarization curves became negligible.

The kinetic zone (low current densities) of the polarization curve is related with reaction kinetic limitations. It can be seen from table 1 that at 0.9 V (low current density) the cell power change slightly after the first hours. It can be concluded that the catalyst area available to promote electrochemical reactions increases along the time and that increase is more significant for the first hours. The middle current densities of the current density-potential curves is related with ohmic losses, the main portion results from the resistance to the proton transport through the PEM. It can be observed from table 1, the cell power at 0.5 V increases with time due to the successive slope reduction associated to the ohmic zone. Additionally, a decrease on the PEM resistance will be also confirmed by the impedance experiments.

Table 1: Cell power values at 0.9 V, 0.6 V and 0.3 V of the MEA at different instants under constant voltage procedure.

	1 h	**3 h**	**5 h**	**7 h**	**9 h**
P (mW) at 0.9 V	305	314	444	447	458
P (mW) at 0.6 V	1108	1211	1365	1418	1443
P (mW) at 0.3 V	825	942	1129	1182	1213

From table 1 it can also be observed that a significant power density increase occurs, from 116.1 mW·cm^{-2} in the first hour to 229.9 mW·cm^{-2} in the last one.

Several impedance spectra at different operating voltages were recorded for each time during constant voltage procedure. This procedure allows evaluating the relevant impedance parameters that quantify the potential losses with time at low and moderate current densities. From figure 1 it can be seen that with time, the Nyquist plots show one arcs, which are associated to the dynamics of the charge transfer. The intersection of the imaginary impedance with the real impedance reflects the solution resistance.

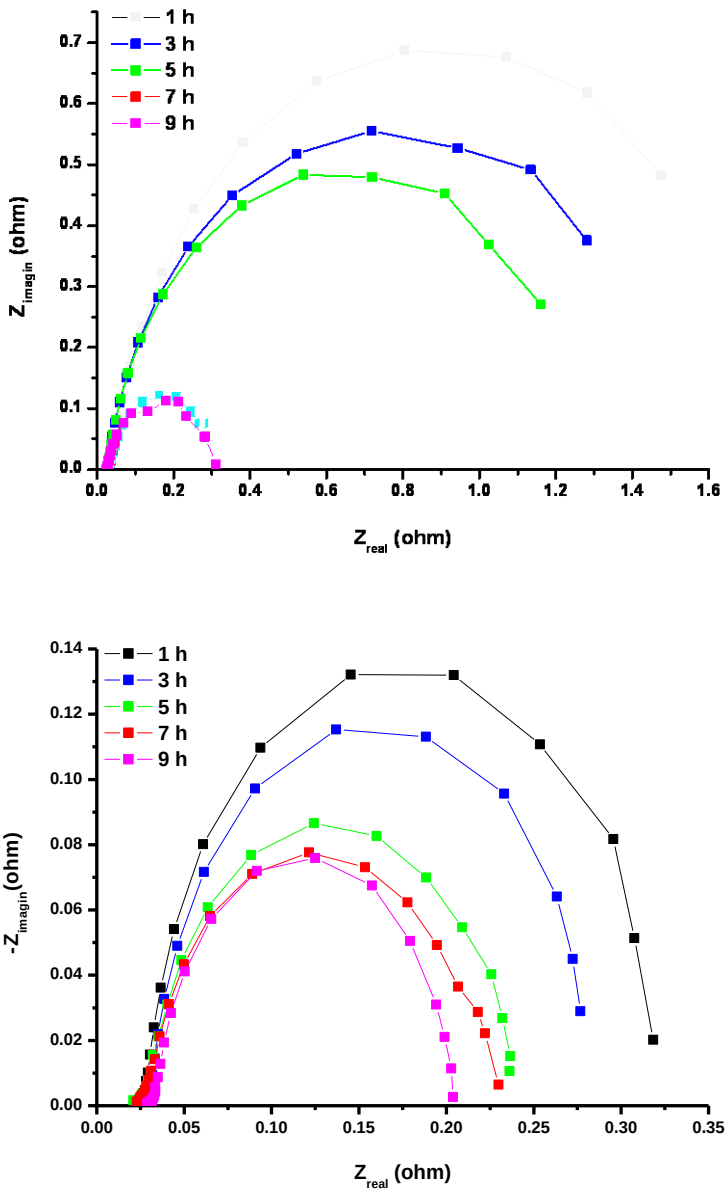

Figure 1: Nyquist plots at different instants of constant voltage 0.6 V procedure, 1, 3, 5, 7 and 9 h at OCV (a) and 0.5 V (b).

It should be pointed out that as the current density increases, the radius of cathode related semicircle decreases, reflecting the increasing driving force for the reduction reaction. It was also observed that the solution resistance changes slightly in a range between OCV and 300 mV. From figure 1 it can be seen that the PEM resistance slightly decreases with time. So, it can be inferred that proton species become much more easily transported across the PEM with time. It is widely accepted that the Nafion proton conductivity and water content are strongly related, obeying to a linear relationship at room temperatures [11]. Constant voltage 0.6 V enable the

PEM to increase its hydration level, favoring this way the protons transport and consequently the power output demands. From figure 1, it also can be seen that, as expected, the charge transfer resistance decreases with time during the constant voltage 0.6 V. The charge transfer resistance is related with the electrochemical reactions that occur at the interface of the PEM and the catalyst layer.

Conclusion

The in-house MEA was applied under constant voltage procedure at 0.6 V and studied by polarization curves and electrochemical impedance spectroscopy. Results indicated that the MEA performance was improved with time. Solution resistance was decreased during the constant voltage process due to the enhancement of the membrane hydration level and the catalyst activity was increased because of impurities removal from the catalyst surface.

Acknowledgment

The support of the Hydrogen & Fuel Cell Laboratory of Tarbiat Modarres University is acknowledged.

References

[1] Mert S.O., Dincer I., Ozcelik Z., “Performance investigation of a transportation PEM fuel cell system”, Int J Hydrogen Energy (2012). 37, 623-33.
[2] Zhu, K., Chen, Y., Han, Z., Zhang, J., Sun, Y., Chinese Journal of Power Sources 26 (2002) 267–269.
[3] Qi, Z., Kaufman, A., “PEM fuel cell PtC dissolution and deposition in Nafion electrolyte”, J Power Sources (2002).111, 181-184.
[4] Bi, W., “PEM fuel cell PtC dissolution and deposition in Nafion electrolyte”, Electrochem. Solid-State Lett (2007). 10, B101-B104.
[5] Shan, J., Yan, X., Sun, X., Hou, Z., Qi, P., Ming, P., “A fast activation method for a fuel cell stack, Chinese Patent, 201010010014.3 (2010).
[6] Lim, T.W., Kim, S.H., Ahn, S.Y., Hong, B.K., Ahn, B.K., “System and method for activating fuel cell, US 2010/0129689 Al, 2010.
[7] Weng, F.-B., Jou, B.-S., Su, A., Chan, S.H., Chi, P.-H., “Design, fabrication and performance analysis of a 200 kW PEM fuel cell short stack”, J. Power Sources (2007). 171, 179-185.
[8] Murthy, M., Sisofo III, N.T., Baczowski, C.A., “Method and device to improve operation of a fuel cell, US 2006/0166051 A1.
[9] Silva, V.B., Rouboa, A., “Hydrogen-fed PEMFC: overvoltage analysis during an activation procedure”, J Electroanal Chem (2012). 671, 58-66.
[10] Zhiani M., Majidi S., Taghiabadi M.M., “Comparative study of on-Line membrane electrode assembly activation procedures in proton exchange membrane fuel cell”, Fuel cells J (2013). 13, 946-55.
[11] Springer, T. E., Zawodzinski T. A., Gottesfeld, S., “Characterization of polymer electrolyte fuel cells using AC impedance spectroscopy”, J Electrochem Soc (1996). 143, 587-99.

8th Iranian Fuel Cell Seminar
FEBRUARY 25,26
2015

Investigation of Electrochemical Impedance Spectroscopy Response of Membrane-Electrode Assembly with Time in the PEMFCs

Somayeh Majidi, Mohammad Zhiani*
Department of Chemistry, Isfahan University of Technology, Isfahan 84156- 83111, Iran
** m_zhiani@cc.iut.ac.ir*

Abstract
The main objective of this study is to understand comprehensively of the impedance behavior of the polymer electrolyte membrane fuel cell (PEMFC) with time under a standard membrane-electrode assembly (MEA) procedure. A procedure was developed by US fuel cell council (USFCC) which contain a combination of constant current and voltage control and cyclic potential processes. The impedance response of MEA was evaluated by the electrical model. Based on the impedance spectra, charge transfer resistance (R_{ct}), mass transfer resistance (R_{mt}) and solution resistance (R_s) were extracted using expanded Randle's analogous circuits. Results indicated that the proton conductivity of the PEM, catalyst area and activity and transportation of reactants to the catalyst surface increase with time.

Keywords: Electrochemical impedance spectroscopy, Membrane-electrode assembly, PEM fuel cell

Introduction

Proton exchange membrane fuel cells (PEMFCs) are promising alternative power sources for various applications due to their high power densities and environmental benefits [1]. Typically, the cell performance increases gradually with time before reaching the steady state. Procedures can be applied during the start-up or after resting periods (restarting).

Murthy et al. [2] recommended monitoring a fuel cell's output current density at 0.6 V and recording it as a function of time during the application of a given conditioning procedure. Yuan et al. investigated constant voltage 0.6 V method [3]. They found (i) higher temperature is more effective in obtaining a high performance, (ii) open circuit voltage relaxation and more cycling steps are not very helpful in accelerating the process, and (iii) higher cycling frequency may reduce the activation time, but is soon followed by degradation. Applying a constant current to condition a fuel cell was also studied with direct methanol fuel cells (DMFCs). Kim et al. [4] investigated the performance of a DMFC (Pt/C for the cathode and PtRu/C for the anode) with time using an impedance technique.

This paper analyzes the behavior of a membrane electrode assembly (MEA) as a function of time along a procedure aiming to understand how this procedure affects the PEM and the catalyst. We present a systematic investigation of the MEA electrochemical impedance response with time. US fuel cell council (USFCC) test protocol [5,6] which contain a combination of constant current and voltage control and cyclic potential procedures was chosen and applied to the MEA. The impedance response of the PEMFC was investigated by an electrical model. Along the time, MEA experiments significant changes that are studied by electrochemical impedance spectroscopy (EIS).

Experiment

The MEAs consisted of a Nafion 212 membrane sandwiched between two gas diffusion electrodes. The anode and cathode catalyst ink were prepared by directly mixing Pt/C (20% wt. Pt, BASF) with a required amount of solvent and Nafion solution (5% wt. solution, EW1000, Aldrich). The catalyst ink was deposited on the surface of the diffusion medium including carbon paper with microporous layer. The Pt loadings on both the anode and cathode were 0.4 mg cm^{-2}. All experiments were conducted on a fuel cell test station (Scribner, 850e).

Pure and fully humidified hydrogen and oxygen were used in anode and cathode sides. Cell temperature was 55 °C. The cathode and anode pressure were 34 kPa. MEA was conditioned by constant current and voltage control and cyclic potential procedures that take 19 h. The MEA performance was investigated every 1-hour by electrochemical impedance spectroscopy. EIS experiments have been carried out at 0.7 V and 0.3 V.

Results and Discussion

USFCC standardized test protocols are widely used by researchers. In this study USFCC protocol which was established in 2007, was applied for conditioning of the MEA. This procedure consists of three steps that mentioned in the experimental section. All obtained EIS plots are shown in figure 1.

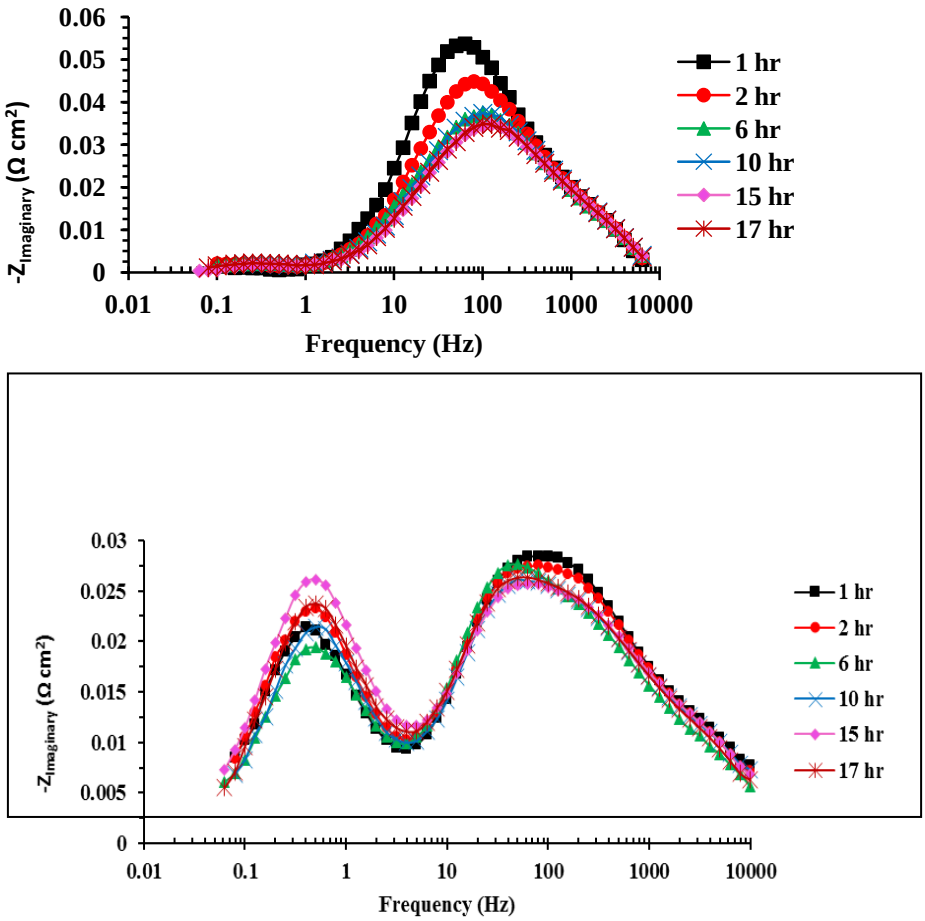

Figure 1: Representation of the impedance versus frequency at different instants of USFCC protocol, 1, 2, 6, 10, 15 and 17 h, at (a) 0.7 V and (b) 0.3 V.

Based on the impedance spectra, charge transfer resistance (R_{ct}), mass transfer resistance (R_{mt}), and R_s can be extracted using two equivalent circuits set up, corresponding to one and two arcs in figure 1a and 1b, respectively [7], where CPE represents the constant phase element. Impedance spectra were fitted by Zview software. The equivalent circuit parameters are listed in table 1. The time constant τ of a particular physical or chemical phenomenon corresponds to the frequency peak of the corresponding arc in the impedance spectra [8]. In table 1**,** τ_{kin} and τ_{dif} are attributed to the time constant of charge and mass transfer processes in the electrode, respectively.

Table 1: Resistance analysis of MEA as a function of time at different instants of USFCC protocol, 1, 2, 6, 10, 15 and 17 h at 55 °C

Voltage	**Parameters**	**Instants times**					
		1	**2**	**6**	**10**	**15**	**17**
0.3	R_{ct} (mΩ)	123	120	117	117	118	117
	CPE1 (mF)	140	145	170	163	170	164
	R_{mt} (mΩ)	50	54	49	47	60	59
	CPE2 (mF)	8452	7387	8254	7691	6318	7068
	τ_{kin} (ms)	15.8	15.8	25.1	25.1	20	20
	τ_{dif} (ms)	3160	2510	2510	2510	2510	2510
	R_s (mΩ)	120	110	92	90	85	85
0.7	R_{ct} (mΩ)	161	136	122	120	113	113
	CPE1 (mF)	51	49	57	53	54	53
	τ_{kin} (ms)	15.8	12.6	10	10	10	10

Table 1 show that a significant charge resistance decrease at 0.7 V occurs from 161 mΩ in the first hour up to 131 mΩ in the last one. Results also indicated that τ_{kin} was decreased along time, suggesting the increase in the rate of oxygen reduction reaction [9].
R_{mt} at 0.3 V was increased at the first 2-h. However, the value of R_{mt} was decreased, after 6-h, along the constant current procedure because water flooding is not occurred at low current density. Results indicated that τ_{diff} was decreased with time, suggesting improvement in the transportation of the reactants to the catalyst surface [10]. Table 1 also show that R_s was decreased with time due to the enhancement of the membrane hydration level [11].

Conclusion

MEA was conditioned using USFCC protocol and studied by EIS technique. EIS spectra were evaluated by electrical circuits and various resistances were extracted using zview software. Results indicated that charge and mass transfer resistance were decreased with time. Solution resistance was decreased with time due to the enhancement of the membrane hydration level and the catalyst activity was increased because of impurities removal from the catalyst surface. The extent of resistance reduction was dependent on the cell voltage along the time.

Acknowledgment
The support of Isfahan University of Technology is acknowledged.

References

[1] Dincer I. “Technical, environmental and exergetic aspects of hydrogen energy systems”, Int J Hydrogen Energy (2002). 27, 265-85.
[2] Murthy, M., Sisofo III, N.T., Baczowski, C.A., Method and device to improve operation of a fuel cell, US 2006/0166051 A1.
[3] Yuan, X., Sun, J. C., Wang, H., Li, H., “Accelerated conditioning for a proton exchange membrane fuel cell”, J Power Sources (2012). 205, 340-4.
[4] Kim, J.-H., Lee, H.-I., Bae, B., Ha, H.Y., Electrochemical analysis of the preconditioning effects on DMFC performance, ECS abstract.
[5] Yuan, X.Z., Zhang, S., Sun, J.C., Wang, H., “A review of accelerated conditioning for a polymer electrolyte membrane fuel cell”, J Power Sources (2011). 196, 9097-106.
[6] USFCC single cell test protocol, Available at http:// www.fchea.org,2007.
[7] Yuan X.Z., Song C., Wang H., Zhang J., “Electrochemical impedance spectroscopy in PEM fuel cells”, Springer, (2009).
[8] Brunetto, C., Moschetto, A., Tina, G., “PEM fuel cell testing by electrochemical impedance spectroscopy”, Electr Pow Syst Res (2009). 79, 17-26.
[9] Silva, V.B., Rouboa, A., “Hydrogen-fed PEMFC: overvoltage analysis during an activation procedure”, J Electroanal Chem (2012). 671, 58-66.
[10] Zhiani M., Majidi S., Taghiabadi M.M., “Comparative study of on-Line membrane electrode assembly activation procedures in proton exchange membrane fuel cell”, Fuel cells J (2013). 13, 946-55.
[11] Zhiani M., Majidi S., “Effect of MEA conditioning on PEMFC performance and EIS response under steady state condition”, Int J Hydrogen Energy (2013). 38, 9819-25.

8th Iranian Fuel Cell Seminar
FEBRUARY 25,26
2015

Analysis of Membrane-Electrode Assembly Performance with Time in the PEMFC

Somayeh Majidi, Mohammad Zhiani*
Department of Chemistry, Isfahan University of Technology, Isfahan 84156- 83111, Iran
** m_zhiani@cc.iut.ac.ir*

Abstract
The main objective of this work is to extract information on the internal behavior of the polymer electrolyte membrane fuel cell with time under a standard membrane-electrode assembly (MEA) procedure. A procedure was developed by US fuel cell council (USFCC) which contain a combination of constant current and voltage control and cyclic potential processes. The MEA performance was evaluated by the analytical model with time. Results indicated that the oxygen reduction kinetic is improved with time, especially in the first few hours. The results also show that ohmic and concentration polarizations are decreased with time. The extent of this reduction depends on the applied voltage or current with time.

Keywords: Performance analysis, Membrane-electrode assembly, PEM fuel cell

Introduction

A newly fabricated PEMFC needs a period to be conditioned, and reach to its best performance. Possible theories have been put forward to explain this phenomena: removal of impurities introduced during the process of manufacturing the MEA, activation of a catalyst that does not participate in the reaction, creation of a transfer passage for reactants to the catalyst [1] and hydration of the membrane and ionomer in catalyst layer [3].

Yuan et al. investigated constant voltage 0.6 V method [4]. They found (i) higher temperature is more effective in obtaining a high performance, (ii) open circuit voltage relaxation and more cycling steps are not very helpful in accelerating the process, and (iii) higher cycling frequency may reduce the activation time, but is soon followed by degradation. Silva et al. applied a procedure setup considering six loading cycles [5]. After each loading cycle, the electrochemical characterization was performed using polarization curves, linear sweep voltammetry, cyclic voltammetry, and electrochemical impedance spectroscopy (EIS).

In this study, we present a systematic investigation of the MEA performance with time. US fuel cell council (USFCC) test protocol [6] which contain a combination of constant current and voltage control and cyclic potential procedures was chosen and applied to the MEA. The performance of the PEMFC was investigated by an analytical model.

Experiment

The MEAs consisted of a Nafion 212 membrane sandwiched between two gas diffusion electrodes. The anode and cathode catalyst ink were prepared by directly mixing Pt/C (20% wt. Pt, BASF) with a required amount of solvent and Nafion solution (5% wt. solution, EW1000, Aldrich). The catalyst ink was deposited on the surface of the diffusion medium including

carbon paper with microporous layer. The Pt loadings on both the anode and cathode were 0.4 mg cm^{-2}. All experiments were conducted on a fuel cell test station (Scribner, 850e). Polarization curve was obtained by scanning of the cell voltage from OCV to 250 mV.
Pure and fully humidified hydrogen and oxygen were used in anode and cathode sides. Cell temperature was 55 °C. The cathode and anode gas pressure were 34 kPa pressure. MEA was conditioned by constant voltage, cyclic potential and constant current procedures that take 19h.

Results and Discussion

USFCC standardized test protocols are widely used by researchers. In this study USFCC protocol which was established in 2007, was applied for conditioning of the MEA. This procedure consists of three steps that mentioned in the experimental section. The MEA performance was investigated every 1-hour during time by i-V curves. In order to obtain comprehensive details for the MEA performance, i-V curves were used in estimating the parameters of a completely analytical model. The model describes the i-V curve with the following equation:

$$V = E_{th\,(PO2,\,PH2,\,T)} - \square_{kin} - \square_{ohm} - \square_{mt} \quad (1)$$

Where V is the real output voltage; E_{thermo} is the thermodynamically predicted voltage; $\square_{kin}$ is the kinetic loss on the cathode; $\square_{ohm}$ is the ohmic loss, and $\square_{mt}$ is the concentration loss on the cathode.The kinetic loss is described by the Tafel equation where a and b are constant experimental parameters [7].

$$\square_{kin}=a+b\ ln(i) \quad (2)$$

The ohmic loss is due to both ionic and electronic resistances within the fuel cell and is expressed as [7]:

$$\square_{ohm}=iR_{ohm} \quad (3)$$

The voltage loss caused by mass transport limitation is expressed by the following theoretical equation where c and d are parameters that have to be evaluated experimentally [7].

$$\square_{mass}=c\ Ln\ (d\ /\ (d-i)) \quad (4)$$

For the applied activation condition, the thermodynamic potential, E_{thermo}, was calculated to be 1.21 V from the modified Nernst equation which takes into account both temperature and pressure values according to [8].
R_{ohm} was obtained when current interrupt testing was implemented on a MEA at each voltage during voltage sweeping in the polarization curve measurements [9]. The obtained ohmic loss values versus current density at different instants (1, 2, 6, 10, 15, and 16 h) during activation procedure are shown in Fig. 1.
According to $\square_{ohmic}$ and E_{thermo} values, the experimental i-V data at different instants (1, 2, 6, 10, 15, and 16 h) during activation procedure were fitted into Equation (1). Fitting was performed using simulated annealing and Broyden-Fletcher-Goldfarb-Shanno (BFGS) optimization algorithms [10]. Fig. 2 and 3 show the predicted kinetic and concentration losses versus current density, respectively.

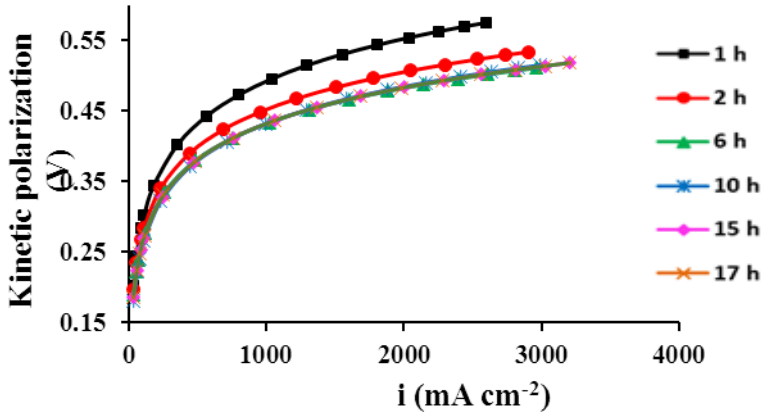

Figure 1: Kinetic polarization versus current density at different instants of USFCC protocol, 1, 2, 6, 10, 15 and 17 h at 55 °C.

Figure 1 show that kinetic polarization was decreased along time. The most extent of kinetic polarization reduction occurred at the first 2-h. While, the value of kinetic loss was constant after 6-h. These results show that catalyst activation occurred during the first 6-h. Low constant current density procedure (final step of USFCC procedure) was not a suitable method for catalyst conditioning at least for a short time.

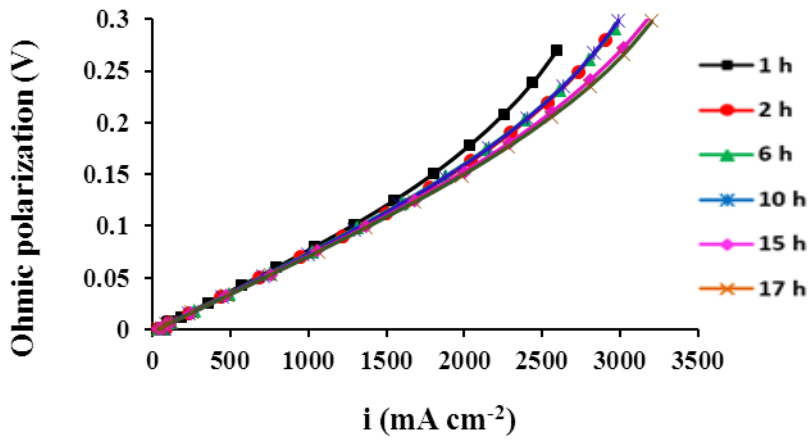

Figure 2: Ohmic polarization versus current density at different instants of USFCC protocol, 1, 2, 6, 10, 15 and 17 h at 55 °C.

Figure 3 show that ohmic polarization was decreased with time due to the enhancement of the membrane hydration level and the catalyst activity.
Figure 2 indicates that curves overlapped during first 6-h. In other words, concentration loss did not change during constant and cyclic voltage procedures. Concentration polarization decreased along the constant current procedure because water flooding is not occurred at low current density. The amount of concentration loss reduction is significant at high current density, about 40 mV.

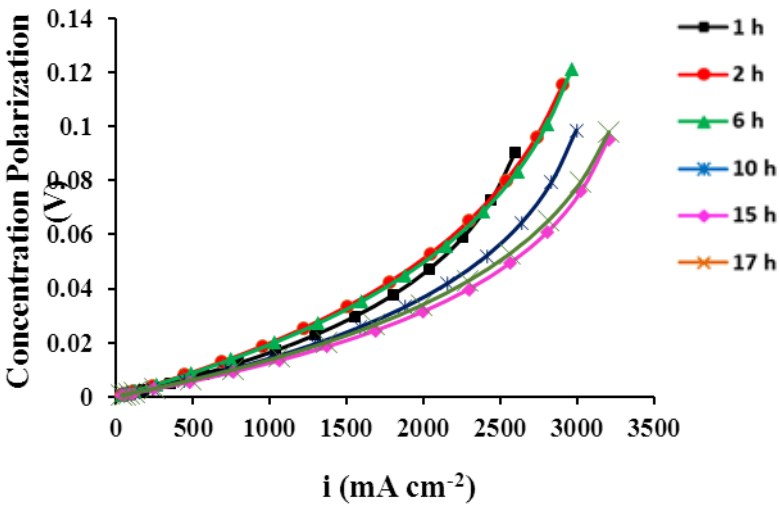

Figure 3: Concentration polarization versus current density at different instants of USFCC protocol, 1, 2, 6, 10, 15 and 17 h at 55 °C.

Conclusion

MEA was activated using USFCC protocol and studied by i-Vs polarization curves. i-V curves were evaluated by an analytical model and parameters attributed to different voltage losses were extracted. Results indicated that kinetic, ohmic and concentration polarization were decreased with time. The extent of polarizations reduction was dependent on the cell voltage along the time.

Acknowledgment

The support of Isfahan University of Technology is acknowledged.

References

[1] Lim, T.W., Kim, S.H., Ahn, S.Y., Hong, B.K, Ahn, B.K., “System and method for activating fuel cell”, US patent 0129689 Al, (2010).
[2] Hallum, R., “Preconditioning membranes of a fuel cell stack”, US Patent 6576356 B1, (2003).
[3] Ren, X., Wilson, M.S., Gottesfeld, S., “High performance direct methanol polymer electrolyte fuel cells”, J Electrochem Soc, (1996). 143, 12-15.
[4] Yuan, X., Sun, J. C., Wang, H., Li, H., “Accelerated conditioning for a proton exchange membrane fuel cell”, J Power Sources, (2012). 205, 340-4.
[5] Silva, V.B., Roubo, A., “In situ activation procedures applied to a DMFC: Analysis and optimization study”, Fuel (2012). 93, 677-83.
[6] USFCC single cell test protocol, Available at http:// www.fchea.org,2007.
[7] Barbir, F., PEM fuel cells (theory and practice). Elsevier Academic Press, (2005).
[8] Cooper, K. R., Smith, M., “Electrical test methods for on-line fuel cell ohmic resistance measurement”, J. Power Sources (2006). 160, 1088-1096.
[9] Larminie, J.R.J., “Current interrupt techniques for circuit modelling”, IEE Colloquium on Electrochemical Measurement, (1994).
[10] Teukolsky, W.H., Vetterling, S.A., Flannery, W.T., “Numerical Recipes: The Art of Scientific Computing”, Cambridge University Press, New York, (2007).

8th Iranian Fuel Cell Seminar
FEBRUARY 25,26
2015

Exploring of the Oxygen Reduction Reaction on the Gas Diffusion Electrode for Zinc Air Fuel Cell

Parisa Akbarian*, Mehdi Kheirmand
Department of Chemistry, Yasouj University, Yasouj, Iran
** Akbarian_parisa@yahoo.com*

Abstract
In this study, a three-layer gas diffusion electrode was made according to the second layer was made of a mixture of carbon black and Teflon with the ratio of 70:30 on a 200µm silver mesh. The third layer that cased of diffusion layer was made of platinum nano-clusters on carbon and Teflon suspension (with the 70:30 ratio). Finally the heat treated electrode was evaluated for oxygen reduction reaction in a three electrode configuration. The performance of electrode was considered in homemade zinc air fuel cell. The results showed that the open circuit voltage of cell was 1.346 V and at the voltage of 0.73 volt; the current density was 166.5 (mA/cm^2).

Keywords: Oxygen reduction reaction, Gas diffusion electrode, Zinc air fuel cell

Introduction

Metal-air fuel cells are electrochemical devices that directly convert the chemical energy stored in metals (e.g., Mg, Al or Zn) into electricity. Compared with hydrogen fuel cells, metal air fuel cells offer many advantages, including facile solid fuel storage, simple system structure and low cost. Due to these intrinsic merits, metal-air fuel cells have gained a great deal of attention and been regarded as promising power sources for application in mobile phones, lights, communication equipments and electric vehicles, etc. [1-5]. Atmospheric oxygen is the oxidant at the cathode of the proton exchange membrane fuel cells (PEMFC) and zinc–air fuel cells (ZAFC) [6-7]. In the most commonly used cathode designs, the oxygen electrode is based on a three-phase reaction zone. Because oxygen is poorly soluble at atmospheric pressure, a three-phase reaction zone is required to provide oxygen in concentrations suitable for higher current densities.

The electrochemical reactions of zinc-air fuel cell can be described as follows [8]:

At the positive (cathode) electrode:

$O_2 + 2H_2O + 4e^- \rightarrow 4OH^-$, $E_0 = 0.40V$ (1)

At the negative (anode) electrode:

$2Zn \rightarrow 2Zn^{2+} + 4e^-$ (2)

$2Zn^{2+} + 4OH^- \rightarrow 2Zn(OH)_2$ $E_0 = -1.25V$ (3)

$2Zn(OH)_2 \rightarrow 2ZnO + 2H_2O$ (4)

Overall cell reaction:

$2Zn + O_2 \rightarrow 2ZnO$ $E_0 = 1.65V$ (5)

In ZAFC, zinc metal as an anode material is abundantly available, inexpensive, non-toxic, safe, and easy to handle and store. Air is an oxygen source to be supplied at the cathode side, while aqueous alkaline solution is an electrolyte. The advantages of zinc air fuel cell are using inexpensive materials of catalysts and separators, the high energy density, stable discharge

voltage and running at ambient temperature. Theoretical specific energy of zinc air cell based on the molecular weight of ZnO is 1085 Wh/kg and 1.65 volts for the theoretical cell voltage [9]. The Oxygen reduction reaction is one of the most important electrochemical reactions because it is the cathodic reaction in fuel cells and metal air batteries, during aerated media corrosion and in some industrial electrolytic processes. For these reasons, research efforts have been focused on developing a proper catalyst and elucidating the mechanism of this reaction [10-12].

Experimental

2.1. Cell Fabrication

The zinc-air fuel cell wrought of zinc anode, cathode and alkaline electrolyte. This Cell has made non-separator and simple.

2.1.1. Gas diffusion electrode fabrication

The zinc-air fuel cell comprised of zinc anode, alkaline electrolyte, and cathode.
Air electrode were fabricated in three layers, a waterproof diffusion layer on the air side and the active layer on the electrolyte side. The first layer is the gas diffusion layer which was made of carbon Vulcan, PTFE, 2-propanol and glycerin by mixing and was sonicated for 20 min until a homogeneous paste was obtained. Then, the above GDL Was placed in an oven at 80 $^{\circ}$C for 3 h, after it has dried for half an hour left in 80 $^{\circ}$C then put 20 min to 100 $^{\circ}$C and 30 min in 120 ºC. Then mesh up a quarter at 300 ºC and a quarter at 340 $^{\circ}$C has put in the oven to stabilized. The PTFE solution: carbon Vulcan ratio was 30:70.

For each electrode, an active layer (AL) was prepared by mixing 31.5 mg Pt/C, 13.5 mg polytetrafluorethylene powder (PTFE) as the hydrophobic catalyst binder, then 10 mL Millipore water and isopropyl alcohol 1:1. This catalyst ink was sonicated for 20 min to obtain a uniform mixture, which was then painted onto the micro porous side of a paper gas diffusion layer (GDL).
Finally these two layers were mobilized on a silver lace as third layer.

2.1.2. Anode

The metal zinc was used as the fuel anode. Anode was in direct contact with the electrolyte and cathode.

2.2. Zinc-air fuel cell test system

The flowing cell testing is focused on cell performance. Electrolyte applique 1.4 M KOH solution.

Results

The results showed that the open circuit voltage of cell was 1.346 V and at the voltage of 0.73 volt; the current density was 166.5 (mA/cm^2).

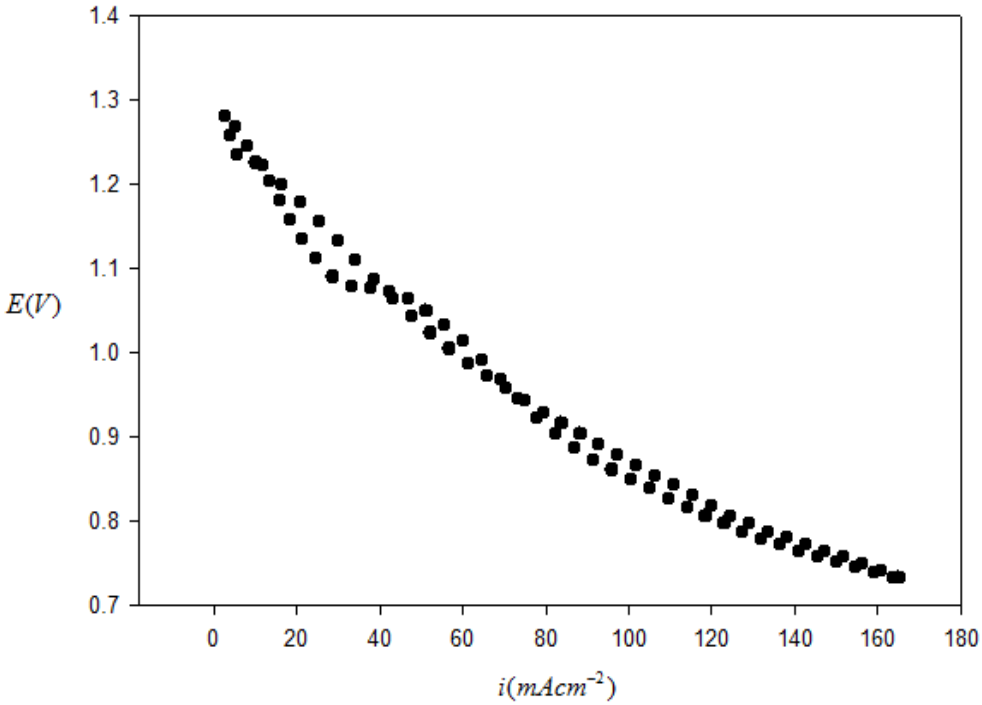

Figure 1. Polarization curve for the zinc-air fuel cell

Conclusions

The experimental study on the improvement of zinc - air fuel cell performance was carried out for non-separator cell. The Cell was made with a good insulation and no leakage was. As you can see from the results of the Cell performance is acceptable.

References

[1] Linden D, Reddy TB. Handbook of batteries. 3rd ed. New York: McGraw-Hill; (2002).
[2] JS. Lee, ST. Kim, RG. Cao, NS. Choi, ML. Liu, KT. Lee, et al. Metal-air batteries with high energy density: Li-air versus Zn-air. Ad Energy Mater, (2011). 1, 34.
[3] Q. Hasvold, H. Henriksen, E. Melvaer, G. Citi, BQ. Johansen, T. Kjqnigsen, et al. Sea-water battery for subsea control systems. J Power Sources. (1997). 65, 253.
[4] MG. Medeiros, RR. Bessette, CM. Deschenes, DW. Atwater. Optimization of the magnesium-solution phase catholyte semi-fuel cell for long duration testing. J Power Sources. (2001). 96, 236.
[5] Q. Hasvold, N. Stqrkersen. Electrochemical power sources for unmanned underwater vehicles used in deep sea survey operations. J Power Sources. (2001). 96, 252.
[6] D.T. Santa Rosa, D.G. Pinto, V.S. Silva, R.A. Silva, C.M. Rangel, High performance PEMFC stack with open-cathode at ambient pressure and temperature conditions, International Journal of Hydrogen Energy. (2007). 32, 4350.
[7] P. Sapkota, H. Kim, Zinc–air fuel cell, a potential candidate for alternative energy, Journal of Industrial and Engineering Chemistry. (2009). 15, 445.
[8] C.K. Yap, T W.C., S.S. Alias, and A.A. Mohamad. Synthesis of zinc oxide by zinc-air system. Journal of Alloys and Compounds. (2009). 484, 934.

[9] R. Othman, W.J. Basirun, A.H. Yahaya, and A.K. Arof. Hydroponics gel as a new electrolyte gelling agent for alkaline zinc air cells. Journal of Power Sources. (2001). 103, 34.
[10] S. Gottsfeld, T.A. Zawodzinski, Advances in Electrochemical science and Engineering. R. C. Alkire, D. M. Kolb, Eds. Vol 5. Wiley-VCH. Weinhim; (1997).
[11] M. R. Tarasevich. Electrokhimiya. (1973). 9, 599.
[12] P. N. Ross. J. Electrochem. Soc. (1979). 126, 78.

بهینه‌سازی جریان سیال در کانال‌های پیل سوختی اکسید جامد صفحه‌ای

رضا خندابی*، رفعت محمّدی

گروه مهندسی مکانیک، دانشگاه اراک
** reza.khondabi@yahoo.com*

چکیده

یکی از مشکلات پیل‌های سوختی اکسید جامد صفحه‌ای توزیع غیریکنواخت سوخت یا هوا در کانال‌های تعبیه‌شده برای عبور آن‌هاست که در نتیجه‌ی آن فرآیند الکتروشیمیایی ناقص انجام شده و ولتاژ تولیدی کاهش می‌یابد. از دیگر مشکلات این نوع پیل‌ها، بالابودن افت فشار سیال در کانال‌ها می‌باشد که باعث افزایش توان کمپرسورهای موردنیاز برای راندن سوخت و هوا در داخل این کانال‌ها و در نتیجه افزایش هزینه‌ی تجهیزات می‌شود. در این مقاله یک مدل محاسباتی برای شبیه‌سازی جریان سیال در شبکه‌ی کانال‌های پیل سوختی صفحه‌ای ارائه شده است. این مدل با منظور نمودن معادلات بقای جرم و مومنتوم، معیارهایی جهت پیش‌بینی افت فشار در هر کانال و برقراری جریان یکنواخت بین کانال‌ها و در نتیجه طراحی بهینه کانال‌ها ارائه می‌کند.

واژه‌های کلیدی: پیل سوختی، مدل‌سازی، شبکه‌ی کانال.

مقدمه

در سال‌های اخیر پیل‌های سوختی به عنوان یکی از تکنولوژی‌های تولید توان با آلایندگی پایین و بازدهی بالا مورد توجه قرار گرفته‌اند. در بین انواع پیل‌های سوختی، پیل‌های اکسید جامد از اهمیت ویژه‌ای برخوردار می‌باشند [۱].یکی از مشکلات این نوع پیل‌ها توزیع غیریکنواخت سوخت یا هوا در کانال‌های تعبیه‌شده برای عبور آن‌ها و در نتیجه فرآیند الکتروشیمیایی ناقص و کاهش ولتاژ تولیدی می‌باشد. مشکل دیگر بالابودن افت فشار سیال در کانال‌ها می‌باشد که باعث افزایش توان پمپ‌ها و کمپرسورهای موردنیاز برای راندن سوخت و هوا در داخل این کانال‌ها و در نتیجه افزایش هزینه‌ی تجهیزات می‌شود.

در تحقیقات مربوط به مدل‌سازی پیل سوختی مدل‌سازی‌های گسترده‌ای برای فهم عملکرد پیل سوختی انجام شده و می‌شود. ایواتا و همکاران [۲]، یک تحلیل جامع از سیستم پیل اکسید جامد صفحه‌ای ارائه کرده‌اند. بورسما و سامز [۳]، یک مدل برای پیش‌بینی جریان در پیل‌ها ارائه کرده‌اند؛ مدل آن‌ها بر پایه‌ی مقاومت هیدرولیک شبکه‌ها استوار است؛ نتایج حاصل از این مدل قابل تعمیم و کلی نمی‌باشند. در این مقاله یک مدل کلی برای طراحی کانال‌های با ابعاد مختلف ارائه می‌شود.

مواد و روش تحقیق

هندسه و معادلات حاکم

در این مقاله مدل‌سازی یک پیل سوختی اکسید جامد صفحه‌ای، در نظر گرفته شده است. محاسبات از نقطه نظر جریان در داخل یک تک لایه، مطرح می‌گردند. تحلیل مربوط به توده نیز مستقیماً از تحلیل لایه پیروی می‌کند. در تحلیل توده، لایه‌ها بخشی از کانال‌هایی در نظر گرفته می‌شود که در یک لایه‌اند و منیفولدها بخشی از هدرها در نظر گرفته می‌شوند. شکل ۱ بخشی از دو لایه پیل صفحه‌ای را نشان می‌دهد. این نوع پیل‌ها از لایه‌های تختی تشکیل شده‌اند که دارای کانال‌هایی برای عبور سوخت و هوا می‌باشند. میان این لایه‌ها آند، کاتد و الکترولیت قرار می‌گیرد. با عبور سوخت و هوا از این لایه‌ها فرآیند الکتروشیمیایی انجام می‌شود. مطابق شکل ۲، سوخت و هوا با عبور از منیفولدهای تغذیه بین لایه‌ها و سپس از طریق هدر تغذیه بین کانال‌ها توزیع می‌شوند و با عبور از کانال‌ها وارد هدر تخلیه و سپس از طریق منیفولد تخلیه از پیل خارج می‌شوند. فضای محاسباتی شامل کانال‌های عبوری، هدر تغذیه و تخلیه و منیفولد تغذیه و تخلیه‌ی سیال (سوخت یا هوا) می‌باشد. در این تحلیل کانال‌های جریان غیر قابل نفوذ در نظر گرفته شده‌اند؛ بدین صورت که از جریان جرم بین کانال‌های اکسیدایزر و سوخت صرفنظر شده است. از این رو چگالی جرمی، ثابت و جریان تراکم‌ناپذیر خواهد بود. علاوه بر این سایر خواص سیال (ویسکوزیته) نیز ثابت در نظر گرفته شده است. همچنین زمانی که سیال یک گاز باشد (هوا یا سوخت تبخیرشده) سرعت جریان خیلی کم و دما تقریباً یکنواخت خواهد ماند. معادلات جرم و مومنتوم به صورت پیوسته، یک‌بعدی و در راستای هدرهای تغذیه و تخلیه نوشته خواهند شد.

آهنگ جریان جرم در کانال

مطابق جریان پایای هایگن پوازی در یک کانال، برای بالانس کردن نیروی به وجود آمده از تنش برشی بین دیواره‌ها، یک تغییر فشار خالص لازم است.

((۱)

که p_{f} و p_{e} به ترتیب فشار در هدر تغذیه و هدر تخلیه را نشان می‌دهند. متغیر دیگر A_{c} می‌باشد که سطح مقطع کانال می‌باشد. P_{c}، محیط کانال و L_{c}، طول کانال می‌باشد.

آهنگ جریان جرم در کانال را می‌توان برحسب اختلاف فشار خالص ورودی و خروجی بدست آورد:

$$\dot{m}_{\mathrm{c}} = \left(\frac{1}{\mathrm{Re}f}\frac{D_{\mathrm{c}}^2 A_{\mathrm{c}}}{2L_{\mathrm{c}}}\frac{\rho}{\mu}\right)(p_{\mathrm{f}} - p_{\mathrm{e}}) = K_{\mathrm{c}}(p_{\mathrm{f}} - p_{\mathrm{e}}) \qquad (۲)$$

که D_{c} قطر هیدرولیک مقطع کانال، A_{c} سطح مقطع کانال، L_{c} طول کانال، ρ و μ به ترتیب چگالی جرمی و ویسکوزیته‌ی دینامیکی سیال، Re عدد رینولدز (بر اساس سرعت متوسط و قطر هیدرولیک)، f ضریب اصطکاک بی‌بعد، p_{f} و p_{e} به ترتیب فشار در هدرهای تغذیه و تخلیه را نشان می‌دهند. ثابت K_{c} نیز نسبت بین آهنگ جریان جرم در کانال و اختلاف فشار ورودی و خروجی را بیان می‌کند. در یک لایه $p_{\mathrm{f}}(z)$ و $p_{\mathrm{e}}(z)$ توابعی از مکان هستند؛ بنابراین براساس توزیع فشار در مسیرها، جریان جرم در هر کانال می‌تواند متفاوت باشد.

همانطور که گفته شد معادلات به صورت معادلات دیفرانسیلی پیوسته استخراج خواهند شد؛ بنابراین لازم است که آهنگ جریان جرم بین مسیرها به صورت یک متغیر پیوسته دوباره بازنویسی شود. آهنگ جریان جرم در واحد طول مسیر، می‌تواند به صورت زیر نوشته شود:

$$\dot{m}_i \quad (۳)$$

که A'_c سطح مقطع کانال در واحد طول مسیر هدر می‌باشد.

معادلات پیوستگی در هدرها

یک حجم کنترل دیفرانسیلی از یک هدر، مطابق شکل ۳، در نظر می‌گیریم. با استفاده از تئوری رینولدز و قانون کلی بقای جرم برای سیستم، معادله‌ی پیوستگی را می‌توان به صورت زیر نوشت:

$$\left(\frac{\mathrm{d}m}{\mathrm{d}t}\right) = \int_{\mathrm{CV}} \left(\frac{\partial \rho}{\partial t} + \boldsymbol{\nabla} \cdot \rho \boldsymbol{V}\right) \mathrm{d}V = \pm \int_{\mathrm{CS}} \dot{m}''_c \, \mathrm{d}A \quad (۴)$$

که $\dot{m}''_c$ شار جرم خارج‌شده از (و یا واردشده به) هدرها از طریق کانال‌های رابط می‌باشد. مساحتی که سیال از طریق آن، کانال را ترک می‌کند (نرمال بر هدر) برابر $\mathrm{d}A = A'_c \mathrm{d}z$ می‌باشد. مطابق شکل ۳ برای کانال مستطیلی، $A'_c = H_c$ می‌باشد. با تقسیم کردن حجم کنترل به طول دیفرانسیلی δz، انتگرال‌ها را می‌توان ثابت در نظر گرفت. با در نظر گرفتن $\delta V = A_h \delta z$ و فرض حالت پایا، جریان یک‌بعدی و تراکم‌ناپذیر رابطه‌ی ۴ به شکل زیر در می‌آید:

$$\frac{\mathrm{d}u}{\mathrm{d}z} = \pm \frac{A'_c}{\rho A_h} \dot{m}''_c = \pm \frac{\dot{m}'_c}{\rho A_h} \quad (۵)$$

با جایگذاری $\dot{m}'_c$ از رابطه‌ی ۳، معادله پیوستگی به شکل زیر در می‌آید:

$$\frac{\mathrm{d}u_h}{\mathrm{d}z} = \pm \frac{K'_c (p_f - p_e)}{\rho A_h} \quad (۶)$$

که اندیس $h = f$ مربوط به هدر تغذیه (با در نظر گرفتن علامت منفی در سمت راست معادله) و اندیس $h = e$ مربوط به هدر تخلیه (با در نظر گرفتن علامت مثبت در سمت راست معادله) می‌باشد.

معادلات مومنتوم در هدرها

در حالت کلی معادله‌ی مومنتوم به صورت زیر می‌باشد:

$$\left(\frac{\mathrm{d}\boldsymbol{P}}{\mathrm{d}t}\right)_{\mathrm{sys}} = \sum \boldsymbol{F} \quad (۷)$$

که متغیرهای این معادله بردار مومنتوم، $\boldsymbol{P} = m\boldsymbol{V}$ و $\boldsymbol{F}$، نیروی اعمال شده به سیستم می‌باشد. متغیر $\boldsymbol{V}$ نیز بردار سرعت می‌باشد. دو نیرو وجود دارد که باید در نظر گرفته شوند. یکی از نیروها ناشی از فشار اعمالی بر مقطع ناحیه‌ی دارای جریان و دیگری ناشی از ویسکوزیته‌ی سیال در تماس با دیواره‌ها می‌باشد. با فرض جریان پایدار و یک‌بعدی و اندکی محاسبات رابطه‌ی ۷ به شکل زیر بازنویسی می‌شود:

$$\int_{\mathrm{CV}} \frac{\partial(\rho u u)}{\partial z} \mathrm{d}V = \int_{\mathrm{CS}} \tau_z \,.\, \boldsymbol{n} \mathrm{d}A - \int_{\mathrm{CS}} \tau_{\mathrm{w}} \mathrm{d}A \tag{۸}$$

اولین انتگرال سمت راست رابطه‌ی ۸ مربوط به نیروی ناشی از تنش اعمالی بر سطح حجم کنترل در راستای جریان می‌باشد؛ در این مورد به طور کلی وابسته به فشار است، $\tau_z = -p$. دومین انتگرال مربوط به نیروی برشی در دیواره‌های کانال می‌باشد. می‌توان برای تبدیل اولین انتگرال سمت راست معادله به انتگرال حجمی از تئوری دیورژانس گائوس استفاده کرد. انتگرال دوم را نیز می‌توان در قالب طول دیفرانسیلی $\mathrm{d}z$، بازنویسی کرد.

$$\int_{\mathrm{CV}} \frac{\partial(\rho u u)}{\partial z} \mathrm{d}V = \int_{\mathrm{CV}} \boldsymbol{\nabla} \,.\, \tau_z \mathrm{d}V - \int_{z} \tau_{\mathrm{w}} P_{\mathrm{h}} \mathrm{d}z \tag{۹}$$

که P_{h} محیط کانال هدر می‌باشد (برای کانال مستطیل‌شکل، $P_{\mathrm{h}} = 2H_{\mathrm{h}} + 2W_{\mathrm{h}}$). با تقسیم حجم کنترل به اجزای خیلی کوچک δz رابطه‌ی ۹ برای جریان تراکم‌ناپذیر به شکل زیر در می‌آید:

$$2\rho u \frac{\mathrm{d}u}{\mathrm{d}z} + \frac{\mathrm{d}p}{\mathrm{d}z} + \frac{P_{\mathrm{h}}}{A_{\mathrm{h}}} \tau_{\mathrm{w}} = 0 \tag{۱۰}$$

در جریان داخل کانال می‌توان تنش برشی در دیواره، τ_{w}، را برحسب ضریب اصطکاکی، که وابسته به ابعاد هدر و خواص سیال می‌باشد، نوشت و در رابطه‌ی ۱۰ جایگذاری کرد،

$$2\rho u_{\mathrm{h}} \frac{\mathrm{d}u_{\mathrm{h}}}{\mathrm{d}z} + \frac{\mathrm{d}p_{\mathrm{h}}}{\mathrm{d}z} + \left(\frac{P_{\mathrm{h}}}{2A_{\mathrm{h}}D_{\mathrm{h}}} \mu \mathrm{Re} f \right) u_{\mathrm{h}} = 0 \tag{۱۱}$$

اندیس $\mathrm{h} = \mathrm{f}$ و $\mathrm{h} = \mathrm{e}$ بترتیب نمایانگر هدر تغذیه و تخلیه می‌باشد.

شرایط مرزی

معادلات پیوستگی و مومنتوم استخراج‌شده (روابط ۶ و ۱۱)، یک دستگاه معادله‌ی چهارگانه، حاوی معادلات دیفرانسیل معمولی، کوپل، غیرخطی و مرتبه اول را تشکیل می‌دهند. معادله‌ی آهنگ جریان جرم نیز یک معادله‌ی اضافی است. از آنجایی که تمام معادلات، معادلات دیفرانسیل معمولی مرتبه اول می‌باشند، هر کدام از آن‌ها یک شرط مرزی و در کل چهار شرط مرزی لازم دارند. مطابق شکل ۴، سرعت در انتهای بسته‌ی هدرها باید صفر باشد،

$$u_{\mathrm{f}}(L_{\mathrm{h}}) = 0 \,, \qquad u_{\mathrm{e}}(0) = 0 \tag{۱۲}$$

فشار منیفولد تخلیه می‌تواند به عنوان فشار مرجع، صفر در نظر گرفته شود. فشار در منیفولد تغذیه یک شرط مرزی از نوع ضمنی می‌باشد که در حین حل باید محاسبه گردد.

$$p_{\mathrm{f}}(0) = p_0 \,, \qquad p_{\mathrm{e}}(L_{\mathrm{h}}) = 0 \tag{۱۳}$$

بی‌بعد سازی

به منظور کلی‌سازی نتایج، می‌توان معادلات را برحسب متغیرهای بی‌بعد نوشت. مقیاس طول مرجع طول هدر، L_{h}، می‌باشد. سرعت مرجع سرعت متوسطی است که به هدر تغذیه وارد و از هدر تخلیه خارج می‌شود که از آهنگ جریان جرم لایه، $\dot{M}_{\mathrm{l}}$، بدست می‌آید.

$$U_{\mathrm{l}} = \frac{\dot{M}_{\mathrm{l}}}{\rho A_{\mathrm{h}}} \tag{۱۴}$$

فشار مرجع یک فشار دینامیکی برحسب سرعت مرجع می‌باشد.

$$p_{\mathrm{ref}} = \rho U_{\mathrm{l}}^2 = \frac{\dot{M}_{\mathrm{l}}^2}{\rho A_{\mathrm{h}}^2} \tag{۱۵}$$

متغیرهای بی‌بعد به صورت زیر تعریف می‌شوند:

$$\hat{z} \tag{۱۶}$$

$$\hat{u} \tag{۱۷}$$

$$\hat{p} \tag{۱۸}$$

با جایگذاری این پارامترهای بی‌بعد در معادلات پیوستگی و مومنتوم و آهنگ جریان جرم، این معادلات به فرم بی‌بعد تبدیل می‌شوند،

$$\frac{d}{} \tag{۱۹}$$

$$2 \tag{۲۰}$$

$$\hat{n} \tag{۲۱}$$

که گروه‌های بی‌بعد Ω_{l}'، Γ_{l} و Ω_{l} به صورت زیر تعریف می‌شوند:

$$\Omega \tag{۲۲}$$

$$I \tag{۲۳}$$

$$\Omega \tag{۲۴}$$

رابطه‌ی بین پارامترهای گسسته، Ω_{l}'، و پیوسته، Ω_{l}، به صورت زیر بدست می‌آید:

$$\Omega_{\mathrm{l}}' = \frac{K_{\mathrm{c}}'\dot{M}_{\mathrm{l}}L_{\mathrm{h}}}{\rho A_{\mathrm{h}}^2} = \frac{K_{\mathrm{c}}\dot{M}_{\mathrm{l}}L_{\mathrm{h}}}{\rho A_{\mathrm{h}}^2 d} = \frac{K_{\mathrm{c}}\dot{M}_{\mathrm{l}}}{\rho A_{\mathrm{h}}^2}N_{\mathrm{c}} = \Omega_{\mathrm{l}}N_{\mathrm{c}} \tag{۲۵}$$

پس تنها دو گروه بی‌بعد مستقل داریم. d فاصله‌ی بین دو کانال مجاور از همدیگر و N_{c} تعداد کانال موجود در یک لایه می‌باشد.

شرایط مرزی بی‌بعد نیز به صورت زیر می‌باشند:

$$\hat{u}_{\mathrm{f}}(1) = 0 \quad , \qquad \hat{u}_{\mathrm{e}}(0) = 0 \tag{۲۶}$$

$$\hat{p}_{\mathrm{f}}(0) = p_0 \, , \qquad \hat{p}_{\mathrm{e}}(1) = 0 \tag{۲۷}$$

تحلیل چند لایه(توده)

تحلیل قبلی برای یک لایه بیان شد؛ یک توده از چند لایه و منیفولدهایی که گاز را تغذیه و تخلیه می‌کنند، تشکیل شده است. یک تحلیل مشابه برای توده وجود دارد. در تحلیل قبلی در سطح لایه فاکتور K_c برای ارتباط بین آهنگ جریان جرم کانال و افت فشار در طول کانال بیان شد. در سطح توده نیز باید یک فاکتور K_l مشابه بیان گردد، طوری که آهنگ جریان جرم لایه به افت فشار بین منیفولدهای تغذیه و تخلیه ارتباط داده شود.

مقدار K_l از حل مسئله‌ی لایه پیروی می‌کند. با تعریف K_l داریم:

$$\Lambda \quad (۲۸)$$

از آنجایی که فشار دود خروجی از لایه به عنوان مرجع در نظر گرفته شده است (شکل ۴)، فقط فشار تغذیه در معادله‌ی بالا دیده می‌شود. با بی‌بعد سازی داریم:

$$\acute{\Lambda} \quad (۲۹)$$

مقدار $\hat{p}_f(0)$ از مسئله‌ی لایه‌ی بی‌بعد بدست می‌آید. با استفاده از تعریف Ω_l داریم:

$$k \quad (۳۰)$$

بنابراین مقدار K_l می‌تواند از حل بی‌بعد برای لایه محاسبه شود. با در دست داشتن مقدار K_l، تحلیل توده‌ی لایه‌ها مشابه تحلیل لایه پیش می‌رود. دو مشخصه‌ی بی‌بعد از نرخ توده و ابعاد منیفولد پیروی می‌کنند،

$$\Omega \quad (۳۱)$$

$$\Gamma \quad (۳۲)$$

در این تعاریف و با توجه به تحلیل، اندیس l برای لایه، با اندیس c برای کانال جایگزین می‌شود. به طور مشابه اندیس m برای منیفولد، با اندیس h برای هدر جایگزین می‌شود.

نتایج و بحث

در این مقاله برای حل معادلات پیوستگی و مومنتوم بدست‌آمده، از نرم‌افزار متلب استفاده شده است. شکل ۵ نتایج مربوط به سرعت و فشار بی‌بعد در هدرهای تغذیه و تخلیه و همچنین آهنگ جریان جرم بی‌بعد در کانال‌ها به ازای یک ترکیب دلخواه از پارامترهای Ω_l، Γ_l و N_c، را نشان می‌دهد. نمودارهای میله‌ای، که به ازای $N_c = ۵۰$ کانال بدست آمده‌اند، جریان جرم بی‌بعد را در هر کانال نشان می‌دهند.

به منظور یک طراحی بهینه، مسئله‌ی بی‌بعد برای تمام ترکیبات محتمل و ضروری Γ_l و $N_c\Omega_l$ حل شده است. شکل ۶ یک نقشه‌ی بی‌بعد است که اطلاعات کمی در مورد لایه بعنوان تابعی از Γ_l و $N_c\Omega_l$ را نشان می‌دهد. کانتورهای یکپارچگی جریان که به صورت زیر تعریف می‌شوند، تفاوت نسبی جریان جرم کانال‌ها را نشان می‌دهند:

$$\frac{\Delta\hat{\dot{m}}_c}{\hat{\dot{m}}_c} = \frac{\max(\hat{\dot{m}}_c) - \min(\hat{\dot{m}}_c)}{\max(\hat{\dot{m}}_c)} \quad (۳۳)$$

این فرض که جریان یکنواخت، برای طراحی لایه مطلوب می‌باشد، منجر به مقدار کوچکی از $\frac{\Delta\hat{\dot{m}}_c}{\hat{\dot{m}}_c}$ می‌گردد (ناحیه‌ی مربوط به $\frac{\Delta\hat{\dot{m}}_c}{\hat{\dot{m}}_c} < ۰/۱$ در شکل ۶). به طور کمی، این ناحیه بین مقادیر زیر محدود شده است:

$$N_c\Omega_l < 5\times10^{-2}, \quad \text{و} \quad 2.5\Gamma_l N_c\Omega_l < 1 \quad (۳۴)$$

در ناحیه‌ی جریان یکنواخت افت فشار بی‌بعد تنها به $N_c\Omega_l$ بستگی دارد، به صورت زیر:

$$\Delta\hat{p} \equiv \frac{\rho A_h^2}{\dot{M}_l^2}\Delta p = \frac{1}{N_c\Omega_l} \quad (۳۵)$$

در ناحیه‌ی بالا و سمت راست کانتورهای یکنواخت، بعضی از کانال‌ها هیچ جریانی ندارند یا جریان در آن‌ها معکوس است. از آنجایی که این نواحی برای کاربرد در پیل‌های سوختی مناسب نیستند، به آن‌ها توجهی نمی‌شود.

شکل ۷ نشان می‌دهد که چگونه توزیع جریان در کانال‌ها برای ترکیبات مختلف Ω_l و Γ_l تغییر می‌کند. توزیع جریان به طور کیفی در نواحی مختلف از جریان غیر یکنواخت، برای مقادیر کم $N_c\Omega_l$ تغییر می‌کند. جایی که کانتورهای یکپارچه به شکل خط‌هایی با شیب رو به پایین دیده می‌شوند، توزیع جریان متقارن است و جریان در کانال‌های مرکزی کمترین مقدار را داراست. برای مقادیر پایین Γ_l ، جایی که کانتورهای یکپارچه به صورت خطوط عمودی دیده می‌شوند، توزیع جریان به طور یکنواخت از یک جریان کمینه نزدیک ورودی تا یک جریان بیشینه نزدیک خروجی افزایش می‌یابد. در ناحیه‌ی خمیده، جایی که کانتورهای یکپارچه از خطوط مورب تا خطوط عمودی، به گوشه تبدیل می‌شوند، توزیع جریان از توزیع کم در مرکز به توزیع یکنواخت افزایشی تغییر می‌کند.

با توجه به معادلات پیوستگی و مومنتوم می‌توان نتیجه گرفت که برای مقادیر خیلی بزرگ Γ_l، ترم درگ در معادله‌ی مومنتوم ترم غالب و ترم هدایتی ناچیز می‌باشد؛ تحت این شرایط جریان غیریکنواخت و متقارن خواهد بود (نقطه‌ی ۵ در شکل ۷). برای مقادیر بسیار کوچک Γ_l، ترم درگ در معادله‌ی مومنتوم قابل چشم‌پوشی و ترم هدایتی ترم غالب می‌باشد و نتایج تنها به Ω_l بستگی دارد؛ در نتیجه جریان غیریکنواخت و نامتقارن خواهد بود (نقطه‌ی ۸ در شکل ۷). رفتار مربوط به مقادیر پایین هر دوی Γ_l و $N_c\Omega_l$، با جایگذاری معادلات پیوستگی در معادلات مومنتوم مشاهده می‌شود،

$$\hat{u}_h[\Gamma_l - 2\Omega_l'(\hat{p}_f - \hat{p}_e)] + \frac{d\hat{p}_h}{d\hat{z}} = 0 \quad (۳۶)$$

که Ω_l (یا Ω_l') و Γ_l هر دو کاملاً کوچکند. تغییرات فشار خیلی کوچک است؛ فشار در هدرهای تغذیه و تخلیه تقریباً یکنواخت است؛ بنابراین جریان کانال شدیداً یکنواخت است (نقطه‌ی ۲ در شکل۷). در نواحی حدود $\Gamma_l \approx ۱۰$ (ناحیه‌ی زانویی‌شکل در شکل۷) که ترم‌های درگ و هدایت هر دو در الگوی جریان دخیل هستند، جریان کانال از الگوی متقارن به غیرمتقارن گذر می‌کند(نقطه‌ی۷ در شکل۷).

بهترین ناحیه برای طراحی حوالی داخل ناحیه‌ی زانویی‌شکل کانتورهای یکپارچه است (حوالی $N_c\Omega_l \approx$ ۰/۰۲ و $\Gamma_l \approx$ ۱). شکل ۷ نتایج مربوط به نقطه‌ای از این ناحیه را نشان می‌دهد. هر چه از این ناحیه دور می‌شویم و به سمت ناحیه‌ی یکنواخت می‌رویم، معمولاً به سمت مقطع هدر بزرگ‌تر می‌رویم و نرخ جریان کمتر و یا افت فشار بیشتر می‌شود که حاصل از ابعاد کانال کوچک (K_c کوچک) است.

نتیجه‌گیری

در این مقاله توزیع جریان سیال در لایه‌های پیل سوختی صفحه‌ای شبیه‌سازی شد و معیارهایی جهت پیش‌بینی افت فشار در هر کانال و برقراری جریان یکنواخت بین کانال‌ها ارائه گردید. نتایج نشان می‌دهند که در حالت $N_c\Omega_l \approx$ ۰/۰۲ و $\Gamma_l \approx$ ۱ بهترین عملکرد از نظر توزیع یکنواخت جریان سیال بین همه کانال‌ها و حداقل افت فشار حاصل می‌شود.

مراجع

1. J. Larminie, A.Dicks, Fuel cell systems explained, second ed., John Wiley & Sons, 2003.
2. M. Iwata, T. Hikosaka, M. Morita, T. Iwanari, K. Onda, Y. Esaki, Y. Sakaki, S. Nagata, “Performance analysis of planar-type unit SOFC considering current and temperature distributions”, Solid State Ionics 132, 2000, 297-308.
3. R.J. Boersma, N.M. Sammes, “Computational analysis of the gas-flow distribution in solid oxide fuel cell stacks”, J. Power Sources 6 , 1996, 215-219.

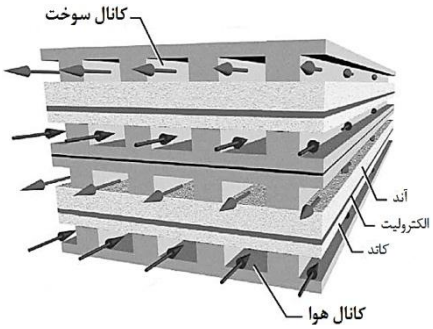

شکل ۱: بخشی از دو لایه پیل سوختی صفحه‌ای

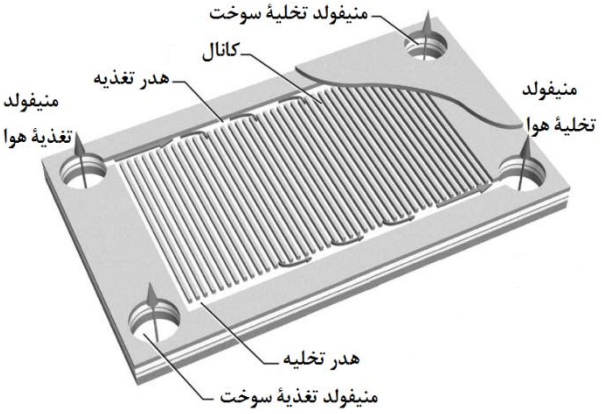

شکل ۲: توزیع جریان در یک تک لایهٔ پیل سوختی

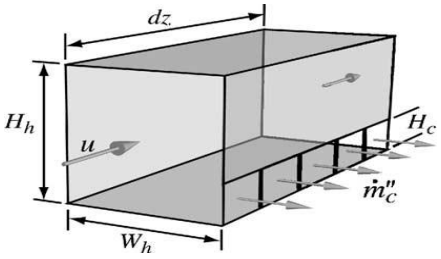

شکل ۳: حجم کنترل دیفرانسیلی از یک هدر

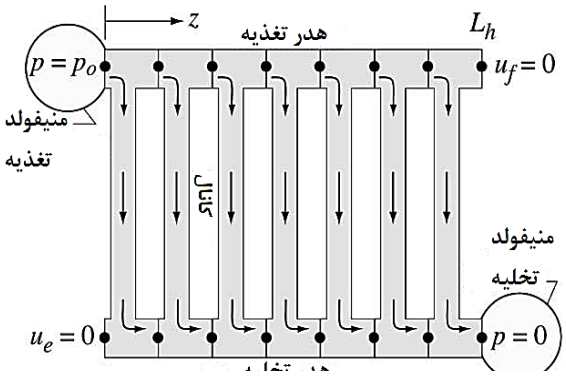

شکل ۴: نمایی از اجزا و شرایط مرزی یک تک لایهٔ پیل سوختی

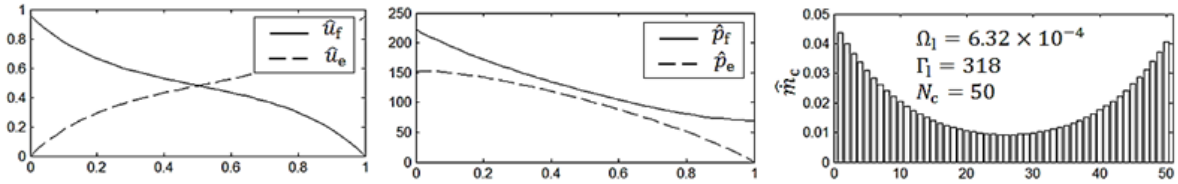

شکل۵: سرعت، فشار و آهنگ جریان جرم بی‌بعد به ازای یک ترکیب دلخواه از متغیرهای Ω_1، Γ_1 و N_c

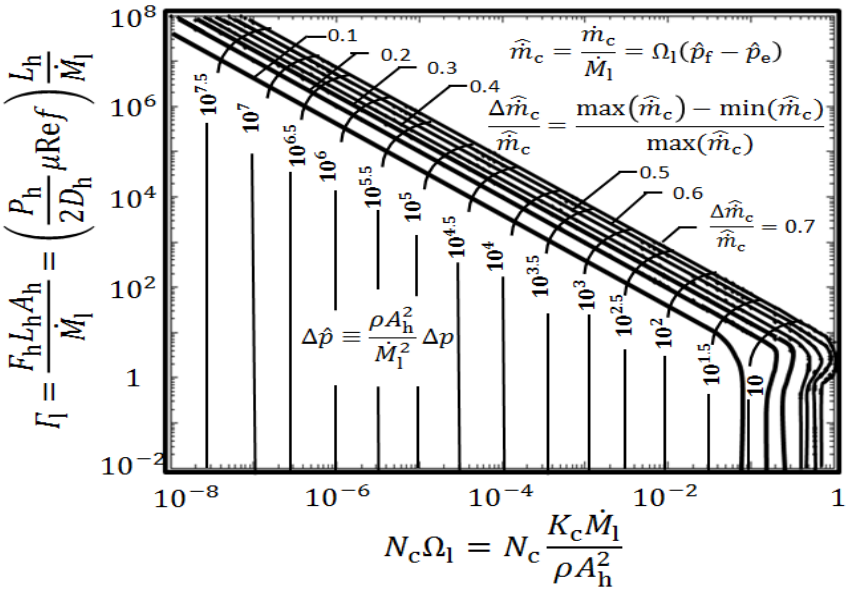

شکل ۶: کانتورهای افت فشار بی‌بعد و یکنواختی جریان کانال برحسب Γ_l و $N_c\Omega_l$

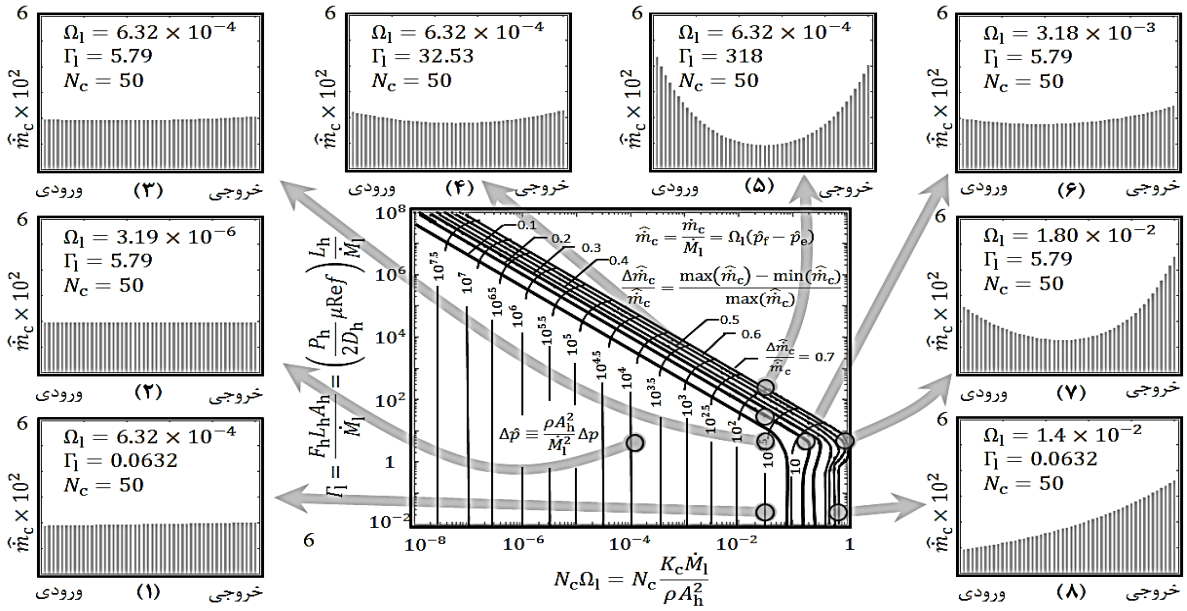

شکل ۷: کانتورهای یکپارچگی جریان بی‌بعد برحسب تابعی از Γ_l و $N_c\Omega_l$- چگونگی توزیع جریان در کانال‌ها برای ترکیبات مختلف Ω_l و Γ_l

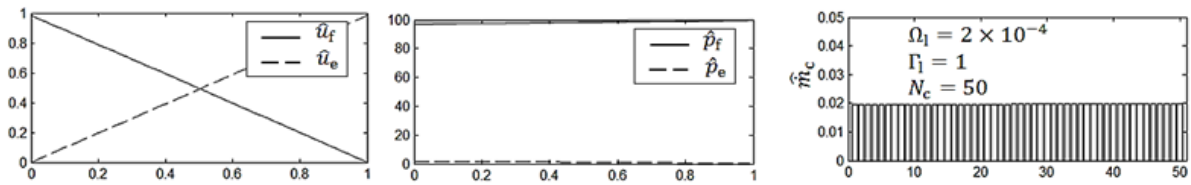

شکل۸: سرعت، فشار و آهنگ جریان جرم بی‌بعد مربوط به حالت بهینه

طیف سنجی الکتروشیمیایی و بررسی توان و ولتاژ پیل سوختی با غشاء خود مرطوب شونده و آند انتها بسته در زمان پرج هیدروژن

محمدرضا نریمانی۱، سعیداصغری۲

۱. دانشکده فنی و مهندسی، دانشگاه آزاد اسلامی، واحد علوم تحقیقات، تهران، ایران
۲. اصفهان، پژوهشکده مواد و انرژی، پژوهشگاه فضایی ، اصفهان، ایران

چکیده

در این پژوهش با استفاده از روش طیف سنجی امپدانس الکتروشیمیایی به بررسی عملکرد یک مونوسل پلیمری با غشاء خود مرطوب شونده و آند انتها بسته پرداخته شده است. در این تحقیق، تاثیر زمان توقف پرج بر عملکرد تک‌پیل مورد ارزیابی قرار گرفت. زمان‌های توقف پرج در نظر گرفته شده برای تحقیق حاضر، ۱ , ۱۰ , ۳۰, ۶۰ و ۱۲۰ ثانیه بود. نتایج حاصل از تست امپدانس الکتروشیمیایی نشان داد که با افزایش زمان توقف پرج هیدروژن، مقاومت اهمی به میزان کمی کاهش یافته است. این کاهش می‌تواند ناشی از تجمع آب در سمت آند و در نتیجه مرطوب شدن بهتر غشاء باشد. همچنین با افزایش زمان توقف پرج، حلقه مربوط به انتقال جرم در طیف امپدانس بازتر شده که نشان از افزایش مقاومت انتقال جرم است. این افزایش مقاومت انتقال جرم ناشی از تجمع قطرات آب در سمت آند و آب‌گرفتگی آن و همچنین تجمع نیتروژن نفوذی از سمت کاتد به سمت آند است.

واژه‌های کلیدی: طیف سنجی الکتروشیمیایی ؛ پرج هیدروژن؛ پیل سوختی پلیمری؛ غشاء خود مرطوب شونده

۱- مقدمه

از میان انواع پیل سوختی به نظر می رسد که پیل های سوختی پلیمری به دلیل دارا بودن زمان راه اندازی کوتاه، چگالی توان به وزن وحجم بالا و دمای عملکرد پایین گزینه مناسبی برای مصارف ایستگاهی، خانگی و حمل و نقل می باشند. در هر صورت موقعیت اقتصادی پیل های سوختی پلیمری به قابلیت اعتماد و رقابتی بودن قیمت آنها در قیاس با دیگر روش های تبدیل و تولید انرژی می باشد. برای دست یابی به این هدف و به منظور بهبود عملکرد و افزایش طول عمر آنها، فهم بهتر تاثیر تمامی پارامترها بر پیل و واکنش ها و پدیده هایی که در پیل سوختی رخ می دهند و همچنین تاثیر آنها بر عملکرد و محدودیت راندمان ضروری است. همواره فهم کامل ترمودینامیک، مکانیک سیالات، دینامیک و واکنش های الکتروشیمیایی درون پیل های سوختی پلیمری چالش بزرگی برای محققان به شمار می آید. با استفاده از روش های عیب یابی می توان از یک طرف به خصوصیات ساختاری و مشخصه های پیل سوختی، مشکلات احتمالی کارکرد و یا هر یک از اجزا دست یافت و از طرف دیگر از نتایج بدست آمده در مدل سازی برای بهینه سازی و کنترل فرآیندهای گوناگون

الکتروشیمیایی و انتقال در پیل های سوختی استفاده نمود. در این تحقیق تاثیر زمان توقف پرج هیدروژن بر روی عملکرد یک مونوسل پلیمری خود مرطوب شونده با آند انتها مورد بررسی قرار گرفت. در این پیل عامل رطوبت ساز در گاز ورودی حذف شده و هیدروژن در سمت آند در چرخه بسته کار می‌کند. برای جلوگیری از انباشتگی ناخالصی در سمت آند و افت کارکرد ناشی از آن، مقداری از گاز داخل چرخه پرج (خارج) می‌شود.

۲- مواد و روش تحقیق

۲-۱ پیل خود مرطوب شونده- آند انتها بسته و پرج هیدروژن:

در حال حاضر غشاء نفیون در پیل سوختی برای عبور پروتون نیاز به حفظ آب دارد. بنابراین برای جلوگیری از خشک شدن غشاء و رسانایی بیش تر غشاء، گازهای ورودی توسط روش های رطوبت سازهای خارجی یا داخلی، مرطوب می شوند. رطوبت ساز های خارجی باعث افزایش وزن و پیچدگی سیستم پیل سوختی و نامناسب برای حمل و نقل می شود. به منظور تحقق بخشیدن به بهره برداری از پیل های سوختی پلیمری، غشاءهای مرکب بسیاری با ویژگی خود مرطوب شوندگی که معایب ذکر شده را ندارند، توسعه داده شده است. در حال حاضر، تمرکز محققان در مورد غشاءهای خود مرطوب شوند در جهات زیر است: (۱)ترکیب کاتالیست Pt و Pt/C در غشاء به ترکیب نفوذ پذیر هیدروژن و اکسیژن برای تولید آب و مرطوب ساختن غشاء (۲) ترکیب اکسیدهای فلزی جاذب رطوبت، مانند: و یا TiO2 در جذب آب (۳) ترکیب برخی از ذرات پروتون – رسانا، مانند ZrP، HPA، SO_4^{-2} ZrO_2 یا $Cs_{2.5}H_{0.5}W_{12}O_{40}$ به منظور بهبود رسانایی پروتون غشاء [۱].

برای دستیابی به کارکرد بهتر پیل سوختی، گازهای واکنش دهنده عموما با نرخ جریان بالاتر از مقدار نیاز به سیستم وارد می شود که این شیوه حالت در جریان نامیده می شود. غلظت آن ها در محل خروجی و در مسیر های داخل پیل بالاتر خواهد بود. از طرف دیگر نرخ جریان بالاتر گازهای واکنش دهنده به خارج شدن آب تولیدی در پیل نیز کمک می کند و مجموعا عملکرد بهتر پیل نتیجه می شود.

هیدروژن می‌تواند دقیقاً با نرخی که مصرف می‌شود، تامین شود و غلظت آن در خروجی صفر خواهد بود که این روش شیوه انتها بسته نامیده می‌شود. اگر هیدروژن فشار بالا در دسترس باشد (مانند هیدروژن در یک مخزن فشار بالا) شیوه انتها بسته به هیچ کنترل کننده‌ای نیاز ندارد، زیرا هیدروژن به اندازه مصرف آن تامین می‌شود و در این حالت ضریب استوکیومتریک برابر یک است. اگر نفوذ هیدروژن از میان غشاء، جریان‌های داخلی هیدروژن و نشتی ها نیز در نظر گرفته شود؛ نرخ جریان هیدروژن ورودی کمی بیشتر از نرخ مصرف هیدروژن برای تولید جریان می‌باشد.

هیدروژن می‌تواند دقیقاً با نرخی که مصرف می‌شود، تامین شود و غلظت آن در خروجی صفر خواهد بود که این روش شیوه انتها بسته نامیده می‌شود. اگر هیدروژن فشار بالا در دسترس باشد (مانند هیدروژن در یک مخزن فشار بالا) شیوه انتها بسته به هیچ کنترل کننده‌ای نیاز ندارد، زیرا هیدروژن به اندازه مصرف آن تامین می‌شود و در این حالت ضریب استوکیومتریک برابر یک است. اگر نفوذ هیدروژن از میان غشاء، جریان‌های داخلی هیدروژن و نشتی ها نیز در نظر گرفته

شود؛ نرخ جریان هیدروژن ورودی کمی بیشتر از نرخ مصرف هیدروژن برای تولید جریان می‌باشد. در شکل (۱) پیچیدگی سیتم در حالت جریان نسبت به حالت انتها بسته در یک توده پیل سوختی را می توان مشاهده نمود.

اگرچه هیدروژن مورداستفاده در پیل سوختی بایستی بسیار خالص باشد ولی مقدار اندک ناخالصی موجود در هیدروژن نیز در طی زمان و با کارکرد مداوم پیل، در سمت آند انباشته می شود. همچنین در پیل سوختی آند بسته در طول کارکرد، نیتروژن و آب مایع در قسمت آند انباشته شده که باعث افت تدریجی ولتاژ می شود. بنابراین جهت به حداقل رساندن میزان این ناخالصی ها، پرچ در سمت هیدروژن لازم است.

۲-۲ روش های عیب یابی و مروری بر مطالعات پیل های سوختی خود مرطوب شونده :

روش های متعددی در زمینه عیب یابی توده های پیل سوختی پلیمری وجود دارند .به طور کلی این روش ها به دو دسته تست های الکتروشیمیایی و تست های فیزیکی / شیمیایی تقسیم می شوند.

روش های روبش جریان[۳۴]، قطع جریان[۳۵]، طیف سنجی امپدانس الکتروشیمیایی، ... در زمره تست های الکتروشیمیایی و روش های اندازه گیری افت فشار، کروماتوگرافی گاز (GC)، تصویر نگاری تشدید مغناطیسی (MRI)، ... در زمره تست های فیزیکی/ شیمیایی قرار می گیرند[۳و۴].

در میان روش ها، عیب یابی غیر مخرب از جایگاه ویژه ای برخوردار است. چرا که بدون ایجاد اغتشاش در عملکرد پیل های سوختی پلیمری می توانند عملکرد آن ها را ارزیابی نمایند. یکی از این روش ها، روش طیف سنجی امپدانس الکتروشیمیایی است که در آن سیگنال کم دامنه جریان یا ولتاژ AC با فرکانس معین به پیل سوختی اعمال شده، دامنه و اختلاف فاز سیگنال پاسخ به صورت تابعی از فرکانس ذخیره می شود. روش های دیگر عیب یابی بسیار دور از حال تعادل عمل می کنند، اما این روش به شرایط عملکرد واقعی و حالت تعادل پیل سوختی نزدیک است. اخیراً محققان مختلفی از این روش برای عیب یابی پیل سوختی استفاده کرده‌اند که از آن جمله می‌توان به گیو(Guo) [۵]، در رابطه با بهینه سازی ساختار مجموعه غشاء الکترود، هالسید (Halseid)[۶] در زمینه بهینه سازی شرایط عملکرد و مقاومت غشاء، سورانو (Ciureanu)، کیم (Kim)، واگنر (Wagner)[۷] در مورد آلاینده های پیل سوختی اشاره نمود.

یانگتیک لی و همکاران در تحقیقی رفتار دینامیکی غشاءی خودمرطوب شونده پلیمری در پیل سوختی را مورد بررسی قرارداده اند[۸].

نمونه‌ای از نمودر نایکوئیست حاصل از تست امپدانس الکتروشیمیایی که بر روی یک پیل سوختی پلیمری صورت پذیرفته است، در شکل (۲) نشان داده شده است. حلقه (۱) مربوط به فرکانس های پایین (1 Hz<f) بوده و معرف پدیده انتقال جرم است. قطر این حلقه نشان دهنده مقدار مقاومت انتقال جرم بوده و غالباً در جریان های بالا که انتقال جرم نقش اساسی را در افت پتانسیل دارد، ظاهر می شود. حلقه (۲) در محدوده فرکانس های متوسط (1 KHz<f<1 Hz) قرار داشته و به دلیل

[34] *Current Sweep*
[35] *Current Interruption*

آنکه از واکنش آرام کاهش اکسیژن تأثیر می پذیرد، غالباً حلقه سینتیک (Kinetic Loop) نامیده می شود و قطر آن معرف مقاومت انتقال بار است. حلقه (۳) مربوط به فرکانس های بالا (F>1 KHz) بوده و به ساختار مجموعه غشاء الکترود وابسته است[۱۰]. هر چند در بعضی از تحقیقات، مقاومت اهمی داخلی و ظرفیت تماس ساختار دانه ای الکترود عامل حلقه فرکانس بالا شناخته شده است[۱۱]. مقاومت اهمی کل پیل سوختی که متشکل از مقاومت اهمی اجزاء تشکیل دهنده پیل سوختی (غشاء، صفحات دو قطبی، ...) و مقاومت تماسی بین این اجزا است، با بخش حقیقی ابتدای حلقه فرکانس بالا (حدود 1KHz) مشخص می شود[۹].

۲-۳ طراحی و ساخت مونوسل

مونوسل ساخته شده شکل (۳) از نوع پلیمری بوده و دارای ابعاد ۴*۱۲/۵ سانتی متر مربع می باشدکه مشخصات آن در جدول (۱) آورده شده است.

۲-٤ دستگاه تست و مشخصات آن

دستگاه تست مورد استفاده شکل (۴) برای انجام آزمایشات بر روی مونو سل در پژوهشکده مواد و انرژی اصفهان طراحی و ساخته شده است، که با ایجاد یک مسیر جانبی در سمت آند جهت تغذیه گاز هیدروژن به پیل، قابل استفاده برای انجام تست بر روی پیل سوختی پلیمری قرار گرفت. این دستگاه تست به طور کلی از سه قسمت تشکیل شده است:

قسمت اول: وظیفه هدایت و تغذیه گازهای واکنش دهنده را بر عهده دارد.

قسمت دوم: وظیفه کنترل پارامترهای مختلف جریان واکنش دهنده ها به پیل را بر عهده دارد که از دو قسمت سخت افزاری و نرم افزاری تشکیل شده است.

قسمت سوم: وظیفه اعمال بار بر روی پیل سوختی و تست الکتریکی پیل تحت بارهای مختلف را بر عهده دارد. ثبت مشخصات ولتاژ و جریان در شرایط مختلف نیز توسط مدار کنترلی انجام می گیرد. در شکل (۴) این دستگاه تست نشان داده شده است.

پارامترهای دخیل در عملکرد پیل طبق جدول (۲) ثابت، پرج هیدروژن در زمان های توقف ۱، ۶۰،۳۰،۱۰ و ۱۲۰ اعمال گردید. برای هر زمان توقف پرج، پس از پایدار شدن شرایط کاری و ولتاژ خروجی، تست امپدانس الکتروشیمیایی صورت پذیرفت. این تست در محدوده فرکانسی ۱ هرتز تا ۱۰۰۰ هرتز صورت پذیرفته و مقدار جریان متناوب درخواستی برابر پنج درصد جریان مستقیم خروجی از پیل تعیین گردید.

۳- نتایج

۳-۱ نمودار نایکویست

همانگونه که از شکل (۵) مشاهده می‌شود، با افزایش زمان پرج هیدروژن، مقاومت اهمی کاهش اندکی می‌یابد. کاهش مقاومت اهمی می تواند ناشی از تجمع بیشتر آب در سمت آند با افزایش زمان توقف پرج است. این تجمع بیشتر آب منجر به مرطوب شدن بیشتر غشاء خود مرطوب شونده شده که خود کاهش مقاومت اهمی غشاء را به دنبال دارد. همچنین با

افزایش زمان توقف پرج، قطر حلقه‌ی انتقال جرم رو به افزایش می‌باشد. به نظر می‌رسد که افزایش انتقال جرم با افزایش زمان توقف پرج ناشی از تجمع آب در سمت آند و وقوع پدیده آب‌گرفتگی در آن و همچنین تجمع نیتروژن نفوذی از سمت کاتد باشد. این مقاومت ها در زمان‌های توقف پرج ۶۰ و ۱۲۰ ثانیه افزایش بیشتری را نشان می‌دهند.

۳-۲ بررسی تغییرات ولتاژ در تست تغییرات زمان توقف پرج

طبق شکل های (۶) تا (۱۰) با افزایش زمان پرج از ۱ ثانیه به بالا با افت ولتاژ مواجه هستیم. هر چه مدت زمان پرج کوتاهتر باشد میزان نوسان فشار در نقاط داخلی توده پیل و دورتر از محل پرج، کمتر بوده و به مرور اثر تغییرات فشار ناشی از پرج محو می شود، یعنی با کاهش مدت زمان پرج، هم میزان افت فشار کمتر می شود و هم در طول کوتاهتری از مسیر آند محسوس خواهد بود.همچمین به افزایش زمان پرج باعث پدیده آبگرفتگی در سطح غشا افزایش یافته است و کاهش ولتاژ را نتیجه می شود.

۳-۳ بررسی تغییرات توان در تست تغییرات پرج در مونوسل مورد آزمایش

با توجه به شکل های (۱۱) تا (۱۵) با افزایش زمان پرج تقریبا توان در حال کاهش است و در زمان پرج ۱۲۰ ثانیه در کمترین توان خود می باشد. که به علت آبگرفتگی و افت فشار در صورت زمان های توقف بیشتر پرج می باشد.

۴- نتیجه گیری:

در این پژوهش عملکرد یک پیل سوختی پلیمری خود مرطوب شونده با آند انتها بسته به کمک روش طیف سنجی امپدانس الکتروشیمیایی مورد ارزیابی قرار گرفت. در طی این تحقیق، زمان توقف پرج هیدروژن بر رفتار امپدانس یک تک پیل مورد ارزیابی قرار گرفت و نتایج زیر حاصل شدند.

- با افزایش زمان پرج هیدروژن، مقاومت اهمی کاهش اندکی می‌یابد. کاهش مقاومت اهمی می تواند ناشی از تجمع بیشتر آب در سمت آند با افزایش زمان توقف پرج است.
- هر چقدر پرج هیدروژن در زمان کمتری رخ دهد کلیه مقاومت های ظاهر شده در پیل نسبت به پرج در ثانیه های بالاتر در کمترین حد ممکن می باشد.
- مدت زمان پرج باید در کمینه زمان ممکن که توسط سیستم قابل فرمان دادن و اجراست در نظر گرفته شود. این زمان، از مشخصات شیر مورد استفاده جهت پرج است. البته از طرف دیگر با کاهش زمان توقف پرج، میزان هدرروی هیدروژن افزایش می‌یابد. بدین منظور بایستی زمان توقف پرج بهینه‌ای یافت که از یک طرف افت ولتاژ ناشی از وقوع پدیده تجمع آب و انباشتگی نیتروژن نفوذی از سمت کاتد به سمت آند کاهش یافته و از طرف دیگر هدر روی هیدروژن به محیط بیرون ناشی از فرایند پرج کاهش یابد.
- عمده مقاومت ظاهر شده در پرج هیدروژن مقاومت انتقال جرم است.

منابع:

1. Zhang, Yu, Huamin Zhang, Cheng Bi, and Xiaobing Zhu. "An inorganic/organic self-humidifying composite membranes for proton exchange membrane fuel cell application." Electrochimica Acta 53, no. 12 (2008): 4096-4103.

2. Chen, Jixin, Jason B. Siegel, and Anna G. Stefanopoulou. "Nitrogen blanketing front equilibria in dead end anode fuel cell operation." In American Control Conference (ACC), 2011, pp. 1524-1529. IEEE, 2011.

3. Wu, Jinfeng, Xiao Zi Yuan, Haijiang Wang, Mauricio Blanco, Jonathan J. Martin, and Jiujun Zhang. "Diagnostic tools in PEM fuel cell research: Part I Electrochemical techniques." International journal of hydrogen energy 33, no. 6 (2008): 1735-1746.

4. Wu, Jinfeng, Xiao Zi Yuan, Haijiang Wang, Mauricio Blanco, Jonathan J. Martin, and Jiujun Zhang. "Diagnostic tools in PEM fuel cell research: part II: physical/chemical methods." International Journal of Hydrogen Energy 33, no. 6 (2008): 1747-1757.

5. Guo, Qingzhi, Maria Cayetano, Yu-min Tsou, Emory S. De Castro, and Ralph E. White. "Study of ionic conductivity profiles of the air cathode of a PEMFC by AC impedance spectroscopy." Journal of The Electrochemical Society 150, no. 11 (2003): A1440-A1449.

6. Halseid, Rune, Preben JS Vie, and Reidar Tunold. "Influence of ammonium on conductivity and water content of Nafion 117 membranes." Journal of the electrochemical society 151, no. 3 (2004): A381-A388.

7. Wagner, N., and E. Gülzow. "Change of electrochemical impedance spectra (EIS) with time during CO-poisoning of the Pt-anode in a membrane fuel cell." Journal of Power Sources 127, no. 1 (2004): 341-347.

8. Lee, Yongtaek, Bosung Kim, and Yongchan Kim. "Effects of self-humidification on the dynamic behavior of polymer electrolyte fuel cells." International Journal of Hydrogen Energy 34, no. 4 (2009): 1999-2007.

9. Lee, Yongtaek, Bosung Kim, and Yongchan Kim. "Effects of self-humidification on the dynamic behavior of polymer electrolyte fuel cells." International Journal of Hydrogen Energy 34, no. 4 (2009): 1999-2007.

10. Study of PEM fuel cell performance by electrochemical impedance spectroscopy Original Research Article International Journal of Hydrogen Energy, Volume 35, Issue 17, September 2010, Pages 9283-9290 Saeed Asghari, Ali Mokmeli, Mahrokh Samavati.

11. Romero-Castanon, T., L. G. Arriaga, and U. Cano-Castillo. "Impedance spectroscopy as a tool in the evaluation of MEA's." Journal of power sources 118, no. 1 (2003): 179-182.

جدول (۱) مشخصات مونوسل طراحی شده

ضخامت غشاء:	۱۸ میکرون
سطح فعال الکترود:	۵۰ سانتی متر مربع

بارگذاری کاتالیست در سمت آند:	۱/۲ میلی گرم بر سانتی متر مربع
بارگذاری کاتالیست در سمت کاتد:	۴/۲ میلی گرم بر سانتی متر مربع
جنس لایه پخش کننده گاز:	کربن کاغذی

جدول(۲) پارامترهای ثابت تست پرچ هیدروژن در مونوسل

دمای کارکرد	۵۰ سانتی گراد
جریان الکتریکی	۵۰ آمپر
فشار در قسمت آند	۰,۱ بار
استوکیومتری هوا	۲

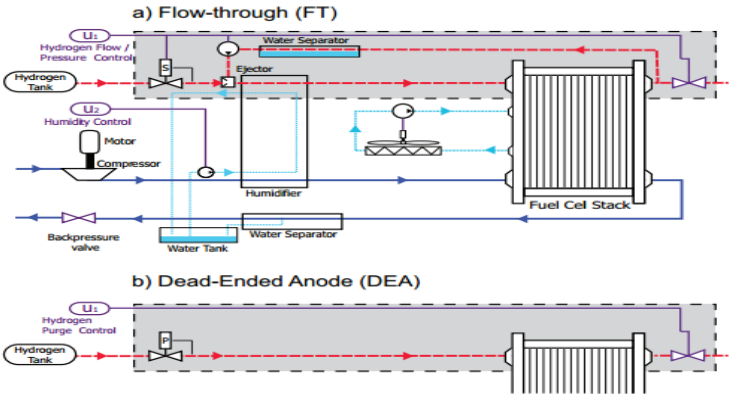

شکل (۱) مقایسه بین پیچیدگی سیستم حالت در جریان(a) و حالت آند انتها بسته(b) درپیل سوختی [۲]

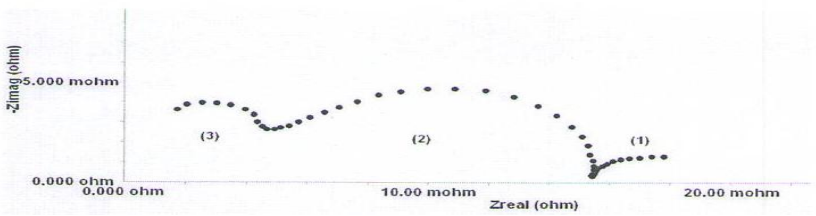

شکل(۲)- نمونه نمودار نایکوئیست پیل سوختی پلیمری با سه حلقه[۹]

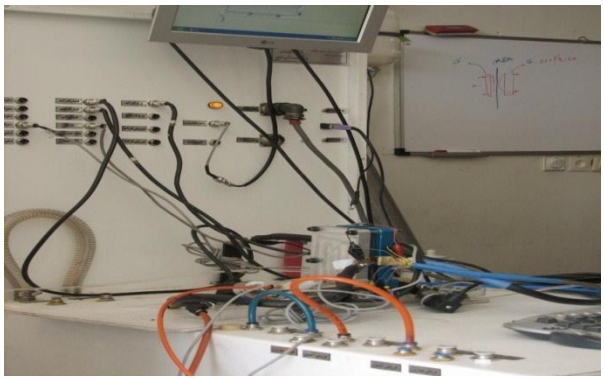

شکل (۳) مونوسل ساخته شده در حین تست

شکل (۴) دستگاه تست پیل سوختی مورد استفاده در پژوهشکده مواد و انرژی

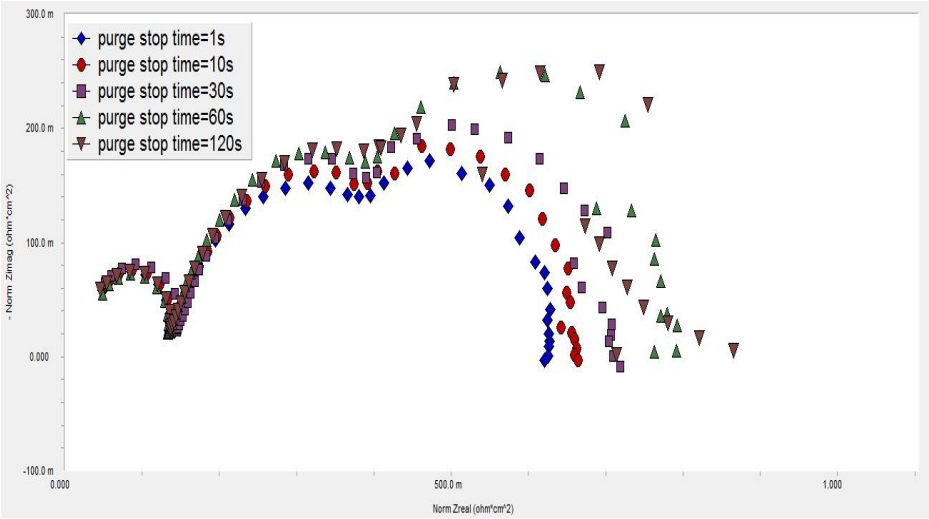

شکل(۵) نمودار نایکویست تست پرج هیدروژن در آزمایش

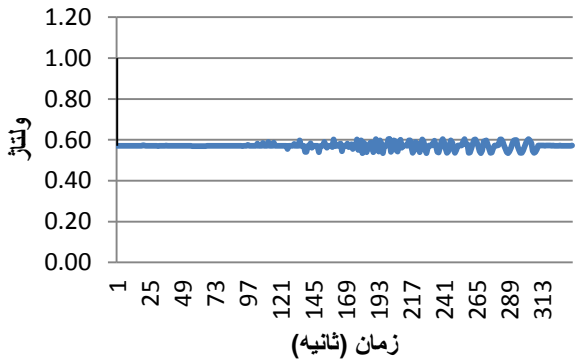

شکل (۶)تغییرات ولتاژ در پرج ۱ ثانیه در تست

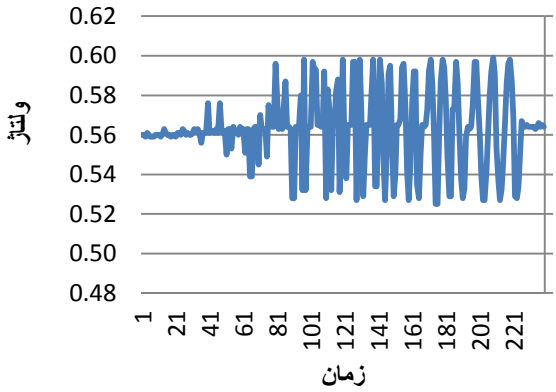

شکل (۷)تغییرات ولتاژ در پرج ۱۰ ثانیه در تست

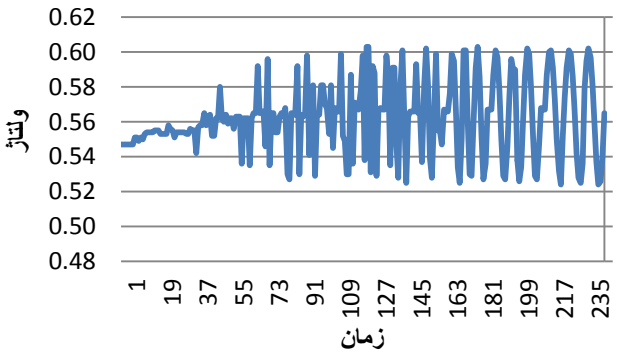

شکل (۸)تغییرات ولتاژ در پرج ۳۰ ثانیه در تست

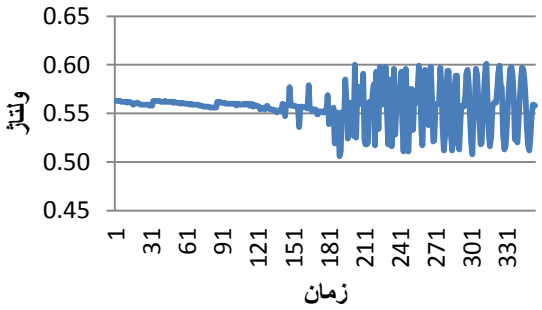

شکل (۹)تغییرات ولتاژ در پرج ۶۰ ثانیه در تست

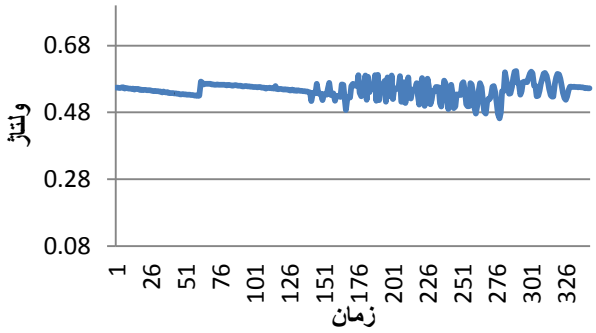

شکل (۱۰)تغییرات ولتاژ در پرج ۱۲۰ ثانیه در تست

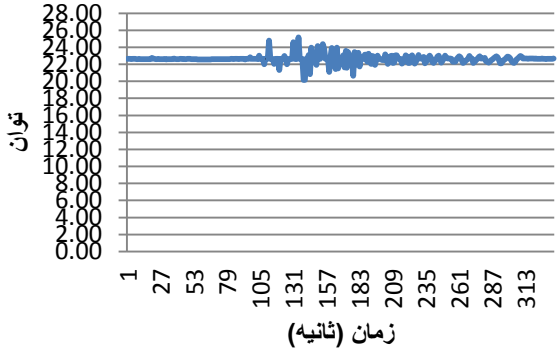

شکل (۱۱)تغییرات توان در پرج ۱ ثانیه در تست انجام گرفته

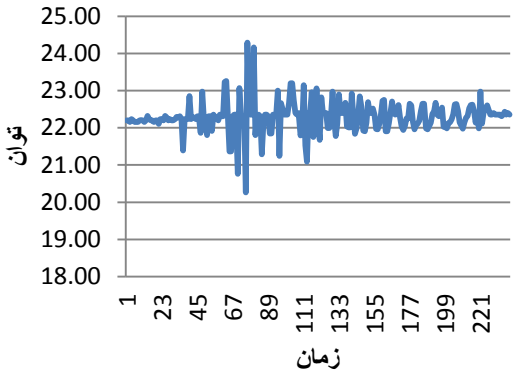

شکل (۱۲)تغییرات توان در پرج ۱۰ ثانیه در تست انجام گرفته

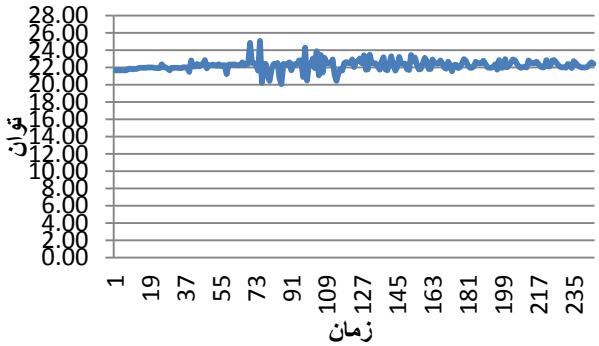

شکل (۱۳)تغییرات توان در پرج ۳۰ ثانیه در تست

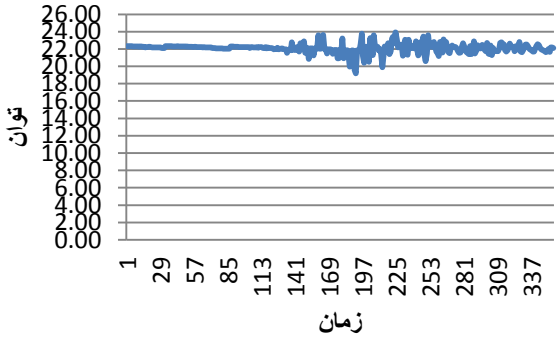

شکل (۱۴)تغییرات توان در پرج ۶۰ ثانیه در تست

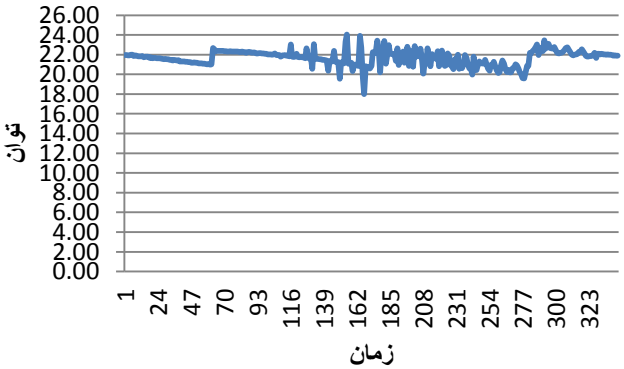

شکل (۱۵) تغییرات توان در پرج ۱۲۰ ثانیه در تست